ARCHIVES OF MECHANICS **Appears since 1949**

Aims and Scope

ARCHIVES OF MECHANICS provides a forum for original research on mechanics of solids, fluids and discrete systems, including the development of mathematical methods for solving mechanical problems. The journal encompasses all aspects of the field, with the emphasis placed on:

- mechanics of materials: elasticity, plasticity, time-dependent phenomena, phase transformation, damage, fracture; physical and experimental foundations, micromechanics, thermodynamics, instabilities
- methods and problems in continuum mechanics: general theory and novel applications, thermomechanics, structural analysis, porous media, contact problems
- dynamics of material systems
- fluid flows and interactions with solids

Address of the Editorial Office:
Institute of Fundamental Technological Research
Świętokrzyska 21
PL 00-049 Warsaw, Poland

Tel.(48-22) 826 60 22, Fax (48-22) 826 98 15, E-mail: publikac@ippt.gov.pl

Abstracted/indexed in:

Applied Mechanics Reviews, Current Mathematical Publications, Mathematical Reviews, MathSci, Zentralblatt für Mathematik, UnCover, Inspec.

http://am.ippt.gov.pl/

Polish Academy of Sciences
Institute of Fundamental Technological Research

Archives of Mechanics

Archiwum Mechaniki Stosowanej

volume 54 issue 5-6

DRUKARNIA BRACI GRODZICKICH

SUBSCRIPTIONS

Address of the Editorial Office: Archives of Mechanics
Institute of Fundamental Technological Research, Świętokrzyska 21
PL 00-049 Warsaw, Poland
Tel. 48 (*prefix*) 22 826 60 22, Fax 48 (*prefix*) 22 826 98 15,
e-mail:publikac@ippt.gov.pl

Subscription orders for all journals edited by IFTR may be sent directly to the Editorial Office of the Institute of Fundamental Technological Research

Subscription rates

Annual subscription rate (2002) including postage is US $ 240.
Please transfer the subscription fee to our bank account: Payee: IPPT PAN,
Bank: PKO SA. IV O/Warszawa,
Account number 12401053-40054492-3000-401112-001.

All journals edited by IFTR are available also through:

- Foreign Trade Enterprise ARS POLONA Krakowskie Przedmieście 7,
  00-068 Warszawa, Poland fax 48 (*prefix*) 22 826 86 73
- RUCH S.A. ul. Towarowa 28,
  00-958 Warszawa, Poland fax 48 (*prefix*) 22 620 17 62
- International Publishing Service Sp. z o.o. ul. Noakowskiego 10 lok. 38
  00-664 Warszawa, Poland tel./fax 48 (*prefix*) 22 625 16 53, 625 49 55

Warunki prenumeraty

Redakcja przyjmuje prenumeratę na wszystkie czasopisma wydawane przez IPPT PAN. Bieżące numery można nabyć, a także zaprenumerować roczne wydanie Archiwum Mechaniki Stosowanej bezpośrednio w Dziale Wydawnictw IPPT PAN, Świętokrzyska 21, 00-049 Warszawa, Tel. 48 (*prefix*) 22 826 60 22; Fax 48 (*prefix*) 22 826 98 15.
Cena rocznej prenumeraty z bonifikatą (na rok 2002) dla krajowego odbiorcy wynosi 300 PLN

Również można je nabyć, a także zamówić (przesyłka za zaliczeniem pocztowym) we Wzorcowni Ośrodka Rozpowszechniania Wydawnictw Naukowych PAN,
00-818 Warszawa, ul. Twarda 51/55, tel. 48 (*prefix*) 22 697 88 35.
Wpłaty na prenumeratę przyjmują także jednostki kolportażowe RUCH S.A. Oddział Krajowej Dystrybucji Prasy, 00-958 Warszawa, ul. Towarowa 28. Konto: PBK. S.A. XIII Oddział Warszawa nr 11101053-16551-2700-1-67. Dostawa odbywa się pocztą lotniczą, której koszt w pełni pokrywa zleceniodawca. Tel. 48 (*prefix*) 22 620 10 39, Fax 48 (*prefix*) 22 620 17 62

Arkuszy wydawniczych 34.5. Arkuszy drukarskich 39.4
Papier offset. kl III 70g. B1.
Oddano do składania w listopadzie 2002 r. Druk ukończono w styczniu 2003 r.
Skład w systemie TEX: E. Jaczyńska.
Druk i oprawa: Drukarnia Braci Grodzickich, Piaseczno ul. Geodetów 47A.

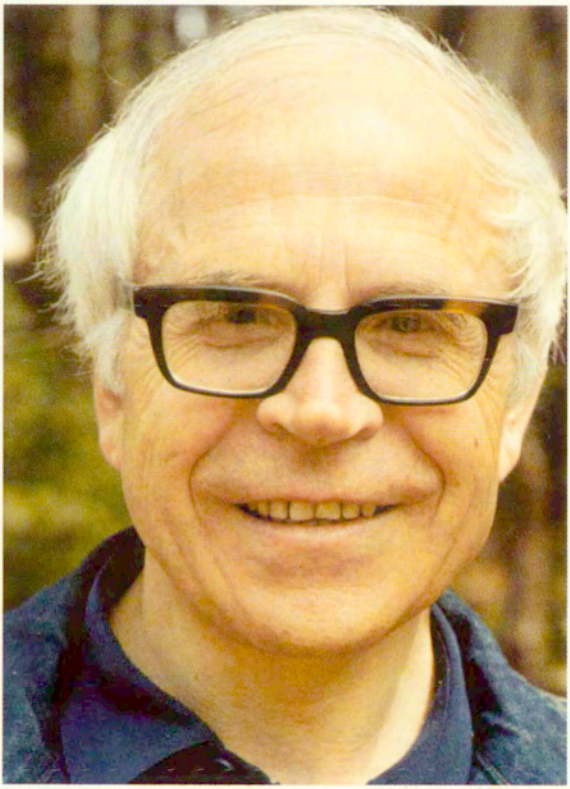

Professor Piotr PERZYNA

A BRIEF SUMMARY OF PROFESSIONAL CAREER OF PROFESSOR PIOTR PERZYNA

Professor Piotr Perzyna was born on August 1, 1931 in the village of Niedźwiada near Łowicz in Poland. He received the M.S. degree in 1956 from the Department of Mechanical Engineering of Warsaw Technical University. He subsequently completed a Ph.D. in Mechanics of Solids at the Institute of Fundamental Technological Research, Polish Academy of Sciences in 1959 under the supervision of Professor Wacław Olszak. The academic year of 1961–1962 he spent abroad working as a Post Doc at Brown University with Professor William Prager. In 1963, he defended his D. Sc (habilitation) thesis.

Since the beginning of his scientific carrier he has been associated with the Institute of Fundamental Technological Research, Polish Academy of Sciences (IPPT PAN). He also held important administrative positions. In 1964 he was promoted to the rank of Associate Professor and the Head of Theory of Viscoplasticity Group, then from 1970 as a Professor, and from 1978 as a Full Professor. In the period 1980–1982 he was a Scientific Director of the Institute; in 1982 he became Head of Department of Theory of Inelastic Materials, Centre of Mechanics. During 1978–1980 he was also the Director of Doctoral Studies at the Institute. In recognition of his achievement he was invited as a Visiting Professor by a number of foreign universities, including University of Kentucky, USA (1969–1970); Université Poitiers, France (1982 and 1985), Brown University, Providence, R.I. (1982), MIT, Cambridge, Mass, U.S.A (1985), Tokyo University, Japan (1986), University of Hannover, Germany (1988–1991).

Professor Perzyna made significant scientific contribution mostly in the field of theory of plasticity, and viscoplasticity, adiabatic shear band, localization and fracture phenomena in solids. He has been particularly interested in high rate effects, thermomechanical couplings, microdamage effects and fracture under dynamic loadings.

Professor Perzyna is the father of a new discipline that is known under the name of "theory of viscoplasticity". His pioneering work in this area has led to the formulation of many interesting projects, both at home and abroad. Of particular interest are the results of the constitutive modeling of inelastic materials with views of the describing the effects of localization and fracture. Professor Perzyna proposed an original concept of describing the above effects through the ther-

modynamic structure with internal parameters (state variables). He chose those parameters very carefully, considering both the physical foundations and the experimental observations. His concepts found wide spread applications to describe analytically phenomena of localization and damage in mono and polycrystals. He succeeded in deriving closed form solutions for the process of localization of plastic and viscoplastic deformations in solids.

More recently Professor Perzyna has been working in the area of instability of the processes of plastic flow and fracture in collaboration, among others, with the Technical University in Poznań and the University of Hannover. He made substantial contributions in the area of computer simulation of the process of plastic flow. The numerical procedures developed by him are stable and therefore are capable of predicting local effects leading to fracture. His work in this area is widely cited and further developed in a number of leading research centers in the USA, England, France, Spain, Denmark, Italy, Holland, Japan, Germany, Argentina, Bulgaria, Romania, and Russia.

Finally, one has to mention two other areas to which Professor Perzyna contributed over the years, that is the thermodynamics of continuous media as well as dynamic and wave effects. One of the first papers in this field was published back in 1963 in the well-established European journal *ZAMP*. "On the propagation of stress waves in a rate sensitive plastic medium", Vol. 14, pp. 241–261, 1963.

The above paper along with another ground breaking publication "The constitutive equations for rate sensitive plastic materials", *Quarterly of Applied Mathematics*, Vol. 15, pp. 321–332, 1963 laid the foundation for the new discipline of viscoplasticity and set up his brilliant international career which lasts until today. Professor Perzyna is the author of three monographs and about 260 original papers. Most of this work has been published in leading international journals.

Since 1964 he has participated and contributed to all IUTAM Congresses and in many international conferences and particularly the ICTAM Symposia and the EUROMECH Colloquia. In 1978, 1980, 1997 and 1998 he organized international courses in CISM, Udine, Italy and between 1981 and 1986 he was a member of the EUROMECH Advisory Committee. He received many distinctions and awards, including the Maximilian Tytus Huber Award in 1960; the award of the Scientific Secretary of the Polish Academy of Sciences in 1974 and 1978. In 1993 he received the Max Planck Research Award in recognition of his contribution to a long-range project conducted with Professor E. Stein at the University of Hannover. In the period 1966–1994 he was a member of the Editorial Committee of the *Archives of Mechanics* and *Engineering Transactions*. At various times he was also a member of the Advisory Board of the *International Journal of Plasticity, International Journal of Impact Engineering, JSME International Journal of Mechanics and Material Engineering,* and the *European Journal of Mechanics*.

Professor Perzyna's contributions to the education of almost two generations of professional colleagues are enormous. He promoted a dozen doctoral theses spanning a period of almost 40 years. The names of his Ph.D. students (in alphabetical order) are:

Angel Baltov, Józef Bejda, Paweł Dłużewski, Aldona Drabik, Kurt Frischmuth, Tadeusz Jeske, Witold Kosiński, Sumio Murakami, Zdzisław Nowak, Anna Pabjanek, Ryszard Pęcherski, Amalia Pielorz, Jacek Rońda, Katarzyna Szmit-Saxton, Tomasz Wierzbicki, Włodzimierz Wojno.

Piotr was a very demanding advisor but also an excellent and highly respected professional colleague and friend. His enthusiasm, high ethical standards, and scientific rigor in his approach to research shaped the minds of generations of his co-workers. Many of his former students and collaborators have become well-established professionals at home and abroad. For example, Dr. Wierzbicki holds the position of Professor at the Massachusetts Institute of Technology; Dr. Baltov is the Scientific Director of the Bulgarian Academy of Sciences; Dr. Murakami is a Professor at Nagoya University; Dr. Kosiński is a Professor and the vice-President for Scientific Affairs of the Polish-Japanese Institute of Information Technology and Dr. Drabik is the vice-President for Students Affairs of the same Institute; Dr. Rońda is a Professor at the Cape Town University, Dr. Saxton is a Professor at the Loyola University, Dr. Pęcherski is a Professor at the Technical University of Kraków, and Dr. Frischmuth is an Associate Professor at Rostock University.

Many colleagues and friends around the world would like to join the above group of Piotr's close collaborators and wish him many happy years in his professional and private life.

Witold Kosiński *Warsaw, Poland*

Tomasz Wierzbicki *Cambridge, MA*

Arch. Mech., **54**, 5-6, pp. 361–371, Warszawa 2002

Linear stability of a 1D flow in porous media under transversal disturbance with adsorption

B. ALBERS

Weierstrass Institute for Applied Analysis and Stochastics
Berlin, Germany
e-mail: albers@wias-berlin.de

Dedicated to Professor Piotr Perzyna
on the occasion of his 70^{th} birthday

IN THIS PAPER we investigate the linear stability behavior of a flow within an adsorption/diffusion model for porous materials summarized in Section 2. We consider a 1D stationary flow through a poroelastic medium which is perturbed by transversal (2D) disturbances with mass exchange. The eigenvalue problem for the first step field equations is solved using a finite-difference scheme. We present the instability regions in dependence on the three most important model parameters, namely the bulk and surface permeability coefficients, and the mass density of the adsorbate on the inner surface.

1. Introduction

AT LEAST TWO kinds of instabilities may appear in porous media: structural instabilities, and flow instabilities. Examples of structural instabilities are piping (the brakedown of a granular medium) or shear band formation. The appearance of Bénard cells or the change from laminar to turbulent flows belong to the class of flow instabilities. All kinds of instability have in common that they appear due to competition of at least two mechanisms. In the case of structural instabilities, e.g. a threshold nonlinearity competes with the permeability of the material. A flow instability arises if a kinematic nonlinearity acts against, for example, viscosity.

This paper is devoted to the investigation of one special type of flow instability. We consider a steady state 1D flow in a porous medium. This defines the base flow on which we superpose a small disturbance with adsorption. The disturbances satisfy equations of the model for multicomponent systems with adsorption (summarized in Section 2 and introduced in [2]). It is considered that a fluid/adsorbate mixture flows through channels of a skeleton. In this case a kinematic nonlinearity acts against the permeability (diffusion) of the medium.

Adsorption processes contribute in a nonlinear way to the field equations, and essentially influence the stability properties.

Small disturbances are inevitably present in any real system but their effect on stable systems is mostly ephemeral. Consider, for example, the influence of wavelike disturbances on the circulation of the athmosphere. As we have shown in earlier works also the superposition of the same flow as this considered in this paper with disturbances without mass exchange led to completely stable situations. But the disturbance with adsorption yields the existence of an instable region which means that adsorption slows down the relaxation process tremendously or even controls the loss of stability of the base flow (see: [3]) for a certain region of permeability coefficients. If the base flow is unstable, the disturbances will grow in amplitude with time and space. However, the values of the permeability coefficient for which the base flow is unstable are much smaller than those used in earlier works.

The region of instability for a transversal disturbance of the base flow with adsorption will be shown in dependence on three important model parameters.

First there appear two different permeability coefficients, namely the bulk permeability coefficient π, and the surface permeability α. While the first one enters the field equations and describes the effective resistance of the skeleton to the flow of the fluid, the latter enters the model through the boundary conditions of the third type, and it accounts for properties of the surface. It is one of the material parameters which determine the fluid velocity. The third parameter, the mass density of the adsorbate on the internal surface ρ_{ad}^{A}, enters the model through the mass source. It is proportional to the size of the internal surface which plays an enormous role for the global rate and amount of adsorption. For different soils it may vary by some orders of magnitude.

2. Adsorption/diffusion model

We investigate the stability behavior of a 1D base flow under perturbations with mass exchange. The disturbance satisfies the following equations of the adsorption/diffusion model introduced e.g. in B. ALBERS [2] Coupling. This model is based on the model with a balance equation for porosity by K. WILMAŃSKI (see e.g. [7, 8]). However, we assume the porosity to be constant so that the model in this work is simpler than the version introduced in the article.

We consider a process of physical adsorption in a three-component porous medium. A fluid-adsorbate mixture flows through the channels of the skeleton. The model takes into account three components: the skeleton, the fluid and an adsorbate which either flows with the same velocity as the fluid through the channels of the skeleton or it settles down on the inner surface of the porous body. Under the assumption of a small concentration of the adsorbate we can

neglect the influence of mass changes of the skeleton. Furthermore we neglect dynamical disturbances of the skeleton.

Mass balances

The mass balance equation for the liquid (fluid and adsorbate phases together) and the concentration balance have the following form:

$$\begin{aligned} &\frac{\partial \rho^L}{\partial t} + \operatorname{div}\left(\rho^L \mathbf{v}^F\right) = \hat{\rho}^A, \\ &\rho^L\left(\frac{\partial c}{\partial t} + \mathbf{v}^F \cdot \operatorname{grad} c\right) = (1-c)\hat{\rho}^A, \end{aligned} \tag{2.1}$$

where ρ^L is the mass density of the liquid phases, i.e. the sum of the mass densities of the fluid and the adsorbate, and c denotes the concentration of the adsorbate in the fluid component. The common velocity of fluid and adsorbate is $\mathbf{v}^F$. The mass balance for the adsorbate is replaced by the concentration balance[1)].

Mass source

According to the model (see [2]) the mass source is given by the relation

$$\hat{\rho}^A = -\frac{m^A}{V}\frac{d\left(\xi f_{int}\right)}{dt} = -\frac{m^A}{V}\left(f_{int}\frac{d\xi}{dt} + \xi\frac{d f_{int}}{dt}\right), \tag{2.2}$$

whose derivation is based on the classical LANGMUIR adsorption theory about *occupied* (ξ) and *bare* $(1-\xi)$ *sites* (see [6]) on the internal surface f_{int} of the solid. V is the representative elementary volume REV and m_A denotes the reference mass of adsorbate per unit of the internal surface area.

[1)] With

$$\frac{\partial}{\partial t}\left[\rho^L\frac{\rho^A}{\rho^L}\right] = \frac{\partial \rho^L}{\partial t}\frac{\rho^A}{\rho^L} + \rho^L\frac{\partial \frac{\rho^A}{\rho^L}}{\partial t}, \quad \text{and} \quad \operatorname{div}\left[\rho^L\frac{\rho^A}{\rho^L}\right]\mathbf{v}^F = \frac{\rho^A}{\rho^L}\operatorname{div}\rho^L\mathbf{v}^F + \rho^L\mathbf{v}^F \cdot \operatorname{grad}\frac{\rho^A}{\rho^L},$$

we get from the mass balance for the adsorbate, i.e. from

$$\frac{\partial \rho^A}{\partial t} + \operatorname{div}\left(\rho^A \mathbf{v}^F\right) = \hat{\rho}^A,$$

the relation:

$$\underbrace{c\left[\frac{\partial \rho^L}{\partial t} + \operatorname{div}\rho^L\mathbf{v}^F\right]}_{\hat{\rho}^A} + \rho^L\left[\frac{\partial c}{\partial t} + \mathbf{v}^F \cdot \operatorname{grad} c\right] = \hat{\rho}^A,$$

From this follows

$$\rho^L\left[\frac{\partial c}{\partial t} + \mathbf{v}^F \cdot \operatorname{grad} c\right] = (1-c)\,\hat{\rho}^A,$$

which is the concentration balance.

The first contribution on the right-hand side of (2.2) describes changes in time of the fraction of occupied sites. It is specified by the Langmuir evolution equation which can be written in the form

$$\frac{\partial \xi}{\partial t} = \left[\frac{cp^L}{p_0}(1-\xi) - \xi\right]\frac{1}{\tau_{ad}}, \tag{2.3}$$

where p^L denotes the partial pressure in the liquid (fluid and adsorbate together), p_0 is a Langmuir reference pressure and τ_{ad} is the characteristic time of adsorption. In the case of time changes of ξ equal to zero the well-known *Langmuir isotherm of occupied sites* follows

$$\xi_L = \frac{\dfrac{cp^L}{p_0}}{1+\dfrac{cp^L}{p_0}}, \tag{2.4}$$

where according to Dalton's law for small concentrations of the adsorbate it is assumed that the partial pressure of the adsorbate $p^A \cong cp^L$.

The other part of (2.2) describes the change of the internal surface. We assumed this change to be coupled with the relaxation of porosity. However, under the assumption of constant porosity it drops out in calculations of this work. This does not influence essentially the results because, as we have shown in earlier works, the Langmuir part of the mass source dominates the part connected with the porosity. Consequently, we obtain the following form of the mass source

$$\hat{\rho}^A = -\rho^A_{ad}\left\{\left[\frac{cp^L}{p_0}(1-\xi) - \xi\right]\frac{1}{\tau_{ad}}\right\}, \tag{2.5}$$

where $\rho^A_{ad} := \dfrac{m^A f_{int}}{V}$ is the mass density of the adsorbate on the internal surface. This is a very important parameter as we know, for example, from BEAR [4] that the internal surface may change by several orders of magnitude. Therefore ρ^A_{ad} is one of those parameters which we alter to see changes in the stability behavior for various porous materials.

Momentum balance

Due to the same velocity of fluid and adsorbate we need only one momentum balance jointly for these both components. We have

$$\frac{\partial \rho^L \mathbf{v}^F}{\partial t} + \operatorname{div}\left(\rho^L \mathbf{v}^F \otimes \mathbf{v}^F + p^L \mathbf{1}\right) = \left(-\pi + \hat{\rho}^A\right)\mathbf{v}^F \approx -\pi \mathbf{v}^F. \tag{2.6}$$

The order of magnitude of π is much higher than that of $\hat{\rho}^A$ so that on the right-hand side of (3.5) $\hat{\rho}^A$ is negligible. Furthermore the permeability coefficient π

and the compressibility parameter κ are assumed to be constant. We assume the flow to be isochoric which leads to the following linear constitutive relation for the pressure in the liquid phase p^L

$$p^L = \overset{0}{p} + \kappa \overset{1}{\rho}. \tag{2.7}$$

Governing equations in 2D

Summing up, the 2D model is governed by the following set of equations

$$\begin{aligned}
&\frac{\partial \rho^L}{\partial t} + \rho^L \left(\frac{\partial v_x^F}{\partial x} + \frac{\partial v_z^F}{\partial z} \right) + v_x^F \frac{\partial \rho^L}{\partial x} + v_z^F \frac{\partial \rho^L}{\partial z} \\
&\qquad = -\frac{\rho_{ad}^A}{\tau_{ad}} \left[\frac{c p^L}{p_0} (1-\xi) - \xi \right], \\
&\rho^L \left[\frac{\partial c}{\partial t} + v_x^F \frac{\partial c}{\partial x} + v_z^F \frac{\partial c}{\partial z} \right] = -(1-c) \frac{\rho_{ad}^A}{\tau_{ad}} \left[\frac{c p^L}{p_0} (1-\xi) - \xi \right], \\
&\frac{\partial \xi}{\partial t} = \left[\frac{c p^L}{p_0} (1-\xi) - \xi \right] \frac{1}{\tau_{ad}}, \\
&\rho^L \left[\frac{\partial v_x^F}{\partial t} + v_x^F \frac{\partial v_x^F}{\partial x} + v_z^F \frac{\partial v_x^F}{\partial z} \right] = -\frac{\partial p^L}{\partial x} - \pi v_x^F, \\
&\rho^L \left[\frac{\partial v_z^F}{\partial t} + v_x^F \frac{\partial v_z^F}{\partial x} + v_z^F \frac{\partial v_z^F}{\partial z} \right] = -\frac{\partial p^L}{\partial z} - \pi v_z^F.
\end{aligned} \tag{2.8}$$

3. Regular perturbation

The stability behavior of the 1D base flow is investigated with respect to transversal (2D) perturbations with mass exchange. For the analysis we use a regular perturbation method restricted to the zeroth and first order contributions. This means that we expect the fields to be a superposition of the base solution (indicated by 0) and a small perturbation (indicated by 1). The solutions have the following structure:

$$\begin{aligned}
&p^F = \overset{0}{p}(x) + \kappa \overset{1}{\rho}(x,z,t), \quad c = \overset{0}{c} + \overset{1}{c}(x,z,t), \quad \xi = \overset{0}{\xi}(x) + \overset{1}{\xi}(x,z,t), \\
&v_x^F = \overset{0}{v} + \overset{1}{v}_x(x,z,t), \quad v_z^F = \overset{1}{v}_z(x,z,t).
\end{aligned} \tag{3.1}$$

3.1. Base solution/zeroth step of perturbation

The base flow satisfies the following set of field equations. It is a steady state one-dimensional flow process in a porous medium,

$$\begin{aligned} &\frac{\partial \rho^F}{\partial t} + \frac{\partial \rho^F v_x^F}{\partial x} = 0, \qquad 0 < x < l \\ &\rho^F \left(\frac{\partial v_x^F}{\partial t} + v_x^F \frac{\partial v_x^F}{\partial x} \right) = -\frac{\partial p^F}{\partial x} - \pi v_x^F . \end{aligned} \tag{3.2}$$

Equations $(3.2)_{1/2}$ are the mass and momentum balances of the fluid. Here, ρ^F is the mass density of the fluid component, v_x^F is the fluid velocity in x-direction and π is the bulk permeability coefficient. The partial pressure in the fluid is denoted by p^F. We investigate solely the steady state processes. Consequently, the base flow does not contain an influence of mass exchange.

It is assumed that a deformed skeleton does not contribute to a dynamical disturbance, and therefore relations for the skeleton are not quoted.

Boundary conditions of this problem have the following form:

$$\begin{aligned} -\rho^F v_x^F\big|_{x=0} &= \alpha \left[p^F\big|_{x=0} - n_E p_l \right], \\ \rho^F v_x^F\big|_{x=l} &= \alpha \left[p^F\big|_{x=l} - n_E p_r \right]. \end{aligned} \tag{3.3}$$

They are of the third type and express the fact that the flow through the boundary of the body depends on the pressure difference of the partial pressure in the fluid (p^F) and the external pressure which works on the fluid (on the left-hand side p_l and on the right-hand side p_r). The permeability of the surface denoted by α is the material property of the system.

For simplicity we assume the base flow to be isochoric. This means that in the zeroth step of perturbation the mass density is constant

$$\overset{0}{\rho} = \text{const} = \rho_0^F . \tag{3.4}$$

This simplification is supported by calculations which we performed in earlier papers on porous media. Bearing $(3.2)_1$ for the zeroth step in mind we obtain that also the fluid velocity in x-direction is constant (denoted by $\overset{0}{v}$ without subscribed x)

$$\overset{0}{v} = \text{const}. \tag{3.5}$$

The stationary form of $(3.2)_2$ allows us to calculate the solution for the partial pressure in the fluid in the zeroth step, $\overset{0}{p}$,

$$\frac{\partial \overset{0}{p}}{\partial x} = -\pi \overset{0}{v} \quad \Longrightarrow \quad \overset{0}{p} = -\pi \overset{0}{v} x + C, \tag{3.6}$$

where C is an integration constant which can be determined by use of the boundary condition on the left-hand side of the system ($x = 0$)

$$-\rho_0^F \overset{0}{v} = \alpha \left[p^F \big|_{x=0} - n_E p_l \right], \tag{3.7}$$

so that we obtain

$$\overset{0}{p} = -\pi \overset{0}{v} x + n_E p_l - \frac{\rho_0^F \overset{0}{v}}{\alpha}. \tag{3.8}$$

As the second boundary condition for $x = l$ we have

$$\rho_0^F \overset{0}{v} = \alpha \left[p^F \big|_{x=l} - n_E p_r \right], \tag{3.9}$$

from which the constant velocity of the zeroth step follows in the form

$$\overset{0}{v} = \frac{\alpha p_d}{2\rho_0^F + \alpha \pi l}, \qquad p_d := n_E (p_l - p_r). \tag{3.10}$$

The base solution forms the zeroth approximation of the above described perturbation. Obviously it depends solely on the x-variable. In addition to the above fields we need in the zeroth step with mass exchange the fields of concentration $\overset{0}{c}$ and of the number of occupied sites $\overset{0}{\xi}$ given by Eq. $(2.8)_{2/3}$.

In the stationary case they reduce to

– concentration balance

$$\rho_0^F \overset{0}{v} \frac{\partial \overset{0}{c}}{\partial x} = -\left(1 - \overset{0}{c}\right) \frac{\rho_{ad}^A}{\tau_{ad}} \left[\overset{0}{c} \frac{\overset{0}{p}}{p_0} \left(1 - \overset{0}{\xi}\right) - \overset{0}{\xi} \right], \tag{3.11}$$

– evolution equation for fraction of occupied sites

$$0 = \overset{0}{c} \frac{\overset{0}{p}}{p_0} \left(1 - \overset{0}{\xi}\right) - \overset{0}{\xi}. \tag{3.12}$$

From (3.12) follows the Langmuir adsorption isotherm which depends, of course, on x

$$\overset{0}{\xi} = \frac{\overset{0}{c} \frac{\overset{0}{p}}{p_0}}{1 + \overset{0}{c} \frac{\overset{0}{p}}{p_0}}. \tag{3.13}$$

On the other hand (3.11) yields $\overset{0}{c} = \text{const.} = c_0$, where c_0 denotes the initial concentration of the adsorbate in the fluid.

3.2. First step of perturbation

For the first step of perturbation (2D) we obtain the following set of equations:

$$(x,z) \in \mathcal{B} := (0,l) \times (-b,b)$$

$$\frac{\partial \overset{1}{\rho}}{\partial t} + \rho_0^F \left(\frac{\partial \overset{1}{v}_x}{\partial x} + \frac{\partial \overset{1}{v}_z}{\partial z} \right) + \overset{0}{v} \frac{\partial \overset{1}{\rho}}{\partial x} = \overset{1}{\hat{\rho}}^A,$$

$$\rho_0^F \left(\frac{\partial \overset{1}{c}}{\partial t} + \overset{0}{v} \frac{\partial \overset{1}{c}}{\partial x} \right) = (1-c_0)\, \overset{1}{\hat{\rho}}^A - \overset{1}{c} \frac{\rho_{ad}^A}{\tau_{ad}} \left[c_0 \frac{\overset{0}{p}}{p_0} \left(1 - \overset{0}{\xi} \right) - \overset{0}{\xi} \right],$$

$$\frac{\partial \overset{1}{\xi}}{\partial t} = \left[\left(1 - \overset{0}{\xi} \right) \left(\frac{c_0 \kappa \overset{1}{\rho}}{p_0} + \overset{1}{c} \frac{\overset{0}{p}}{p_0} \right) - \left(1 + c_0 \frac{\overset{0}{p}}{p_0} \right) \overset{1}{\xi} \right] \frac{1}{\tau_{ad}}, \tag{3.14}$$

$$\rho_0^F \left[\frac{\partial \overset{1}{v}_x}{\partial t} + \overset{0}{v} \frac{\partial \overset{1}{v}_x}{\partial x} \right] = -\kappa \frac{\partial \overset{1}{\rho}}{\partial x} - \pi \overset{1}{v}_x,$$

$$\rho_0^F \left[\frac{\partial \overset{1}{v}_z}{\partial t} + \overset{0}{v} \frac{\partial \overset{1}{v}_z}{\partial x} \right] = -\kappa \frac{\partial \overset{1}{\rho}}{\partial z} - \pi \overset{1}{v}_z,$$

with

$$\overset{1}{\hat{\rho}}^A = -\frac{\rho_{ad}^A}{\tau_{ad}} \left[\left(1 - \overset{0}{\xi} \right) \left(\frac{c_0 \kappa \overset{1}{\rho}}{p_0} + \overset{1}{c} \frac{\overset{0}{p}}{p_0} \right) - \overset{1}{\xi} \left(1 + c_0 \frac{\overset{0}{p}}{p_0} \right) \right]. \tag{3.15}$$

The following boundary conditions are considered:

$$\begin{aligned} -\rho^F v_x^F \big|_{x=0} &= \alpha \left[p^F \big|_{x=0} - n_E p_l \right], \\ \rho^F v_x^F \big|_{x=l} &= \alpha \left[p^F \big|_{x=l} - n_E p_r \right], \end{aligned} \qquad v_z^F \big|_{z=\pm b} = 0. \tag{3.16}$$

The two conditions on the left-hand side corresponding to the momentum balance in x-direction are already introduced in (3.3). They describe in the above explained way the in- and outflow in x-direction of the liquid to the porous body of length l. But we consider also the flow in z-direction. We assume the fields to be periodic in this direction with period $2b$. Application of a Fourier ansatz yields that the two boundary conditions on the right-hand side of (3.16) corresponding to the momentum balance in z-direction are automatically fulfilled.

In the first step of perturbation boundary conditions (3.16) have the form

$$\begin{aligned} -\rho_0^F \overset{1}{v}_x \big|_{x=0} - \overset{0}{v}\, \overset{1}{\rho} \big|_{x=0} &= \alpha\kappa\, \overset{1}{\rho} \big|_{x=0}, \\ \rho_0^F \overset{1}{v}_x \big|_{x=l} + \overset{0}{v}\, \overset{1}{\rho} \big|_{x=l} &= \alpha\kappa\, \overset{1}{\rho} \big|_{x=l}, \end{aligned} \qquad \overset{1}{v}_z \big|_{z=\pm b} = 0. \tag{3.17}$$

4. Wave ansatz for the disturbance

The perturbations in the first step are expressed in terms of the following simple wave ansatz:

$$\begin{gathered} \overset{1}{\rho} = \mathrm{e}^{\omega t}\bar{\rho}(x)\cos kz, \quad \overset{1}{v}_x = \mathrm{e}^{\omega t}\bar{v}_x(x)\cos kz, \quad \overset{1}{v}_z = \mathrm{e}^{\omega t}\bar{v}_z(x)\sin kz, \\ \overset{1}{c} = \mathrm{e}^{\omega t}\bar{c}(x)\cos kz, \quad \overset{1}{\xi} = \mathrm{e}^{\omega t}\bar{\xi}(x)\cos kz, \end{gathered} \tag{4.1}$$

where $\bar{\rho}(x), \bar{v}_x(x), \bar{v}_z(x), \bar{c}(x)$ and $\bar{\xi}(x)$ are the amplitudes of the disturbances, ω is the frequency, possibly complex, and k the real wave number defined as

$$k := \frac{\Pi m}{b}, \qquad \Pi = 3.1415... \tag{4.2}$$

The Fourier ansatz in z-direction follows from the structure of the boundary conditions.

After insertion of this ansatz into the field equations (2.8) we have

$$\begin{aligned} &\omega\bar{\rho} + \rho_0^F\left(\frac{\partial\bar{v}_x}{\partial x} + k\bar{v}_z\right) + \overset{0}{v}\frac{\partial\bar{\rho}}{\partial x} \\ &\qquad = -\frac{\rho_{ad}^A}{\tau_{ad}}\left[\left(\frac{c_0\kappa\bar{\rho}}{p_0} + \bar{c}\frac{\overset{0}{p}}{p_0}\right)\left(1-\overset{0}{\xi}\right) - \bar{\xi}\left(1 + c_0\frac{\overset{0}{p}}{p_0}\right)\right], \\ &\rho_0^F\left(\omega\bar{c} + \overset{0}{v}\frac{\partial\bar{c}}{\partial x}\right) = -(1-c_0)\frac{\rho_{ad}^A}{\tau_{ad}}\left[\left(\frac{c_0\kappa\bar{\rho}}{p_0} + \bar{c}\frac{\overset{0}{p}}{p_0}\right)\left(1-\overset{0}{\xi}\right)\right. \\ &\qquad \left. -\bar{\xi}\left(1 + c_0\frac{\overset{0}{p}}{p_0}\right)\right] - \frac{\rho_{ad}^A}{\tau_{ad}}\bar{c}\left[c_0\frac{\overset{0}{p}}{p_0}\left(1-\overset{0}{\xi}\right) - \overset{0}{\xi}\right], \\ &\omega\bar{\xi} = \left[\left(\bar{\rho}\frac{c_0\kappa}{p_0} + \bar{c}\frac{\overset{0}{p}}{p_0}\right)\left(1-\overset{0}{\xi}\right) - \bar{\xi}\left(1 + c_0\frac{\overset{0}{p}}{p_0}\right)\right]\frac{1}{\tau_{ad}}, \\ &\rho_0^F\left(\omega\bar{v}_x + \overset{0}{v}\frac{\partial\bar{v}_x}{\partial x}\right) = -\kappa\frac{\partial\bar{\rho}}{\partial x} - \pi\bar{v}_x, \\ &\rho_0^F\left(\omega\bar{v}_z + \overset{0}{v}\frac{\partial\bar{v}_z}{\partial x}\right) = k\kappa\bar{\rho} - \pi\bar{v}_z. \end{aligned} \tag{4.3}$$

Dispersion relation

We have to analyse the following dispersion relation:

$$(\omega\mathsf{I} + \mathfrak{A})\,\mathbf{u} + \mathfrak{B}\mathbf{u}' = 0, \tag{4.29}$$

with

$$\mathbf{u} = \left(\bar{\rho}, \bar{c}, \bar{\xi}, \bar{v}_x, \bar{v}_z\right)^T, \quad \mathbf{u}' = \left(\frac{\partial \bar{\rho}}{\partial x}, \frac{\partial \bar{c}}{\partial x}, \frac{\partial \bar{\xi}}{\partial x}, \frac{\partial \bar{v}_x}{\partial x}, \frac{\partial \bar{v}_z}{\partial x}\right)^T,$$

$$\mathsf{I} = \begin{pmatrix} 1 & 0 & 0 & 0 & 0 \\ 0 & 1 & 0 & 0 & 0 \\ 0 & 0 & 1 & 0 & 0 \\ 0 & 0 & 0 & 1 & 0 \\ 0 & 0 & 0 & 0 & 1 \end{pmatrix}, \quad \mathfrak{B} := \begin{pmatrix} \overset{0}{v} & 0 & 0 & \rho_0^F & 0 \\ 0 & \overset{0}{v} & 0 & 0 & 0 \\ 0 & 0 & 0 & 0 & 0 \\ \frac{\kappa}{\rho_0^F} & 0 & 0 & \overset{0}{v} & 0 \\ 0 & 0 & 0 & 0 & \overset{0}{v} \end{pmatrix}, \tag{4.30}$$

$$\mathfrak{A} := \begin{pmatrix} \frac{\rho_{ad}^A}{\tau_{ad}} \frac{c_0 \kappa}{p_0} \left(1 - \overset{0}{\xi}\right) & \frac{\rho_{ad}^A}{\tau_{ad}} \frac{\overset{0}{p}}{p_0} \left(1 - \overset{0}{\xi}\right) \\ \frac{1 - c_0}{\rho_0^F} \frac{\rho_{ad}^A}{\tau_{ad}} \frac{c_0 \kappa}{p_0} \left(1 - \overset{0}{\xi}\right) & \frac{1 - c_0}{\rho_0^F} \frac{\rho_{ad}^A}{\tau_{ad}} \frac{\overset{0}{p}}{p_0} \left(1 - \overset{0}{\xi}\right) + \frac{1}{\rho_0^F} \frac{\rho_{ad}^A}{\tau_{ad}} \left[c_0 \frac{\overset{0}{p}}{p_0} \left(1 - \overset{0}{\xi}\right) - \overset{0}{\xi}\right] \\ -\frac{c_0 \kappa}{p_0} \left(1 - \overset{0}{\xi}\right) \frac{1}{\tau_{ad}} & -\frac{\overset{0}{p}}{p_0} \left(1 - \overset{0}{\xi}\right) \frac{1}{\tau_{ad}} \\ 0 & 0 \\ -k \frac{\kappa}{\rho_0^F} & 0 \end{pmatrix}$$

$$\begin{pmatrix} -\frac{\rho_{ad}^A}{\tau_{ad}} \left(1 + c_0 \frac{\overset{0}{p}}{p_0}\right) & 0 & \rho_0^F k \\ -\frac{1 - c_0}{\rho_0^F} \frac{\rho_{ad}^A}{\tau_{ad}} \left(1 + c_0 \frac{\overset{0}{p}}{p_0}\right) & 0 & 0 \\ \left(1 + c_0 \frac{\overset{0}{p}}{p_0}\right) \frac{1}{\tau_{ad}} & 0 & 0 \\ 0 & \frac{\pi}{\rho_0^F} & 0 \\ 0 & 0 & \frac{\pi}{\rho_0^F} \end{pmatrix}$$

and boundary conditions

$$\begin{aligned} \bar{v}_x|_{x=0} &= -\frac{\alpha\kappa + \overset{0}{v}}{\rho_0^F} \bar{\rho}|_{x=0}, \\ \bar{v}_z|_{z=\pm b} &= 0. \\ \bar{v}_x|_{x=l} &= \frac{\alpha\kappa - \overset{0}{v}}{\rho_0^F} \bar{\rho}|_{x=l}, \end{aligned} \tag{4.31}$$

Condititions in z-direction are fulfilled automatically due to ansatz (4.1).

5. Numerical investigation

We solve the eigenvalue problem for ω, using a second order finite difference scheme in a equidistant mesh (length of the body l divided into n parts of length h). The derivatives of disturbances are written as central differences $\left(\frac{\partial u}{\partial x} = \frac{u(x+h) - u(x-h)}{2h}\right)$ for inner mesh points, or as asymmetric ones for the first $\left(\frac{\partial u}{\partial x} = \frac{u(x+h) - u(x)}{h}\right)$ and the last point $\left(\frac{\partial u}{\partial x} = \frac{u(x) - u(x-h)}{h}\right)$. For this linear eigenvalue problem we obtain $5n+3$ eigenvalues ω_i (number of linear equations: $5(n+1)$-2). The exponential form of the ansatz (4.1) yields that the base flow is stable if all real parts of ω_i are negative and unstable if at least one of the $5n+3$ real parts is positive.

For a chosen pair (α, ρ_{ad}^A) we calculate $\max(Re(\omega))$ in dependence on π. In order to consider the precision of numerical calculations only those real parts of eigenvalues are considered whose absolute value is greater than 10^{-5}. We have determined this value by comparison of results for the same parameters running once a program without mass exchange and once a program with mass exchange where mass exchange was switched off. Many authors who solve eigenvalue problems numerically using a finite-difference scheme complain about slowly converging procedures (e.g. [5]) from which it follows that calculations for a large value of elements are necessary. In our case we do not observe such problems: Comparison of analytical and numerical results (without mass exchange) shows that the small number of 10 elements is sufficient to obtain a good agreement of results in the scope of the just mentioned precision.

In the calculations we use the data of the following two tables. The data are typical for geotechnical applications. In Table 1 parameters for a flow process without adsorption are given, in Table 2 these quantities are given which enter the model due to the adsorption process:

Table 1. Typical model parameters for flow processes in soils.

Length, width of the body l, b	1m	equilibrium porosity n_E	0.23
Compressibility κ	$2.25 \cdot 10^6 \frac{m^2}{s^2}$	Initial mass density ρ_0^L	$2.3 \cdot 10^2 \frac{kg}{m^3}$
Pressure left-h.s. p_l	110kPa	Pressure right-h.s. p_r	100kPa
Pressure difference working	on the fluid	$p_d = n_E(p_l - p_r)$	2.3kPa

Table 2. Additional model parameters for adsorption processes in soils.

Initial concentration c_0	10^{-3}
Langmuir pressure p_0	10 kPa
Charact. time of adsorp. τ_{ad}	1s

In the following Fig. 1 we show the results of the stability analysis. The domain of instability is shown in 3D in dependence on the bulk permeability π, the surface permeability α, and the coefficient ρ_{ad}^{A} characterizing adsorption properties of the internal surface. The last coefficient may change by a few orders of magnitude because it is proportional to the internal surface. Below we see the 2D projections of the instability region.

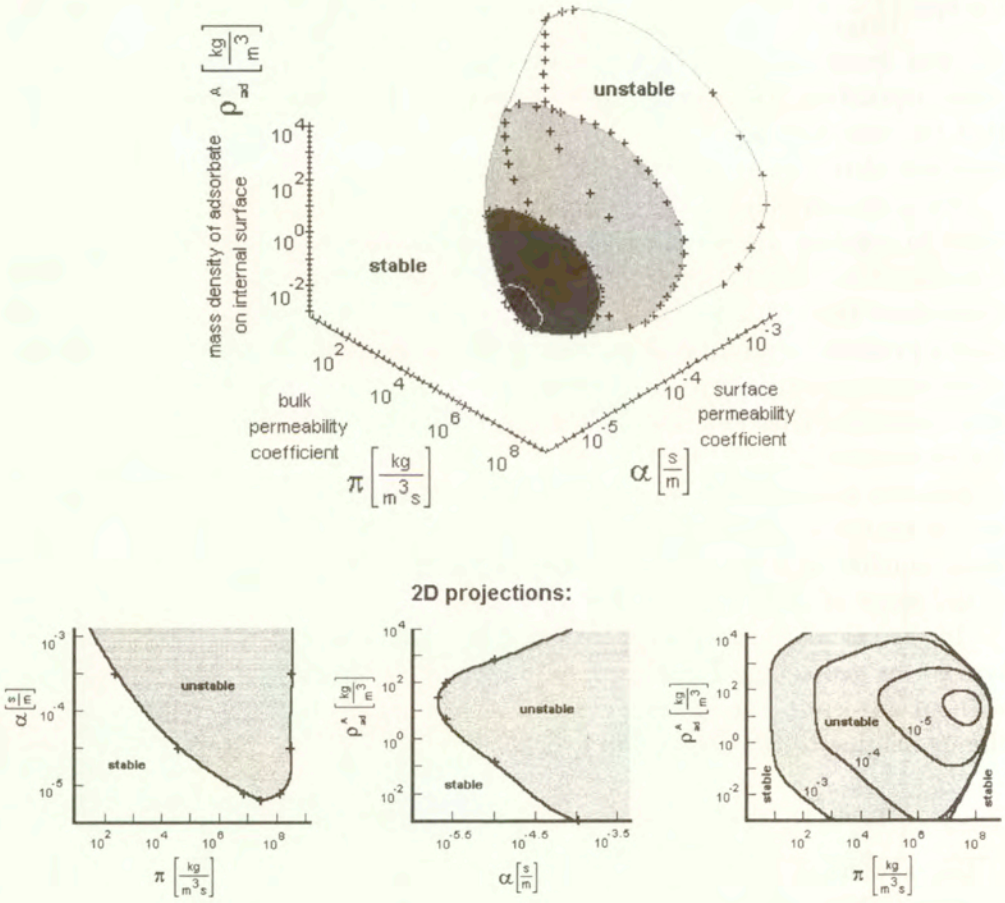

FIG. 1. Numerical result for transversal disturbance with mass exchange.

Transversal disturbance with mass exchange yields an instability of the steady state flow for some ranges of parameters. While for small values of π the border of this region strongly varies with the surface permeability parameter α (see the third 2D projection), on the side of large π the unstable region is limited by a value of π app. $10^{8.548}$. For greater values of π the base flow is stable for any α. In

the range of extremally large π not shown any more in the figure there appears again an instability for all values of α. However, the model is not applicable in this range any more. In addition, the numerical procedure is not stable any more for such very large values of π.

With decreasing α also the region of π decreases for which the flow is unstable until the value $\alpha \approx 10^{-5.690}$ is reached where the base flow is stable in the whole range of π (see the first 2D projection). A similar behavior exists in dependence on ρ_{ad}^{A} (see second 2D projection): the range of ρ_{ad}^{A} for which the flow is unstable decreases with decreasing α. For smaller values than $\alpha \approx 10^{-5.690}$ the flow is stable for any ρ_{ad}^{A}. It is worth mentioning that parameters which have been used for the works quoted earlier lie all in the stable region.

6. Properties of some other disturbances of the base flow

As in many other known cases of flow instabilities, a 1D disturbance either without or with mass exchange does not produce any instability of our base flow. The same is valid for a 2D disturbance without mass exchange. Results for these disturbances are shown in the paper [1]. Although there appears no region of instability for the three mentioned disturbances results show important features of the relaxation behavior. For the 1D and 2D disturbances without mass exchange even an analytical investigation was feasible which gave hints for the numerical approach also of this work.

From the stable cases we know that the relaxation properties do not change monotonously with the permeability π. They possess rather two different ranges. In the range of smaller values of π the relaxation is determined by a real part of the complex root, while for larger π this root does not possess the imaginary part. It means that the perturbation causes vibrations in the range of smaller π, whose frequencies cover the whole discrete spectrum. For values of π greater than this of the turning point, the disturbance is only damped but the damping is smaller than that predicted by the resistance to the diffusion $\left(\text{i.e.} < \frac{\pi}{\rho_0^F}\right)$. The position of the turning point is determined by the compressibility coefficient of the fluid. We refer to [3] where this property is discussed. In general the damping is the smallest (i.e. the relaxation is the slowest) for large and small values of π.

Calculations for different disturbances made it evident that the mass exchange slows down the relaxation even by a few orders of magnitude. This effect is related to the characteristic time of adsorption τ_{ad}. Little can be said about its experimental values for porous materials because most experiments are conducted in quasistatic conditions. In [3] we show the influence of τ_{ad} on the relaxation properties. As expected, the disturbances relax faster for smaller characteristic times τ_{ad} but even for a very short time of adsorption $\tau_{ad} = 10^{-5}$s

this relaxation is considerably longer than in the case of no mass exchange. For the current work we used a value of $\tau_{ad} = 1$s as in all earlier works on adsorption.

Results for the 2D disturbance without mass exchange reveal the same behavior as these for the 1D perturbation. Admittedly there appear additional solutions but they do neither have influence on the stability behavior nor on the relaxation properties. In general the relaxation in the 2D case without mass exchange is faster than in the 1D case. Anyway it is interesting that the 2D disturbance with mass exchange yields an instability while the 1D disturbance with adsorption does not.

7. Conclusions

In this work we have shown that for transversal disturbances with mass exchange of the 1D steady state flow through the porous material there appears a region of parameters π, α, and ρ_{ad}^A in which the base flow is unstable. This is not the case with respect to a linear longitudinal disturbance without and with mass exchange and to a linear transversal disturbance without mass exchange. For the three latter disturbances the base flow is stable in the whole range of control permeability parameters π, and α.

This shows that a disturbance with adsorption has a great influence on the stability behavior of the base flow. While adsorption already in the case of 1D disturbances decreases the maximum values of real parts by some orders of magnitude, for the 2D disturbances it even decides whether the base flow is stable or unstable.

The existing unstable region for the disturbance investigated in this paper appears in the region of π where in the case of the other disturbances (1D without and with mass exchange, 2D without mass exchange) appear complex roots and thus vibrations. The range of instability corresponds to higher velocities for the same pressure difference due to a lower resistance of the boundary. Simultaneously it corresponds to a lower "internal friction" πv_x^F in momentum balance equation due to lower values of permeability π.

The work has shown that the order of magnitude of parameters which were used in earlier works on this model were determined correctly and lie in stable regions of the model.

References

1. B. ALBERS, *Relaxation analysis and linear stability vs. adsorption in porous materials,* WIAS-Preprint No. 721, accepted for publication in Continuum Mech. Thermodyn., 2002.

2. B. ALBERS, *Coupling of adsorption and diffusion in porous and granular materials. A 1-D Example of the boundary value problem,* Arch.Appl.Mech. **70**, 7, 519–531, 2000.

3. B. ALBERS, K. WILMAŃSKI, *Relaxation properties of a 1D flow through a porous material without and with adsorption*, WIAS-Preprint No. 707, 2001.

4. J. BEAR, *Dynamics of fluids in porous media*, American Elsevier Publishing Company 1972, also: Dover Publications, 1988.

5. A. GILMAN, J. BEAR, *The influence of free convection on soil salinization in arid regions*, Transport in Porous Media, **23**, 275–301, 1996.

6. S. J. GREGG, K. S. W. SING, *Adsorption, surface area and porosity*, Academic Press, London, 1982.

7. K. WILMAŃSKI, *Porous media at finite strains. The new model with the balance equation for porosity*, Arch. Mech., **48**, 4, 591–628, 1996.

8. K. WILMAŃSKI, *A thermodynamic model of compressible porous materials with the balance equation of porosity*, Transport in Porous Media, **32**, 21–47, 1998.

Received June 28, 2002; revised version August 16, 2002.

Arch. Mech., **54**, 5-6, pp. 377–387, Warszawa 2002

A numerical framework for continuum damage - discontinuum transition

R. DE BORST[1] and M. A. ABELLAN[2]

[1] *Koiter Institute Delft, Delft University of Technology,*
P.O. Box 5058, NL-2600 GB Delft, The Netherlands,
e-mail: R.deBorst@LR.TUDelft.nl

[2] *LTDS-ENISE - UMR CNRS 5513,*
Ecole Nationale d'Ingénieurs de Saint-Etienne,
58, rue Jean Parot, F-42023 Saint-Etienne, France,
e-mail: abellan@enise.fr

Dedicated to Professor Piotr Perzyna
on the occasion of his 70^{th} birthday

A FRAMEWORK is derived for the proper and consistent description of a discontinuity (a crack) as the result of a damaging process in a continuous medium. The damaging process in the continuous medium is described using a gradient-enhanced damage theory, so that well-posedness of the boundary-value problem is maintained until the damage process is completed and a discontinuity arises. At that moment the partition-of-unity property of finite element shape functions is exploited to partition the displacement field into two continuous fields, separated via a Heaviside function. It is demonstrated that the additional boundary conditions that arise in a gradient-enhanced damage theory, can be accounted for in a natural and transparent manner.

1. Introduction

THE FAILURE behaviour of many engineering materials can be classified as quasi-brittle. Prominent examples are concrete and ceramics, but also most fibre-reinforced materials behave as such. The salient characteristic common in failure of these materials is that, ahead of a macroscopically observable crack, there is a rather large fracture process zone, in which micro-cracks initiate, grow and coalesce. This observation prevents the use of linear elastic fracture mechanics. Indeed, from a physical point of view, a model in which the micro-cracking ahead of the crack tip would be modelled as a degrading continuum, e.g., using continuum damage mechanics, while the macroscopic crack would be captured as a true discontinuity, would be most appealing. It is precisely such an approach that we will describe in this contribution.

For the micro-cracking ahead of the crack tip, we shall use a smeared, or continuum approach. In particular, we shall employ a standard isotropic damage model, e.g., [4]. However, since standard damage models lack an internal length scale, the governing equations in the fracture process zone can lose ellipticity during quasi-static loadings. To remedy this, the model must be enhanced by a form of non-locality [3] or by adding viscosity [5]. Herein, we employ the second gradient of the equivalent strain measure of the damage model for this purpose [7], [8]. For numerical solutions of non-local and gradient-enhanced models, a very fine discretisation is required, since the spacing of nodes or grid points must be smaller than the characteristic or internal length scale of the continuum in order to resolve the strains in the fracture processes zone properly.

In isotropic damage models, the material locally loses all coherence when the damage parameter ω becomes equal to one. Then, the governing partial differential equations that arise from the equilibrium, the kinematic and the constitutive equations, lose meaning for a continuum and a discrete crack arises. In fact, a 'vanishing' length scale then arises, since a discrete crack has a zero width. To capture such a 'zero' length scale using numerical techniques designed for continuum problems is impossible. However, traditional finite element techniques can be adapted to cope with this when use is made of the partition-of-unity property of the shape functions of finite elements [1]. Then, the displacement field can be written as the sum of two continuous displacement fields, which are separated via a Heaviside function and a crack, i.e. a discontinuity in an otherwise smooth displacement field, can be described in an exact manner. Following the work of BELYTSCHKO and BLACK [2] for linear elastic fracture mechanics and WELLS *et al.* [9], [10] for cohesive-zone models and application to viscoplasticity, this concept is now applied to form a true discontinuity at the end of a process in which a gradient-enhanced damage model has been used to describe the initiation, growth and coalescence of micro-cracks.

The paper will first give a succinct summary of the implicit gradient damage model. Then, the development leading to the introduction of a discontinuity in a gradient-enhanced continuum will be outlined. Special attention will be given to the treatment of the additional boundary condition, which arises due to the introduction of the gradient term, at the internal boundary, i.e. at the crack.

2. Gradient-enhanced damage model

We start the discussion by recalling the governing equations of the so-called implicit gradient-enhanced damage model, originated by Peerlings *at al.* [7], [8]. In it, the equilibrium equation (in the absence of body forces):

$$\text{div } \boldsymbol{\sigma} = \mathbf{0} \tag{2.1}$$

and the kinematic relation (for small strains)

$$\boldsymbol{\epsilon} = \nabla^s \mathbf{u} \tag{2.2}$$

with $\mathbf{u}$ being the displacement field and the superscript s denoting the symmetric part of the gradient operator, are augmented by an injective relation between the stress tensor $\boldsymbol{\sigma}$ and the strain tensor $\boldsymbol{\epsilon}$:

$$\boldsymbol{\sigma} = (1 - \omega)\, \mathbf{D}^e : \boldsymbol{\epsilon} \tag{2.3}$$

In equation (2.3) $\mathbf{D}^e$ is the elasticity tensor with the virgin elastic constants E (Young's modulus) and ν (Poisson's ratio). ω is a monotically increasing damage parameter, with an initial value 0, for the intact material, and an ultimate value 1, at complete loss of material coherence. It is a function of a history parameter κ:

$$\omega = \omega(\kappa) \tag{2.4}$$

with κ linked to a non-local strain measure $\bar{\epsilon}$ via a loading function

$$f = \bar{\epsilon} - \kappa \tag{2.5}$$

such that loading occurs if $f = 0$, $\dot{f} = 0$ and $\omega < 1$. Formally, the loading-unloading process can be captured by the Kuhn-Tucker conditions:

$$f\,\dot{\kappa} = 0\,, \qquad f \leq 0, \qquad \dot{\kappa} \geq 0. \tag{2.6}$$

The non-local strain measure is coupled to a local strain measure $\tilde{\epsilon}$ via a Helmholtz equation:

$$\bar{\epsilon} - c\,\nabla^2 \bar{\epsilon} = \tilde{\epsilon} \tag{2.7}$$

with c denoting a material parameter with the dimension of length squared, and $\tilde{\epsilon}$ a function of the strain tensor:

$$\tilde{\epsilon} = \tilde{\epsilon}(\boldsymbol{\epsilon}). \tag{2.8}$$

The equilibrium equation (2.1), the kinematic equation (2.2) and the constitutive model (2.3)–(2.8) are complemented by the boundary conditions

$$\boldsymbol{\sigma} \cdot \mathbf{n}_{\partial\Omega} = \mathbf{t}_p \qquad \text{and} \qquad \mathbf{u} = \mathbf{u}_p \tag{2.9}$$

on complementary parts of the boundary $\partial\Omega_t$ and $\partial\Omega_u$, with $\partial\Omega = \partial\Omega_t \cup \partial\Omega_u$ and $\partial\Omega_t \cap \partial\Omega_u = \emptyset$, while for the non-local strain $\bar{\epsilon}$ the natural boundary condition

$$\frac{\partial \bar{\epsilon}}{\partial n} \equiv \mathbf{n}_{\partial\Omega} \cdot \nabla \bar{\epsilon} = 0 \tag{2.10}$$

with the unit normal vector $\mathbf{n}_{\partial\Omega}$ at the boundary $\partial\Omega$, is commonly assumed [6].

3. Transition to a discontinuity

When $\omega = 1$, the material has lost all coherence. At this moment, the governing equations for the continuous medium lose validity and a discrete crack arises. Then, the displacement field can be written as

$$\mathbf{u}(\mathbf{x},\ t)\ =\ \mathbf{u}^a(\mathbf{x},\ t)\ +\ H_{\partial\Omega^d}(\mathbf{x})\ \mathbf{u}^b(\mathbf{x},\ t) \tag{3.1}$$

with $\mathbf{u}^a$ and $\mathbf{u}^b$ denoting the continuous displacement fields, and $H_{\partial\Omega^d}$ a Heaviside function centered at the discontinuity $\partial\Omega^d$ which separates the Ω^+ domain from the Ω^- domain ($\Omega = \Omega^+ \cap \Omega^-$). At this discontinuity a normal $\mathbf{n}_{\partial\Omega^d}$ is defined such that it points to the Ω^+ domain. From Eq. (3.1) the strain field can be derived as:

$$\boldsymbol{\epsilon}(\mathbf{x},\ t)\ =\ \nabla^s\mathbf{u}^a(\mathbf{x},\ t)\ +\ H_{\partial\Omega^d}(\mathbf{x})\ \nabla^s\mathbf{u}^b(\mathbf{x},\ t) +\ \delta_{\partial\Omega^d}\ \left(\mathbf{u}^b \otimes \mathbf{n}_{\partial\Omega^d}\right)^s \tag{3.2}$$

with $\delta_{\partial\Omega^d}$ the Dirac function at $\partial\Omega^d$. Again, the superscript s denotes the symmetric part.

Consistent with the decomposition (3.1) we now partition the field that describes the non-local strain measure as:

$$\bar{\epsilon}(\mathbf{x},\ t)\ =\ \bar{\epsilon}^a(\mathbf{x},\ t)\ +\ H_{\partial\Omega^d}(\mathbf{x})\ \bar{\epsilon}^b(\mathbf{x},\ t) \tag{3.3}$$

where, as emphasised by PEERLINGS *et al.* [6], the boundary condition is also applied at the internal boundary $\partial\Omega^d$.

We now cast the governing equations (2.1) and (2.7) in a weak format by multiplying them by test functions $\boldsymbol{\eta}$ and ξ, respectively, and integrating over the body. When adopting a BUBNOV-GALERKIN approach, we have, cf. Eqs. (3.1) and (3.3):

$$\boldsymbol{\eta}\ =\ \boldsymbol{\eta}^a\ +\ H_{\partial\Omega^d}\ \boldsymbol{\eta}^b, \tag{3.4}$$

$$\xi\ =\ \xi^a\ +\ H_{\partial\Omega^d}\ \xi^b, \tag{3.5}$$

where the dependence on $\mathbf{x}$ and t has been left out for clarity of notation. Thus, the weak forms become:

$$\int_\Omega \left(\boldsymbol{\eta}^a\ +\ H_{\partial\Omega^d}\ \boldsymbol{\eta}^b\right)^T\ \left(\mathbf{L}^T\ \boldsymbol{\sigma}\right)\ d\Omega\ =\ 0, \tag{3.6}$$

$$\int_\Omega \left(\xi^a\ +\ H_{\partial\Omega^d}\ \xi^b\right)\ \left(\bar{\epsilon}\ -\ c\ \nabla^2\bar{\epsilon}\ -\ \tilde{\epsilon}\right)\ d\Omega\ =\ 0, \tag{3.7}$$

where a change has been made to matrix-vector notation, with $\mathbf{L}$ denoting a differential operator matrix, for 2D:

$$\mathbf{L} = \begin{bmatrix} \dfrac{\partial}{\partial x} & 0 \\ 0 & \dfrac{\partial}{\partial y} \\ \dfrac{\partial}{\partial y} & \dfrac{\partial}{\partial x} \end{bmatrix}. \tag{3.8}$$

Use of the divergence theorem and the boundary conditions (2.9) and (2.10) gives in lieu of equations (3.6) and (3.7):

$$\int_\Omega \left[\mathbf{L}\,\eta^a + H_{\partial\Omega^d}\,\mathbf{L}\,\eta^b\right]^T \sigma\, d\Omega + \int_\Omega \delta_{\partial\Omega^d} \left(\mathbf{L}^*\,\eta^b\right)^T \sigma\, d\Omega = \int_{\partial\Omega} \left(\eta^a + H_{\partial\Omega^d}\,\eta^b\right)^T \mathbf{t}_p\, d(\partial\Omega), \tag{3.9}$$

$$\int_\Omega \left(\xi^a + H_{\partial\Omega^d}\,\xi^b\right) \bar{\epsilon}\; d\Omega + \int_\Omega c \left(\nabla\xi^a + H_{\partial\Omega^d}\,\nabla\xi^b\right)^T \nabla\bar{\epsilon}\, d\Omega + \int_\Omega c\,\delta_{\partial\Omega^d}\,\xi^b\,\mathbf{n}_{\partial\Omega^d}^T\,\nabla\bar{\epsilon}\; d\Omega = \int_\Omega \left(\xi^a + H_{\partial\Omega^d}\,\xi^b\right) \tilde{\epsilon}\, d\Omega, \tag{3.10}$$

with $\mathbf{L}^*$ defined as

$$\mathbf{L}^* = \begin{bmatrix} n_x & 0 \\ 0 & n_y \\ n_y & n_x \end{bmatrix}. \tag{3.11}$$

Using the general distribution property

$$\int_\Omega \delta_{\partial\Omega^d} \ldots d\Omega = \int_{\partial\Omega^d} \ldots d(\partial\Omega) \tag{3.12}$$

and

$$\int_\Omega H_{\partial\Omega^d} \ldots d\Omega = \int_{\Omega^+} \ldots d\Omega \tag{3.13}$$

we rewrite equations (3.9) and (3.10) as:

$$(3.14)\quad \int_\Omega (\boldsymbol{\eta}^a)^T \mathbf{L}^T \boldsymbol{\sigma}\, d\Omega + \int_{\Omega^+} \left(\boldsymbol{\eta}^b\right)^T \mathbf{L}^T \boldsymbol{\sigma}\, d\Omega + \int_{\partial\Omega^d} \left(\boldsymbol{\eta}^b\right)^T (\mathbf{L}^*)^T \boldsymbol{\sigma}\, d(\partial\Omega) = \int_{\partial\Omega} \left(\boldsymbol{\eta}^a + H_{\partial\Omega^d}\, \boldsymbol{\eta}^b\right)^T \mathbf{t}_p\, d(\partial\Omega),$$

$$(3.15)\quad \int_\Omega \xi^a\, \bar{\epsilon}\, d\Omega + \int_{\Omega^+} \xi^b\, \bar{\epsilon}\, d\Omega + \int_\Omega c\, (\nabla\xi^a)^T\, \nabla\bar{\epsilon}\, d\Omega + \int_{\Omega^+} c\, \left(\nabla\xi^b\right)^T \nabla\bar{\epsilon}\, d\Omega + \int_{\partial\Omega^d} c\, \xi^b\, \mathbf{n}_{\partial\Omega^d}^T\, \nabla\bar{\epsilon}\, d(\partial\Omega) = \int_\Omega \xi^a\, \tilde{\epsilon}\, d\Omega + \int_{\Omega^+} \xi^b\, \tilde{\epsilon}\, d\Omega.$$

After complete decohesion of the bulk material, the internal crack or discontinuity that then arises is stress-free. Accordingly, for the interface traction $\mathbf{t}_{\partial\Omega^d}$, it holds that

$$(3.16)\quad \mathbf{t}_{\partial\Omega^d} \equiv (\mathbf{L}^*)^T\, \boldsymbol{\sigma} = \mathbf{0}.$$

Thus, the third integral in Eq. (3.15) cancels. Similarly, the fifth integral of Eq. (3.16) cancels because of the boundary condition (2.10), which, as has been emphasised by PEERLINGS *et al.* [6], must also hold at the internal boundary $\partial\Omega^d$. Thus, we obtain instead of Eqs. (3.15) and (3.16):

$$(3.17)\quad \int_\Omega (\boldsymbol{\eta}^a)^T \mathbf{L}^T \boldsymbol{\sigma}\, d\Omega + \int_{\Omega^+} \left(\boldsymbol{\eta}^b\right)^T \mathbf{L}^T \boldsymbol{\sigma}\, d\Omega = \int_{\partial\Omega} (\boldsymbol{\eta}^a)^T\, \mathbf{t}_p\, d(\partial\Omega) + \int_{\partial\Omega} H_{\partial\Omega^d}\, \left(\boldsymbol{\eta}^b\right)^T\, \mathbf{t}_p\, d(\partial\Omega),$$

$$(3.18)\quad \int_\Omega \xi^a\, \bar{\epsilon}\, d\Omega + \int_{\Omega^+} \xi^b\, \bar{\epsilon}\, d\Omega + \int_\Omega c\, (\nabla\xi^a)^T\, \nabla\bar{\epsilon}\, d\Omega + \int_{\Omega^+} c\, \left(\nabla\xi^b\right)^T \nabla\bar{\epsilon}\, d\Omega = \int_\Omega \xi^a\, \tilde{\epsilon}\, d\Omega + \int_{\Omega^+} \xi^b\, \tilde{\epsilon}\, d\Omega.$$

4. Spatial discretisation

For the spatial discretisation we use a standard Bubnov-Galerkin approach, so that the test and trial functions are in the same space:

$$\mathbf{u} = \mathbf{N}\,(\mathbf{a} + H_{\partial\Omega^d}\,\mathbf{b}), \tag{4.1}$$

$$\boldsymbol{\eta} = \mathbf{N}\,(\mathbf{w} + H_{\partial\Omega^d}\,\mathbf{z}), \tag{4.2}$$

$$\bar{\epsilon} = \bar{\mathbf{N}}\,(\mathbf{e} + H_{\partial\Omega^d}\,\mathbf{g}), \tag{4.3}$$

$$\xi = \bar{\mathbf{N}}\,(\mathbf{f} + H_{\partial\Omega^d}\,\mathbf{h}) \tag{4.4}$$

where the partition-of-unity property of the shape functions contained in $\mathbf{N}$ and $\bar{\mathbf{N}}$ has been exploited. The arrays $\mathbf{a}$ and $\mathbf{e}$ contain the "regular" nodal degrees-of-freedom of the displacements and the non-local strain measure, while $\mathbf{b}$ and $\mathbf{g}$ contain the part that is due to the enhancement. Inserting Eqs. (4.1)–(4.4) into Eqs. (3.18)–(3.19) and setting:

$$\mathbf{B} = \mathbf{L}\,\mathbf{N} \quad \text{and} \quad \bar{\mathbf{B}} = \nabla\bar{\mathbf{N}} \tag{4.5}$$

gives, after requiring that the result holds for all admissible $\mathbf{w}$, $\mathbf{z}$, $\mathbf{f}$ and $\mathbf{h}$:

$$\int_{\Omega} \mathbf{B}^T\,\boldsymbol{\sigma}\,d\Omega = \int_{\partial\Omega} \mathbf{N}^T\,\mathbf{t}_p\,d(\partial\Omega), \tag{4.6}$$

$$\int_{\Omega^+} \mathbf{B}^T\,\boldsymbol{\sigma}\,d\Omega = \int_{\partial\Omega} H_{\partial\Omega^d}\,\mathbf{N}^T\,\mathbf{t}_p\,d(\partial\Omega), \tag{4.7}$$

$$\int_{\Omega} (\bar{\mathbf{N}}^T\,\bar{\mathbf{N}} + c\,\bar{\mathbf{B}}^T\,\bar{\mathbf{B}})\,d\Omega\,\mathbf{e} + \int_{\Omega^+} (\bar{\mathbf{N}}^T\,\bar{\mathbf{N}} + c\,\bar{\mathbf{B}}^T\,\bar{\mathbf{B}})\,d\Omega\,\mathbf{g} = \int_{\Omega} \bar{\mathbf{N}}^T\,\tilde{\epsilon}\,d\Omega, \tag{4.8}$$

$$\int_{\Omega^+} (\bar{\mathbf{N}}^T\,\bar{\mathbf{N}} + c\,\bar{\mathbf{B}}^T\,\bar{\mathbf{B}})\,d\Omega\,\mathbf{e} + \int_{\Omega^+} (\bar{\mathbf{N}}^T\,\bar{\mathbf{N}} + c\,\bar{\mathbf{B}}^T\,\bar{\mathbf{B}})\,d\Omega\,\mathbf{g} = \int_{\Omega^+} \bar{\mathbf{N}}^T\,\tilde{\epsilon}\,d\Omega. \tag{4.9}$$

To facilitate the linearisation process, needed for an incremental-iterative procedure in a Newton-Raphson sense, we define:

$$\mathbf{f}_a^{\text{int}} = \int_{\Omega} \mathbf{B}^T\,\boldsymbol{\sigma}\,d\Omega, \tag{4.10}$$

$$\mathbf{f}_b^{\text{int}} = \int_{\Omega^+} \mathbf{B}^T \boldsymbol{\sigma}\, d\Omega, \tag{4.11}$$

$$\mathbf{f}_a^{\text{ext}} = \int_{\partial\Omega} \mathbf{N}^T \mathbf{t}_p \; d(\partial\Omega), \tag{4.12}$$

$$\mathbf{f}_b^{\text{ext}} = \int_{\partial\Omega} H_{\partial\Omega^d}\, \mathbf{N}^T \mathbf{t}_p \; d(\partial\Omega), \tag{4.13}$$

$$\mathbf{f}_e = \int_{\Omega} \mathbf{N}^T \tilde{\epsilon}\, d\Omega, \tag{4.14}$$

$$\mathbf{f}_g = \int_{\Omega^+} \mathbf{N}^T \tilde{\epsilon}\, d\Omega, \tag{4.15}$$

and

$$\mathbf{K}_{ee} = \int_{\Omega} \left(\bar{\mathbf{N}}^T \bar{\mathbf{N}} + c\, \bar{\mathbf{B}}^T \bar{\mathbf{B}}\right) d\Omega \tag{4.16}$$

$$\mathbf{K}_{eg} = \int_{\Omega^+} \left(\bar{\mathbf{N}}^T \bar{\mathbf{N}} + c\, \bar{\mathbf{B}}^T \bar{\mathbf{B}}\right) d\Omega \tag{4.17}$$

Then, Eqs. (4.6)–(4.9) can be cast in the following format:

$$\mathbf{f}_a^{\text{int}} = \mathbf{f}_a^{\text{ext}}, \tag{4.18}$$

$$\mathbf{f}_b^{\text{int}} = \mathbf{f}_b^{\text{ext}}, \tag{4.19}$$

$$\mathbf{K}_{ee}\, \mathbf{e} + \mathbf{K}_{eg}\, \mathbf{g} = \mathbf{f}_e, \tag{4.20}$$

$$\mathbf{K}_{eg}\, \mathbf{e} + \mathbf{K}_{eg}\, \mathbf{g} = \mathbf{f}_g. \tag{4.21}$$

5. Consistent linearisation

To solve the coupled discrete Eqs. (4.18)–(4.21), a Newton-Raphson procedure is normally employed, which requires a linearisation of the set. Equation (4.18) can be linearised as follows, cf. Eq. (2.3),

$$\begin{aligned}(5.1)\qquad \boldsymbol{\sigma}_j &= \boldsymbol{\sigma}_{j-1} + d\boldsymbol{\sigma} \\ &= \boldsymbol{\sigma}_{j-1} + (1 - \omega_{j-1})\,\mathbf{D}^e\, d\boldsymbol{\epsilon} - d\omega\,\mathbf{D}^e\,\boldsymbol{\epsilon}_{j-1} \\ &= \boldsymbol{\sigma}_{j-1} + (1 - \omega_{j-1})\,\mathbf{D}^e\,\mathbf{B}\,(d\mathbf{a} + H_{\partial\Omega^d}\, d\mathbf{b}) - d\omega\,\mathbf{D}^e\,\boldsymbol{\epsilon}_{j-1}.\end{aligned}$$

Since

$$(5.2)\qquad d\omega = \frac{d\omega}{d\kappa}\,\frac{d\kappa}{d\bar{\epsilon}}\,\bar{\mathbf{N}}\,(d\mathbf{e} + H_{\partial\Omega^d}\, d\mathbf{g}),$$

we have for $\boldsymbol{\sigma}_j$

$$\begin{aligned}(5.3)\qquad \boldsymbol{\sigma}_j = \boldsymbol{\sigma}_{j-1} &+ (1 - \omega_{j-1})\,\mathbf{D}^e\,\mathbf{B}\,(d\mathbf{a} + H_{\partial\Omega^d}\, d\mathbf{b}) \\ &- \mathbf{D}^e\,\boldsymbol{\epsilon}_{j-1}\,\frac{d\omega}{d\kappa}\,\frac{d\kappa}{d\bar{\epsilon}}\,\bar{\mathbf{N}}\,(d\mathbf{e} + H_{\partial\Omega^d}\, d\mathbf{g})\end{aligned}$$

and the linearised form of (4.18) becomes:

$$(5.4)\qquad \mathbf{K}_{aa}\, d\mathbf{a} + \mathbf{K}_{ab}\, d\mathbf{b} + \mathbf{K}_{ae}\, d\mathbf{e} + \mathbf{K}_{ag}\, d\mathbf{g} = \mathbf{f}_a^{\text{ext}} - \mathbf{f}_{a,j-1}^{\text{int}}$$

where

$$(5.5)\qquad \mathbf{K}_{aa} = \int_\Omega \mathbf{B}^T\,(1 - \omega_{j-1})\,\mathbf{D}^e\,\mathbf{B}\, d\Omega,$$

$$(5.6)\qquad \mathbf{K}_{ab} = \int_{\Omega^+} \mathbf{B}^T\,(1 - \omega_{j-1})\,\mathbf{D}^e\,\mathbf{B}\, d\Omega,$$

$$(5.7)\qquad \mathbf{K}_{ae} = -\int_\Omega \mathbf{B}^T\,\mathbf{D}^e\,\boldsymbol{\epsilon}_{j-1}\,\frac{d\omega}{d\kappa}\,\frac{d\kappa}{d\bar{\epsilon}}\,\bar{\mathbf{N}}\, d\Omega,$$

$$(5.8)\qquad \mathbf{K}_{ag} = -\int_{\Omega^+} \mathbf{B}^T\,\mathbf{D}^e\,\boldsymbol{\epsilon}_{j-1}\,\frac{d\omega}{d\kappa}\,\frac{d\kappa}{d\bar{\epsilon}}\,\bar{\mathbf{N}}\, d\Omega.$$

In a similar fashion, we obtain for Eq. (4.19)

$$(5.9)\qquad \mathbf{K}_{ab}\, d\mathbf{a} + \mathbf{K}_{ab}\, d\mathbf{b} + \mathbf{K}_{ag}\, d\mathbf{e} + \mathbf{K}_{ag}\, d\mathbf{g} = \mathbf{f}_b^{\text{ext}} - \mathbf{f}_{b,j-1}^{\text{int}}\,.$$

Finally, $\mathbf{f}_e$ can be linearised using

$$d\tilde{\epsilon} = \left(\frac{d\tilde{\epsilon}}{d\boldsymbol{\epsilon}}\right)^T \mathbf{B}\ (d\mathbf{a} + H_{\partial\Omega^d}\, d\mathbf{b}) \tag{5.10}$$

so that Eqs. (4.20) and (4.21) turn into:

$$\mathbf{K}_{ea}\, d\mathbf{a} + \mathbf{K}_{ga}\, d\mathbf{b} + \mathbf{K}_{ee}\, d\mathbf{e} + \mathbf{K}_{eg}\, d\mathbf{g} = \mathbf{f}_{e,j-1} - \mathbf{K}_{ee}\, \mathbf{e}_{j-1} - \mathbf{K}_{eg}\, \mathbf{g}_{j-1} \tag{5.11}$$

and

$$\mathbf{K}_{ga}\, d\mathbf{a} + \mathbf{K}_{ga}\, d\mathbf{b} + \mathbf{K}_{eg}\, d\mathbf{e} + \mathbf{K}_{eg}\, d\mathbf{g} = \mathbf{f}_{g,j-1} - \mathbf{K}_{eg}\, \mathbf{e}_{j-1} - \mathbf{K}_{eg}\, \mathbf{g}_{j-1}\,, \tag{5.12}$$

$$\mathbf{K}_{ea} = -\int_\Omega \bar{\mathbf{N}}^T \left(\frac{d\tilde{\epsilon}}{d\boldsymbol{\epsilon}}\right)^T \mathbf{B}\, d\Omega, \tag{5.13}$$

$$\mathbf{K}_{ga} = -\int_{\Omega^+} \bar{\mathbf{N}}^T \left(\frac{d\tilde{\epsilon}}{d\boldsymbol{\epsilon}}\right)^T \mathbf{B}\, d\Omega. \tag{5.14}$$

Summarising Eqs. (5.4), (5.9), (5.11) and (5.12) in a matrix-vector format, we obtain:

$$\begin{bmatrix} \mathbf{K}_{aa} & \mathbf{K}_{ab} & \mathbf{K}_{ae} & \mathbf{K}_{ag} \\ \mathbf{K}_{ab} & \mathbf{K}_{ab} & \mathbf{K}_{ag} & \mathbf{K}_{ag} \\ \mathbf{K}_{ea} & \mathbf{K}_{ga} & \mathbf{K}_{ee} & \mathbf{K}_{eg} \\ \mathbf{K}_{ga} & \mathbf{K}_{ga} & \mathbf{K}_{eg} & \mathbf{K}_{eg} \end{bmatrix} \begin{bmatrix} d\mathbf{a} \\ d\mathbf{b} \\ d\mathbf{e} \\ d\mathbf{g} \end{bmatrix} = \begin{pmatrix} \mathbf{f}_a^{ext} - \mathbf{f}_{a,j-1}^{int} \\ \mathbf{f}_b^{ext} - \mathbf{f}_{b,j-1}^{int} \\ \mathbf{f}_{e,j-1} - \mathbf{K}_{ee}\, \mathbf{e}_{j-1} - \mathbf{K}_{eg}\, \mathbf{g}_{j-1} \\ \mathbf{f}_{g,j-1} - \mathbf{K}_{eg}\, \mathbf{e}_{j-1} - \mathbf{K}_{eg}\, \mathbf{g}_{j-1} \end{pmatrix}. \tag{5.15}$$

6. Concluding remarks

A theoretical framework has been given for the description of a truly discontinuous crack arising as the result of a damaging process involving initiation, growth and coalescence of micro-cracks. For the latter process, a gradient-enhanced damage model has been utilised. An example representing the proposed method will be presented in a forthcoming publication.

Acknowledgements

Financial support of the European Union to the second author under the TMR-project "Spatio-Temporal Instabilities in Solids" is gratefully acknowledged.

References

1. I. Babuska, J.M. Melenk, *The partition of unity method*, Int. J. Num. Meth. Eng., **40**, 727–758, 1997.
2. T. Belytschko, T. Black, *Elastic crack growth in finite elements with minimal remeshing*, Int. J. Num. Meth. Eng., **45**, 5, 601–620, 1999.
3. R. de Borst, *Some recent issues in computational failure mechanics*, Int. J. Num. Meth. Eng., **52**, 63–95, 2001.
4. R. de Borst and M.A. Gutiérrez, *A unified framework for concrete damage and fracture models with a view to size effects*, Int. J. Fracture, **95**, 261–277, 1999.
5. M. K. Duszek-Perzyna, P. Perzyna, E. Stein, *Adiabatic shear localization in elastic-plastic damaged solids*, Int. J. Plasticity, **8**, 361–384, 1992.
6. R.H.J. Peerlings, R. de Borst, W.A.M. Brekelmans, M.G.D. Geers, *Localisation issues in local and nonlocal continuum approaches to fracture*, European Journal of Mechanics: A/Solids, **21**, 175–189, 2002.
7. R.H.J. Peerlings, R. de Borst, W.A.M. Brekelmans and H.P.J. de Vree, *Gradient-enhanced damage for quasi-brittle materials*, Int. J. Num. Meth. Eng., **39**, 3391–3403, 1996.
8. R.H.J. Peerlings, R. de Borst, W.A.M. Brekelmans, H.P.J. de Vree and I. Spree, *"Some observations on localisation in non-local and gradient damage models"*, European Journal of Mechanics: A/Solids, **15**, 937–954, 1996.
9. G.N. Wells, L.J. Sluys, *A new method for modelling cohesive cracks using finite elements*, Int. J. Num. Meth. Eng., **50**, 12, 2667–2682, 2001.
10. G.N. Wells, L.J. Sluys, R. de Borst, *Simulating the propagation of displacement discontinuities in a regularised strain-softening medium*, Int. J. Num. Meth. Eng., **53**, 1235–1256, 2002.

Received May 10, 2002; revised version September 7, 2002.

Arch. Mech., **54**, 5-6, pp. 389–410, Warszawa 2002

A new integration procedure for thermo-elasto-viscoplasticity

W. DORNOWSKI

Institute of Fundamental Technological Research,
Polish Academy of Sciences,
Świętokrzyska 21, 00-049 Warsaw, Poland
e-mail: wdorn@ippt.gov.pl

Dedicated to Professor Piotr Perzyna
on the occasion of his 70^{th} birthday

A NUMERICAL INTEGRATION algorithm for thermo-elasto-viscoplastic constitutive equations is presented. This algorithm satisfies the principle of material objectivity with respect to the total motion (translation, rotation and strain) of a material element. For this purpose, the properties of convective description are used. The explicit-implicit integration scheme for the plastic flow rule plays the crucial role in the proposed algorithm. The method of determining the stress state for inelastic deformations is based on the iterative solution of the dynamic yield condition with respect to the norm of the viscoplastic deformation rate tensor. The constitutive model being the subject of numerical analyses is described. Results of numerical calculations, which show an excellent performance of the proposed procedure, are presented.

1. Introduction

CONTEMPORARY DEVELOPMENT of computer technologies gives hope that a more realistic numerical simulation of deformation and fracture processes for metal structures will be possible in the near future. The effective execution of such a simulation demands an analysis of detailed problems connected with the theoretical investigation and experimental identification of constitutive models for structural materials. The applied numerical method as well as the spatial modelling of structures and their loads must be carefully considered too.

The main objective of the paper is to formulate a numerical integration algorithm for thermo-elasto-viscoplastic constitutive relations. In this formulation, the material objectivity in relation to the total motion (translation, rotation and deformation) of a structural element is postulated. The proposed algorithm can be used for the numerical analysis of large deformations and fracture of metal structural elements under monotonic or cyclic loadings.

Numerical integration procedures for elasto-viscoplastic constitutive relations, applied in the finite element or finite difference methods, are based on

the additive structure of these relations. In these procedures, two fundamental parts may be distinguished. In the first part, the so-called elastic trial state, represented by a point of the stress space, is determined. If this point lies beyond the elastic region determined by the yield surface, this means that the plastic flow process is achieved locally. Thus, the principal problem of the second part is to determine the stress state represented by a point of the actual yield surface.

The numerical integration algorithms for elasto-viscoplastic or elasto-plastic constitutive relations, which exist in the literature, differ in manners of determining the stress state for the inelastic deformation. In the procedure for plastically incompressible materials (J_2 flow theory), originally proposed in [33], the flow stresses are determined by the orthogonal projection of trial stresses onto the yield surface. Generalisations of this algorithm for plastic materials with linear isotropic and kinematic hardening have been proposed in [17, 18, 27].

Other generalisations have been referred to a wider class of materials described by non-associative plastic flow rules, arbitrary yield criteria and more complicated hardening laws. In addition, a general elastic response is considered, not restricted to constant elasticities. In such cases, the path of stress projection is already not represented by the straight line in the stress space and it has to be determined numerically. Algorithms of this type are based on the so-called return mapping method [3, 22, 31, 32]. In this method, as a result of integration of elastic equations, the elastic prediction is obtained to determine the initial conditions for plastic equations. Relaxation relations for both stresses and internal state variables define the plastic correction, which is necessary to assure the plastic consistency. The numerical relaxation process is carried out in a step-by-step fashion. At each iteration the yield function is linearized around the current values of state variables. The linearized yield function is represented by a plane contained in the stress space. In order to determine the next iteration the stresses are projected onto this plane. In the limit, such a plane becomes tangent to the yield surface and plastic consistency is restored.

From the computational standpoint, the central issue to be addressed concerns the numerical integration of the constitutive model in such a manner that the resulting discrete equations identically satisfy the principle of material frame indifference. Satisfaction of this fundamental restriction leads to the so-called incrementally objective algorithms [15, 26, 29]. The material objectivity for the superimposed spatial rigid body motion has been considered most often.

Constitutive equations, which are assumed to be the object of the numerical analysis, are presented in Sec. 2. Within the framework of the rate-type covariance, material structure with a finite set of the internal state variables, the viscoplastic effects, plastic strain induced anisotropy (kinematic hardening), micro-damage mechanisms, isotropic hardening, plastic spin effects as well as thermomechanical couplings are taken into account.

The proposed numerical integration algorithm for the given constitutive equations is presented in Sec. 3. Properties of the convective description are used. In the convective coordinate system the rates of spatial tensor fields, objective with respect to the arbitrary spatial diffeomorphism (regular motion), are represented by matrices of partial time derivatives of suitable components of these fields [5]. This property directly leads to the incremental expressions, which are objective in the above sense. The explicit-implicit integration scheme for the plastic flow rule is the essential part of the proposed algorithm. The method of determination of the flow stresses is based on the iterative solution of the dynamic yield condition with respect to the norm of the viscoplastic deformation rate tensor.

A numerical example is presented in Sec. 4. In this example, the capability of the discussed algorithm is shown. A thin steel plate with a narrow notch performed perpendicularly to its edge is analysed numerically by means of the finite difference method. The dynamic cyclic load is assumed. The so-called low-cycle fatigue regime is considered. The evolution of greatest stress regions forming in the neighbourhood of the initial notch is analysed. The numerical simulation of evolutions of plastic zones, temperature, microdamage and plastic rotation in vicinity of the developing fatigue crack is carried out. The adiabatic process is considered.

Final comments and conclusions are presented in Sec. 5.

2. Constitutive foundations

Most of metals show simultaneously plastic and viscous effects. Viscous effects appear most clearly in fast changing processes, but they also influence essentially the rheological phenomena. Physical processes lying at the bases of viscoplastic phenomena have a complicated nature and they depend mostly on the movement of dislocations and on changes of distributions of the dislocation density. Besides, temperature of a material influences strongly the movement of dislocations and the changes of their densities, and thus the viscoplastic phenomena. Temperature activates or breaks these processes [24, 25].

In viscoplasticity, unlike in plasticity, the dependence of plastic deformations is postulated not only on the path of loading, but also on the phenomena of the time scale. This means that viscoplastic materials show simultaneously the sensitivity to the path of loading and to the rate of deformation. In this manner, different magnitudes of the plastic deformations will be obtained for different loading paths and for different deformation rates. The fact, that these two different material sensitivities correspond to two different forms of the internal dissipation, should find a reflection in the constitutive modelling.

Except for viscoplasticity, the effects such as micro-damage, plastic strain-induced anisotropy (kinematic hardening), isotropic hardening, the plastic spin

and the thermomechanical couplings are taken into account [10, 11]. The considerations are limited to the fast changing, adiabatic processes. The spatial description is assumed as physically most natural. Such an approach has also a reason, which results from the application of constitutive equations to the description of plastic flow processes in the actual state.

The considered constitutive relations can be written in the following, comfortable for an incremental analysis, form:

Evolution equation for the Kirchhoff stress tensor τ [5, 6, 11, 12]

$$L_{\mathbf{v}}\boldsymbol{\tau} = L^e : \mathbf{d} - L^e : \mathbf{d}^p - L^{th}\dot{\vartheta} - \mathbf{k} - \mathbf{s}. \tag{2.1}$$

In the above equation the tensorial measure of the stress rate is the Lie derivative of the tensor $\boldsymbol{\tau}$. In the mechanics of continuous media, the notion of the Lie derivative is connected with the material objectivity of rates of spatial tensor fields with respect to the diffeomorphism (regular motion) [11, 20]. The total deformation rate tensor $\mathbf{d}$ and the inelastic deformation rate tensor $\mathbf{d}^p$ are measures of strain rates, which are objective in the above sense. By L^e and L^{th} we denote the tensor of elastic moduli (fourth rank tensor) and the thermal expansion tensor (second rank tensor), respectively. The symbol $\dot{\vartheta}$ denotes the rate of temperature.

Expressions

$$\mathbf{k} = \mathbf{d}^p \cdot \boldsymbol{\tau} - \boldsymbol{\tau} \cdot \mathbf{d}^p, \quad \mathbf{s} = \boldsymbol{\omega}^p \cdot \boldsymbol{\tau} - \boldsymbol{\tau} \cdot \boldsymbol{\omega}^p \tag{2.2}$$

describe the covariant effect and the influence of a plastic spin $\boldsymbol{\omega}^p$, respectively [7].

Plastic flow rule

$$\mathbf{d}^p = \bar{\Lambda}(\tilde{\boldsymbol{\tau}}' + A\mathrm{tr}\tilde{\boldsymbol{\tau}}\mathbf{g}). \tag{2.3}$$

The scalar multiplier $\bar{\Lambda}$ is given by the relation

$$\bar{\Lambda} = \frac{1}{T_m}\langle\Phi(\cdot)\rangle\,(2\tilde{J}_2' + 3A^2\tilde{J}_1^2)^{-1/2}, \tag{2.4}$$

where T_m denotes the relaxation time and Φ is the empirical overstress function [23]. The second invariant of a relative stress deviator $\tilde{\boldsymbol{\tau}}' = \boldsymbol{\tau}' - \boldsymbol{\alpha}'$ is denoted by $\tilde{J}_2'$, and $\tilde{J}_1$ denotes the first invariant of the relative stress $\tilde{\boldsymbol{\tau}} = \boldsymbol{\tau} - \boldsymbol{\alpha}$. The back stress tensor $\boldsymbol{\alpha}$ determines the actual position of the yield surface centre in the stress space and it is the measure of kinematic hardening. Thus, the relative stress expresses the difference between the point of loading and the yield surface centre. By $\mathbf{g}$ the metric tensor of the convective coordinate system is denoted.

The magnitude

$$A = 2\left[n_1(\vartheta) + n_2(\vartheta)\xi\right] \tag{2.5}$$

describes the influence of temperature-dependent micro-damage mechanisms on the plastic flow direction. The scalar parameter ξ expresses the volumetric participation of microdamages in the material.

Equation for the plastic spin [2] has the form

$$\omega^p = \bar{\eta}(\boldsymbol{\alpha} \cdot \mathbf{d}^p - \mathbf{d}^p \cdot \boldsymbol{\alpha}). \tag{2.6}$$

The postulated equation describes the dependence of the plastic spin on the plastic strain-induced anisotropy. Therefore, the plastic spin may be of significance in problems of the cyclic plasticity (accumulation of the plastic rotation at cyclic loads).

Evolution equations for internal state variables [6, 8]

$$L_{\mathbf{v}}\boldsymbol{\mu} = \hat{\mathbf{m}} \tag{2.7}$$

The vector of evolution functions $\hat{\mathbf{m}}$ is determined by analyses of the examined physical processes. It is postulated that the internal state vector $\boldsymbol{\mu}$ has the form $\mu = (\xi, \alpha)$. Evolution equation for temperature (adiabatic process) [9, 19] is

$$\dot{\vartheta} = \frac{\bar{\chi}}{\rho c_p}\tau : \mathbf{d}^p + \frac{\bar{\bar{\chi}}}{\rho c_p}\Xi, \tag{2.8}$$

where ρ is the mass density in the actual configuration, c_p denotes the specific heat, Ξ determines the evolution function for internal micro-damage mechanisms (nucleation, growth and coalescence). By $\bar{\chi}$ and $\bar{\bar{\chi}}$ the irreversibility coefficients are denoted.

Making the operation $\mathbf{d}^p : \mathbf{d}^p$, the dynamic yield criterion is obtained as follows

$$\begin{gathered}\Theta = \left\{\tilde{J}_2' + \left[n_1(\vartheta) + n_2(\vartheta)\xi\right]\tilde{J}_1^2\right\}^{1/2} - \kappa\left[1 + \Phi^{-1}\left(T_m \left\|\mathbf{d}^p\right\|\right)\right] = 0, \\ \left\|\mathbf{d}^p\right\| = \left(\mathbf{d}^p : \mathbf{d}^p\right)^{1/2},\end{gathered} \tag{2.9}$$

where κ is the isotropic hardening-softening function. A more detailed discussion of the presented constitutive model can be found in the quoted papers, where wide bibliographic references to the considered problems are presented.

3. A numerical integration algorithm

To construct an incrementally objective algorithm the properties of convective description [13, 14, 21] is used. In this description the rate of spatial tensor field, objective with respect to an arbitrary spatial diffeomorphism (regular motion), is represented by the matrix of partial time derivatives of suitable components of such a field. This property directly leads to the incremental expressions, which are objective in the above sense. For example, in the implicit expression the objective increments of strains and stresses have the following convective representations:

$$\underset{(n)}{\mathbf{d}}\,\Delta t \cong \Delta e_{ij}(\underset{(n)}{\mathbf{g}^i} \otimes \underset{(n)}{\mathbf{g}^j}) \,, \quad \underset{(n)}{L_{\mathbf{v}}\boldsymbol{\tau}}\,\Delta t \cong \Delta \tau^{ij}(\underset{(n)}{\mathbf{g}_i} \otimes \underset{(n)}{\mathbf{g}_i}), \tag{3.1}$$

where

$$\Delta e_{ij} = \underset{(n)}{e_{ij}} - \underset{(n-1)}{e_{ij}} \,, \quad \Delta \tau^{ij} = \underset{(n)}{\tau^{ij}} - \underset{(n-1)}{\tau^{ij}} \tag{3.2}$$

are the increments of convective components of the Euler strain tensor and the Kirchhoff stress tensor, respectively. The defined increments refer to the time increment $\Delta t^{n-1,n} = t^n - t^{n-1}$ (for simplification of the notation the index $(n\text{-}1,n)$ is omitted).

For comparison, in the spatial description referred to the fixed, rectangular system of coordinates $\{x^i\}$ with a basis $\{\mathbf{e}_i\}$, $i = 1,2,3$, the suitable stress increment has the following form:

$$\underset{(n)}{L_{\mathbf{v}}\boldsymbol{\tau}}\,\Delta t \cong \left(\Delta \tau^{ij} + \left.\frac{\partial \tau^{ij}}{\partial x^k}\right|_{(n)} \underset{(n)}{v^k}\,\Delta t - \underset{(n)}{\tau^{kj}} \left.\frac{\partial v^i}{\partial x^k}\right|_{(n)} \Delta t - \underset{(n)}{\tau^{ik}} \left.\frac{\partial v^j}{\partial x^k}\right|_{(n)} \Delta t \right) (\mathbf{e}_i \otimes \mathbf{e}_j), \tag{3.3}$$

where v^i are components of the spatial velocity field. The numerical integration procedure based on the increment (3.3) needs additional calculation of the stress and velocity gradients. In the convective approach this troublesome necessity is not performed. As a result, less complicated and thus more efficient algorithm can be obtained.

In the numerical integration algorithm presented below for the specified constitutive equations the convective approach is just used. Incremental relationships determining the elastic trial state $\breve{\boldsymbol{\tau}}$ ($\mathbf{d}^e = \mathbf{d}$), separated into volumetric and deviatoric parts, have the following form:

$$\operatorname{tr}(\underset{(n)}{L_{\mathbf{v}}\breve{\boldsymbol{\tau}}})\Delta t = (2\mu + 3\lambda)\operatorname{tr}\underset{(n)}{\mathbf{d}}\,\Delta t, \quad \underset{(n)}{L_{\mathbf{v}}\breve{\boldsymbol{\tau}}'}\,\Delta t = 2\mu\,\underset{(n)}{\mathbf{d}'}\,\Delta t, \tag{3.4}$$

where

$$\operatorname{tr}(L_{\mathbf{v}}\overset{\smile}{\boldsymbol{\tau}})\Delta t = \underset{(n)}{\overset{\cdot}{\overset{\smile}{\boldsymbol{\tau}}}}{}^{ij}\,\Delta t\, g_{ij} \cong \Delta\overset{\smile}{\boldsymbol{\tau}}{}^{ij}\, g_{ij}\ ,$$

$$\mathrm{L}_{\mathbf{v}}\overset{\smile}{\boldsymbol{\tau}}{}'\,\Delta t = \underset{(n)}{\overset{\cdot}{\overset{\smile}{\boldsymbol{\tau}}}}{}'^{ij}\,\Delta t(\mathbf{g}_i \otimes \mathbf{g}_j) \cong \Delta\overset{\smile}{\boldsymbol{\tau}}{}'^{ij}(\mathbf{g}_i \otimes \mathbf{g}_j)\ ,$$

$$\operatorname{tr}\mathbf{d}\,\Delta t = \dot{e}_{ij}\,\Delta t\, g^{ij} \cong \Delta e_{ij}\, g^{ij}\ , \tag{3.5}$$

$$\begin{aligned}\mathbf{d}'\,\Delta t &= d'_{kl}\,\Delta t(\overset{k}{\mathbf{g}} \otimes \mathbf{g}^l)\\ &= \dot{e}'_{kl}\,\Delta t\, g^{ki}\, g^{lj}(\mathbf{g}_i \otimes \mathbf{g}_j) \cong \Delta\, e'_{kl}\, g^{ki}\, g^{lj}(\mathbf{g}_i \otimes \mathbf{g}_j)\ .\end{aligned}$$

By μ and λ the Lamé constants are denoted. It is noteworthy that the product $\dot{e}'_{kl}\, g^{ki}\, g^{lj}$ in Eq. $(3.5)_4$ can not be prescribed as $\dot{e}'^{ij}$, because $\dot{e}'^{ij} = \overbrace{e'_{kl}g^{ki}g^{lj}}^{\cdot} = \dot{e}'_{kl}g^{ki}g^{lj} + e'_{kl}\dot{g}^{ki}g^{lj} + e'_{kl}g^{ki}\dot{g}^{lj}$. Besides, convective components $\dot{e}^{ij}$ do not represent the deformation rate tensor $\mathbf{d}$. They represent another objective rate measure of the Euler strain tensor, i.e. $L_{\mathbf{v}}\mathbf{e} = \dot{\mathbf{e}} - \mathbf{e}\cdot\mathbf{l}^T - \mathbf{l}\cdot\mathbf{e} = \dot{e}^{ij}(\mathbf{g}_i \otimes \mathbf{g}_j)$ [5]. Therefore, the incremental equations (3.4) for the elastic trial state are prescribed in the covariant basis of the convective reference frame.

In the proposed algorithm the following matrix notation for suitable tensor representations is used (for the simplification of notation the index (n) is omitted):

$$\begin{gathered}\mathbf{g} = [g_{ij}]_{3\times3},\quad \mathbf{g}^{-1} = [g^{ij}]_{3\times3},\quad \boldsymbol{\tau} = [\tau^{ij}]_{3\times3},\quad \overset{\smile}{\boldsymbol{\tau}} = [\overset{\smile}{\tau}{}^{ij}]_{3\times3},\\ \Delta\boldsymbol{\tau} = [\Delta\tau^{ij}]_{3\times3},\quad \Delta\overset{\smile}{\boldsymbol{\tau}} = [\Delta\overset{\smile}{\tau}{}^{ij}]_{3\times3},\quad \boldsymbol{\alpha} = [\alpha^{ij}]_{3\times3},\quad \mathbf{d}^p = [d^p_{ij}]_{3\times3},\\ \Delta\mathbf{e} = [\Delta e_{ij}]_{3\times3},\quad \Delta\mathbf{e}^p = [\Delta e^p_{ij}]_{3\times3},\\ \boldsymbol{\omega}^p = [\omega^{pij}]_{3\times3},\quad \mathbf{k} = [k^{ij}]_{3\times3},\quad \mathbf{s} = [s^{ij}]_{3\times3}.\end{gathered} \tag{3.6}$$

At last, the incremental equations for the elastic trial state take the matrix form

$$\operatorname{tr}(\Delta\overset{\smile}{\boldsymbol{\tau}}\mathbf{g}) = (2\mu + 3\lambda)\operatorname{tr}(\Delta\mathbf{e}\mathbf{g}^{-1})\quad \Delta\overset{\smile}{\boldsymbol{\tau}}{}' = 2\mu\mathbf{g}^{-1}\Delta\mathbf{e}'\mathbf{g}^{-1}. \tag{3.7}$$

From Eq. (3.7) the increments of trial stresses in a time interval $[t^{n-1}, t^n]$ are determined. According to the following expressions, the trial stresses may be

determined for a time instant t^n:

$$\text{tr}(\breve{\boldsymbol{\tau}}\mathbf{g}) = \text{tr}(\underset{(n-1)}{\breve{\boldsymbol{\tau}}}\,\mathbf{g}) + \text{tr}(\Delta\breve{\boldsymbol{\tau}}\mathbf{g}), \qquad \breve{\boldsymbol{\tau}}' = \underset{(n-1)}{\breve{\boldsymbol{\tau}}'} + \Delta\breve{\boldsymbol{\tau}}'. \tag{3.8}$$

These stresses are used to check the yield condition.

$$\varphi = \hat{\varphi}(\breve{\boldsymbol{\tau}}, \underset{(n-1)}{\mu}, \underset{(n-1)}{\vartheta}, \underset{(n-1)}{\kappa}). \tag{3.9}$$

If $\varphi \leq 0$ the elastic process takes place and

$$\text{tr}(\boldsymbol{\tau}\mathbf{g}) = \text{tr}(\breve{\boldsymbol{\tau}}\mathbf{g}) \,, \quad \boldsymbol{\tau}' = \breve{\boldsymbol{\tau}}'. \tag{3.10}$$

Internal state variables, temperature and the hardening-softening function remain unchanged, i.e. $\mu = \underset{(n-1)}{\mu}$, $\vartheta = \underset{(n-1)}{\vartheta}$ and $\kappa = \underset{(n-1)}{\kappa}$.

If $\varphi > 0$ the inelastic process is achieved locally. Then, the suitable relationships of elasto-viscoplasticity should be considered. In order to describe the incremental form of the plastic flow rule (2.3) the following mixed (explicit-implicit) approach is proposed:

$$\text{tr}\mathbf{d}^p \Delta t = 3\Delta\bar{\Lambda} \underset{(n-1)}{A}\, \text{tr}(\boldsymbol{\tau} - \underset{(n-1)}{\boldsymbol{\alpha}}), \quad \mathbf{d}'^p \Delta t = \Delta\bar{\Lambda}(\boldsymbol{\tau}' - \underset{(n-1)}{\boldsymbol{\alpha}}'), \tag{3.11}$$

where

$$\text{tr}\,\mathbf{d}'^p\,\Delta t = \Delta e^p_{ij}\, g^{ij}, \quad \mathbf{d}'^p\,\Delta t = \Delta e'^p_{kl}\, g^{ki}\, g^{lj}(\mathbf{g}_i \otimes \mathbf{g}_j), \quad \Delta\bar{\Lambda} = \bar{\Lambda}\Delta t. \tag{3.12}$$

All magnitudes prescribed at the right-hand side of equations (3.11), except the stresses, are defined for a time instant t^{n-1} at the beginning of the time step. In this sense, the incremental formulas (3.11) are explicit for internal state variables $\underset{(n-1)}{\xi}$ and $\underset{(n-1)}{\alpha}$, and implicit for stresses. In the matrix notation for suitable tensorial representations, the analysed law takes the form

$$\begin{aligned} &\text{tr}(\Delta\mathbf{e}^p\mathbf{g}^{-1}) = 3\Delta\bar{\Lambda} \underset{(n-1)}{A}\, \text{tr}[(\boldsymbol{\tau} - \underset{(n-1)}{\boldsymbol{\alpha}})\mathbf{g}], \\ &\mathbf{g}^{-1}\Delta\mathbf{e}'^p\,\mathbf{g}^{-1} = \Delta\bar{\Lambda}(\boldsymbol{\tau}' - \underset{(n-1)}{\boldsymbol{\alpha}}'). \end{aligned} \tag{3.13}$$

The incremental form of the evolution equation for the Kirchhoff stress tensor (2.1) in the matrix notation is

$$\begin{aligned} \text{tr}(\Delta\boldsymbol{\tau}\mathbf{g}) = {} & (2\mu + 3\lambda)\text{tr}(\Delta\mathbf{e}\mathbf{g}^{-1}) - (2\mu + 3\lambda)\text{tr}(\Delta\mathbf{e}^p\mathbf{g}^{-1}) \\ & - 3(2\mu + 3\lambda)\theta\, \underset{(n-1)}{\dot{\vartheta}}\, \Delta t - [\text{tr}(\underset{(n-1)}{\mathbf{k}}\,\mathbf{g}) + \text{tr}(\underset{(n-1)}{\mathbf{s}}\,\mathbf{g})]\Delta t, \end{aligned} \tag{3.14}$$

$$\Delta\boldsymbol{\tau}' = 2\mu\mathbf{g}^{-1}\Delta\mathbf{e}'\mathbf{g}^{-1} - 2\mu\mathbf{g}^{-1}\Delta\mathbf{e}'^p\mathbf{g}^{-1} - (\underset{(n-1)}{\mathbf{k}}' + \underset{(n-1)}{\mathbf{s}}')\Delta t.$$

Taking into account the relationships of the elastic trial state (3.7) it can be noticed that the first components at the right-hand sides of equations (3.14) express the increments of trial stresses. Substituting Eq. (3.7) and Eq. (3.13) into Eq. (3.14) gives the following system of algebraic equations:

$$\text{(3.15)}\quad \operatorname{tr}(\boldsymbol{\tau}\mathbf{g}) = \operatorname{tr}(\underset{(n-1)}{\boldsymbol{\alpha}}\,\mathbf{g}) + \frac{1}{1+3(2\mu+3\lambda)\Delta\bar{\Lambda}\underset{(n-1)}{A}}\Big\{\operatorname{tr}[(\breve{\boldsymbol{\tau}} - \underset{(n-1)}{\boldsymbol{\alpha}})\mathbf{g}]$$

$$- 3(2\mu+3\lambda)\theta\underset{(n-1)}{\dot{\vartheta}}\Delta t - [\operatorname{tr}(\underset{(n-1)}{\mathbf{k}}\,\mathbf{g}) + \operatorname{tr}(\underset{(n-1)}{\mathbf{s}}\,\mathbf{g})]\Delta t\Big\},$$

$$\boldsymbol{\tau}' = \underset{(n-1)}{\boldsymbol{\alpha}'} + \frac{1}{1+2\mu\Delta\bar{\Lambda}}\Big[\breve{\boldsymbol{\tau}}' - \underset{(n-1)}{\boldsymbol{\alpha}'} - (\underset{(n-1)}{\mathbf{k}'} + \underset{(n-1)}{\mathbf{s}'})\Delta t\Big].$$

This system will be appointed with respect to the scalar multiplier $\Delta\bar{\Lambda}$ when the dynamic yield condition (2.9) will be taken into account,

$$\text{(3.16)}\qquad \Theta = f(\boldsymbol{\tau}, \underset{(n-1)}{\boldsymbol{\alpha}}, \underset{(n-1)}{\xi}, \underset{(n-1)}{\vartheta}) - \underset{(n-1)}{\kappa}\,[1+\Phi^{-1}(T_m\,\|\mathbf{d}^p\|)] = 0.$$

Owing to nonlinearity of this condition, $\Delta\bar{\Lambda}$ has to be determined by an iterative method (e.g. Newton's method). In accordance with Eq. (3.16) the norm of the inelastic deformation rate tensor $\mathbf{d}^p$ is updated at each iteration. For this purpose, the incremental form (3.13) of the inelastic flow rule is used. The iterative procedure of determination of the multiplier $\Delta\bar{\Lambda}$ determines the non-linear path of projection of the trial stress onto the actual yield surface.

After the end of the iterative procedure the temperature ϑ at a time instant t^n is calculated,

$$\text{(3.17)}\qquad \vartheta = \underset{(n-1)}{\vartheta} + \Delta\vartheta, \quad \Delta\vartheta = \frac{\bar{\chi}}{\underset{(n-1)}{\rho}\,c_p}\operatorname{tr}(\boldsymbol{\tau}\Delta\mathbf{e}^p) + \frac{\bar{\bar{\chi}}}{\underset{(n-1)}{\rho}\,c_p}\underset{(n-1)}{\Xi}\,\Delta t.$$

Next, the following magnitudes are determined: the internal state variables

$$\text{(3.18)}\qquad \boldsymbol{\mu} = \underset{(n-1)}{\boldsymbol{\mu}} + \Delta\boldsymbol{\mu}, \quad \Delta\boldsymbol{\mu} = \hat{\mathbf{m}}(\boldsymbol{\tau}, \underset{(n-1)}{\boldsymbol{\mu}}, \vartheta)\Delta t,$$

the plastic spin

$$\text{(3.19)}\qquad \boldsymbol{\omega}^p = \bar{\eta}(\boldsymbol{\alpha}\mathbf{d}^p\mathbf{g}^{-1} - \mathbf{g}^{-1}\mathbf{d}^p\boldsymbol{\alpha}),$$

and tensors of the covariant and plastic spin effects:

$$\text{(3.20)}\qquad \mathbf{k} = \mathbf{g}^{-1}\mathbf{d}^p\boldsymbol{\tau} - \boldsymbol{\tau}\mathbf{d}^p\mathbf{g}^{-1}, \quad \mathbf{s} = \boldsymbol{\omega}^p\mathbf{g}\boldsymbol{\tau} - \boldsymbol{\tau}\mathbf{g}\boldsymbol{\omega}^p.$$

The proposed approach gives very good results for calculations with a small time step as in the explicit finite element or finite difference methods that operate with small time steps because of the stability condition. Operating with a greater time step becomes quite possible in the implicit, unconditionally stable methods. In such cases, the implicit forms of relationships (3.13) and (3.14) should be considered, i.e. such in which $\underset{(n)}{\boldsymbol{\mu}}$, $\underset{(n)}{\mathbf{k}}$, $\underset{(n)}{\mathbf{s}}$ and $\underset{(n)}{\dot{\vartheta}}$ are determined at the end of a time step. As a result the system of non-linear, algebraic equations is obtained instead of the system of equations (3.15). From the viewpoint of numerical calculations the solution of such a system is much more expensive (time-consuming).

To describe the analysed method in the form of a numerical algorithm it is assumed that the non-linear equation (3.16) is solved by means of the iterative Newton's method.

1. Geometric update

$$\Delta\mathbf{e} = \mathbf{e} - \underset{(n-1)}{\mathbf{e}}.$$

2. Elastic trial state

$$\mathrm{tr}(\Delta\breve{\boldsymbol{\tau}}\mathbf{g}) = (2\mu + 3\lambda)\mathrm{tr}(\Delta\mathbf{e}\mathbf{g}^{-1}), \quad \Delta\breve{\boldsymbol{\tau}}' = 2\mu\mathbf{g}^{-1}\Delta\mathbf{e}'\mathbf{g}^{-1}$$

$$\mathrm{tr}(\breve{\boldsymbol{\tau}}\mathbf{g}) = \mathrm{tr}(\underset{(n-1)}{\breve{\boldsymbol{\tau}}}\,\mathbf{g}) + \mathrm{tr}(\Delta\breve{\boldsymbol{\tau}}\mathbf{g}), \quad \breve{\boldsymbol{\tau}}' = \underset{(n-1)}{\breve{\boldsymbol{\tau}}'} + \Delta\breve{\boldsymbol{\tau}}'.$$

3. Check the yield condition

$$\hat{\varphi}(\breve{\boldsymbol{\tau}}, \underset{(n-1)}{\boldsymbol{\mu}}, \underset{(n-1)}{\vartheta}, \underset{(n-1)}{\kappa}) \leq 0\ ?$$

YES: $\mathrm{tr}(\boldsymbol{\tau}\mathbf{g}) = \mathrm{tr}(\breve{\boldsymbol{\tau}}\mathbf{g})$, $\boldsymbol{\tau}' = \breve{\boldsymbol{\tau}}'$,

$$\boldsymbol{\mu} = \underset{(n-1)}{\boldsymbol{\mu}}, \quad \vartheta = \underset{(n-1)}{\vartheta}, \quad \kappa = \underset{(n-1)}{\kappa} \rightarrow \text{EXIT}$$

NO: $i = 1$, $\Delta\bar{\Lambda}^{(i-1)} = \Delta\underset{(n-1)}{\bar{\Lambda}}$.

4. Stresses in the inelastic state

$$\mathrm{tr}(\boldsymbol{\tau}^{(i)}\mathbf{g}) = \mathrm{tr}(\underset{(n-1)}{\boldsymbol{\alpha}}\,\mathbf{g}) + \frac{1}{1 + 3(2\mu + 3\lambda)\Delta\bar{\Lambda}^{(i-1)}\underset{(n-1)}{A}}\Big\{\mathrm{tr}[(\breve{\boldsymbol{\tau}} - \underset{(n-1)}{\alpha})\mathbf{g}]$$

$$- 3(2\mu + 3\lambda)\theta\,\underset{(n-1)}{\dot{\vartheta}}\,\Delta t - [\mathrm{tr}(\underset{(n-1)}{\mathbf{k}}\,\mathbf{g}) + tr(\underset{(n-1)}{\mathbf{s}}\,\mathbf{g})]\Delta t\Big\},$$

$$\boldsymbol{\tau}'^{(i)} = \underset{(n-1)}{\boldsymbol{\alpha}'} + \frac{1}{1 + 2\mu\Delta\bar{\Lambda}^{(i-1)}}\left[\breve{\boldsymbol{\tau}}' - \underset{(n-1)}{\boldsymbol{\alpha}'} - (\underset{(n-1)}{\mathbf{k}'} + \underset{(n-1)}{\mathbf{s}'})\Delta t\right].$$

5. Viscoplastic strain increment

$$\operatorname{tr}(\Delta \mathbf{e}^{p(i)}\mathbf{g}^{-1}) = 3\Delta\bar{\Lambda}^{(i-1)} \underset{(n-1)}{A}\, \operatorname{tr}[(\boldsymbol{\tau}^{(i)} - \underset{(n-1)}{\alpha})\mathbf{g}]$$

$$\mathbf{g}^{-1}\Delta \mathbf{e}'^{p(i)}\,\mathbf{g}^{-1} = \Delta\bar{\Lambda}^{(i-1)}(\boldsymbol{\tau}'^{(i)} - \underset{(n-1)}{\overset{\prime}{\alpha}}),$$

6. Viscoplastic deformation rate tensor

$$\mathbf{d}^{p(i)} = \Delta \mathbf{e}^{p(i)}/\Delta t\,, \quad \left\|\mathbf{d}^{p(i)}\right\| = (\mathbf{g}^{-1}\mathbf{d}^{p(i)}\mathbf{g}^{-1}\mathbf{d}^{p(i)})^{1/2},$$

7. Scalar multiplier $\Delta\bar{\Lambda}$(Newton's method)

$$\Delta\bar{\Lambda}^{(i)} = \Delta\bar{\Lambda}^{(i-1)} - \left[\frac{\partial\Theta(\Delta\bar{\Lambda}^{(i-1)})}{\partial\Delta\bar{\Lambda}^{(i-1)}}\right]^{-1}\Theta(\Delta\bar{\Lambda}^{(i-1)}),$$

8. Check the convergence

$$\left|\Delta\bar{\Lambda}^{(i)} - \Delta\bar{\Lambda}^{(i-1)}\right| \leq \mathrm{TOL}\ ?$$

YES: $\operatorname{tr}(\boldsymbol{\tau}\mathbf{g}) = \operatorname{tr}(\overset{\smile}{\boldsymbol{\tau}}^{(i)}\mathbf{g})$, $\boldsymbol{\tau}' = \overset{\smile}{\boldsymbol{\tau}}^{\prime(i)}$, $\mathbf{d}^p = \mathbf{d}^{p(i)}$, $\Delta\mathbf{e}^p = \Delta\mathbf{e}^{p(i)}$ go to **9**

NO: $i \leftarrow i+1$ go to **4**

9. Temperature

$$\vartheta = \underset{(n-1)}{\vartheta} + \frac{\bar{\chi}}{\underset{(n-1)}{\rho}\, c_p}\operatorname{tr}(\boldsymbol{\tau}\Delta\mathbf{e}^p) + \frac{\bar{\bar{\chi}}}{\underset{(n-1)}{\rho}\, c_p}\,\underset{(n-1)}{\Xi}\,\Delta t,$$

10. Internal state variables

$$\boldsymbol{\mu} = \underset{(n-1)}{\boldsymbol{\mu}} + \hat{\mathbf{m}}(\boldsymbol{\tau}, \underset{(n-1)}{\boldsymbol{\mu}}, \vartheta)\Delta t,$$

11. Covariant and plastic spin effects

$$\boldsymbol{\omega}^p = \bar{\eta}(\boldsymbol{\alpha}\mathbf{d}^p\mathbf{g}^{-1} - \mathbf{g}^{-1}\mathbf{d}^p\boldsymbol{\alpha}),$$

$$\mathbf{k} = \mathbf{g}^{-1}\mathbf{d}^p\boldsymbol{\tau} - \boldsymbol{\tau}\mathbf{d}^p\mathbf{g}^{-1},$$

$$\mathbf{s} = \boldsymbol{\omega}^p\mathbf{g}\boldsymbol{\tau} - \boldsymbol{\tau}\mathbf{g}\boldsymbol{\omega}^p,$$

12. Other magnitudes, which depend on the inelastic deformation (isotropic hardening-softening function, density of the material etc...)

In numerical implementations the derivative contained in the Newton's formula (Point **7**) is usually calculated in an approximate way.

A mathematical proof of the convergence and stability of the presented method is an extremely difficult task. First of all, the geometrical and physical nonlinearities decide about this. Such essential features as the convergence and stability can be shown in a numerical way, solving the particular initial-boundary value problem. Such a numerical proof of the convergence and stability of that algorithm is presented in [7] for certain problem of the localized plastic deformation. The example presented below also confirms the convergence and stability of the proposed method for large number of the time increments.

4. Numerical example

The finite element [16] or finite difference [28] methods are frequently used in numerical analyses of deformation of structural elements. These methods differ in manners of space-time discretization and in approximation of functions of the evolution problem. Other numerical methods are also developed to use the possibility of effective simulation of fragmentation of structural elements [1].

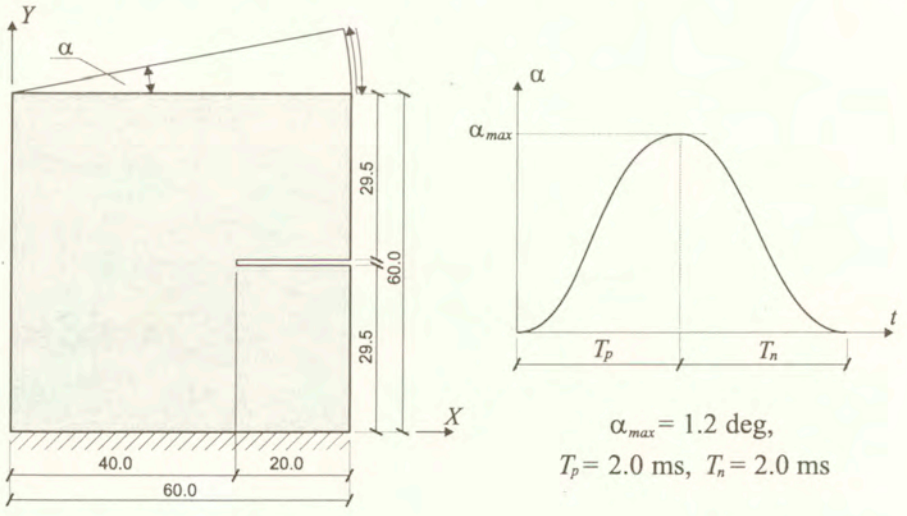

FIG. 1. Geometry and kinematic constraints of the thin steel plate with sharp notch.

The problem of fatigue crack propagation in a thin steel plate (AISI 4340) is used to illustrate the correctness of the proposed algorithm [9]. In the plate, a narrow initial notch (20 x 1 mm) is made (Fig. 1). The cyclic load realised by a rigid turn of the upper edge in relation to its left end is assumed. This load is represented by positive cycles with the amplitude $\alpha_{\max} = 1.2$ deg and with

the constant period $T = 4.0$ ms. The tensile strain time T_p and the compressive strain time T_n, are equal (Fig. 1). The number of cycles is assumed to be $N = 40$. The bottom edge of the plate ($Y = 0$) is fixed completely.

The analysis is carried out by use of the finite difference method with the explicit integration scheme with respect to time. In order to observe the local effects with great precision, a dense regular difference net (64 x 64 = 4096 nodes) is assumed. The time step assuring the stability of numerical procedure is $\Delta t = 0.1416$ μs. It leads to the total number of time increments equal to 1129943.

The isotropic work-hardening-softening function κ is postulated as [9]

$$\kappa = \hat{\kappa}(\in^p, \vartheta, \xi) \tag{4.1}$$
$$= \{\kappa_s(\vartheta) - [\kappa_s(\vartheta) - \kappa_0(\vartheta)] \exp[-\delta(\vartheta) \in^p]\} [1 - (\xi/\xi_F)^{\beta(\vartheta)}],$$

where

$$\kappa_0(\vartheta) = \kappa_0^* - \kappa_0^{**}\bar{\vartheta}, \quad \kappa_s(\vartheta) = \kappa_s^* - \kappa_s^{**}\bar{\vartheta},$$
$$\delta(\vartheta) = \delta^* - \delta^{**}\bar{\vartheta}, \quad \beta(\vartheta) = \beta^* - \beta^{**}\bar{\vartheta}, \quad \bar{\vartheta} = (\vartheta - \vartheta_0) \,/\, \vartheta_0. \tag{4.2}$$

The material parameters κ_0 and κ_s denote the yield stress and the stress at which the strain hardening saturates, respectively. The coefficients δ and β are material hardening parameters. All the material parameters are functions of temperature as in (4.2).

Thus isotropic hardening-softening effects are described by a nonlinear function depending on the equivalent plastic deformation, temperature and on the microdamage. This function determines also the local failure criterion. Let us assume that for $\xi = \xi_F$ a catastrophe takes place, that is $\kappa = \hat{\kappa}(\in^p, \vartheta, \xi)|_{\xi=\xi_F} = 0$. It means that for $\xi = \xi_F$ the material loses its carrying capacity. Such an approach is very useful to correct simulation of the fatigue crack propagation in the range of the low-cycle fatigue.

The evolution equation for the kinematic hardening parameter $\boldsymbol{\alpha}$ is assumed in the form [5]

$$L_{\mathbf{v}}\boldsymbol{\alpha} = \frac{1}{T_m} \left\langle \Phi\left(\frac{f}{\kappa} - 1\right) \right\rangle [\zeta_1(\xi, \vartheta)\mathbf{P} + \zeta_2(\xi, \vartheta)\boldsymbol{\alpha}] \tag{4.3}$$

with

$$\zeta_1(\xi, \vartheta) = \zeta_1^* - \zeta_1^{**}\bar{\vartheta}, \; \zeta_2(\xi, \vartheta) = \zeta_2^* - \zeta_2^{**}\bar{\vartheta}. \tag{4.4}$$

The kinematic hardening law (4.3) leads to the nonlinear stress-strain relation with characteristic saturation effect. The material function $\zeta_1(\xi, \vartheta)$ for $\xi = \xi_0$ and $\vartheta = \vartheta_0$ can be interpreted as an initial value of the kinematic hardening modulus

while the material function $\zeta_2(\xi, \vartheta)$ determines the character of nonlinearity of the kinematic hardening. The particular forms of the functions ζ_1 and ζ_2 have to take into account the degradation nature of the influence of the intrinsic micro-damage process on the evolution of anisotropic hardening.

The evolution equation for the porosity ξ is postulated as

$$\dot{\xi} = (\dot{\xi})_{\text{grow}} = \frac{g^*(\vartheta, \xi)}{T_m \kappa_0} \left[\tilde{I}_g - \tau_{eq}(\vartheta, \xi, \in^p) \right] \tag{4.5}$$

where [4]

$$g^*(\xi, \vartheta) = c_1(\vartheta) \frac{\xi}{1 - \xi}, \quad \tilde{I}_g = b_1 \tilde{J}_1 + b_2 \sqrt{\tilde{J}_2'},$$

$$\tau_{eq}(\vartheta, \xi, \in^p) = c_2(\vartheta)(1 - \xi) \ln \frac{1}{\xi} \{2\kappa_s(\vartheta) - [\kappa_s(\vartheta) - \kappa_0(\vartheta)] F(\xi_0, \xi, \vartheta)\},$$

$$c_1(\vartheta) = \text{const}, \quad c_2(\vartheta) = \text{const}, \tag{4.6}$$

$$F(\xi, \xi_0, \vartheta) = \left(\frac{\xi_0}{1 - \xi_0} \frac{1 - \xi}{\xi} \right)^{\frac{2}{3}\delta} + \left(\frac{1 - \xi}{1 - \xi_0} \right)^{\frac{2}{3}\delta}.$$

By $T_m \kappa_0$ we denote the dynamic viscosity of a material, $g^*(\vartheta, \xi)$ represents the void growth material function and takes into account the void interaction, $\tau_{eq}(\vartheta, \xi, \in^p)$ is the porosity, temperature and equivalent viscoplastic strain-dependent void growth threshold stress, $\tilde{I}_g$ defines the stress intensity invariant for growth, b_1 and b_2 are the material constants.

Based on the best curve fitting of the experimental results for AISI 4340 steel, the identification of the material constants has been done [9], cf. Table 1.

Table 1. Material constants for AISI 4340 steel

$\kappa_s^* = 809$ MPa	$\kappa_s^{**} = 228$ MPa	$\kappa_0^* = 598$ MPa	$\kappa_0^{**} = 168$ MPa
$\delta^* = 14.00$	$\delta^{**} = 3.94$	$\beta^* = 9.00$	$\beta^{**} = 2.53$
$\vartheta_0 = 293$ K	$\xi_F = 0.20$	$\rho_0 = 7850 \text{kg/m}^3$	$\mu = 76.92$ GPa
$\lambda = 115.38$ GPa	$\theta = 12 \cdot 10^{-6} \text{k}^{-1}$	$T_m = 2.5$ ms	$m = 1$
$\zeta_1^* = 15.00$ MPa	$\zeta_1^{**} = 4.22$ MPa	$\zeta_2^* = 69.60$ MPa	$\zeta_2^{**} = 19.60$ MPa
$c_1 = 0.202$	$c_2 = 6.7 \cdot 10^{-2}$	$b_1 = 1.0$	$b_2 = 1.30$
$\xi_0 = 6 \cdot 10^{-4}$	$\bar{\chi} = 0.85$	$\bar{\bar{\chi}} = 0.0$	$c_p = 455$ J / kg K

The distribution of the Mises stress for chosen instants during two deformation cycles is shown in Fig. 2. The results illustrate the formation of the greatest stress zones in the vicinity of the initial notch. The characteristic unsymmetrical distribution of these zones is a result of the assumed boundary conditions.

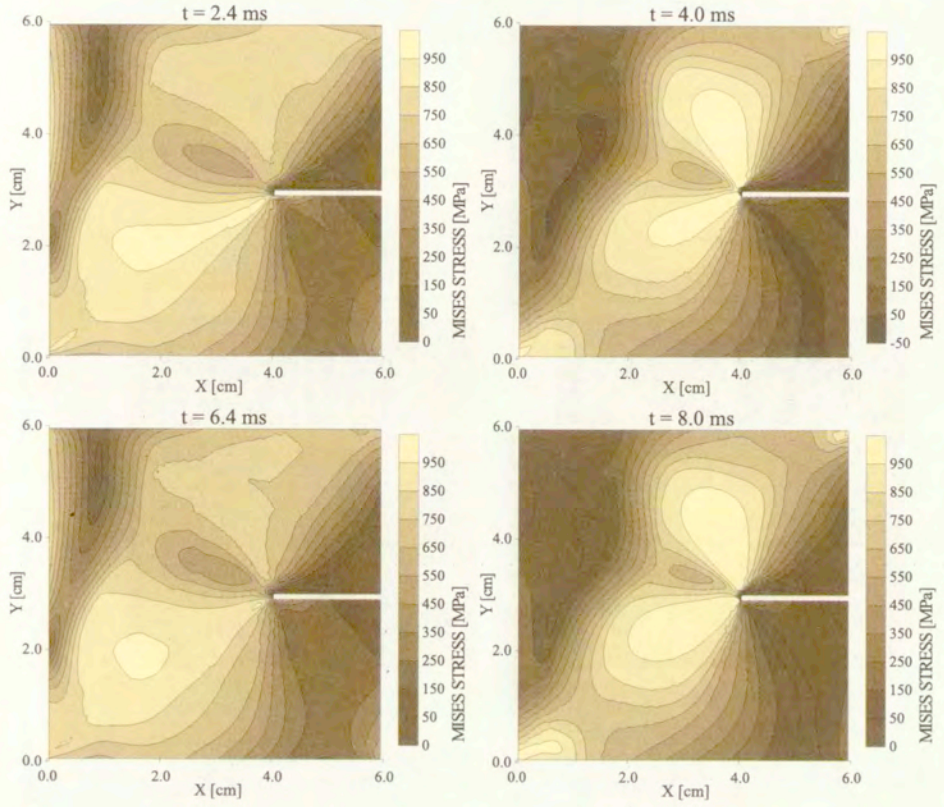

FIG. 2. Distribution of the norm of the Kirchhoff stress for chosen instants during two deformation cycles.

In Fig. 3 the evolution of the plastic equivalent deformation in the vicinity of the developed fatigue macrocrack is presented. In the initial part of the cyclic deformation process (several cycles), the plastic zone has a characteristic shape (seed of a maple). Such a form of the plastic zone has been observed experimentally. For the advanced cyclic deformation process (i.e., when the number of cycles is increased) the plastic zone is very much restricted to the vicinity of the macrocrack. The macrocrack direction is consistent with the least radius direction of the initial plastic zone. The strong concentration of plastic deformations has been seen on the front of the macrocrack.

The evolution of temperature for the considered adiabatic process is shown in Fig. 4. Zones of increased temperature correspond to the plastic zones. The maximum value of temperature is $\vartheta_{\max} = 1092$ K. The effect of such a strong heating of the material results from its mechanical properties, i.e. the high strength steel ($R_m = 1400$ MPa).

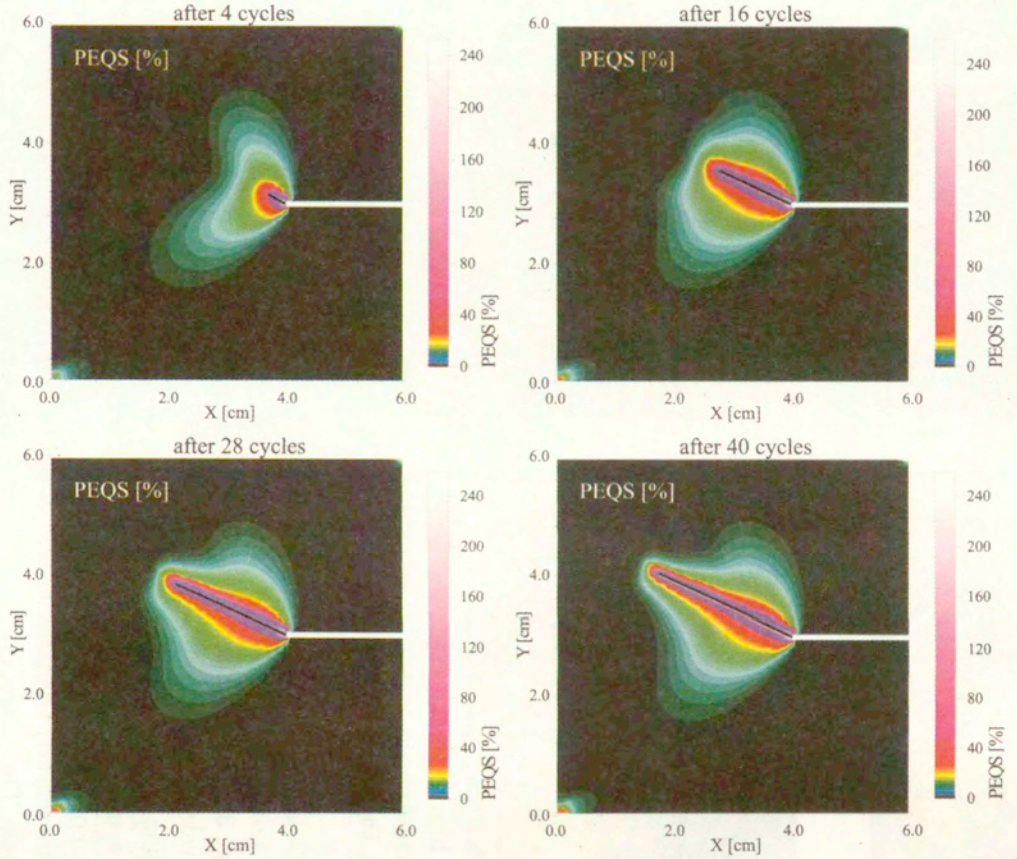

FIG. 3. Evolution of the equivalent plastic deformation in the vicinity of the developed fatigue damage.

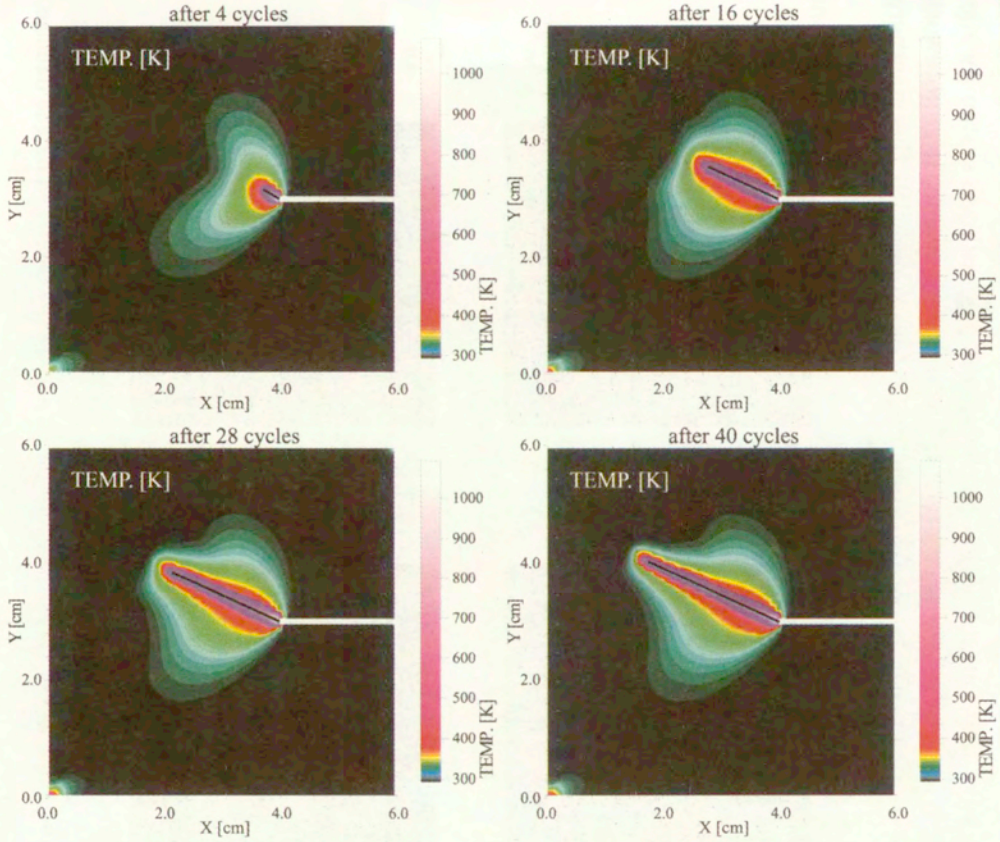

FIG. 4. Evolution of temperature in the vicinity of the developed fatigue damage.

In Fig. 5 the evolution of microdamage is presented. The domain of microdamage is limited to the vicinity of the macrocrack. This effect is a result of the strong concentration of the microdamage process on the front of the macrocrack. The complex evolution of the plastic rotation is shown in Fig. 6. In the domain lying above the macrocrack the plastic rotation has negative value, i.e. the rotation in the left direction in relation to the assumed coordinate system, while in the domain lying below the macrocrack it has a positive value. It is noteworthy that the border between these two domains is consistent with the macrocrack direction.

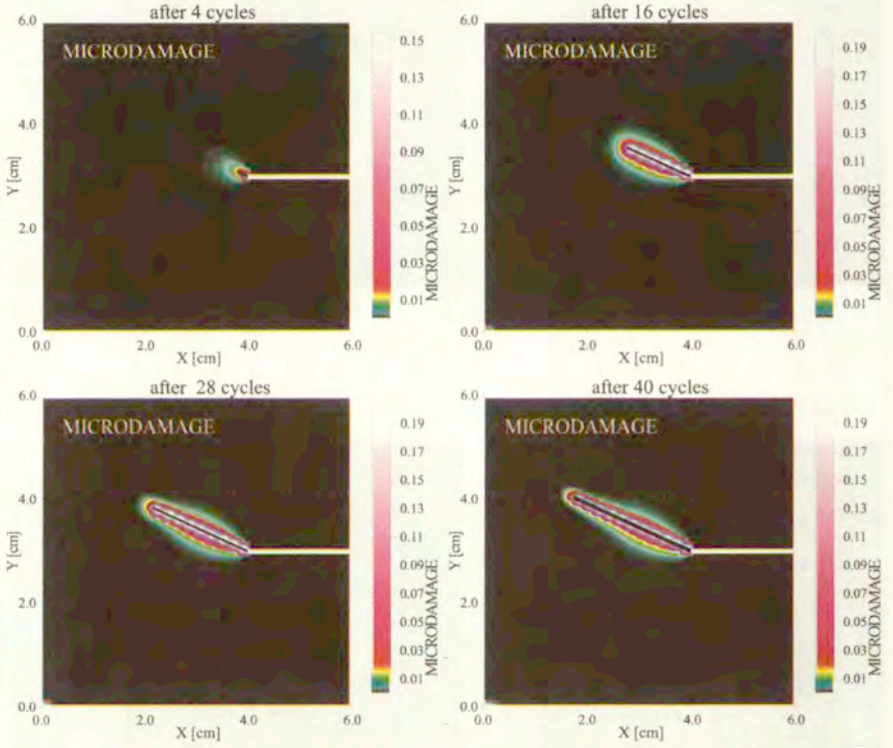

FIG. 5. Evolution of the microdamage in the vicinity of the developed fatigue damage.

The analyzed fatigue damage process at high temperature is very complex. The experimental observations performed in [30] show that the decrease in fatigue life is associated with a change in the fracture mode from transgranular to intergranular cracking. The microdamage kinetics interacts with thermal and load changes to make failure of solids a highly rate, temperature and history-dependent, nonlinear process. The incorporation of these effects in the presented constitutive model required considering the general constitutive structure with internal state variables for polycrystalline solids.

The constitutive description of internal micro-damage process required a special care [4]. This process was treated as a sequence of nucleation, growth and coalescence of microcracks. Evolution equations based on the concept of threshold stresses for nucleation and growth processes are assumed. It made possible the correct description of damage fatigue accumulation.

It is noteworthy that the presented description of the thermodynamical process of inelastic flow is internally regularized [19], in this case the time of mechanical relaxation is a regularization parameter. From a computational standpoint this property is of a very important significance, because it assures the unique numerical solution.

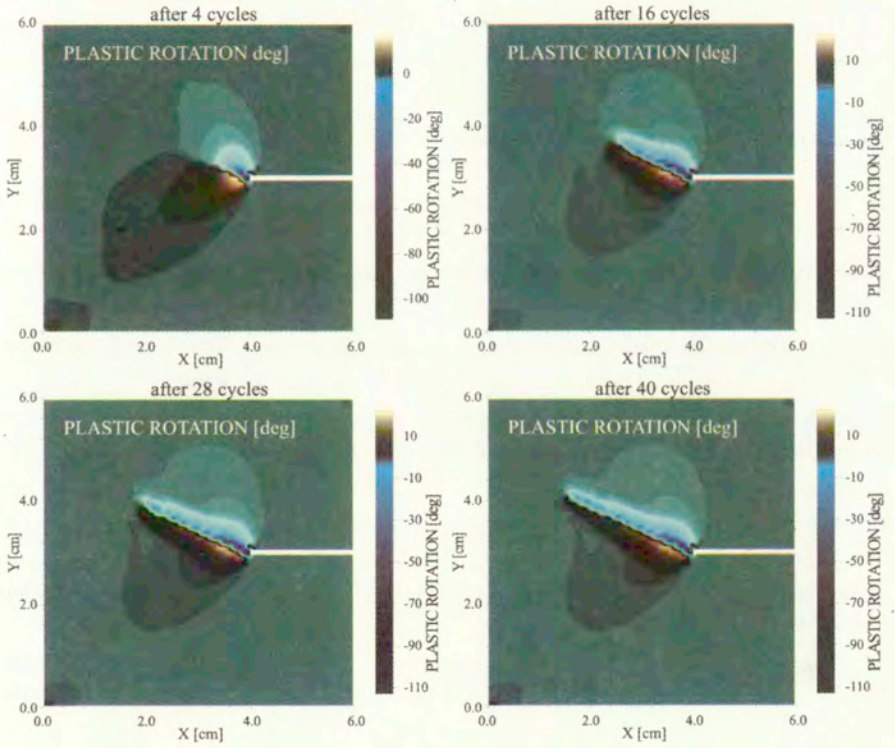

FIG. 6. Evolution of the plastic rotation in the vicinity of the developed fatigue damage.

5. Final comments

The performed numerical simulations of the dynamic, cyclic loading process have proven the usefulness of the proposed numerical integration algorithm in the investigation of localized fatigue fracture phenomena. The material objec-

tivity with respect to the total motion (translation, rotation and strain) of a material element is preserved. The way in which the incremental form of the plastic flow rule is obtained and the way of determining the flow stresses decide on the originality of the algorithm and differentiate it from the return mapping algorithms.

The proposed algorithm is very effective and it can be used to the numerical analysis of large deformations and fracture in metal structural elements under monotonic loadings too.

Acknowledgement

The paper has been prepared within the research programme sponsored by the Committee of Scientific Research under Grant 7T07A00616.

References

1. T. BELYTSCHKO and M. TABBARA, *Dynamic fracture using element-free Galerkin methods*, International Journal for Numerical Methods in Engineering, **39**, 923–938, 1996.
2. Y. F. DAFALIAS, *Corotational rates for kinematic hardening at large plastic deformations*, J. Appl. Mech., **50**, 561–565, 1983.
3. W. DORNOWSKI, *A constitutive model for a cyclically loaded material with microdamages*, Bull. MUT, **2**, 95–117, 1998.
4. W. DORNOWSKI, *Influence of finite deformations on the growth mechanism of microvoids contained in structural metals*, Arch. Mech., **51**, 71–86, 1999.
5. W. DORNOWSKI, *Numerical simulations of plastic flow processes under cyclic dynamic loadings*, MUT 2598/99, Warsaw 1999.
6. W. DORNOWSKI and P. PERZYNA, *Constitutive modeling of inelastic solids for plastic flow process under cyclic dynamic loadings*, Journal of Engineering Materials and Technology, ASME, **121**, 210–220, 1999.
7. W. DORNOWSKI and P. PERZYNA, *Localization phenomena in thermo-viscoplastic flow processes under cyclic dynamic loadings*, Computer Assisted Mechanics and Engineering Sciences, **7**, 117–160, 2000.
8. W. DORNOWSKI and P. PERZYNA, *Numerical simulations of thermo-viscoplastic flow processes under cyclic dynamic loadings*, In: Proc. Euromech Colloquium 383, Inelastic Analysis of Structures under Variable Loads: Theory and Engineering Applications D. WEICHERT and G. MAIER [Eds.], Kluwer Academic Publishers, 69–94, 2000.
9. W. DORNOWSKI and P. PERZYNA, *Localized fracture phenomena in thermo-viscoplastic flow processes under cyclic dynamic loadings*, Acta Mechanica, **30**, 1–23, 2001.
10. M. DUSZEK and P. PERZYNA, *Plasticity of damage solids and shear band localization*, Ingenieur-Archiv., **58**, 380–392, 1988.
11. M. K. DUSZEK and P. PERZYNA, *The localization of plastic deformation in thermoplastic solids*, Int. J. Solids Structures, **27**, 11, 1419–1443, 1991.

12. M. K. DUSZEK-PERZYNA and P. PERZYNA, *Adiabatic shear band localization in elastic-plastic single crystals*, Int. J. Solids Structures, **30**, 61–89, 1993.

13. A. E. GREEN and W. ZERNA, *Theoretical elasticity*, Second Edition, Clarendon Press, Oxford 1960.

14. R. HILL, *Aspects of invariance in Solid Mechanics*, Advances in Applied Mechanics, **18**, 1–75, 1978.

15. T. J. R. HUGHES and J. WINGET, *Finite rotation effects in numerical integration of rate constitutive equations arising in large-deformation analysis*, International Journal for Numerical Methods in Engineering, **15**, 9, 1413-1418, 1980.

16. M. KLEIBER and C. WOŹNIAK, *Nonlinear mechanics of structures*, PWN, Warsaw, Kluwer Academic Publishers, Dordrecht/Boston/London, 1991.

17. R. D. KRIEG and S. W. KEY, *Implementation of a time dependent plasticity theory into structural computer programs*, Constitutive Equations in Viscoplasticity, Computational and Engineering Aspects, J.A. STRICKLIN and K.J. SACZLSKI [Eds.], AMD-20, ASME, New York 1976.

18. R. D. KRIEG and D. B. KRIEG, *Accuracies of numerical solution methods for the elastic-perfectly plastic model*, Journal of Pressure Vessel Technology, ASME, **99**, 1977.

19. T. ČODYGOWSKI and P. PERZYNA, *Localized fracture in inelastic polycrystalline solids under dynamic loading processes*, Int. J. Damage Mechanics, **6**, 364-407, 1997.

20. J. E. MARSDEN and T. J. R. HUGHES, *Mathematical Foundations of Elasticity*, Prentice-Hall, Englewood Cliffs, NY 1983.

21. A. NEEDLEMAN and V. TVERGAARD, *Finite element analysis of localization plasticity*, [in:] Finite Elements, Vol V: Special problems in solid mechanics, J. T. ODEN and G. F. CAREY [Eds.], Prentice-Hall, Englewood Cliffs, New Jersey 1984.

22. M. ORTIZ and J. C. SIMO, *An analysis of a new class of integration algorithms for elasto-plastic constitutive relations*, International Journal for Numerical Methods in Engineering, **23**, 353–366, 1986.

23. P. PERZYNA, *The constitutive equations for rate sensitive plastic materials*, Q. Appl. Math., **20**, 321–332, 1963.

24. P. PERZYNA, *Theory of viscoplasticity*, PWN, Warsaw 1966.

25. P. PERZYNA, *Thermodynamics of inelastic materials*, PWN, Warsaw 1978.

26. P. PINSKY, M. ORTIZ and K. S. PISTER, *Numerical integration of rate constitutive equations in finite deformation analysis*, Computer Methods in Applied Mechanics and Engineering, **40**, 137–158, 1983.

27. J. R. RICE and D. M. TRACEY, *Computational fracture mechanics*, In Proceedings of the Symposium on Numerical Methods in Structural Mechanics, S. J. FENVES [Ed.], Academic Press, Urbana Illinois 1973.

28. R. D. RICHTMYER and K. W. MORTON, *Difference methods for initial-value problems*, Interscience Publishers, 2^{nd} edition, New York 1967.

29. R. RUBINSTEIN and S. N. ATLURI, *Objectivity of incremental constitutive relations over finite time step in computational finite deformation analyses*, Computer Methods in Applied Mechanics and Engineering, **36**, 1983.

30. D. SIDEY and L. F. COFFIN, *Low-cycle fatigue damage mechanisms at high temperature*, Fatigue Mechanisms, Proceedings of an ASTM-NBS-NSF symposium, Kansas City, Mo., May 1978, J. T. FONG [Ed.], ASTM STP 675. American Society for Testing and Materials, 528–568, 1979.

31. J. C. SIMO and M. ORTIZ, *A unified approach to finite deformation elastoplasticity based on the use of hyperelastic constitutive equations*, Computer Methods in Applied Mechanics and Engineering, **49**, 221-245, 1985.

32. J. C. SIMO, *Algorithms for static and dynamic multiplicative plasticity that preserve the classical return mapping schemes of the infinitesimal theory*, Computer Methods in Applied Mechanics and Engineering, **99**, 61-112, 1992.

33. M. L. WILKINS, *Calculation of elastic-plastic flow*, In Methods of Computational Physics 3, Editors B. Alder *et. al.*, Academic Press, New York 1964.

Received May 28, 2002; revised version September 19, 2002.

Arch. Mech., **54**, 5-6, pp. 411–423, Warszawa 2002

On importance of imperfections in plastic strain localization problems in materials under impact loading

A. GLEMA, T. ŁODYGOWSKI

Institute of Structural Engineering,
Poznań University of Technology,
ul. Piotrowo 5, 60-965 Poznań, Poland

Dedicated to Professor Piotr Perzyna
on the occasion of his 70^{th} birthday

THE WORK is the continuation of Professor Piotr Perzyna achievements in the description and analysis of the phenomenon of plastic strain localization. The ductile materials under impact loading are in focus of interest. In particular, the influence of initial imperfections on the final pattern of localization is elaborated. The computer simulations were performed in the environment of ABAQUS program.

1. Introduction

THE DESCRIPTION of plastic strain localization phenomena has been focus of research for at least the last two decades. The phenomenon is clearly observed in ductile and brittle materials as well as in soils. Localization as a precursor of failure is usually accompanied by other phenomena such like, for example, heat generation and transfer (for ductile materials loaded by impact) or fluid flow in zones of localized deformations (for soils). When trying to propose the adequate description of the phenomena, the crucial point is to choose the constitutive structure which would be the closest to the observed properties but still formulated in the frame of continuum mechanics. The careful experimental observations prove that the plastic strain localization observed on the level of continuum is a very complex phenomenon which in fact, is a kind of homogenization of changes that are observed on other scales (mezo-, macro- or nano). In many cases under consideration, the localization of plastic strains is strongly connected with softening which could be the next source of difficulties that arise in the process of solution. The crucial question that has to be answered is the well-posedness of the system of governing equations; for discussions see [7, 20, 27]. There are different approaches to the solution of the problem in the frame of plasticity and continuum formulation. All of them introduce, implicitly or explicitly, internal length scale and are viewed as regularization methods. Depending on

the process (static or dynamic), type of localization (necking or shear bands) and the main properties of materials (ductile or brittle), the different methods can successfully describe the phenomena. In computations the attention is focused on assigning the place, time and the width of localization zones. Of course, all of them strongly depend on geometry of the specimens, boundary and initial conditions including the characteristic of loading. The important feature which differs the treatment, and which follows the computations, the static cases versus dynamic, is the necessity of introducing any imperfection (geometric or constitutive) which is the source of appearing of the first plastic strain localization. For dynamic cases (impact loading) in computations, one can avoid these imperfections and the choice of the localization form depends then on waves interaction which in a natural way introduce the heterogeneity, and properly describes the merit of the phenomenon. In the work, the problem of plastic strain localization in materials under impact loading is studied. Particularly, the influence of introducing the imperfections, both geometrical in the form of additional internal boundaries and constitutive in the form of inclusions, on the pattern of localized plastic strains is elaborated and documented in the numerical examples.

2. Numerical treatment of localization phenomena

The review of the papers that approaches the description of plastic zones was done in many works viewing the problem from different standpoints; see e.g. [19]. Some classical formulations, e. g. [3] or [12] defined the fundamental criteria for creation the pattern of localized deformations (shear bands). The main point was to recognize the change of the type of governing equations, for statics, from elliptic into parabolic. In the described process this change was identified with the final state of the specimen. The analysis could not be continued. When introducing the softening behavior of the material in computations, there appeared numerical problems which were recognized as mesh dependence; see [5]. To avoid this pathological form the authors started to introduce different forms of regularization, first on the level of finite element formulation. The so-called embedded elements [5, 9, 11], which usually explicitly declared the width of localization partially allowed to avoid this loss of stability in the FE solutions. The drawback of the proposition was the necessary explicit knowledge on the width of localization which obviously is not constant for the material and depends on the boundary conditions and loadings. The other works [22] stressed the mathematical side of constitutive form. No matter if the authors accepted non-local constitutive description [6], gradient-type theories [15], plastic-damage [36], rate-dependence [7, 24, 27] or coupled fields [21, 23] they always introduced the form of regularization. After this enrichment the system of equations becomes well-posed, it means the solution is unique and stable, and the type of the system of

incremental equations that describe the process remains unchanged in the whole range of interests. It could be also proved that all the constitutive formulations introduce the dispersive character of the media [13, 27]. For metals under very fast loading (impact), it is reasonable to accept the viscous properties of the material. Rate-dependence introduces the regularization and is physically well documented in dozens of experiments; see e. g. [16] The simple constitutive form useful for practical applications was originally proposed by [4]. The modification of this form is widely used [24, 25] in industrial applications. The mathematically consistent form of constitutive visco-plastic behavior was originally proposed by PERZYNA [1, 2, 7]. This formulation which is also used in this work introduces the relaxation time of mechanical disturbances T_m which is simultaneously the constitutive parameter and a mathematical regularization parameter. In this formulation the internal scale parameter is introduced implicitly. The profits that arise from using the proposed constitutive structure were discussed by the authors in [27, 32, 35]. The important fact is that it is not necessary to use any type of imperfection to reach localization in a specimen which is, in a natural way, the result of constitutive properties and the boundary value problem characteristic. In the work the attention is focused on showing how strong the influence of imperfections can be. How the imperfection attracts the localization zones and eventually, how it could be controlled to achieve the expected behavior of the specimen.

3. Elasto-thermo-plastic formulation

The material under consideration exhibits strain softening as a result of temperature rise or/and evolution of porosity. Both of these effects for classical rate-independent plastic strain formulation with negative stress-strain constitutive relation lead to ill-posed problems and in consequence, to non-unique results in numerical applications [14].

An adiabatic flow process written in the evolution form can be presented as follows:

$$
\begin{aligned}
&\dot{\phi} = \boldsymbol{v},\\
&\dot{\boldsymbol{v}} = \frac{1}{\rho^0(1-\xi_0)}\left(\frac{\boldsymbol{\tau}}{\rho}\mathrm{grad}\rho + \mathrm{div}\boldsymbol{\tau} - \frac{\boldsymbol{\tau}}{1-\xi}\mathrm{grad}\xi\right),\\
&\dot{\rho} = \frac{\rho}{1-\xi}\Xi - \rho\mathrm{div}\boldsymbol{v},\\
&\dot{\boldsymbol{\tau}} = \left[\mathcal{L}^e - \frac{1}{c_p\rho_{Ref}}\vartheta\mathcal{L}^{th}\frac{\partial\boldsymbol{\tau}}{\partial\vartheta}\right] : \mathrm{sym}D\boldsymbol{v} + 2\mathrm{sym}\left(\boldsymbol{\tau} : \frac{\partial\boldsymbol{v}}{\partial\mathbf{x}}\right)\\
&\quad - \left[\left(\frac{\chi^*}{\rho(1-\xi)c_p}\mathcal{L}^{th}\boldsymbol{\tau} + \mathcal{L}^e + \mathbf{g}\boldsymbol{\tau} + \boldsymbol{\tau}\mathbf{g}\right) : \mathbf{P}\right]\frac{1}{T_m}\left\langle\left(\frac{f}{\kappa} - 1\right)^m\right\rangle
\end{aligned}
\tag{3.1}
$$

$$
\begin{aligned}
&- \frac{\chi^{**}\mathcal{L}^{th}}{\rho(1-\xi)c_p}\Xi,\\
&\dot{\xi} = \Xi,\\
&\dot{\vartheta} = \frac{\vartheta}{c_p\rho_{Ref}}\frac{\partial\boldsymbol{\tau}}{\partial\vartheta} : \mathrm{sym}D\boldsymbol{v} + \frac{\chi^{*}}{\rho(1-\xi)c_p}\boldsymbol{\tau} : \mathbf{P}\frac{1}{T_m}\langle\left(\frac{f}{\kappa}-1\right)^{m}\rangle\\
&+ \frac{\chi^{**}}{\rho(1-\xi)c_p}\Xi;
\end{aligned}
\tag{3.1}
$$

[cont.]

where at the left-hand side consequently appear the rates of scalar values (mass density ρ, porosity ξ and temperature ϑ), vectorial (displacement ϕ and velocity $\boldsymbol{v}$) and tensorial quantities (Kirchhoff stress $\boldsymbol{\tau}$). For detailed discusion see also [27].

Let us restrict our consideration to elastic-viscoplastic associative model allowing for finite deformations. For the plastic part of the total deformation rate tensor $\boldsymbol{\varepsilon}^p$ ($\boldsymbol{\varepsilon} = \boldsymbol{\varepsilon}^e + \boldsymbol{\varepsilon}^p$) we postulate the evolution equation with the elastic-viscoplastic model of the material [20], and the tensor function $\boldsymbol{P}$ is defined for associative plasticity

$$
\boldsymbol{\varepsilon}^p = \lambda\cdot\boldsymbol{P}, \qquad \lambda = \frac{1}{T_m}\langle\Phi(f-\kappa)\rangle), \qquad \boldsymbol{P} = \frac{\partial f}{\partial\tau}.
\tag{3.2}
$$

In the above, T_m denotes the relaxation time for mechanical disturbances, κ is the isotropic work hardening/softening parameter, Φ denote the empirical overstress functions, $\langle\cdot\rangle$ denotes the so-called McCauly bracket and τ is the Kirchhoff stress tensor and f represents the plastic yield function [27, 35].

The different alternative hardening/softening forms of material function κ can be assumed including the effects of porosity nucleation and growth [20, 27].

Following Perzyna's achievements [1, 2, 8] we postulate the overstress viscoplastic function Φ in the form

$$
\Phi(f-\kappa) = (f-\kappa)^m \qquad \text{where} \quad m = 1, 3, 5, \ldots
\tag{3.3}
$$

We restrict our numerical tests to the initial boundary value problems for which the time scale covers only a fraction of a second and for this reason, adiabatic inelastic flow process describes sufficiently close the physical phenomena which appear.

The boundary conditions for surface traction and displacement are defined on the separate boundaries, assuming that the heat flux prescribed on the whole boundary is equal to zero and the initial conditions for all variables are given at time $t = 0$.

The whole physical and mathematical structure of the analytical and numerical model has the wave nature [13, 17].

4. Numerical Examples - Impact tension of rectangular metal specimen

As a reference (perfect) specimen, thin plate loaded by dynamic impulse is taken into computations. The constitutive relation incorparates thermal softening of the yield stress or the evolution of porosity. Twodimensional shell model is applied. The dimensions of the plate are as follows: length 25.4 mm and width 12.7 mm. The thickness of the specimen is 0.33 mm. The impact loading is defined by kinematic conditions. The bottom side of the specimen is fixed (all possible displacements) and the longitudinal velocity of 20 m/s is applied at all nodes of the top side (see Fig. 1a). Both vertical boundaries are free, without any constraints. The space discretization shown in Fig. 1b consists of finite element mesh of square elements: 80 along the length and 40 along the width. The constitutive parameters used in computations are: Young's modulus 200,000 MPa, Poisson ratio $\nu = 0.3$, strength stress 1634 MPa, initial mass density $\rho_0 = 7850\,\mathrm{kg/m^3}$. The inelastic heat fraction 0.9, specific heat 460 J/kg ^{0}C defines the part of

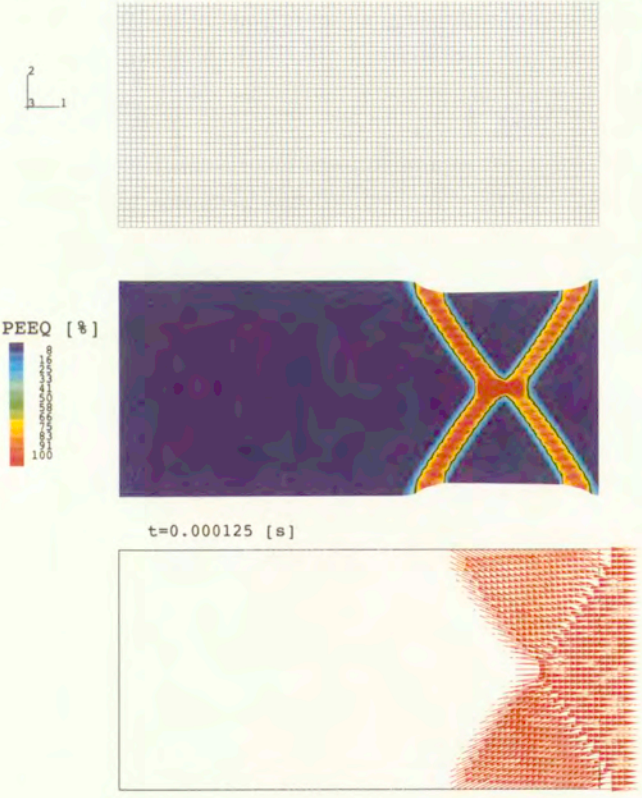

FIG. 1. Mesh, plastic equivalent strain distribution and vector plot of velocity for 2D model.

thermally dissipated energy. The strength stress decreases nonlinearly to the value of 1016 MPa when temperature grows to 610°C. Density evolution describes the softening character of the material in range of void volume ratio $0.004 \div 0.3$. The fundamental relaxation time is $T_m = 2.5\,\mu s$. The whole process time is equal to $t = 50\,\mu s$. Process time is discretized for increments of the order $0.01\,\mu s$. The stability criteria for explicit procedure and physical requirements for wave propagation are satisfied.

There are two different groups of models under the investigation. The first one contains the computations in case of no imperfections: material, geometrical nor numerical. The next one contains the analyses with considered material inclusions.

4.1. Perfect specimen

The final distribution of plastic equivalent strains and vector plots of velocities at the end of the process are shown in Fig. 1c, 5a. The achieved zones of localization are insensitive to the finite element mesh accepted for computations.

The place of localization is well recognized when looking at the plot of material point velocity.

The next two figures, Figs. 2–3, report the studies of the sensitivity and qualitative changes in the behavior of a specimen for different relaxation times T_m. If the relaxation time T_m tends to 0, the material becomes not dispersive and the energy is dissipated only due to plasticity. The plots in Fig. 2 show the differen-

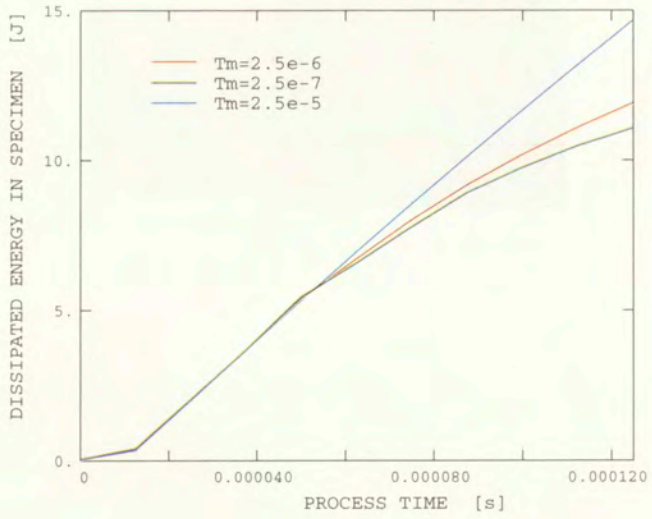

FIG. 2. History of the total structure dissipated energy for 2D model for different viscosity.

ces in the amount of energy which is related to the dispersive character of the viscoplastic medium [28, 30]. Figure 3 presents the distribution of plastic strains along the axis of symmetry of the specimen for different relaxation times. If the time is relatively long, the localization remains very much diffused ($T_m = 2.5 * 10^{-5}$ s). The gradient of velocity [35] splits the specimen into two parts fixing the place of localization. When using longer relaxation time, the gradient is not so sharp. The transition zone is more diffused. At the final state of deformation we can observe the clear division of the specimen into two zones where the velocities of material points vanish (left-hand side), while only the rest of the specimen moves.

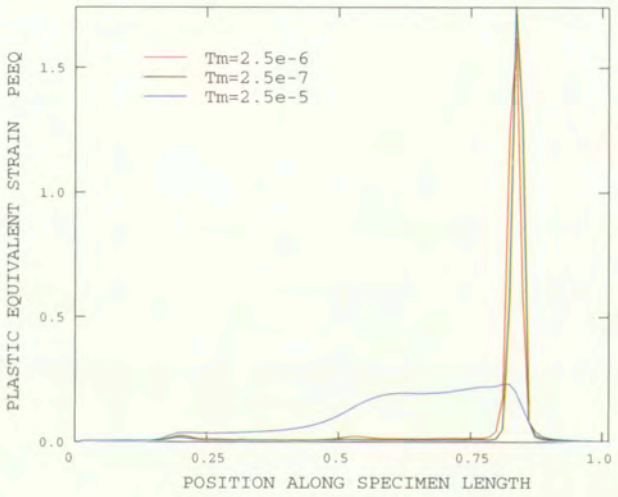

FIG. 3. Plastic strain localization for 2D model for different viscosity.

4.2. Specimen with material imperfection

In the following analyses we consider the models that contain the imperfection. The results concerning the cases with inclusions in the center of the specimen were presented in [33]. The single, material or geometrical, inclusion influenced the solution, due to the reflection and interaction of waves. The pattern and placement of localization became different than for computations with no imperfections.

We are studying three models with material inclusions. The inclusion is defined by smaller Young's modulus associated with six finite elements. All other parameters remain the same. For all cases under consideration the imperfection breakes the symmetry of the IBV problem. The assumed places of imperfections are presented in Fig. 5. For the case 1, Fig. 5b, the inclusion is located in the

middle of specimen on its left edge. For case 2, the imperfection is displaced toward the center of the specimen. In case 3, the imperfection stays at the left edge, but is moved toward the bottom constrained side.

The results, as before, are represented by plastic equivalent strain and plots of velocity vectors. Three time instants represent the history of deformations and

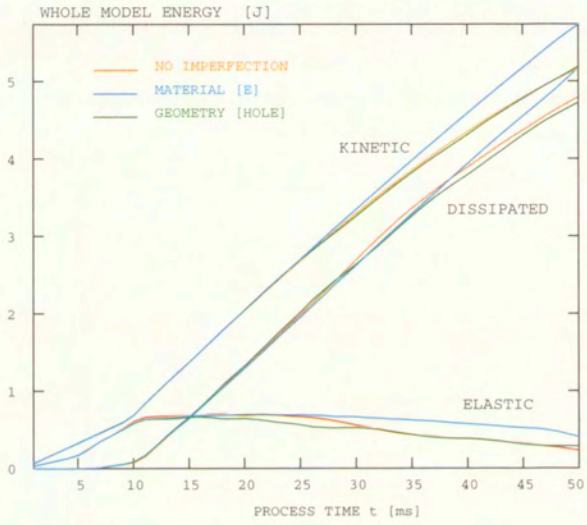

FIG. 4. Plot of energy history – division of kinetic energy into dissipated and recoverable in the whole process for three models: without imperfection, with material inclusion and with central hole [32].

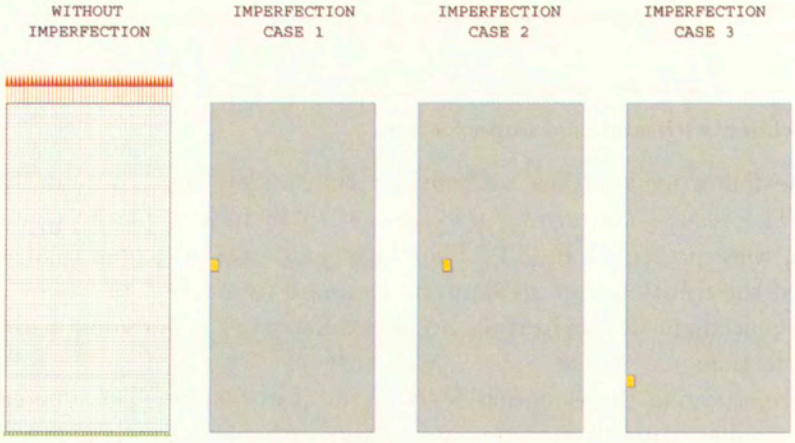

FIG. 5. Schema of initial-boundary conditions for 2D plate under tension (a), cases of material inclusions (b), (c), (d).

are taken to display the specific points of the process evolution. Figure 6 shows the distribution of equivalent plastic deformations and velocity field for the process time equal to $t = 20\,\mu s$. The next Fig. 7 shows the same quantities for the process time equal to $t = 30\,\mu s$. The final state for time equal to $t = 50\,\mu s$ is presented in Fig. 8. For each case of imperfection, comparing with the perfect specimen, it is clearly seen that the imperfection influences both the velocity history and plastic deformation and finally the localization pattern.

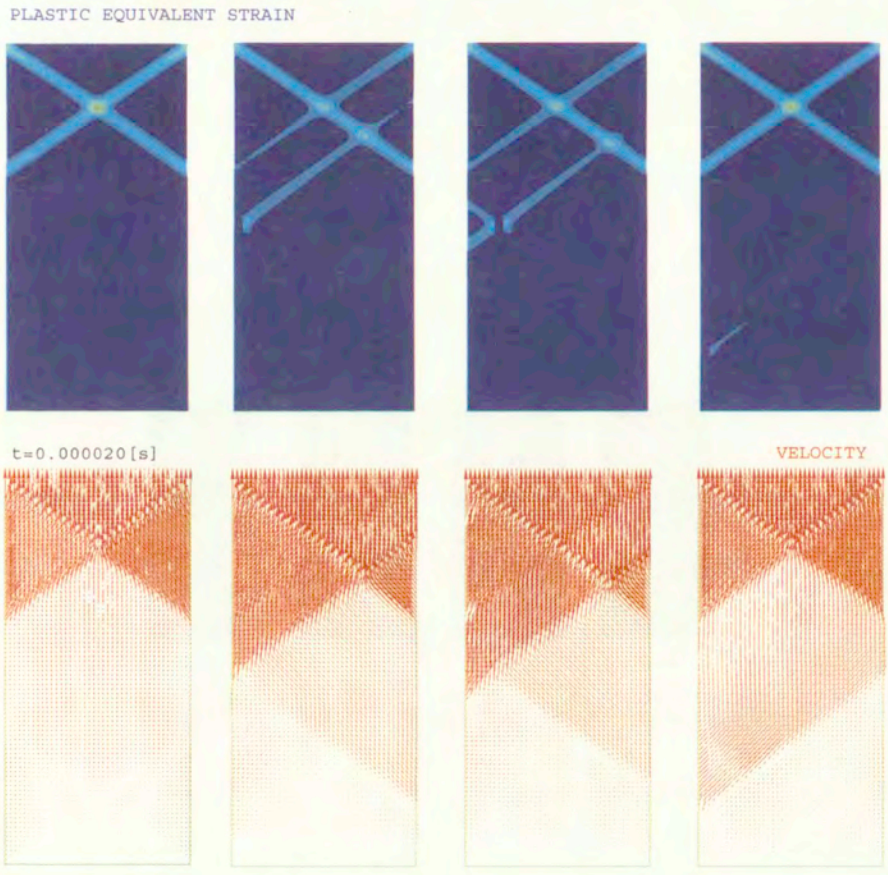

FIG. 5. Equivalent plastic strain distribution for process time $t = 20\mu s$ in the model without imperfection (a), and models with material inclusions (b), (c) (d).

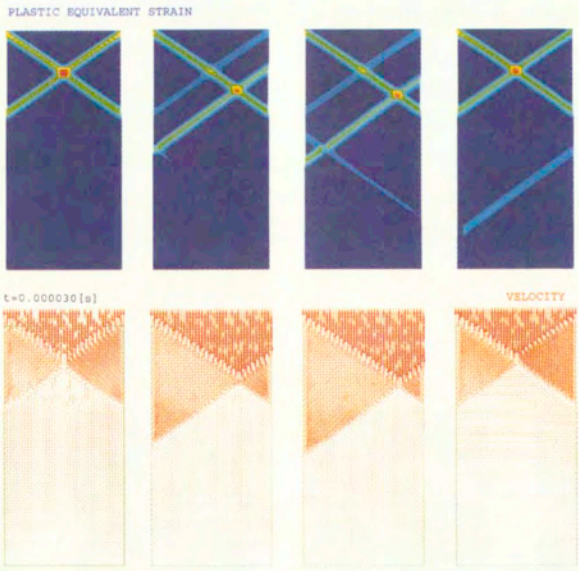

FIG. 7. Equivalent plastic strain distribution for process time $t = 20\mu s$ in the model without imperfection (a), and models with material inclusions (b), (c) (d).

FIG. 8. Equivalent plastic strain distribution for process time $t = 20\mu s$ in the model without imperfection (a), and models with material inclusions (b), (c) (d).

5. Conclusions

The usual practice in computations, for rate-independent formulations, is to assume the initial imperfections which will guarantee the initiation of the strain localization. It is not possible to continue the computations without this introductory imperfections. The result of this assumption is always connected with the loss of symmetry which is enforced and its form strongly depends on the imperfection. One can expect a different form of localization for every single imperfection.

For dynamic processes when using rate-dependent constitutive form, even for symmetric initial-boundary-value problems the localization pattern is finally achieved as a result of waves interaction. In these cases the process of localized deformations will appear and will be growing without any artificial accelerators. In the cases studied in the paper the numerical tests were performed on perfect structure (2D plate) and we have obtained the symmetry in the behavior of the specimen and also we have compared the results with those where the inclusions were consciously introduced. The changes in the localization forms and the amount of energy that is dissipated during the whole process of deformations were in the focus of authors' interest.

It is clearly seen that the next step, in the near future, should concentrate on designing the patterns of inclusions which would generate for example the maximum amount of energy dissipated during the deformation process. The solution of this optimization problem is of crucial practical value.

References

1. P. PERZYNA, *The constitutive equations for rate sensitive plastic materials.* Quart. Appl. Math, **20**, 321–332, 1963.
2. P. PERZYNA, *Thermodynamic theory of viscoplasticity.* Advances in Applied Mechanics, **11**, 313–354, 1971.
3. J. W. RUDNICKI, J. R. RICE, *Conditions for the localization of deformations in pressure-sensitive dilatant materials*, Journal of Mechanical Physics of Solids, **23**, 371–394, 1975.
4. J. LITOŃSKI, *Plastic flow of a tube under adiabatic torsion*, Bulletin PAS, Technical Sciences, **25**,1, 7, 1977.
5. S. PIETRUSZCZAK, Z. MRÓZ, *Finite element analysis of deformation of strain-softening materials*, International Journal of Numerical Methods in Engineering, **17**, 327–334, 1981.
6. Z. P. BAZANT, T. B. BELYTSCHKO, T. P. CHANG, *Continuum theory for strain softening*, Journal of Engineering Mechanics, **110**, 1666–1692, 1984.
7. P. PERZYNA, *Constitutive modelling of dissipative solids for postcritical behaviour and fracture*, ASME Journal of Engineering Materials and Technology, **106**, 410–419, 1984.
8. P. PERZYNA, *Internal state variable description of dynamic fracture of ductile solids*, International Journal of Solids and Structures, **22**, 797–818, 1986.

9. T. BELYTSCHKO, J. FISH, T. ENGELMANN, *A finite element with embedded localization zones*, Computer Methods in Applied Mechanics and Engineering, **70**, 1, 59–89, 1988.

10. Z. P. BAZANT, G. PIJAUDIER-CABOT, *Nonlocal continuum damage, localisation instability and convergence* Journal of Applied Mechanics, **55**, 287–293, 1988.

11. M. KLISIŃSKI, K. RUNESSON, S. STURE, *Finite element with inner softening band*, Journal of Engineering Mechanics, **17**, 3, 575–587, 1991.

12. D. BIGONI, T. HÜCKEL, *Uniqueness and localization*, Part I and II, International Journal of Solids and Structures, **28**, 197–213, 1991.

13. L. J. SLUYS, *Wave propagation, localisation and dispersion in softening solids*, TU Delft, 1992.

14. P. PERZYNA, *Instability phenomena and adiabatic shear band localization in thermoplastic flow processes*, Acta Mechanica, **106**, 173–205, 1994.

15. J. PAMIN, *Gradient-dependent plasticity in numerical simulation of localization phenomena*, TU Delft, 1994.

16. J. R. KLEPACZKO, *An experimental technique for shear testing at high and very high strain rates; the case of mild steel*, International Journal of Impact Engineering, **15**, 25, 1994.

17. P. PERZYNA, *Interactions of elastic-viscoplastic waves and localization phenomena in solids*, IUTAM Symposium on Nonlinear Waves in Solids, Victoria, Canada, August 15-20, 1993, J.L. WEGNER and F.R. NORWOOD [Eds.], ASME, 114–121, 1995.

18. F. ARMERO, K. GARIKIPATI, *An analysis of strong discontinuities in multiplicative finite strain plasticity and their relation with the numerical simulation of strain localization in solids*, International Journal of Solids and Structures, **33**, 2863–2885, 1996.

19. T. ŁODYGOWSKI, *Theoretical and numerical aspects of plastic strain localization*, Poznań University of Technology, 1996.

20. T. ŁODYGOWSKI, P. PERZYNA, *Numerical modelling of localized fracture of inelastic solids in dynamic loading processes*, International Journal of Numerical Methods in Engineering, **40**, 4137–4158, 1997.

21. J. PAMIN, R. DE BORST, *Simulation of crack spacing using a reinforced concrete model with an internal length parameter*, Archive of Applied Mechanics, **68**, 613–625, 1998.

22. P. PERZYNA, *Constitutive modelling of dissipative solids for localization and fracture*, P. PERZYNA [Ed.], Localization and fracture phenomena in inelastic solids, CISM Courses and Lectures No 386, Spinger, Wien New York, 1998.

23. R. DE BORST, J. PAMIN, M. G. D. GEERS, *On coupled gradient-dependent plasticity and damage theories with a view to localization analysis*, European Journal of Mechanics A/Solids, **18**, 939–962, 1999.

24. J. R. KLEPACZKO, M. KLOSAK, *Numerical study of critical impact velocity in shear*, European Journal of Mechanics A/Solids, **18**, 93–113, 1999.

25. M. KLOSAK, T. ŁODYGOWSKI, J. R. KLEPACZKO, *Remarks on numerical estimation of the critical impact velocity in shear*, Computer Assisted Mechanics and Engineering Sciences, **8**, 579–593, 1999.

26. W. DORNOWSKI, P. PERZYNA, *Constitutive modeling of inelastic solids for plastic flow process under cyclic dynamic loadings, of microvoids contained in structural metals*, ASME Journal of Engineering Materials and Technology, **121**, 210–220, 1999.

27. A. GLEMA, T. ŁODYGOWSKI, P. PERZYNA, *Interaction of deformation waves and localization phenomena in inelastic solids*, Computer Methods in Applied Mechanics and Engineering, **183**, 123-140, 2000.

28. A. GLEMA, *Dispersive waves in solid mechanics of elasto-visco-plastic material*, Fifth International Conference on Mathematical and Numerical Aspects of Wave Propagation, Santiago de Compostela, Spain, July 10-14, 2000, 153–157, 2000.

29. K. GARIKIPATI, J.R. HUGHES, *Embedding a micromechanical law in the continuum formulation: a multiscale approach applied to discontinuous solutions*, International Journal for Civil and Structural Engineering, **1**, 64–78, 2000.

30. A. GLEMA, T. ŁODYGOWSKI, P. PERZYNA, *The role of dispersion for the description of strain localization in materials under impact loading*, ECCMM 2001 - European Conference on Computational Mechanics, June 26-29, 2001, Cracow 2001.

31. R. W. LEWIS, A. R. KHOEI, *Numerical analysis of strain localization in metal powder-forming processes*, International Journal of Numerical Methods in Engineering, **52**, 489–501, 2001.

32. A. GLEMA, T. ŁODYGOWSKI, P. PERZYNA, *Numerical treatment of plastic strain localization phenomena*, Fourteenth U.S. National Congress of Applied Mechanics, Blacksburg, Virginia, USA, June 23–28, 2002.

33. A. GLEMA, *Wave propagation in elasto-viscoplastic solids for advanced impact deformation with softening*. Proceedings of the Fifth World Congress on Computational Mechanics (WCCM V), July 7-12, 2002, Vienna, Austria, H. A. MANG, F. G. RAMMERSTORFER, J. EBERHARDSTEINER, [Eds.], Publisher: Vienna University of Technology, Austria, ISBN 3-9501554-0-6, http://wccm.tuwien.ac.at, 2002.

34. W. DORNOWSKI, P. PERZYNA, *Localized fracture phenomena in thermo-visco-plastic flow processes under cyclic loading*, Acta Mechanica, **155**, 233–255, 2002.

35. A. GLEMA, T. ŁODYGOWSKI, P. PERZYNA, *The waves interaction and the role of dispersion the analysis of plastic strain localization in materials under impact loading*, Computer Methods in Applied Mechanics and Engineering, [submitted], 2002.

36. G. Z. VOYIADJIS, R. J. DORGA, *Gradient Formulation in coupled damage-plasticity*, Archives of Mechanics, [submitted], 2002.

Received August 6, 2002; revised version October 25, 2002.

Arch. Mech., **54**, 5-6, pp. 425–437, Warszawa 2002

On the reduction of constants in plane elasticity with eigenstrains

I. JASIUK and S. D. BOCCARA

The George W. Woodruff School of Mechanical Engineering,
Georgia Institute of Technology,
Atlanta, GA 30332-0405, U.S.A.

Dedicated to Professor Piotr Perzyna
on the occasion of his 70^{th} birthday

IN THIS PAPER the reduced parameter dependence in linear plane elasticity with eigenstrains (transformation strains) is studied. The focus is on simply connected inhomogeneous materials and two-phase materials with perfectly bonded interfaces. In the analysis we rely on the result of CHERKAEV, LURIE and MILTON (Proc. Roy. Soc. Lond. A 438, 519-529, 1992), and we show that the stress field is invariant under a shift in area bulk and shear compliances, if the eigenstrains obey certain conditions. The analysis can be extended to multiply connected inhomogeneous materials and materials with slipping interfaces.

1. Introduction

IN THIS PAPER we focus on linear plane elasticity with eigenstrains to study a reduced parameter dependence. In the terminology of MURA [1] eigenstrains may represent nonelastic strains such as thermal expansion, plastic strain, phase transformation, initial strain, and other. The classical work pointing out the reduced dependence of stresses on elastic constants in plane elasticity was performed by MICHELL [2]. He showed that for materials with holes, the in-plane stress fields are independent of elastic constants, provided that the loading is in terms of prescribed tractions and that there are no net forces on internal boundaries. This result was utilized in an experimental technique called photoelasticity. DUNDURS [3–4] extended Michell's result to planar two-phase materials and showed that stress fields depend on only two non-dimensional constants, instead of three, if the composite material is subjected to tractions. This concept was generalized to multi-phase materials by NEUMEISTER [5]. CHERKAEV, LURIE and MILTON [6] showed that the stress field in two-dimensional (planar) elasticity is invariant under a shift in elastic bulk and shear compliances, which is directly related to the Dundurs result, and they extended the concept of reduced parameter dependence to effective elastic moduli. This latter work,

referred to as the CLM result, inspired a number of follow-up studies in the context of planar elasticity [7–15]. The present paper extends these earlier results to the linear plane elasticity with eigenstrains. The CLM concept was also found applicable to planar Cosserat materials [16], planar piezoelectric materials [17], planar electromagnetic thermoelastic materials [18, 19], and was explored for three-dimensional elasticity [20, 21].

First, we briefly present the main definitions of three-dimensional elasticity with eigenstrains, following the notation of MURA [1]. The total strain ε_{ij} is the sum of the elastic strain e_{ij} and the eigenstrain ε^*_{ij}

$$\varepsilon_{ij} = e_{ij} + \varepsilon^*_{ij}, \qquad i,j = 1,2,3. \tag{1.1}$$

The total strain ε_{ij}, for infinitesimal deformations, is related to displacements as $\varepsilon_{ij} = (u_{i,j} + u_{j,i})/2$ and is compatible. For linear elastic materials the elastic strain components are related to stress σ_{ij} by Hooke's law as

$$\sigma_{ij} = C_{ijkl} e_{kl} = C_{ijkl} (\varepsilon_{kl} - \varepsilon^*_{kl}) \tag{1.2}$$

where C_{ijkl} is the elastic stiffness tensor.

The inverse of expression (1.2) is

$$e_{ij} = S_{ijkl} \sigma_{kl} \tag{1.3}$$

where $S_{ijkl} = (C_{ijkl})^{-1}$ is the elastic compliance tensor. Using Eq. (1.1), Eq. (1.3) can be written in the form

$$\varepsilon_{ij} = S_{ijkl} \sigma_{kl} + \varepsilon^*_{ij}. \tag{1.4}$$

Note that all quantities may depend on the spacial position $\mathbf{x}$. This dependence representation is omitted for simplicity of notation.

In elasticity with eigenstrains the material is assumed to be free from any external forces and surface constraints. If these conditions of free surface are not satisfied, the stress field can be obtained by a superposition of the stress of a free body and the stress obtained from the solution of a given boundary value problem with nonzero external forces or boundary conditions.

The stresses must satisfy the equations of equilibrium

$$\sigma_{ij,j} = 0 \quad i,j = 1,2,3 \tag{1.5}$$

and traction free-boundary condition

$$\sigma_{ij} n_j = 0. \tag{1.6}$$

Following MURA [1], by substituting Eq. (1.2) into Eq. (1.5) and assuming homogeneous material, we have

$$C_{ijkl}\varepsilon_{kl,j} = C_{ijkl}\varepsilon^*_{kl,j} \tag{1.7}$$

and by substituting Eq. (1.2) into Eq. (1.6) we obtain

$$C_{ijkl}\varepsilon_{kl}n_j = C_{ijkl}\varepsilon^*_{kl}n_j. \tag{1.8}$$

Note that in the absence of eigenstrain ($\varepsilon^*_{kl} = 0$), the left-hand side of Eq. (1.7) corresponds to $\sigma_{ij,j}$ and the left-hand side of Eq. (1.8) to $\sigma_{ij}n_j$. Thus, Eq. (1.7) is in the form $\sigma_{ij,j} = -X_i$ where $X_i = -C_{ijkl}\varepsilon^*_{kl,j}$ and Eq. (1.8) is in the form $\sigma_{ij}n_j = t_i$ where $t_i = C_{ijkl}\varepsilon^*_{kl}n_j$. Therefore, the contribution of eigenstrain ε^*_{ij} to the equations of equilibrium (1.7) is mathematically equivalent to a body force, and contribution to the boundary conditions (1.8) is similar to a surface force.

In the next sections we focus on the planar elasticity with eigenstrains, assuming isotropy in elastic properties. In addition we relax the boundary condition (1.6) and admit nonzero tractions to make the formulation more general. This will not change our conclusions on the reduced parameter dependence.

Note that a special case of elasticity with eigenstrains is the uncoupled thermoelasticity when the eigenstrain ε^*_{ij} is defined as

$$\varepsilon^*_{ij} = \alpha_{ij}\Delta T \quad \alpha_{ij} = 0 \text{ if } i \neq j \quad i,j = 1,2,3, \tag{1.9}$$

where α_{ij} is thermal expansion coefficient and ΔT is temperature change. We will refer to this special case in examples.

2. Governing equations of plane elasticity with eigenstrains

The governing equations of linear plane elasticity with eigenstrains in the absence of body forces in a domain D are as follows:

i) The equations of equilibrium in terms of stresses

$$\frac{\partial\sigma_{xx}}{\partial x} + \frac{\partial\sigma_{xy}}{\partial y} = 0 \quad \frac{\partial\sigma_{xy}}{\partial x} + \frac{\partial\sigma_{yy}}{\partial y} = 0. \tag{2.1}$$

ii) Constitutive equations (1.4), assuming isotropy, accommodating both plane strain and plane stress, and including eigenstrains

$$4\varepsilon_{xx} = 2S\sigma_{xx} + (A - S)(\sigma_{xx} + \sigma_{yy}) + 4\varepsilon^*_{xx} + 4\eta\varepsilon^*_{zz},$$

$$4\varepsilon_{xy} = 2S\sigma_{xy} + 4\varepsilon^*_{xy}, \tag{2.2}$$

$$4\varepsilon_{yy} = 2S\sigma_{yy} + (A - S)(\sigma_{xx} + \sigma_{yy}) + 4\varepsilon^*_{yy} + 4\eta\varepsilon^*_{zz},$$

where A and S denote the bulk and shear compliances respectively, defined by

$$A = \frac{\kappa - 1}{2G}, \qquad S = \frac{1}{G}. \tag{2.3}$$

Here G denotes the shear modulus and κ is the Kolosov constant defined in terms of the Poisson's ratio as

$$\begin{aligned} \kappa &= 3 - 4\nu, \qquad \eta = \nu \text{ (plane strain)}, \\ \kappa &= \frac{3 - \nu}{1 + \nu}, \qquad \eta = 0 \text{ (plane stress)}. \end{aligned} \tag{2.4}$$

iii) Pointwise (local) compatibility in terms of total strains

$$\frac{\partial^2 \varepsilon_{yy}}{\partial x^2} - 2\frac{\partial^2 \varepsilon_{xy}}{\partial x \partial y} + \frac{\partial^2 \varepsilon_{xx}}{\partial y^2} = 0 \qquad \text{in } D. \tag{2.5}$$

These equations are subject to boundary conditions on S, the boundary of domain D. In this paper we focus on the boundary value problems involving applied tractions

$$t_x = \sigma_{xx} n_x + \sigma_{xy} n_y \qquad t_y = \sigma_{xy} n_x + \sigma_{yy} n_y \qquad \text{on } S. \tag{2.6}$$

3. Inhomogeneous materials

First, we consider an inhomogeneous, isotropic, simply connected body D subjected to spacially varying eigenstrains ε^*_{ij} and traction boundary conditions (2.6). Using Eqs. (2.1) and (2.2), and assuming that both compliances and eigenstrains are smoothly varying functions of position, the compatibility condition (2.5) can be expressed in terms of stresses as

$$\begin{aligned} \nabla^2 [(A + S)(\sigma_{xx} + \sigma_{yy})] - 2\frac{\partial^2 S}{\partial x^2}\sigma_{xx} - 2\frac{\partial^2 S}{\partial y^2}\sigma_{yy} - 4\frac{\partial^2 S}{\partial x \partial y}\sigma_{xy} = -4\frac{\partial^2 \varepsilon^*_{yy}}{\partial x^2} \\ - 4\frac{\partial^2 \varepsilon^*_{xx}}{\partial y^2} + 8\frac{\partial^2 \varepsilon^*_{xy}}{\partial x \partial y} - 4\nabla^2 \eta \varepsilon^*_{zz} - 8\frac{\partial \eta}{\partial x}\frac{\partial \varepsilon^*_{zz}}{\partial x} - 8\frac{\partial \eta}{\partial y}\frac{\partial \varepsilon^*_{zz}}{\partial y} - 4\eta\nabla^2 \varepsilon^*_{zz}, \end{aligned} \tag{3.1}$$

where $\eta = \nu = \frac{1}{2}(1 - A/S)$ for plane strain and $\eta = 0$ for plane stress. Thus, the unknown planar stress components σ_{xx}, σ_{xy}, and σ_{yy} can be determined from the equilibrium equations (2.1), the compatibility condition (3.1) and boundary conditions (2.6). From these governing equations only Eq. (3.1) contains elastic compliances. Thus, in our investigation on reduced parameter dependence we focus on Eq. (3.1).

Following CHERKAEV, LURIE and MILTON [6] we seek the conditions for the invariance of the planar stresses with respect to the shift in shear and bulk compliances in this class of boundary value problems. In particular, the general form of the shift in elastic compliances, introduced by DUNDURS and MARKENSCOFF [8] is considered

$$\overline{A} = mA + a + bx + cy, \qquad \overline{S} = mS - a - bx - cy, \tag{3.2}$$

where a, b, c, and m are arbitrary constants provided that the compliances remain non-negative. In this analysis, in addition to the plane stress and plane strain cases, which lead to different results, the distinction is made between the cases when $m = 1$ and $m \neq 1$.

For the plane stress case and $m = 1$, Eq. (3.1) remains unchanged under the linear shift (3.2), i.e. the planar stress components remain unchanged, for any ε^*_{ij}, and thus there is a reduced parameter dependence.

For the plane strain case and $m = 1$, Eq. (3.1) remains invariant under the linear shift (3.2) when

$$\nabla^2 \eta \varepsilon^*_{zz} + 2\frac{\partial \eta}{\partial x}\frac{\partial \varepsilon^*_{zz}}{\partial x} + 2\frac{\partial \eta}{\partial y}\frac{\partial \varepsilon^*_{zz}}{\partial y} + \eta \nabla^2 \varepsilon^*_{zz} = 0. \tag{3.3}$$

For the special case of uniform eigenstrains, the condition (3.3) is satisfied provided that

$$\varepsilon^*_{zz} = 0 \quad \text{or} \quad \nabla^2 \eta = 0, \tag{3.4}$$

while for the case of a homogeneous material the condition (3.3) is satisfied if

$$\nabla^2 \varepsilon^*_{zz} = 0 \quad \text{or} \quad \eta = 0. \tag{3.5}$$

Recall that $\eta = \nu$ for plane strain case.

For the case of plane stress and $m \neq 1$, Eq. (3.1) is invariant under the shift (3.2) if

$$\frac{\partial^2 \varepsilon^*_{yy}}{\partial x^2} - 2\frac{\partial^2 \varepsilon^*_{xy}}{\partial x \partial y} + \frac{\partial^2 \varepsilon^*_{xx}}{\partial y^2} = 0, \tag{3.6}$$

while for the plane strain case and $m \neq 1$, the linear shift is only possible when

$$(3.7) \quad \frac{\partial^2 \varepsilon^*_{yy}}{\partial x^2} - 2\frac{\partial^2 \varepsilon^*_{xy}}{\partial x \partial y} + \frac{\partial^2 \varepsilon^*_{xx}}{\partial y^2} + \nabla^2 \eta \varepsilon^*_{zz} + 2\frac{\partial \eta}{\partial x}\frac{\partial \varepsilon^*_{zz}}{\partial x} + 2\frac{\partial \eta}{\partial y}\frac{\partial \varepsilon^*_{zz}}{\partial y} + \eta \nabla^2 \varepsilon^*_{zz} = 0.$$

For multiply connected materials the compatibility condition (3.1) is a necessary but not a sufficient condition for the existence of continuous displacements. Thus, for such materials in addition to (3.1), the global compatibility conditions in the form of line integrals (called Cesaro integrals) need to be included. More details on this procedure are given in [8, 15]; the analysis presented there can be extended to multiply connected materials with eigenstrains. This class of problems is not addressed in this paper.

Next, two special cases are considered.

CASE 1. Assume a homogeneous material with uniform eigenstrains subject to zero traction boundary conditions. In this case the eigenstrains may represent thermal strains defined by Eq. (1.9) and the problem reduces to the case of uncoupled linear thermoelasticity for homogeneous materials. The governing equation (3.1) becomes

$$\nabla^2 (\sigma_{xx} + \sigma_{yy}) = 0$$

subject to zero tractions in the plane. This boundary value problem is satisfied identically by zero stresses, as expected. Thus, the concept of the reduced parameter dependence has no relevance for this boundary value problem.

CASE 2. Assume a homogeneous material with non-uniform eigenstrains subject to traction boundary conditions. Eq. (3.1) takes the form

$$(3.8) \quad (A + S) \nabla^2 (\sigma_{xx} + \sigma_{yy}) = -4\frac{\partial^2 \varepsilon^*_{yy}}{\partial x^2} + 8\frac{\partial^2 \varepsilon^*_{xy}}{\partial x \partial y} - 4\frac{\partial^2 \varepsilon^*_{xx}}{\partial y^2} - 4\eta \nabla^2 \varepsilon^*_{zz}.$$

In general, for this case, the stresses are non-zero, and the concept of reduced parameter dependence applies, subject to conditions on eigenstrains given in this section.

A related work addressing residual stresses in isotropic materials is due to HOGER [22]. It that reference, residual stress is defined as the stress present in a body in an unloaded reference configuration. In this definition there are no body forces and no surface tractions acting on material. For such class of problems in an isotropic material "the residual stresses must commute with all proper orthogonal tensors", and therefore have a restricted form of a hydrostatic pressure. For zero tractions on the boundary this stress must be identically zero. Thus, it is concluded in [22] that an isotropic body can support no residual stress.

In our case the stress is caused by external eigenstrains which, as mentioned in Sec. 1, are mathematically equivalent to body forces and surface tractions. Thus, the stress fields in our formulation differ from those in [22]. More specifically, the stresses have the unrestricted form, which is related to the unrestricted form of applied eigenstrains. The form of eigenstrains is determined solely by the physical problem considered. Thus, for nonuniform applied eigenstrains, the stresses are in general nonuniform and nonzero. This agrees with the statement in [22] that nonzero residual stress must be nonuniform.

4. Two-phase materials with perfectly bonded interfaces

Next, we consider the case of a domain consisting of two discontinuous phases 1 and 2, subjected to eigenstrains. We assume perfect bonding boundary conditions on the boundary between the two phases, and we assume traction boundary conditions applied on the outer boundary. Using the stress formulation, the governing equations are Eq. (3.1) for phase 1

$$
\begin{aligned}
(4.1)\quad \nabla^2\left[(A_1+S_1)\left(\sigma_{xx}^{(1)}+\sigma_{yy}^{(1)}\right)\right] - 2\frac{\partial^2 S_1}{\partial x^2}\sigma_{xx}^{(1)} - 2\frac{\partial^2 S_1}{\partial y^2}\sigma_{yy}^{(1)} - 4\frac{\partial^2 S_1}{\partial x \partial y}\sigma_{xy}^{(1)} \\
= -4\frac{\partial^2 \left(\varepsilon_{yy}^*\right)_1}{\partial x^2} - 4\frac{\partial^2 \left(\varepsilon_{xx}^*\right)_1}{\partial y^2} + 8\frac{\partial^2 \left(\varepsilon_{xy}^*\right)_1}{\partial x \partial y} - 4\nabla^2\eta_1 \left(\varepsilon_{zz}^*\right)_1 \\
- 8\frac{\partial \eta_1}{\partial x}\frac{\partial \left(\varepsilon_{zz}^*\right)_1}{\partial x} - 8\frac{\partial \eta_1}{\partial y}\frac{\partial \left(\varepsilon_{zz}^*\right)_1}{\partial y} - 4\eta_1\nabla^2\left(\varepsilon_{zz}^*\right)_1,
\end{aligned}
$$

and the analogous equation for phase 2, the equilibrium equations (2.1) applied for each phase, and boundary conditions (2.6).

Following [8, 23], for a domain consisting of two discontinuous phases (denoted by 1 and 2), the perfect bonding boundary conditions on the boundary S_{12} between these phases involve

a) the continuity of normal tractions

$$
(4.2)\qquad \sigma_{nn}^{(1)} = \sigma_{nn}^{(2)} \qquad \text{on } S_{12},
$$

b) the continuity of tangential tractions

$$
(4.3)\qquad \sigma_{ns}^{(1)} = \sigma_{ns}^{(2)} \qquad \text{on } S_{12},
$$

c) the continuity of change in curvature $\Delta K_1 = \Delta K_2$, which in terms of

stresses has the form

$$(4.4)\quad \frac{\partial}{\partial n}\left[(A_2+S_2)\,\sigma_{ss}^{(2)}\right]-\frac{\partial}{\partial n}\left[(A_1+S_1)\,\sigma_{ss}^{(1)}\right]$$
$$-\left[(A_2-A_1)+3\,(S_2-S_1)\right]\frac{\partial \sigma_{ns}}{\partial s}$$
$$-4\frac{\partial}{\partial s}\,(S_2-S_1)\,\sigma_{ns}+\left\{\frac{\partial}{\partial n}\left[(A_2-A_1)-(S_2-S_1)\right]+2K\,(A_2-A_1)\right\}\sigma_{nn}$$
$$-8\frac{\partial}{\partial s}\left[(\varepsilon_{sn}^{*})_2-(\varepsilon_{sn}^{*})_1\right]+\frac{\partial}{\partial n}\left\{4\left[(\varepsilon_{ss}^{*})_2-(\varepsilon_{ss}^{*})_1\right]+4\left[\eta_2\,(\varepsilon_{zz}^{*})_2-\eta_1\,(\varepsilon_{zz}^{*})_1\right]\right\}$$
$$+K\left\{4\left[(\varepsilon_{nn}^{*})_2-(\varepsilon_{nn}^{*})_1\right]+4\left[\eta_2\,(\varepsilon_{zz}^{*})_2-\eta_1\,(\varepsilon_{zz}^{*})_1\right]\right\}=0 \quad \text{on} \quad S_{12}$$

where K is curvature,

d) the continuity of stretch strains $\varepsilon_{ss}^{(1)}=\varepsilon_{ss}^{(2)}$, which expressed in terms of stresses gives

$$(4.5)\quad (A_2+S_2)\,\sigma_{ss}^{(2)}-(A_1+S_1)\,\sigma_{ss}^{(1)}+\left[(A_2-A_1)-(S_2-S_1)\right]\sigma_{nn}$$
$$+4\left[(\varepsilon_{ss}^{*})_2-(\varepsilon_{ss}^{*})_1\right]+4\left[\eta_2\,(\varepsilon_{zz}^{*})_2-\eta_1\,(\varepsilon_{zz}^{*})_1\right]=0 \quad \text{on} \quad S_{12},$$

where subscripts and superscripts 1 and 2 denote quantities in phases 1 and 2, respectively, and n and s are normal and tangential directions in plane as defined by DUNDURS [23]. Note that the last two boundary conditions (4.4) and (4.5) replace the conventional conditions involving the continuity of normal and tangential displacements

$$(4.6)\qquad u_n^{(1)}=u_n^{(2)} \qquad u_s^{(1)}=u_s^{(2)}.$$

Next we explore the conditions for stress invariance. For two phase materials the linear shift (3.2) takes on the form

$$(4.7)\quad \begin{aligned} \overline{A}_1 &= mA_1+a+bx+cy \qquad \overline{S}_1 = mS_1-a-bx-cy,\\ \overline{A}_2 &= mA_2+a+bx+cy \qquad \overline{S}_2 = mS_2-a-bx-cy. \end{aligned}$$

Note that only the boundary conditions (4.4) – (4.5) depend on compliances. Thus, we explore the invariance under a shift by focusing on these two conditions.

For the case of plane stress and $m=1$, Eqs. (4.2) – (4.5) are invariant under the linear shift (4.7) for any eigenstrain ε_{ij}^{*} in phase 1 and 2.

For the case of plane strain and $m=1$ the linear shift is possible if

$$(4.8)\qquad \eta_1\,(\varepsilon_{zz}^{*})_1=\eta_2\,(\varepsilon_{zz}^{*})_2\,.$$

For the plane stress case and $m \neq 1$ the boundary condition (4.4) does not change under a linear shift if

$$(4.9)\quad -2\frac{\partial}{\partial s}\left[(\varepsilon^*_{sn})_2 - (\varepsilon^*_{sn})_1\right] + \frac{\partial}{\partial n}\left[(\varepsilon^*_{ss})_2 - (\varepsilon^*_{ss})_1\right] + K\left[(\varepsilon^*_{nn})_2 - (\varepsilon^*_{nn})_1\right] = 0$$

and the boundary condition (4.5) remains unchanged under a shift if

$$(4.10)\qquad (\varepsilon^*_{ss})_1 = (\varepsilon^*_{ss})_2 .$$

For plane strain case and $m \neq 1$ Eq. (4.4) is invariant if

$$(4.11)\quad -2\frac{\partial}{\partial s}\left[(\varepsilon^*_{sn})_2 - (\varepsilon^*_{sn})_1\right] + \frac{\partial}{\partial n}\left\{\left[(\varepsilon^*_{ss})_2 - (\varepsilon^*_{ss})_1\right] + \left[\eta_2 (\varepsilon^*_{zz})_2 - \eta_1 (\varepsilon^*_{zz})_1\right]\right\}$$
$$+ K\left\{\left[(\varepsilon^*_{nn})_2 - (\varepsilon^*_{nn})_1\right] + \left[\eta_2 (\varepsilon^*_{zz})_2 - \eta_1 (\varepsilon^*_{zz})_1\right]\right\} = 0 \quad \text{on} \quad S_{12}$$

and Eq. (4.5) is invariant if

$$(4.12)\qquad \left[(\varepsilon^*_{ss})_2 - (\varepsilon^*_{ss})_1\right] + \left[\eta_2 (\varepsilon^*_{zz})_2 - \eta_1 (\varepsilon^*_{zz})_1\right] = 0 \quad \text{on} \quad S_{12},$$

Thus, if (4.12) is used, the condition (4.11) reduces to

$$(4.13)\quad -2\frac{\partial}{\partial s}\left[(\varepsilon^*_{sn})_2 - (\varepsilon^*_{sn})_1\right] + K\left\{\left[(\varepsilon^*_{nn})_2 - (\varepsilon^*_{nn})_1\right]\right.$$
$$\left. + \left[\eta_2 (\varepsilon^*_{zz})_2 - \eta_1 (\varepsilon^*_{zz})_1\right]\right\} = 0.$$

In addition, the conditions on the invariance of Eq. (4.1) and on its counterpart for phase 2 must be satisfied for all the four cases discussed. These conditions are analogous to those in Sec. 3.

Note that the results presented in this section are applicable for both simply and multiply connected two phase materials. It has been shown by MARKENSCOFF [24] that for multiply connected materials with perfectly bonded interfaces, the Cesaro integrals do not need to be considered. Also, the results for two phase materials, discussed in this section, can be extended to multiphase materials in a straightforward way.

To illustrate the concepts presented in this section we include in the Appendix an example involving a single elastic circular inclusion embedded in the elastic matrix subjected to uniform eigenstrains, and more specifically – to a uniform temperature change.

5. Conclusions

We showed the reduced parameter dependence in the in-plane stress fields in the problems governed by plane elasticity with eigenstrains, if the eigenstrains

satisfy the given conditions. Note that there are no conditions needed for the plane stress case for the form of shift with $m = 1$. These results can be applied for two-phase materials to linear plane uncoupled thermoelasticity, where eigenstrains are uniform and represent the product of the thermal expansion coefficient and temperature change. The analysis can also be extended to multi-phase materials with perfectly bonded interfaces, two-phase (or multi-phase) materials with slipping interfaces [25], and inhomogeneous multiply connected materials.

The reduced parameter dependence is of importance in parametric studies, both experimental and theoretical. It can be used as a check for numerical and analytical calculations, it reduces the number of output parameters, and facilitates the presentation of results. It results in savings in time, space and resources.

Acknowledgement

I.J. gratefully acknowledges the support of the National Science Foundation through the grants CMS-9753075 and CMS-0085137.

Appendix

The analytical linear elastic solution for radial stresses due to a small circular homogeneous inclusion made of phase 2 of radius a embedded in a homogeneous matrix of phase 1 and subjected to a uniform temperature change ΔT is given by

$$\sigma_{rr}^{(1)} = \frac{2\left[\alpha_1\left(1+\eta_1\right) - \alpha_2\left(1+\eta_2\right)\right]\Delta T a^2}{\dfrac{\kappa_2 - 1}{2G_2} + \dfrac{1}{G_1}} \frac{1}{r^2} \tag{A.1}$$

and

$$\sigma_{rr}^{(2)} = \frac{\left[\alpha_1\left(1+\eta_1\right) - \alpha_2\left(1+\eta_2\right)\right]\Delta T}{\dfrac{\kappa_2 - 1}{2G_2} + \dfrac{1}{G_1}}, \tag{A.2}$$

where subscripts and superscripts 1 and 2 denote the matrix and inclusion respectively, and α is the coefficient of thermal expansion. κ is the Kolosov constant defined in Eq. (2.4) and G is a shear modulus. If we express this solution in a contracted form using the definitions (2.3), we have

$$\sigma_{rr}^{(1)} = \frac{2\left[\alpha_1\left(1+\eta_1\right) - \alpha_2\left(1+\eta_2\right)\right]\Delta T a^2}{A_2 + S_1} \frac{1}{r^2} \tag{A.3}$$

and

$$\sigma_{rr}^{(2)} = \frac{\left[\alpha_1\left(1+\eta_1\right) - \alpha_2\left(1+\eta_2\right)\right]\Delta T}{A_2 + S_1} \tag{A.4}$$

Note that the eigenstrains, defined in Eq. (1.9), are

$$(\varepsilon^*_{rr})_1 = (\varepsilon^*_{\theta\theta})_1 = (\varepsilon^*_{zz})_1 = \alpha_1 \Delta T \tag{A.5}$$

$$(\varepsilon^*_{rr})_2 = (\varepsilon^*_{\theta\theta})_2 = (\varepsilon^*_{zz})_2 = \alpha_2 \Delta T \tag{A.6}$$

and

$$\varepsilon^*_{rr} = \varepsilon^*_{nn} \qquad \varepsilon^*_{\theta\theta} = \varepsilon^*_{ss}. \tag{A.7}$$

Note that the stresses are invariant under the transformation (4.7) subject to conditions discussed in Sec. 4.

Thus, for plane stress case and $m = 1$, the in-plane stresses are invariant under the shift (4.7) and there is a reduced parameter dependence.

For plane stress case and $m \neq 1$, the condition (3.6) applied to $\left(\varepsilon^*_{ij}\right)_1$ and $\left(\varepsilon^*_{ij}\right)_2$ is satisfied automatically, but the conditions (4.9) and (4.10) impose

$$(\varepsilon^*_{rr})_1 = (\varepsilon^*_{rr})_2 \qquad (\varepsilon^*_{\theta\theta})_1 = (\varepsilon^*_{\theta\theta})_2. \tag{A.8}$$

The condition (5.8) implies $\alpha_1 = \alpha_2$, which gives a zero stress field. Thus, the reduced parameter dependence does not hold for this case. This conclusion can easily be verified by analyzing Eqs. (5.3) – (5.4).

For plane strain case and $m = 1$, the conditions (3.4) and (4.8) are satisfied if

$$(\varepsilon^*_{zz})_1 = (\varepsilon^*_{zz})_2 = 0 \tag{A.9}$$

Thus, there is parameter dependence subject to the condition (5.9).

For the plane strain case and $m \neq 1$, the condition (3.7) is satisfied for any eigenstrain value, while the conditions (4.12) and (4.13) are satisfied only if

$$(\varepsilon^*_{rr})_1 = (\varepsilon^*_{rr})_2 \qquad (\varepsilon^*_{\theta\theta})_1 = (\varepsilon^*_{\theta\theta})_2 \qquad (\varepsilon^*_{zz})_1 = (\varepsilon^*_{zz})_2 \tag{A.10}$$

which implies $\alpha_1 = \alpha_2$, and thus the zero stress field. Therefore, the reduced parameter dependence does not hold for this case.

References

1. T. MURA, *Micromechanics of defects in solids*, 2nd ed., Martinus Nijhoff, Dordrecht 1987.
2. J. H. MICHELL, *On the direct determination of stress in an elastic solid, with application to the theory of plates*, Proc. Lond. Math. Soc. **31**, 100–125, 1899.
3. J. DUNDURS, *Effect of elastic constants on stress in a composite under plane deformation*, J. Compos. Mater. **1**, 310–322, 1967.

4. J. DUNDURS, *Discussion of paper by D.B. Bogy*, J. Appl. Mech. **36**, 650–652, 1969.

5. J. M. NEUMEISTER, *On the role of elastic constants in multiphase contact problems*, J. Appl. Mech. **59**, 328–334, 1992.

6. A. CHERKAEV, K. LURIE, G.W. MILTON, *Invariant properties of the stress in plane elasticity and equivalence classes of composites*. Proc. R. Soc. Lond. A **438**, 519–529, 1992.

7. M. F. THORPE, I. JASIUK, *New results in the theory of elasticity for two-dimensional composites*. Proc. R. Soc. Lond. A**438**, 531–544, 1992.

8. J. DUNDURS, X. MARKENSCOFF, *Invariance of stresses under a change in elastic compliances*, Proc. R. Soc. Lond. A **443**, 289–300, 1993.

9. B. MORAN, M. GOSZ, *On the constitutive response of fiber composites with imperfect interfaces*. In Advanced Composites: Design, Materials and Processing Technologies (Proc. 8th Annual ASM/ESD Advanced Composites Conference), pp. 261–266. ASM International 1992.

10. B. MORAN, M. GOSZ, *Stress invariance in plane anisotropic elasticity*, Modelling Simul. Mater. Sci. Engng. **2**, 677–688, 1994.

11. Q.-S. ZHENG, K. C. HWANG, *Reduced dependence of defect compliance on matrix and inclusion elastic properties in two-dimensional elasticity*, Proc. R. Soc. Lond. A **452**, 2493–2507, 1996.

12. Q.-S. ZHENG, K.C. HWANG, *Two-dimensional elastic compliances of materials with holes and microcracks*, Proc. R. Soc. Lond. A **453**, 353–364, 1997.

13. J. DUNDURS, I. JASIUK, *Effective elastic moduli of composite materials: Reduced parameter dependence*, Appl. Mech. Rev., **50** (Part 2), S39–S43, 1997.

14. I. JASIUK, J. DUNDURS, M. JIANG, *On the reduced parameter dependence of the Mori-Tanaka theory*, Mater. Sci. & Engng. A, **285**, 130–135, 2000.

15. X. MARKENSCOFF, I. JASIUK, *On multiple-connectivity and the reduction of constants for composites with body forces*, Proc. R. Soc. Lond. A **454**, 1357–1369, 1998.

16. M. OSTOJA-STARZEWSKI, I. JASIUK, *Stress invariance in planar Cosserat elasticity*, Proc. R. Soc. Lond. A **451**, 453–470, 1995.

17. T. CHEN, *Further results on invariant properties of the stress in plane elasticity and its extension to piezoelectricity*, Mech. Res. Comm. **22**, 251–256, 1995.

18. Q.-S. ZHENG, T. CHEN, *Generalized plane deformation of electromagnetic thermoelastic solids I. Correspondence and invariance shifts*, Proc. R. Soc. Lond. A **455**, 1283–1299, 1999.

19. Q.-S. ZHENG, T. CHEN, *Generalized plane deformation of electromagnetic thermoelastic solids II. Further results on invariance shifts and reduced dependencies*, Proc. R. Soc. Lond. A **455**, 1301–1314, 1999.

20. A. N. NORRIS, *Stress invariance and redundant moduli in three-dimensional elasticity*, Proc. R. Soc. Lond. A **455**, 4097–4116, 1999.

21. G. K. HU, G. J. WENG, *A new derivative on the shift property of effective elastic compliances for planar and three-dimensional composites*, Proc. R. Soc. Lond. A **457**, 1675–1684, 2001.

22. A. HOGER, *On the residual stress possible in an elastic body with material symmetry*, Arch. Rat. Mech. Anal. **88**, 271–289, 1985.

23. J. DUNDURS, *Boundary conditions at Interface. In Micromechanics and inhomogeneity*, The Toshio Mura Anniversary Volume, G. J. WENG, M. TAYA and H. ABE [Eds.], pp. 109–114. New York: Springer-Verlag, 1990.

24. X. MARKENSCOFF, *A note on strain jump conditions and Cesaro integrals for bonded and slipping inclusions*, J. Elasticity, **45**, 33–44, 1996.

25. S. D. BOCCARA, *An investigation of micropolar moduli and characteristic lengths of heterogeneous materials and a reduction of constants in plane elasticity with eigenstrains*, M.Sc. Thesis, Georgia Institute of Technology, 1998.

Received May 5, 2002; revised version October 2, 2002.

Arch. Mech., **54**, 5-6, pp. 439–457, Warszawa 2002

Thermomechanical coupled waves in a viscoplastic medium

K. FRISCHMUTH [1], W. KOSIŃSKI [2]

[1] *Fachbereich Mathematik, Universität Rostock,*
Universitätsplatz 1, D–18051 Rostock, Germany
e-mail: kurt.frischmuth@mathematik.uni-rostock.de

[2] *Research Center, Polish–Japanese Institute of Information Technology*
ul. Koszykowa 86, PL-02-008 Warszawa, Poland
e-mail: wkos@pjwstk.edu.pl

Dedicated to Professor Piotr Perzyna
on the occasion of his 70^{th} birthday

IDEAS OF PERZYNA'S theory of material systems in the cases of viscoplastic materials and heat conductors are elaborated. Both theories are based on the notion of a *method of preparation*. They are combined into one coupled model for an elasto-viscoplastic heat conductor. We study its behavior by numerically calculating solutions for plane waves passing through a body.

Key words: visco-plastic materials, hyperbolic systems, nonlinear wave propagation, method of preparation

1. Introduction

FOR AN ELASTO-VISCOPLASTIC body, stress depends on the present *configuration*, and additionally, on *irreversible deformations* accumulated in the past. Perzyna introduced the notion of a *method of preparation* to summarize all information that is given on top of the actual configuration, which allows to determine the present response of the studied material [1].

The description of the method of preparation may contain information that is eventually not needed – as opposed to the notion of a *state* – which by definition must be minimal [2, 3]. Thus a description by the method of preparation may be more convenient. In particular, the method of preparation may be given in terms of the whole *history* of a sample, or comprised in form of just a finite number of essential quantities, the *internal variables* or *state parameters,* cf. [3]. Sometimes it may be useful to have access to both descriptions, cf. [5, 6 7].

We demonstrate the concept of a method of preparation in the case of an elasto-viscoplastic material, for a rigid heat conductor and for a coupled thermomechanical model. For the sake of simplicity we refrain from technicalities and,

initially, we confine ourselves to 1D models. Then a 3D generalization will be done together with some thermodynamic background for the model equations introduced.

2. General setup of the theory of materials

Constructing mathematical models of real behavior of material objects we use a framework which has its source in the system theory. The accurate setup of such a framework one can find in the papers of W. NOLL [8.9]. There the concepts of state, configuration and evolution function as well as response functions have been used. The approach presented by Noll was *intrinsic*, in the sense that the concepts are independent of the observer and of the description used (i.e. material or spatial). Such a level of abstraction is suitable when a global system approach is used, which is open for further specification.

It was Perzyna who almost at the same time introduced the concept of a *method of preparation* to the theory of materials. The method of preparation together with the configuration form the state of a material element in Noll's approach. *Response functions* are defined on the collection of all states. Inputs (*processes* in Noll's terminology) applied to a material element (or a material system) being at a given state, result in an evolution of the state, and consequently in a new response. The evolution of states forced by inputs (processes), governed in Noll's approach by his *evolution function*, is described in Perzyna's approach by a particular operator responsible for the evolution of the method of preparation, while the actual configuration is contained in the value of the input (process) at the actual time.

A second substantial contribution of P. Perzyna to the theory of materials was the first application of the concept of *internal state variables* (*parameters*) to viscoplasticity theory. After the pioneering paper of K. C. VALANIS who for the first time in the world literature in 1967 formulated the thermodynamic setup of internal state variables for inelestic materials in [10] (later on a celebrated paper by COLEMAN and GURTIN [11] appeared), PERZYNA with his coworker W. WOJNO introduced in [12] the inelastic strain tensor $\boldsymbol{C}^i$ for the description of viscoplastic flow in the complete nonlinear setup of a thermodynamic theory.

The method of preparation of the actual configuration contains all information necessary to give at the given state a unique response value of the material element. The choice of a particular form of the description – or better to say, a particular class of response functions – is crucial for the choice of the method of preparation. Sometimes it can be the whole past (or summed) history of the configuration, represented by a function defined on the infinite domain $[0, \infty)$, in other cases just the rate of change of configuration is taken into account.

In particular, the above approach can be applied to mechanics – the configuration being a tensorial measure of deformation, to thermodynamics – the configuration being the collection of a tensorial measure of deformation, the absolute temperature and possibly its gradient. Further applications can be found in electro-magnetic fields, diffusion, filtration and so on, where configurations may contain more quantities. In each case the pure *constitutive theory* has to be compatible with *invariancy requirements*. This has to be studied in the context of appropriate *balance equations*. For a one-dimensional setting, this will be demonstrated on the examples of the next three sections. In the framework we are going to use the method of preparation given by two quantities: a tensorial and scalar one (in the 3D thermodynamic case), both are called internal state variables. The first one will represent a measure of inelastic (permanent) deformation of the material element, as in Perzyna's and Wojno's approach, while the second one is a thermal state variable, called in our previous paper a *new temperature scale*, which represents a summed history of the temperature. For both variables *evolution equations* are introduced in the form of ordinary differential equations (ODEs) for each fixed material point (element).

3. Elasto-viscoplastic material

For simplicity as well as for the purpose of the present paper, first the 1D case will be considered. Introducing u as the displacement of a material point X in the case of the mechanical model we identify the configuration with the partial derivative $\partial u/\partial X =: m$ and introduce C_p as a method of preparation. The scalar quantity C_p is an internal state variable, identified with plastic, better to say, inelastic strain, which requires an ODE to govern its evolution. In the context of Noll's theory the pair (m, C_p) can be regarded as a state. Then the *response* function $\hat{S}$ is introduced giving the stress S of the material element (point)

$$S = \hat{S}(m, C_p) \; . \tag{3.1}$$

The evolution of the method of preparation is defined by the so-called kinetic function Ω appearing on the right-hand side of the evolution equation for the internal state variable C_p. We have the Cauchy problem

$$\dot{C}_p = \Omega(m, C_p) \; , \quad C_p(0) = C_p^0 \; , \tag{3.2}$$

where $\dot{C}_p$ denotes the partial derivative with respect to time t at the constant particle X. A particular solution to the equation can be found as a function of time t if an input (a process) in form of a time-dependent configuration $m(t)$ is given as well as an initial condition C_p^0. For the internal variable C_p the kinetic function Ω needs to be identified on the basis of experimental observations and suitable physical identifications. Usually the following is assumed [13]:

- *elastic range:* if the actual stress is small there is no *yielding*, the state variable C_p does not change, i.e. Ω vanishes;
- *yielding:* if the stress reaches the *plastic limit* κ_0 (or *yield stress*), C_p changes, increases or decreases according to the sign of S. While in the pure plasticity (i.e. in the rate-independent case), the yield stress may never be exceeded, in viscoplasticity we may have *over-stress*, and there is a relation between this over-stress and the rate of plastic flow, i.e.

$$\Omega(m, C_p) = \Phi(\hat{S}(m, C_p); \kappa_0) \tag{3.3}$$

  with some function Φ and a parametric dependence on κ_0;
- *viscosity:* we have rate-dependence due to the evolution equation for the plastic strain.

If we assume vanishing body forces, the first balance law, called the conservation of momentum $\rho_0 v$, where $v = \dot{u}$ denotes the velocity and ρ_0 the reference mass density, together with the geometric and evolution equations, may be expressed by

$$\dot{m} = v_{,X} , \tag{3.4}$$

$$\dot{v} = \frac{1}{\rho_0} \hat{S}(m, C_p)_{,X} , \tag{3.5}$$

$$\dot{C}_p = \Omega(m, C_p) . \tag{3.6}$$

This system (3.4 – 3.6) is suitable for time-integration. Note that here all right-hand sides depend only on the *local state* $U = (v, m, C_p)^T$, and on its first partial derivatives $U_{,X}$. This can be brought to the general form

$$\dot{U} + f(U)_{,X} = b(U) \tag{3.7}$$

with the flux term f and the source term b. In this form we will solve this system in Sec. 7.2 and its thermo-mechanical generalization in Sec. 7.3. Note that for the hyperbolic system (3.4 – 3.6) the *local state* is the *state* extended by the *local velocity*.

As an easy example, consider the balance equations with constitutive equations for stress S and plastic flow speed Ω determined by

$$S = E(m - C_p), \tag{3.8}$$

$$\dot{C}_p = \Omega = \Phi(S; \kappa_0), \tag{3.9}$$

where E is Young's modulus and Φ is a (regularized) indicator function of the interval $[-\kappa_0, \kappa_0]$. Here we denote by κ_0 the yield stress, for smaller values of S

there is practically no flow, above we have a dramatic increase of flow speed. As an example we take

$$\Phi(S, \kappa_0) = \text{sign}\,(S)\text{pos}\,abs\,((S - \kappa_0)^n)$$

with pos$(\cdot)$ denoting the positive part of the real input argument. For implementation, the absolute value, sign and positive part have been regularized in the way proposed in [14].

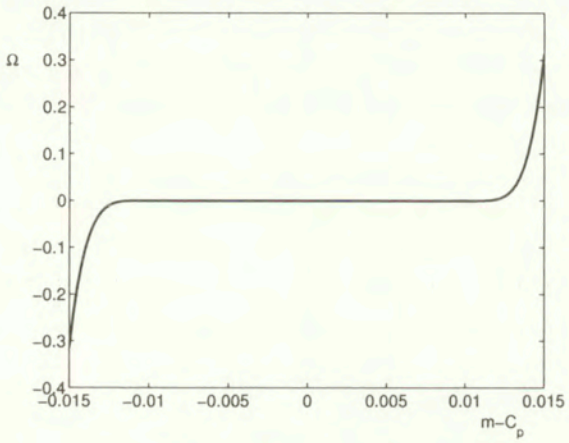

FIG. 1. Flow speed as function of $m - C_p$.

It is worthwhile to note that in the plasticity theory usually *incompressibility* is assumed. However, for the considered 1D theory this is of no consequence.

4. Heat conduction

Several technological situations at moderate and high temperatures (such as distribution of temperature around propagating cracks [15], and temperature distribution in solid materials due to laser pulse train of a very short duration [16]) and many physical experiments at low temperatures (cf. [17, 18, 19, 20, 21, 22]), show the necessity of taking into account the wave structure of the heat transport.

There are several phenomenological approaches aimed at a new heat conduction equation that could describe the mentioned phenomena. Some of them are reviewed in the papers [23, 24, 25]. The present approach keeps a proportionality law ([26]) between the heat flux q and the spatial gradient of a thermal internal state variable β in the form

$$q = -\alpha\beta_{,x}\ , \tag{4.1}$$

with a proportionality coefficient α which may depend on ϑ. Here the lower case x denotes the spatial position of the material point X. (Notice that in the case of a deformable material body x is the position after the displacement u, i.e. $x = u + X$). The classical Fourier law, on the other hand, is

$$q = -k(\vartheta)\vartheta_{,x} \tag{4.2}$$

where the heat conduction coefficient $k(\vartheta)$ can depend, in general, on the absolute temperature ϑ. The scalar internal state variable β will represent the history of the temperature in the sense that its value at the present time will be a solution to an initial-value problem for a suitable ODE in which the right-hand side is a function of (at least) ϑ and β. Let us notice that in the linear case such an ODE can have the form:

$$\dot{\beta} = \frac{1}{\tau}(\vartheta - \beta), \text{ with initial condition } \beta(0) = \beta^0\,, \tag{4.3}$$

where the coefficient τ is called the *thermal relaxation time*. If we perform spatial differentiation in (4.3) and make use of (4.1) we get

$$\tau\dot{q} + q = -\alpha\vartheta_{,x}\ . \tag{4.4}$$

The last equation can be regarded as a modification of the Fourier law if the heat conductivity coefficient $k(\vartheta)$ is identified with α and one has added to (4.2) a term in which the time derivative of the heat flux q is multiplied by the coefficient τ. If one omits introducing the thermal internal state variable β, the last equation (4.4) becomes the well-know *telegraph equation* which is the governing equation of the so-called *rate type approach* modelling heat conduction, and is called the MAXWELL-CATTANEO-VERNOTTE-KALISKI equation ([27, 28, 29, 30, 31]). It is interesting to add that the approach based on the last equation can be obtained as a particular case of the summed temperature–gradient history approach proposed by the authors of [32].

There are some drawbacks in applying the equation (4.4) to the thermodynamic theory of thermomechanics, especially because of the internal dissipation inequality. The present author (W. K.) with PERZYNA in [33] (and later in [34] in a more general setup) calculated for the first time finite speeds of thermal (and thermo-mechanical) waves in the framework of a thermodynamic theory with internal state variables. Later on COLEMAN *et al.* [35] repeated the first results of Kosiński and Perzyna from 1972 in a slightly different set-up, without referring to the internal state variable approach and to the original paper [33].

The model proposed in [26] is based on a different procedure than the derivation of the wave-type heat propagation equation; in fact it is somehow a next generation of [33], [34]. In that model a scalar internal state variable β has

been introduced to represent at the same time a history of the thermodynamic temperature and the potential for its gradient. In the course of obtaining the consequences for the laws of thermodynamics, a modified Fourier-type law was found, leading to finite speeds of propagation of thermal and thermo-mechanical waves. The model has been mostly applied to heat conductors in 1D and 3D cases and to thermo-elastic solids (cf. [36, 37], and the literature given in [38]). Its similarities to other models are shown in [39, 40] (cf. also [23, 25]). In terms of the material description in the last approach, the state is formed by the configuration, composed of the temperature ϑ and the method of preparation. The latter is composed of the (thermal) internal state variable β, and its spatial gradient $\partial\beta/\partial x = p$. The state is a triple (ϑ, β, p), while the response is composed of two quantities: the internal energy e and the heat flux q, i.e. the pair (e, q). For the evolution of the method of preparation we have at our disposal two differential equations, written in a general form as:

$$\dot{\beta} = F(\vartheta, \beta) , \tag{4.5}$$

$$\dot{p} = F_1(\vartheta)_{,x} + F_2'(\beta)p \tag{4.6}$$

with

$$F(\vartheta, \beta) = F_1(\vartheta) + F_2(\beta) \text{ and } F_2'(\beta) = dF_2(\beta)/d\beta .$$

For the response function we may write

$$e = \hat{e}(\vartheta, \beta, p) \text{ and } q = \hat{q}(\vartheta, \beta, p) . \tag{4.7}$$

Note that both variants have a drawback: the classical one based on (4.4) needs an initial condition for the heat flux q, the semi-empirical ([39]) theory ([14–15]) requires initial data for β. (Notice that the initial condition for p can be calculated from the initial condition for β by simple differentiation.) We conclude this subsection with a formulation of the first order system for the one-dimensional case. We introduce the vector of thermodynamic unknowns as $V = (e, \beta, p)^T$ with the *internal energy* e, the *semi-empirical temperature* β and the gradient of the latter $p = \nabla\beta$, in the one-dimensional case $p = \beta_{,x}$.

We assume a one-to-one relation between absolute temperature ϑ and internal energy e, e.g. given by Debye's law $e = e_4\vartheta^4 + e_0\vartheta$ or simple proportionality, $e = c_v\vartheta$. Together with the previous constitutive relation (4.1) in the form $q = -\alpha(\vartheta)p$, and by adding the energy balance $\dot{e} = -q_{,x} + r$, we obtain the system

$$\begin{pmatrix} \dot{e} \\ \dot{\beta} \\ \dot{p} \end{pmatrix} = \begin{pmatrix} -q_{,x} \\ 0 \\ F_{1,x} \end{pmatrix} + \begin{pmatrix} r \\ F_1 + F_2 \\ F_2'p \end{pmatrix} . \tag{4.8}$$

Here r denotes the known external heat source density, and $F_1 = F_1(\vartheta), F_2 = F_2(\beta)$.

5. Elasto-viscoplastic heat conductor

In this section the governing system of equations is formulated for the 1D case. The theory is based on thermodynamics of heat conduction in a viscoplastic medium with over-stress function. Such a function is known from Perzyna's model of viscoplasticity (cf. [3, 4, 13]. We assume here that this function is independent of the gradient of β. Due to thermodynamics, the stress appearing in it is not the total second Piola-Kirchhoff stress tensor as calculated from the free energy function by the potential relation, but its so-called *instantaneous part* $\boldsymbol{S}_{RI}$, in which the gradient of β has been neglected (no coupling with $\nabla\beta$). Consequently, we assume that the evolution equation for the inelastic strain tensor $\boldsymbol{C}_p$ is given by the polynomial over-stress function

$$\Omega(\boldsymbol{S}_{RI}, \vartheta) = \gamma^* \left(\frac{\sqrt{J_2}}{\kappa(\vartheta)} - 1 \right)^n \frac{\partial \sqrt{J_2}}{\partial \boldsymbol{S}^D_{RI}} = \gamma^* \left(\frac{\sqrt{J_2}}{\kappa(\vartheta)} - 1 \right)^n \frac{\boldsymbol{S}^D_{RI}}{\sqrt{J_2}} \tag{5.1}$$

in which the yield stress κ as well as the viscosity coefficient γ^* may depend on the temperature ϑ, and $\boldsymbol{S}^D_{RI}$ is the deviatoric part of the instantaneous stress tensor $\boldsymbol{S}_{RI}$, with J_2 as its second invariant. In the present 1D case $J_2 = \sqrt{\frac{2}{3}}\, abs(S_R)$.

Finally, we collect all equations and formulate them as a system of PDEs which a vector of unknowns $\boldsymbol{U}$ has to satisfy. Restricting ourselves to the 1D case we assume the notations: S as S^1_1 component of the first Piola-Kirchhoff stress tensor $\boldsymbol{S}$ and E for the component E_{11} of the elastic part of the Lagrange strain tensor $\boldsymbol{E}^e$, writing C_p for the component C_{11p} of the tensor internal state variable $\boldsymbol{C}_p$, and we put S_R for the S^{11}_{RI} component of the stress tensor $\boldsymbol{S}_{RI}$ appearing in the definition of Perzyna's over-stress function, q_κ as the only component of the reference heat flux vector $\boldsymbol{q}_\kappa$ and p for the first component of the spatial gradient of β, $p = \nabla\beta$. Since $1 + m$ is the F_{11} component of the deformation gradient $\boldsymbol{F}$, we get

$$E = \frac{(1+m)^2 - C_p}{2}\,. \tag{5.2}$$

Let us assume that the free energy ψ is (an isotropic, in 3 D case) function of the strain m, inelastic strain (i.e. internal state variable) C_p, gradient of β and temperature ϑ , i.e.

$$\psi = \hat{\psi}(m, \vartheta, \beta_{,x}, C_p)\,. \tag{5.3}$$

Repeating our assumptions from [38, 41] telling that:

(1) the heat flux is linear in the gradient of β, cf. (4.1),

(2) the specific heat is independent of the gradient of β, and adding two more assumptions here, namely:

(3) elastic properties are independent of the inelastic strain and are expressed by the strain-temperature-stress relations of a neo-Hookean material,

(4) the specific heat is of 3rd order in temperature,

we end up with the following partition of the free energy function:

$$\hat{\psi}(m,\vartheta,p,C_p) = \psi_1(E,\vartheta) + \psi_2(m,p,\vartheta) \tag{5.4}$$

where the first mechanical part of ψ_1 is quadratic in E and bilinear in $\vartheta - \vartheta_0$ and E, while ψ_2 must possess the form

$$\psi_2(m,p,\vartheta) = 0.5\psi_{20}\,\vartheta\,p^2\,m, \tag{5.5}$$

where the factor 0.5 is introduced for convenience only. The linearity of the heat flux in p(cf.(4.1)), and the independence of the coefficient α of the strain m together with the above assumptions lead to the specification of the coefficient and the form of ψ_1

$$\psi_1(E,\vartheta) = c_1^2E^2 - \frac{\gamma}{\rho_0}(\vartheta-\vartheta_0)E - c_{v0}\,\vartheta\,(\ln\frac{\vartheta}{\vartheta_0} - 1) - \frac{1}{12}\,c_{v3}\frac{\vartheta^4}{\vartheta_0^3} - \eta_0\,(\vartheta-\vartheta_0)\,, \tag{5.6}$$

with $\alpha(\vartheta) = \rho_0\,\psi_{20}\vartheta^2F'(\vartheta)$ and constants $\psi_{20}, \gamma, \vartheta_0, c_{v0}, c_{v3}, \eta_0$. The dependence of α on F_1' turns out to be a consequence of the second law of thermodynamics, together with the following stress-temperature-strain relation

$$\begin{aligned} S &= \rho_0\frac{\partial\psi}{\partial m} - \rho_0 p\frac{\partial\psi_2}{\partial p}m^{-1} \\ &= \left[\rho_0 c_1^2\frac{(1+m)^2 - C_p}{2} - \gamma(\vartheta-\vartheta_0)\right](1+m) - \frac{1}{2}\rho_0\,\vartheta\,\psi_{20}\,p^2\,, \end{aligned} \tag{5.7}$$

where $c_1^2 = (\lambda + 2\mu)/\rho_0$, with λ and μ as Lamé's constants.

On the other hand, the thermodynamic identity between the internal energy (per unit mass) ϵ, the free energy ψ and the entropy $\eta = -\partial\psi/\partial\vartheta$, which is of the form $\epsilon = \psi + \vartheta\eta$, applied to (5.4–5.6) gives the following expression for ϵ

$$\hat{\epsilon}(E,\vartheta) = \frac{c_1^2}{2}E^2 + \frac{\gamma}{\rho_0}\vartheta_0 E + c_{v0}\,\vartheta + \frac{1}{4}\,c_{v3}\frac{\vartheta^4}{\vartheta_0^3} + \eta_0\,\vartheta_0\,. \tag{5.8}$$

For the first component of the instantaneous stress $\boldsymbol{S}_{RI}$ we have

$$S_R = \rho_0(1+m)^{-1}\frac{\partial\psi_1}{\partial m} = \left[\rho_0 c_1^2\frac{(1+m)^2 - C_p}{2} - \gamma(\vartheta-\vartheta_0)\right]. \tag{5.9}$$

For the inelastic strain we have (cf. (5.1))

$$\dot{C}_p = \gamma^* \left(\frac{abs(S_R)}{\sqrt{\frac{3}{2}}\,\kappa} - 1 \right)^n \frac{S_R}{\sqrt{\frac{2}{3}}\,abs(S_R)} \,. \tag{5.10}$$

For the only nontrivial heat flux component q_κ we have

$$q_\kappa = -\rho_0 \psi_{20} \vartheta^2 \frac{\partial F(\beta, \vartheta)}{\partial \vartheta} p \,. \tag{5.11}$$

For β we have the evolution equation

$$\dot{\beta} = F, \quad \text{with} \quad F(\vartheta, \beta) = F_1(\vartheta) + F_2(\beta) \tag{5.12}$$

and for its material gradient $\pi := \beta_{,X} = p(1+m)$, the so-called prolongated equation (cf. (4.6)),

$$\dot{\pi} = F_1(\vartheta)_{,X} + F_2'(\beta) p (1+m) \,. \tag{5.13}$$

The above constitutive functions are now restricted by the second law of thermodynamics expressed in terms of the *residual dissipation inequality*

$$-\frac{\rho_0}{\vartheta} \left[\frac{\partial F}{\partial \beta} \frac{\partial \psi}{\partial p} p + \frac{\partial \psi}{\partial C_P} \Omega(S_R, \vartheta) \right] \geq 0 \,, \tag{5.14}$$

in which the function Ω is the right-hand side of Eq. (5.10). The balance equations, in this case of linear momentum and energy, will be

$$\dot{v} = \frac{1}{\rho_0} S_{,X} + b \,, \tag{5.15}$$

$$\dot{\left(\rho_0 \epsilon + \frac{\rho_0}{2} v^2\right)} + (q_\kappa - vS)_{,X} = \rho_0 r + \rho_0 v\, b \,, \tag{5.16}$$

where r and b represent heat sources and body forces, respectively. The equations are accompanied by the geometrical compatibility equation

$$\dot{m} = v_{,X} \,. \tag{5.17}$$

6. Numerical results

For hyperbolic systems, we may apply the well-known explicit time-stepping schemes due to Lax-Friedrich, Osher or Lax-Wendroff. While the first mentioned

methods have the advantage of monotonicity, and hence converge to entropy solutions, the Lax-Wendroff scheme is second order accurate and converges faster – at the price of possible violations of monotonicity and artificial oscillations near the wave fronts. We solve the sample problems by an *ad hoc* hybrid combination of the mentioned methods to find a compromise between speed and stability.

We present here in Fig. 2 the resulting data for the mechanical quantities, velocity and strain. There is a wave running from left to right which results from applying a short pressure impulse at the left boundary, which results in a compression wave.

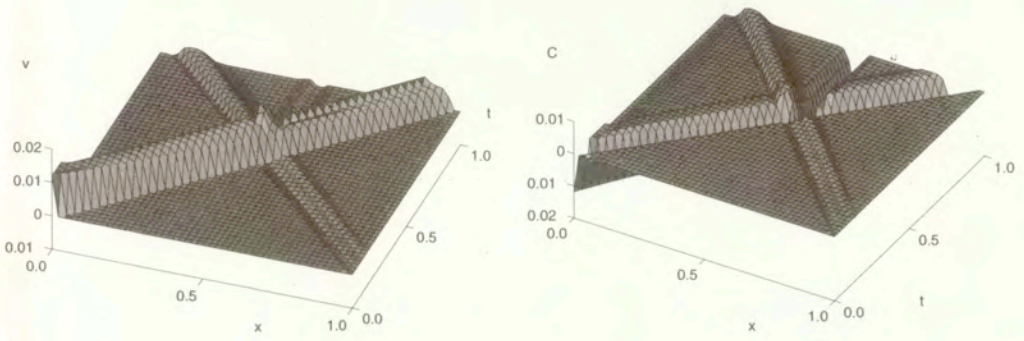

FIG. 2. Velocity and strain.

At the same time, a heat impulse occurs at the right boundary. It runs as a wave from right to left, and it it affects also visibly the mechanical submodel. In the Fig. 3, we depict the temperature increment together with the heat flux. Here the hyperbolic character of the heat transition model becomes obvious.

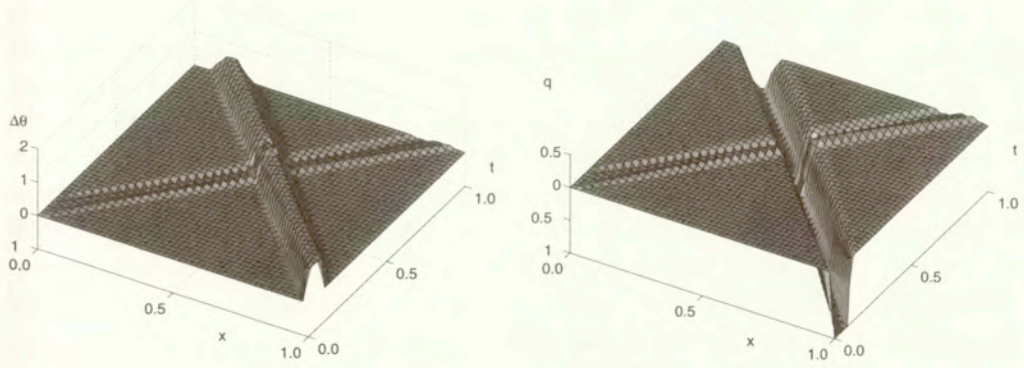

FIG. 3. Temperature and heat flux.

Finally, in Fig. 4 we show the residual deformations, i.e. the internal variable C_p. Note that we have permanent deformations first where the mechanical wave originates. However, due to the nonlinear coupling with the thermal wave, at elevated temperature the state re-enters the plastic range after the crossing point.

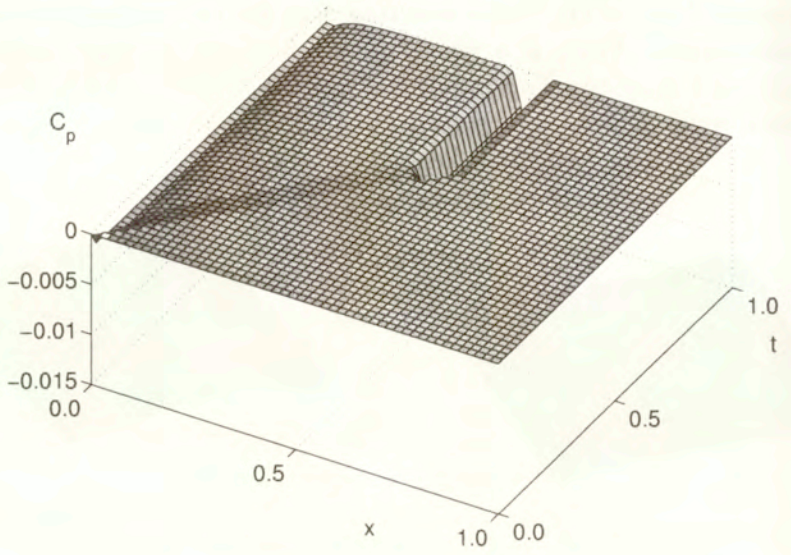

FIG. 4. Permanent deformation.

7. Generalizations

We have presented just the one-dimensional implementations of the general theory. Further, we have limited ourselves to the minimum number of couplings to obtain a non-trivial thermo-mechanical theory. That way it was possible to present the ideas behind the general theory in a particularly clear manner. At this stage, we want to give just some hints as to the full three-dimensional formulation of the theory. However, it has to be mentioned that a major problem is the identification of material parameters/functions for each real material at hand. To keep this paper self-contained, we quote some of the foundations of thermodynamics of an inelastic material with the modified Fourier law presented in [42] (cf. also [38], [43]) and repeat the most important consequences of that presentation. The case of 3D thermo-mechanics at finite strains requires to introduce instead of scalar quantities the following variables:

- $\boldsymbol{F}$ – the deformation gradient tensor;
- the Lagrange strain tensor $\boldsymbol{E}$ related to $\boldsymbol{F}$ by $\boldsymbol{E} = 0.5(\boldsymbol{F}^T\boldsymbol{F} - \boldsymbol{I})$;

- the actual mass density ρ related to the reference mass density ρ_0 by the law $\rho_0 = J\rho$, with $J = \det \boldsymbol{F}$;
- the symmetric Cauchy stress tensor $\boldsymbol{T}$ related to the first Piola-Kirchhoff stress tensor $\boldsymbol{S}$ by the identity $\boldsymbol{S} = J\boldsymbol{T}\boldsymbol{F}^{-T}$ while the
- second Piola-Kirchhoff stress tensor $\boldsymbol{S}_R$ is given by the identity $\boldsymbol{S}_R = \boldsymbol{F}^{-1}\boldsymbol{S}$;
- the particle velocity $\boldsymbol{v}$,
- the heat flux vector $\boldsymbol{q}$, related to the reference heat flux $\boldsymbol{q}_\kappa$ by the identity $\boldsymbol{q}_\kappa = J\boldsymbol{q}\boldsymbol{F}^{-T}$.

We assume that the spatial gradient grad $\beta = \nabla\beta$ and the inelastic strain tensor $\boldsymbol{C}_p$ appears in the constitutive equations for free energy ψ, entropy η, stress $\boldsymbol{S}$ and heat flux $\boldsymbol{q}_\kappa$ as the method of preparation:

$$
\begin{aligned}
\psi &= \psi^*(\boldsymbol{F}, \vartheta, \nabla\vartheta, \nabla\beta, \boldsymbol{C}_p), \qquad \eta = \eta^*(\boldsymbol{F}, \vartheta, \nabla\vartheta, \nabla\beta, \boldsymbol{C}_p),\\
\boldsymbol{S} &= \boldsymbol{S}^*(\boldsymbol{F}, \vartheta, \nabla\vartheta, \nabla\beta, \boldsymbol{C}_p), \qquad \boldsymbol{q}_\kappa = \boldsymbol{Q}^*(\boldsymbol{F}, \vartheta, \nabla\beta, \boldsymbol{C}_p).
\end{aligned} \tag{7.1}
$$

For the internal state variables – the scalar β and the tensor $\boldsymbol{C}_p$ – the evolution equations have the form (cf. (3.6), (2.61))

$$
\dot{\beta} = F(\vartheta, \beta)\,, \tag{7.2}
$$

$$
\dot{\boldsymbol{C}}_p = \Omega^*(\boldsymbol{F}, \vartheta, \boldsymbol{C}_p)\,. \tag{7.3}
$$

Notice that the independence of the heat flux of the actual value of the temperature gradient is crucial for the development of a hyperbolic model. Now the second law of thermodynamics

$$
\rho_0(\dot{\eta}\vartheta - \dot{\epsilon}) + \boldsymbol{S}\cdot\dot{\boldsymbol{F}} - \vartheta^{-1}\boldsymbol{q}_\kappa\cdot \mathrm{Grad}\vartheta \geq 0, \tag{7.4}
$$

is used to get the following potential–type consequences :

$$
\begin{aligned}
\mathbf{0} &= \partial\psi^*/\partial\nabla\vartheta, \qquad \boldsymbol{S} = \rho_0\left[\partial\psi^*/\partial\boldsymbol{F} - \nabla\beta\otimes(\partial\psi^*/\partial\nabla\beta)\boldsymbol{F}^{-T}\right],\\
\eta &= -\partial\psi^*/\partial\vartheta, \qquad \boldsymbol{q}_\kappa = -\rho_0(\vartheta\partial F/\partial\vartheta)(\partial\psi^*/\partial\nabla\beta)\boldsymbol{F}^{-T},
\end{aligned} \tag{7.5}
$$

and a reduced inequality, with F substituted from (7.2) and Ω^* from (7.3),

$$
-\rho_0\left[(\partial F/\partial\beta)(\partial\psi^*/\partial\nabla\beta)\cdot\nabla\beta + (\partial\psi^*/\partial\boldsymbol{C}_p)\cdot\Omega^*\right] \geq 0. \tag{7.6}
$$

The first three identities of (7.5) are well-known, the last one is rather not typical (cf. [34]). The stress potential relation in $(7.5)_2$ contains two components: the first component is rather classical, while the second one represents the direct

coupling between mechanical and thermal fields in which an extra stress term appears. Substituting $\boldsymbol{q}_\kappa$ into the stress relation in (7.5) and (7.6) we get a new potential relation for the Piola-Kirchhoff stress (in terms of the heat flux) and a residual inequality, both in terms of the heat flux. Here this potential relation is presented together with the relation for the second Piola-Kirchhoff stress $\boldsymbol{S}_R$ in terms of $\nabla\beta$ and the actual heat flux vector, all in a general anisotropic case.

$$
\begin{aligned}
\boldsymbol{S} &= \rho_0 \partial\psi^*/\partial\boldsymbol{F} + (\vartheta\partial F/\partial\vartheta)^{-1}(\nabla\beta \otimes \boldsymbol{q}_\kappa), \\
\boldsymbol{S}_R &= \rho_0 \boldsymbol{F}^{-1}\left[\partial\psi^*/\partial\boldsymbol{F} - \nabla\beta \otimes (\partial\psi^*/\partial\nabla\beta)\boldsymbol{F}^{-T}\right], \\
\boldsymbol{q} &= -\rho\vartheta(\partial\psi^*/\partial\nabla\beta)(\partial F/\partial\vartheta)\ .
\end{aligned} \tag{7.7}
$$

Let us assume in $(7.7)_3$ a linear relation with respect to $\nabla\beta$. Then due to the principle of material frame indifference this will be true if the free energy function is of the form

$$
\psi^* = \psi_1^*(\boldsymbol{B}, \vartheta, \boldsymbol{C}_p) + 0.5\psi_2^*(\boldsymbol{B}, \vartheta, \boldsymbol{C}_p)\nabla\beta \cdot \nabla\beta, \tag{7.8}
$$

where the factor 0.5 has been assumed for convenience only, with $\boldsymbol{B} = \boldsymbol{F}\boldsymbol{F}^T$; assuming this, Eq. $(7.7)_3$ turns into

$$
\boldsymbol{q} = -\alpha^*(\boldsymbol{B}, \vartheta, \boldsymbol{C}_p)\nabla\beta \ \text{ with } \ \alpha^*(\boldsymbol{B}, \vartheta, \boldsymbol{C}_p) = \rho\vartheta\partial F/\partial\vartheta\ \psi_2^*(\boldsymbol{B}, \vartheta, \boldsymbol{C}_p)\ . \tag{7.9}
$$

In the present case, the independence of the free energy function of β leads to splitting the function $F(\vartheta, \beta)$ into two independent terms

$$
F(\vartheta, \beta) = F_1(\vartheta) + F_2(\beta). \tag{7.10}
$$

Moreover, in the linear case (7.9) the proportionality material coefficient α^* has to be independent of both strains, i.e.

$$
\alpha^*(\boldsymbol{B}, \vartheta, \boldsymbol{C}_p) = \alpha^*(\vartheta), \quad \psi_2^*(\boldsymbol{B}, \vartheta, \boldsymbol{C}_p) = \psi_{21}^*(\vartheta)J \ \text{ and } \ \boldsymbol{q} = -\alpha^*(\vartheta)\ \nabla\beta, \tag{7.11}
$$

with $\psi_{21}^* \geq 0$.

If the internal energy $\epsilon^* = \psi^* + \vartheta\eta^*$ is independent of $\nabla\beta$ then the function ψ_{21}^* is linear in ϑ, i.e. $\psi_{21}^*(\vartheta) = \psi_{20}\vartheta$. In this case Eq. $(7.7)_1$ due to (7.8) will take the form

$$
\boldsymbol{S} = 2\rho_0(\partial\psi_1^*/\partial\boldsymbol{B})\boldsymbol{F} + \rho_0\psi_{20}\vartheta J(0.5|\nabla\beta|^2\boldsymbol{I} - \nabla\beta \otimes \nabla\beta)\boldsymbol{F}^{-T}, \tag{7.12}
$$

or equivalently, using $(7.11)_3$,

$$
\boldsymbol{S} = 2\rho_0(\partial\psi_1^*/\partial\boldsymbol{B})\boldsymbol{F} + \rho_0\frac{\psi_{20}\vartheta J}{\alpha^*(\vartheta)^2}(0.5|\boldsymbol{q}|^2\boldsymbol{I} - \boldsymbol{q} \otimes \boldsymbol{q})\boldsymbol{F}^{-T}\ , \tag{7.13}
$$

with $\alpha^*(\vartheta) = \rho_0\psi_{20}^*\vartheta^2 F_1'(\vartheta)$.

Let us notice that even in this simplified case the stress–strain-temperature relation has an extra term due to the thermo-mechanical coupling; this term can be called an *extra thermal stress*. This contribution can have a substantial meaning in describing thermo-mechanical coupling phenomena in viscoplastic materials. We assume for the material the property of *isotropy*. Hence, the free energy function can be expressed in terms of the right Cauchy-Green stress tensor $\boldsymbol{C}$ instead of the left one $\boldsymbol{B}$. Moreover, for the mechanical response a neo-Hookean type of behavior is assumed, however, in terms of the so-called elastic strain tensor $\boldsymbol{E}^e$ defined by

$$\boldsymbol{E}^e = 0.5(\boldsymbol{F}^T\boldsymbol{F} - \boldsymbol{C}_P)\ . \tag{7.14}$$

Then for the free energy function we will have

$$\psi(\boldsymbol{F}, \vartheta, \operatorname{grad}\beta, \boldsymbol{C}_P) = \psi_1(\boldsymbol{E}^e, \vartheta) + \psi_2(\boldsymbol{F}, \nabla\beta, \vartheta), \tag{7.15}$$

in which in ψ_1 the first part is quadratic and isotropic in $\boldsymbol{E}^e$:

$$\frac{\lambda}{2\rho_0}(\operatorname{tr}\boldsymbol{E}^e)^2 + \frac{\mu}{\rho_0}\operatorname{tr}(\boldsymbol{E}^e)^2 \tag{7.16}$$

while the thermo-mechanical coupling is bilinear in both variables, i.e.

$$-\frac{\gamma}{\rho_0}(\vartheta - \vartheta_0)\operatorname{tr}\boldsymbol{E}^e\,. \tag{7.17}$$

Assuming, moreover, that the specific heat is of 3rd order in temperature and independent of $\nabla\beta$, we can write

$$\begin{aligned}\psi_1(\boldsymbol{E}^e, \vartheta) = {} & \frac{\lambda}{2\rho_0}(\operatorname{tr}\boldsymbol{E}^e)^2 + \frac{\mu}{\rho_0}\operatorname{tr}(\boldsymbol{E}^e)^2 - \frac{\gamma}{\rho_0}(\vartheta - \vartheta_0)\operatorname{tr}\boldsymbol{E}^e \\ & - c_{v0}\,\vartheta\,(\ln\frac{\vartheta}{\vartheta_0} - 1)\ - \frac{1}{12}\,c_{v3}\frac{\vartheta^4}{\vartheta_0^3} - \eta_0\,(\vartheta - \vartheta_0).\end{aligned} \tag{7.18}$$

The second part we assume in the form already used in our previous paper (cf. [41])

$$\psi_2(\boldsymbol{F}, \nabla\beta, \vartheta) = 0.5\psi_{20}\vartheta\nabla\beta\cdot\nabla\beta\det\boldsymbol{F}. \tag{7.19}$$

Due to the potential relation $\eta = -\partial\psi/\partial\vartheta$ and the relation between the internal and free energies $\epsilon^* = \psi + \eta\vartheta$, the internal energy is independent of $\nabla\beta$ and has the form

$$\begin{aligned}\epsilon^*(\boldsymbol{E}^e, \vartheta) = {} & \frac{\lambda}{2\rho_0}(\operatorname{tr}\boldsymbol{E}^e)^2 \\ & + \frac{\mu}{\rho_0}\operatorname{tr}(\boldsymbol{E}^e)^2 + \frac{\gamma}{\rho_0}\vartheta_0\operatorname{tr}\boldsymbol{E}^e + c_{v0}\vartheta + \frac{1}{4}\,c_{v3}\frac{\vartheta^4}{\vartheta_0^3} + \eta_0\,\vartheta_0.\end{aligned} \tag{7.20}$$

Due to thermodynamical consequences for the first Piola-Kirchhoff stress tensor $\boldsymbol{S}$ we obtain the following stress–strain-temperature relation

$$\boldsymbol{S} = \lambda\ \mathrm{tr}\boldsymbol{E}^e\boldsymbol{F} + 2\mu\boldsymbol{F}\boldsymbol{E}^e - \gamma(\vartheta - \vartheta_0)\boldsymbol{F} + \rho_0\ \psi_{20}\vartheta\ J\ (0.5|\nabla\beta|^2\boldsymbol{I} - \nabla\beta\otimes\nabla\beta)\boldsymbol{F}^{-T}. \tag{7.21}$$

For the instantaneous stress tensor $\boldsymbol{S}_{RI}$ being equal to $\boldsymbol{S}_R = \boldsymbol{F}^{-1}\boldsymbol{S}$ at vanishing $\nabla\beta$ we get from (7.21)

$$\boldsymbol{S}_{RI} = \rho_0\ \boldsymbol{F}^{-1}\frac{\partial\psi_1(\boldsymbol{F},\vartheta)}{\partial\boldsymbol{F}} = \lambda\mathrm{tr}\boldsymbol{E}^e\boldsymbol{I} + 2\mu\boldsymbol{E}^e - \gamma(\vartheta - \vartheta_0)\boldsymbol{I}\ . \tag{7.22}$$

This stress tensor is used in the defintion of the over-stress function and the evolution equation for the inelastic strain (cf. (5.1) and (7.3)).

8. Conclusions

More than 20 years after the publication of Perzyna's book [3] on viscoplasticity, the theory laid down there is still alive, and there are still challenging new problems in this field.

Thanks to tremendous progress in computational methods, today it is possible to realize numerically some of the concepts developed theoretically in the period of rapid development of the viscoplastic material models.

Acknowledgement

Both authors wish to express their gratitude to Piotr Perzyna for introducing them into the world of inelastic materials. A part of the work on this paper has been done when the second author (W. K.) stayed at Fachbereich Mathematik, Universität Rostock, supported by the Alexander von Humboldt Stiftung.

References

1. P. PERZYNA and W. KOSIŃSKI, *A mathematical theory of materials,* Bull. Acad. Pol. Sci., Sér. Sci. Techn. **21**, 12, 1017–1024, 1974.
2. W. KOSIŃSKI and P. PERZYNA, *The unique material structures*, Bull. Acad. Pol. Sci., Ser. Sci. Tech. **21**, 12, 1025–1032, 1974.
3. P. PERZYNA, *Thermodynamics of inelastic materials* [in Polish], PWN, Warszawa, 1978.
4. P. PERZYNA, *Interactions of elastic-viscoplastic waves and localization phenomena in solids*, in IUTAM Sypmosium on Nonlinear Waves in Solids, August 15-20, 1993, Victoria, Canada J.L. WEGNER and F. R.NORWOOD [Eds.] ASME, pp. 114–121, 1995.

5. K. FRISCHMUTH and W. KOSIŃSKI, On the asymptotic rest property. Arch. Mech., **34**, 4, 515–521, 1982.

6. K. FRISCHMUTH and P. PERZYNA , *Thermodynamics of the modified material structure with internal state variables*, Arch. Mech., **35**, 2, 279–286, 1983.

7. K. FRISCHMUTH, W. KOSIŃSKI, and P.PERZYNA, *Remarks on mathematical theory of materials*, Arch. Mech. **38**, 1–2, 59–69, 1986.

8. W. NOLL, *A new mathematical theory of simple materials*, Arch. Ratl. Mech. Anal., **48**, 1, 1–48, 1972.

9. W. NOLL, *Lectures on the foundations of continuum mechanics and thermodynamics*, Arch. Ratl. Mech. Anal., **52**, 1, 62–92, 1973.

10. K. C. VALANIS, *Unified theory of thermomechanical behavior of viscoplastic materials*, [in:] Symp. Mech. Behav. Mater. Dyn. Loads, San Antonio 1967, Springer, New York, pp. 343–364, 1968.

11. B. D. COLEMAN and M. E. GURTIN, *Thermodynamics with internal state variables*, J. Chem. Phys. **47**, 597–613, 1967.

12. P. PERZYNA, W. WOJNO, *Thermodynamics of a rate sensitive plastic material*, Arch. Mech. Stos., **20**, 5, 491–511, 1968.

13. P. PERZYNA, *The constitutive equations for rate-sensitive plastic materials*, Quart. Appl. Math. **20**, 4, 321–332, 1963.

14. K. FRISCHMUTH, *Regularization methods for non-smooth dynamical problems*, [in:] "Dynamical Problems in Mechanical Systems IV", Proc. of the 4th Polish-German Workshop, July 30 – August 4, 1995 in Berlin, R. BOGACZ, G. P. OSTERMEYER and K. POPP [Eds.], IPPT PAN, Warsaw, pp. 99–108, 1996.

15. D. Y. TZOU, *Shock wave formation around a moving heat source in a solid with finite speed of heat propagation*, Int. J. Heat Mass Transfer **32**, 10, 1979, 1989.

16. JR. L.G. HECTOR, W.-S. KIM, M. N. ÖZISIK, *Hyperbolic heat conduction due to a mode locked laser pulse train*, Int. J. Engng. Sci., **30**, 12, 1731–1744, 1992.

17. C. C. ACKERMAN, B. BERTMAN, H. A. FAIRBANK, R. A. GUYER, *Second sound in solid helium*, Phys. Rev. Letters, **16**, 789–791, 1966.

18. H. E. JACKSON, C. T. WALKER, T. F. MCNELLY, *Second sound in NaF*, Phys. Rev. Letters, **25**, 1, 26–28, 1970.

19. H. E. JACKSON, and C. T. WALKER, *Thermal conductivity, second sound, and phonon-phonon interactions in NaF*, Physical Review B, **3**, 4, 1428–1439, 1971.

20. V. NARAYANAMURTI, R. C. DYNES, *Observation of second sound in Bismuth*, Phys. Rev. Letters, **28**, 22, 1461–1465, 1972.

21. Y. M. PAO, D. K. BANERJEE, *Thermal pulses in dielectric crystals*, Lett. Appl. Engng. Sci. **1**, 33–41, 1973.

22. W. DREYER, H. STRUCHTRUP, *Heat pulse experiments revisited*, Continuum Mech. Thermodyn., **5**, 3–50, 1993.

23. D. S. CHANDRASEKHARAIAH, *Hyperbolic thermoelasticity: A review of recent literature*, Applied Mechanics Review, **51**, 12, 1, 705–729, 1998.

24. D. D. JOSEPH, L. PREZIOSI, *Heat waves*, Rev. Mod. Phys. **61**, 41, 1–62, 1989, Addendum, Rev. Mod. Phys. **62**, 2, 375–392, 1990.

25. D. JOU, J. CASAS-VÁZQUEZ, G. LEBON, *Extended irreversible thermodynamics revisited* (1988–98), Rep. Prog. Phys., **62**, 1035–1142, 1999.

26. W. KOSIŃSKI, *Elastic waves in the presence of a new temperature scale*, in "Elastic Wave Propagation"M. F. MCCARTHY and M. HAYES [Eds.], Elsevier Science (North Holland), 629–634, New York 1989.

27. J. C. MAXWELL, *On the dynamical theory of gases*, Phil. Trans. Royal. Soc. London **157**, 49–101, 1867.

28. C. CATTANEO, *Sulla conduzione del calore*, Atti Sem. Mat. Fis. Univ. Modena, **3**, 83–101, 1948.

29. C. CATTANEO, *Sur une forme de l'equation de la chaleur, èliminant le paradoxe d'une propagation instantanée*, Comp. Rend. Sci., **247**, 431–433, 1958.

30. M. P. VERNOTTE, *Les paradoxes de la theorie continue de l'equation de la chaleur*, Comp. Rend. Sci., **246**, 3154–3155, 1958.

31. S. KALISKI, *Wave equation of heat conduction*, Bull. Acad. Polon. Sci., Série Sci. Tech., **13**, 4, 211–219, 1965.

32. M. E. GURTIN, A. C. PIPKIN, *A general theory of heat conduction with finite wave speeds*, Arch. Ratl. Mech. Anal., **31**, 113–126, 1968.

33. W. KOSIŃSKI, P. PERZYNA, *Analysis of acceleration waves in materials with internal parameters*, Arch. Mech., **24**, 4, 1972, 629–643, 1972.

34. W. KOSIŃSKI, *Thermal waves in inelastic bodies*, Arch. Mech., **23**, 733–748, 1975.

35. B. D. COLEMAN M. FABRIZIO, R. OWEN, *On the thermodynamics of second sound in dielectric crystals*, Arch. Ratl. Mech. Anal., **80**, 2, 135–158, 1982.

36. K. FRISCHMUTH, V. A. CIMMELLI, *Numerical reconstruction of heat pulse experiments*, Int. J. Engng. Sci., **33**, 2, 209–215, 1995.

37. M. ARCISZ, W. KOSIŃSKI, *Hugoniot relations and heat conduction laws*, J. Thermal Stresses, **19**, 1, 17–37, 1996.

38. W. KOSIŃSKI, *Hyperbolic framework for thermoelastic materials*, Arch. Mech., **50**, 3, 423–450, 1998.

39. V. A. CIMMELLI, W. KOSIŃSKI, *Nonequilibrium semi-empirical temperature in materials with thermal relaxation*, Arch. Mech., **43**, 6, 753–767, 1991.

40. V. A. CIMMELLI, W. KOSIŃSKI and K. SAXTON, *Modified Fourier law – comparison of two approaches*, Arch. Mech., **44**, 4, 409–415, 1992.

41. W. KOSIŃSKI, K. FRISCHMUTH, *Thermomechanical coupled waves in a nonlinear medium*, Wave Motion, **34**, 1, 131–141, 2001.

42. W. KOSIŃSKI, *A modified hyperbolic framework for thermoelastic materials with damage*, [in:] Problems of Environmental and Damage Mechanics, Proc. of the XXXI Polish Solid Mechanics Conference SolMec'96, Mierki near Olsztyn, September 9–14, 1996, W. KOSIŃSKI, R. DE BOER and D. GROSS [Eds.], IPPT PAN, Warszawa, 157–172, 1997.

43. W. KOSIŃSKI, *Thermodynamics of continua with heat waves*, [in:] Thermoelastic Problems and Thermodynamics of Continua, Proc. of the 1995 Joint ASME Applied Mechanics and Materials Summer Meeting, Los Angeles, California, June 28-30, 1995, UCLA, L. BROCK [Ed.], AMD Vol. 198, American Society of Mechanical Engineers, New York, 19–25, 1995.

Received July 26, 2002; revised version November 12, 2002.

Arch. Mech., **54**, 5-6, pp. 459–478, Warszawa 2002

Visco-plasticity of polycrystalline tantalum - rational phenomenology in constitutive modeling

J. R. KLEPACZKO

Metz University,
Laboratory of Physics and Mechanics of Materials,
Ile du Saulcy, 57045 Metz, France,
e-mail: klepaczko@lpmm.univ-metz.fr

Dedicated to Professor Piotr Perzyna
on the occasion of his 70^{th} birthday

CONSTITUTIVE MODELING based on the so-called rational phenomenology (materials science approach) has been applied to take into account strain hardening, strain-rate sensitivity, thermal effects and evolution of microstructure in a polycrystalline tantalum. A wide range of strain rate in shear (10^{-4} 1/s $< \dot{\Gamma} <$ 5*10^3 1/s) and homologous temperature ($0.05 < \Theta < 0.2$) is considered. Behavior of tantalum is understood as an example for BCC polycrystalline metals. The constitutive modeling provided a possibility to determine all material constants via the experimental results obtained on thin tubular specimens using a fast hydraulic machine and a torsion Hopkinson bar. Finally, the model predictions are demonstrated by numerical simulations for different history paths in strain rate and temperature.

1. Introduction

POLYCRYSTALLINE TANTALUM, symbol Ta, BBC crystalline structure, melting point T_m = 3290 K, density ρ = 15.0 [g/cm^3], and heat capacity at 25^o C : C_p = 0.140 [J/g K], is used in many industries and not only in military applications. Its very high plasticity is very attractive in many applications, for example in cumulative charges.

Application of tantalum in extreme conditions demands extensive numerical calculations with relatively good precision. Unfortunately, practically in all cases very simple constitutive relations are used for such a purpose with pure phenomenological parameters. It is clear that more advanced approaches must be introduced in order to improve numerical calculations. Because of more efficient numerical codes and much faster computers which have been introduced recently, more advanced constitutive modeling can be used in those codes. For example, the so-called MTS model (Mechanical Threshold Stress), [1], has more recently been applied to tantalum and tantalum-tungsten alloys [2]. Still more

advanced constitutive modeling has been proposed in the series of papers by this author, [3-7]. All constitutive relations derived on the basis of materials science are founded on the concept of thermal activation processes, for example [8-11].

It is well established that plastic deformation of crystalline materials is accomplished by motion of dislocations. Dislocations are generated, multiplied, and partly annihilated during plastic deformation occurring with a specified strain rate. Velocities of edge and screw dislocations substantially increase, sometimes by several orders of magnitude, when the effective shear stress is increased above the threshold level, for example [13]. Thermal motion of atoms is manifested by temperature. The thermal vibrations with Debye frequency $\nu_D \approx 10^{13}\ 1/s$, and the vibration energy $W = kT$, where k is the Boltzmann constant and T is the absolute temperature, assist in most of the dislocation processes and cause certain rate and temperature effects in plasticity. Some processes are athermal, that is the energy of thermal vibration is not high enough to activate a process. For example, the thermal vibrations of atoms cannot play any role in generation of the dislocations by the Frank-Read multiplication mechanism, since the threshold energy is much higher than that could be supplied by the thermal vibrations, [14]. On the contrary, the movement of dislocations can be thermally activated with the assistance of the effective shear stress τ^* acting on the glide plane, [10]. In the simplest case the fundamental relation has been established between the shear strain Γ, shear strain rate $\dot{\Gamma}$ on the glide plane, the absolute temperature T and the effective shear stress τ^*, in the form of Arrhenius relation

$$\dot{\Gamma} = \dot{\Gamma}_0 \exp\left[\exp(-\frac{\Delta G(\tau*)}{kT})\right] \tag{1.1}$$

where $\dot{\Gamma}_0$ is the frequency factor related to the characteristic frequency of vibration of the moving dislocation and to the Debye frequency, $\Delta G(\tau^*)$ is the energy activation or free Gibbs energy, [8-12]. The relation in the form of the effective stress versus absolute temperature provides fundamental information on the nature of a thermally activated process of plastic deformation. If the expression for the energy of activation is linearized with respect of the effective stress, that is

$$\Delta G = G_0 - (\tau - \tau_\mu)\, v* \qquad \text{where} \quad \tau* = \tau - \tau_\mu, \tag{1.2}$$

the total shear stress τ on the slip plane can be written as

$$\tau = \tau_\mu + \frac{G_0}{v*}\left[1 - \frac{kT}{G_0} \ln\left(\frac{\dot{\Gamma}_0}{\dot{\Gamma}}\right)\right]. \tag{1.3}$$

The stress component τ_μ is called the athermal stress or the internal stress. The activation volume v* can be defined in general as

$$v* = -\frac{\partial \Delta G}{\partial \tau*}. \tag{1.4}$$

In the case of linearization, the activation volume is determined with respect to the total stress τ

$$v = -\frac{\partial \Delta G}{\partial \tau} \quad \text{and} \quad v = v^*. \tag{1.5}$$

Relation $((5.4)_3)$ can be rewritten in the following form:

$$\tau = \tau_\mu + \tau_0^* \Big[1 - \frac{MkT}{G_0} \log\Big(\frac{\dot{\Gamma}_0}{\dot{\Gamma}}\Big)\Big] \tag{1.6}$$

where M = 2.3026 (conversion factor to decimal logarithm) and $\tau_0^* = G_0/v^*$ is the threshold shear stress at $T = 0$ or $\dot{\Gamma} = \dot{\Gamma}_0$. Since the thermally activated component of the shear stress must be always positive, the following condition must be imposed on Eq. (1.6):

$$\frac{MkT_C}{G_0} \log\Big(\frac{\dot{\Gamma}_0}{\dot{\Gamma}_C}\Big) \geq 1 \quad \text{or} \quad T_C \log\Big(\frac{\dot{\Gamma}_0}{\dot{\Gamma}_C}\Big) \geq \frac{G_0}{Mk}. \tag{1.7}$$

Values of the critical absolute temperature T_C and critical strain rate $\dot{\Gamma}_C$ define the critical point on the $(T, \dot{\Gamma})$ plane. If $T > T_C$ or $\dot{\Gamma} < \dot{\Gamma}_C$ then $\tau = \tau_\mu$.

In reality, the linear case may by a good approximation at relatively low temperatures. For example in Fig. 1 is shown the change in flow stress of a single crystal of tantalum with temperature at the strain rate $8*10^{-5}$ 1/s, the data reconstituted after [15] for three levels of shear strain: 0.01, 0.04 and 0.08. It is interesting to note, as it was stated in [15], that the changes of the flow stress with temperature are independent of the crystal orientation. Such behavior can be explained by the existence of a single thermally activated process true for all orientations. It is well known that for BCC metals the adequate process is the kinetics of the dislocation movement over the Peierls potential, [8.12]. In BCC metals the Peierls potential is relatively high, this is the potential of the lattice itself. Figure 1 shows also that the strain hardening, not taken into account in the analysis given above, must be considered in more advanced versions of constitutive modeling. The simplest approach is to include all strain hardening effects into the internal stress τ_μ. This concept leads to a variety of models proposed by different authors. The set of such models can be written as

$$\tau = \tau(\Gamma_p, T) + \tau_0^* [1 - \frac{MkT}{G_0} \log(\frac{\dot{\Gamma}_0}{\dot{\Gamma}_p})] \tag{1.8}$$

where Γ_p is the plastic shear strain.

Even if the strain hardening effects on the flow stress are included as it is done in Eq. (1.8), this simple approach is not capable of accounting for variety of effects related to micro-structural evolution at different strain rates and

temperatures, for example [3, 16, 17]. Those effects had been studied for many decades and they have provided many data which should be included into more advanced constitutive modeling. One of such approaches is presented in the next part of this paper.

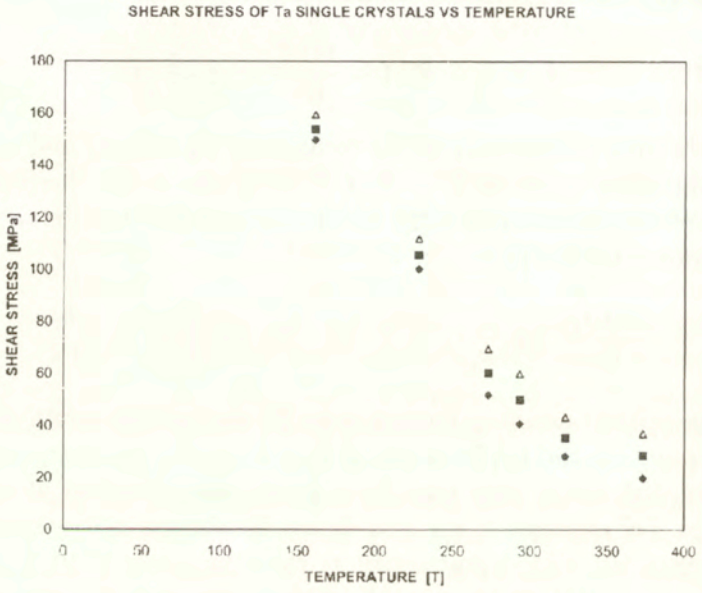

FIG. 1. Changes in flow stress of single crystals of Ta with temperature at $\dot{\Gamma} = 8 * 10^{-5}$ 1/s, reanalyzed data after [15].

2. The constitutive formalism

The constitutive modeling applied to polycrystalline tantalum is based on a consistent approach to the kinetics of macroscopic plastic flow of metals with BCC and FCC structures. The approach is called "the rational phenomenology", [18]. All variables and parameters are defined as physically based. However, the microscopic variables are used in the macroscopic scale as the mean ones, for example density of dislocations, with no statistical specification how the transition into the mean values was obtained. It is believed that such an approach is justified for statistics of large numbers. The set of relations between particular variables and parameters combined in a specific order is called the constitutive formalism. Although in general the same or similar standard relations known in materials science are applied, their combination and use decide about efficiency and logic of the formalism.

In the approach presented here the constitutive formalism is applied with the *one* constitutive variable that is the total dislocation density ρ. It is assumed that plastic deformation in shear is the fundamental mode in metals plasticity. It is assumed further that at constant microstructure the flow stress τ consists of two components: the internal stress τ_μ and the effective stress τ^*, thus

$$\tau = \tau_\mu[s_i, h(\dot{\Gamma}_p, T)]_{STR} + \tau^*[(s_i, \dot{\Gamma}_p, T)]_{STR} \tag{2.1}$$

where s_i is a number, so far unspecified, of internal state variables which define the current microstructure, [5, 6], $h(\dot{\Gamma}_p, T)$ is the thermal-mechanical history of plastic deformation, Γ_p and $\dot{\Gamma}_p$ are, respectively, plastic shear strain and plastic shear strain rate. In the next part of the paper the subscript "p" will be omitted. It is important to note that the plastic strain does not enter directly into relation (2.9). Plastic strain can not be assumed in the materials science approach as an independent variable, or argument in constitutive relations, since the process of defect accumulation (plastic strain) depends on the past thermal-mechanical history. In relation (2.1) the internal stress τ_μ is caused, therefore, by the long-range, strong obstacles to dislocation motion, and the effective stress τ^* is due to thermally activated short-range obstacles. In fact, the internal stress τ_μ must be indirectly rate- and temperature-dependent via dislocation rearrangement and annihilation (recovery), during the whole process of plastic deformation.

In the case of *one* internal state variable assumed here as the total dislocation density ρ, Eq. (2.1) can be simplified to the form

$$\tau = \tau_\mu[\rho, h(\dot{\Gamma}, T)] + \tau^*(\rho_m, \dot{\Gamma}, T) \tag{2.2}$$

where ρ_m is the mobile dislocation density. In the one-variable approach the mobile dislocation density is directly related to the total density by the relation

$$\rho_m = f\,\rho, \qquad f \leq 1. \tag{2.3}$$

In general, the microstructure can be characterized by five instantaneous quantities: ρ, ρ_m , d, D and Δ, where ρ and ρ_m are the mean values over few subgrains, d, D and Δ are respectively, the subgrain diameter, the grain diameter and the mean distance between the twins, [5, 6]. The explicit form for the internal stress τ_μ can be written for a constant temperature as follows, [5, 6]

$$\tau_\mu = \alpha_1\,\mu\,b\,\sqrt{\rho} + \alpha_2\,\mu\left(\frac{b}{d(\rho)}\right)^{\delta} + \alpha_3\,\mu\left(\frac{b}{D}\right) + \alpha_4\,\mu\left(\frac{b}{\Delta}\right). \tag{2.4}$$

The first three terms in Eq. (2.4) are related respectively to dislocation-long range obstacle interaction, evolution of sub-grain size d and the effect of grain diameter D, so-called the Hall-Petch term. The fourth term accounts for twin

formation typically observed at very low temperatures or at very high strain rates. The constants α_1, α_2, α_3, and α_4 are the interaction constants showing the fraction contribution of each micro-mechanism to the total value of the internal stress τ_μ, b is the modulus of the Burgers vector . The power δ in the second term has a dual nature, $\delta = 1.0$ for cells and small sub-grains with large mis-orientations, and $\delta = 1/2$ for "ideal" sub-grains in thermally recovered metals, [19]. Finally, μ is the shear modulus. Although evolution of sub-grains and twins are observed in BCC metals, their contribution is assumed here as the second order effect. The effect of grain diameter D is automatically included into the generalized interaction coefficient α. Equation (2.4) can be rewritten in the following form:

$$\tau_\mu = \mu b \sqrt{\rho} \left\{ \alpha_1 + \alpha_2 [b \rho d(\rho)]^{-1/2} + \alpha_3 [b \rho D]^{-1/2} + \alpha_4 [b \rho \Delta]^{-1/2} \right\} \tag{2.5}$$

The expression in the large brackets of Eq. (2.5) can be understood as a generalized coefficient $\alpha(\rho, d, D, \Delta)$ of interaction between dislocations and *all* long-range obstacles used frequently in analyses of the experimental data. With this simplification, the final form for the internal stress τ_μ and for a constant temperature case applied in this modeling, can be written as follows:

$$\tau_\mu = \alpha_0 \mu(T) b \sqrt{\rho[h(\dot{\Gamma}, T)]}, \tag{2.6}$$

where α_0 is the interaction constant at T = 0. The dislocation-obstacle interaction must be modified to include temperature-dependent changes of elastic constants. One possibility is a simple empirical relation

$$\mu(T) = \mu_0 (1 - At - BT^2) \tag{2.7}$$

where A and B are the constants, with condition $\mu(T_m) = 0$, where T_m is the melting temperature. Due to the thermal softening of the lattice, the interaction constant is also temperature-dependent

$$\alpha(T) = \alpha_0 \frac{\mu(T)}{\mu_0}. \tag{2.8}$$

All equations outlined above constitute the fundamental framework for the first part of the constitutive formalism. The most important problem arises now, how to model the micro-structural evolution at different strain rates and temperatures.

3. Kinetics of micro-structural evolution, the internal stress

It is well established that during plastic deformation of metals at different strain rates and temperatures, the rate of strain hardening may vary substan-

tially. If the strain rate and temperature is changed during the process of deformation, such variations are the source of strain rate and temperature history effects, [3, 16, 17]. One possibility is to introduce micro-structural evolution in the modeling by a set of ordinary differential equations of the first order. Each equation describes evolution of an internal state variable as a function of plastic strain. In a general case of such modeling five differential equations should be introduced for five internal state variables, ρ_i, ρ_m, d, D, Δ, where the total dislocation density ρ is split into the immobile density ρ_i and the mobile density ρ_m

$$\rho = \rho_i + \rho_m. \tag{3.1}$$

Since in BCC metals the evolution of the mobile dislocation density is very important, both densities must be accounted for. Some propositions and discussions of the evolution equations can be found elsewhere, [3-7]. A general notion is adopted that the evolution of microstructure can be described by the accumulation kinetics of defects, in the present case- of dislocations. Of course, the process of accumulation depends on the strain rate and temperature. It is assumed that the general form of evolution equation is given by

$$\frac{d\rho}{d\Gamma} = M_{eff}(\rho, \dot{\Gamma}, T), \tag{3.2}$$

where M_{eff} is the effective multiplication rate of dislocations, [20]. A simple equation for structural evolution has been derived in the following form, [5],

$$\frac{d\rho}{d\Gamma} = M_{II}(\dot{\Gamma}) - k_a(\dot{\Gamma}, T)\,(\rho - \rho_0) \tag{3.3}$$

where M_{II} is the multiplication factor at small plastic strains and $k_a(\dot{\Gamma}, T)$ is the rate and temperature- dependent annihilation factor, ρ_0 is the initial dislocation density. For BCC metals the multiplication factor M_{II} can be assumed as a constant at not very high strain rates and up to the temperature where annihilation micro-mechanisms (recovery) start to be intensified. The explicit mathematical form for k_a has been proposed for FCC metals in [5] and adapted for BCC structures in [21] as follows:

$$k_a(\dot{\Gamma}, T) = k_0 \left(\frac{\dot{\Gamma}}{\dot{\Gamma}_0}\right)^{-2m_0(\dot{\Gamma}, T_a)} \tag{3.4}$$

where k_0 and m_0 are the annihilation constants at $T = 0$, m_0 is the absolute rate sensitivity of strain hardening, $\dot{\Gamma}_0$ and T_a are respectively the frequency factor and the transition temperature. If $T \leq T_a$ or $\dot{\Gamma} \geq \dot{\Gamma}_0$ then $k_a = k_0$.

When temperature and strain rate are constant, the evolution Eq. (3.3) can be integrated with the initial conditions $\rho = \rho_0$ at $\Gamma = 0$ and solution for ρ can be found in the closed form

$$\rho(\dot{\Gamma}, T) = \rho_0 + \frac{M_{II}}{k_a[h(\dot{\Gamma}, T)]}[1 - \exp(-k_a[h(\dot{\Gamma}, T)])]. \tag{3.5}$$

If the temperature is lower than T_a, Eq. (3.5) reduces to the simpler form with $k_a = k_0$ and then the explicit form for the internal stress τ_μ is

$$\tau_\mu = \alpha(T)\,\mu_0\,b\left[\rho_0 + \frac{M_{II}}{k_0}[1 - \exp(-k_0\,\Gamma)]\right]^{1/2}, \qquad T \leq T_a. \tag{3.6}$$

It may be noted that Eq. (3.6) predicts a saturation of the internal stress at large strains. The internal stress at saturation is

$$\tau_\mu(\Gamma \to \infty) = \alpha_0\,\mu(T)\,b\left[\rho_0 + \frac{M_{II}}{k_a(\dot{\Gamma}, T)}\right]^{1/2}, \qquad T \geq T_a. \tag{3.7}$$

$$\tau_\mu(\Gamma \to \infty) = \alpha_0\,\mu(T)\,b\left[\rho_0 + \frac{M_{II}}{k_0}\right]^{1/2}, \qquad T \leq T_a. \tag{3.8}$$

A more exact evolution relation suitable for larger strains can be written as follows:

$$\frac{d\rho}{d\Gamma} = M_{II}(\Gamma) + \left[k_a(\dot{\Gamma}, T)(\rho - \rho_0)\right]^{1/2} - k_a(\dot{\Gamma}, T)(\rho - \rho_0). \tag{3.9}$$

Although differential Eq. (3.8) can be integrated for constant strain rate and temperature, the inversion to find the dislocation density $\rho(\Gamma)$ is only numerically possible.

In conclusion, the approximation (3.6) assumes the absence of the rate sensitivity of strain hardening, [22], at temperatures lower than T_a. At temperatures higher than T_a the rate sensitivity of strain hardening is present and intensifies as the strain rate decreases. It may be noted that the internal stress τ_μ is temperature-dependent even at $T < T_a$ due to the temperature-dependence of the interaction constant α via temperature-dependence of the elastic constants. It has been shown previously that the approximation of the internal stress is sufficiently exact for BCC micro-structures, for example mild steels, [4, 5, 6].

4. Kinetics of micro-structural evolution, the effective stress

The effective stress τ^*, directly related to the instantaneous rate sensitivity, [22], can be determined by inversion of the generalized Arrhenius relation, [3],

$$\dot{\Gamma} = \nu_k(\rho_m, T) \exp\left[-\frac{\Delta G(\tau^*, T, \rho_m)}{kT}\right] \tag{4.1}$$

where ν_k is the frequency factor and ΔG_k is the free energy of activation, k is the Boltzmann constant. It has been shown, for example in [8, 9, 12], that dislocations in BCC structures move by the thermally activated formation and propagation of kink pairs over the Peierls potential. A universal relation between ΔG_k and τ^* has been proposed in [12] in the form

$$\Delta G_k = 2H_k(T)\left[1 - \left(\frac{\tau^*}{\tau_p^*(T)}\right)^p\right]^q, \tag{4.2}$$

where p and q are constants that characterize the shape of a thermally activated obstacle, and in this case the Peierls potential, $2H_k$ is the total activation energy necessary to form a double kink and overcome the potential, $\tau_p * (T)$ is the Peierls stress. Both constants are temperature-dependent through the temperature changes of the elastic shear modulus, thus

$$2H_k(T) = 2H_k^0 \frac{\mu(T)}{\mu_0} \quad \text{and} \quad \tau_p^*(T) = \tau_p^0 \frac{\mu(T)}{\mu_0}, \tag{4.3}$$

where H_k^0, τ_p^0, and μ_0 are respectively the activation energy, Peierls stress, and shear modulus, all in 0 K.

When the dislocation kinetics is controlled by thermally activated overcoming of obstacle, one obtains the pre-exponential factor in the following form, [11],

$$\nu(\rho_m, T) = \rho_m \frac{bA(T)}{L(T)}\left(\frac{b}{2l(T)}\nu_D\right) \tag{4.4}$$

l is the length of the dislocation segment involved in the thermal activation, A is the area swept out by the mobile dislocation following the successful attempt, ν_D is the vibration frequency of the lattice (Debye frequency). Therefore ρ_m indicates the number of places where the thermal activation occurs, $\nu_i = (b/2L(T))\nu_D$, ν_i is the vibration frequency of the pinned dislocation of length L involved in the event, $l < L$. For the case of double kink, the pre-exponential factor can be written as

$$\nu_k = n\,\rho_m\,b^2\,\nu_D \quad \text{and} \quad n = \frac{a\,L}{2\,l_c^2}, \tag{4.5}$$

l_c is the critical length of the kink segment of dislocation. Assuming that $A = La$ and $a = b$, n becomes the non-dimensional coefficient characterizing the geometry of the double kink formation, [4]. In general, the dislocation length L is much greater than the dislocation segment l involved in the thermal activation.

The second internal state variable that enters the pre-exponential factor is the mobile dislocation density ρ_m. Since even in relatively pure BCC metals the stationary dislocations are pinned, for example by Cottrell atmospheres, [23], evolution of the mobile dislocation density must be accounted for. One, and the simplest, possibility is to assume $\rho_m = f\rho$, where f is the fraction of the total density, $f < 1$; f may change as a function of ρ and temperature. Although it can be shown that the constant value of f gives satisfactory quantitative results, more exact analyses of experimental data, mostly for steels, indicate that the fraction f is a more complicated function of ρ, $\dot{\Gamma}$ and T. At relatively low homologous temperatures, and under the assumption that the evolution of the mobile dislocation density is independent of the immobile density, a differential equation introduced in [4] has the following form:

$$\frac{d\rho_m}{d\rho} = \frac{\beta}{\rho} \tag{4.6}$$

where β is the material constant. The solution of (4.6) with the initial conditions $\rho_m = \rho_{m0}$ at $\rho = \rho_0$ has the following form:

$$\rho_m = \rho_{m0} + \beta \ln\left(\frac{\rho}{\rho_0}\right). \tag{4.7}$$

Thus, the evolution of the mobile dislocation density is a complicated function of plastic strain since in Eq. (4.7) the solution for ρ , Eq. (3.5) or (3.6), depends on the temperature domain of deformation. Thus, the solution for ρ must be introduced into (4.7). It is interesting to mention that the limit of the mobile dislocation density ρ_m is the saturation level of the total density with $f = 1$, $\rho_m(M/k_a)$

$$\rho_m\left(\frac{M_{II}}{k_a}\right) = \rho_{m0} + \beta\frac{k_a}{M_{II}} \ln\left(\frac{M_{II}}{\rho_0 k_a}\right), \quad \rho_{m0} < \rho < M_{II}/k_a. \tag{4.8}$$

The solution for the mobile dislocation density makes it possible to determine the pre exponential factor in Eq. (4.5) and define completely the effective stress τ^*. After introduction of (4.2) and (4.5) into (4.1) and inversion, the explicit expression for τ^* is obtained

$$\tau^*(\rho, \dot{\Gamma}, T) = \tau_p^* \left\{1 - \left[\frac{kT}{2H_k} \log\left(\frac{n\rho_m b^2 \nu_D}{\dot{\Gamma}}\right)\right]^{1/q}\right\}^{1/p}. \tag{4.9}$$

The total stress is defined by Eq. (2.2). In this manner the model is complete including the following Eqs. (2.6), (2.7), (2.8), (3.1), (3.4), (3.5), (4.2), (4.3), (4.5), (4.7) and (4.9). The total number of constants is 21, including the absolute physical constants: $b, H_k, n, p, q, T_m, \mu_0, \nu_D$ and τ_p^0, total 9, which can be found theoretically from physical analyses; the rest, that is 12 constants, are the constants related directly to specific material behavior and conditions of deformation.

5. Constitutive modeling of polycrystalline tantalum

The constitutive formalism applied in the case of tantalum is similar to the simplified constitutive model applied earlier to mild steels, [4]. The rate sensitivity of strain hardening is neglected, that means that relatively low homologous temperatures are considered, and the following relations are applied: (2.6), (2.7), (2.8), (3.1), (3.6), (4.2), (4.3), (4.5) and (4.7). The constants have been identified from experiments.

Experiments reported in [24] have been performed at room temperature on thin tubular specimens of annealed polycrystalline Ta in LPMM-Metz on a fast hydraulic machine, and in CEA-DAM (the French Atomic Energy Commission) on a Split Hopkinsion Torsion Bar (SHTB). Those two experimental setups permitted to cover the shear strain rates from $3*10^{-4}$ 1/s to $3*10^{2}$ 1/s not only at constant imposed values but also in the changed-strain-rate mode, that is from low to high and from high to low strain rates. The strain rate changes from lower to higher and from higher to lower strain rate were applied with the loading-unloading procedure for two initial pre-strains. The final results reproduced after [24] are shown in Fig. 2 and Fig. 3. The behavior is typical for polycrystalline BCC metals. At low strain rate, $3*10^{-4}$ 1/s, relatively high strain-hardening is observed, but at $3*10^{2}$ 1/s the rate of strain-hardening is positive at lower strains, say up to 0.3 and then zero or even negative. It may be mentioned that at strain rates higher than ~50 1/s the process of plastic deformation is practically adiabatic and about 90% of plastic work is converted into heat. Since BBC metals are very sensitive to temperature, as it is shown in Fig. 1, the decrement of stress due to adiabatic heating is not negligible and in order to compare $\tau(\Gamma)$ at different strain rates, specially at lower and at higher ones, the high strain-rate curves should be converted into isothermal conditions. A more exact discussion and a simple method of conversion were given in [17]. In the present analysis the conversion is neglected because only simplified modeling is analyzed numerically. Experiments with changed strain rates confirmed for tantalum the existence of the strain rate history effects revealed earlier for soft steels, [17, 25]. A change of strain rate from low to high values produces "overshoot" of flow stress, that is the flow stress is higher at the same strain rate as that applied in a constant

strain, rate deformation. In the case of tantalum strain rate change from $3*10^{-4}$ 1/s to $3*10^{2}$ 1/s, Fig. 2, and from $1.5*10^{-2}$ 1/s to $3*10^{2}$ 1/s produces rather small overshoots. On the contrary, change of strain rate from high to low, that is from $3*10^{2}$ 1/s to $3*10^{-4}$ 1/s, revealed a substantial "undershoot", that is all $\tau(\Gamma)$ curves are lower than that obtained at the same constant strain rate. Those strain rate history effects are quite opposite than those observed many times in various of FCC metals, for example [3, 5, 16]. It is clear that specific strain-rate history effects are found in tantalum.

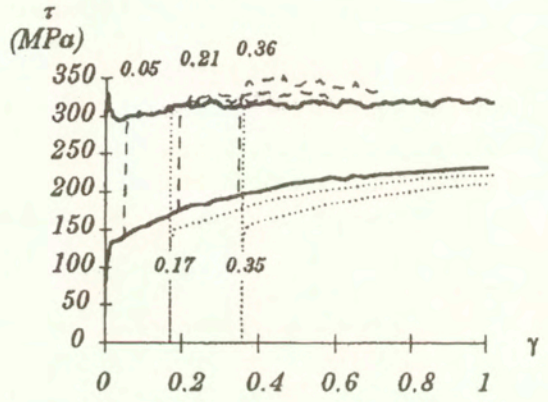

FIG. 2. Results of torsion experiments on polycrystalline Ta at two strain rates: $\dot{\Gamma} = 3.10^{-4}$ 1/s and $\dot{\Gamma} = 3 * 10^{2}$ 1/s; Constant and changed strain rates at three levels of prestrain, after [24].

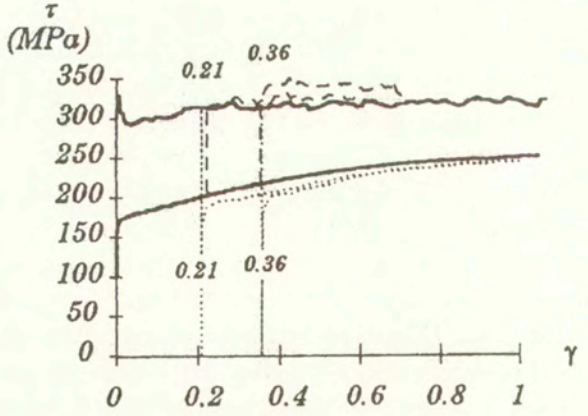

FIG. 3. Results of torsion experiments on polycrystalline Ta at two strain rates: $\dot{\Gamma} = 1.5 * 10^{-2}$ 1/s and $\dot{\Gamma} = 3 * 10^{2}$ 1/s; Constant and changed strain rates at two levels of prestrain, after [24].

The main task of this study was to apply a simplified version of the constitutive formalism with a possibility to model not only the behavior at constant strain rates but also the strain-rate history effects. The micro-structural evolution of the internal stress, dependent on strain-rate and temperature, has been neglected. The evolution of the internal stress is rate independent and was taken into account by relation (3.6). A complete set of relations describing the effective stress was used in numerical modeling, that is Eqs. (4.7) and (4.9).

In order to identify all material constants at $T = 300$ K it was assumed that $\tau^* \approx 0$ at strain rate 10^{-4} 1/s and the coefficient of interaction is $\alpha = 0.5$, for example [12]. The elastic shear modulus at RT is assumed as $\mu = 72$ GPa, and the Burgers vector b = $2.86*10^{-8}$ cm. By application of the optimization procedure by the least square method the following values of the material constants have been found: $\rho_0 = 1.25*10^{10}$ 1/cm^2, $M_{II} = 9.8*10^{11}$ 1/cm^2, $k_a = 2.2$. Those values permit to calculate the internal stress at RT.

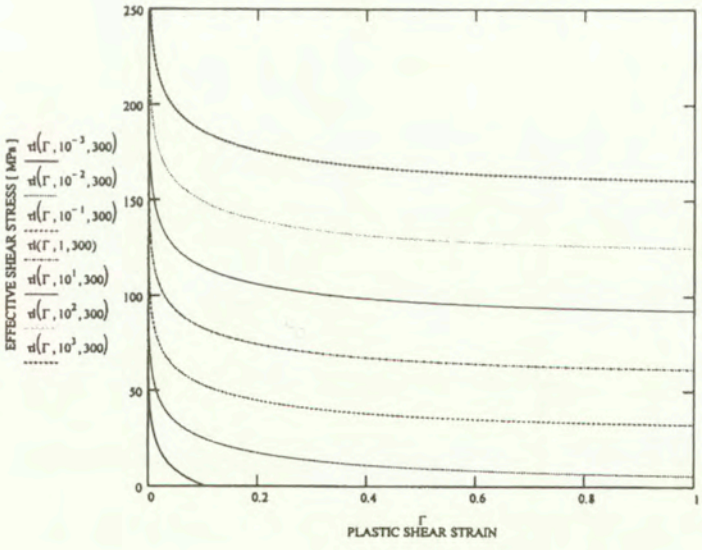

FIG. 4. Numerical calculation of the effective shear stress τ^* for Ta with plastic shear strain for 9 shear strain rates from $\dot{\Gamma} = 3 * 10^{-4}$ 1/s to $\dot{\Gamma} = 10^3$ 1/s, T=300 K.

In order to estimate the effective stress, values of the constants p and q were obtained from the literature data reporting the rate and temperature-sensitivity of Ta, [24], as $p = 1$ and $q = 8/5$, the energy of the obstacle $\Delta G_0 = 0.62$ eV. The Peierls shear stress at $T = 0$ K has been assumed as $\tau_p{}^* = 515$ MPa. The second set of constants allows to calculate the effective stress at RT. The effective stress τ^* at $T = 300$ K is shown as a function of shear strain in Fig. 4 for different strain

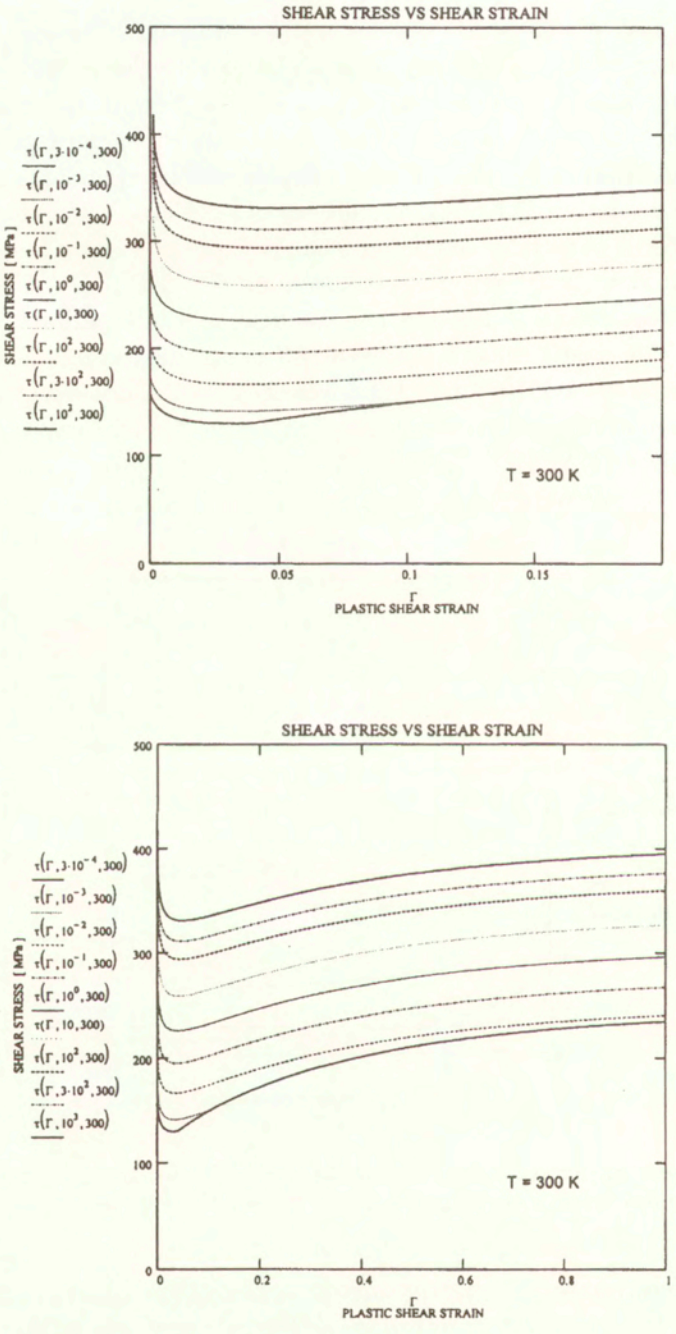

FIG. 5. Numerical calculation of the flow stress τ for Ta with plastic strain for 9 shear strain rates, steps in strain rate are the same as in Fig. 4, $T = 300$ K; (a) range of strain from 0 to 0.2. (b) range of strain from 0 to 1.0.

rates from $3*10^{-4}$ 1/s to 10^3 1/s. At low strain rates the effective stress relaxes very quickly to zero at specific strain which could be obtained from the condition: $\tau^* = 0$ at $(\dot{\Gamma}_C, T_C)$. In tantalum, as in all BCC metals, the rate-sensitivity of the effective stress is very high, [25].

The result of calculations of the flow stress at different strain rates, the same as assumed for τ^* calculations, is shown in Fig. 5.

Because all curves are calculated at $T = 300$ K and the thermal softening occurring normally at higher strain rates is neglected, the curves at strain rates 10 1/s, 10^2 1/s and $3*10^2$1/s show slightly higher rate of strain hardening than in experiments.

However, the stress levels for lower strains (a less intense adiabatic heating) are almost exactly the same as a found experimentally. The upper and lower yield stress is also determined. Although the material constants have been estimated for RT, the model includes also all features of temperature-dependence at medium and low temperatures. The temperature effect on the flow stress is shown in Fig. 6 for two levels of shear strain, $\Gamma = 0$ and $\Gamma = 1.0$, and three values of strain rate: $3*10^{-4}$ 1/s, $3*10^2$ 1/s and $5*10^3$ 1/s. As expected, the critical points $(\dot{\Gamma}_C, T_C)$ at different strain rates are shifted to higher temperatures.

Another important part of the modeling is a question how to depict the strain rate history effects. An attempt reported in [26] to approximate the same experimental data was not so successful in the sense that some constants should be adjusted to the current conditions. Here a hypothesis is pursued that when the strain rate is increased, more and more mobile dislocations are generated. This assumption will lead to history-sensitive pre-exponential factor ν_k, Eq. (4.5). The differential equation for evolution of the mobile dislocation density, Eq. (4.6), does not encompass directly the strain rate. Therefore, this equation has been modified in the following way

$$\frac{d\rho_m}{d\rho_i} = \frac{\beta}{\rho_i} + C(\dot{\Gamma}). \tag{5.1}$$

Solution with the initial conditions: $\rho_m = \rho_{m0}$ when $\rho_i = \rho_{i0}$ is in the form

$$\rho_m(\rho_i, \Gamma, \dot{\Gamma}) = \rho_{m0} + \beta \ln\left(\frac{\rho_i(\Gamma)}{\rho_{i0}}\right) + (\rho_i(\Gamma) - \rho_{i0})C(\dot{\Gamma}). \tag{5.2}$$

Since this approach is purely empirical the explicit expression for $C(\dot{\Gamma})$ is assumed as

$$C(\dot{\Gamma}) = \eta \ln\left(\frac{\dot{\Gamma}}{\dot{\Gamma}_0}\right). \tag{5.3}$$

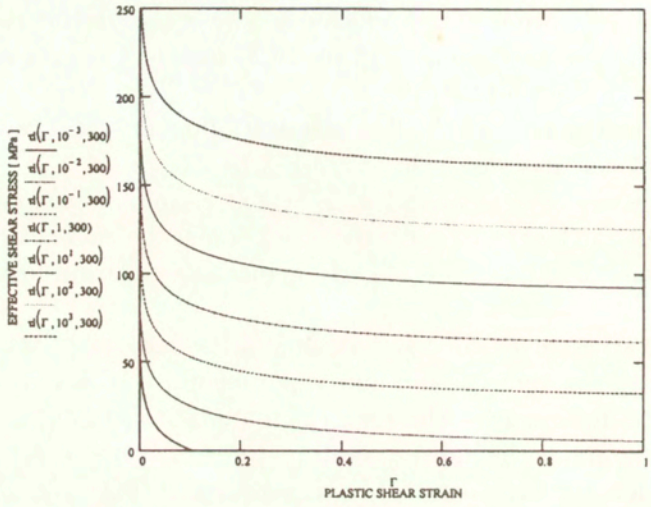

FIG. 6. Numerical calculation of the flow stress for Ta with temperature for two levels of strain and three strain rates: $\dot{\Gamma}$= 3*10^{-4} 1/s, 3*10^{2} 1/s and 5*10^{3} 1/s.

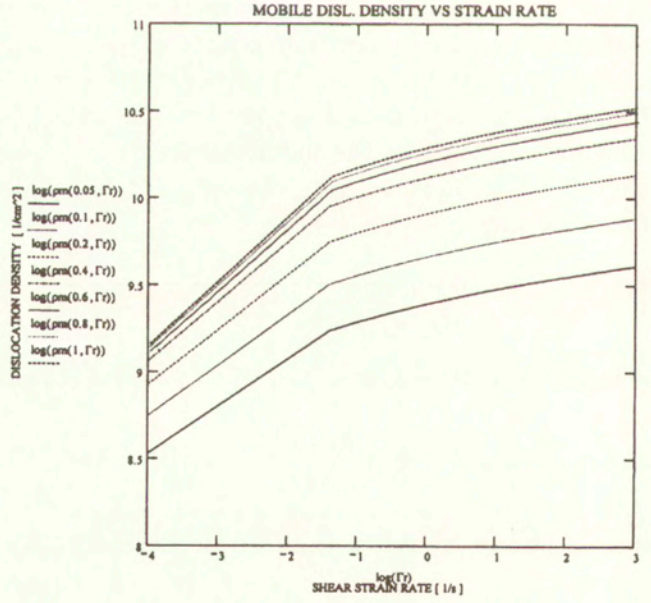

FIG. 7. Mobile dislocation density calculated after Eqs. (5.2) and (5.3) in $\log(\rho_m)$ [1/cm^2] vs. log ($\dot{\Gamma}$) [1/s] for 7 different strains from 0.05 to 1.0.

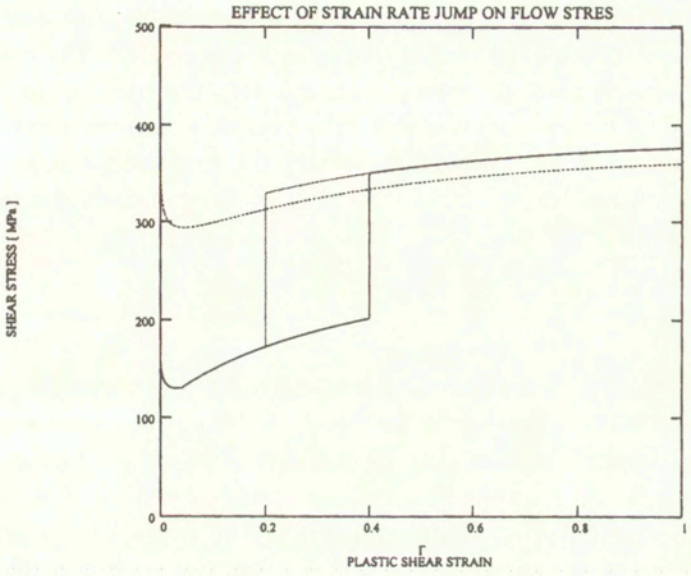

FIG. 8. Schematic simulation of strain rate jump test from $\dot{\Gamma}$ $3*10^{-4}$ 1/s to $3*10^{2}$ 1/s for two prestrains Γ : 0.2 and 0.4.

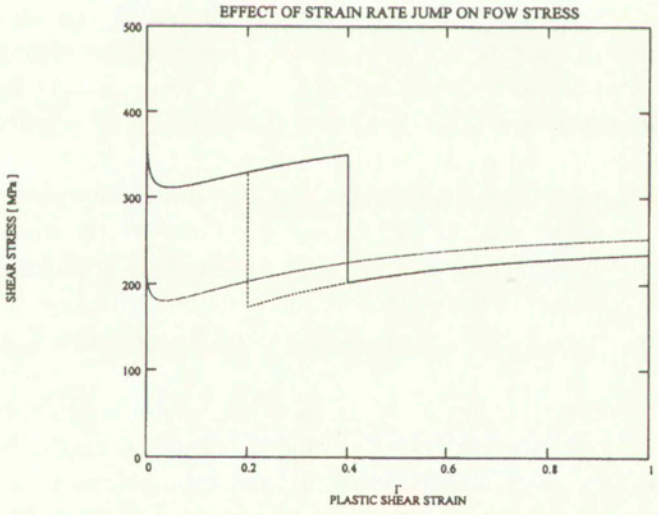

FIG. 9. Schematic simulation of strain rate jump test from $\dot{\Gamma}$ $3*10^{2}$1/s to $3*10^{-4}$ 1/s for two prestrains Γ : 0.2 and 0.4.

With the constants $\beta = 10^{9}$ cm $^{-2}$ and $\eta = 5*10^{-2}$, the evolution of the mobile dislocation density in the double logarithmic scale for different levels of

strain is shown in Fig. 7. That relation was used to calculate the strain rate jump tests from $3*10^{-4}$ 1/s to $3*10^{2}$ 1/s at two strains: 0.2 and 0.4. The result is shown in Fig. 8. Similar calculations were performed with the jump from $3*10^{2}$ 1/s to $3*10^{-4}$ 1/s, the result is shown in Fig. 9. It is clear that those artificial simulations yield results as expected, the overshoot and the undershoot are obtained. Of course, in the future a more vigorous analysis is needed from the point of view of materials science.

6. Conclusions

It has been shown that the constitutive formalism in its simplified form can approach visco-plastic behavior of polycrystalline tantalum at low as well as at relatively high strain rates. In this version of modeling, all material constants have been identified and applied in numerical analyses. As it is shown in Fig. 6, the simplified model has its limits concerning the range of temperature. The temperature limit is estimated as $T \approx 400$ K. The room temperature constitutes for tantalum the homologous temperature $\Theta_{RT} = 0.091$ and 400 K yields $\Theta = 0.122$. Thus, the modeling of visco-plasticity around room temperature is practically limited to the low temperature behavior. A complete model should include rate and temperature-dependent dislocation annihilation and rearrangement in the form of Eqs. (3.4) and (3.5). However, the simplified version can approach quantitatively the shear stress – shear strain characteristics within wide ranges of strains and strain rates. Of course, use of the formalism in 3D is possible, especially in the more advanced numerical calculations, by application of some visco-plasticity theory, for example [27, 28].

Since some applications of polycrystalline tantalum takes place frequently in the form of plates after cold rolling, a problem of anisotropy arises, for example [29,30]. In the 1D formalism presented here the isotropy is assumed, however it is important to mention that the interaction constant α in Eqs. (2.6) and (3.6) has a directional character and an anisotropy can be introduced directly in that way.

In general, constitutive formalisms based on the materials science approach should be introduced into variety of advanced numerical codes. Such modeling includes evolution of microstructure at different strain rates and temperatures, a very important factor at high strain rates.

References

1. P. S. FOLLANSBEE and U. F. KOCKS, *A constitutive description of the deformation of copper based on the use of mechanical threshold stress as an internal state variable,* Acta Metallurgica, **36**, 81, 1988.

2. S. R. CHEN and G. T.GRAY III, *Constitutive behavior of tantalum and tantalum-tungsten alloys,* Met. Trans. **27A**, 2994, 1996.

3. J. R. KLEPACZKO, *Thermally activated flow and strain rate history effects for some polycrystalline fcc metals,* Material Science and Engineering, **18,** 121, 1975.

4. J. R. KLEPACZKO, *An engineering model for yielding and plastic flow of ferritic steels,* in: High Energy Rate Fabrication, ASME, 45, New York 1984.

5. J. R. KLEPACZKO, *Modeling of structural evolution at medium and medium strain rates, FCC and BCC metals,* [in:]Constitutive Relations and Their Physical Basis, Riso Natl. Laboratory, 387, Roskilde, Denmark, 1987.

6. J. R. KLEPACZKO, *A general approach to rate sensitivity and constitutive modeling of fcc and bcc metals,* [in:] Impact: Effects of Fast Transient Loadings, A.A.Balkema, Rotterdam, Netherlands, 3, 1988.

7. J. R. KLEPACZKO, *Constitutive modeling in dynamic plasticity based on physical state variables: A review,* [in:] Int. Conf. on Mechanical and Physical Behaviour of Materials under Dynamic Loading, Les editions de physique, Les Ulis, France, C3-553, 1988.

8. J. FRIEDEL, *Les Dislocations, Gauthier-Villars,* Paris, English translation: Addison - Wesley, Reading, Massachsetts, 1964.

9. H. CONRAD, *Thermally activated deformation in metals,* Journal of Metals, **16**, 582, 1964.

10. A. SEEGER, *The mechanism of glide and work hardening in FCC and HCP metals,* in: Dislocations and Mechanical Properties of Crystals, p.271, J.Wiley, New York, 1957.

11. B. DE MEESTER, C. YIN, M. DONNER and H. CONRAD, *Thermally activated deformation in solids,* in: Rate Processes in Plastic Deformation of Materials, ASM, New York, 175, 1974.

12. U. F. KOCKS, A. S. ARGON and M. F. ASHBY, *Thermodynamics and Kinetics of Slip,* Pergamon Press, Oxford, England 1975.

13. W. G. JOHNSTON and J. J. GILMAN, *Dislocation velocities, dislocation densities, and plastic flow in lithium fluoride crystals,* Journal of Applied Physics, **31**, 632, 1959.

14. F. C. FRANK and W. T. READ, *Multiplication process for slow moving dislocations,* Physics Review, **79**, 772, 1950.

15. B. MORDIKE, *Plastic deformation of zone refined tantalum single crystals,* Zeitschrift fur Metallkunde, **53**, 586, 1962.

16. J. R. KLEPACZKO and J. DUFFY, *Strain rate and temperature memory effects for some polycrystalline FCC metals,* Proc. Conf. on Mechanical Properties of Materials at High Rates of Strain, Ser. No. 21, The Institute of Physics, Oxford, England p. 91, 1974.

17. J. R. KLEPACZKO and J. DUFFY, *Strain rate history effects in Body-Centered-Cubic metals,* in: Mechanical Testing for Deformation Model Development, ASTM STP 765, ASTM, p. 251, 1974.

18. H. J. FROST and M. F. ASHBY, *Deformation-mechanism maps: the plasticity and creep of metals and ceramics,* Pergamon Press, Oxford 1982.

19. F. R. N. NABARRO, *Work hardening in face-centered cubic single crystals,* [in:] Strength of Metals and Alloys, Proc. International Symposium CMA-7, Pergamon Press, **3**, p.545, Oxford 1986.

20. J. J. GILMAN, *Micromechanics of flow of solids,* Mc Graw-Hill, New York 1969.

21. N. E. ZEGHIB, *Etude experimentale et modelisation de la deformation plastique tenant compte du vieillissement dynamique, cas ses aciers doux,* These de Doctorat, Universite de Metz, France, 1990.

22. J. R. KLEPACZKO and C. Y. CHIEM, *On rate sensitivity of FCC metals, instantaneous rate sensitivity and rate sensitivity of strain hardening,* Journal of the Mechanics and Physics of Solids, **34**, 29, 1986.

23. A. H. COTTRELL, *Dislocations and plastic flow in crystals,* Oxford University Press, London 1953.

24. F. BUY, *Etude experimentale et modelisation du comportement plastique d'un tanatle. Prose en compte de la vitesse de deformation et du trajet de chargement,* These de Doctorat, Universite de Metz, France, 1996.

25. J. R.KLEPACZKO, *The relation of thermally activated flow in BCC metals and ferritic steels to strain rate history effects,* Technical Report, Division of Engineering, Brown University, Providence, (April 1981).

26. F. BUY, J. FARRE, J. R. KLEPACZKO and G. TALABART, *Evaluation of the parameters of constitutive model for b.c.c. metals based on thermal activation,* [in:] Proc. of Int.Conf. on Mechanical and Physical Behavior of Materials under Dynamic Loading, Coll.C3, Les editions de physique, Les Ulis, France, p. C3-631, 1997.

27. P. PERZYNA, *The constitutive equations for rate-sensitive materials,* Quart. Applied Mathematics, **20**, 321, 1963.

28. S. R. BODNER, *Unified plasticity for engineering applications,* Kluwer Academic- Plenum Publishers, New York 2002.

29. S. I. WRIGHT, G. T. GRAY III and A. D. ROLLET, *Textural and microstructural gradient effects on the mechanical behavior of a tantalum plate,* Met. Mat. Trans., **25A**, 1025, 1994.

30. P. J. MAUDLIN, J. F. BINGERT, J. W. HOUSE and S. R. CHEN, *On the modeling of the Taylor cylinder test for orthotropic textured materials: experiments and simulations,* Int. Journal of Plasticity, **15**, 139, 1999.

Received June 3, 2002.

Arch. Mech., **54**, 5-6, pp. 479–495, Warszawa 2002

On the added mass effect for porous media

W. KOSIŃSKI [1], J. KUBIK [2], K. HUTTER[3]

[1] *Research Center, Polish–Japanese Institute of Information Technology*
ul. Koszykowa 86, PL-02-008 Warszawa, Poland
e-mail: wkos@pjwstk.edu.pl

[2] *Institute of Environmental Mechanics and Applied Computer Science*
University of Bydgoszcz,
ul. Chodkiewicza 30, 85-064 Bydgoszcz, Poland
e-mail: kubik@ab-byd.edu.pl

[3] *Institut für Mechanik,*
Technische Universität Darmstadt
Hochschulstr. 1, 64289 Darmstadt, Germany
e-mail: hutter@mechanik.tu-darmstadt.de

Dedicated to Professor Piotr Perzyna
on the occasion of his 70^{th} birthday

CONSIDER A POROUS solid skeleton saturated with N fluid constituents. To describe the saturation condition and the immiscibility of the mixture constituents (phases), $N+1$ volume fraction parameters are introduced. In the energy equation an added mass effect is incorporated in the form of a constitutive assumption. This allows to include, on the phenomenological level, the influence of the pore structure of the solid constituent on the kinetic energy formulation of the whole mixture. Its consequences are deduced; they lead to a new form of the kinetic energy in the balance law of energy, from which a new form of motion equations are deduced. A particular case of one fluid component in the isotropic case is considered.

1. Introduction

IN ANALYSIS of the mechanical behaviour of multiphase media such as porous solids filled with one or a number of fluids, one of the key problems is to establish the proper description of the interphase force (internal body force) accounting for the local interaction of the constituents with each other.

Modelling such materials has been a subject of wide discussion through the last three decades and is based mostly upon the fundamental notions of the *classical mixture theory*, TRUESDELL and TOUPIN [22], BOWEN [8], and its reformulated form – the *theory of interacting continua*, GREEN and NAGHDI [14, 8].

In this case a fluid-filled porous medium is treated as a superposition of two miscible continua: solid and fluid, characterized by two independent velocity fields: $\mathbf{v}^s$ and $\mathbf{v}^f$. In such an approach the microstructure of the solid–fluid mixture is not taken into account in formulating the balance equations and constitutive relations. However, it has been observed that in a number of typical multiphase media, consisting of an identifiable porous matrix and a fluid filling its pores, the internal geometrical pore structure strongly influences the behaviour of the phases, especially the pore fluid phase, inducing an inhomogeneity of the micro-velocity fields. This effect is regarded to be of prime importance in understanding the acoustic properties of porous media saturated with fluids.

In most papers treating the problems of fluid flow through deformable porous solids, the solid–fluid interaction force is taken to depend on the relative macro–velocities of phases (the Stokes drag force) and on respective density gradients. However, a more realistic modelling of such media, in a non-stationary case, should take into account fluctuations of the micro–velocity fields of the fluid phases, which have a strong influence on the solid-fluid force interaction by creating inertial couplings between the constituents represented by virtual or added mass force.

The basic concept of an added mass force can be easily understood by considering the change in kinetic energy of the fluid surrounding an accelerating material object (see the Fig. 1). The classical result, when the effects of any viscous forces are not considered, is that the acceleration of the object induces a resisting force at this object proportional to the mass of the displaced fluid and the acceleration of the object.

Such an approach was applied in some works, mainly for isotropic systems, by introducing on the macroscopic level a suitable form of the kinetic energy (e.g. M. A. BIOT [3,4,5], D. LHUILLIER [20], O. COUSSY [11], A. BEDFORD *et al.* [1], B. YAVARI and A. BEDFORD [25], D. DREW *et al.* [12], G. B. WALLIS [23], J. A. GEURST [13]).

The present study is concerned with the added mass force during accelerated flows of N fluids through a porous solid. The problem of dynamic coupling is generalized and extended to saturated porous media with an anisotropic internal pore structure. In the present approach, individual physical properties of immiscible constituents play an important role in transport phenomena.

In previous publications of one of us as well as in a number of other papers (cf. [6,7,8,9,10,16,17,18,19,21]) devoted to modelling fluid-saturated porous solids, the immiscibility effect has been incorporated into the description by introducing a parameter of volume porosity characterizing the volume fraction of the fluid constituent. In the present paper our aim is to state a more fundamental approach, from which the existence of quantities describing the motion of

the so-called virtual components will follow as a mathematical consequence of a constitutive assumption.

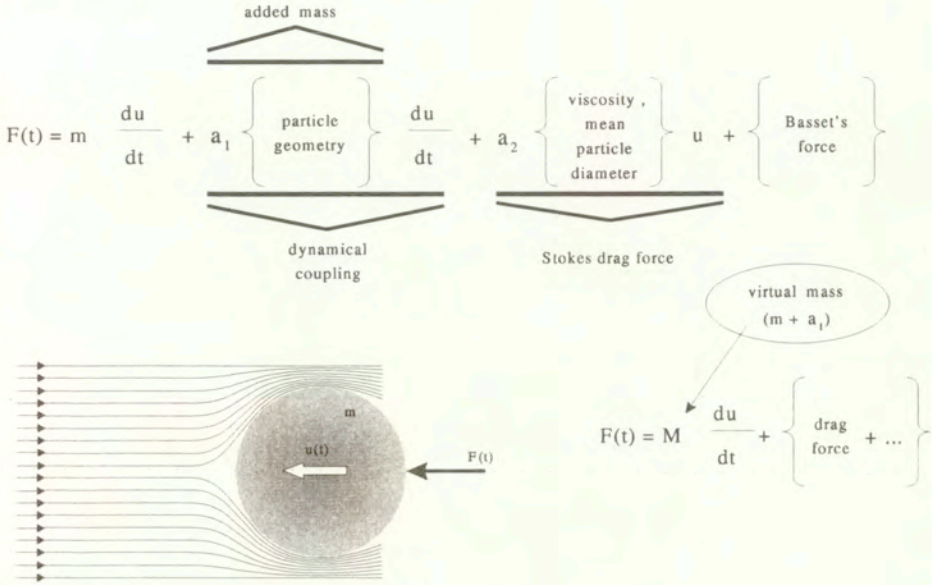

FIG. 1. Added mass and force effect.

2. Kinematic relations

In this section we repeat the main model assumptions of the author of the previous paper [18], however, with some generalization by admitting N pore fluid constituents.

Consider a mixture of $N+1$ constituents and let s and $\alpha = 1, 2, ..., N$, be indices identifying these constituents. Assume that one of the constituents, i.e. s, is a solid, while the remaining are of fluid type (liquid or gas). The difficulty in describing the kinematics is that each of the constituents (or phases) performs its own motion that, however, the spatial placement in the present configuration is assumed to be occupied by all constituents. We regard then the physical space as a 3D Euclidean space $\mathbb{E}$ and the domain $B \subset \mathbb{E}$ which is occupied by the constituents as an open set in $\mathbb{E}$ with boundary ∂B.

For our considerations at the macro-scale we make use of the local volume average field quantities defined over REV (Representative Elementary Volume – compare, for example [15, 24]) for each phase of the medium.

If Ω represents the averaging region containing the solid part Ω^s and the pore region Ω^p filled with fluid, (see Fig. 2), we have

$$\Omega = \Omega^s \cup \Omega^p, \tag{2.1}$$

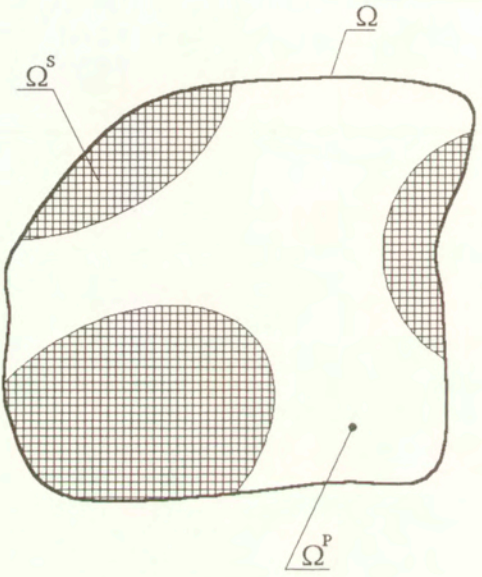

FIG. 2. Averaging region of porous medium (REV).

and one can define the volume fraction ratios

$$n^s = \frac{|\Omega^s|}{|\Omega|}, \quad n^p = n^f = \frac{|\Omega^p|}{|\Omega|} =: f_v, \tag{2.2}$$

for the solid and fluid phase, respectively, where f_v is the volume porosity, and the following condition is satisfied

$$n^s + n^p = 1 .$$

We consider the porous solid as fully saturated with the fluid phase. The pore-fluid phase may, in general, consist of $\alpha = 1, 2, ..., N$ fluid type components, and therefore we have

$$\Omega^p = \bigcup_{\alpha=1}^{N} \Omega^\alpha . \tag{2.3}$$

In such a case one can introduce volume fraction ratios for each fluid phase, i.e.,

$$\frac{|\Omega^\alpha|}{|\Omega|} = n^\alpha . \tag{2.4}$$

Obviously, n^α is constrained by

$$\sum_{\alpha=1}^{N} n^\alpha = f_v \ , \tag{2.5}$$

and introducing the saturation parameters

$$\frac{n^\alpha}{f_v} = s^\alpha \ , \quad \alpha = 1, ..., N, \tag{2.6}$$

one takes

$$\sum_{\alpha=1}^{N} s^\alpha = 1 \ . \tag{2.7}$$

3. Phase density and linear momentum

We assume for any phase that the microscopic quantities are defined at the pore or grain scale, and we denote them by double upper case indices, say $\rho^{\alpha\alpha}$ and $v^{\alpha\alpha}$ for the mass density and the velocity, respectively. Hence the bulk and effective volume average quantities can be defined with the help of them as their corresponding integral mean values (averages). For the solid phase we may neglect the fluctuations of mass density and velocity from their averages, so that we have for the mass density

$$\rho^s := \langle \rho^{ss} \rangle = \frac{1}{|\Omega^s|} \int_{\Omega^\alpha} \rho^{ss} d\Omega = \rho^{ss} \tag{3.1}$$

and similarly for the velocity

$$\mathbf{v}^{ss} = \mathbf{v}^s \ . \tag{3.2}$$

However, for the bulk solid partial density we can write

$$\bar{\rho}^s := \frac{1}{|\Omega|} \int_{\Omega^s} \rho^{ss} d\Omega = n^s \rho^s = (1 - f_v)\rho^s, \tag{3.3}$$

and the local form of linear momentum for the porous skeleton is

$$\mathbf{l}^s = \frac{1}{|\Omega|} \int_{\Omega^s} \rho^{ss} \mathbf{v}^{ss} d\Omega = n^s \rho^s \mathbf{v}^s = \bar{\rho}^s \mathbf{v}^s \ . \tag{3.4}$$

For the fluid components their pore velocities are strongly inhomogeneous in Ω^p (cf. Fig. 3 when one microscopic fluid component velocity $\mathbf{v}^{ff}$ is present) but the mass density fluctuations are small and will be disregarded in the further analysis, i.e.

$$\rho^{\alpha\alpha} = \rho^{\alpha}, \qquad \alpha = 1, ..., N \ . \tag{3.5}$$

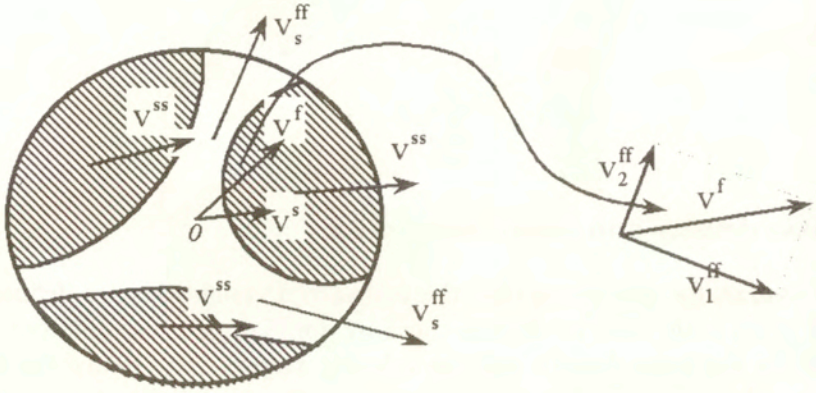

FIG. 3. Velocity scheme for the micro and macro-components.

For each fluid phase the bulk partial mass density $\bar{\rho}^{\alpha}$ and the corresponding saturation parameter s^{α} are coupled in the following relation:

$$\frac{1}{|\Omega|}\int_{\Omega^{\alpha}} \rho^{\alpha\alpha} d\Omega = s^{\alpha}\bar{\rho}^{\alpha} \ , \quad \alpha = 1, ..., N$$

$$\text{where} \qquad \bar{\rho}^{\alpha} = f_v \rho^{\alpha} = f_v \frac{1}{|\Omega^{\alpha}|}\int_{\Omega^{\alpha}} \rho^{\alpha\alpha} d\Omega. \tag{3.6}$$

The density of the fluid linear momentum is defined as

$$\mathbf{I}^{\alpha} = \frac{1}{|\Omega|}\int_{\Omega^{\alpha}} \rho^{\alpha\alpha}\mathbf{v}^{\alpha\alpha} d\Omega = \rho^{\alpha} n^{\alpha}\mathbf{v}^{\alpha} = s^{\alpha}\bar{\rho}^{\alpha}\mathbf{v}^{\alpha} \ . \tag{3.7}$$

Note that this relation also defines $\mathbf{v}^{\alpha}$ in terms of $\mathbf{v}^{\alpha\alpha}$ and n^{α}; $\mathbf{v}^{\alpha}$ is obviously a "barycentric" mean of $\mathbf{v}^{\alpha\alpha}$. If the pores are filled with a one-component fluid, i.e., $N = 1$ and if $\alpha \equiv f$, then $s^f = 1$ and $n^{\alpha} = n^f = f_v$, and we arrive at a porous solid saturated with one physical fluid.

The mass density for the whole system is

$$\rho = \bar{\rho}^s + \sum_{\alpha=1}^{N} s^\alpha \bar{\rho}^\alpha \,, \tag{3.8}$$

and the density of the linear momentum is

$$\boldsymbol{l} = \boldsymbol{l}^s + \sum_\alpha \boldsymbol{l}^\alpha = \bar{\rho}^s \mathbf{v}^s + \sum_\alpha s^\alpha \bar{\rho}^\alpha \mathbf{v}^\alpha \,. \tag{3.9}$$

4. Kinetic energy

The local form of the kinetic energy for the solid phase, when the assumption (3.1) is taken into account, can be exactly described by the average solid velocity $\mathbf{v}^s$ in the form

$$E^s = \frac{1}{2}\frac{1}{|\Omega|}\int_{\Omega^s} \rho^{ss}\mathbf{v}^{ss}\cdot\mathbf{v}^{ss}d\Omega = \frac{1}{2}\bar{\rho}^s\mathbf{v}^s\cdot\mathbf{v}^s, \tag{4.1}$$

that represents the total kinetic energy of the particles of the solid skeleton in Ω. However, for any fluid component flowing through the pores, the fluctuations of the pore velocity are of the order of the average component velocity as a result of the influence of the pore structure, and the α-component of the kinetic energy expressed by the phase velocity $\boldsymbol{v}^\alpha$ only, does not represent the total kinetic energy of that fluid component, i.e.,

$$\frac{1}{2}\frac{1}{|\Omega|}\int_{\Omega^\alpha} \rho^{\alpha\alpha}\mathbf{v}^{\alpha\alpha}\cdot\mathbf{v}^{\alpha\alpha}d\Omega \neq \frac{1}{2}s^\alpha\bar{\rho}^\alpha\mathbf{v}^\alpha\cdot\mathbf{v}^\alpha \,. \tag{4.2}$$

To describe the total kinetic energy reflecting the real motion of the α-component at the pore level, one can follow the approach of BIOT [6], BEDFORD and DRUMHELLER [1] and KUBIK [17] and assume this contribution to the energy to consist of two parts:

1. K_d – the part, responsible for the contribution of the average velocity field of the particular fluid components

$$K_d = \frac{1}{2}\sum_\alpha s^\alpha\bar{\rho}^\alpha\mathbf{v}^\alpha\cdot\mathbf{v}^\alpha \qquad \alpha = 1,...,N \,, \tag{4.3}$$

2. K_n – the part, responsible for the inhomogeneity of the velocity fields at the pore level, caused by the pore structure (as well as some other effects of the fluid

components) and expressed by means of the α-component velocities relative to the skeleton

$$K_n = \frac{1}{2}\sum_{\alpha} s^{\alpha}\bar{\rho}^{\alpha}(\mathbf{v}^{\alpha} - \mathbf{v}^{s}) \cdot \boldsymbol{A}^{\alpha}(\mathbf{v}^{\alpha} - \mathbf{v}^{s}) \,, \quad \text{where} \quad \alpha = 1, ..., N \,, \tag{4.4}$$

where the symmetric tensors $\boldsymbol{A}^{\alpha}$ represent the influence of the geometrical structure of the pores on the kinematics of the flow, and assumed to be positive definite. The non–diagonal part K_n expressed by the tensors $\boldsymbol{A}^{\alpha}$ has to satisfy the principle of the material objectivity, since their existence is a constitutive assumption.

With the use of the above expressions, the kinetic energy of the system composed of the porous skeleton saturated with N fluid components is

$$E = \frac{1}{2}\bar{\rho}^{s}\mathbf{v}^{s} \cdot \mathbf{v}^{s} + \frac{1}{2}\sum_{\alpha} s^{\alpha}\bar{\rho}^{\alpha}\mathbf{v}^{\alpha} \cdot \mathbf{v}^{\alpha} + \frac{1}{2}\sum_{\alpha} s^{\alpha}\bar{\rho}^{\alpha}(\mathbf{v}^{\alpha} - \mathbf{v}^{s}) \cdot \boldsymbol{A}^{\alpha}(\mathbf{v}^{\alpha} - \mathbf{v}^{s}) \,. \tag{4.5}$$

Introducing the macroscopic relative velocity $\mathbf{u}^{\alpha}$,

$$\mathbf{u}^{\alpha} = \mathbf{v}^{\alpha} - \mathbf{v}^{s} \,, \tag{4.6}$$

one can reformulate the energy of the considered system as follows

$$\begin{aligned} E = {} & \frac{1}{2}\bar{\rho}^{s}\mathbf{v}^{s} \cdot \mathbf{v}^{s} \\ & + \frac{1}{2}\left\{\sum_{\alpha} s^{\alpha}\bar{\rho}^{\alpha}[\mathbf{v}^{s} \cdot \mathbf{v}^{s} + 2\mathbf{v}^{s} \cdot \mathbf{u}^{\alpha} + \mathbf{u}^{\alpha} \cdot \mathbf{u}^{\alpha} + \mathbf{u}^{\alpha} \cdot \mathbf{A}^{\alpha}\mathbf{u}^{\alpha}]\right\} \\ & = \frac{1}{2}\bar{\rho}^{s}\mathbf{v}^{s} \cdot \mathbf{v}^{s} + \frac{1}{2}\left\{\sum_{\alpha} s^{\alpha}\bar{\rho}^{\alpha}[\mathbf{v}^{s} \cdot \mathbf{v}^{s} + 2\mathbf{v}^{s} \cdot \mathbf{u}^{\alpha} + \mathbf{u}^{\alpha}(1 + \mathbf{A}^{\alpha})\mathbf{u}^{\alpha}]\right\} , \end{aligned} \tag{4.7}$$

where the motion of the solid phase is singled out.

Since each tensor $\mathbf{1} + \mathbf{A}^{\alpha}$ is symmetric and non-singular, we can define a new second order symmetric tensor $\mathbf{P}^{\alpha}$, for each α, such that

$$\mathbf{1} + \mathbf{A}^{\alpha} = (\mathbf{P}^{\alpha})^{-1} f_v \quad \text{or} \quad \mathbf{P}^{\alpha} = (1 + \mathbf{A}^{\alpha})^{-1} f_v \,. \tag{4.8}$$

Using the tensor $\mathbf{P}^{\alpha}$ we may define a new relative velocity field for the α-component

$$\overset{\alpha}{\mathbf{u}} = (\mathbf{P}^{\alpha})^{-1}\mathbf{u}^{\alpha} f_v \,. \tag{4.9}$$

Each $\mathbf{P}^\alpha$ reflects the effect of the tortuosity of the pore structure of the skeleton on the fluid pore velocity.

Applying relation (4.9) in (4.7) yields

$$E = \frac{1}{2}\bar{\rho}^s \mathbf{v}^s \cdot \mathbf{v}^s + \frac{1}{2}\sum_\alpha \bar{\rho}^\alpha s^\alpha [\mathbf{v}^s \cdot \mathbf{v}^s + 2\frac{1}{f_v}(\mathbf{P}^\alpha \overset{\alpha}{\boldsymbol{u}}) \cdot \mathbf{v}^s + \frac{1}{f_v}(\boldsymbol{P}^\alpha \overset{\alpha}{\boldsymbol{u}}) \cdot \overset{\alpha}{\boldsymbol{u}}] \tag{4.10}$$

and after some rearranging, we obtain the canonical representation for the kinetic energy of the system

$$\begin{aligned} E &= \frac{1}{2}\bar{\rho}^s \mathbf{v}^s \cdot \mathbf{v}^s \\ &+ \frac{1}{2}\sum_\alpha s^\alpha \bar{\rho}^\alpha \left[\mathbf{v}^s \cdot (\mathbf{1} - \frac{1}{f_v}\mathbf{P}^\alpha)\mathbf{v}^s + \overset{\alpha}{\mathbf{v}} \cdot (\mathbf{1} - \frac{1}{f_v}\mathbf{P}^\alpha) \overset{\alpha}{\mathbf{v}}\right] \\ &= \frac{1}{2}\left\{\mathbf{v}^s \cdot \left[\bar{\rho}^s \mathbf{1} + \sum_\alpha s^\alpha \bar{\rho}^\alpha (\mathbf{1} - \frac{1}{f_v}\mathbf{P}^\alpha)\right]\mathbf{v}^s + \sum_\alpha \overset{\alpha}{\mathbf{v}} \cdot (s^\alpha \bar{\rho}^\alpha \frac{1}{f_v}\mathbf{P}^\alpha) \overset{\alpha}{\mathbf{v}}\right\}, \end{aligned} \tag{4.11}$$

where

$$\overset{\alpha}{\mathbf{v}} = \mathbf{v}^s + \overset{\alpha}{\mathbf{u}} \ . \tag{4.12}$$

Taking the above representation into account one can define the so-called **virtual constituents** of the system. The first virtual constituent is composed of the skeleton and those parts of the fluid components which move at the skeleton velocity $\mathbf{v}^s$, the partial density of which is

$$\overset{s}{\mathbf{M}} = \left[\bar{\rho}^s \mathbf{1} + \sum_\alpha s^\alpha \bar{\rho}^\alpha (\mathbf{1} - \frac{1}{f_v}\mathbf{P}^\alpha)\right]; \tag{4.13}$$

the remaining virtual constituents have partial densities

$$\overset{\alpha}{\mathbf{M}} = s^\alpha \bar{\rho}^\alpha \frac{1}{f_v}\mathbf{P}^\alpha \ , \quad \alpha = 1, ..., N, \tag{4.14}$$

and they move with the corresponding velocities $\overset{\alpha}{\boldsymbol{v}}$. Consequently, the linear momentum for the first virtual constituent takes the form

$$\overset{s}{\mathbf{L}} = \overset{s}{\mathbf{M}}\, \boldsymbol{v}^s = \left[\bar{\rho}^s \mathbf{1} + \sum_\alpha s^\alpha \bar{\rho}^\alpha (\mathbf{1} - \frac{1}{f_v}\mathbf{P}^\alpha)\right]\mathbf{v}^s \ , \tag{4.15}$$

and the α-constituent linear momentum written by means of partial densities and the velocities of the virtual constituents will be

$$\overset{\alpha}{\mathbf{L}} = s^\alpha \bar{\rho}^\alpha \frac{1}{f_v}\mathbf{P}^\alpha \overset{\alpha}{\mathbf{v}} \ . \tag{4.16}$$

At the same time the canonical representation of the kinetic energy will be

$$E = \frac{1}{2} \overset{s}{\mathbf{v}} \cdot \overset{s}{\mathbf{M}} \overset{s}{\mathbf{v}} + \frac{1}{2} \sum_{\alpha} \overset{\alpha}{\mathbf{v}} \cdot \overset{\alpha}{\mathbf{M}} \overset{\alpha}{\mathbf{v}} , \tag{4.17}$$

where

$$\begin{aligned} &\overset{\alpha}{\mathbf{v}} = \mathbf{v}^s + \overset{\alpha}{\mathbf{u}} , \ \mathbf{u}^\alpha = (\mathbf{v}^\alpha - \mathbf{v}^s), \\ &\overset{\alpha}{\mathbf{u}} = (\mathbf{1} + \mathbf{A}^\alpha)\mathbf{u}^\alpha = (\mathbf{P}^\alpha)^{-1}\mathbf{u}^\alpha f_v . \end{aligned} \tag{4.18}$$

One can now prove that the mass densities and the linear momentum densities of the virtual constituents of the porous solid, filled with a multicomponent fluid, satisfy the following conditions:

- for mass densities

$$\overset{s}{\mathbf{M}} + \sum_{\alpha} \overset{\alpha}{\mathbf{M}} = \bar{\rho}^s \mathbf{1} + \sum_{\alpha} s^\alpha \bar{\rho}^\alpha \left(\mathbf{1} - \frac{1}{f_v} \mathbf{P}^\alpha \right) + \sum_{\alpha} s^\alpha \bar{\rho}^\alpha \frac{1}{f_v} \mathbf{P}^\alpha = \bar{\rho}^s \mathbf{1} + \sum_{\alpha} s^\alpha \bar{\rho}^\alpha \mathbf{1} , \tag{4.19}$$

- for linear momentum

$$\overset{s}{\mathbf{M}} \mathbf{v}^s + \sum_{\alpha} \overset{\alpha}{\mathbf{L}} = \left[\bar{\rho}^s \mathbf{1} + \sum_{\alpha} s^\alpha \bar{\rho}^\alpha \left(\mathbf{1} - \frac{1}{f_v} \mathbf{P}^\alpha \right) \right] \mathbf{v}^s + \sum_{\alpha} s^\alpha \bar{\rho}^\alpha \frac{1}{f_v} \mathbf{P}^\alpha \overset{\alpha}{\mathbf{v}}, \tag{4.20}$$

and since $\overset{\alpha}{\mathbf{v}} = \mathbf{v}^s + \overset{\alpha}{\mathbf{u}}$, we have

$$\overset{s}{\mathbf{M}} \mathbf{v}^s + \sum_{\alpha} \overset{\alpha}{\mathbf{L}} = \left[\left(\bar{\rho}^s \mathbf{1} + \sum_{\alpha} s^\alpha \bar{\rho}^\alpha \mathbf{1} \right) \right] \mathbf{v}^s + \sum_{\alpha} s^\alpha \bar{\rho}^\alpha \frac{1}{f_v} \boldsymbol{P}^\alpha \overset{\alpha}{\mathbf{u}} = \left[\bar{\rho}^s \mathbf{v}^s + \sum_{\alpha} s^\alpha \bar{\rho}^\alpha \mathbf{v}^\alpha \right] . \tag{4.21}$$

Notice that for an isotropic pore structure simplifications occur, i.e., $\boldsymbol{P}^\alpha = \lambda^\alpha \mathbf{1}$, with λ^α as a structural permeability parameter for each α, and

$$\overset{s}{\mathbf{M}} = \left[\bar{\rho}^s + \sum_{\alpha} s^\alpha \bar{\rho}^\alpha (1 - \kappa^\alpha) \right] \mathbf{1}, \quad \overset{\alpha}{\mathbf{M}} = s^\alpha \bar{\rho}^\alpha \kappa^\alpha \mathbf{1}, \quad \alpha = 1, ..., N, \tag{4.22}$$

where $\kappa^\alpha = \lambda^\alpha / f_v$ can be called the pore structure parameter corresponding to the α-th fluid constituent. The case of $N = 1$ has already been discussed in [9, 17], where for a fluid-saturated porous skeleton the following representation of the velocity of the virtual components was obtained

$$\overset{\alpha}{\mathbf{v}} = \overset{f}{\mathbf{v}} \quad \text{with} \quad \overset{f}{\mathbf{v}} = \mathbf{v}^s + \frac{1}{\kappa}(\mathbf{v}^f - \mathbf{v}^s) \ , \ \text{or} \ \mathbf{v}^f = (1-\kappa)\mathbf{v}^s + \kappa \overset{f}{\mathbf{v}}, \tag{4.23}$$

with only one $\alpha \equiv f$, and $\mathbf{v}^1 = \mathbf{v}^f$, the velocity of a one-component fluid and $\kappa = \kappa^1$, the pore structure parameter, and with the partial mass densities of the virtual components

$$\overset{s}{\mathbf{M}} = (\bar{\rho}^s + (1-\kappa)\ \bar{\rho}^f)\ \mathbf{1} \ , \quad \overset{f}{\mathbf{M}} = \kappa \bar{\rho}^f\ \mathbf{1} \ . \tag{4.24}$$

5. Mass continuity equations

For a porous skeleton and a pore fluid with chemically inert components, the local form of the balance equations of mass can be written in the form

$$\frac{\partial \bar{\rho}^s}{\partial t} + \operatorname{div}(\bar{\rho}^s \mathbf{v}^s) = 0 \ , \tag{5.1}$$

$$\frac{\partial s^\alpha \bar{\rho}^\alpha}{\partial t} + \operatorname{div}(s^\alpha \bar{\rho}^\alpha \mathbf{v}^\alpha) = 0, \quad \alpha = 1, ..., N. \tag{5.2}$$

When the virtual division of the system is considered, the local form of the balance equations of mass are

$$\frac{\partial \overset{s}{\mathbf{M}}}{\partial t} + \operatorname{div}(\mathbf{1} \otimes \overset{s}{\mathbf{M}}\ \mathbf{v}^s) = \overset{s}{\mathbf{H}}, \tag{5.3}$$

$$\frac{\partial \overset{\alpha}{\mathbf{M}}}{\partial t} + \operatorname{div}(\mathbf{1} \otimes \overset{\alpha}{\mathbf{M}} \overset{\alpha}{\mathbf{v}}) = \overset{\alpha}{\boldsymbol{H}}, \tag{5.4}$$

where $\alpha = 1, 2, ..., N$, while $\overset{s}{\mathbf{H}}$ and $\overset{\alpha}{\mathbf{H}}$ are mass supply functions that will be subsequently identified. Eq. (5.3), when (4.13) and (5.1) are taken into account can be rewritten in the following form

$$\frac{\partial}{\partial t}\left\{\sum_\alpha s^\alpha \bar{\rho}^\alpha \left(\mathbf{1} - \frac{1}{f_v}\mathbf{P}^\alpha\right)\right\} + \operatorname{div}\left\{\mathbf{1} \otimes \left[\sum_\alpha s^\alpha \bar{\rho}^\alpha \left(\mathbf{1} - \frac{1}{f_v}\boldsymbol{P}^\alpha\right)\right] \mathbf{v}^s\right\} = \overset{s}{\mathbf{H}} \ . \tag{5.5}$$

Equation (5.3), when (4.14) and (5.2) are used yields

$$\frac{\partial}{\partial t}\left\{s^\alpha \bar{\rho}^\alpha \frac{1}{f_v}\mathbf{P}^\alpha\right\} + \operatorname{div}\left\{\mathbf{1}\otimes\left[s^\alpha \bar{\rho}^\alpha \frac{1}{f_v}\mathbf{P}^\alpha \overset{\alpha}{\mathbf{v}}\right]\right\} = \overset{\alpha}{\mathbf{H}}, \tag{5.6}$$

$$\frac{\partial}{\partial t}\{s^\alpha \bar{\rho}^\alpha \mathbf{1}\} + \operatorname{div}\left\{s^\alpha \bar{\rho}^\alpha\left[\mathbf{1}\otimes\mathbf{v}^s + \frac{1}{f_v}\mathbf{1}\otimes\mathbf{P}^\alpha \overset{\alpha}{\mathbf{u}}\right]\right\} = \mathbf{0}\,. \tag{5.7}$$

By subtraction (5.6) from (5.5) one obtains

$$\frac{\partial}{\partial t}\left\{s^\alpha \bar{\rho}^\alpha\left(\mathbf{1} - \frac{1}{f_v}\mathbf{P}^\alpha\right)\right\} + \operatorname{div}\left\{s^\alpha \bar{\rho}^\alpha \mathbf{1}\otimes\left(\mathbf{1} - \frac{1}{f_v}\mathbf{P}^\alpha\right)\mathbf{v}^s\right\} = -\overset{\alpha}{\mathbf{H}}\,, \tag{5.8}$$

and for any component α, but when summing over all $\alpha = 1, 2, ..., N$, we have

$$\frac{\partial}{\partial t}\left\{\sum_\alpha s^\alpha \bar{\rho}^\alpha\left(\mathbf{1} - \frac{1}{f_v}\mathbf{P}^\alpha\right)\right\} + \operatorname{div}\left\{\sum_\alpha s^\alpha \bar{\rho}^\alpha \mathbf{1}\otimes\left(\mathbf{1} - \frac{1}{f_v}\mathbf{P}^\alpha\right)\mathbf{v}^s\right\} = -\sum_\alpha \overset{\alpha}{\mathbf{H}}\,. \tag{5.9}$$

Comparing (5.9) and (5.5) we find that the mass supplies satisfy the condition

$$\overset{s}{\mathbf{H}} + \sum_\alpha \overset{\alpha}{\mathbf{H}} = \mathbf{0}\,, \tag{5.10}$$

which shows that during the motion of the system the first virtual component moving at the skeleton velocity interchanges its mass with the remaining virtual components. It can be shown that the mass supply functions can be written as

$$\overset{s}{\mathbf{H}} = -\sum_\alpha \overset{\alpha}{\mathbf{H}} = \bar{\rho}^s \frac{D^s}{Dt}\left\{\frac{1}{\bar{\rho}^s}\sum_\alpha s^\alpha \bar{\rho}^\alpha\left(\mathbf{1} - \frac{1}{f_v}\mathbf{P}^\alpha\right)\right\}\,, \tag{5.11}$$

where $\dfrac{D^s}{Dt} = \dfrac{\partial}{\partial t} + \mathbf{v}^s \cdot \operatorname{grad}\,.$

For an isotropic pore structure, for which

$$\boldsymbol{P}^\alpha = \lambda^\alpha \mathbf{1} = \kappa^\alpha f_v \mathbf{1}$$

we obtain the continuity equations

$$\frac{\partial}{\partial t}\left\{\sum_{\alpha} s^{\alpha}\bar{\rho}^{\alpha}(1-\kappa^{\alpha})\right\} + \operatorname{div}\left\{\left[\sum_{\alpha} s^{\alpha}\bar{\rho}^{\alpha}(1-\kappa^{\alpha})\right]\mathbf{v}^{s}\right\} = \mathbf{H}^{s}$$

$$\frac{\partial}{\partial t}\{s^{\alpha}\bar{\rho}^{\alpha}\kappa^{\alpha}\} + \operatorname{div}\{s^{\alpha}\bar{\rho}^{\alpha}\kappa^{\alpha}\mathbf{v}^{\alpha}\} = \mathbf{H}^{\alpha}$$

with the condition

$$\overset{s}{\mathbf{H}} + \sum_{\alpha} \overset{\alpha}{\mathbf{H}} = 0.$$

For the mass supply function we have

$$\overset{s}{\mathbf{H}} = -\sum_{\alpha} \overset{\alpha}{\mathbf{H}} = \bar{\rho}^{s}\frac{D^{s}}{Dt}\left\{\frac{1}{\bar{\rho}^{s}}\sum_{\alpha} s^{\alpha}\bar{\rho}^{\alpha}(1-\kappa^{\alpha})\right\}.$$

6. Motion equations for an isotropic porous solid filled with a one-component fluid, $N = 1$

For $N = 1$ a porous solid-fluid composition forms a mixture composed of two virtual components with corresponding velocities $\overset{s}{\mathbf{v}}$ and $\overset{f}{\mathbf{v}}$, (4.23), and densities $\overset{s}{M}$ and $\overset{f}{M}$, (4.24). (Note that now $\overset{s}{\mathbf{M}} = \overset{s}{M}\,\mathbf{1}$ and $\overset{f}{\mathbf{M}} = \overset{f}{M}\,\mathbf{1}$.) Now, having defined the virtual components we associate the stress vector $\overset{k}{\mathbf{t}}$ $(k = s, f)$ with each of the components in such a way that the scalar product $\overset{k}{\mathbf{t}} \cdot \overset{k}{\mathbf{v}}$ represents the rate of work of a particular component per unit area of a surface bounding the bulk material. These can be derived from the condition that the total rates of mechanical work for virtual and physical components are equal,

$$\overset{s}{\mathbf{t}} \cdot \overset{s}{\mathbf{v}} + \overset{f}{\mathbf{t}} \cdot \overset{f}{\mathbf{v}} = \mathbf{t}^{s} \cdot \mathbf{v}^{s} + \mathbf{t}^{f} \cdot \mathbf{v}^{f}\,. \tag{6.1}$$

Thus, using (4.23), the relations between $\overset{k}{\mathbf{t}}$ and $\mathbf{t}^{\alpha}$ are

$$\overset{s}{\mathbf{t}} = \mathbf{t}^{s} + (1-\kappa)\mathbf{t}^{f}, \quad \overset{f}{\mathbf{t}} = \kappa\mathbf{t}^{f} \tag{6.2}$$

and for the stress tensors we have

$$\overset{s}{\mathbf{T}} = \mathbf{T}^{s} + (1-\kappa)\mathbf{T}^{f}, \quad \overset{f}{\mathbf{T}} = \kappa\mathbf{T}^{f} \tag{6.3}$$

where the identity $\mathbf{t}^{\alpha} = \mathbf{T}^{\alpha}\mathbf{n}$ was used, with $\mathbf{n}$ as the unit normal to a surface element on which the stress tensors are defined.

Now, motion equations for the virtual components may be obtained from the energy balance for the whole solid–fluid composition by applying invariance conditions under the superposed rigid body translations. Therefore we write the energy balance in the following form:

$$
\begin{aligned}
(6.4)\quad & \int_V \frac{\partial}{\partial t}\left(\bar{\rho}^s e^s + \bar{\rho}^f e^f + \frac{1}{2}\left(\overset{s}{M}\overset{s}{\mathbf{v}}\cdot\overset{s}{\mathbf{v}} + \overset{f}{M}\overset{f}{\mathbf{v}}\cdot\overset{f}{\mathbf{v}}\right)\right) dV \\
& + \int_S \left(e^s\bar{\rho}^s\,\overset{s}{\mathbf{v}} + e^f\left[\left(\bar{\rho}^f - \overset{s}{M}\right)\overset{s}{\mathbf{v}} + \overset{f}{M}\overset{f}{\mathbf{v}}\right] + \frac{1}{2}\left[\left(\overset{s}{M}\overset{s}{\mathbf{v}}\cdot\overset{s}{\mathbf{v}}\right)\overset{s}{\mathbf{v}} + \left(\overset{f}{M}\overset{f}{\mathbf{v}}\cdot\overset{f}{\mathbf{v}}\right)\overset{f}{\mathbf{v}}\right]\right) \\
& \cdot \mathbf{n}dS = \int_V \left(\overset{s}{M}\,\mathbf{b}\cdot\overset{s}{\mathbf{v}} + \overset{f}{M}\,\mathbf{b}\cdot\overset{f}{\mathbf{v}}\right) dV + \int_S \left(\overset{s}{\mathbf{t}}\cdot\overset{s}{\mathbf{v}} + \overset{f}{\mathbf{t}}\cdot\overset{f}{\mathbf{v}}\right) dS
\end{aligned}
$$

where e^s and e^f stand for the internal energies per unit mass of the skeleton and the fluid, respectively, and where the external body forces $\overset{s}{M}\,\mathbf{b}$ and $\overset{f}{M}\,\mathbf{b}$ contribute by their rate of work contribution, i.e., $\overset{s}{M}\,\mathbf{b}\cdot\overset{s}{\boldsymbol{v}}$ and $\overset{f}{M}\,\mathbf{b}\cdot\overset{f}{\boldsymbol{v}}$, respectively.

Using (4.24) and continuity equations (5.3) and (5.4) and applying invariance conditions under rigid body translations, we obtain the equations of motion

$$
\begin{aligned}
(6.5)\quad & \operatorname{div}\overset{s}{\mathbf{T}} + \overset{s}{M}\,\mathbf{b} + \overset{s}{\boldsymbol{\pi}} = \overset{s}{M}\,\frac{\overset{s}{\mathbf{D}}}{Dt}\,\overset{s}{\mathbf{v}} + \frac{1}{2}\,\overset{s}{M}\left(\overset{f}{\mathbf{v}} - \overset{s}{\mathbf{v}}\right) \\
& \operatorname{div}\overset{f}{\mathbf{T}} + \overset{f}{M}\,\boldsymbol{b} + \overset{f}{\boldsymbol{\pi}} = \overset{f}{M}\,\frac{\overset{f}{\mathbf{D}}}{Dt}\,\overset{f}{\mathbf{v}} + \frac{1}{2}\,\overset{s}{M}\left(\overset{f}{\mathbf{v}} - \overset{s}{\mathbf{v}}\right)
\end{aligned}
$$

where $\overset{s}{\boldsymbol{\pi}} = -\overset{f}{\boldsymbol{\pi}}$ represents the viscous interaction force and the force $\frac{1}{2}\,\overset{s}{M}\,\mathbf{u} = \frac{1}{2}\,\overset{s}{M}\left(\overset{f}{\mathbf{v}} - \overset{s}{\mathbf{v}}\right)$ results from the mass exchange between the virtual components. The equations of motion for the physical components are

$$
\begin{aligned}
(6.6)\quad & \operatorname{div}\mathbf{T}^s + \bar{\rho}^s\mathbf{b} + \boldsymbol{\pi}^s = \bar{\rho}^s\frac{D^s}{Dt}\mathbf{v}^s, \\
& \operatorname{div}\mathbf{T}_c^f + \bar{\rho}^f\mathbf{b} + \boldsymbol{\pi}^f = \bar{\rho}^f\frac{D^f}{Dt}\mathbf{v}^f\,,
\end{aligned}
$$

where the interphase interaction force has the form

$$
\begin{aligned}
\boldsymbol{\pi}^s = -\boldsymbol{\pi}^f = -\frac{1}{\kappa}\left(\overset{f}{\boldsymbol{\pi}} + \mathbf{T}^f \operatorname{grad}\kappa\right) \\
+ (1-\kappa)\,\bar{\rho}^f \left\{ \frac{D^f}{Dt}\mathbf{v}^f - \frac{D^s}{Dt}\mathbf{v}^s + \frac{D^f}{Dt}\left[\left(\frac{1}{\kappa}-1\right)\mathbf{u}\right] \right. \\
\left. + \left(\frac{1}{\kappa}-1\right)\mathbf{u}\cdot\operatorname{grad}\left[\mathbf{v}^f + \left(\frac{1}{\kappa}-1\right)\mathbf{u}\right]\right\} \\
+ \left(1-\frac{1}{2\kappa}\right)\left\{\frac{1}{\kappa}\mathbf{u}\,\bar{\rho}^s \frac{D^s}{Dt}\left[\frac{\bar{\rho}^f(1-\kappa)}{\bar{\rho}^s}\right]\right\},
\end{aligned}
\tag{6.7}
$$

and

$$
\mathbf{T}_c^f = \mathbf{T}^f - \left(\frac{1}{\kappa}-1\right)\bar{\varrho}^f\left(\mathbf{v}^s - \mathbf{v}^f\right)\otimes\left(\mathbf{v}^s - \mathbf{v}^f\right)
$$

is the so-called complete stress tensor of the fluid phase.

The second and third terms of the right–hand side of (6.7) represent the inertial coupling between the solid and the fluid phases due to fluctuations of the micro-velocity field of the pore fluid that have been taken into account within the description. It is worth noticing that if $\kappa = 1$ the fluctuations are disregarded and the inertial coupling vanishes.

7. Concluding remarks

In this paper we considered a porous solid skeleton saturated with N fluid constituents. In the authors' opinion the individual physical properties of the immiscible constituents as well as the geometrical structure of the pores play an important role in describing transport phenomena through porous materials. The present approach to represent the kinetic energy of the medium at the macro-continuum scale takes into account the immiscibility effect and the non-homogeneity of the fluids' micro-velocities $\mathbf{v}^{ff} - \mathbf{v}^s$. The constitutive assumption regarding the extra contribution of those velocities to the kinetic energy of the fluid flow through the pores at the macro-scale are made in the form of the sum (4.3). In this way the added mass effect appears: the mass densities (4.13) and (4.14) of the virtual components satisfy the mass balance equation with non-vanishing production terms (cf. (5.3)–(5.4)) and the additional inertial solid-fluid interaction in the equations of motion (6.6) is evident. As a consequence we arrived at the total representation of the kinetic energy (4.11).

The tensors $\mathbf{A}^\alpha$ and consequently the tensors $\mathbf{P}^\alpha$ are related to the structure of the pores of the medium – the most important parameter describing the

structure is the tortuosity parameter. Its appearence in the papers of Biot, Bedford *et al.* and Kubik was mostly restricted to the isotropic case. However, the present approach introducing a tensorial characterisation of the structure brings for the first time the consqeuent derivation of the added mass effect without any restrictions concerning the size of strain and the fluid in the pores.

Acknowledgements

The research on the paper has been conducted by W. Kosiński and J. Kubik under the grants from the State Committee for Scientific Research (KBN, Poland) No. 7 T07A 05 115 and No. 8 T11F 017 18 (of W. Kosiński). The research of K. Hutter was performed during his stay in Poland as the recipient of the Alexander–von–Humboldt Fellowship of the Foundation for the Polish Science.

References

1. A. BEDFORD and D. C. DRUMHELLER, *Theories of immiscible and structured mixtures*, Int. J. Engng Sci., **21**, 8, 863–960, 1983.
2. A. BEDFORD, R. D. COSTLEY, M. STERN, *On the drag and virtual mass coefficients in Biot's equations*, J. Acoust.Soc. Am., **76**, 6, 1804–1809, 1983.
3. M. A. BIOT, *Theory of propagation of elastic waves in fluid saturated porous soli*, J. Acous. Soc. Am., **28** 9, 168–191, 1956.
4. M. A. BIOT, *Generalized theory of acoustic propagation in porous dissipative media*, J. Acoust. Soc. Am., **9**, 34, 1254–1264, 1962.
5. M. A. BIOT, *Mechanics of deformation and acoustic propagation in porous media*, J. Appl. Phys., **4**, 33, 1482–1498, 1962.
6. M. A. BIOT, *Theory of finite deformations of porous solids*, Ind. Univ. Math. J., **21**, 7, 597–620, 1972.
7. R. M. BOWEN, *Compressible porous media models by use of the theory of mixtures*, Int. J. Engng Sci., **20**, 697–735, 1982.
8. R. M. BOWEN, *Diffusion models implied by the theory of mixtures*, [in:] Rational Thermodynamics, C. Truesdell, 2 ed Edition, pp. 237–263, Springer, New York, 1984.
9. M. CIESZKO, and J. KUBIK, *Constitutive relations and internal equilibrium condition for fluid-saturated porous solids. Nonlinear theory*, Arch. Mech. **48**, 5, 893–910, 1996.
10. M. CIESZKO, J. KUBIK, *Constitutive relations and internal equilibrium condition for fluid–saturated porous solid. Linear description*, Arch. Mech. **48**, 5, 911–923, 1996.
11. O. COUSSY, *Thermomechanics of saturated porous solids in finite deformation*, Eur. J. Mech, A/Solids **8**, 1, 1–14, 1989.
12. D. DREW, L. CHENG, R. T. LAHEY, *The analysis of virtual mass effects in two-phase flow*, Int. J. Multiphase Flow, 5, 233–242, 1979.

13. J. A. GEURST, *Virtual mass in two-phase bubbly flow*, Physica, 129A, 233–261, 1985.

14. A. E. GREEN and P. M. NAGHDI, *A dynamical theory of interacting continua*, Int. J. Engng Sci., **3**, 231–241, 1965.

15. M. HASSANIZADEH AND W. G. GRAY, *General conservation equations for multiphase systems. Averaging procedure*, Adv. Water Res., **2**, 131–144, 1979.

16. M. KACZMAREK and J. KUBIK, *Determination of material constants of fluid–saturated porous solid* (in Polish), Engng Trans., **33**, 4, 589–609, 1985.

17. J. KUBIK, *On internal coupling in dynamic equations of fluid–saturated porous solid*, Int. J. Engng Sci., **24**, 981–989, 1986.

18. J. KUBIK, *Pore structure in dynamic behaviour of saturated materials*, Transport in Porous Media, **9**, 15–24, 1992.

19. J. KUBIK, M. CIESZKO, M. KACZMAREK, 2000 *Fundamentals of Dynamics of saturated porous media* (in Polish), IPPT PAN, Warszawa 2000.

20. D. LHUILLIER, *Phenomenology of inertia effects in a dispersed solid-fluid mixture*, Int. J. Multiphase Flow, **11**, 4, 427–444, 1985.

21. G. SZEFER, *Nonlinear problems of consolidation theory*, [in:] Problems de Reologie, Symposium Franco–Polonaise, Kraków 1977, pp. 585–604, PWN, Warszawa 1980.

22. C. TRUESDELL and R. A. TOUPIN, *The classical field theories*, [in:] Handbuch der Physik, vol. III/I. pp. 226–793, Springer-Verlag, Berlin–Göttingen–Heidelberg, 1960.

23. G. B. WALLIS, *On Geurst's equations for inertial coupling in two-phase flow*, in Two Phase Flows and Waves, D. D. JOSEPH, D. G. SCHAEFFER [Ed.], Springer-Verlag, pp. 150–164, 1990.

24. S. WHITAKER, *Flow in porous media I: A theoretical derivation of Darcys' law*, Transport in Porous Media, **1**, 3–25, 1986.

25. B. YAVARI, A. BEDFORD, *Computation af the Biot drag and virtual mass coefficients*, Int. J. Multiphase Flow, **14**, 1–12, 1988.

Received June 21, 2002; revised version November 29, 2002.

Arch. Mech., **54**, 5-6, pp. 497–523, Warszawa 2002

Energy-based limit conditions for transversally isotropic solids

K. KOWALCZYK and J. OSTROWSKA-MACIEJEWSKA

Institute of Fundamental Technological Research
Polish Academy of Sciences,
Świętokrzyska 21, 00-049 Warsaw

Dedicated to Professor Piotr Perzyna
on the occasion of his 70^{th} birthday

USING AN EXAMPLE of transversal isotropy, the limit condition having an energy interpretation for anisotropic bodies proposed by J. RYCHLEWSKI [11] has been illustrated. Transversal isotropy is characterized by the highest degree of symmetry, for which the spherical tensor is not any more the eigenstate of the compliance tensor $\mathbf{C}$. In the case when the spectral decomposition of the compliance tensor $\mathbf{C}$ is taken as a main energy-orthogonal decomposition, the limit condition representing a generalization of the Maxwell-Huber-Mises condition is obtained. For a prescribed form of the limit tensor $\mathbf{H}$, the Mises condition is presented in the form of a sum of elastic energies corresponding to uniquely defined energy-orthogonal parts of stress with certain weights, representing the limiting values of those energies. The effect of Burzyński's condition on the form of anisotropy and on the limit condition is discussed. Experimental tests are proposed which could be useful in determining the physical parameters describing the transversal isotropy.

1. Introduction

IN THE MECHANICS of continuous media, in formulating the constitutive equations, an important role is played by the conditions which limit the region of applicability and validity of these equations. These are usually certain criteria limiting the material strength measures, without any detailed analysis of the state of stress. Hence, it may be the passage from linear to nonlinear elasticity, the limit of appearing of the irreversible deformations (plasticity), appearing of viscosity or other structural changes of the material.

Most of the known limit conditions have a definite energy interpretation, i.e. they are certain limitations imposed on the energy (or its parts).

We are thus discussing the truly classical materials, in which the infinitesimal strain $\boldsymbol{\varepsilon}$ causes the stress $\boldsymbol{\sigma}$ according to Hooke's law

$$\boldsymbol{\varepsilon} = \mathbf{C} \cdot \boldsymbol{\sigma}, \quad \boldsymbol{\sigma} = \mathbf{S} \cdot \boldsymbol{\varepsilon}, \tag{1.1}$$

$$\mathbf{C} \circ \mathbf{S} = \mathbf{S} \circ \mathbf{C} = \mathbb{I}_S, \tag{1.2}$$

where the fourth-rank tensors $\mathbf{C}$, $\mathbf{S}$, $\mathbb{I}_S$ are the compliance, stiffness and unit tensors respectively, of certain symmetry. In indicial notation expressions (1.1) and (1.2) assume the form:

$$\varepsilon_{ij} = C_{ijkl}\sigma_{kl}, \quad \sigma_{mn} = S_{mnij}\varepsilon_{ij}, \tag{1.3}$$

$$S_{ijmn}C_{mnkl} = C_{ijmn}S_{mnkl} = \frac{1}{2}(\delta_{ik}\delta_{jl} + \delta_{il}\delta_{jk}). \tag{1.4}$$

From Hooke's law (1.1) it follows that *the elastic energy density* Φ is given by

$$\Phi(\boldsymbol{\sigma}) \equiv \frac{1}{2}\boldsymbol{\sigma}\cdot\boldsymbol{\varepsilon} = \frac{1}{2}\boldsymbol{\sigma}\cdot\mathbf{C}\cdot\boldsymbol{\sigma} = \frac{1}{2}\boldsymbol{\varepsilon}\cdot\mathbf{S}\cdot\boldsymbol{\varepsilon}. \tag{1.5}$$

In the case of isotropy, energy Φ may be presented in the form of a sum of the energy connected with the change of volume $\Phi(\sigma\mathbf{I})$ and the change of shape $\Phi(\mathbf{s})$, namely

$$\Phi(\boldsymbol{\sigma}) = \Phi(\sigma\mathbf{I}) + \Phi(\mathbf{s}) = \frac{1}{2K}\sigma^2 + \frac{1}{4G}\mathbf{s}\cdot\mathbf{s}, \tag{1.6}$$

where $\sigma = \frac{1}{3}\operatorname{tr}\boldsymbol{\sigma}$ and $\mathbf{s} = \boldsymbol{\sigma} - \sigma\mathbf{I}$.

Hooke's law (1.1) describes the behaviour of the material within the elastic range, i.e. as long as the strength condition does not reach the critical value.

The objective of this paper is to formulate the limit condition for anisotropic bodies.

M. T. HUBER [5], on defining the limit criterion for isotropic bodies, assumed that only the distortion energy decided on passing of the material to the plastic state, i.e. only the part $\Phi(\mathbf{s})$ of the elastic energy $\Phi(\boldsymbol{\sigma})$ (1.6) enters the yield condition. This concept of assuming the distortion energy to be responsible for appearance of the plastic deformations, can be also found in the papers by MISES [16] and HENCKY [2].

The limit condition

$$\frac{1}{h}\Phi(\mathbf{s}) \leq 1, \quad \text{where} \quad h = \frac{k^2}{2G} \tag{1.7}$$

is equivalent to

$$\mathbf{s}\cdot\mathbf{s} = 2k^2 \tag{1.8}$$

and is well known in the literature as the Huber-Mises-Hencky condition. It is one of the most frequently applied conditions for isotropy.

J. RYCHLEWSKI, on preparing the paper [12] for print, found a private letter written by C. MAXWELL to Lord KELVIN in 1855 [7], suggesting that the condition of appearing of plastic strains is reaching of a certain limiting value by the distortion energy $\Phi(\mathbf{s})$. Hence RYCHLEWSKI, in his paper [12], proposed to call the condition (1.7) *the Maxwell-Huber-Mises limit state condition.*

When the linear-elastic anisotropic bodies are dealt with, we must decide upon a proper generalization of the Maxwell-Huber-Mises condition (1.7).

In case of anisotropic bodies, there is no physical reason to consider the hydrostatic state as a state playing a decisive role in formulation of the strength measures. For bodies with a definite type of anisotropy, the tensor characterizing the anisotropic structure may prove to be the characteristic tensor. The spherical part of the stress tensor may thus enter the limit condition.

When an arbitrary anisotropy (1.1) is considered, the decomposition of energy into the parts connected with the change of volume $\Phi(\sigma\mathbf{I})$ and the change of shape $\Phi(\mathbf{s})$ (1.6) is impossible.

From Eq. (1.5) it follows that for anisotropy (1.1)

$$2\Phi(\boldsymbol{\sigma}) = \boldsymbol{\sigma} \cdot \mathbf{C} \cdot \boldsymbol{\sigma} = \sigma^2 \mathbf{I} \cdot \mathbf{C} \cdot \mathbf{I} + \mathbf{s} \cdot \mathbf{C} \cdot \mathbf{s} + 2\mathbf{I} \cdot \mathbf{C} \cdot \mathbf{s}. \tag{1.9}$$

When

$$\mathbf{I} \cdot \mathbf{C} \cdot \mathbf{s} \neq 0, \tag{1.10}$$

decomposition of the energy $\Phi(\boldsymbol{\sigma})$ into $\Phi(\sigma\mathbf{I})$ and $\Phi(\mathbf{s})$ is not possible.

In the corresponding literature we can find the attempts of discriminating the spherical parts of a stress tensor also for the anisotropic bodies. Huber's pupil, W. BURZYŃSKI, in his Ph.D. dissertation [1], formulated the hypothesis that there is no physical reason against the introduction of the decomposition of the elastic energy into these two components $\Phi(\sigma\mathbf{I})$ and $\Phi(\mathbf{s})$ (1.6) in the case of anisotropic bodies as well.

The Burzynski hypothesis is equivalent to assuming in Eq. (1.9) the condition

$$\mathbf{I} \cdot \mathbf{C} \cdot \mathbf{s} = 0, \tag{1.11}$$

what means that all anisotropic bodies are *voluminally isotropic.*

The unit tensor $\mathbf{I}$ is then the eigenstate for the compliance tensor $\mathbf{C}$, i.e.

$$\mathbf{C} \cdot \mathbf{I} = \lambda \mathbf{I}. \tag{1.12}$$

In the arbitrary Cartesian coordinate system with orthonormal base $\mathbf{m}_k$, condition (1.12) is equivalent to the set of the equations:

$$C_{1211} + C_{1222} + C_{1233} = 0, \tag{1.13}$$

$$C_{1311} + C_{1322} + C_{1333} = 0, \tag{1.14}$$

$$C_{2311} + C_{2322} + C_{2333} = 0, \tag{1.15}$$

$$C_{1111} - C_{2222} = C_{2233} - C_{1133}, \tag{1.16}$$

$$C_{1111} - C_{3333} = C_{2233} - C_{1122}. \tag{1.17}$$

Equations (1.13) – (1.17) represent certain constraints imposed on the type of anisotropy. The number of independent components of the compliance tensor $\mathbf{C}$ is then reduced from 21 to 16.

The Burzynski conditions (1.13) – (1.17) are satisfied identically in cases of isotropy and in materials with cubic symmetry. In other cases the conditions introduce certain additional limitations.

Certain attempts of formulating the limit criteria for some classes of anisotropy were made in papers [8, 9]. The problem has been solved completely by J. RYCHLEWSKI in the paper [12].

Rychlewski, looking for the limit condition in the form proposed by MISES [17]

$$\boldsymbol{\sigma} \cdot \mathbf{H} \cdot \boldsymbol{\sigma} \leq 1, \tag{1.18}$$

introduced the notion of *energy-orthogonal* states of stress and proved that every condition of the form (1.18) had an energetic sense. It means that each quadratic criterion (1.18) has a definite energy-based interpretation.

It is a pity that paper [12] of such a fundamental importance, has not appeared in English translation till now. The paper [12] in its present form doesn't contain any examples of application of the obtained results to the derivation of the limit conditions for some types of anisotropy.

This paper is aimed at following the way of reasoning of RYCHLEWSKI [12] in formulating the limit condition (1.18) for the case of transversal isotropy.

Transversal isotropy is selected because it is the type of anisotropy characterized by the highest symmetry properties, for which the spherical tensor is no more a proper elastic state.

2. Main energy-orthogonal decomposition

According to the definition given in paper [12] two states of stress $\boldsymbol{\alpha}, \boldsymbol{\beta} \in S$ are called *energy-orthogonal* if

$$\boldsymbol{\alpha} \times \boldsymbol{\beta} \equiv \boldsymbol{\alpha} \cdot \mathbf{C} \cdot \boldsymbol{\beta} = 0. \tag{2.1}$$

Equality (2.1) means that the state of stress $\boldsymbol{\alpha}$ does not perform any work on the deformations produced by the state of stress $\boldsymbol{\beta}$ and vice versa.

It is easy to prove that the proper elastic states of the compliance tensor $\mathbf{C}$ are energy-orthogonal as well (see also [13, 14]).

It is well known that the proper states of $\mathbf{C}$ [11] corresponding to various elastic moduli (Kelvin moduli) are orthonormal

$$\boldsymbol{\omega}_K \cdot \boldsymbol{\omega}_L = \delta_{KL}. \tag{2.2}$$

If

$$\mathbf{C} \cdot \boldsymbol{\omega}_K = \lambda^{-1} \boldsymbol{\omega}_K \tag{2.3}$$

then

$$\boldsymbol{\omega}_L \cdot \mathbf{C} \cdot \boldsymbol{\omega}_K = \boldsymbol{\omega}_L \cdot \lambda^{-1} \boldsymbol{\omega}_K = \lambda^{-1} \delta_{LK} \tag{2.4}$$

and for $K \neq L$

$$\boldsymbol{\omega}_L \cdot \mathbf{C} \cdot \boldsymbol{\omega}_K = 0. \tag{2.5}$$

Equation (2.5) means that the spectral decomposition [11] is at the same time the energy-orthogonal decomposition. It is not true inversely. The spectral decomposition in RYCHLEWSKI's paper [12] was called *the main energy-orthogonal decomposition.*

The approach to the problem of formulation of a quadratic limit condition (1.18) will be illustrated here by an example of transversal isotropy.

In order to find the main energy-orthogonal decomposition, the spectral decomposition must be determinated first.

Transversal isotropy was already considered in papers [9] and [11]. In those papers the main energy-orthogonal decomposition was used. It means that elastic and plastic properties were dependent.

The material is called *transversally isotropic* if it contains a certain direction $\mathbf{k} \otimes \mathbf{k}$ such that all shearings of the type

$$\begin{matrix} \boldsymbol{\tau} & = & \mathbf{a} \otimes \mathbf{k} + \mathbf{k} \otimes \mathbf{a}, \\ \boldsymbol{\tau} & = & \mathbf{a} \otimes \mathbf{b} + \mathbf{b} \otimes \mathbf{a} \end{matrix} \quad , \quad \text{where} \quad \mathbf{a} \cdot \mathbf{k} = \mathbf{b} \cdot \mathbf{k} = \mathbf{a} \cdot \mathbf{b} = 0 \tag{2.6}$$

are the eigenstates for the compliance tensor $\mathbf{C}$.

The anisotropic elastic properties are represented by the fourth-rank tensor $\mathbf{C}$. In this paper we will follow the notation representing the elastic coefficients as a second-rank tensor in a six-dimensional space. Stress and strain are considered then as vectors in a six-dimensional Cartesian space as well as second-rank tensors in three-dimensional Cartesian reference system.

The space S of symmetric tensors of second-rank is six-dimensional. Base (polybase) of this space will be created by six linearly independent tensors. If in a physical space the base has the form of a orthonormal triad of vectors $\mathbf{m}_k$ selected so that $\mathbf{m}_3 = \mathbf{k}$, then the bases in S are formed by dyads $\mathbf{m}_k \otimes \mathbf{m}_l$.

There are infinite number of polybases in S. As the most natural base in S we consider the orthonormal polybase $\mathbf{e}_\beta \in S$ $(\beta = I, II, ..., VI)$ of the form

$$\mathbf{e}_I = \mathbf{m}_1 \otimes \mathbf{m}_1 \sim \begin{bmatrix} 1 & 0 & 0 \\ 0 & 0 & 0 \\ 0 & 0 & 0 \end{bmatrix}, \tag{2.7}$$

$$\mathbf{e}_{II} = \mathbf{m}_2 \otimes \mathbf{m}_2 \sim \begin{bmatrix} 0 & 0 & 0 \\ 0 & 1 & 0 \\ 0 & 0 & 0 \end{bmatrix}, \tag{2.8}$$

$$\mathbf{e}_{III} = \mathbf{k} \otimes \mathbf{k} \sim \begin{bmatrix} 0 & 0 & 0 \\ 0 & 0 & 0 \\ 0 & 0 & 1 \end{bmatrix}, \tag{2.9}$$

$$\mathbf{e}_{IV} = \frac{1}{\sqrt{2}}(\mathbf{m}_2 \otimes \mathbf{k} + \mathbf{k} \otimes \mathbf{m}_2) \sim \frac{1}{\sqrt{2}} \begin{bmatrix} 0 & 0 & 0 \\ 0 & 0 & 1 \\ 0 & 1 & 0 \end{bmatrix}, \tag{2.10}$$

$$\mathbf{e}_V = \frac{1}{\sqrt{2}}(\mathbf{k} \otimes \mathbf{m}_1 + \mathbf{m}_1 \otimes \mathbf{k}) \sim \frac{1}{\sqrt{2}} \begin{bmatrix} 0 & 0 & 1 \\ 0 & 0 & 0 \\ 1 & 0 & 0 \end{bmatrix}, \tag{2.11}$$

$$\mathbf{e}_{VI} = \frac{1}{\sqrt{2}}(\mathbf{m}_1 \otimes \mathbf{m}_2 + \mathbf{m}_2 \otimes \mathbf{m}_1) \sim \frac{1}{\sqrt{2}} \begin{bmatrix} 0 & 1 & 0 \\ 1 & 0 & 0 \\ 0 & 0 & 0 \end{bmatrix}. \tag{2.12}$$

Three-by-three matrices representing the components of the tensors $\mathbf{e}_\beta$ are taken in the base $\mathbf{m}_k$.

In order to discuss the Burzynski conditions (1.13) – (1.17) it will be more convenient to consider another polybase $\mathbf{a}_\alpha \in S$ in which the spherical tensor is discriminated. The remaining tensors are deviators.

Tensors $\mathbf{a}_\alpha \in S$ $(\alpha = I, II, ..., VI)$ also form the orthonormal base in S and can be written as follows

$$\mathbf{a}_I = \frac{1}{\sqrt{3}}(\mathbf{m}_1 \otimes \mathbf{m}_1 + \mathbf{m}_2 \otimes \mathbf{m}_2 + \mathbf{k} \otimes \mathbf{k}) \sim \frac{1}{\sqrt{3}} \begin{bmatrix} 1 & 0 & 0 \\ 0 & 1 & 0 \\ 0 & 0 & 1 \end{bmatrix}, \tag{2.13}$$

$$\mathbf{a}_{II} = \frac{1}{\sqrt{2}}(\mathbf{m}_1 \otimes \mathbf{m}_1 - \mathbf{m}_2 \otimes \mathbf{m}_2) \sim \frac{1}{\sqrt{2}} \begin{bmatrix} 1 & 0 & 0 \\ 0 & -1 & 0 \\ 0 & 0 & 0 \end{bmatrix}, \tag{2.14}$$

$$\mathbf{a}_{III} = \frac{1}{\sqrt{6}}(\mathbf{m}_1 \otimes \mathbf{m}_1 + \mathbf{m}_2 \otimes \mathbf{m}_2 - 2\mathbf{k} \otimes \mathbf{k}) \sim \frac{1}{\sqrt{6}} \begin{bmatrix} 1 & 0 & 0 \\ 0 & 1 & 0 \\ 0 & 0 & -2 \end{bmatrix}, \tag{2.15}$$

$$\mathbf{a}_{IV} = \mathbf{e}_{IV}, \tag{2.16}$$

$$\mathbf{a}_{V} = \mathbf{e}_{V}, \tag{2.17}$$

$$\mathbf{a}_{VI} = \mathbf{e}_{VI}. \tag{2.18}$$

The basis $\mathbf{a}_\alpha$ and $\mathbf{e}_\beta$ are connected by the rotation $Q_{\alpha\beta}$ in six-dimensional space, namely

$$\mathbf{a}_\alpha = Q_{\alpha\beta}\mathbf{e}_\beta, \tag{2.19}$$

where the matrix $Q_{\alpha\beta}$ has the form

$$Q_{KL} = \begin{bmatrix} \frac{1}{\sqrt{3}} & \frac{1}{\sqrt{3}} & \frac{1}{\sqrt{3}} & 0 & 0 & 0 \\ \frac{1}{\sqrt{2}} & -\frac{1}{\sqrt{2}} & 0 & 0 & 0 & 0 \\ \frac{1}{\sqrt{6}} & \frac{1}{\sqrt{6}} & -\frac{2}{\sqrt{6}} & 0 & 0 & 0 \\ 0 & 0 & 0 & 1 & 0 & 0 \\ 0 & 0 & 0 & 0 & 1 & 0 \\ 0 & 0 & 0 & 0 & 0 & 1 \end{bmatrix}. \tag{2.20}$$

In the case of transversal isotropy the fourth-rank compliance tensor $\mathbf{C}$, which has components C_{ijkl} relative to the base $\mathbf{m}_k$, is represented in the polybase $\mathbf{e}_\beta$ by the following six-by-six matrix [15]:

$$\mathbf{C} \sim C_{\alpha\beta} = \begin{bmatrix} C_{1111} & C_{1122} & C_{1133} & 0 & 0 & 0 \\ C_{1122} & C_{1111} & C_{1133} & 0 & 0 & 0 \\ C_{1133} & C_{1133} & C_{3333} & 0 & 0 & 0 \\ 0 & 0 & 0 & 2C_{1313} & 0 & 0 \\ 0 & 0 & 0 & 0 & 2C_{1313} & 0 \\ 0 & 0 & 0 & 0 & 0 & C_{1111} - C_{1122} \end{bmatrix}. \tag{2.21}$$

It means that transversal isotropy is described by only five independent components of $\mathbf{C}$, namely

$$C_{1111}, \quad C_{3333}, \quad C_{1122}, \quad C_{1133}, \quad C_{1313}. \tag{2.22}$$

The matrix $C_{\alpha\beta}$ (2.21) after rotation (2.20) will change its form according to the formula

$$\tilde{C}_{MN} = Q_{M\alpha} C_{\alpha\beta} Q_{N\beta}. \tag{2.23}$$

The matrix $\tilde{C}_{MN}$ represents the tensor $\mathbf{C}$ in the polybase $\mathbf{a}_\alpha$ and can be expressed as

$$\mathbf{C} \sim \tilde{C}_{MN} \tag{2.24}$$

$$= \begin{bmatrix} A & 0 & B & 0 & 0 & 0 \\ 0 & C_{1111} - C_{1122} & 0 & 0 & 0 & 0 \\ B & 0 & D & 0 & 0 & 0 \\ 0 & 0 & 0 & 2C_{1313} & 0 & 0 \\ 0 & 0 & 0 & 0 & 2C_{1313} & 0 \\ 0 & 0 & 0 & 0 & 0 & C_{1111} - C_{1122} \end{bmatrix}.$$

The following notations are introduced:

$$A = \frac{1}{3}(2C_{1111} + 2C_{1122} + 4C_{1133} + C_{3333}), \tag{2.25}$$

$$B = \frac{\sqrt{2}}{3}(C_{1111} + C_{1122} - C_{1133} - C_{3333}), \tag{2.26}$$

$$D = \frac{1}{3}(C_{1111} + C_{1122} - 4C_{1133} + 2C_{3333}). \tag{2.27}$$

In order to construct the main energy-orthogonal decomposition of the space S for transversal isotropy, spectral decomposition of elasticity tensor has to be found out.

Spectral decomposition of elasticity tensor [11] opens completely new possibilities for comparing elastic materials. The spectral decomposition of the compliance tensor $\mathbf{C}$ is known if there are known all eigenvalues $\frac{1}{\lambda_K}$ and eigenstates $\boldsymbol{\omega}_K$ of $\mathbf{C}$.

Elastic moduli λ_K (eigenvalues of the stiffness tensor $\mathbf{S}$) will be called after Rychlewski – *the Kelvin moduli*. For the eigenvalue $\frac{1}{\lambda^*}$ of multiplicity one,

the proper state $\boldsymbol{\omega}^*$ – eigentensor corresponding to it, is given uniquely by the following relation

$$\mathbf{C} \cdot \boldsymbol{\omega}^* = \frac{1}{\lambda^*}\boldsymbol{\omega}^*. \tag{2.28}$$

In this case the orthogonal projector $\mathbf{P}^*$ has the form

$$\mathbf{P}^* = \boldsymbol{\omega}^* \otimes \boldsymbol{\omega}^*. \tag{2.29}$$

When Kelvin moduli are not distinct, i.e. there are some eigenvalues of multiplicity two, three or more, then there exist infinite number of possible eigentensors from which the basic eigentensors may be selected. They create the proper subspaces P_K [11]. The subspace P_K contains all proper elastic states corresponding to the elastic modulus λ_K. The orthogonal projectors $\mathbf{P}_K$ defined uniquely, map the space S onto subspaces P_K.

$$\mathbf{P}_K \cdot \boldsymbol{\sigma} = \boldsymbol{\sigma}_K \in P_K. \tag{2.30}$$

In the polybase $\boldsymbol{\omega}_K$ – eigentensors, which are selected so that the form an orthonormal set in six-dimensional space, the matrix six-by-six for $\mathbf{C}$ has a diagonal form with eigenvalues on the diagonal.

From (2.24) it is implied that for transversal isotropy, the following components

$$2C_{1313}, \quad C_{1111} - C_{1122} \tag{2.31}$$

are eigenvalues for $\mathbf{C}$ of multiplicity two. If we denote respectively by

$$\frac{1}{\lambda_3} = 2C_{1313}, \quad \frac{1}{\lambda_4} = C_{1111} - C_{1122}, \tag{2.32}$$

then the proper subspaces P_3 and P_4 corresponding to them are two-dimensional. They are created by tensors of the following form:

$$\boldsymbol{\sigma}_3 \sim \begin{pmatrix} 0 & 0 & p \\ 0 & 0 & q \\ p & q & 0 \end{pmatrix} \in P_3, \quad \boldsymbol{\sigma}_4 \sim \begin{pmatrix} u & v & 0 \\ v & -u & 0 \\ 0 & 0 & 0 \end{pmatrix} \in P_4. \tag{2.33}$$

An orthonormal base in the subspace P_3 may be taken as follows:

$$\boldsymbol{\omega}_{III} = \mathbf{e}_V = \frac{1}{\sqrt{2}}(\mathbf{m}_1 \otimes \mathbf{k} + \mathbf{k} \otimes \mathbf{m}_1), \tag{2.34}$$

$$\boldsymbol{\omega}_{IV} = \mathbf{e}_{IV} = \frac{1}{\sqrt{2}}(\mathbf{m}_2 \otimes \mathbf{k} + \mathbf{k} \otimes \mathbf{m}_2). \tag{2.35}$$

Two tensors of the form

$$\boldsymbol{\omega}_V = \mathbf{a}_{II} = \frac{1}{\sqrt{2}}(\mathbf{e}_I - \mathbf{e}_{II}) = \frac{1}{\sqrt{2}}(\mathbf{m}_1 \otimes \mathbf{m}_1 - \mathbf{m}_2 \otimes \mathbf{m}_2), \tag{2.36}$$

$$\boldsymbol{\omega}_{VI} = \mathbf{e}_{VI} = \frac{1}{\sqrt{2}}(\mathbf{m}_1 \otimes \mathbf{m}_2 + \mathbf{m}_2 \otimes \mathbf{m}_1) \tag{2.37}$$

may be selected as a base in P_4 .

Two distinct Kelvin moduli λ_1 and λ_2 are obtained from the characteristic equation

$$\det \begin{pmatrix} A - \frac{1}{\lambda} & B \\ B & D - \frac{1}{\lambda} \end{pmatrix} = \left(\frac{1}{\lambda}\right)^2 - (A+D)\frac{1}{\lambda} + AD - B^2 = 0. \tag{2.38}$$

Both moduli λ_1 and λ_2 are of multiplicity one and have the form

$$\lambda_1^{-1} = \frac{1}{2}\left[A + D - \sqrt{(A-D)^2 + 4B^2}\right], \tag{2.39}$$

$$\lambda_2^{-1} = \frac{1}{2}\left[A + D + \sqrt{(A-D)^2 + 4B^2}\right]. \tag{2.40}$$

The parameters A, B, D are described by relations (2.25) – (2.27).

The proper states corresponding to λ_1 and λ_2 (2.39) – (2.40) create two one-dimensional subspaces P_1 and P_2. They are orthogonal to each other and orthogonal to P_3 and P_4.

From (2.24) it is implied that the eigentensors, proper states $\boldsymbol{\omega}_I$ and $\boldsymbol{\omega}_{II}$ corresponding to λ_1 and λ_2, may be obtained from the tensors $\mathbf{a}_I$ (2.13) and $\mathbf{a}_{III}$ (2.15), by rotation, namely

$$\boldsymbol{\omega}_I = \cos(\aleph - \aleph_0)\mathbf{a}_I + \sin(\aleph - \aleph_0)\mathbf{a}_{III}, \tag{2.41}$$

$$\boldsymbol{\omega}_{II} = -\sin(\aleph - \aleph_0)\mathbf{a}_I + \cos(\aleph - \aleph_0)\mathbf{a}_{III}, \tag{2.42}$$

where

$$\aleph_0 \Rightarrow \quad \tan\aleph_0 = \sqrt{2} \tag{2.43}$$

and

$$\tan 2(\aleph - \aleph_0) = \frac{2B}{A-D} \quad (A \neq D). \tag{2.44}$$

Thus substituting values of $\mathbf{a}_I$ and $\mathbf{a}_{III}$ into (2.41) – (2.42) we immediately arrive at the result

$$\boldsymbol{\omega}_I = \frac{1}{\sqrt{2}}\left[\sin\aleph\mathbf{I} + \sqrt{3}\sin(\aleph_0 - \aleph)\mathbf{k}\otimes\mathbf{k}\right], \tag{2.45}$$

$$\boldsymbol{\omega}_{II} = \frac{1}{\sqrt{2}}\left[\cos\aleph\mathbf{I} - \sqrt{3}\cos(\aleph_0 - \aleph)\mathbf{k}\otimes\mathbf{k}\right]. \tag{2.46}$$

Tensors $\boldsymbol{\omega}_I$ and $\boldsymbol{\omega}_{II}$ in the base $\mathbf{m}_k$ have the following matrix representations:

$$\begin{aligned}\boldsymbol{\omega}_I &\sim \frac{1}{\sqrt{2}}\begin{pmatrix}\sin\aleph & 0 & 0\\ 0 & \sin\aleph & 0\\ 0 & 0 & \sqrt{2}\cos\aleph\end{pmatrix},\\ \boldsymbol{\omega}_{II} &\sim \frac{1}{\sqrt{2}}\begin{pmatrix}\cos\aleph & 0 & 0\\ 0 & \cos\aleph & 0\\ 0 & 0 & -\sqrt{2}\sin\aleph\end{pmatrix}.\end{aligned} \tag{2.47}$$

Finally the spectral decomposition of the compliance tensor $\mathbf{C}$ (1.1) for the transversal isotropy has the form:

$$\begin{aligned}\mathbf{C} &= \frac{1}{\lambda_1}\mathbf{P}_1 + \frac{1}{\lambda_2}\mathbf{P}_2 + \frac{1}{\lambda_3}\mathbf{P}_3 + \frac{1}{\lambda_4}\mathbf{P}_4\\ &= \frac{1}{\lambda_1}\boldsymbol{\omega}_I\otimes\boldsymbol{\omega}_I + \frac{1}{\lambda_2}\boldsymbol{\omega}_{II}\otimes\boldsymbol{\omega}_{II} + \frac{1}{\lambda_3}(\boldsymbol{\omega}_{III}\otimes\boldsymbol{\omega}_{III} + \boldsymbol{\omega}_{IV}\otimes\boldsymbol{\omega}_{IV})\\ &\quad + \frac{1}{\lambda_4}(\boldsymbol{\omega}_V\otimes\boldsymbol{\omega}_V + \boldsymbol{\omega}_{VI}\otimes\boldsymbol{\omega}_{VI}).\end{aligned} \tag{2.48}$$

The Kelvin moduli λ_1, λ_2, λ_3 i λ_4 are given by formulae (2.32) and (2.39) – (2.40).

The spectral decomposition of the space $S = P_1\oplus P_2\oplus P_3\oplus P_4$ is in the same time the main energy-orthogonal decomposition. Hence transversal isotropy is described now by λ_1, λ_2, λ_3, λ_4 and $\aleph$ instead of the parameters (2.22).

Decomposing a stress $\boldsymbol{\sigma}\in S$ into the parts $\boldsymbol{\sigma}_K$, $\boldsymbol{\sigma}_K = \mathbf{P}_K\cdot\boldsymbol{\sigma}$ in the proper subspaces P_K we obtain that

$$\boldsymbol{\sigma} = \boldsymbol{\sigma}_1 + \boldsymbol{\sigma}_2 + \boldsymbol{\sigma}_3 + \boldsymbol{\sigma}_4, \quad \boldsymbol{\sigma}_K\in P_K. \tag{2.49}$$

The above decomposition has a unique form. Since this decomposition is energy-orthogonal as well, then the elastic energy $\Phi(\boldsymbol{\sigma})$ (1.5) may be written as the following sum:

$$\Phi(\boldsymbol{\sigma}) = \Phi(\boldsymbol{\sigma}_1) + \Phi(\boldsymbol{\sigma}_2) + \Phi(\boldsymbol{\sigma}_3) + \Phi(\boldsymbol{\sigma}_4) \tag{2.50}$$

where

$$\Phi(\boldsymbol{\sigma}_1) = \frac{1}{2}\boldsymbol{\sigma}_1 \cdot \mathbf{C} \cdot \boldsymbol{\sigma}_1 = \frac{1}{2\lambda_1}\boldsymbol{\sigma}_1 \cdot \boldsymbol{\sigma}_1 = \frac{1}{4\lambda_1}\left[\sin \aleph \mathrm{tr}\boldsymbol{\sigma} + \sqrt{3}\sin(\aleph_0 - \aleph)\mathbf{k} \cdot \boldsymbol{\sigma} \cdot \mathbf{k}\right]^2, \tag{2.51}$$

$$\Phi(\boldsymbol{\sigma}_2) = \frac{1}{2}\boldsymbol{\sigma}_2 \cdot \mathbf{C} \cdot \boldsymbol{\sigma}_2 = \frac{1}{2\lambda_2}\boldsymbol{\sigma}_2 \cdot \boldsymbol{\sigma}_2 = \frac{1}{4\lambda_2}\left[\cos \aleph \mathrm{tr}\boldsymbol{\sigma} - \sqrt{3}\cos(\aleph_0 - \aleph)\mathbf{k} \cdot \boldsymbol{\sigma} \cdot \mathbf{k}\right]^2, \tag{2.52}$$

$$\Phi(\boldsymbol{\sigma}_3) = \frac{1}{2}\boldsymbol{\sigma}_3 \cdot \mathbf{C} \cdot \boldsymbol{\sigma}_3 = \frac{1}{2\lambda_3}\boldsymbol{\sigma}_3 \cdot \boldsymbol{\sigma}_3 = \frac{1}{2\lambda_3}\left[(\mathbf{m}_1 \cdot \boldsymbol{\sigma} \cdot \mathbf{k})^2 + (\mathbf{m}_2 \cdot \boldsymbol{\sigma} \cdot \mathbf{k})^2\right], \tag{2.53}$$

$$\Phi(\boldsymbol{\sigma}_4) = \frac{1}{2}\boldsymbol{\sigma}_4 \cdot \mathbf{C} \cdot \boldsymbol{\sigma}_4 = \frac{1}{2\lambda_4}\boldsymbol{\sigma}_4 \cdot \boldsymbol{\sigma}_4 = \frac{1}{2\lambda_4}\left\{[(\mathbf{m}_1 \cdot \boldsymbol{\sigma} \cdot \mathbf{m}_1) - (\mathbf{m}_2 \cdot \boldsymbol{\sigma} \cdot \mathbf{m}_2)]^2 + 4(\mathbf{m}_1 \cdot \boldsymbol{\sigma} \cdot \mathbf{m}_2)^2\right\}. \tag{2.54}$$

From (2.50) – (2.54) it is implied that

$$\begin{aligned} 2\Phi(\boldsymbol{\sigma}) = \boldsymbol{\sigma} \cdot \mathbf{C} \cdot \boldsymbol{\sigma} = {} & \frac{1}{2\lambda_1}\left[\sin \aleph \mathrm{tr}\boldsymbol{\sigma} + \sqrt{3}\sin(\aleph_0 - \aleph)\mathbf{k}\boldsymbol{\sigma}\mathbf{k}\right]^2 \\ & + \frac{1}{2\lambda_2}\left[\cos \aleph \mathrm{tr}\boldsymbol{\sigma} - \sqrt{3}\cos(\aleph_0 - \aleph)\mathbf{k}\boldsymbol{\sigma}\mathbf{k}\right]^2 \\ & + \frac{1}{\lambda_3}\left[(\mathbf{m}_1 \cdot \boldsymbol{\sigma} \cdot \mathbf{k})^2 + (\mathbf{m}_2 \cdot \boldsymbol{\sigma} \cdot \mathbf{k})^2\right] \\ & + \frac{1}{\lambda_4}\left\{[(\mathbf{m}_1 \cdot \boldsymbol{\sigma} \cdot \mathbf{m}_1) - (\mathbf{m}_2 \cdot \boldsymbol{\sigma} \cdot \mathbf{m}_2)]^2 + 4(\mathbf{m}_1 \cdot \boldsymbol{\sigma} \cdot \mathbf{m}_2)^2\right\}. \end{aligned} \tag{2.55}$$

The limit condition of the Mises type (1.18) representing a generalization of the Maxwell-Huber-Mises condition for transversal isotropy may be taken in the form [9]:

$$\frac{1}{h_1}\Phi(\boldsymbol{\sigma}_1) + \frac{1}{h_2}\Phi(\boldsymbol{\sigma}_2) + \frac{1}{h_3}\Phi(\boldsymbol{\sigma}_3) + \frac{1}{h_4}\Phi(\boldsymbol{\sigma}_4) \leq 1 \tag{2.56}$$

where h_α are energy limits of elasticity $\Phi(\boldsymbol{\sigma}_\alpha)$ (2.51) – (2.54).

It means that the limit criterion (2.56) bounds the weighted sum of stored energies, corresponding to uniquely defined, energy–orthogonal parts of stress. Taking the yield condition in the form (2.56) we assumed that the tensors $\mathbf{C}$ and $\mathbf{H}$ were coaxial.

Let us denote by $\mathbf{M}$ the dyad $\mathbf{k} \otimes \mathbf{k}$ i.e.

$$\mathbf{M} = \mathbf{k} \otimes \mathbf{k}, \tag{2.57}$$

then the elastic energies $\Phi(\boldsymbol{\sigma}_K)$ may be expressed in the invariant form [10]:

$$\Phi(\boldsymbol{\sigma}_1) = \frac{1}{4\lambda_1}\left[\sqrt{2}\cos\aleph\left(\mathrm{tr}\mathbf{M}\mathbf{s} + \frac{1}{3}\mathrm{tr}\boldsymbol{\sigma}\right) - \sin\aleph\left(\mathrm{tr}\mathbf{M}\mathbf{s} - \frac{2}{3}\mathrm{tr}\boldsymbol{\sigma}\right)\right]^2, \tag{2.58}$$

$$\Phi(\boldsymbol{\sigma}_2) = \frac{1}{4\lambda_2}\left[\cos\aleph\left(\frac{2}{3}\mathrm{tr}\boldsymbol{\sigma} - \mathrm{tr}\mathbf{M}\mathbf{s}\right) - \sqrt{2}\sin\aleph\left(\mathrm{tr}\mathbf{M}\mathbf{s} + \frac{1}{3}\mathrm{tr}\boldsymbol{\sigma}\right)\right]^2, \tag{2.59}$$

$$\Phi(\boldsymbol{\sigma}_3) = \frac{1}{\lambda_3}\left[\mathrm{tr}\mathbf{M}\mathbf{s}^2 - (\mathrm{tr}\mathbf{M}\mathbf{s})^2\right], \tag{2.60}$$

$$\Phi(\boldsymbol{\sigma}_4) = \frac{1}{2\lambda_4}\left[\mathrm{tr}\mathbf{s}^2 - 2\mathrm{tr}\mathbf{M}\mathbf{s}^2 + \frac{1}{2}(\mathrm{tr}\mathbf{M}\mathbf{s})^2\right]. \tag{2.61}$$

Denoting by σ_{ij} components of a stress tensor $\boldsymbol{\sigma}$ in the base $\mathbf{m}_k$, the following symbols can be introduced:

$$r = \frac{1}{2 + (1-\gamma)^2}\left(\sigma_{11} + \sigma_{22} + (1-\gamma)\sigma_{33}\right), \tag{2.62}$$

$$s = \frac{1-\gamma}{2(2+(1-\gamma)^2)}\left(\sigma_{11} + \sigma_{22} - \frac{2}{1-\gamma}\sigma_{33}\right), \tag{2.63}$$

$$u = \frac{1}{2}\left(\sigma_{11} - \sigma_{22}\right), \tag{2.64}$$

$$v = \sigma_{12}, \quad p = \sigma_{13}, \quad q = \sigma_{23}, \tag{2.65}$$

and

$$1 - \gamma = \sqrt{2}\cot\aleph. \tag{2.66}$$

The graphical illustration of the parts of stress $\boldsymbol{\sigma}_K \in P_K$ (2.49) is presented in Fig. 1.

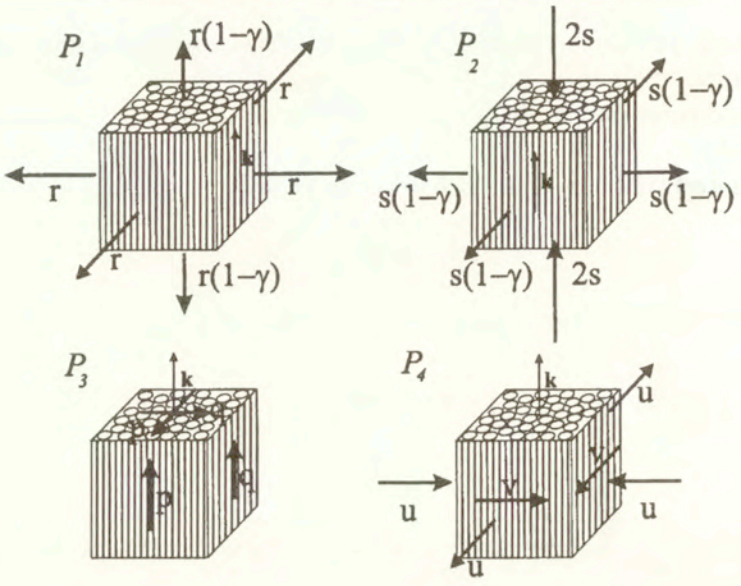

FIG. 1. Graphical illustration of subspaces P_K of the proper states of $\mathbf{C}$ for transversally isotropic solids.

3. Safe states of stress

The energy is the most universal physical notion. The idea that the stored elastic energy is an appropriate measure of the mechanical behaviour of the elastic material is quite widely acceptable.

The classical Maxwell-Huber-Mises condition (1.7) limits the distortion energy only. Consequently, plastic deformations occur in the plastic shaping process and are not accompanied by volume changes. It means that the spherical parts of stress tensors are safe.

In case of anisotropic bodies, there is no physical reason to consider the hydrostatic state as a safe stress. Depending on the type of anisotropy, different states can be taken as safe stresses. Using an example of transversal isotropy we assume that two different states of stresses are safe.

The limit condition (2.56) which is based on the main energy-orthogonal decomposition is discussed. If energy limit of elasticity h_K tends to infinity ($h_K \to \infty$) then the subspace P_K consists of safe stresses. In contrast, while a state of stress $\boldsymbol{\sigma}_K^* \in P_K$ ($\boldsymbol{\sigma}_K^*$ is a proper state) is a safe stress then the energy $\Phi(\boldsymbol{\sigma}_K^*)$ does not enter the limit condition. It means that h_K, an elasticity limit for $\Phi(\boldsymbol{\sigma}_K^*)$, tends to infinity.

The situation becomes more complicated if the proposed safe stress is not a proper state for the compliance tensor $\mathbf{C}$. Still the limit conditions (2.56) is under consideration.

Now let us assume that the hydrostatic pressure is the safe stress as it is for isotropy. We remind that the spherical tensor is not a proper state for transversal isotropy. Now, we consider two different states of stress

$$\boldsymbol{\sigma}^a = \sigma_a \mathbf{I} + \mathbf{s}, \quad \boldsymbol{\sigma}^b = \sigma_b \mathbf{I} + \mathbf{s}, \quad \sigma_a \neq \sigma_b, \tag{3.1}$$

with the same deviatoric parts $\mathbf{s}$ and different isotropic parts.

Since it has been assumed that the hydrostatic pressure is safe, the function (2.56) in the limit state should have the same value for both states of stress, namely

$$\frac{1}{h_1}\Phi(\boldsymbol{\sigma}_1^a)+\frac{1}{h_2}\Phi(\boldsymbol{\sigma}_2^a)+\frac{1}{h_3}\Phi(\boldsymbol{\sigma}_3^a)+\frac{1}{h_4}\Phi(\boldsymbol{\sigma}_4^a) = \frac{1}{h_1}\Phi(\boldsymbol{\sigma}_1^b)+\frac{1}{h_2}\Phi(\boldsymbol{\sigma}_2^b)+\frac{1}{h_3}\Phi(\boldsymbol{\sigma}_3^b)+\frac{1}{h_4}\Phi(\boldsymbol{\sigma}_4^b), \tag{3.2}$$

where $\boldsymbol{\sigma}_K^a = \mathbf{P}_K \cdot \boldsymbol{\sigma}^a$ and $\boldsymbol{\sigma}_K^b = \mathbf{P}_K \cdot \boldsymbol{\sigma}^b$. The above condition, after using Eqs. (2.51) – (2.52) can be rewritten in the form

$$\frac{1}{h_1}(\Phi(\boldsymbol{\sigma}_1^a) - \Phi(\boldsymbol{\sigma}_1^b)) + \frac{1}{h_2}(\Phi(\boldsymbol{\sigma}_2^a) - \Phi(\boldsymbol{\sigma}_2^b)) = 0. \tag{3.3}$$

Finally, after substituting (2.51) – (2.52) into (3.3) and taking advantage of the fact that $\sigma_a \neq \sigma_b$ we obtain the following equation:

$$\frac{1}{6}(\sigma_a + \sigma_b)\left[\frac{\cos^2(\aleph-\aleph_0)}{\lambda_1 h_1} + \frac{\sin^2(\aleph-\aleph_0)}{\lambda_2 h_2}\right] + \frac{\sin 2(\aleph-\aleph_0)}{2\sqrt{3}}(\mathbf{s}\cdot\mathbf{a}_{III})\left[\frac{1}{\lambda_1 h_1} - \frac{1}{\lambda_2 h_2}\right] = 0, \tag{3.4}$$

which should be satisfied by any σ_a, σ_b and $\mathbf{s}$. In particular it is convenient to assume that for $\mathbf{s} = 0$, two following cases are considered:

$$\sigma_b = -\sigma_a \quad \text{and} \quad \sigma_b \neq -\sigma_a. \tag{3.5}$$

By combining the above assumptions we obtain from (3.4) the following conditions:

- $\dfrac{1}{h_1} = \dfrac{1}{h_2} = 0, \quad$ when $\aleph \neq \aleph_0$

- $\dfrac{1}{h_1} = 0$ and $\dfrac{1}{h_2} \neq 0$, when $\aleph = \aleph_0$ (the spherical tensor is the proper state of $\mathbf{C}$).

We note that for $\aleph \neq \aleph_0$ the spherical tensor can be a safe state only then when the subspace $P_1 \oplus P_2 \in S$ is the subspace of safe stresses.

As an example of transversally isotropic materials, the fibre-reinforced composites are considered.

Let us suppose that tensions in the privileged fiber direction $\mathbf{k}$ are safe stresses. It means that the fibres are inextensible or they are much stronger than the matrix material. In a general case the tension in the $\mathbf{k}$ direction is not a proper state for transversal isotropy.

Now, we consider the following two states of stress

$$\boldsymbol{\sigma}^c = \sigma_c \mathbf{k} \otimes \mathbf{k} + \mathbf{p}, \quad \boldsymbol{\sigma}^d = \sigma_d + \mathbf{p}, \quad \sigma_c \neq \sigma_d \quad \text{and} \quad \mathbf{k} \cdot \mathbf{p} \cdot \mathbf{k} = 0 \tag{3.6}$$

only with different projectors on the $\mathbf{k}$ direction.

Using the analogous way as above we conclude that the state $a\mathbf{k} \otimes \mathbf{k}$ is safe only when:

- $\dfrac{1}{h_1} = \dfrac{1}{h_2} = 0$, for $\aleph \neq 0$,
- $\dfrac{1}{h_1} = 0$ and $\dfrac{1}{h_2} \neq 0$, for $\aleph = 0$ (it means that the state $a\mathbf{k} \otimes \mathbf{k}$ is the proper state for $\mathbf{C}$).

We note that for $\aleph \neq 0$ the obtained conditions are, at the same time, the conditions which are satisfied when all stress states from the subspace $P_1 \oplus P_2$ are safe, including the states for which $\mathbf{k} \cdot \boldsymbol{\sigma} \cdot \mathbf{k} = 0$.

In the real material the assumptions that the spherical tensor and the tension in the $\mathbf{k}$ direction are safe states do not necessary implicate that any state of stress $\boldsymbol{\sigma} \in P_1 \oplus P_2$ for which $\mathrm{tr}\boldsymbol{\sigma} = 0$ or $\mathbf{k} \cdot \boldsymbol{\sigma} \cdot \mathbf{k} = 0$ is safe.

The proposed yield condition (2.56) is one of the possible generalizations of the Maxwell-Huber-Mises condition for the case of anisotropy. We have established it for anisotropic bodies for which elastic and plastic properties are dependent, namely the tensors $\mathbf{C}$ and $\mathbf{H}$ are coaxial. In a general case the fourth-rank tensor $\mathbf{H}$ proposed by MISES [17] can be assumed to be arbitrary.

4. Physical interpretation of material parameters for transversally isotropic solids

Transversal isotropy is described by the following five parameters: four Kelvin moduli – λ_1, λ_2, λ_3, λ_4 and one stiffness distributor $\aleph$.

In order to determine these parameters some experimental tests should be proposed. The values of the moduli λ_3 and λ_4 can be determined without special

difficulties. Taking for each of them two states of stress from the subspace P_3 or P_4 respectively, we find relations between stresses and strains (see Fig.2). Hence, it is implied that λ_3 and λ_4 are as follows:

$$\tan\varphi_1 = \lambda_3, \quad \tan\varphi_2 = \lambda_4 \tag{4.1}$$

where the angles φ_1 and φ_2 are shown in Fig. 2.

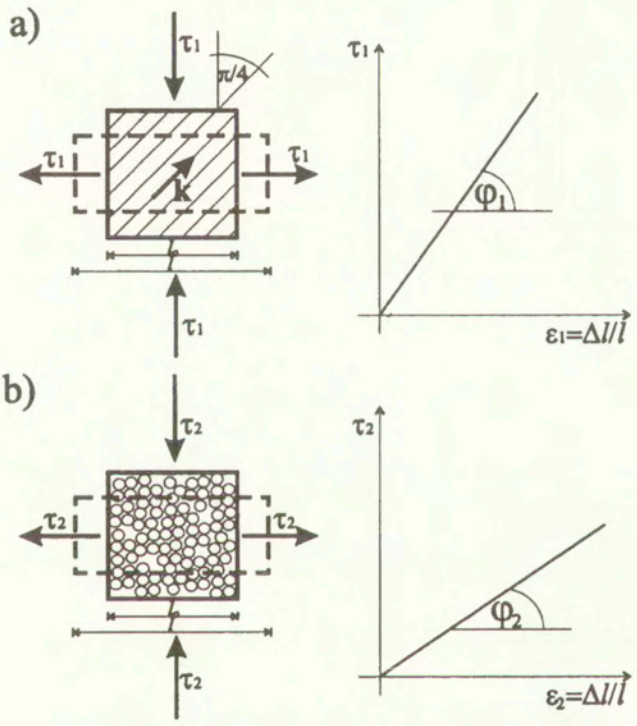

FIG. 2. Proposed experimental tests useful in determining the Kelvin moduli λ_3(a) and λ_4(b).

Calculations of the remaining three parameters are more complicated. We propose the experimental tests illustrated in Fig. 3 together with the obtained stress-strain relations.

Both the proposed states of stress have the orthogonal projections onto subspaces P_1 and P_2.

For simplicity, the following notations are introduced:

$$r_3 = \frac{\varepsilon_l}{\varepsilon_a} = \frac{\varepsilon_{33}}{\varepsilon_{11}}, \quad \text{(Fig. 3a)}; \quad r_4 = \frac{\varepsilon_b}{\varepsilon_h} = \frac{\varepsilon_{11}}{\varepsilon_{33}}, \quad \text{(Fig. 3b)}; \quad \bar{r} = r_3 - 2r_4. \tag{4.2}$$

If the value of $\bar{r}$ is known then the stiffness distributor $\aleph$ can be found from the relation

$$\cot 2\aleph = \frac{\sqrt{2}}{4}\bar{r}. \tag{4.3}$$

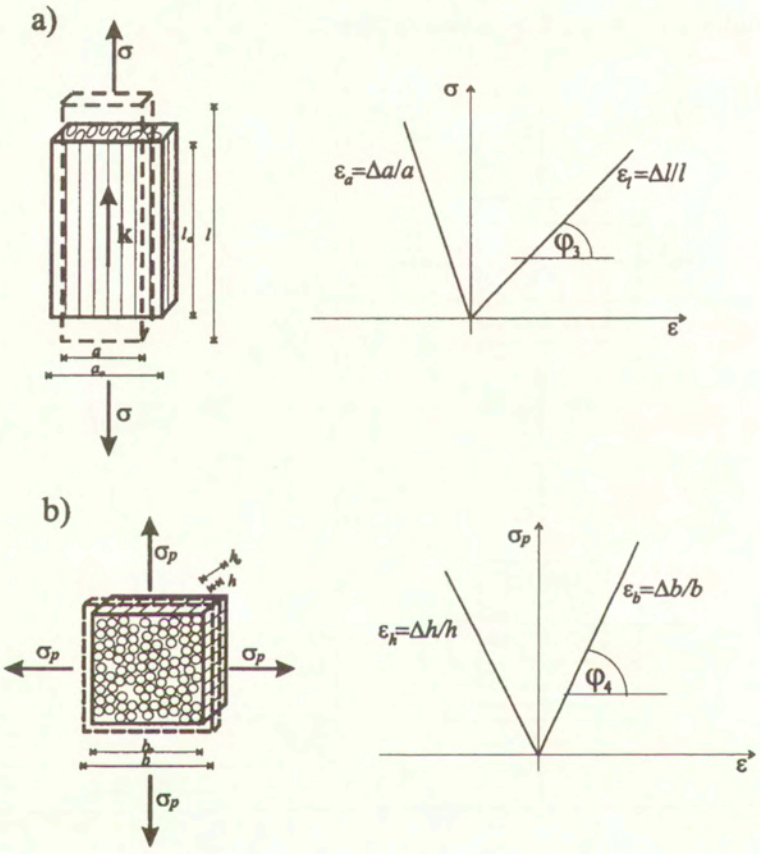

FIG. 3. Proposed experimental tests useful in determining the Kelvin moduli λ_1 and λ_2 as well as the stiffness distributor $\aleph$.

We note that $\bar{r} = -1$ for cubic symmetry and isotropy.

The Kelvin moduli λ_1 and λ_2 for a known value of the stiffness distributor $\aleph$ are given by the formulae

$$\lambda_1 = \frac{(1-\cot^2\aleph)\tan\varphi_3\tan\varphi_4}{\tan\varphi_3 - \cot^2\aleph\tan\varphi_4}, \tag{4.4}$$

$$\lambda_2 = \frac{(1-\cot^2\aleph)\tan\varphi_3\tan\varphi_4}{\tan\varphi_4 - \cot^2\aleph\tan\varphi_3}. \tag{4.5}$$

Let us consider two special cases of transversal isotropy, depending on the value of $\aleph$, namely:

- $\aleph = \aleph_0$,
- $\aleph = 0$.

From Eqs. (2.44) – (2.45) it is implied that for $\aleph = \aleph_0$ the spherical tensor is a proper state and $B = 0$. Consequently we conclude that the Burzynski conditions (1.13) – (1.17) are satisfied. In this case the number of independent material parameters reduces to four.

On the other hand when $\aleph = 0$, tension in the direction $\mathbf{k}$ is a proper state (see Fig. 3a) and we have $\varepsilon_a = \varepsilon_{11} = \varepsilon_{22} = 0$. From Eqs. (2.44) and (2.25) it is implied that $C_{1133} = 0$. We should emphasize that in both cases some extra constraints are imposed on the material because the stiffness distributor is determined.

Carrying on the proposed experimental tests (see Fig. 2 and Fig. 3) until permanent deformation or damage appear, we can determine the values of elasticity limits h_K in the limit condition (2.56). The elastic energies in the limit state for each of the tests can be expressed as follows:

$$\Phi_1 = \tau_1^* \varepsilon_1^*, \quad \Phi_2 = \tau_2^* \varepsilon_2^*, \quad \Phi_3 = \frac{1}{2}\sigma^* \varepsilon_l^*, \quad \Phi_4 = \sigma_p^* \varepsilon_b^*, \tag{4.6}$$

where $(.)^*$ denote the values of the stresses and strains in the limit state (see Fig. 2 and Fig. 3).

Thus substituting the found stiffness distributor value into the formulas (2.51) – (2.54) we obtain

$$h_1 = \frac{(k_1 - k_2)\Phi_3\Phi_4}{4(2k_1 - k_2 + 1)\Phi_4 - (2 - k_1)\Phi_3},$$
$$h_2 = \frac{(k_1 - k_2)\Phi_3\Phi_4}{4(2k_1 - k_2 - 1)\Phi_4 + (2 - k_1)\Phi_3}, \tag{4.7}$$

$$h_3 = \Phi_1, \quad h_4 = \Phi_2, \tag{4.8}$$

where the following parameters are introduced:

$$k_1 = \cos 2\aleph \left(1 + \frac{4}{\bar{r}r_3}\right), \quad k_2 = \cos 2\aleph \left(1 + \frac{2}{\bar{r}r_4}\right). \tag{4.9}$$

We note that the state of stress is safe if for sufficiently high value of it the limit condition is not reached.

5. The Mises limit condition for transversal isotropy

The limit condition proposed in Sec. 2 is based on the main energy-orthogonal decomposition. It is in some sense a generalization of the Maxwell-Huber-Mises yield condition for anisotropic materials. Formulating that condition we have assumed that elastic and limit properties are mutually dependent. Tensor $\mathbf{C}$ and $\mathbf{H}$ are coaxial. In real materials they can be arbitrary.

MISES [16, 17] proposed the limit condition in the form

$$\mathbf{s} \cdot \mathbf{H} \cdot \mathbf{s} \leq 1. \tag{5.1}$$

It means that he introduced the fourth rank limit tensor $\mathbf{H}$ responsible for limit properties. Besides, he assumed that the spherical part of stress tensor is safe.

When anisotropic materials are considered, there is no physical reason to privilege the spherical tensor. This assumption is in common use in hydrodynamics and isotropy.

Rychlewski [12] introduced the limit condition (1.18) which is in some sense a generalization of Mises one (5.1). He considered the quadratic form $\boldsymbol{\sigma} \cdot \mathbf{H} \cdot \boldsymbol{\sigma} \geq 0$ instead of (5.1). According to the proposed condition, the stress $\hat{\boldsymbol{\sigma}}$ is safe if the following condition

$$\hat{\boldsymbol{\sigma}} \cdot \mathbf{H} \cdot \hat{\boldsymbol{\sigma}} = 0 \tag{5.2}$$

is satisfied.

We should emphasize that MISES did not bind up the condition (5.2) with stored elastic energy. Rychlewski [12], considering two quadratic forms (1.5) and (1.8), i.e.

$$\boldsymbol{\sigma} \cdot \mathbf{C} \cdot \boldsymbol{\sigma} \quad \text{and} \quad \boldsymbol{\sigma} \cdot \mathbf{H} \cdot \boldsymbol{\sigma}, \tag{5.3}$$

proved the theorem that any stress measures of the form (5.3) have uniquely determined energy-based interpretation and they may be decomposed into the following sums:

$$\frac{1}{2}\boldsymbol{\sigma} \cdot \mathbf{C} \cdot \boldsymbol{\sigma} = \Phi(\boldsymbol{\sigma}) = \Phi(\tilde{\boldsymbol{\sigma}}_1) + \Phi(\tilde{\boldsymbol{\sigma}}_2) + \ldots + \Phi(\tilde{\boldsymbol{\sigma}}_\chi), \tag{5.4}$$

$$\boldsymbol{\sigma} \cdot \mathbf{H} \cdot \boldsymbol{\sigma} = \frac{1}{\tilde{h}_1}\Phi(\tilde{\boldsymbol{\sigma}}_1) + \frac{1}{\tilde{h}_2}\Phi(\tilde{\boldsymbol{\sigma}}_2) + \ldots + \frac{1}{\tilde{h}_\chi}\Phi(\tilde{\boldsymbol{\sigma}}_\chi), \tag{5.5}$$

where

$$\boldsymbol{\sigma} = \tilde{\boldsymbol{\sigma}}_1 + \ldots + \tilde{\boldsymbol{\sigma}}_\chi, \quad \chi \leq 6 \quad \text{and} \quad \tilde{\boldsymbol{\sigma}}_\alpha \times \tilde{\boldsymbol{\sigma}}_\beta = \begin{cases} 0, & \alpha \neq \beta \\ 2\Phi(\tilde{\boldsymbol{\sigma}}_\alpha), & \alpha = \beta. \end{cases} \tag{5.6}$$

It means that $\tilde{\boldsymbol{\sigma}}_\alpha$ are energy-orthogonal states of stress (2.1), while the parameters $\tilde{h}_\alpha$ are energy limits of elasticity $\Phi(\tilde{\boldsymbol{\sigma}}_\alpha)$. We should emphasize that the states of stress (5.6) need not be orthogonal, i.e. $\tilde{\boldsymbol{\sigma}}_\alpha \cdot \tilde{\boldsymbol{\sigma}}_\beta \neq 0$ for $\alpha \neq \beta$.

The purpose of this work is to demonstrate the limit condition of the form (5.5) for transversal isotropy. Using Rychlewski's approach proposed in paper [12] we will find the energy-orthogonal decomposition of the space S (5.6) and moduli $\tilde{h}_\alpha$.

The quadratic form (5.2)b may be rewritten in the form

$$\boldsymbol{\sigma} \cdot \mathbf{H} \cdot \boldsymbol{\sigma} = \boldsymbol{\sigma} \times (\mathbf{S} \circ \mathbf{H} \circ \mathbf{S}) \times \boldsymbol{\sigma} \tag{5.7}$$

where the definition of the energy scalar product (2.1) and the condition (1.2) were used.

Fourth-rank tensor $\mathbf{S} \circ \mathbf{H} \circ \mathbf{S}$ realizes a symmetric linear transformation of the space of symmetric second-rank tensors S into itself, i.e.

$$(\mathbf{S} \circ \mathbf{H} \circ \mathbf{S}) \times \boldsymbol{\alpha} = \boldsymbol{\beta}, \quad \boldsymbol{\alpha}, \boldsymbol{\beta} \in S. \tag{5.8}$$

Tensor $\boldsymbol{\kappa}$ is a proper state of the operator (5.8) if

$$(\mathbf{S} \circ \mathbf{H} \circ \mathbf{S}) \times \boldsymbol{\kappa} = \frac{1}{2\tilde{h}} \boldsymbol{\kappa}. \tag{5.9}$$

The operator $\mathbf{S} \circ \mathbf{H} \circ \mathbf{S}$ is a symmetric one, thus there is a set of energy-orthogonal tensors $\boldsymbol{\kappa}_\alpha$ corresponding to the values $\frac{1}{2\tilde{h}_\alpha}$

$$\boldsymbol{\kappa}_\alpha \times \boldsymbol{\kappa}_\beta = \delta_{\alpha\beta}. \tag{5.10}$$

Equation (5.9) after using the definition of energy scalar product (2.1) and multiplying left-sided by $\mathbf{C}$, takes the form

$$(\mathbf{H} - \frac{1}{2\tilde{h}} \mathbf{C}) \cdot \boldsymbol{\kappa} = \mathbf{0}. \tag{5.11}$$

States $\boldsymbol{\kappa}$ create the kernel of the operator $\mathbf{H} - \frac{1}{2\tilde{h}} \mathbf{C}$ but moduli $\tilde{h}$ are determined from the equation

$$\det(\mathbf{H} - \frac{1}{2\tilde{h}} \mathbf{C}) = 0. \tag{5.12}$$

If the moduli $\tilde{h}_\alpha$ are distinct, the energy-orthogonal states corresponding to them have unique form. For multiple moduli $\tilde{h}_\alpha$ the energy-orthogonal states $\boldsymbol{\kappa}_\alpha$ form the subspaces $H_\alpha \subset S$.

Let us denote by $\mathbf{P}_\alpha^H$ $(\alpha = 1, ..., \chi)$ the projectors of a stress tensor $\boldsymbol{\sigma}$ onto the energy-orthogonal subspaces H_α; then

$$\tilde{\boldsymbol{\sigma}}_\alpha = \mathbf{P}_\alpha^H \times \boldsymbol{\sigma}, \quad \tilde{\boldsymbol{\sigma}}_\alpha \in H_\alpha. \tag{5.13}$$

We want to emphasize that the tensors $\mathbf{C}$ and $\mathbf{H}$ in (5.11) are mutually independent.

Usually, some coupling of elastic properties with the limit ones is observed. For instance, it can be assumed that $\mathbf{C}$ and $\mathbf{H}$ are co-axial [12] that is they have the same eigentensors. In this case solution of Eq. (5.11) becomes simplified. For transversally isotropic materials it leads to Eq. (2.56) given in the Sec. 2.

In this section we will focus on the case of transversally isotropic material for which tensors $\mathbf{C}$ and $\mathbf{H}$ are not coaxial. We only assume that the orientation of the preference direction $\mathbf{k}$ is the same for material in the elastic range as well as in the limit state. The matrix representation of the compliance tensor $\mathbf{C}$ has the form (2.21) or (2.24) according to the basis.

HILL in 1948 [3, 4] proposed the yield condition of the form (5.1) for material with orthotropic symmetry. It was expressed by six independent components of the limit tensor $\mathbf{H}$. When transversal isotropy is considered, the number of independent components of $\mathbf{H}$ reduces to three [6]. Therefore the matrix representations of $\mathbf{H}$ in the polybases (2.7) – (2.12) and (2.13) – (2.18) respectively are as follows:

$$\mathbf{H} \sim \frac{1}{2}\begin{bmatrix} g+n & g-n & -2g & 0 & 0 & 0 \\ g-n & g+n & -2g & 0 & 0 & 0 \\ -2g & -2g & 4g & 0 & 0 & 0 \\ 0 & 0 & 0 & 2m & 0 & 0 \\ 0 & 0 & 0 & 0 & 2m & 0 \\ 0 & 0 & 0 & 0 & 0 & 2n \end{bmatrix} \tag{5.14}$$

and

$$\mathbf{H} \sim \begin{bmatrix} 0 & 0 & 0 & 0 & 0 & 0 \\ 0 & n & 0 & 0 & 0 & 0 \\ 0 & 0 & 3g & 0 & 0 & 0 \\ 0 & 0 & 0 & m & 0 & 0 \\ 0 & 0 & 0 & 0 & m & 0 \\ 0 & 0 & 0 & 0 & 0 & n \end{bmatrix}. \tag{5.15}$$

Notations are taken from the HILL paper [3].

It is easy to prove that the spherical tensor is a safe state. Then the equation (3.2) is satisfied. We note that the matrix representation of $\mathbf{H}$ (5.15) in the base $\mathbf{a}_k$ has a diagonal from. It means that the tensors $\mathbf{a}_k$ are the proper states for $\mathbf{H}$

and the componenets $3g$, m and n on the diagonal are the proper values. For the spherical state the corresponding proper value is equal to 0.

In order to obtain the energy-orthogonal decomposition (5.6), the matrix representations of $\mathbf{C}$ and $\mathbf{H}$ in the base $\mathbf{a}_K$ are used, Eq. (5.12) reduces to the form

$$\frac{1}{2\tilde{h}}\left[A(3g-\frac{1}{2\tilde{h}}D)+\frac{1}{2\tilde{h}}B^2\right]\left[m-\frac{1}{\tilde{h}}C_{1313}\right]^2 \left[n-\frac{1}{2\tilde{h}}(C_{1111}-C_{1122})\right]^2=0. \tag{5.16}$$

The solution of the above equation is created by two roots of multiplicity two and two single ones. The double roots have the form:

$$\tilde{h}_3=\frac{C_{1313}}{m}=\frac{1}{2\lambda_3 m},\quad \tilde{h}_4=\frac{C_{1111}-C_{1122}}{2n}=\frac{1}{2\lambda_4 n}. \tag{5.17}$$

The proper states $\boldsymbol{\kappa}$ corresponding to the proper values (5.17) form two subspaces $H_3=P_3$ and $H_4=P_4$, respectively. Both subspaces are two-dimensional. They consist of the tensors of the form (2.33).

An energy-orthogonal base in the subspace H_3 may be taken as follows

$$\boldsymbol{\kappa}_{III}=\sqrt{\lambda_3}\boldsymbol{\omega}_{III},\quad \boldsymbol{\kappa}_{IV}=\sqrt{\lambda_3}\boldsymbol{\omega}_{IV}, \tag{5.18}$$

and in the subspace H_4 the base may be selected as

$$\boldsymbol{\kappa}_V=\sqrt{\lambda_4}\boldsymbol{\omega}_V,\quad \boldsymbol{\kappa}_{VI}=\sqrt{\lambda_4}\boldsymbol{\omega}_{VI}. \tag{5.19}$$

Two single roots of Eq. (5.16) have the following form:

$$\tilde{h}_1\to\infty,\quad \tilde{h}_2=\frac{AD-B^2}{6Ag}=\frac{1}{6\lambda_1\lambda_2 Ag}. \tag{5.20}$$

The energy-orthogonal states $\boldsymbol{\kappa}$ corresponding to them are given by formulae

$$\boldsymbol{\kappa}_1=\frac{1}{\sqrt{A}}\mathbf{a}_I,\quad \boldsymbol{\kappa}_2=\sqrt{\frac{B^2}{A(AD-B^2)}}\left(\mathbf{a}_I-\frac{A}{B}\mathbf{a}_{III}\right). \tag{5.21}$$

The subspaces H_1 and H_2 are one-dimensional.

The projectors $\mathbf{P}_\alpha^H$ of stress tensor $\boldsymbol{\sigma}$ onto the subspaces H_α can be expressed as

$$\begin{aligned}\mathbf{P}_1^H &= \frac{1}{A}\mathbf{a}_I\otimes\mathbf{a}_I,\\ \mathbf{P}_2^H &= \frac{B^2}{A(AD-B^2)}\left(\mathbf{a}_I-\frac{A}{B}\mathbf{a}_{III}\right)\otimes\left(\mathbf{a}_I-\frac{A}{B}\mathbf{a}_{III}\right),\\ \mathbf{P}_3^H &= \lambda_3\mathbf{P}_3,\quad \mathbf{P}_4^H=\lambda_4\mathbf{P}_4\end{aligned} \tag{5.22}$$

On substituting (5.22) into (5.13) we obtain the energy-orthogonal stresses $\tilde{\boldsymbol{\sigma}}_\alpha$. We see that $\tilde{\boldsymbol{\sigma}}_3 = \boldsymbol{\sigma}_3$ and $\tilde{\boldsymbol{\sigma}}_4 = \boldsymbol{\sigma}_4$. It means that they have the same form as for the main energy-orthogonal decomposition (see Fig. 1c, d and formulae (2.64–2.65)).

In order to find the stresses $\tilde{\boldsymbol{\sigma}}_1$ and $\tilde{\boldsymbol{\sigma}}_2$, the following scalar parameters are introduced

$$\tilde{s} = \frac{1}{6}(\sigma_{11} + \sigma_{22} - 2\sigma_{33}) \quad \text{and} \quad \mu' = \frac{\sqrt{2}B}{A}. \tag{5.23}$$

The stresses $\tilde{\boldsymbol{\sigma}}_1$ and $\tilde{\boldsymbol{\sigma}}_2$ are illustrated in Fig. 4 (we remind that $\sigma = \frac{1}{3}\operatorname{tr}\boldsymbol{\sigma}$).

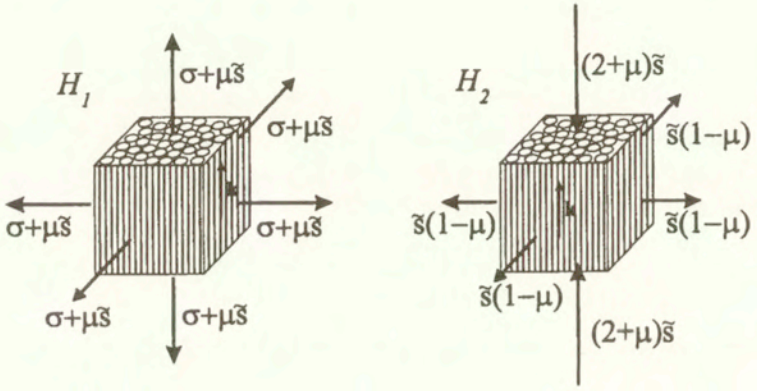

FIG. 4. Subspaces H_1 and H_2 of energy-orthogonal states $\tilde{\boldsymbol{\sigma}}_1$ and $\tilde{\boldsymbol{\sigma}}_2$ for transversally isotropic material connected with the limit tensor $\mathbf{H}$ (5.14)-(5.15).

While the moduli $\tilde{h}_\alpha$ and stresses $\tilde{\boldsymbol{\sigma}}_\alpha$ are given the limit condition of Mises type (5.5) for the limit tensor $\mathbf{H}$ (5.15) takes the form

$$\frac{1}{\tilde{h}_2}\Phi(\tilde{\boldsymbol{\sigma}}_2) + \frac{1}{\tilde{h}_3}\Phi(\tilde{\boldsymbol{\sigma}}_3) + \frac{1}{\tilde{h}_4}\Phi(\tilde{\boldsymbol{\sigma}}_4) \leq 1. \tag{5.24}$$

Since $\tilde{h}_1 \to \infty$, the stress $\tilde{\boldsymbol{\sigma}}_1 \in H_1$ is safe and the part of energy $\Phi(\tilde{\boldsymbol{\sigma}}_1)$ has no influence on the limit condition (5.24).

The energies $\Phi(\tilde{\boldsymbol{\sigma}}_3)$ and $\Phi(\tilde{\boldsymbol{\sigma}}_4)$ are given by formulae (2.53) and (2.54). However, the energies $\Phi(\tilde{\boldsymbol{\sigma}}_1)$ and $\Phi(\tilde{\boldsymbol{\sigma}}_2)$ may be expressed as follows:

$$2\Phi(\tilde{\boldsymbol{\sigma}}_1) = \tilde{\boldsymbol{\sigma}}_1 \times \tilde{\boldsymbol{\sigma}}_1 = 3A(\sigma + \mu\tilde{s})^2, \tag{5.25}$$

$$2\Phi(\tilde{\boldsymbol{\sigma}}_2) = \tilde{\boldsymbol{\sigma}}_2 \times \tilde{\boldsymbol{\sigma}}_2 = \frac{6(AD - B^2)}{A}\tilde{s}^2. \tag{5.26}$$

Analysing the obtained result we note that the stresses $\tilde{\boldsymbol{\sigma}}_2$, $\tilde{\boldsymbol{\sigma}}_3$ and $\tilde{\boldsymbol{\sigma}}_4$ do not cause elastic volume changes.

If the hydrostatic pressure is the only acting stress then the corresponding stress tensor $\boldsymbol{\sigma} = \tilde{\boldsymbol{\sigma}}_1 \in H_1$ is safe.

On the other hand, assuming that the considered state of stress $\boldsymbol{\sigma}$ has the following properties $\sigma = u = v = p = q = 0$ and $\tilde{s} \neq 0$ (see (2.64)–(2.65) and (5.23)), we obtain that $\boldsymbol{\sigma} \in H_1 \oplus H_2$, and the part of energy $\Phi(\tilde{\boldsymbol{\sigma}}_1)$ has no influence on the limit condition.

Considering the state of stress $\boldsymbol{\sigma}$ for which

$$\sigma = -\mu\tilde{s}, \tag{5.27}$$

we note that no part of the stress tensor is a safe state. In spite of $\mathrm{tr}\boldsymbol{\sigma} \neq 0$ we have that $\Phi(\tilde{\boldsymbol{\sigma}}_1) = 0$ and the total elastic energy $\Phi(\boldsymbol{\sigma})$ enters the limit condition.

We should emphasize that for two states of stress with different spherical parts only, the values of the quadratic form $(5.3)_2$ are equal.

The tensors $\mathbf{C}$ and $\mathbf{H}$ are coaxial if the stiffness distributor $\aleph = \aleph_0$ $(B = 0)$. Then the spherical tensor is a proper state for both tensors.

6. Summary

Using the example of transversal isotropy, the limit condition of the Mises type having an energy-based interpretation has been obtained. Following the approach proposed by J. Rychlewski, the limit condition was given in the form of weighted sum of stored energies corresponding to uniquely defined energy-orthogonal parts of stress.

Without special difficulties the presented approach may be adopted to the problem of formulating the limit condition for other types of anisotropy.

In the general case tensors $\mathbf{C}$ and $\mathbf{H}$ are independent. This property allows to consider different types of symmetry in elastic and limit states. Assuming some form of coupling of elastic and plastic properties, the solution of the problem becomes simplified.

We note that the presented approach may be applied to the problem of describing the plastic anisotropy evolution in the material, which changes its properties when passing from elastic to plastic state. Then we may assume that the evolution of moduli h_α or $\tilde{h}_\alpha$ depends on dissipation of energy connected with irreversible deformations.

Acknowledgement

Most of the results reported in the present paper were obtained in the framework of the research supported by the grant of Committee of the Scientific Research, No 5 TO7A 031 22, headed by W. Gambin.

References

1. W. T. BURZYŃSKI, *Study of the strength hypotheses,* [in Polish] Lwow, 1928/also „Collected Papers", **1**, PWN, Warszawa 1982.

2. H. HENCKY, *Zur Theorie plastischer Deformationen und der hierdurch im Material hervorgerufenen Nachspannungen,* ZAMM, **4**, 323–334, 1924.

3. R. HILL, *A theory of the yielding and plastic flow of anisotropic metals,* Proc. Roy. Soc., 193 (Ser.A) 281–297, 1948.

4. R. HILL, *Mathematical theory of plasticity,* Oxford: Clarendon Press, 1950.

5. M. T. HUBER. *Distortion strain energy as a measure of strength of the material,* [in Polish] Czas. Tech. XXII, Lwow 1904/also „Papers", **1, 2,** 3–20, PWN Warszawa 1956. Czas. Techn., XXII, Lwów 1904. (Pisma I-II, s. 3-20, PWN, Warszawa 1956).

6. S. JEMIOŁO and K. KOWALCZYK, *Invariant formulation and spectral decomposition of Hill's anisotropic yield condition* [in Polish], Prace Naukowe PW, Budownictwo, z. 133, 87–123, 1999.

7. J. C. MAXWELL, *Proc. Cambridge Phil. Soc.*, **32**, 1936 (also Origins of Clerk Maxwell's electric ideas as described in familiar letters to William Thompson, ed. by Sir J. Larmor, Cambridge at Univ. Press, 1937).

8. W. OLSZAK and J. OSTROWSKA-MACIEJEWSKA, *The plastic potential in the theory of anisotropic elastic-plastic solids,* Engng. Fracture Mech., **21**, 4, 625–632, 1985.

9. J. OSTROWSKA-MACIEJEWSKA and J. RYCHLEWSKI, *Plane elastic and limit states in anisotropic solids,* Arch. Mech., **40**, 4, 79–386, 1988.

10. B. RANIECKI and Z. MRÓZ, *On the strain-induced anisotropy and texture in rigid-plastic solids,* Inelastic Solids and Structures (Antoni Sawczuk memorial volume), Prineridge Press, Swansea, U.K., 1990.

11. J. RYCHLEWSKI, *"CEIIINOSSSTTUV", Mathematical structure of elastic bodies,* [in Russian], Technical Report 217, Inst. Mech. Probl. USSR Acad. Sci., Moscow, 1983.

12. J. RYCHLEWSKI, *Elastic energy decomposition and limit criteria* [in Russian], Advances in Mechanics, **7**, 3, 1984.

13. J. RYCHLEWSKI, *On Hook's law* [in Russian], PMM, **48**, 420–435, 1984. See translation Prikl. Matem. Mekhan., **48**, 303-314, 1984.

14. J. RYCHLEWSKI, *Unconventional approach to linear elasticity,* Arch. Mech., **47**, 2, 149–171, 1995.

15. S. SUTCLIFFE, *Spectral decomposition of the elasticity tensor,* J. Appl. Mech., **59**, 4, 762–773, 1992.

16. R. VON MISES, *Mechanik der festen Körper im plastisch deformablen Zustand, Nachrichten der Königlichen Gesellschaft der Wissenschaften zu Göttingen,* Math-Phys. **1**, 4, 582–592, 1913.

17. R. VON MISES, *Mechanik der plastischen Formänderung von Kristallen,* Zeitschrift für Angewandte Mathematik und Mechanik, 8, 161–185, 1928.

Received February 15, 2002; revised version August 26, 2002.

Arch. Mech., **54**, 5-6, pp. 525–552, Warszawa 2002

Material instabilities in fiber-reinforced nonlinearly elastic solids under plane deformation

J. MERODIO[1] and R. W. OGDEN[2]

[1] *Department of Structural and Mechanical Engineering,*
E.T.S. Ing. Industriales y Tel.,
University of Cantabria, 39005, Santander, Spain
e-mail: merodioj@unican.es

[2] *Department of Mathematics, University of Glasgow*
Glasgow G12 8QW, UK
e-mail: rwo@maths.gla.ac.uk

Dedicated to Professor Piotr Perzyna
on the occasion of his 70^{th} birthday

MATERIAL INSTABILITIES in fiber-reinforced nonlinearly elastic solids are examined under plane deformation. In particular, the materials under consideration are isotropic nonlinearly elastic models augmented by a function that accounts for the existence of a unidirectional reinforcing. This function describes the anisotropic (transversely isotropic) character of the material and is referred to as a *reinforcing model*. The onset of failure is signalled by the loss of ellipticity of the governing differential equations. Previous work has dealt with the analysis of specific reinforcing models and has established that the loss of ellipticity for such augmented isotropic materials requires *contraction* in the reinforcing direction. The loss of ellipticity was related to fiber kinking. Here we generalize these results and establish *sufficient* conditions for the ellipticity of the governing equations of equilibrium for more general reinforcing models to be guaranteed. We also establish *necessary* conditions for failure of ellipticity. The incipient loss of ellipticity is interpreted in terms of fiber kinking, fiber de-bonding, fiber splitting and matrix failure in fiber-reinforced composite materials. Attention is restricted to incompressible materials in this paper.

Key words: Fiber failure, fiber kinking, fiber de-bonding, fiber splitting, matrix failure, loss of ellipticity, reinforcing models, anisotropy.

1. Introduction

FAILURE MECHANISMS in composite materials which consist of an isotropic base material with unidirectional reinforcement have received increased attention in the last few years. These failure mechanisms include fiber kinking [1–8], fiber splitting [9], fiber de-bonding [10] and matrix failure [11–12]. These analyses provide different theories to capture and explain the failure modes for the mate-

rials under consideration. However, a unified approach to the prediction of fiber instability or fiber failure in fiber-reinforced composite materials is lacking.

In this paper, our objective is to present a continuum-mechanical model in the setting of nonlinear elasticity theory that captures and predicts the material instabilities mentioned above for particular fiber-reinforced materials. For this purpose, a sufficiently general (transversely isotropic) strain energy depending on deformation invariants that penalize deformation in a particular, direction, serves as the material model. The onset of failure is heralded by the loss of ellipticity of the governing differential equations [6–8].

For a given strain-energy function the loss of ellipticity condition determines both the *deformation* associated with the existence of surfaces of weak discontinuity and the *direction of the normal* to that surface. Surfaces of weak discontinuity (or weak surfaces) are surfaces across which the second derivative of the deformation field is discontinuous, while across a fully developed (or strong) surface of discontinuity the first derivative (i.e. the deformation gradient) suffers a finite jump. In the present analysis we relate the angle between the weak surface normal and the fiber-reinforcement direction to a particular failure mechanism. The argument is summarized as follows. Under fiber *contraction* the onset of fiber kinking is associated with weak surfaces that lie close to the normal to the direction of fiber reinforcement [1]. Thus, if the loss of ellipticity analysis yields a weak surface perpendicular to the fiber under fiber contraction, the associated fiber failure is identified as fiber kinking. By contrast, for fiber de-bonding the angle between the weak surface and the fiber reinforcement is close to zero [10]. For fiber kinking combined with fiber splitting, the simultaneous existence of weak surfaces close to and normal to the fiber direction is required [9]. Matrix failure arises under fiber *extension* and is associated with weak surfaces perpendicular to the fiber reinforcement [11–12]. These various possibilities are depicted in Fig. 1.

Constitutive equations that suffer a loss of ellipticity have been studied in a variety of contexts (see, for example, [6–8] [13–20]). In particular, the loss of ellipticity of some particular transversely isotropic nonlinear elastic materials under *plane* deformations has been examined in [7, 8, 18, 19]. The procedure used in these analyses is the following. An isotropic base material is augmented by a uniaxial reinforcement in what is referred to as the *fiber direction*. The plane of deformation contains the fiber reinforcement. In [7–8] and [18] the isotropic base material considered is a neo-Hookean material (incompressible), while in [19] it is the special Blatz-Ko material (compressible). In each case the same reinforcing model was used to characterize the anisotropy of the constitutive equation: the so-called *standard reinforcing model*. As is well known, the neo-Hookean model retains ellipticity at all deformations. By contrast, the Blatz-Ko material loses ellipticity at sufficiently large deformations both in tension and compression

(see, for example, [16]). Nevertheless, these papers conclude that the standard fiber reinforcement "weakens" the material in fiber compression since the loss of ellipticity involves fiber contraction, while it "strengthens" the material in fiber tension. In tension the loss of ellipticity can be avoided for a reinforcement of sufficient strength. Furthermore, the analysis of [7–8] interpreted the loss of ellipticity in terms of kink-band phenomena for fiber-reinforced materials. Here, we follow the same procedure and define the strain energy as consisting of an isotropic base material augmented by a reinforcing model. For the latter, two general classes of functions are examined.

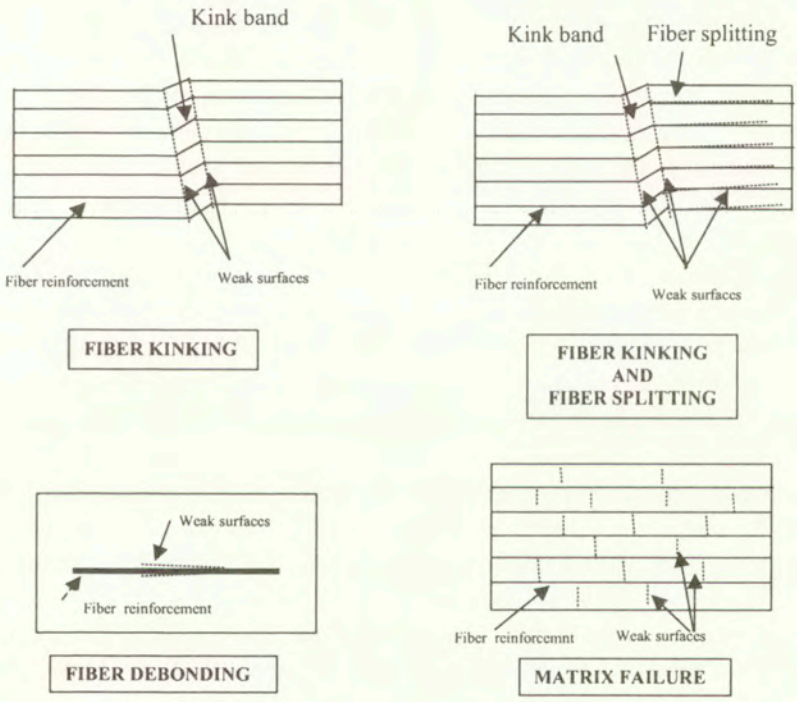

FIG. 1. Kinematics of fiber kinking, fiber kinking with fiber splitting, fiber de-bonding and matrix failure in fiber reinforced composite materials. The boundary of the kink band in the incipient fiber kinking mechanism is interpreted as a weak surface and is close to the normal direction of the fiber reinforcement (upper left figure). In the fiber kinking combined with fiber splitting there is also a weak surface in the direction of the fiber reinforcement (upper right figure). Fiber de-bonding is associated with weak surfaces close to the fiber reinforcement direction (lower left figure). Matrix failure is associated with weak surfaces normal to the fiber reinforcement (lower right figure

In three dimensions, two independent deformation invariants, denoted I_4 and I_5, are sufficient to characterize the anisotropic nature of a transversely isotropic material. These are additional to the usual three invariants I_1, I_2, I_3 of

the Cauchy-Green deformation tensors required for isotropy in a compressible material (for an incompressible material $I_3 \equiv 1$). The invariant I_4 represents the square of the stretch in the direction of the fiber reinforcement. The standard reinforcing model is a quadratic function that depends only on I_4. The invariant I_5 is also related to the fiber stretch but additionally registers the reaction of the reinforcement to shear deformations and to deformations of surface area elements normal to the fiber direction. Under plane deformations with the fiber direction in the considered plane I_4 and I_5 are no longer independent and the material response depends only on I_1 $(= I_2)$ and I_4 (in the case of incompressibility). The ellipticity analysis for a general strain-energy function restricted to the plane in question then depends on only one anisotropic invariant. Nevertheless, each of I_4 and I_5 will be considered separately in the reinforcement model since each adds a distinct anisotropic character to the isotropic base material.

The paper is organized as follows. In Sec. 2, the material model is introduced and the ellipticity, strong ellipticity and loss of ellipticity conditions for the governing differential equations are summarized. Specialization to plane strain is discussed in Sec. 2.5. In Sec. 3, the ellipticity status of a general reinforcing model depending on I_4 is established. It is shown that failure of ellipticity is to be expected in fiber compression. In particular, under fiber contraction the incipient loss of ellipticity is interpreted in terms of fiber kinking. Failure can also occur in fiber extension if the reinforcing model loses convexity, in which case fiber de-bonding is an appropriate interpretation of the associated failure mode. Convex reinforcing models are discussed briefly in Sec. 3.2. The analysis in Sec. 3 is carried out for a general fiber-reinforcement orientation within the plane of deformation. This allows us, additionally, to make a qualitative analysis of the ellipticity status of a reinforcement consisting of two fiber families in the plane of deformation. This is discussed in Sec. 3.3.

In Sec. 4, our study focuses briefly on the invariant I_5. Under fiber contraction it is found that failure of ellipticity may occur in two different modes, which may be associated with fiber kinking and fiber splitting. In fiber extension under a suitable simple shear deformation, de-bonding is again a possible failure mode if the reinforcing model is non-convex. A weak surface may also arise perpendicular to the fiber direction and this is interpreted as matrix failure. These examples of failure modes are not exhaustive. Fiber de-bonding and matrix failure are also possible failure modes under fiber extension if the base material loses ellipticity, whether or not the reinforcing model is convex. In Sec. 5 we summarize and discuss briefly the results obtained in the previous sections.

2. The material model and ellipticity

2.1. Description of the deformation

Let $\mathbf{X}$ denote the position vector of a material particle in the stress-free reference configuration and let $\mathbf{x}$ denote the location of the particle in the deformed configuration. The deformation gradient tensor $\partial\mathbf{x}/\partial\mathbf{X}$ is denoted $\mathbf{F}$. The left and right Cauchy-Green deformation tensors, respectively $\mathbf{B}$ and $\mathbf{C}$, are given by

$$\mathbf{B} = \mathbf{F}\mathbf{F}^T, \quad \mathbf{C} = \mathbf{F}^T\mathbf{F}, \tag{2.1}$$

and the principal (isotropic) invariants of $\mathbf{C}$ (equivalently of $\mathbf{B}$) are defined by

$$I_1 = \operatorname{tr}\mathbf{C}, \quad I_2 = I_3 \operatorname{tr}(\mathbf{C}^{-1}), \quad I_3 = \det\mathbf{C}. \tag{2.2}$$

Let the unit vector $\mathbf{A}$ define the direction of fiber reinforcement in the undeformed configuration. The combination of $\mathbf{A}$ and $\mathbf{C}$ introduces two additional (in general independent) invariants, denoted I_4 and I_5, which are defined by

$$I_4 = \mathbf{A}\cdot(\mathbf{C}\mathbf{A}), \quad I_5 = \mathbf{A}\cdot(\mathbf{C}^2\mathbf{A}). \tag{2.3}$$

Let the vector $\mathbf{a}$ result from the action of $\mathbf{F}$ on $\mathbf{A}$, so that

$$\mathbf{a} = \mathbf{F}\mathbf{A}. \tag{2.4}$$

For a homogeneous deformation $\mathbf{a}$ is the image of $\mathbf{A}$ in the deformed configuration. On use of (2.4) and (2.1) we may therefore write (2.3) as

$$I_4 = \mathbf{a}\cdot\mathbf{a}, \quad I_5 = \mathbf{a}\cdot(\mathbf{B}\mathbf{a}). \tag{2.5}$$

In terms of the principal stretches $(\lambda_1, \lambda_2, \lambda_3)$ of the deformation we have

$$I_1 = \lambda_1^2 + \lambda_2^2 + \lambda_3^2, \quad I_2 = I_3(\lambda_1^{-2} + \lambda_2^{-2} + \lambda_3^{-2}), \quad I_3 = \lambda_1^2\lambda_2^2\lambda_3^2, \tag{2.6}$$

$$I_4 = \lambda_1^2 A_1^2 + \lambda_2^2 A_2^2 + \lambda_3^2 A_3^2 = a_1^2 + a_2^2 + a_3^2, \tag{2.7}$$

$$I_5 = \lambda_1^4 A_1^2 + \lambda_2^4 A_2^2 + \lambda_3^4 A_3^2 = \lambda_1^2 a_1^2 + \lambda_2^2 a_2^2 + \lambda_3^2 a_3^2 \tag{2.8}$$

where (A_1, A_2, A_3) are the components of $\mathbf{A}$ referred to the principal axes of $\mathbf{C}$, and (a_1, a_2, a_3) those of $\mathbf{a}$ referred to the principal axes of $\mathbf{B}$. It is clear from the above that $\sqrt{I_4}$ is the stretch in the direction $\mathbf{A}$ of the fiber reinforcement. Therefore the invariant I_4 registers deformations that modify the length of the fiber. The invariant I_5 has no similar simple interpretation in general and it

depends on both changes in the fiber length and shearing strains. However, the following connection is of interest. From the Cayley-Hamilton theorem for $\mathbf{C}$, namely

$$\mathbf{C}^3 - I_1\mathbf{C}^2 + I_2\mathbf{C} - I_3\mathbf{I} = \mathbf{0}, \tag{2.9}$$

we obtain

$$I_5 = I_1 I_4 - I_2 + \mathbf{A} \cdot (\mathbf{C}^*\mathbf{A}), \tag{2.10}$$

where $\mathbf{I}$ is the identity tensor and $\mathbf{C}^* = I_3\mathbf{C}^{-1}$ is the adjugate of $\mathbf{C}$. Since a reference surface area element of unit magnitude with normal in the direction $\mathbf{A}$ transforms to $\sqrt{I_3}\mathbf{F}^{-T}\mathbf{A}$ (Nanson's formula), the final term in (2.10) is interpreted as the square of the ratio of deformed to undeformed surface area elements and could be used as an alternative to I_5 as a measure of the influence of reinforcement.

2.2. Strain energy and stress

According to SPENCER [21], for an elastic material without internal constraints the most general strain-energy function for a homogeneous transversely isotropic nonlinear elastic solid depends only on the invariants $(I_1, I_2, I_3, I_4, I_5)$. In this paper we focus on *incompressible* elastic materials, so that $I_3 \equiv 1$ and hence

$$\lambda_1\lambda_2\lambda_3 = 1. \tag{2.11}$$

As a result only four independent invariants remain, and we write the strain energy per unit reference volume as

$$W = W(I_1, I_2, I_4, I_5). \tag{2.12}$$

The nominal stress tensor $\mathbf{S}$ is calculated from the strain energy W in the form

$$\mathbf{S} = \frac{\partial W}{\partial \mathbf{F}} - p\,\mathbf{F}^{-1}, \tag{2.13}$$

where p is the Lagrange multiplier associated with the incompressibility constraint $\det\mathbf{F} = 1$. To make this explicit in respect of (2.12) we require the formulas

$$\frac{\partial I_1}{\partial \mathbf{F}} = 2\mathbf{F}^T, \quad \frac{\partial I_2}{\partial \mathbf{F}} = 2I_1\mathbf{F}^T - 2\mathbf{F}^T\mathbf{F}\mathbf{F}^T, \tag{2.14}$$

$$\frac{\partial I_4}{\partial \mathbf{F}} = 2\mathbf{A} \otimes \mathbf{F}\mathbf{A}, \quad \frac{\partial I_5}{\partial \mathbf{F}} = 2(\mathbf{A} \otimes \mathbf{F}\mathbf{C}\mathbf{A} + \mathbf{C}\mathbf{A} \otimes \mathbf{F}\mathbf{A}), \tag{2.15}$$

and hence

$$\mathbf{S} = 2W_1\mathbf{F}^T + 2W_2(I_1\mathbf{I} - \mathbf{C})\mathbf{F}^T + 2W_4\mathbf{A}\otimes\mathbf{FA} + 2W_5(\mathbf{A}\otimes\mathbf{FCA} + \mathbf{CA}\otimes\mathbf{FA}) - p\mathbf{F}^{-1}, \tag{2.16}$$

where the subscripts $1, 2, 4, 5$ on W indicate differentiation with respect to I_1, I_2, I_4, I_5, respectively, and $\mathbf{I}$ is again the identity tensor.

The corresponding expression for the Cauchy stress tensor $\sigma = \mathbf{FS}$ is

$$\sigma = 2W_1\mathbf{B} + 2W_2(I_1\mathbf{I} - \mathbf{B})\mathbf{B} + 2W_4\mathbf{a}\otimes\mathbf{a} + 2W_5(\mathbf{a}\otimes\mathbf{Ba} + \mathbf{Ba}\otimes\mathbf{a}) - p\mathbf{I}, \tag{2.17}$$

The energy function and the stress must vanish in the reference configuration (where $I_1 = I_2 = 3$ and $I_4 = I_5 = 1$) and it therefore follows that

$$W(3,3,1,1) = 0, \quad 2W_1(3,3,1,1) + 4W_2(3,3,1,1) - p_0 = 0, \tag{2.18}$$

$$W_4(3,3,1,1) + 2W_5(3,3,1,1) = 0, \tag{2.19}$$

where p_0 is the value of p in that configuration. Conditions on the second derivatives of W at $(3,3,1,1)$ for consistency with the classical linear theory of transversely isotropic elasticity may be obtained but we omit the details here for the three-dimensional case. For the simpler case of plane strain the appropriate connections will be noted in Sec. 2.5.

2.3. Equilibrium and ellipticity

The equation of equilibrium in the absence of body forces has the form $\operatorname{Div}\mathbf{S} = \mathbf{0}$ and may be written in the component form

$$\mathcal{A}_{\alpha i\beta j}x_{j,\alpha\beta} - p_{,i} = 0, \tag{2.20}$$

where

$$\mathcal{A}_{\alpha i\beta j} = \frac{\partial^2 W}{\partial F_{i\alpha}\partial F_{j\beta}}, \tag{2.21}$$

Greek indices being associated with the components of $\mathbf{X}$ and Roman indices with those of $\mathbf{x}$. The subscripts following a comma indicate differentiation with respect to the relevant coordinate.

The linearized equations governing a small incremental deformation superimposed on a homogeneous finite deformation have a similar structure to (2.20) and may be written

$$\mathcal{A}_{\alpha i\beta j}u_{j,\alpha\beta} - \bar{p}_{,i} = 0, \tag{2.22}$$

where $\mathbf{u}$, with components (u_1, u_2, u_3), is the incremental displacement and $\bar{p}$ is the corresponding increment in p. The incremental incompressibility condition is

$$\operatorname{div}\mathbf{u} = 0. \tag{2.23}$$

If we regard $\mathbf{u}$ as a function of the deformed position $\mathbf{x}$ and we introduce the updated version $\mathcal{A}_{0piqj}$ of the components $\mathcal{A}_{\alpha i\beta j}$, then the incremental equations may be written

$$\mathcal{A}_{0piqj}u_{j,pq} - \bar{p}_{,i} = 0, \tag{2.24}$$

where (see, for example, [23])

$$\mathcal{A}_{0piqj} = F_{p\alpha}F_{q\beta}\mathcal{A}_{\alpha i\beta j}. \tag{2.25}$$

Now consider incremental deformations of the form

$$\mathbf{u} = \mathbf{m}\,\mathrm{e}^{\mathrm{i}k\mathbf{n}\cdot\mathbf{x}}, \quad \bar{p} = q\,\mathrm{e}^{\mathrm{i}k\mathbf{n}\cdot\mathbf{x}}, \tag{2.26}$$

where $\mathbf{m}$ is the amplitude vector, k is the 'wave' number and $\mathbf{n}$ is a constant unit vector. On substitution into the Eq. (2.24) this leads to

$$\mathbf{Q}(\mathbf{n})\mathbf{m} + \mathrm{i}q\mathbf{n} = \mathbf{0}, \tag{2.27}$$

where the *acoustic tensor* $\mathbf{Q}(\mathbf{n})$ has components defined by

$$Q_{ij} = \mathcal{A}_{0piqj}n_p n_q, \tag{2.28}$$

and the vectors $\mathbf{m}$ and $\mathbf{n}$ satisfy the orthogonality condition

$$\mathbf{m}\cdot\mathbf{n} = 0 \tag{2.29}$$

resulting from the incompressibility constraint (2.23)

It follows that for an incremental deformation of the form (2.26) to be admissible the equality

$$\mathcal{A}_{0piqj}n_p n_q m_i m_j \equiv [\mathbf{Q}(\mathbf{n})\mathbf{m}]\cdot\mathbf{m} = 0 \tag{2.30}$$

must hold, where, without loss of generality, $\mathbf{m}$ has been taken to be a unit vector. For a non-trivial solution this equation, together with (2.24), defines a pair of (unit) vectors $\mathbf{m}$ and $\mathbf{n}$.

If the Eqs. (2.20) (or 2.24)) are *elliptic* then no such solutions exist. The condition for ellipticity is that

$$\mathcal{A}_{0piqj} n_p n_q m_i m_j \neq 0 \tag{2.31}$$

for all vectors $\mathbf{m} \neq \mathbf{0}$, $\mathbf{n} \neq \mathbf{0}$ such that $\mathbf{m} \cdot \mathbf{n} = 0$.

A stronger requirement is the *strong-ellipticity condition*

$$\mathcal{A}_{0piqj} n_p n_q m_i m_j > 0 \quad \mathbf{m} \neq 0,\ \mathbf{n} \neq 0,\ \mathbf{m} \cdot \mathbf{n} = 0. \tag{2.32}$$

The analysis of Eq. (2.31) for specific forms of the energy function W furnishes the ellipticity status of that particular strain energy. A deformation gradient $\mathbf{F}$ satisfying (2.31) for every pair of unit vectors $\mathbf{m}$ and $\mathbf{n}$ such that $\mathbf{m} \cdot \mathbf{n} = 0$ is said to be an *elliptic deformation* for that W. If all possible deformations for a particular material are elliptic then the material itself is referred to as an *elliptic material* (the isotropic neo-Hookean material is an example of an elliptic material). On the other hand, if, for some pair of orthogonal unit vectors $\mathbf{m}$ and $\mathbf{n}$, a deformation gradient $\mathbf{F}$ satisfies Eq. (2.30), then the deformation is said to be non-elliptic for that material model. Furthermore, the unit vector $\mathbf{n}$ is identified as the normal vector to a surface (in the deformed configuration), referred to as a *weak surface*, across which some of the differentiability properties required in the derivation of the equilibrium equations are not satisfied by some or all the variables involved. The pre-image of $\mathbf{n}$ is $\mathbf{N} = \mathbf{F}^T \mathbf{n}$, which is not

2.4. Reinforcing model

If an incompressible isotropic elastic material is reinforced with unidirectional reinforcing then the augmented strain-energy function may be written

$$W = W(I_1, I_2, I_4, I_5) = W_{\text{iso}}(I_1, I_2) + W_{\text{fib}}(I_4, I_5). \tag{2.33}$$

The first term in (2.33) represents the *isotropic base material*, while the second term is the so-called *reinforcing model*, the subscript standing for „fiber" reinforcement. This strain energy must be consistent with the conditions (2.18) and (2.19).

In what follows we shall restrict W_{fib} to functions that depend only on one invariant. Section 3 will be concerned with I_4 reinforcement and it will be convenient to write $W_{\text{fib}}(I_4, I_5) = F(I_4)$, while in Sec. 4 the focus will be on I_5 reinforcement and we will write $W_{\text{fib}}(I_4, I_5) = G(I_5)$.

In the literature (see [18] and [19]) use has been made of the so-called *standard reinforcing model* defined by the function

$$F(I_4) = \alpha(I_4 - 1)^2, \quad F'(I_4) = 2\alpha(I_4 - 1), \quad F''(I_4) = 2\alpha, \tag{2.34}$$

where $\alpha > 0$ is an anisotropy parameter which is a measure of the strength (or degree) of anisotropy. The standard reinforcing model penalizes deformation in the fiber direction and is a convex function of I_4. In [18] – [19], for α sufficiently large, loss of ellipticity was found in fiber compression, i.e. for $I_4 < 1$. On the other hand, the considered materials gain stability in fiber extension. In Sec. 3 we generalize these results and provide a unified derivation of necessary and sufficient conditions for the ellipticity status of $F(I_4)$, regardless of the fiber orientation in the plane of deformation.

At this point we note that the contribution of the term W_4 to the Cauchy stress (2.17) gives a traction component $2I_4W_4$ in the deformed fibre direction. Thus, for the reinforcing model $F(I_4)$ this contribution is positive (negative) in fiber extension (contraction) provided

$$F'(I_4) > 0 \ (< 0) \quad \text{for} \quad I_4 > 1 \ (< 1), \quad F'(1) = 0. \tag{2.35}$$

It may also be appropriate to take

$$F'(I_4) \to -\infty \, (\infty) \quad \text{as} \quad I_4 \to 0 \, (\infty), \tag{2.36}$$

although we note that the standard model Eq. (2.29) does not satisfy the lower of these limits. Similarly, the contribution of the term W_5 to the Cauchy stress gives a traction component $4I_5W_5$ and hence, for the reinforcing model $G(I_5)$, the traction in the fiber direction is positive (negative) according to whether I_5 is greater than or less than unity, provided

$$G'(I_5) > 0 \ (< 0) \quad \text{for} \quad I_5 > 1 \ (< 1), \quad G'(1) = 0. \tag{2.37}$$

Analogously to (2.36) we take

$$G'(I_5) \to -\infty \, (\infty) \quad \text{as} \quad I_5 \to 0 \, (\infty). \tag{2.38}$$

We emphasize that $I_5 > 1$ does not in general correspond to fiber extension. In what follows we shall adopt the inequalities (2.35) – (2.38).

2.5. Restriction to plane strain

Our concern in this paper is the ellipticity analysis of the materials introduced above under the plane strain restriction, with the fiber reinforcement lying in the considered plane. We aim to derive conditions on $F(I_4)$ and $G(I_5)$ that provide a qualitative understanding of the ellipticity status of the model (2.33).

We take the plane in question to correspond to the (X_1, X_2) coordinate plane so that the basic finite deformation is such that $x_3 = X_3$ with (x_1, x_2) independent of X_3. The incremental displacement field $\mathbf{u}$ is then such that $u_3 = 0$,

with (u_1, u_2) depending only on x_1 and x_2. It follows that $F_{13} = F_{23} = F_{31} = F_{32} = 0$ and $F_{33} = 1$, and, for the components of $\mathbf{C}$, $C_{13} = C_{23} = 0$ and $C_{33} = 1$.

The out-of-plane principal stretch is now $\lambda_3 = 1$ and, by incompressibility, $\lambda_1\lambda_2 = 1$. Hence, the invariants (2.6) reduce to

$$I_2 = I_1 = \lambda_1^2 + \lambda_2^2 + 1, \quad I_3 = 1. \tag{2.39}$$

The fiber direction $\mathbf{A}$ lies in the (X_1, X_2) plane, and therefore

$$I_4 = \lambda_1^2 A_1^2 + \lambda_2^2 A_2^2, \quad I_5 = \lambda_1^4 A_1^2 + \lambda_2^4 A_2^2. \tag{2.40}$$

The important connection

$$I_5 = (I_1 - 1)I_4 - 1 \tag{2.41}$$

then follows, while the specialization of (2.10) leads to

$$\mathbf{A} \cdot (\mathbf{C}^*\mathbf{A}) = I_1 - I_4 - 1. \tag{2.42}$$

Thus, when restricted to plane strain, the strain, energy $W(I_1, I_2, I_4, I_5)$ of a fiber-reinforced incompressible elastic material (i.e. a transversely isotropic incompressible elastic material) can be represented in terms of two independent invariants, and we write

$$\hat{W}(I_1, I_4) = W(I_1, I_1, I_4, (I_1 - 1)I_4 - 1). \tag{2.43}$$

Let $\mathbf{F}$ now denote the in-plane restriction of the deformation gradient. We then have

$$\frac{\partial I_1}{\partial \mathbf{F}} = 2\mathbf{F}^T, \quad \frac{\partial I_4}{\partial \mathbf{F}} = 2\mathbf{A} \otimes \mathbf{F}\mathbf{A}, \tag{2.44}$$

specializing $(2.14)_1$ and $(2.15)_1$. The corresponding plane restriction of the nominal stress tensor is then given by

$$\mathbf{S} = 2\hat{W}_1\mathbf{F}^T + 2\hat{W}_4\mathbf{A} \otimes \mathbf{F}\mathbf{A} - \hat{p}\mathbf{F}^{-1}, \tag{2.45}$$

where, in general, $\hat{p}$ differs from the p in (2.16). Note that the only out-of-plane component of nominal stress (S_{33}) has to be calculated from (2.16) and is not given by (2.45).

Restrictions on $\hat{W}$ in the reference configuration analogous to those given for W in (2.18) and (2.19) are

$$\hat{W}(3,1) = 0, \quad 2\hat{W}_1(3,1) - \hat{p}_0 = 0, \quad \hat{W}_4(3,1) = 0, \tag{2.46}$$

where $\hat{p}_0$ is the value of $\hat{p}$ in the reference configuration.

Comparison with the corresponding classical linear theory (see, for example, [22], p. 160) shows that

$$2\hat{W}_1(3,1) + \hat{W}_{44}(3,1) = (c_{11} + c_{33} - 2c_{13})/4, \quad \hat{W}_1(3,1) = c_{44}/2, \tag{2.47}$$

where $c_{11}, c_{13}, c_{33}, c_{44}$ are the constants arising in the classical theory (this notation being appropriate for reinforcement aligned in the x_3 direction).

For the $\hat{W}$ defined above the components of $\mathcal{A}_{\alpha i \beta j}$ are explicitly

$$\begin{aligned}\mathcal{A}_{\alpha i \beta j} = {} & 4\hat{W}_{11}F_{i\alpha}F_{j\beta} + 2\hat{W}_1\delta_{ij}\delta_{\alpha\beta} + 4\hat{W}_{14}(F_{i\alpha}F_{j\gamma}A_\beta + F_{j\beta}F_{i\gamma}A_\alpha)A_\gamma \\ & + 4\hat{W}_{44}F_{i\gamma}F_{j\delta}A_\alpha A_\beta A_\gamma A_\delta + 2\hat{W}_4 A_\alpha A_\beta \delta_{ij},\end{aligned} \tag{2.48}$$

and, by use of (2.25), the updated version of this is given by

$$\begin{aligned}\mathcal{A}_{0piqj} = {} & 4\hat{W}_{11}B_{pi}B_{qj} + 2\hat{W}_1\delta_{ij}B_{pq} + 4\hat{W}_{14}(B_{pi}a_j a_q + B_{qj}a_i a_p) \\ & + 4\hat{W}_{44}a_p a_q a_i a_j + 2\hat{W}_4 a_p a_q \delta_{ij}.\end{aligned} \tag{2.49}$$

In (2.48) and (2.49) and henceforth, the indices take the values 1 and 2 only.

In terms of components of $\mathbf{m}$ and $\mathbf{n}$ referred to the principal axes of $\mathbf{B}$, the strong ellipticity condition (2.32), specialized to two dimensions, becomes

$$\begin{aligned}& 2\hat{W}_{11}(\lambda_1^2 - \lambda_2^2)^2 n_1^2 n_2^2 + \hat{W}_1(\lambda_1^2 n_1^2 + \lambda_2^2 n_2^2) \\ & \qquad + 4\hat{W}_{14}(\lambda_1^2 - \lambda_2^2)n_1 n_2(n_1 a_1 + n_2 a_2)(n_2 a_1 - n_1 a_2) \\ & \qquad + 2\hat{W}_{44}(n_1 a_1 + n_2 a_2)^2(n_2 a_1 - n_1 a_2)^2 + \hat{W}_4(n_1 a_1 + n_2 a_2)^2 > 0,\end{aligned} \tag{2.50}$$

where the orthogonality $\mathbf{m} \cdot \mathbf{n} = 0$ has been used to write $m_1 = n_2, m_2 = -n_1$.

The inequality (2.50) must hold for all (n_1, n_2) such that $n_1^2 + n_2^2 = 1$. For the special case of an *isotropic* material this inequality reduces to

$$2\hat{W}_{11}(\lambda_1^2 - \lambda_2^2)^2 n_1^2 n_2^2 + \hat{W}_1(\lambda_1^2 n_1^2 + \lambda_2^2 n_2^2) > 0, \tag{2.51}$$

for all considered (n_1, n_2), and this can be rearranged as

$$(I_1 + 1)[\hat{W}_1 + 2(I_1 - 3)\hat{W}_{11}]n_1^2 n_2^2 + \hat{W}_1(\lambda_1 n_1^2 - \lambda_2 n_2^2)^2 > 0. \tag{2.52}$$

It then follows immediately that necessary and sufficient conditions for this to hold are

$$\hat{W}_1 > 0, \quad 2(I_1 - 3)\hat{W}_{11} + \hat{W}_1 > 0 \tag{2.53}$$

(see, for example, [20]; alternative (and equivalent) inequalities in terms of the stretches can be found in [23]). In general, however, the inequalities (2.53) are not necessary, and certainly not sufficient, for (2.50) to hold.

It is interesting to note that when evaluated in the reference configuration, the inequality (2.50) reduces to

$$\hat{W}_1(3,1) + 2\hat{W}_{44}(3,1)(n_1a_1 + n_2a_2)^2(n_2a_1 - n_1a_2)^2 > 0 \tag{2.54}$$

for all unit vectors (n_1, n_2), with $\mathbf{a} = \mathbf{A}$. For this to hold, the necessary and sufficient conditions are easily seen to be

$$\hat{W}_1(3,1) > 0, \quad 2\hat{W}_1(3,1) + \hat{W}_{44}(3,1) > 0. \tag{2.55}$$

We assume that the inequalities (2.55) hold. Thus, by continuity, strong ellipticity holds in some neighbourhood of the reference configuration and on any path of deformation from the reference configuration strong ellipticity holds until a deformation is met at which strong ellipticity just fails. This happens (if at all) when a point is reached at which strict inequality is replaced by

$$\begin{aligned} 2\hat{W}_{11}(\lambda_1^2 - \lambda_2^2)^2 n_1^2 n_2^2 + \hat{W}_1(\lambda_1^2 n_1^2 + \lambda_2^2 n_2^2) \\ + 4\hat{W}_{14}(\lambda_1^2 - \lambda_2^2) n_1 n_2 (n_1a_1 + n_2a_2)(n_2a_1 - n_1a_2) \\ + 2\hat{W}_{44}(n_1a_1 + n_2a_2)^2(n_2a_1 - n_1a_2)^2 + \hat{W}_4(n_1a_1 + n_2a_2)^2 \geq 0 \end{aligned} \tag{2.56}$$

with equality holding for one or more unit vectors (n_1, n_2).

3. The effect of I_4 reinforcement

3.1. Reinforcing model

With the restriction to plane strain we now consider the strain energy

$$\hat{W}(I_1, I_4) = W_{\text{iso}}(I_1) + W_{\text{fib}}(I_4) \tag{3.1}$$

in which an isotropic base material with strain energy $W_{\text{iso}}(I_1)$ is augmented by the reinforcing model $W_{\text{fib}}(I_4) = F(I_4)$. This is the plane strain specialization of (2.39) with I_5 omitted. For this separable form of energy (the dependence of $\hat{W}$ on I_1 and I_4 being decoupled) the strong ellipticity condition (2.50) reduces to

$$\begin{aligned} 2\hat{W}_{11}(\lambda_1^2 - \lambda_2^2)^2 n_1^2 n_2^2 + \hat{W}_1(\lambda_1^2 n_1^2 + \lambda_2^2 n_2^2) \\ + (\mathbf{a}\cdot\mathbf{n})^2[\hat{W}_4 + 2(\mathbf{a}\times\mathbf{n})^2\hat{W}_{44}] > 0. \end{aligned} \tag{3.2}$$

We note that $(\lambda_1^2-\lambda_2^2)^2 = (I_1-3)(I_1+1)$ and that the first two terms in (3.2) are independent of $\mathbf{A}$ and I_4. The third and fourth terms depend on the deformation through $\mathbf{a} = \mathbf{FA}$ and I_4.

We now assume that the isotropic base material satisfies the strong ellipticity inequalities (2.53). (The effect of relaxation of one or more of these inequalities will be discussed later.) Then

$$W'_{\rm iso}(I_1) > 0, \quad W'_{\rm iso}(I_1) + 2(I_1 - 3)W''_{\rm iso}(I_1) > 0, \tag{3.3}$$

the prime indicating differentiation with respect to I_1. Note that in the reference configuration the inequalities (3.3) reduce to the single inequality $W'_{\rm iso}(3) > 0$.

With reference to (3.2) we see that since $\mathbf{n}$ may be chosen so that $\mathbf{a}\cdot\mathbf{n} = 0$, the ellipticity status of the model (3.1) depends on the sign of

$$\hat{W}_4 + 2(\mathbf{a}\times\mathbf{n})^2\hat{W}_{44} \equiv F'(I_4) + 2(\mathbf{a}\times\mathbf{n})^2F''(I_4), \tag{3.4}$$

where a prime denotes differentiation with respect to I_4. In view of $(2.48)_3$ we have $F'(1) = 0$. Since we may choose $\mathbf{n}$ so that $\mathbf{a}\times\mathbf{n} = \mathbf{0}$, it is clear that for (3.4) to be non-negative it is necessary that $F'(I_4) \geq 0$. If also $F''(I_4) \geq 0$ then (3.4) is non-negative for all (n_1, n_2). If, on the other hand, $F''(I_4) < 0$ then

$$F'(I_4) + 2(\mathbf{a}\times\mathbf{n})^2F''(I_4) \geq F'(I_4) + 2I_4F''(I_4).$$

It follows that (3.4) is non-negative if and only if

$$F'(I_4) \geq 0, \quad F'(I_4) + 2I_4F''(I_4) \geq 0. \tag{3.5}$$

Thus, sufficient conditions for (3.2) are clearly (3.5) together with (3.3).

3.1.1. The ellipticity status of $F(I_4)$. Here we are concerned with the ellipticity status of the reinforcing model $F(I_4)$ and its influence on the overall ellipticity of the energy function (3.1). Without loss of generality we may take $F(1) = 0$. Hence, recalling (2.35), the restrictions on F in the reference configuration are

$$F(1) = 0, \quad F'(1) = 0, \quad 2W'_{\rm iso}(3) + F''(1) > 0, \tag{3.6}$$

the latter following from (2.55). This is certainly satisfied if $F''(1) \geq 0$, which, in fact, follows from (2.35).

Because of the factor $(\mathbf{n}\cdot\mathbf{a})^2$ in (3.2), in isolation from the isotropic base material, $F(I_4)$ always loses ellipticity since $\mathbf{n}$ may be chosen so that $\mathbf{n}\cdot\mathbf{a} = 0$. For all other $\mathbf{n}$, the contribution of F to (3.2) is strictly positive if and only if

$$F'(I_4) > 0, \quad F'(I_4) + 2I_4F''(I_4) > 0. \tag{3.7}$$

Of course, the first of these inequalities fails in the reference configuration, while strict inequality in the second is also lost in the reference configuration if $F''(1) = 0$.

We note here that the terms involving I_4 in (3.2) may be written as

$$I_4\{(\hat{\mathbf{a}}\cdot\mathbf{n})^4F'(I_4) + (\hat{\mathbf{a}}\cdot\mathbf{n})^2(\hat{\mathbf{a}}\times\mathbf{n})^2[F'(I_4) + 2I_4F''(I_4)]\}, \tag{3.8}$$

where $\hat{\mathbf{a}} = \mathbf{a}/|\mathbf{a}|$. It is useful to consider (3.8) as quadratic in $x = (\mathbf{n}\cdot\hat{\mathbf{a}})^2$ with $0 \leq x \leq 1$. Then, (3.8) is written simply as

$$f(x) \equiv -ax^2 + (a+b)x, \tag{3.9}$$

where

$$a = 2I_4^2F''(I_4), \quad b = I_4F'(I_4). \tag{3.10}$$

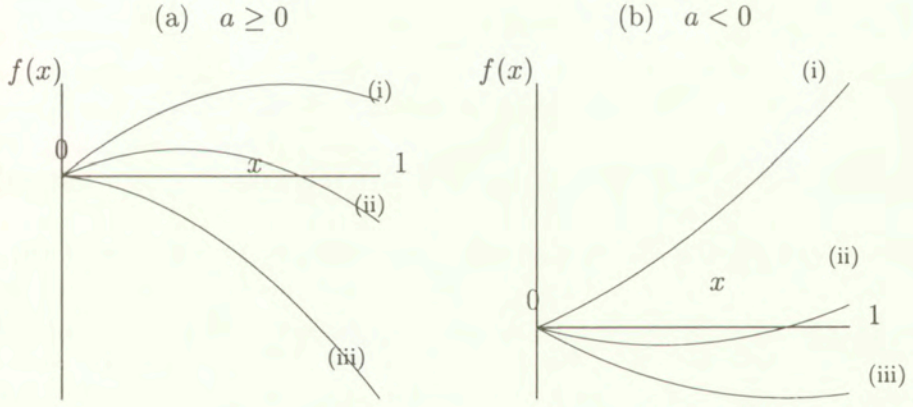

FIG. 2. Properties of the function $f(x)$ for $x = (\mathbf{n}\cdot\hat{\mathbf{a}})^2$: (a) $a \geq 0$ with (i) $b > 0$, (ii) $b < 0$, $a + b > 0$, (iii) $a + b < 0$; (b) $a < 0$ with (i) $a + b > 0$, (ii) $b > 0$, $a + b < 0$, (iii) $b < 0$.

Noting that $f(0) = 0, f(1) = b$ and $f'(0) = a + b$ we show the behaviour of $f(x)$ in Figs. 2(a) and 2(b) for $a \geq 0$ and $a < 0$ respectively. It is clear from Fig. 2(a) that for $F''(I_4) \geq 0$ the expression (3.8) first becomes negative as soon as $F'(I_4)$ becomes negative, and that it is negative for a range of values of x near 1 (i.e. where $\mathbf{n}$ is nearly parallel to $\mathbf{a}$) provided $F'(I_4) + 2I_4F''(I_4) > 0$. For $F'(I_4) + 2I_4F''(I_4) \leq 0$ it is negative for all $x \in (0, 1]$. Figure 2(b) is applicable

for fiber extension. The expression (3.8) first becomes negative (near $x = 0$) as $F'(I_4) + 2I_4F''(I_4)$ changes from positive to negative, which is relevant for functions F that are non-convex ($F''(I_4) < 0$ for some I_4).

For the standard reinforcing model (2.34), $F'(I_4) > 0$ if and only if $I_4 > 1$, while $F'(I_4) + 2I_4F''(I_4) > 0$ if and only if $I_4 > 1/3$. Deformation gradients $\mathbf{F}$ satisfying $I_4 < 1/3$ are not of interest since ellipticity will be lost at a larger value of $I_4 < 1$ on a path from $I_4 = 1$.

3.1.2. Overall ellipticity. Our goal is to determine the set of deformation gradients, denoted E, containing the undeformed configuration for which it is possible to construct a parametrized family of (plane) deformation gradients $\mathbf{F}$ such that ellipticity of $\hat{W}$ is not lost at an intermediate deformation on a path of deformation from the undeformed configuration. We refer to E as the *effective elliptic region* for $\hat{W}$. Since we assume that strong ellipticity holds in the reference configuration it follows that strong ellipticity holds within E. The boundary of E, denoted $\partial\mathsf{E}$, is defined by the loss of strong ellipticity condition, i.e. by the set of deformation gradients $\mathbf{F}$ for which (2.56) holds for one or more unit vectors $\mathbf{n}$ with (2.50) holding for all other $\mathbf{n}$. This boundary is therefore associated with breakdown of (strong) ellipticity. Since the isotropic base material is assumed to be strongly elliptic it is clear that a necessary condition for the breakdown of ellipticity of an elliptic isotropic nonlinearly elastic solid augmented with $F(I_4)$ is that, for $\mathbf{F} \in \mathsf{E}$, either $F'(I_4) < 0$ or $F'(I_4) + 2I_4F''(I_4) < 0$ on some path of deformation before the boundary $\partial\mathsf{E}$ is reached.

It is worth pointing out here that (3.2)is *quartic* in the components (n_1, n_2) and can be rearranged as a quartic in a single variable (e.g., n_1/n_2) with values between $-\infty$ and $+\infty$. Necessary and sufficient conditions for such a quartic to be positive can be written down explicitly, but they are extremely complicated and not easy to interpret. It is therefore appropriate to examine the influence of (3.8 on the inequality (3.2). This is particularly important for strong reinforcement in which the magnitude of (3.8) dominates (3.2).

At this point it is appropriate to consider the ellipticity status of $W_{\rm iso}$ on the same basis as that of F and we write the left-hand side of (2.51) as

$$i(x) \equiv -ax^2 + (a + b - c)x + c, \tag{3.11}$$

where again $x = n_1^2$ and the notation a, b, c is defined by

$$a = 2(I_1 + 1)(I_1 - 3)W''_{\rm iso}(I_1), \quad b = \lambda_1^2 W'_{\rm iso}(I_1), \quad c = \lambda_2^2 W'_{\rm iso}(I_1), \tag{3.12}$$

the definitions of a and b being different from those appearing in (3.10). Figure 3 shows the behaviour of $i(x)$. In Fig. 3(a) $b > 0$ (and hence $c > 0$). Strong ellipticity holds for the upper curve, corresponding to $a > 0$ (i.e. $W''_{\rm iso}(I_1) > 0$),

and the middle curve, for which $a < 0$ but $W'_{\text{iso}}(I_1)+2(I_1-3)W''_{\text{iso}}(I_1)$ is positive. Ellipticity is lost as the latter term passes through zero, and the lower curve corresponds to $W'_{\text{iso}}(I_1)+2(I_1-3)W''_{\text{iso}}(I_1) < 0$. In Fig. 3 (b) we have $b < 0$ (and $c < 0$) and $i(x)$ is negative except for an intermediate range of values of x when $a > 0$ and $W'_{\text{iso}}(I_1) + 2(I_1 - 3)W''_{\text{iso}}(I_1) \geq 0$.

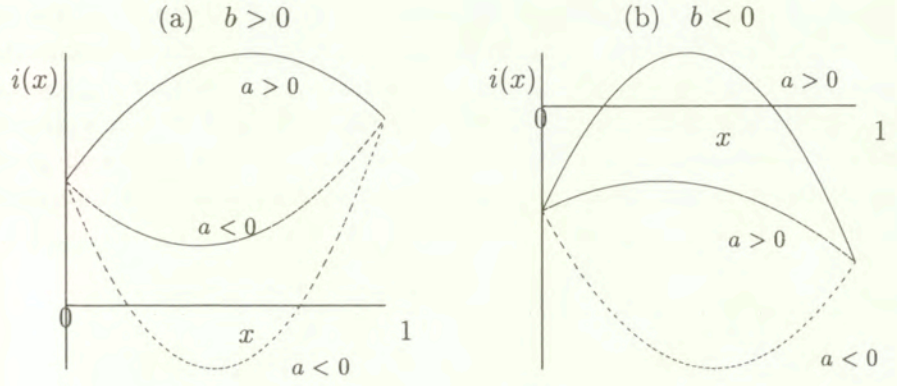

FIG. 3. Properties of the function $i(x)$ for $x = n_1^2$: (a) $b > 0$; (b) $b < 0$. In each case there is a maximum if $a > 0$ and a minimum if $a < 0$.

REMARK 1. Weak surfaces cannot be aligned with the fiber reinforcement axis since then we would have $\mathbf{n} \cdot \mathbf{a} = 0$ and, because of the assumed strong ellipticity of the isotropic base material, the inequality (3.2) holds, as indeed does (2.50). Weak surfaces are the only possible carriers of discontinuity for the equilibrium Eqs. (2.22) or (2.24). Therefore, no surface of discontinuity, either weak or fully developed (i.e. strong [7, 8]) can be aligned with the fiber direction. In [7], for the standard reinforcing model, this result was established for weak and strong surfaces with a particular deformation on one side of the surface, namely a deformation for which the (reference) fiber direction is a Lagrangian principal direction (i.e. an eigenvector of $\mathbf{C}$).

REMARK 2. If $F''(I_4) \geq 0$, *fiber kinking*, is the relevant failure mechanism under compressive strain in the fiber direction ($I_4 < 1$). It suffices to show that the weak surface at breakdown of ellipticity is normal to the fiber. If $\mathbf{n}$ is parallel to $\mathbf{a}$ then (3.8) reduces to

$$I_4 F'(I_4), \tag{3.13}$$

which is easily shown to be the least value of (3.8) whatever the sign of $F'(I_4) + 2I_4F''(I_4)$. However, with reference to Fig. 2(a) we see that (3.8) first becomes negative on a path of deformation from the reference configuration (where $I_4 = 1$) as I_4 decreases with $F'(I_4) + 2I_4F''(I_4) > 0$ and this negative value decreases with I_4. Thus, breakdown of ellipticity occurs as I_4 decreases from 1 when the negative value of $I_4F'(I_4)$ balances the positive value of the first pair of terms in (3.2) with $\mathbf{n} = \hat{\mathbf{a}}$. If $\mathbf{a}$ is an eigenvector of $\mathbf{B}$ then this happens for $n_2 = 0$ and (3.8) reduces to $I_4F'(I_4) + \lambda_1^2 W'_{\text{iso}}(I_1)$. Since, by strong ellipticity of the base material, $W'_{\text{iso}}(I_1) > 0$, this will vanish for some $I_4 < 1$ even for reinforcements of moderate strength. For very strong reinforcement it will vanish for I_4 close to 1. Suppose the deformation consists of a simple shear of amount γ in a direction normal to the reference direction of the fiber superimposed on a pure shear with stretch λ in the same direction. For simplicity, let $\mathbf{A} = \mathbf{e}_1$. Then, the components of the deformation gradient are

$$\begin{pmatrix} \lambda & 0 \\ \gamma\lambda & \lambda^{-1} \end{pmatrix}, \tag{3.14}$$

and

$$\mathbf{a} = \mathbf{FA} = \begin{pmatrix} \lambda \\ \gamma\lambda \end{pmatrix}. \tag{3.15}$$

Since $\mathbf{n} = \hat{\mathbf{a}}$ the angle, θ say, that the weak surface makes with the $\mathbf{e}_1$ axis (measured counterclockwise) is given by $\tan\theta = -1/\gamma$, while $I_4 = \lambda^2(1 + \gamma^2)$. Clearly, as γ increases λ must decrease in order to maintain $I_4 < 1$. If $\gamma > 0$ then $\pi/2 < \theta < \pi$ while if $\gamma < 0$ we have $0 < \theta < \pi/2$. Thus, as γ increases from 0 the weak surface rotates from the vertical (aligned with $\mathbf{e}_2$) counterclockwise (as does the fiber with changing deformation), and if γ decreases from 0 the surface rotates clockwise. We emphasize that larger values of $|\gamma|$ require smaller values of λ for loss of ellipticity.

REMARK 3. If $F''(I_4) < 0$ and $F'(I_4) + 2I_4F''(I_4) > 0$ then there can be no loss of ellipticity, but if $F'(I_4) + 2I_4F''(I_4) < 0$ then the (negative) minimum value of (3.8) is

$$\frac{(F' + 2I_4F'')^2}{8I_4F''} \tag{3.16}$$

whether $F' > 0$ or $F' < 0$, and it occurs for

$$(\mathbf{n} \cdot \mathbf{a})^2 = \frac{F' + 2I_4F''}{4F''} \tag{3.17}$$

(see Fig. 2(b)). Loss of ellipticity occurs first, however, in fiber extension with $F'(I_4) > 0$ when $F'(I_4) + 2I_4F''(I_4)$ passes from positive to negative. This, of course, requires loss of convexity of F.

Thus, in fiber *extension* ($I_4 > 1$) ellipticity can fail, if again $\mathbf{a}$ is an eigenvector of $\mathbf{B}$, when $\mathbf{n} \cdot \mathbf{a}$ is small since the negative contribution to (2.45) then balances the positive contribution due to W'_{iso} provided the reinforcement is sufficiently strong. In this case the weak surface is close to parallel to the fiber direction and the relevant failure mechanism can be interpreted as de-bonding.

It is interesting to note that in this case the contribution of $F(I_4)$ to the component of nominal traction, s say, in the fiber direction is, from (2.45), $2I_4^{1/2}F'(I_4)$. Hence, $\mathrm{d}s/\mathrm{d}I_4 = I_4^{-1/2}[F'(I_4) + 2I_4F''(I_4)]$ and thus failure of ellipticity is associated with s passing through a maximum during fiber extension.

Figure 4 shows a schematic of the possible failure mechanisms for $I_4 < 1$ and $I_4 > 1$ and the associated properties of $F(I_4)$.

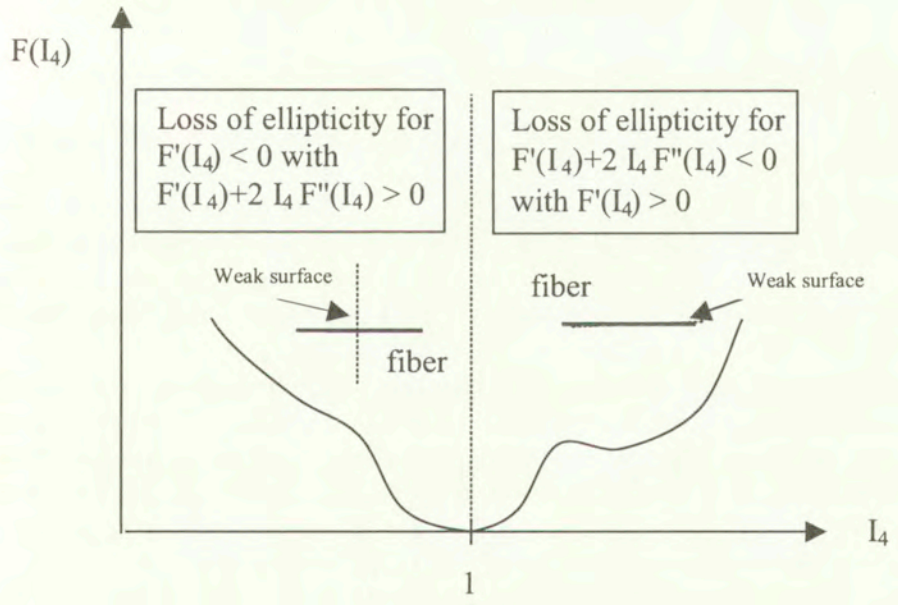

FIG. 4. Loss of ellipticity associated with the properties of $F(I_4)$ in the case of a strongly elliptic isotropic base material. Under compression in the fiber direction, the associated weak surface is normal to the fiber as appropriate for the fiber kinking mechanism. Under fiber extension, the weak surface is close to the fiber direction, as in fiber de-bonding.

REMARK 4. As discussed previously, for $\mathbf{n} \cdot \mathbf{a} = 0$ ellipticity cannot fail if W_{iso} is strongly elliptic. However, it is worth noting here that if W_{iso} is allowed to lose ellipticity then this can happen for $\mathbf{n}$ such that $\mathbf{n} \cdot \mathbf{a} = 0$, i.e. when the weak

surface coincides with the fiber direction. This is independent of the properties of the reinforcing model $F(I_4)$ and is not therefore depicted in Fig. 4.

3.2. Ellipticity of convex I_4 reinforcement

In this section we are concerned with convex reinforcing models, so that $F''(I_4) \geq 0$. Suppose that $F(I_4) = \alpha f(I_4)$, where $\alpha\,(>0)$ is an anisotropy parameter, as in the standard reinforcing model (2.34), then loss of ellipticity requires fiber contraction since $F'(I_4) \geq 0$ and $F''(I_4) \geq 0$ in fiber extension. Furthermore, the breakdown of ellipticity for the considered materials, i.e. models with an elliptic isotropic base material, satisfies a nesting property with respect to the parameter α. The result is stated as follows.

PROPOSITION. If $\mathbf{F}$ is on the ellipticity boundary $\partial\mathsf{E}$ for α_1 and $\alpha_2 > \alpha_1$ then $\mathbf{F} \notin \mathsf{E}$ for α_2.

P r o o f. This follows easily from (3.2), which we now write as

$$2W''_{\rm iso}(I_1)(\lambda_1^2-\lambda_2^2)^2n_1^2n_2^2 + W'_{\rm iso}(I_1)(\lambda_1^2n_1^2+\lambda_2^2n_2^2) + \alpha(\mathbf{a}\cdot\mathbf{n})^2[f'(I_4)+2(\mathbf{a}\times\mathbf{n})^2f''(I_4)] > 0. \tag{3.18}$$

By hypothesis $2W''_{\rm iso}(I_1)(\lambda_1^2-\lambda_2^2)^2n_1^2n_2^2 + W'_{\rm iso}(I_1)(\lambda_1^2n_1^2+\lambda_2^2n_2^2) > 0$. Now consider that the left-hand side of (3.17) vanishes for the deformation gradient $\mathbf{F}$ when $\alpha = \alpha_1$ and for a specific $\mathbf{n}$, but is otherwise non-negative. It follows that for this $\mathbf{F}$ and $\mathbf{n}$ the left-hand side of (3.17) is negative for $\alpha_2 > \alpha_1$. Hence, $\mathbf{F} \notin \mathsf{E}$ for $\alpha = \alpha_2$.

In [18] this nesting property of $\mathbf{F}$ giving rise to the breakdown of ellipticity was illustrated for the standard reinforcing model (2.34) by reference to plots in (C_{11}, C_{12}, α)-space. Furthermore, it may be shown that the asymptotic form of the breakdown of ellipticity curves in (C_{11}, C_{12}, α)-space as α and $C_{12} \to \infty$ is $I_4 = C_{11} \to 1/3$. We recall that in Sec. 3.1 it was noted that $I_4 = 1/3$ is associated with vanishing of $F'(I_4) + 2I_4F''(I_4)$ in respect of (2.34).

If the isotropic base material is non-elliptic, however, then the effect of the anisotropic parameter is as follows. Two possibilities have to be considered depending on the fiber stretch. If the fiber is under contraction then the nesting property is as in the case of an elliptic base material. If the fiber is subject to extension with a deformation gradient $\mathbf{F}$, then if $\mathbf{F} \in \mathsf{E}$ for α_1, then $\mathbf{F} \in \mathsf{E}$ is elliptic for $\alpha_2 > \alpha_1$. Therefore, deformation gradients giving rise to breakdown of ellipticity are nested with respect to α in fiber contraction, while the elliptic regions are nested with respect to α in fiber extension. This allows us to conclude that an elliptic isotropic base material augmented with a convex reinforcing model gains stability in fiber extension while it is weakened in fiber contraction. Similarly,

as α increases, i.e. as the degree of anisotropy increases, the solid becomes more stable in fiber extension, but less stable in fiber compression.

3.3. The case of two reinforcing models

The general analysis above does not depend on the fiber orientation in the plane of deformation. This allows us to consider simultaneously the qualitative effect of more than one fiber direction on the ellipticity status of an augmented isotropic base material. The undeformed angles of the fibers have an important role since a deformation gradient $\mathbf{F}$ may generate contraction in one of the fibers and extension in the other, for example. The analysis could include several fibers and several reinforcing models. However, here we focus on the simple case of two fibers and the influence of their relative orientation under a deformation gradient corresponding to (plane) pure homogeneous strain. Thus,

$$\mathbf{F} = \lambda \mathbf{e}_1 \otimes \mathbf{e}_1 + \lambda^{-1} \mathbf{e}_2 \otimes \mathbf{e}_2, \tag{3.19}$$

where $\mathbf{e}_1, \mathbf{e}_2$ are the (in-plane) Cartesian unit basis vectors.

Let the fibers be defined by the convex reinforcing models $F_1(I_4^{(1)})$ and $F_2(I_4^{(2)})$ so that $W_{\text{fib}} = F_1(I_4^{(1)}) + F_2(I_4^{(2)})$. Without loss of generality we take fiber 1 to be aligned with $\mathbf{e}_1$ in the undeformed configuration and hence $I_4^{(1)} = \lambda^2$. Let the direction of fiber 2 be given by the angle ϕ relative to the $\mathbf{e}_1$ direction in the undeformed configuration. Because of symmetry it is sufficient to consider $0 < \phi < \pi/2$. Then, we have

$$I_4^{(2)} = \lambda^2 \cos^2 \phi + \lambda^{-2} \sin^2 \phi. \tag{3.20}$$

A preliminary step is to consider for which angles ϕ fiber 2 is in contraction or extension for a given λ. We consider separately the ranges of angles $0 < \phi < \pi/4$ and $\pi/4 < \phi < \pi/2$. Then it is easily seen that, for $0 < \phi < \pi/4$,

$$\begin{aligned} &\text{if} \quad 0 < \lambda < \tan\phi \quad \text{or} \quad \lambda > 1 \quad \text{then} \quad I_4^{(2)} > 1, \\ &\text{if} \quad \tan\phi < \lambda < 1 \quad \text{then} \quad I_4^{(2)} < 1, \end{aligned} \tag{3.21}$$

with $I_4^{(2)} = 1$ corresponding to $\tan\phi = \lambda$. For $\pi/4 < \phi < \pi/2$ the corresponding inequalities are

$$\begin{aligned} &\text{if} \quad 0 < \lambda < 1 \quad \text{or} \quad \tan\phi < \lambda \quad \text{then} \quad I_4^{(2)} > 1, \\ &\text{if} \quad 1 < \lambda < \tan\phi \quad \text{then} \quad I_4^{(2)} < 1, \end{aligned} \tag{3.22}$$

with again $I_4^{(2)} = 1$ corresponding to $\tan\phi = \lambda$.

For this double reinforcement the strong ellipticity inequality (3.2) becomes

$$2W''_{\rm iso}(I_1)(\lambda_1^2-\lambda_2^2)^2n_1^2n_2^2+W'_{\rm iso}(I_1)(\lambda_1^2n_1^2+\lambda_2^2n_2^2) + (\mathbf{a}\cdot\mathbf{n})^2[W'_{\rm fib}(I_4)+2(\mathbf{a}\times\mathbf{n})^2W''_{\rm fib}(I_4)]>0. \tag{3.23}$$

If $\lambda<1$ then fiber 1 is under contraction and $F_1(I_4^{(1)})$ is non-elliptic and contributes a negative quantity $I_4F_1'(I_4^{(1)})$ to (3.23) when $\mathbf{n}\times\mathbf{e}_1=\mathbf{0}$. If fiber 2 is in extension it contributes a positive term to (3.23) and counteracts the effect of fiber 1. If it is of sufficient magnitude this may have the effect of restoring strong ellipticity. On the other hand, if fiber 2 is under contraction then it contributes a negative term to (3.23) and enhances the prospects of loss of ellipticity. It follows that compared with the material with a single reinforcement, the doubly-reinforced, material gains stability if fiber 2 is such that $\pi/4<\phi<\pi/2$. For $\lambda>1$, the opposite state of affairs applies: fiber 1 is in extension and contributes a positive term to (3.23). Then, if fiber 2 is under contraction its contribution to $W_{\rm fib}$ is such that ellipticity may be lost, but if fiber 2 is extended then $W_{\rm fib}$ is strongly elliptic. The loss of ellipticity can be avoided if fiber 2 is such that $0<\phi<\pi/4$.

4. The effect of I_5 reinforcement

In this section we consider the reinforcing model

$$\hat{W}(I_1,I_4)=W_{\rm iso}(I_1)+W_{\rm fib}(I_5), \tag{4.1}$$

where I_4 has been replaced by I_5 in (3.1) and we recall that $I_5=(I_1-1)I_4-1$. Thus, while in (3.1) I_1 and I_4 are decoupled in (4.1) there is a coupling of I_1 and I_4 through I_5. For convenience, we write $G(I_5)=W_{\rm fib}(I_5)$ and we analyze the reinforcing model $G(I_5)$, again with the restriction to plane deformations. We will show that no particular property of the reinforcing model enables loss of ellipticity of $G(I_5)$ to be avoided, unlike the situation for $F(I_4)$.

The domain for I_5 is $0<I_5<\infty$ and the condition $I_5=1$ is satisfied in many configurations (in addition to the undeformed configuration) depending on the fiber orientation in the undeformed configuration. It necessarily entails fiber contraction since, without loss of generality, if we consider $\mathbf{A}=\mathbf{e}_1$ then, $I_5=C_{11}^2+C_{12}^2=1$ if and only if $I_4=C_{11}<1$ provided $C_{12}\neq0$ and therefore necessarily involves the shearing indicator C_{12}. It is worth noting that in general (in plane strain) it follows from the connection (2.41) that $I_4\geq1$ implies $I_5\geq1$ while $I_5\leq1$ implies $I_4\leq1$ (in particular, note that $I_5=1$ implies $I_4\leq1$, with equality if and only if the material is undeformed). These implication do not go

the other way. This can be seen by noting that the counterpart of the expression (3.20) for I_5, obtained by replacing λ by λ^2, is

$$I_5 = \lambda^4 \cos^2\phi + \lambda^{-4}\sin^2\phi. \tag{4.2}$$

Thus, by reference to (3.21) and (3.22), for $0 < \phi < \pi/4$,

$$\begin{aligned} &\text{if} \quad 0 < \lambda < \sqrt{\tan\phi} \quad \text{or} \quad \lambda > 1 \quad \text{then} \quad I_5 > 1, \\ &\text{if} \quad \sqrt{\tan\phi} < \lambda < 1 \quad \text{then} \quad I_5 < 1, \end{aligned} \tag{4.3}$$

and for $\pi/4 < \phi < \pi/2$:

$$\begin{aligned} &\text{if} \quad 0 < \lambda < 1 \quad \text{or} \quad \sqrt{\tan\phi} < \lambda \quad \text{then} \quad I_5 > 1, \\ &\text{if} \quad 1 < \lambda < \sqrt{\tan\phi} \quad \text{then} \quad I_5 < 1, \end{aligned} \tag{4.4}$$

with $I_5 = 1$ corresponding to $\tan\phi = \lambda^2$ in each case.

On substitution of (4.1) into (3.2) we obtain

$$\begin{aligned} 2W''_{\rm iso}(I_1)(\lambda_1^2 - \lambda_2^2)^2 n_1^2 n_2^2 + W'_{\rm iso}(I_1)(\lambda_1^2 n_1^2 + \lambda_2^2 n_2^2) \\ + 2G''(I_5)\left[I_4(\lambda_1^2 - \lambda_2^2)n_1 n_2 + (I_1 - 1)(\mathbf{n}\cdot\mathbf{a})(\mathbf{a}\times\mathbf{n})_3\right]^2 \\ + G'(I_5)\left[(I_1 - 1)(\mathbf{n}\cdot\mathbf{a})^2 + I_4(\lambda_1^2 n_1^2 + \lambda_2^2 n_2^2)\right. \\ \left. + 4(\lambda_1^2 - \lambda_2^2)n_1 n_2 (\mathbf{n}\cdot\mathbf{a})(\mathbf{a}\times\mathbf{n})_3\right] > 0, \end{aligned} \tag{4.5}$$

where $(\mathbf{a}\times\mathbf{n})_3 = a_1 n_2 - a_2 n_1$.

We note two special cases of (4.5). First, we note that if $\mathbf{n}\cdot\mathbf{a} = 0$ then the terms in G in (4.5) reduce to

$$2G''(I_5)\left[I_4(\lambda_1^2 - \lambda_2^2)n_1 n_2\right]^2 + I_4 G'(I_5)(\lambda_1^2 n_1^2 + \lambda_2^2 n_2^2), \tag{4.6}$$

while if $\mathbf{n}\times\mathbf{a} = \mathbf{0}$ they reduce to

$$2G''(I_5)\left[I_4(\lambda_1^2 - \lambda_2^2)n_1 n_2\right]^2 + I_4 G'(I_5)(\lambda_1^2 n_1^2 + \lambda_2^2 n_2^2 + \lambda_1^2 + \lambda_2^2). \tag{4.7}$$

REMARK 5. In Sec. 3.1 it was pointed out that $F(I_4)$ does not admit a weak surface aligned with the fiber direction. This is not the case for $G(I_5)$, as we now show. We recall from (2.37) that $G'(I_5) < 0$ for $I_5 < 1$. Thus, if either $n_1 = 0$ or $n_2 = 0$, for example, the expression (4.6) is negative when $I_5 < 1$, in which case $I_4 < 1$ and the fiber is under contraction. Thus, ellipticity can fail for $I_5 < 1$. If $n_1 = 0$ ($a_2 = 0$) this corresponds to a weak surface parallel to the fiber direction and may be associated with fiber splitting [9].

REMARK 6. The case of (4.7) with $n_2 = 0$ and $a_2 = 0$ may be associated with a weak surface normal to the fiber direction. Thus, failure of ellipticity under fiber contraction can correspond to fiber kinking, as for the $F(I_4)$ reinforcement.

REMARK 7. If the degree of anisotropy is sufficiently strong then the terms in G dominate the left-hand side of (4.5) and hence loss of ellipticity cannot be avoided under contraction if I_5 is sufficiently small. Deformations satisfying $I_5 = 1$ involve $C_{11} < 1$ and $C_{12} \neq 0$ simultaneously. We can therefore conclude that for deformation gradients satisfying $I_4 = C_{11} < 1$ and $I_5 \leq 1$ the material is expected to lose ellipticity.

REMARK 8. Note that the coefficient of $G'(I_5)$ in (4.5) is not sign definite, so that failure of ellipticity can occur even if $G''(I_5) \geq 0$, i.e. if G is convex.

For the special case when $\mathbf{a}$ is an eigenvector of $\mathbf{B}$ the behaviour of the terms in G in (4.5) can be seen as follows. Let $\hat{\mathbf{a}}$ be the first eigenvector of $\mathbf{B}$. Then, $\mathbf{n} \cdot \hat{\mathbf{a}} = n_1$ and $(\hat{\mathbf{a}} \times \mathbf{n})_3 = n_2$ and the terms in G may be written as

$$g(x) \equiv -ax^2 + (a+b)x + c, \tag{4.8}$$

where $x = n_1^2$ and

$$a = 4I_4[2\lambda_1^4 I_4 G''(I_5) + (\lambda_1^2 - \lambda_2^2)G'(I_5)], \tag{4.9}$$

$$b = 2I_4\lambda_1^2 G'(I_5), \quad c = I_4\lambda_2^2 G'(I_5). \tag{4.10}$$

Note that the definitions of a, b and c differ from those in (3.12).

Figure 5 shows the behaviour of $g(x)$, which is very similar to that of $i(x)$ shown in Fig. 3 except that a, b, c are different. Figure 5 (a) corresponds to fiber contraction and it is clear that the negative contribution of the terms in G to (4.5) near $x = 0$ and $x = 1$ will balance the positive contribution from strongly elliptic W_{iso} whenever the reinforcement is sufficiently strong. In fiber extension, corresponding to Fig. 5 (b), loss of ellipticity requires $a < 0$, but this is not sufficient since the minimum value of $g(x)$ must be negative. If this is the case then loss of ellipticity occurs at an intermediate value of x. It follows from (4.6) and (4.7) that the weak surface is neither close to the fiber axis nor close to the normal to the fiber. It is not clear how to interpret the associated failure mechanism in this situation.

An illustration of a possible situation in which $\mathbf{a}$ is not an eigenvector is provided by simple shear. Consider, in particular, a simple shear deformation in which the direction of shear is perpendicular to the undeformed fiber direction. For definiteness we take $\mathbf{A} = \mathbf{e}_2$ and consider the simple shear with amount of shear γ so that $\mathbf{a} = \gamma\mathbf{e}_1 + \mathbf{e}_2$ and hence $I_4 = 1 + \gamma^2$, $I_5 = 1 + 3\gamma^2 + \gamma^4$. If $\mathbf{a} \cdot \mathbf{n} = 0$

then $\mathbf{n} = (-\mathbf{e}_1 + \gamma\mathbf{e}_2)/\sqrt{I_4}$ and the contribution of the terms in G to (4.5) is then

$$2I_4G''(I_5)\gamma^4(\gamma^2+4) + G'(I_5)(\lambda^2+\gamma^2\lambda^{-2}). \tag{4.11}$$

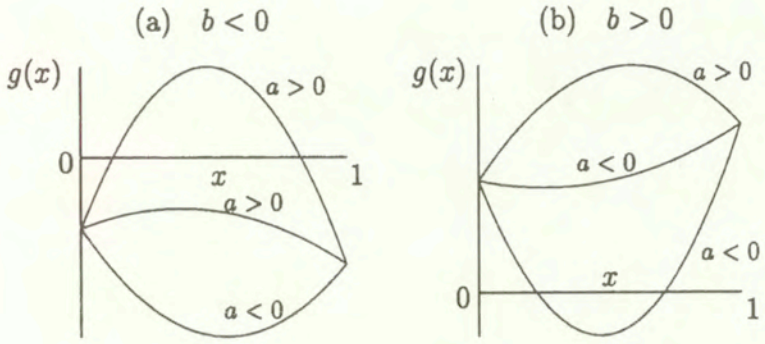

FIG. 5. Properties of the function $g(x)$ for $x = n_1^2$.

REMARK 9. It follows from (4.11) that for a simple shear deformation in which the direction of shear is not parallel to the fiber direction (and, in particular, when it is perpendicular to the fiber direction) a necessary condition for loss of ellipticity (if the base material is strongly elliptic) is $G''(I_5) < 0$. In this case the weak surface is parallel to the fiber direction and de-bonding is the appropriate failure mechanism.

REMARK 10. If, instead of $\mathbf{a}\cdot\mathbf{n} = 0$, $\mathbf{n}$ is parallel to $\mathbf{a}$ then a similar situation to that described in Remark 9 ensues. In this case the weak surface is perpendicular to the fiber direction and the appropriate failure mechanism is matrix failure.

REMARK 11. If the isotropic base material loses ellipticity with W'_{iso} becoming negative then overall ellipticity can fail either for $\mathbf{n}\cdot\mathbf{a} = 0$ or $\mathbf{n}\times\mathbf{a} = \mathbf{0}$. With reference to (4.5), it can be seen that this can occur for $G'(I_5)$ and $G''(I_5)$ with appropriate signs.

Figure 6 shows a schematic of the possible failure mechanisms for $I_5 < 1$ and $I_5 > 1$ and the associated properties of $G(I_5)$.

5. Discussion and Summary

This analysis has been motivated by instability phenomena in fiber-reinforced composite materials and has focused on failure prediction. The materials considered are isotropic base materials augmented by a function that accounts for

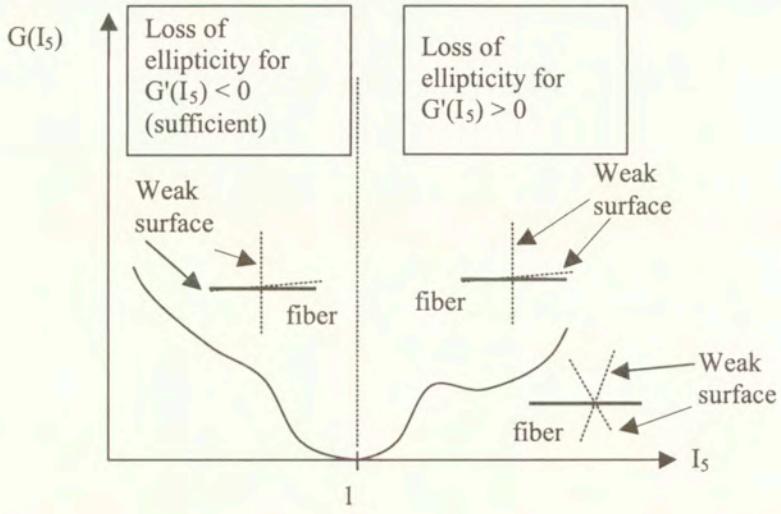

FIG. 6. Loss of ellipticity associated with $G(I_5)$ for the case of a strongly elliptic isotropic base material.

the existence of fiber reinforcement (the reinforcing model). The onset of failure is associated with loss of ellipticity of the governing differential equations. A detailed analysis of the ellipticity status of the I_4 reinforcing model has been given. In particular, in Sec. 3 simple conditions that guarantees the ellipticity of the I_4 reinforcing model has been determined. It was found that loss of ellipticity (and hence fiber failure) is expected under fiber contraction. Fiber failure may also occur under fiber extension if the reinforcing model is non-convex. In Sec. 4, the I_5 reinforcing model has been considered briefly and its effect on the loss of ellipticity has been illustrated in some simple cases. We have indicated how the breakdown of ellipticity may be related to different fiber failure mechanisms.

It should be emphasized that we have focused on instabilities associated with loss of ellipticity in a homogeneous material homogeneously deformed so that boundary conditions are not involved. We have not considered other types of instability such as buckling, which, under appropriate boundary conditions, may be initiated prior to loss of ellipticity.

References

1. B. BUDIANSKY and N. A. FLECK, *Compressive failure of fiber composites*, J. Mech. Phys. Solids, **41**, 183–211, 1993.

2. B. BUDIANSKY, N. A. FLECK and J. C. AMAZIGO, *On kink-band propagation in fiber composites*, J. Mech. Phys. Solids, **9**, 1637–1653, 1998.

3. P. M. MORAN and C. F. SHIH, *Kink band formation and band broadening in ductile matrix fiber composites: experiments and analysis*, Int. J. Solids Structures, **35**, 1709–1722, 1998.

4. S. KYRIAKIDES, R. ARSECULERANE, E. PERRY and K. M. LIECHTI, *On the compressive failure of fiber reinforced composites*, Int. J. Solids Structures, **32**, 689–738, 1995.

5. T. J. VOGLER and S. KYRIAKIDES, *Initiation and axial propagation of kink bands in fiber composites*, Acta Metall. Mater., **45**, 2443–2454, 1997.

6. H. M. JENSEN and J. CHRISTOFFERSEN, *Kink band formation in fiber reinforced materials*, J. Mech. Phys. Solids, **45**, 1121–1136, 1997.

7. J. MERODIO and T. J. PENCE, *Kink surfaces in a directionally reinforced neo-Hookean material under plane deformation: I. Mechanical equilibrium*, J. Elasticity, **62**, 119–144, 2001.

8. J. MERODIO and T. J. PENCE, *Kink surfaces in a directionally reinforced neo-Hookean material under plane deformation: II. Kink band stability and maximally dissipative band broadening*, J. Elasticity, **62**, 145–170, 2001.

9. S. H. LEE, C. S. YERRAMALLI, A. M. WAAS, *Compressive splitting response of glass-fiber reinforced unidirectional composites*, Composites Science and Technology, **60**, 2957–2966, 2000.

10. M. R. PIGGOTT, *Why interface testing by single-fibre methods can be misleading*, Composites Science and Technology, **57**, 965–974, 1997.

11. T. OKABE, J. KOMOTORI, M. SHIMIZU, N. TAKEDA, *Mechanical behavior of SiC fiber reinforced brittle-matrix composites*, Journal of Material Science, **34**, 3405–3412, 1999.

12. K. LIAO and K. L. REIFSNIDER, *A tensile model for unidirectional fiber-reinforced brittle matrix composite*, Int. J. Fracture, **106**, 95–115, 2000.

13. J. K. KNOWLES and E. STERNBERG, *On the ellipticity of the equations of nonlinear elastostatics for a special material*, J. Elasticity, **5**, 341–361, 1975.

14. L. ZEE and E. STERNBERG, *Ordinary and strong ellipticity in the equilibrium theory of incompressible hyperelastic solids*, Arch. Rat. Mech. Anal., **83**, 50–90, 1983.

15. P. ROSAKIS, *Ellipticity and deformations with discontinuous gradients in plane elastostatics of compressible solids*, Arch. Rat. Mech. Anal., **109**, 1–37, 1990.

16. C. O. HORGAN, *Remarks on ellipticity for the generalized Blatz-Ko constitutive model for a compressible nonlinearly elastic solid*, J. Elasticity, **42**, 165–176, 1996.

17. J. K. KNOWLES and E. STERNBERG, *On the failure of ellipticity and the emergence of discontinuous deformation gradients in plane finite elastostatics*, J. Elasticity, *8*, 329–379, 1978.

18. G. Y. QIU and T. J. PENCE, *Loss of ellipticity in plane deformations of a simple directionally reinforced incompressible nonlinearly elastic solid*, J. Elasticity, **49**, 31–63, 1997.

19. N. TRIANTAFYLLIDIS and R. C. ABEYARATNE, *Instability of a finitely deformed fiber-reinforced elastic material*, J. Appl. Mech., **50**, 149–156, 1983.

20. R. C. ABEYARATNE, *Discontinuous deformation gradients in plane finite elastostatics of incompressible materials*, J. Elasticity, **10**, 255–293, 1980.

21. A. J. M. SPENCER, *Deformations of fibre-reinforced materials*, Oxford University Press, 1972.

22. A. E. H. LOVE, *A treatise on the mathematical theory of elasticity*, 4th Edition, Dover Publications, New York 1944.

23. R. W. OGDEN, *Non-linear elastic deformations*, Ellis Horwood, Chichester 1984.

Received July 23, 2002.

Arch. Mech., **54**, 5-6, pp. 553–575, Warszawa 2002

Wave solution for an impulsively loaded rigid-plastic circular membrane

M. MIHAILESCU-SULICIU [1], T. WIERZBICKI [2]

[1] *Institute of Mathematics,*
Romanian Academy of Sciences

[2] *Massachusetts Institute of Technology*
Cambridge, Massachusetts

Dedicated to Professor Piotr Perzyna
on the occasion of his 70^{th} birthday

TRANSIENT RESPONSE of a clamped rigid-perfectly plastic circular membrane subjected to central impulse loading is formulated as a wave propagation problem. A closed-form solution for transverse deflections is derived by neglecting the radial motion as well as the circumferential stress in the constitutive law but retaining finite deflections and slopes. The final shape of the membrane is obtained in terms of the magnitude of the applied impulse and the radius of the centrally loaded area.

Notations

ρ_0, ρ	=	initial and actual mass density per unit initial and current area of the membrane
R, r	=	initial and current radius
w	=	transverse displacement
t	=	time
p	=	pressure load per unit current area
σ_r, σ_θ	=	Cauchy stress components
σ_0	=	uniaxial yield stress
$\varepsilon_1, \varepsilon_2$	=	strain measures
σ_1, σ_2	=	stress measures conjugated to $\varepsilon_1, \varepsilon_2$
R_1	=	radius of central loaded area
R_0	=	radius of the plate
I_0	=	impulse per unit area
I	=	total impulse imparted to the plate
ξ	=	$\dfrac{R}{R_0}$, dimensionless radial coordinates
ξ_0	=	$\dfrac{R_1}{R_0}$, dimensionless central radius
τ	=	$\dfrac{c_0 t}{R_0}$, dimensionless time

$c_0 = \sqrt{\frac{\sigma_o}{\rho_0}}$, plastic transverse wave velocity

$\omega = \frac{w}{R_0}$, dimensionless plate deflection

$h =$ plate thickness

$s = \frac{\sigma_1}{\sigma_o}$, dimensionless stress

$v = \frac{\partial \omega}{\partial \tau}$

$u = \frac{\partial \omega}{\partial \xi}$

$V = \frac{I_0}{c_0 \rho_0 h}$, dimensionless impulse.

1. Introduction

Several decades of research on dynamic inelastic response of structures brought an important understanding of many factors that govern the deformation and failure of beams, plates, and shells. Perhaps the most comprehensive review of the methods and solutions pertaining to this subject was compiled by JONES [1]. Circular plates have been regarded as the prototype of a thin-walled structure on which various modeling concepts could be conveniently studied. Early work on plates was concerned with determining the transient and permanent deflection profile and relating it to material properties and temporal and spatial variation of the external dynamic loading applied in the form of a projectile impact, pressure loading or an ideal impulse [2, 3, 4, 5]. For a comprehensive review of the relevant literature, the reader is referred to the survey paper by JONES [6].

In a special level of complexity, failure of plates has become an important topic of research. It was shown through extensive testing that plates may fail either through necking followed by fracture (as in sheet metal forming) or through out-of-plane shear. JONES [7, 8] was first to offer a theoretical description of these phenomena, while NURICK and his co-workers contributed significantly to this problem through small-scale testing [9, 10, 11].

One of the present authors (T. W.) has been actively involved in the development of solution methods for dynamically loaded inelastic plates over more than 30 years. Early efforts were restricted to small deflection bending theory of viscoplastic plates subjected to a uniformly distributed impulsive loading (FLORENCE, WIERZBICKI [12]) and projectile impact (KELLY, WIERZBICKI [13]). These results have been extended to the range of moderately large deflection by WIERZBICKI and KELLY [14] and SYMONDS and WIERZBICKI [15], where the theoretical solution was correlated with tests. In a much more recent development, the momentum conservation approach was used to derive an approximate

solution for large transient deformations of plates subjected to central explosive loading, WIERZBICKI and NURICK [16], and to mass impact, WIERZBICKI and HOO FATT [17]. It was shown by SYMONDS and WIERZBICKI [15] that large dynamic deformations of rigid-plastic plates subjected to an axisymmetric impulsive loading are governed by the homogeneous wave equation in the polar coordinate system. By contrast to the elastic formation, the initial-boundary value problem is subjected to an unloading condition that brings to the problem an interesting nonlinearity.

In previous attempts to treat this problem, analytically approximate solutions were derived. The mode solution with error minimization was developed in Ref. [15]. The method of eigenvalue expansion developed originally by WIERZBICKI [18] was applied in Ref. [16] while the momentum conservation approach was proposed in Ref. [17].

The objective of the present paper is to derive an exact solution of the problem using the method of characteristics. This method was very popular in the literature before the final element method came onto the scene in the seventies. Many important practical problems for inelastic solids and structures were solved using this method. A good source of information on this technique can be found in a classical book by CRISTESCU [19].

On the practical side, the present solution gives a distribution of maximum radial strains along the plate radius and the permanent deflection profile of the plate. Based on these results, predictions can be made on the onset of fracture as a function of the magnitude of the applied impulse and the radius of the centrally loaded area.

The authors believe that the subject of the paper nicely fits into this special anniversary volume of the Archives of Mechanics. The first author spent four months as a doctoral fellow back in the 60s in the Laboratory of Viscoplasticity directed by Professor Perzyna. The second author was the Ph.D. student of Professor Perzyna and worked closely with him during the period 1961 through 1981. By submitting this manuscript to the Archives of Mechanics, we would like to pay tribute to our wonderful teacher, mentor, and professional colleague. The present paper makes indeed a connection between the present time and Piotr's early work on the application of the newly developed by him theory of viscoplasticity. Back in 1963, after returning from his extended stay at Brown University, Piotr published two groundbreaking papers. The first of the series presented a unified, phenomenological theory of viscoplasticity (The constitutive equations for rate sensitive plastic materials, *Quarterly Applied Mathematics*, Vol. 20, pp. 321-332, 1963). The second dealt with propagation of spherical and cylindrical waves in the viscoplastic medium (On the propagation of stress waves in a rate sensitive plastic medium, *ZAMP,* Vol. 14, pp. 241-261, 1963). Our exposure to this subject, a mathematical rigor that has characterized all Piotr's

work ever since and relation to the world of physics, made a long-lasting effect on our professional careers in these formative years. We take this opportunity to wish Piotr many happy and productive years and continuing success in his new world of fracture.

2. Formulation of the problem

The problem of the transverse motion of a rigid-perfectly plastic finite circular membrane is formulated and solved in this paper. We extend here the wave solution obtained in [20] for the transverse motion of a rigid-perfectly plastic string on a plastic foundation to the case of a circular membrane.

The circular membrane of a finite radius R_o is considered initially at rest on a plane and at $t = 0+$ an impulsive transverse load is applied over a central circular zone of radius R_1, Fig. 1.

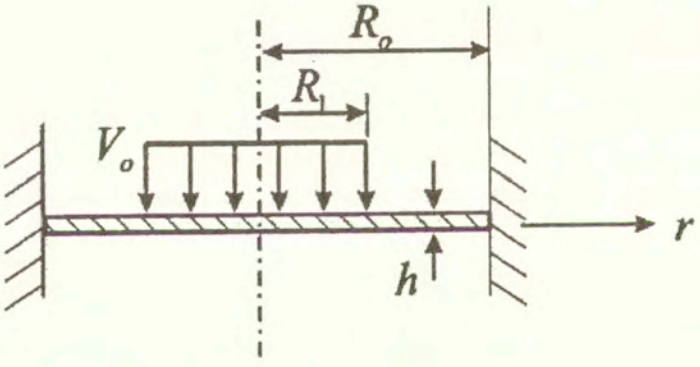

FIG. 1. Plate geometry and loading configuration.

In order to obtain a closed-form solution, it is assumed that the radial displacements are neglected. Also the circumferential stress is disregarded in the constitutive law. In order to simplify the problem, a *material* description with appropriate measures of stresses and strains is used in this work. A similar set of assumptions were also made in [17] to obtain a closed-form solution of a circular membrane impacted by a rigid projectile. In the present work, following a similar technique as in [20], the impulsive loading problem is transformed into a simpler but discontinuous initial-value problem. The piecewise smooth solution (i.e., the vertical displacement of the membrane) can then be constructed by using a complete analysis of the first and second order waves. The resulting permanent deflections depend on magnitude and spatial distribution of the applied impulse.

The stress profile is not always unique but this loss of uniqueness in stresses does not affect the strain, velocity, and displacement distribution in the membrane, which are unique. As an example, deflection and normalized deflection profiles are determined for several values of the radius of a centrally loaded area.

We consider a plane circular membrane clamped at the edge and subjected to the impact of a uniform transversal pressure p suddenly applied over a central part of the plate of radius $R_1 < R_o$. The pressure is held constant during a time interval $t_o > 0$ and then is suddenly removed. The problem is axi-symmetric and therefore the actual position of each particle of the membrane is completely described by its actual radius r and actual transversal displacement w,both r and w being functions of the initial radius R and the time t. We are interested in impulsive loading so we assume that for each fixed time interval t_o, the uniform applied pressure $p(t_o)$ is such that the product $t_o\, p(t_o)$ remains constant when t_o decreases, i.e., we have

$$\lim_{t_o \to 0} t_o p(t_o) = I_o = \text{const}, \qquad I_o = \rho_o V_o. \tag{2.1}$$

In the limiting case $t_o = 0$, the pressure loading problem is converted to the impulsive loading problem, i.e., an initial-boundary problem with a discontinuous initial velocity (see for instance [20] and also [21]).

The balance of momentum and the balance of mass in Lagrangean descriptions (according to MUNDAY and NEWITT [21], see also [19]) give rise to the following equations:

$$\rho_0 R \frac{\partial^2 r}{\partial t^2} = -\sigma_\theta \frac{ds}{dR} + \frac{\partial}{\partial R}\left(r\,\sigma_r \frac{dR}{ds}\frac{\partial r}{\partial R}\right),$$

$$\rho_0 R \frac{\partial^2 w}{\partial t^2} = \frac{\partial}{\partial R}\left(r\,\sigma_r \frac{dR}{ds}\frac{\partial w}{\partial R}\right), \tag{2.2}$$

$$\rho_r \frac{ds}{dR} = \rho_0 R,$$

where $r = r(R,t)$, $w = (R,t)$ represent the equation of the actual meridian curve of the membrane and

$$\mathrm{ds} = \left\{ \left(\frac{\partial r}{\partial R}\right)^2 + \left(\frac{\partial w}{\partial R}\right)^2 \right\}^{1/2} dR. \tag{2.3}$$

is the element of arc length of this curve; ρ_o and ρ are the initial and actual mass density per unit area, while σ_r and σ_θ are the actual meridian and circumferential (Cauchy) stress components respectively (on unit actual area). We use the

following strain measures:

$$2\varepsilon_1 = \left(\frac{\partial r}{\partial R}\right)^2 + \left(\frac{\partial w}{\partial R}\right)^2 - 1,$$

$$2\varepsilon_2 = \frac{r^2}{R^2} - 1, \tag{2.4}$$

with the corresponding conjugated stress measures with respect to the mechanical power

$$\sigma_1 = \sigma_r \frac{r}{R}\left\{\left(\frac{\partial r}{\partial R}\right)^2 + \left(\frac{\partial w}{\partial R}\right)^2\right\}^{-1/2},$$

$$\sigma_2 = \sigma_\theta \frac{R}{r}\left\{\left(\frac{\partial r}{\partial R}\right)^2 + \left(\frac{\partial w}{\partial R}\right)^2\right\}^{1/2}. \tag{2.5}$$

Equation $((5.3)_2)$ then becomes

$$\rho_o R\frac{\partial^2 r}{\partial t^2} = \frac{\partial}{\partial R}\left(\sigma_1 R\frac{\partial r}{\partial R}\right) - \frac{r}{R}\sigma_2 .$$

$$\rho_o R\frac{\partial^2 w}{\partial t^2} = \frac{\partial}{\partial R}\left(\sigma_1 R\frac{\partial w}{\partial R}\right). \tag{2.6}$$

$$\rho\{(1+2\varepsilon_1)(1+2\varepsilon_2)\}^{1/2} = \rho_o .$$

The initial and boundary conditions are

$$(r,w)(R,0) = (R,0), \quad R \in (0,R_0),$$

$$\frac{\partial r}{\partial t}(R,0) = 0, \quad R \in (0,R_0),$$

$$\frac{\partial w}{\partial t}(R,0) = \begin{cases} -\dfrac{I_0}{\rho_0 h}, & R \in (0,R_1), \\ 0, & R \in (R_1,R_0), \end{cases} \tag{2.7}$$

$$w(R_0,t) = 0, t > 0.$$

The membrane is assumed to be rigid-perfectly plastic, with a uniaxial flow stress σ_o.

In order to get a closed-form solution of the above problem, two additional hypotheses are introduced: (i) there is no radial displacement, i.e., $r(R,t) \equiv R$

for $R \in (0, R_o)$ and $t > 0$; and, (ii) σ_2 is sufficiently small to be neglected in the constitutive relation. Both of these additional assumptions are very restrictive; the first one may be proper for clamped boundary conditions, while the second one is not adequate near the center of the membrane where by symmetry the circumferential stress is in fact equal to the meridian stress. Consequently, as it will be seen in the following, the solution of this simplified problem differs (at least in the neighborhood of the center of the membrane) from the experimentally observed one.

Under the assumptions (i) and (ii) the initial boundary value problem is simplified as follows:

$$\rho_o R \frac{\partial^2 w}{\partial t^2} = \frac{\partial}{\partial R}\left(\sigma_1 R \frac{\partial w}{\partial R}\right),$$

$$2\varepsilon_1 = \left(\frac{\partial w}{\partial R}\right)^2,$$

$$\frac{\partial \varepsilon_1}{\partial t} = \begin{cases} 0 \text{ for } \sigma_1 \in (0, \sigma_o) \text{ or } \sigma_1 = \sigma_o, \ \dfrac{\partial \sigma_1}{\partial t} < 0, \\ > 0 \text{ for } \sigma_1 = \sigma_o, \ \dfrac{\partial \sigma_1}{\partial t} = 0, \end{cases}$$

(2.8)
$$w(R, 0) = 0, R \in (0, R_o)$$

$$\frac{\partial w}{\partial t}(R, 0) = \begin{cases} -\dfrac{I_o}{\rho_o h}, & R \in (0, R_1) \\ 0, & R \in (R_1, R_o) \end{cases}$$

$$w(R_o, t) = 0, t > 0$$

where $\sigma_o = \text{const}$ is the uniaxial yield stress.

With the following notations:

$$\xi = \frac{R}{R_0}, \quad \xi_0 = \frac{R_1}{R_0}, \quad \tau = \frac{c_o t}{R_0}, \quad c_o = \left[\frac{\sigma_o}{\rho_o}\right]^{1/2}$$

(2.9)
$$\omega = \frac{w}{R_0}, \quad s = \frac{\sigma_1}{\sigma_o}, \quad V = \frac{I_o}{c_o \rho_o h}$$

$$u = \frac{\partial \omega}{\partial \xi}, \quad v = \frac{\partial \omega}{\partial \tau}.$$

a dimensionless form of problem (2.8) transformed to a system of first order PDE's is

$$\xi \frac{\partial v}{\partial \tau} = \frac{\partial}{\partial \xi}(\xi s u), \frac{\partial u}{\partial \tau} = \frac{\partial v}{\partial \xi}$$

$$\omega(\xi, 0) = 0, \xi \in (0,1)$$

(2.10)

$$v(\xi, 0) = \begin{cases} -V, \xi \in (0, \xi_o) \\ 0, \ \xi \in (\xi_o, 1), \end{cases}$$

$$\omega(1, \tau) = 0, \tau > 0.$$

The natural boundary condition at the plate center requires vanishing of the total shear force, i.e., $\lim_{\xi \to 0} 2\pi \xi s u = 0$. This is satisfied as long as the product su remains finite as $\xi \to 0$. It can be shown by inspection that the present solution does satisfy the above boundary condition.

3. Solution of the problem

The initial discontinuity in velocity generates a discontinuous solution and therefore, in order to construct this solution, a complete analysis of all possible shock waves, rarefaction waves, and acceleration (second order) waves is necessary. This has been done in the earlier publication dealing with the impulsively-loaded string (see [20]). The main difference with the present problem being that rarefaction waves are possible in the membrane, at $\xi = 0$.

The discontinuity in the initial condition$(10)_4$ gives rise at $(\xi_o, 0)$ to two shock waves S_1 and S_2 with constant propagation speeds $d\xi/d\tau = 1$ and $d\xi/d\tau = -1$ respectively (see Fig. 2).

No initial conditions for the stress have been prescribed but the initial values of s are of no consequence on the behavior of u and v for $\tau > 0$ and therefore they need not to be given in the mathematical problem (2.10). Indeed, a horizontal shock wave at $\tau = 0$ (which leaves u and v unchanged) will force s to jump at $(\xi_o, 0)$ from its initial values to the value $s = 1$ in order to make possible the propagation of S_1 and S_2. Furthermore, the only possible acceleration wave at $(\xi_o, 0)$ is a vertical one (note that acceleration waves superposed on shock waves are not taken into consideration). Thus, the shock wave jump relations give the limit values, at $(\xi_o, 0)$, of u and v beyond the two shocks, i.e.

$$u = \frac{V}{2}, \quad v = -\frac{V}{2}$$

while the jump conditions for the first derivatives of u, v, and s give the limit values at $(\xi_o, 0)$ of $\frac{\partial u}{\partial \tau}$ and $\frac{\partial s}{\partial \tau}$ beyond the two shocks, namely $\frac{\partial u}{\partial \tau} = \frac{\partial s}{\partial \tau} = 0$.

Therefore, there is no way to decide whether beyond the shocks there is a rigid region (i.e., with $\frac{\partial \varepsilon}{\partial \tau} \equiv 0$) or a plastic region (i.e., with $\frac{\partial \varepsilon}{\partial \tau} > 0$).

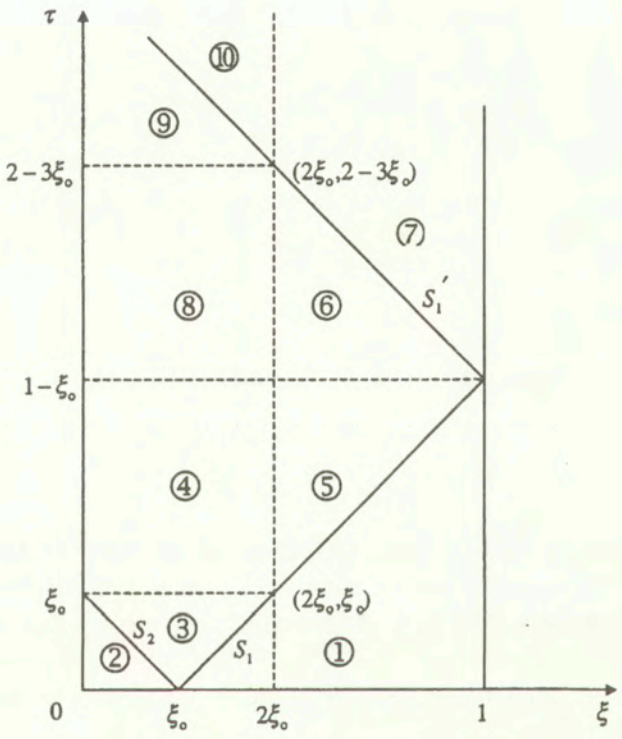

FIG. 2. A phase plane diagram showing converging (S_2) and diverging (S_1) wave initiated from ξ_o and the reflected wave (S_1').

Now, according to $(2.10)_{1-2}$ and the initial and boundary conditions, in the whole region ahead of S_1 the solution is $u \equiv v \equiv 0$, while in the whole region ahead of S_2 the solution is $u \equiv 0, v \equiv -V$. On the other hand, if a plastic region extends beyond the shocks, i.e., $s = 1$, $\frac{\partial \varepsilon}{\partial \tau} > 0$, a simple analysis of the solution in this case shows that the limit values of the strain ε on S_2 (beyond the shock) are rapidly increasing in time to infinity (at $\xi = 0$) while v is rapidly decreasing to $-\infty$. The conclusion is then that beyond the shocks S_1 and S_2 there has to be a rigid region with $\frac{\partial \varepsilon}{\partial \tau} = 0$ which implies $u(\xi, \tau) = u(\xi)$ and $v(\xi, \tau) = v(\tau)$ in that region.

From now on the technique employed to calculate u, v,and s in a rigid region is quite simple: equation $(2.10)_1$ is integrated with respect to ξ between the

boundaries of the region (where $s = 1$) to get an ordinary differential equation for $v(\tau)$. Consequently $u(\xi, \tau) = u(\xi)$ can be calculated from its values on the boundary of the rigid region. In order to illustrate this technique we perform the explicit calculations for the first case.

We denote by "1" the region ahead of S_1, by "2" the region ahead of S_2, and by "3" the region beyond the two shocks. The solution in the first two regions can be readily obtained:

Region "1"

$$u(\xi,\tau) = v(\xi,\tau) = 0, \quad \tau \in (0, \min(1-\xi_o, \xi_o)),$$
$$\omega(\xi,\tau) = 0, \quad \xi \in (\xi_o + \tau, 1) \tag{3.1}$$

Region "2"

$$u(\xi,\tau) = 0 \quad \tau \in (0, \min(1-\xi_o, \xi_o)),$$
$$v(\xi,\tau) = -V \quad \xi \in (0, \xi_o - \tau), \tag{3.2}$$
$$\omega(\xi,\tau) = -V\tau.$$

It is interesting to observe that there is no unique solution for $s$in these two regions, but this has no influence on the values of u and v. Furthermore, in order to calculate the solution in region "3", one only needs the values of s on S_1 and S_2 (as s does not jump across these two shocks) which are equal to 1 for any choice of the stress solution in regions "1" and "2". Now, in order to calculate $v(\xi,\tau) = v(\tau)$ in region "3", Eq. (2.10) is integrated with respect to ξ between $\xi_1 = \xi_o - \tau$ and $\xi_2 = \xi_o + \tau$ (i.e., between S_2 and S_1) to give

$$\frac{1}{2}\{(\xi_o+\tau)^2 - (\xi_o-\tau)^2\}\frac{dv(\tau)}{d\tau} \tag{3.3}$$
$$= (\xi_o+\tau)(su)(\xi_o+\tau,\tau) - (\xi_o-\tau)(su)(\xi_o-\tau,\tau)$$

where the values of u, v, and s are those of region "3". But $s(\xi_o+\tau,\tau) = s(\xi_o-\tau,\tau) = 1$, and from the jump relations across S_1 and S_2 we have

$$u_3(\xi_o+\tau,\tau) = -v_3(\xi_o+\tau,\tau),$$
$$u_3(\xi_o-\tau,\tau) = v_3(\xi_o-\tau,\tau) + V. \tag{3.4}$$

Introducing (3.4) into (3.3), the following differential equation is obtained for $v(t)$:

$$\tau\frac{dv}{d\tau} + v = V\frac{\tau-\xi_o}{2\xi_o}, \quad v(0) = -\frac{V}{2} \tag{3.5}$$

with the solution

$$v(\tau) = \frac{V(\tau - 2\xi_o)}{4\xi_o}.$$

The values of $u(\xi, \tau) = u(\xi)$ are then determined by means of (3.4) and (3.5)

$$u(\xi, \tau) = \frac{V(3\xi_o - \xi)}{4\xi_o}, \qquad \xi \in (\xi_o - \tau, \xi_o + \tau) \tag{3.6}$$

while the stress s is calculated by integrating Eq. (2.10) with respect to ξ from $\xi_1 = \xi_o - \tau$ to $\xi_2 = \xi$ (and $\xi_1 = \xi$ and $\xi_2 = \xi_o + \tau$ respectively) and using (3.5) and (3.6); one gets

$$s(\xi, \tau) = \frac{\xi^2 + 3(\xi_o^2 - \tau^2)}{2\xi(3\xi_o - \xi)}. \tag{3.7}$$

The expression of the deflection $\omega(\xi, \tau)$ in region "3" may be calculated either from u or from v since $u = \dfrac{\partial \omega}{\partial \xi}$ and $v = \dfrac{\partial \omega}{\partial \tau}$. The complete solution is then:

Region "3"

$$\begin{aligned}
u(\xi, \tau) &= \frac{V(3\xi_0 - \xi)}{4\xi_0}, \\
v(\xi, \tau) &= \frac{V(\tau - 2\xi_0)}{4\xi_0}, \\
s(\xi, \tau) &= \frac{\xi^2 + 3(\xi_0^2 - \tau^2)}{2\xi(3\xi_0 - \xi)}, \\
\omega(\xi, \tau) &= \frac{V}{4}\left\{3(\xi - \xi_0) - \tau - \frac{1}{2\xi_0}\left(\xi^2 - (\xi_0 - \tau)^2\right)\right\}.
\end{aligned} \tag{3.8}$$

At this stage one has to treat separately the cases $\xi_o < 1 - \xi_o$ (i.e., $\xi_o < \frac{1}{2}$) and $\xi_o > 1 - \xi_o$ (i.e., $\xi_o > \frac{1}{2}$) as they depend on which one of the two shocks S_1 and S_2 is the first to reach the boundary $\xi = 1$ and the center $\xi = 0$, respectively. Of interest here is the final shape of the membrane after all its points have stopped, i.e., $\omega(\xi, \tilde{\tau})$ for $\tilde{\tau}$ the smallest τ with $v(\xi, \tilde{\tau}) = 0$ for all $\xi \in (0, 1)$. Experiments show [6] that under impulsive transversal loading, the transversal velocity of the membrane $v(\xi, \tau)$ maintains a constant sign (which is negative in the present notation). Therefore transversal velocity and acceleration do vanish at the same time. In order to address the physical problem, the loading-unloading

criterion must be introduced. It is assumed that whenever the instantaneous velocity vanishes at a given point $v(\xi,\tau)=0$, it must stay so for the duration of the motion. Then a rigid region will propagate over the membrane until the velocity vanishes at all points of the membrane; at that moment $\tilde{\tau}$ calculations are stopped, even if $\dfrac{\partial v}{\partial \tau} > 0$. The resulting deflections are called permanent deflection of the membrane.

2_1 CASE $\xi_o < \dfrac{1}{2}$

The solution (3.8) for region "3" remains valid up to $\tau=\xi_o$ when S_2 reaches the center $\xi=0$ of the membrane. Then, at $(0,\xi_o)$ a rarefaction fan appears in Region "3" for the stress s, with $s(\eta)=\dfrac{1}{\eta}$, $\eta=\dfrac{\xi}{\tau-\xi_o}$, $\eta\in(-\infty,-1)$, i.e., between S_2 and $\tau=\xi_o$; this rarefaction wave will "kill" the shock wave S_2 as it makes s decrease from the value $s=1$ to the value $s=0$. Indeed, we now have a Goursat problem for $(2.10)_{1-2}$ at $(0,\xi_o)$, between $\tau=\xi_o$ (i.e., $\eta=+\infty$) and $\xi=0$ (i.e., $\eta=0$), with $(su)(\eta=0)=0$ from the boundary condition at $\xi=0$ and $(u,v,s)(\eta=+\infty)=(\dfrac{3V}{4},-\dfrac{V}{4},0)$ as the limit values calculated from (3.8); but u can no longer be equal to zero at the center $\xi=0$ since $u(\eta=+\infty)=\dfrac{3V}{4}>0$ and the constitutive law does not allow ε to decrease, so $s(\eta=0)$ has to vanish. Therefore S_2 can not be reflected at $(0,\xi_o)$ as there exists no wave mechanism which allows $s(\eta)$ to increase from $s=0$ at $\eta=+\infty$ to the value $s=1$ at $\eta=1$ (and thus to permit a reflected shock wave to propagate) and subsequently decrease from $s=1$ at $\eta=1$ to $s=0$ at $\eta=0$. The only wave that starts propagating at $(0,\xi_o)$ is a horizontal acceleration wave $\tau=\xi_o$ which has to change the sign of $\dfrac{\partial s}{\partial \tau}$ since $\dfrac{\partial s}{\partial \tau}(\xi,\xi_o)$ given by (3.8) is negative in the neighborhood of $\xi=0$ while $\xi\to 0$ $s(\xi,\xi_o)=0$. This horizontal second order wave gives rise to a vertical acceleration wave at $(2\xi_o,\xi_o)$ where it meets the shock S_1. So for $\tau\in(\xi_o,1-\xi_o)$ there are two new regions: "4" and "5" (see Fig. 1), both of them being rigid regions and, following the same technique as that employed to calculate the solution in region "3", one gets

Region "4"

$$
\begin{aligned}
u(\xi,\tau) &= \frac{V(3\xi_0-\xi)}{4\xi_0},\\
v(\xi,\tau) &= -\frac{V\xi_0^2}{(\xi_0+\tau)^2}, \qquad \xi\in(0,2\xi_0), \quad \tau\in(\xi_0,1-\xi_0),\\
s(\xi,\tau) &= \frac{4\xi_0^3\xi}{(3\xi_0-\xi)(\xi_0+\tau)^3},
\end{aligned}
\tag{3.9}
$$

(3.9) [cont.]
$$\omega(\xi,\tau)=\frac{V\xi_0^2}{\xi_0+\tau}-\frac{V}{8\xi_0}\left(3\xi_0^2+(\xi-3\xi_0)^2\right),$$

Region "5"

$$u(\xi,\tau)=\frac{V\xi_o^2}{\xi^2},$$

$$v(\xi,\tau)=-\frac{V\xi_o^2}{(\xi_o+\tau)^2} \qquad \tau\in(\xi_o,1-\xi_o) \quad \xi\in(2\xi_o,\xi_o+\tau),$$

(3.10)
$$v(\xi,\tau)=-\frac{V\xi_o^2}{(\xi_o+\tau)^2},$$

$$s(\xi,\tau)=\frac{\xi^3}{(\xi_o+\tau)^3},$$

$$\omega(\xi,\tau)=V\xi_o^2\left(\frac{1}{\xi_o+\tau}-\frac{1}{\xi}\right).$$

Now the shock wave S_1 reaches the edge of the membrane at $\tau=1-\xi_o$ and is reflected as the shock wave S_1' while a horizontal acceleration wave $\tau=1-\xi_o$ is also generated at $(1,1-\xi_o)$ in order to change the sign of $\frac{\partial s}{\partial\tau}$ and make $\frac{\partial s}{\partial\tau}$ increase again in time for $\tau>1-\xi_o$, in order to allow the propagation of S_1'. The limit value of the derivatives at $(1,-\xi_o)$ in region "7" (see Fig. 1) is

$$\frac{\partial u}{\partial\tau}=-V\xi_o^2\left(1+\frac{\partial s}{\partial\tau}\right)$$

and therefore $\frac{\partial u}{\partial\tau}=0$, $\frac{\partial s}{\partial\tau}=-1$ and region "7" is again a rigid region with $v(\xi,\tau)=v(\tau)=0$ since $v=0$ at the edge $\xi=1$. One can proceed further by calculating the solution in regions "6" and "8" and then in region "7". This gives, respectively

Region "6"

$$u(\xi,\tau) = \frac{V\,\xi_o^2}{\xi^2},$$

$$v(\xi,\tau) = V\,\xi_o^2\left\{\frac{1}{(2-\xi_o-\tau)^2} - 2\right\}$$

(3.11) $$\tau \in (1-\xi_o, 2-3\,\xi_o) \quad \tau \in (2\,\xi_o, 2-\xi_o-\tau),$$

$$s(\xi,\tau) = \frac{\xi^3}{\xi_o^2(2-\xi_o-\tau)^3},$$

$$\omega(\xi,\tau) = V\,\xi_o^2\left\{\frac{1}{2-\xi_o-\tau} - \frac{1}{\xi} + 2(1-\xi_o-\tau)\right\}.$$

Region "8"

(3.12)

$$u(\xi,\tau) = \frac{V(3\,\xi_o-\xi)}{4\,\xi_o},$$

$$v(\xi,\tau) = V\,\xi_0^2\left\{\frac{1}{(2-\xi_o-\tau)^2} - 2\right\} \quad \rho \in (0, 2\,\xi_o) \quad \tau \in (1-\xi_o, 2-3\,\xi_o),$$

$$s(\xi,\tau) = \frac{4\,\xi_o^3\,\xi}{(3\,\xi_o-\xi)(2-\xi_o-\tau)^3},$$

$$\omega(\xi,\tau) = V\,\xi_0^2\left\{\frac{1}{2-\xi_o-\tau} + 2(1-\xi_o-\tau)\right\} - \frac{V}{8\,\xi_o}\left\{3\,\xi_o^2 + (\xi-3\,\xi_o)^2\right\}.$$

Region "7"

$$u(\xi,\tau) = 2V\,\xi_o^2 \quad \tau \in (1-\xi_o, 2-3\,\xi_o) \quad \xi \in (2-\xi_o-\tau, 1),$$

(3.13) $$v(\xi,\tau) = 0 \quad \text{and} \quad \omega(\xi,\tau) = 2V\,\xi_o^2(\xi-1),$$

$$\tau \in (2-3\,\xi_o, 2-\xi_o) \quad \xi \in (2\,\xi_o, 1),$$

It can be noted that v may now vanish in regions "6" and "8" so two subcases should be considered.

2.1a For $\xi_o \in (0, \frac{1}{2\sqrt{2}})$ it is found that $v(\xi,\tilde{\tau}) = 0$ in regions "6" and "8",

with $\tilde{\tau} = 2 - \xi_o - \frac{1}{\sqrt{2}} < 2 - 3\xi_o$ and the final shape of the membrane is given by

$$\omega(\xi,\tilde{\tau}) = \begin{cases} 2(\sqrt{2}-1)V\xi_o^2 - \frac{V}{8\xi_o}(3\xi_o^2 + (\xi - 3\xi_o)^2), \xi \in (0, 2\xi_o) \\ V\xi_o^2\left\{2(\sqrt{2}-1) - \frac{1}{\xi}\right\}, \xi \in (2\xi_o, \frac{1}{\sqrt{2}}) \\ 2V\xi_o^2(\xi - 1), \xi \in (\frac{1}{\sqrt{2}}, 1) \end{cases} \tag{3.14}$$

2.1b For $\xi_o \in (\frac{1}{2\sqrt{2}}, \frac{1}{2})$, v remains negative in regions "6" and "8" up to $\tau = 2 - 3\xi_o$ so one has to calculate the solution in regions "9" and "10"

Region "9"

$$u(\xi,\tau) = \frac{V(3\xi_o - \xi)}{4\xi_o},$$

$$v(\xi,\tau) = \frac{V}{2\xi_o}\left(2 - \tau - \frac{5}{2}\xi_o - 4\xi_o^3 - 3\xi_o \ln\frac{2-\tau-\xi_o}{2\xi_o}\right),$$

$$\omega(\xi,\tau) = -\frac{V}{8\xi_o}(\xi - 3\xi_o)^2$$

$$+\frac{V}{2\xi_o}\left(-3\xi_o(\tau - 2 + \xi_o)\ln\frac{2-\xi_o-\tau}{2\xi_o} - \frac{\tau^2}{2} - \tau(4\xi_o^3 - \frac{\xi_o}{2} - 2)\right.$$

$$\left. -4\xi_o^4 + 4\xi_o^3 + \frac{25}{4}\xi_o^2 - \xi_o - 2\right), \tag{3.15}$$

$$\tau \in (2 - 3\xi_o, 2 - \xi_0), \quad \xi \in (0, 2 - \xi_o - \tau).$$

Region "10"

$$u(\xi,\tau) = \frac{V}{4\xi_o}\left\{8\xi_o^3 + 6\xi_o - 3\xi + 6\xi_o \ln\frac{\xi}{2\xi_o}\right\}$$

$$v(\xi,\tau) = 0$$

$$\omega(\xi,\tau) = \frac{V}{8\xi_o}\left\{3\xi^2 - 16\xi_o^3\right\} + 16\xi_o^3 - 12\xi_o^2 - 12\xi_o\xi\ln\frac{\xi}{2\xi_o} \tag{3.16}$$

$$\tau \in (2 - 3\xi_o, 2 - \xi_o), \quad \xi \in (2 - \xi_o - \tau, 2\xi_o)$$

The expression of v in region "9" implies that there exists a unique $\tilde{\tau} \in (2-3\xi_o,\ 2-\xi_o)$ such that $v(\xi,\tilde{\tau})=0$ in region "9" and $\tilde{\tau}$ is the solution of the algebraic equation.

$$2\mu - 3\ln\mu = \frac{3}{2} + 4\xi_o^2,\quad \mu = \frac{2-\tilde{\tau}-\xi_o}{2\xi_o} \in (0,1). \tag{3.17}$$

The motion of the membrane does therefore stop before S_1' reaches the center $\xi=0$ and the final shape of the membrane is given by $\omega(\xi,\tilde{\tau})$ calculated from $(3.16)_3$ for region "10" and $(3.15)_3$, $(3.13)_3$ for regions "9" and "7" respectively, i.e.

$$\omega(\xi,\tilde{\tau}) \tag{3.18}$$

$$= \begin{cases} -\dfrac{V}{8\xi_0}(\xi-3\xi_0)^2 \\ \qquad +\dfrac{V}{2\xi_0}\left(\dfrac{\tilde{\tau}^2}{2}+2(2\xi_0-1\tilde{\tau}-4\xi_0^3+\dfrac{35}{4}\xi^2-8\xi_0+2\right), & \xi\in(0,\dfrac{1}{\sqrt{2}}) \\ -\dfrac{V}{8\xi_0}\left(3\xi^2-16\xi_0^3\xi+16\xi_0^3-12\xi_0^2-12\xi_0\xi\ln\dfrac{\xi}{2\xi_0}\right), & \xi\in(\dfrac{1}{\sqrt{2}},2\xi_0) \\ 2V\xi_o^2(\xi-1), & \xi\in(2\xi_0,1) \end{cases}$$

2.2 Case $\xi_o = \frac{1}{2}$

In this case, for the regions "1", "2", and "3" (see Fig. 3), the solution is the same as for the case $\xi_0 < \frac{1}{2}$, i.e., it is given by (3.1), (3.2), and (3.8) respectively where $\xi_0 = \frac{1}{2}$.

Region "4"'

$$\begin{aligned} u(\xi,\tau) &= \frac{V(3-2\xi)}{4}, \qquad \tau\in(\frac{1}{2},\frac{3}{2}), \\ v(\xi,\tau) &= V\left(\frac{1}{4}-\tau-\frac{3}{2}\ln\frac{3-2\tau}{2}\right), \quad \rho\in(0,\frac{3}{2}-\tau), \\ \omega(\xi,\tau) &= \frac{V}{4}\left(-\xi^2+3\xi-2\tau^2+7\tau-5-3(2\tau-3)\ln\frac{3-2\tau}{2}\right). \end{aligned} \tag{3.19}$$

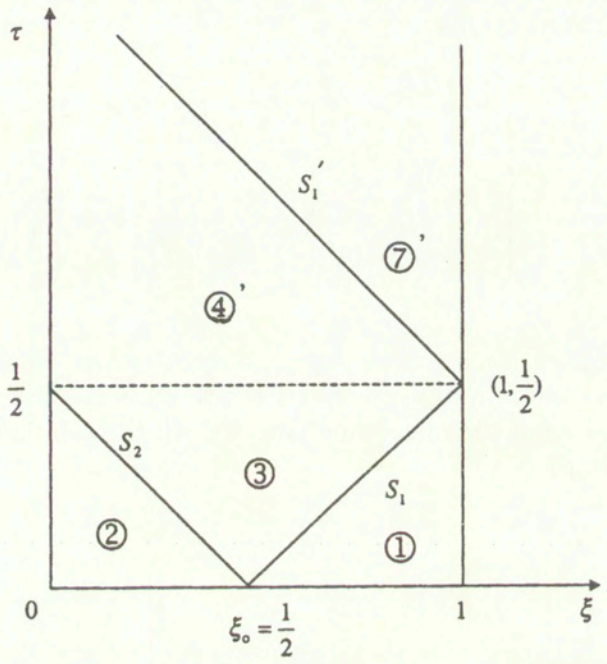

FIG. 3. A special case of the wave solution shown in Fig. 2 in which $\xi_o = 1/2$.

Region "7"'

$$u(\xi,\tau) = V\left(2 - \frac{3}{2}\xi + \frac{3}{2}\ln\xi\right),$$

$$v(\xi,\tau) = 0, \quad \tau \in (\frac{1}{2},\frac{3}{2}) \quad \xi \in (\frac{3}{2} - \tau, 1), \tag{3.20}$$

$$\omega(\xi,\tau) = \frac{V}{4}\left(-3\xi^2 + 2\xi + 1 + 6\xi\ln\xi\right).$$

There exists a unique value $\tilde{\tau} \in (\frac{1}{2},\frac{3}{2})$, i.e. before the shock wave S_1' reaches the center $\xi = 0$, such that $v(\xi,\tilde{\tau})$ in Region "4", namely $\tilde{\tau}$, is the solution of the algebraic equation

$$\frac{3}{2}\ln\frac{3-2\tilde{\tau}}{2} + \tilde{\tau} = \frac{1}{4}. \tag{3.21}$$

The membrane stops moving at $\tau = \tilde{\tau}$ and its final shape is given by $(3.19)_3$ and $(3.20)_3$, that is

$$\omega(\xi,\tilde{\tau}) = \begin{cases} \dfrac{V}{4}\left(-\xi^2+3\xi-2\tilde{\tau}^2+7\tilde{\tau}-5-3(2\tilde{\tau}-3)\ln\dfrac{3-2\tilde{\tau}}{2}\right), \\ \qquad\qquad\qquad\qquad \xi\in\left(0,\dfrac{3}{2}-\tilde{\tau}\right), \\ \dfrac{V}{4}\left(-3\xi^2+2\xi+1+6\xi\ln\xi\right), \quad \xi\in\left(\dfrac{3}{2}-\tilde{\tau}1\right). \end{cases} \tag{3.22}$$

2.3 CASE $\xi_o = 1$

There is only one initially generated shock wave in this case, namely S_2, starting at the edge of the membrane (see Fig. 4); the solution in region "2" is given by (3.2) and

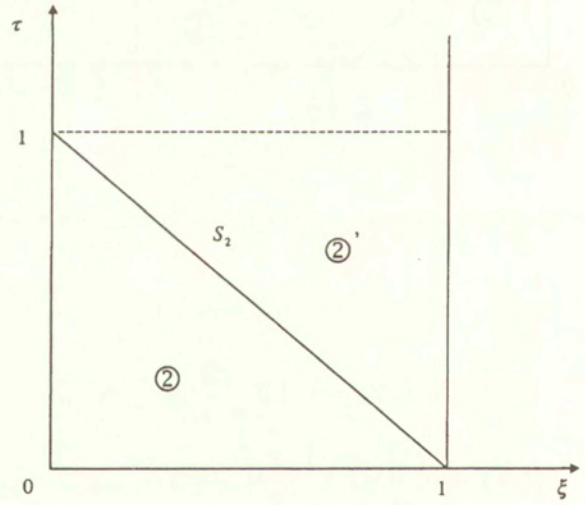

FIG. 4. Degenerated wave picture on the phase plane in the case of $\xi_o = 1$ showing one converging wave.

Region "2"

$$\begin{aligned} &u(\xi,\tau) = V, \\ &v(\xi,\tau) = 0, \qquad\qquad \tau\in(0,1), \\ &s(\xi,\tau) = \frac{1-\tau}{\xi}, \qquad \xi\in(1-\tau,1), \\ &\omega(\xi,\tau) = V(\xi-1). \end{aligned} \tag{3.23}$$

The motion stops at $\tilde{\tau} = 1$ and the final shape of the membrane is therefore given by

$$\omega(\xi, 1) = V(\xi - 1), \quad \xi \in (0, 1), \tag{3.24}$$

4. Discussion

Despite its apparent formal character, the present solution brings a wealth of interesting information about transient response of thin plates. According to the present wave approach, the deflected shape of the plate depends strongly on the value of the dimensional radius of loading $\xi_o = R_0/R$. There are three regions of ξ_o and in each of them a different set of equations describes the deflected shape. In the region $\xi_o \in \left(0, 1/2\sqrt{2}\right)$, Eq. (3.14) applies. Then the region $\xi_o \in \left(1/2\sqrt{2}, 1/2\right)$ is governed by Eq. (3.16). Finally, the solution for $\xi_0 = 1$ is given by Eq. (3.24). A comparison of deflected shapes for five different values of the parameter ξ_o is shown in Fig. 5. It is seen that the smaller the dimensional radius of impulsive

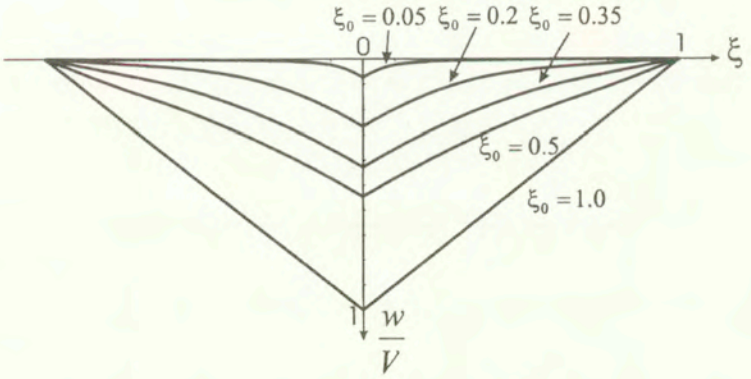

FIG. 5. Dimensionless deflection profiles of the membrane for different values of the radius of the impulsive loading.

loading ξ_o is, the more localized deformations are around the plate center. It is interesting to plot the dimensionless maximum central amplitude and $(w/V)_{\max}$ versus the value of the parameter ξ_o(Fig. 6).

It is seen that the above relationship is almost linear except for the initial slightly curved portion. As mentioned earlier, the nonlinearity of the problem comes not from the wave solution but rather from the unloading condition. For the rigid-perfectly plastic material, unloading occurs whenever a velocity of the given particle of the beam becomes zero. The equation of the unloading wave is given by Eq. (3.17) which is a nonlinear algebraic equation. However, when the

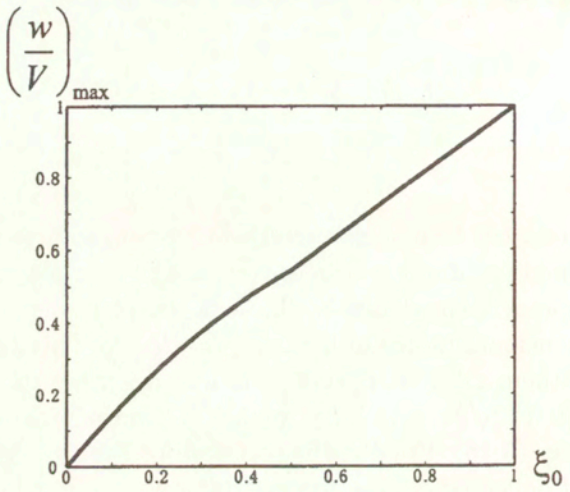

FIG. 6. A plot of the dimensionless maximum central deflection of the plate as a function of the radius of the impassive loading.

unloading time $\bar{\tau}$ is plotted against the parameter ξ_o, the unloading boundary is seen to be composed of two portions of almost straight lines as shown in Fig. 7.

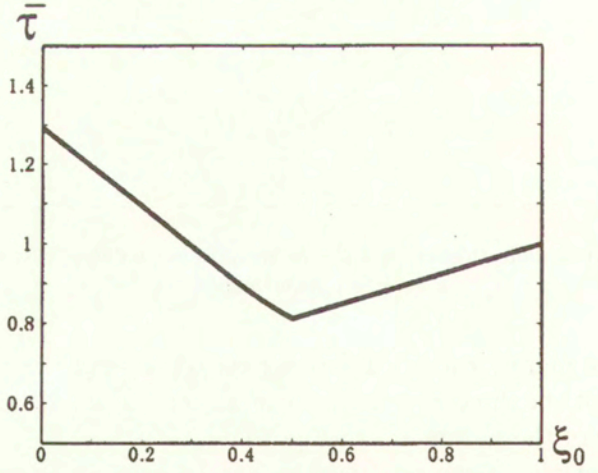

FIG. 7. The dependence of the so-called "time-to-rest" on the radius of the impulsive loading.

So far considered was the case when the amplitude of the initial velocity V was independent of the radius of the impulsive loading. It is interesting to

rearrange the solution and assume that the total impulse imparted to the plate, defined by

$$V_{\text{total}} = \pi \xi^2 V \tag{4.1}$$

is held constant. Under this condition, the dimensionless maximum central amplitude is no longer an increasing function as it was in the case shown in Fig. 6 but is a decreasing function of the parameter ξ_o (see Fig. 8).

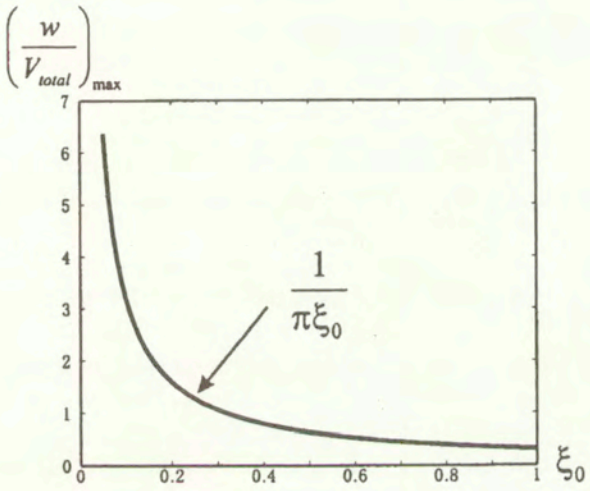

FIG. 8. The dependence of dimensionless maximum central deflection on the parameter ξ_o for a constant value of the total applied impulse V_{total} .

Finally, it should be noted that the maximum slope of the deflected shape is always constant in the range $\xi_o \in (0, 1/2)$ and is equal to $\omega' = 3V/4$. Then in the range $\xi_o \in (1/2, 1)$ the slope will increase and assume a maximum value at $\xi_o = 1$. In the theory of thin membranes the radial strain is defined by $\varepsilon = 1/2\,(w')^2$. With this definition and using the calculated slope, it is possible to make an estimation on the maximum strain developed in the membrane as a result of the impulsive loading. The membrane will fracture when the strain reaches a critical value ε_f, that is when

$$V_{\text{cric}} = \sqrt{\frac{32}{9}\varepsilon_f} \tag{4.2}$$

where V_{cric} denotes critical velocity to fracture.

In conclusion, it must be stated that the present analysis provides the first closed form solution of the problem of impulsively loaded thin plates loaded by

an explosive material distributed around the center part of the plate. TEELING-SMITH and NURICK [11] performed a series of tests of impulsively loaded thin plates and determined experimentally the deflected shapes. A comparison of the present theory with those tests will be done in a future publication.

Acknowledgement

The authors would like to thank Dr. I. Suliciu for the helpful discussions during this research work and Mr. X. Teng for his assistance in making all graphs of the deformed shape.

References

1. N. JONES, *Structural Impact*, Cambridge University Press, 1989.
2. H. G. HOPKINS and W. PRAGER, *The load carrying capacity of circular plates*, J. Mech. Phys. Solids, **2**, pp. 1–13, 1953.
3. P. S. SYMONDS, *Survey of methods of analysis for plastic deformation of structures under dynamic loading*, Brown University Report BU/NSRDC/1–67, 1967. W. Johnson, Impact Strength of Materials. E. Arnold, London and Crane Russak, New York, 1972.
4. N. JONES *Recent progress in the dynamic plastic behavior of structures, Shock and Vibration Digest*; Part 1, **10** (2.9), 21–33, 1978; Part 2, **10** (2.10), 13–19, 1978; Part 3, 13 (2.10), 3-16, 1981); Part 4, **17** ($(5.3)_2$), 35–47, 1985.
5. A. L. FLORENCE, *Circular Plate under a uniformly distributed impulse*, Int. J. Solids and Structures, **2**, 37–47, 1996.
6. N. JONES, *Recent studies on the dynamic plastic behavior of structures*, Applied Mechanics Review, Vol. 42, No. 4, April 1989, ASME Book No. AMR053.
7. N. JONES, *Plastic failure of ductile beams loaded dynamically*, Trans. ASME, J. Engng. for Industry, **98B** (1), 131–136, 1976.
8. N. JONES and C. JONES, *Inelastic failure of fully clamped beams and circular plates under impact loading*, Proc. Instn. Mech. Engrs, Vol. 216, Part C, *J. Mech. Engng. Sciences*, 133–149, 2002.
9. G. N. NURICK, and J. B. MARTIN, *Deformation of thin plates subjected to impulsive loading – a review, Part I: theoretical considerations* International Journal of Impact Engineering, Vol. 8, No. 2, 159–170, 1989.
10. G. N. NURICK, and J. B. MARTIN, *Deformation of thin plates subjected to impulsive loading – a review, Part II: experimental studies*, International Journal of Impact Engineering, Vol. 8, No. 2, 171–186, 1989.
11. R. G. TEELING-SMITH, and G. N. NURICK, *The deformation and tearing of circular plates subjected to impulsive loads*, International Journal of Impact Engineering, Vol. 11, No. 1, 77–92, 1991.
12. T. WIERZBICKI and A. L. FLORENCE, *A theoretical and experimental investigation of impulsively loaded clamped circular viscoplastic plates*, International Journal of Solids and Structures, Vol. 6, No. 5, 553–568, 1970.

13. J. K. KELLY and T. WIERZBICKI, *Motion of a circular viscoplastic plate subject to projectile impact*, *ZAMP*, Vol. 18, No. 2, 236–246, 1967.

14. T. WIERZBICKI and J. M. KELLY, *Finite deflection of a circular viscoplastic plate subject to projectile impact*, International Journal of Solids and Structures, Vol. 4, No. 11, 1081–1092, 1968.

15. P. S. SYMONDS and T. WIERZBICKI, *Membrane mode solutions for impulsively loaded circular plates*, Journal of Applied Mechanics, Vol. 46, No. 1, 1979.

16. T. WIERZBICKI and G. N. NURICK, *Large deformation of thin plates under localized impulsive loading*, International Journal of Impact Engineering, Vol. 18, No. 7–8, 899–918, 1996.

17. T. WIERZBICKI and M. S. HOO FATT, *Deformation and perforation of a circular membrane due to rigid projectile impact*, in *PVP*, Vol. 225, Dynamic Response of Structures to High-Energy Excitation, [Eds.] T. L. GEERS and Y. S. SHIN, ASME Book No. H00717, 1991.

18. T. WIERZBICKI, *Application of an eigenfunction expansion method in plasticity*, Journal of Applied Mechanics, Vol. 41, No. 2, 448–452, 1974.

19. N. CRISTESCU, *Dynamic Plasticity*, North-Holland, 1967.

20. M. MIHAILECU-SULICIU, I. SULICIU, T. WIERZBICKI, and M. S. HOO FATT, *Transient response of an impulsively loaded plastic string on a plastic foundation*, Quarterly of Applied Mathematics, Vol. LIV, No. 2, 327–343, 1996.

21. G. MUNDAY and D. M. NEWITT, *The deformation of transversely loaded disks under dynamic loads*, Phil. Trans. Roy. Soc., London, A, 1–30, 1963.

Received July 24, 2002; revised version November 14, 2002.

Arch. Mech., **54**, 5-6, pp. 577–602, Warszawa 2002

Plastic wave propagation in Hopkinson bar - revisited

M. MIĆUNOVIĆ[1] and A. BALTOV[2]

[1] *Faculty of Mechanical Engineering, University of Kragujevac, Sestre Janjica 6a, 34000 Kragujevac, Yugoslavia*
e-mail: mmicun@EUnet.yu

[2] *Institute of Mechanics, Bulgarian Academy of Sciences bl. 4, Acad. G. Bontchev str., 1113 Sofia, Bulgaria*
e-mail: baltov@imbm.bas.bg

Dedicated to Professor Piotr Perzyna on the occasion of his 70^{th} birthday

THE SUBJECT OF this paper is an analysis of the experimental Hopkinson bar technique when such a device consists of a short tensile or shearing specimen surrounded by two very long elastic bars [1]. Unlike the commonly applied by-pass analysis which attempts to draw conclusions from the behaviour of elastic bars, we attempt to take into account real plastic waves inside the specimen with several hundreds of reflections. A quasi rate-independent as well as a more general, rate-dependent tensor function model for AISI 316H calibrated in [19] are applied. Some special slightly perturbed elastic incident and reflected waves in elastic bars served to simulate the starting solutions. The numerical results have shown a good agreement with experimentally observed homogeneous strain state throughout the specimen during the process. Lindholm's procedure for finding specimen stress and strain by such a by-pass procedure is criticized.

1. Introduction

THE GOAL of this paper is to revisit the standard techniques for analysis of the Hopkinson bar testing technique, taking into account plastic wave propagation inside the standard (extremely short) tension specimen, as well as elastic waves propagating along the very long incident-reflected wave bar and the transmitted wave bar. The strains inside the specimen are large and reach up to 60%. The evolution equation for plastic stretching tensor was calibrated in [19] on the basis of the experiments performed in dynamic testing laboratory of the JRC-Ispra, Italy [1, 2, 3], with classical tension specimen as well as "bichierrino" shear specimen (consisting of two rigid cylinders connected by the gauge part - a thin circular crown explained in detail in [4]) made of austenitic stainless steel AISI 316H, in the range of strain rates $[10^{-3}, 10^{3}]s^{-1}$.

2. Preliminaries

Before proceeding, clear stress and strain measures are necessary. It is commonly accepted that in addition to the undeformed configuration $\mathcal{B}_0$ and the instant deformed configuration $\mathcal{B}$, an intermediate local reference configuration $\mathcal{B}_N$ is introduced. Then Kroener's decomposition rule holds [9]

$$\mathbf{F} = \mathbf{F}_E \mathbf{F}_P \tag{2.1}$$

where $\mathbf{F}$ – the deformation gradient tensor, $\mathbf{F}_E$ – the elastic distortion tensor, and $\mathbf{F}_P$ – the plastic distortion tensor, mapping respectively $\mathcal{B}_0 \to \mathcal{B}$, $\mathcal{B}_N \to \mathcal{B}$ and $\mathcal{B}_0 \to \mathcal{B}_N$. The name "distortion" is used to underline the fact that $\mathbf{F}_E$ and $\mathbf{F}_P$ are incompatible, i.e. compatibility conditions applied to a metric tensor of $\mathcal{B}_N$ are not satisfied (cf. e.g. [13]). Let us apply polar decomposition on plastic distortion i.e. $\mathbf{F}_P = \mathbf{R}_P \mathbf{U}_P = \mathbf{V}_P \mathbf{R}_P$, where $\mathbf{R}_P$ is the plastic rotation tensor $\mathbf{U}_P$ and $\mathbf{V}_P$ are the right and the left plastic stretch tensors. In the subsequent sections it will be especially convenient to use logarithmic plastic strain by making use of the definition:

$$\mathbf{e}_P = \ln \mathbf{V}_P = \frac{1}{2} \ln \left(\mathbf{F}_P \mathbf{F}_P^T \right). \tag{2.2}$$

It is traceless when plastic volume change is negligible (which takes place whenever damage such as creep, low-cycle-fatigue, irradiation creep etc. is not taken into account). It is worth of note that this holds true for large plastic strains as well. As another strain measure, the Lagrangean elastic strain will be used

$$\mathbf{E}_E = \frac{1}{2} \left(\mathbf{F}_E^T \mathbf{F}_E - \mathbf{1} \right). \tag{2.3}$$

Both measures are referred to the vectorial base vectors of $\mathcal{B}_N$. Another tensor connected also with the configuration $\mathcal{B}_N$, being of importance for the following considerations, is the plastic stretching tensor:

$$\mathbf{D}_P = \frac{1}{2} \left(\dot{\mathbf{F}}_P \mathbf{F}_P^{-1} + \mathbf{F}_P^{-T} \dot{\mathbf{F}}_P^T \right), \tag{2.4}$$

where the superposed dot stands for material differentiation with respect to time holding considered particle fixed.

According to the assumption that the elastic strain is caused and escorted by the corresponding stress tensor, Hooke's law holds for the mapping $\mathcal{B}_N \to \mathcal{B}$ and it should be written in an invariant way connected with the intermediate referential configuration $\mathcal{B}_N$. For this aim, aside stress tensor present in $\mathcal{B}$ – configuration, called Cauchy stress (or "true" stress), we quote also the first and second Piola-Kirchhoff stress tensor [28]:

$$\mathbf{T}_R = \det(\mathbf{F})\, \mathbf{T} \mathbf{F}^{-T}, \quad \mathbf{S} = \det(\mathbf{F_E})\, \mathbf{F}_E^{-1} \mathbf{T} \mathbf{F}_E^{-T}, \tag{2.5}$$

respectively. The first of them is connected with $\mathcal{B}$ and $\mathcal{B}_0$ and often it is named the engineering stress, whereas the second one is referred to the natural state local configuration $\mathcal{B}_N$. If the elastic strain is much smaller than the finite total strain, then Hooke's law reads:

$$\mathbf{S} = \mathcal{H} : \mathbf{E}_E. \tag{2.6}$$

Fourth rank tensor $\mathcal{H}$ consisting of material constants should depend in general on temperature as well as on principal invariants of the (traceless) plastic strain tensor.

$$\pi_2 = tr\left\{\mathbf{e}_P^2\right\}, \quad \pi_3 = tr\left\{\mathbf{e}_P^3\right\}. \tag{2.7}$$

Two basic tensor constituents of the subsequent evolution equations are the plastic strain tensor and the second Piola-Kirchhoff stress tensor defined above. Thus, the relevant tensor generators are (the subscript d is used to denote the deviatoric part of a second rank tensor) [28, 21]:

$$\begin{gathered} \mathbf{H}_1 = \mathbf{S}_d, \quad \mathbf{H}_2 = \left(\mathbf{S}_d^2\right)_d, \quad \mathbf{H}_3 = \mathbf{e}_P, \quad \mathbf{H}_4 = \left(\mathbf{e}_P^2\right)_d, \\ \mathbf{H}_5 = \left(\mathbf{S}_d\mathbf{e}_P + \mathbf{e}_P\mathbf{S}_d\right)_d, \quad \mathbf{H}_6 = \left(\mathbf{S}_d\mathbf{e}_P^2 + \mathbf{e}_P^2\mathbf{S}_d\right)_d, \\ \mathbf{H}_7 = \left(\mathbf{S}_d^2\mathbf{e}_P + \mathbf{e}_P\mathbf{S}_d^2\right)_d, \end{gathered} \tag{2.8}$$

while the corresponding principal and mixed invariants will also be necessary in the sequel:

$$\begin{gathered} s_2 = tr\left(\mathbf{S}_d^2\right), \quad s_3 = tr\left(\mathbf{S}_d^3\right), \quad \mu_1 = tr\left(\mathbf{S}_d\mathbf{e}_P\right), \\ \mu_2 = tr\left(\mathbf{S}_d\mathbf{e}_P^2\right), \quad \mu_3 = tr\left(\mathbf{S}_d^2\mathbf{e}_P\right), \quad \mu_4 = tr\left(\mathbf{S}_d^2\mathbf{e}_P^2\right), \\ \gamma \equiv \left\{s_2, s_3, \pi_2, \pi_3, \mu_1, \mu_2, \mu_3, \mu_4\right\}. \end{gathered} \tag{2.9}$$

As usual, some of the above principal invariants are used here to denote the intensities of the corresponding tensors

$$S = \sqrt{s_2}, \quad \dot{\pi} = \left(\mathbf{D}_P : \mathbf{D}_P\right)^{1/2}, \quad \pi = \int_0^\tau \dot{\pi}\left(\tau'\right)\, d\tau'. \tag{2.10}$$

In the terminology of experimental plasticity, in a slightly different form

$$\sigma^{eq} = S\sqrt{\frac{3}{2}}, \quad \dot{\varepsilon}_P^{eq} = \dot{\pi}\sqrt{\frac{2}{3}}, \quad \varepsilon_P^{eq} = \pi\sqrt{\frac{2}{3}}, \tag{2.11}$$

they are commonly named *equivalent stress*, *equivalent plastic strain* (i.e. accumulated plastic strain) and *equivalent plastic strain rate*.

3. Experimental evidence and evolution equations

It has been known by experimentalists for a long time that initial yield stress depends on the strain rate or on the stress rate such that at higher stress rates, initial yield stress is larger. On the other hand, Rabotnov in his book has suggested that there exists the phenomenon of delayed yielding inherent at some metals and alloys, i.e. it means that stress exceeds its static value after elapsing of a certain time interval called the delay time. According to such an assumption, in the paper [19] the following integral equation

$$\pi(\tau) = \int_0^{\tau} J(\tau - \tau') \frac{DS(\tau')}{D\tau'} d\tau' \equiv \int_0^{\tau} \psi(\tau, \tau') \, d\tau' \tag{3.1}$$

was postulated and calibrated.

If plastic deformation commences at time τ^* so that initial stress time rate equals

$$S(\tau^*) \equiv Y_0 \left(\frac{DS(\tau)}{D\tau}\bigg|_{\tau=\tau^*} \right), \tag{3.2}$$

then the initial yield stress depends on the initial time rate of stress. Accordingly, the kernel in the above integral equation should read

$$J(\tau - \tau') = \begin{cases} 0, & \tau < \tau^*, \\ \exp(-\mathcal{M}), & \tau \geq \tau^*. \end{cases} \tag{3.3}$$

Applying this expression for kernel to the above integral equation, the following representation is acquired:

$$\dot{\pi}(\tau) = J(0) \frac{DS(\tau)}{D\tau} = \begin{cases} 0, & \tau < \tau^*, \\ \exp(-\mathcal{M}) \sqrt{2/3} \; \dot{\sigma}^{eq}(\tau), & \tau \geq \tau^*. \end{cases} \tag{3.4}$$

The integral appearing in (3.1) is the Riemann integral. Indeed, it is not difficult to show that it is uniformly bounded on $[0, \tau]$. On the other hand, a linear relationship between $D\pi/D\tau$ and $DS/D\tau$ was found in [19] in the form:

$$\frac{D\pi}{D\tau} = \exp(-\mathcal{M}) \frac{DS}{D\tau} \tag{3.5}$$

with a material constant $\mathcal{M}$ holding both for tension and shear of AISI 316H so that [19]:

$$\mathcal{M}_{\text{tension}} \approx \mathcal{M}_{\text{shear}} \approx \mathcal{M} = 6.8645. \tag{3.6}$$

The agreement of these values with the corresponding values obtained in the case of tension as well as shear is considerable, i.e. discrepancy between $\mathcal{M}_{\text{tension}}$ and $\mathcal{M}_{\text{shear}}$ amounts approximately to 0.3% at a very large range of strain rates $D\pi/D\tau \in [10^{-3}, 10^{3}]\ s^{-1}$. Thus it is expected that $\mathcal{M}$ is a material constant for AISI 316H. [1)]

If the triggering value of the invariant S (cf. $(2.10)_1$) where plasticity onset happens is denoted by Y, then the simplest nonlinear dependence of Y on the initial stress rate could be given by the following equation:

$$Y = Y_0 + Y_1 \left(\frac{DS(\tau)}{D\tau}\bigg|_{\tau=\tau^*} \right)^m . \tag{3.7}$$

Its statical value Y_0 depends on the accumulated plastic strain accounting in such a way for the strain hardening effect. The other two quantities appearing above, namely Y_1 and m, are constants giving rise to the simplest way of nonlinear stress rate hardening.

It has been shown by experiments on AISI 316H (by means of traditional tension specimen, *"bicchierino"*-type specimen as well as a cruciform specimen) that the plastic stretching tensor is not perpendicular to the yield surface (cf. [3]). Taking such an evidence into account, some constitutive models have been compared and calibrated in the paper [19]. Since such a deviation from normality is not large (as relatively simple and yet general enough to be concordant with experiments) normality model introduced by Rice in [27] based on a loading function normality and generalized to tensor functions is accepted here. Similar evolution equation was derived by Ziegler from the principle of least irreversible force. Such an equation reads:

$$\mathbf{D}_P = \Lambda \left(\frac{\partial \Omega}{\partial \mathbf{S}} \right)_d . \tag{3.8}$$

This relationship has been made explicit in the papers [18, 20] in such a way to include the dependence of the loading function on the stress tensor and plastic strain as representatives of Rice's PIR (pattern of internal rearrangements). More precisely,

$$\Omega = \hat{\Omega}(\mathbf{S}, \varepsilon_P) = \tilde{\Omega}(\gamma) \tag{3.9}$$

[1)] Instead of $\mathcal{M}$ the value of this material constant may be more conveniently expressed (for $\tau \geq \tau^*$) by means of the integral kernel

$$J(0) \approx 1.044 \times 10^{-3} [MPa^{-1}]$$

allowing for explicit dimensions.

and stress derivatives of this function necessarily lead to the tensor generators (2.8).

On the other hand, the above consideration on the time delay of plastic yielding and dependence of the yield stress on the stress rate, allow further specialization of (3.8) by means of

$$\Lambda = \frac{DS}{D\tau} J(0)\,\phi(\pi). \tag{3.10}$$

The simplest evolution equation nonlinear in the stress tensor reads then (cf. (2.8)):

$$\mathbf{D}_P = \frac{DS}{D\tau} \exp(-\mathcal{M})\,\eta(S-Y)\,\phi(\pi)\left(c_1\mathbf{S}_d + c_2\left(\mathbf{S}_d^2\right)_d\right), \tag{3.11}$$

where $\eta(S-Y) = 1$ for $S > Y$ and $\eta(S-Y) = 0$ otherwise (the Heaviside function), and the strain function $\phi(\pi)$ might be either unity or some function aimed to take into account the strain hardening such as:

$$\phi(\pi) = \pi^{\lambda}$$

where, obviously for $\lambda \neq 0$, we have a nonlinear π-dependance. Such a model with only four material constants $\{\mathcal{M}, c_1, c_2, \lambda\}$ was calibrated in [19] leading to a high correlation coefficient 0.9683 for tension and shear in the very large strain rate range $D\pi/D\tau \in \left[10^{-3}, 10^{3}\right] s^{-1}$. The evolution equation (3.11) may be written as follows:

$$\mathbf{D}_P = \frac{DS}{D\tau} \exp(-\mathcal{M})\,\eta(S-Y)\,\phi(\pi) \sum_{\alpha=1}^{7} \Gamma_\alpha(\gamma)\,\mathbf{H}_\alpha, \tag{3.12}$$

where the loading function

$$\Omega = \frac{1}{2}c_1 s_2 + \frac{1}{3}c_2 s_3$$

leads to $\Gamma_1 = c_1$, $\Gamma_2 = c_2$, $\Gamma_\alpha = 0$ $(\alpha > 2)$, while the tensor generators $\mathbf{H}_\alpha$ $(\alpha = 1, ..., 7)$ are shown above in (2.8). Such a model could be named as *quasi-rate-independent*. This means that if we multiply (3.11) by $d\tau$, then this equation becomes incremental. However, it should be taken into account that Y depends on $DS/D\tau$ what means that time rates influence the plastic stretching tensor.

A more general rate-dependent model in its simplest form might be given by [19]

$$\mathbf{D}_P = \eta(S-Y)\,\phi(\pi) \sum_{\alpha=1}^{7} \left(\Gamma_\alpha(\gamma)\,\frac{DS}{D\tau}\exp(-\mathcal{M}) + \Gamma_\alpha^{\#}(\gamma)\right)\mathbf{H}_\alpha \tag{3.13}$$

where, additionally $\Gamma_1^{\#} = c_3, \Gamma_2^{\#} = c_4, \Gamma_\alpha^{\#} = 0\,(\alpha > 2)$. Necessarily, by experimental evidence, the constants c_3, c_4 must be much smaller than c_1, c_2 (cf. (3.5)). Its advantage with respect to (3.12) is that for slow processes it covers the case when the stress rate vanishes while inelastic creep strain rate is different from zero. In our considerations dealing with high strain rates it is not so important to take these additional terms into account.

4. Longitudinal plastic waves

Consider inelastic deformation in an isotropic straight cylindrical bar with circular cross-section whose longitudinal material coordinate is $\zeta \in [0, L]$ and the other material coordinates ξ, η are also Cartesian. It is assumed in the sequel that during all the considered time interval $\tau \in [0, T]$, deplanation of the cross-sections is negligible. Thus, all material points belonging initially to a normal cross section belong to the same section during all the motion. Therefore, $\zeta = \text{const}$ stands for a cross-section with such fixed material points. Moreover, it is assumed that shears are also negligible. Then the deformation gradient tensor and plastic distortion tensor have the following forms:

$$\mathbf{F} = \begin{Bmatrix} 1+\omega & 0 & 0 \\ 0 & 1+\omega & 0 \\ 0 & 0 & 1+\varepsilon \end{Bmatrix},$$

(4.1)

$$\mathbf{F}_P = \begin{Bmatrix} (1+\varepsilon_P)^{-1/2} & 0 & 0 \\ 0 & (1+\varepsilon_P)^{-1/2} & 0 \\ 0 & 0 & 1+\varepsilon_P \end{Bmatrix}.$$

Logarithmic plastic strain tensor and plastic stretching are then obtained as follows:

$$\mathbf{e}_P = \sqrt{\frac{3}{2}} \ln(1+\varepsilon_P)\ \mathbf{N}, \quad \text{where} \quad \mathbf{N} = \sqrt{\frac{1}{6}} \begin{Bmatrix} -1 & 0 & 0 \\ 0 & -1 & 0 \\ 0 & 0 & 2 \end{Bmatrix}, \tag{4.2}$$

so that

$$\mathbf{D}_P = \dot{\pi}\,\mathbf{N} \quad \text{with} \quad \dot{\pi} \equiv \|\mathbf{D}_P\| = (\mathbf{D}_P : \mathbf{D}_P)^{1/2} = \sqrt{\frac{3}{2}} \frac{D}{D\tau} \ln(1+\varepsilon_P). \tag{4.3}$$

In such a case of special geometry and strain conditions we have $\mathbf{D}_P = D\mathbf{e}_P/D\tau$. Of course, such a relationship would not hold in a general case. The unit tensor $\mathbf{N}$ with the properties $\|\mathbf{N}\| = (\mathbf{N} : \mathbf{N})^{1/2} = 1$ is here introduced for convenience.

If only the longitudinal Cauchy stress component $T_{33} \equiv \sigma$ differs from zero, then from Hooke's law written with respect to the $\mathcal{B}_N$-configuration, i.e.

$$\mathbf{E}_E = \frac{1}{E}\left((1+\nu)\ \mathbf{S} - \nu \mathbf{1}\ tr\mathbf{S}\right) \tag{4.4}$$

(E, ν are elastic constants for isotropic body), we get the only non-zero components of the Piola-Kirchhoff tensors $(2.5)_2$ in the form:

$$S_{33} = E\,E_{E33} = \sigma\ (1+\omega)^2\,\frac{(1+\varepsilon_P)^2}{1+\varepsilon},\quad T_{R33} = \sigma\ (1+\omega)^2 = E\,E_{E33}\frac{1+\varepsilon}{(1+\varepsilon_P)^2},$$

where

$$E_{E33} = \frac{1}{2}\left(\left(\frac{1+\varepsilon}{1+\varepsilon_P}\right)^2 - 1\right) \equiv \frac{1}{2}\left((1+\varepsilon_E)^2 - 1\right)$$

is the corresponding longitudinal elastic strain component being very small for steels ($|E_{E33}| \ll 1$). On the other hand, from $S_{11} = S_{22} = 0$ we get the lateral total stretch by means of the formula

$$(1+\omega)^2 = \frac{1 - 2\nu E_{E33}}{1+\varepsilon_P}.$$

The equation of balance of linear momentum written with respect to the undeformed reference configuration $\mathcal{B}_0$ reads:

$$\frac{\partial}{\partial \zeta} T_{R33} = \rho_0 \frac{Dv_3}{D\tau}, \tag{4.5}$$

where ρ_0 is the mass density in the undeformed configuration $\mathcal{B}_0$, v_3 is the longitudinal component of the velocity vector in spatial coordinates with respect to the deformed configuration $\mathcal{B}$, and T_{R33} is given above.

In order to complete the field equations of the problem, the following geometric relation:

$$\frac{\partial v_3}{\partial \zeta} = \frac{D\varepsilon}{D\tau}, \tag{4.6}$$

is necessary. Let us introduce non-dimensional time t and non-dimensional longitudinal material coordinate Z by means of the formulae:

$$Z = \frac{\zeta}{L},\quad t = \frac{\tau}{T}, \tag{4.7}$$

such that $Z \in [0,1]$, $t \in [0,1]$ and $V = \dfrac{T}{L} v_3$ is the corresponding non-dimensional velocity.

Now, the balance law (4.5) by means of (4.6) and (4.7) may be transformed into

$$\frac{DV}{Dt} = \frac{c_0^2}{2}\frac{\partial}{\partial Z}\left(\frac{1+\varepsilon_E}{1+\varepsilon_P}\left((1+\varepsilon_E)^2-1\right)\right), \tag{4.8}$$

where

$$c_0^2 = \frac{E}{\rho_0}\left(\frac{T}{L}\right)^2 \tag{4.9}$$

is the *non-dimensional elastic wave speed* of the linearized wave equation. Indeed, in the elastic range, $\varepsilon_P = 0$, such that (4.8) together with the following non-dimensional equation

$$\frac{\partial V}{\partial Z} = \frac{D\varepsilon}{Dt}, \tag{4.10}$$

obtained from the geometric relation (4.6), give elastic wave equation. However, if plastic strain rate does not vanish, then an additional equation is necessary. Such an equation is (3.13) rewritten in its non-dimensional form. Therefore, Eqs. (4.8), (4.10) and such a transformed Eq. (3.13) are collected into the following set of nonlinear partial differential equations of the first order:

$$\frac{\partial \mathcal{U}}{\partial t} + \mathcal{A}(\mathcal{U})\frac{\partial \mathcal{U}}{\partial Z} = \mathcal{B}^{\#}(\mathcal{U}), \tag{4.11}$$

where

$$\mathcal{U} = \begin{Bmatrix} V \\ \varepsilon \\ \varepsilon_P \end{Bmatrix}, \quad \mathcal{B}^{\#}(\mathcal{U}) = \begin{Bmatrix} 0 \\ 0 \\ \eta T b^{\#} \end{Bmatrix},$$

$$\mathcal{A}(\mathcal{U}) = \begin{Bmatrix} 0 & -c_0^2\, a_{12} & -c_0^2\, a_{13} \\ -1 & 0 & 0 \\ -\eta\, a_{31} & 0 & 0 \end{Bmatrix}. \tag{4.12}$$

In the above expressions for the matrix $\mathcal{A}$ and the column-vector $\mathcal{B}^{\#}$, the following scalar functions are introduced:

$$2(1+\varepsilon_P)^2 a_{12} = 3(1+\varepsilon_E)^2 - 1,\ (1+\varepsilon_P)^2 a_{13} = -(1+\varepsilon_E)\left(2(1+\varepsilon_E)^2 - 1\right),$$

$$a_{31} = \frac{(1+\varepsilon_E)\mathcal{D}}{1-(1+\varepsilon_E)^2\mathcal{D}\eta}, \quad \mathcal{D} = \sqrt{\frac{2}{3}}\exp(-\mathcal{M})\, E\, \pi^{\lambda}\left(C_1\, s + C_2\, s^2\right),$$

$$b^{\#} = \sqrt{\frac{2}{3}}(1+\varepsilon_P)\frac{\left(C_3\, s + C_4\, s^2\right)\pi^{\lambda}}{1-(1+\varepsilon_E)^2 D\eta}. \tag{4.13}$$

Here the Heaviside function is denoted by $\eta = \eta(S - Y)$ and the non-dimensional second Piola-Kirchhoff stress

$$s = \frac{S_{33}}{Y_0|_{\varepsilon_P=0}} = \frac{1}{Y_0|_{\varepsilon_P=0}} E E_{E33} \tag{4.14}$$

is scaled by means of the initial yield stress at the boundary of the original (virgin) elastic range such that the reduced material constants (cf. (3.12) and (3.13)) are introduced as follows:

$$C_\alpha = \frac{c_\alpha}{Y_0|_{\varepsilon_P=0}},\ \alpha \in \{1,3\} \quad \text{and} \quad C_\beta = \frac{c_\beta}{\sqrt{6}\, Y_0|_{\varepsilon_P=0}},\ \beta \in \{2,4\}. \tag{4.15}$$

Let us assume a solution of the homogeneous part of (3.11) in the form $\mathcal{U} = \mathcal{U}_0 \exp(Z - \lambda t)$, i.e. as a wave propagating along the Z-axis at a speed $\lambda \equiv c$. With such an assumption, Eq. (4.11) is reduced to

$$(\mathcal{A} - \lambda 1)\,\mathcal{U}_0 = 0. \tag{4.16}$$

Since the solutions of the characteristic equation

$$\det(\mathcal{A} - \lambda 1) = -\lambda^3 + \lambda\, c_0^2\,(a_{12} + \eta\, a_{13} a_{31}) = 0 \tag{4.17}$$

are real and different, i.e.

$$\lambda_1 = 0, \quad \lambda_{2/3} = \pm c_0\,(a_{12} + \eta\, a_{13} a_{31})^{1/2} \tag{4.18}$$

the wave equation is hyperbolic. It should be noted that one of the solutions vanishes.

Consider now more closely the initial elastic range characterized by $\varepsilon_P = \varepsilon_{P0} = 0$. The above solutions of (4.11) reduce for this very special case to a very simple expression for the initial nonlinear wave speed:

$$c_0^{el} = c_0\, a_{12}^{1/2} = c_0 \left(1 + 3\varepsilon_E + \frac{3}{2}\varepsilon_E^2\right)^{1/2}. \tag{4.19}$$

Of course, in this special case elastic and total strains coincide. In a subsequent elastic range characterized by means of $\varepsilon_P = \varepsilon_{P0} = \text{const} \neq 0$ we would have plastic strain-dependent *nonlinear elastic wave speed* as follows:

$$c^{el} = c_0\, a_{12}^{1/2} = \frac{c_0}{|1 + \varepsilon_{P0}|} \left(1 + 3\varepsilon_E + \frac{3}{2}\varepsilon_E^2\right)^{1/2}. \tag{4.20}_1$$

Taking into account that for steels $|\varepsilon_E| \ll 1$, we note that in a subsequent elastic range with advanced previous plastic strains, the corresponding elastic

wave speed is predicted to be considerably smaller than the elastic wave speed in the initial elastic range. Such a proposition could serve as a basis for an experimental check of validity of the constitutive model proposed and calibrated in [19] and applied here. Concerning the character of such a wave, we see from the derivative of the elastic wave speed i.e.

$$(4.20)_2 \qquad \frac{dc^{el}}{d\varepsilon} = \frac{3\,(1+\varepsilon_E)\,c^{el}}{2\left(1+3\varepsilon_E+\frac{3}{2}\varepsilon_E^2\right)} > 0,$$

that an acceleration wave could be transformed into a shock wave if large elastic strains were possible. However, this cannot happen since much slower plastic wave appears immediately after a yield surface crossing.

Indeed, if $S > Y$, then plastic strain changes with time so that $\eta = \eta\,(S-Y) = 1$ and *plastic wave speed* c may be expressed by the following expression (cf. (4.14) and (4.18)):

$$(4.21) \quad c = c^{el}\left(1+\frac{a_{13}a_{31}}{a_{12}}\,\eta\right)^{1/2}$$

$$= c^{el}\left(1-\eta\frac{2\,(1+\varepsilon_E)\left(2\,(1+\varepsilon_E)^2-1\right)}{3\,(1+\varepsilon_E)^2-1}\,\frac{(1+\varepsilon_E)\,\mathcal{D}}{1-(1+\varepsilon_E)^2\,\mathcal{D}\eta}\right)^{1/2}.$$

Let us note that $c < c^{el}$. For advanced plastic strains we may even neglect elastic strain in the above relationship which leads to

$$c \approx c^{el}\left(\frac{1-2\mathcal{D}\eta}{1-\mathcal{D}\eta}\right)^{1/2}.$$

Thus, for a very long rod excited at one of its ends, the plastic wave front is always delayed behind an elastic precursor wave travelling with the speed c^{el} characteristic for the elastic range to which the state of material at that instant belongs.

It is worth to note that the special case of the above approximate relation when $\mathcal{D} \approx 0.5$ leads to vanishing of the plastic wave speed and this should give rise to a localization onset according to [24].

Let us now introduce left $l_{(\alpha)}$, $\alpha \in \{1,2,3\}$, and right $r_{(\beta)}$, $\beta \in \{1,2,3\}$, (column-type) eigenvectors of the Eq. (4.16) i.e.

$$(4.22) \qquad l_{(\alpha)}^T\left(\mathcal{A}\,(\mathcal{U}) - \lambda_{(\alpha)}1\right) = 0 \quad \text{and} \quad \left(\mathcal{A}\,(\mathcal{U}) - \lambda_{(\beta)}1\right) r_{(\beta)} = 0,$$

which are orthogonal to each other i.e. $l_{(\alpha)}^T r_{(\beta)} = 0$ if $\alpha \neq \beta$. They form the

matrices

$$\left\{ \begin{array}{c} l^T_{(1)} \\ l^T_{(2)} \\ l^T_{(3)} \end{array} \right\} = \left\{ \begin{array}{ccc} 0 & -\eta\, a_{31} & 1 \\ 1 & -c_0^2\, a_{12}/c & -c_0^2\, a_{13}/c \\ 1 & c_0^2\, a_{12}/c & c_0^2\, a_{13}/c \end{array} \right\}, \tag{4.23}$$

$$\left\{ \begin{array}{ccc} r_{(1)} & r_{(2)} & r_{(3)} \end{array} \right\} = \left\{ \begin{array}{ccc} 0 & 1/2 & 1/2 \\ -(c_0/c)^2\, a_{13} & -1/2c & 1/2c \\ (c_0/c)^2\, a_{12} & -\eta\, a_{31}/2c & \eta\, a_{31}/2c \end{array} \right\}. \tag{4.24}$$

Suppose now that instead of the material coordinate Z and time t, new coordinates r and $s \equiv t$ are introduced by means of

$$r(Z,t) = \text{const.} \tag{4.25}$$

They are *characteristics* for the *loading acceleration wave* whose front $Z = \hat{Z}(t)$ moves at the speed (cf. (4.22))

$$\frac{d\hat{Z}}{dt} = \lambda_{(2)}, \quad \lambda_{(2)} = c, \quad c = -\frac{\partial r/\partial t}{\partial r/\partial Z}, \tag{4.26}$$

such that

$$\left(\mathcal{A}(\mathcal{U}) - \lambda_{(\alpha)} 1\right) \left[\frac{\partial \mathcal{U}}{\partial r}\right] = 0 \;\Rightarrow\; \left[\frac{\partial V}{\partial r}\right] = -c \left[\frac{\partial \varepsilon}{\partial r}\right], \tag{4.27}$$

$$\left[\frac{\partial \varepsilon_P}{\partial r}\right] = \eta\, a_{31} \left[\frac{\partial \varepsilon}{\partial r}\right]$$

hold. In the above relationships $[\partial \mathcal{U}/\partial r]$ denotes the jump of $\partial \mathcal{U}/\partial r$ passing from one side of the characteristic (4.25) to its opposite side.

Let us transform the wave Eq. (4.11) by introducing new independent variables i.e. $\{r,t\}$ instead of $\{Z,t\}$, and multiply such a transformed equation from the left side by the corresponding left eigenvector $l^T_{(2)}$. In such a way we obtain the so-called *interior equation*

$$l^T_{(2)} \frac{\partial \mathcal{U}}{\partial t} = l^T_{(2)} \mathcal{B}^{\#}(\mathcal{U}), \tag{4.28}$$

which holds along each characteristic (4.25) governing the change of the solution vector $\mathcal{U}$ along it. Obviously, the solution vector $\mathcal{U}$ is constant along a characteristic for the quasi-rate-independent model (3.12). In other words, such a wave is

said to be *simple* (cf. [22] page 145). For the more general rate-dependent model (2.14) a change of the solution vector along a characteristic is very small since constants $\Gamma_\alpha^\# = \{c_3, c_4\}$ are much smaller than $\Gamma_\alpha = \{c_1, c_2\}$.

Let us derive an equation governing the spatial and temporal changes of $[\partial \mathcal{U}/\partial r]$. First, transforming the wave equation from $\{Z, t\}$ to $\{r, t\}$ and differentiating such a transformed equation by r, we get

$$(4.29)\quad (\mathcal{A}(\mathcal{U}) - c\,1)\frac{\partial^2 \mathcal{U}}{\partial r^2}\frac{\partial r}{\partial Z} + \frac{\partial \mathcal{U}^T}{\partial r^2}\frac{\partial}{\partial \mathcal{U}}(\mathcal{A}(\mathcal{U}) - c\,1)\frac{\partial \mathcal{U}}{\partial r}\frac{\partial r}{\partial Z} + \frac{\partial^2 \mathcal{U}}{\partial r\,\partial t} = \frac{\partial \mathcal{B}^\#}{\partial \mathcal{U}}\frac{\partial \mathcal{U}}{\partial r}.$$

If this equation is multiplied by $l_{(2)}^T$ and the orthogonality of $l_{(\alpha)}$ and $r_{(\beta)}$ is remembered, then after taking jumps of all the terms, the above equation becomes:

$$(4.30)\qquad \frac{\partial}{\partial t}\left[\frac{\partial \varepsilon}{\partial r}\right] + \mu_1\left[\frac{\partial \varepsilon}{\partial r}\right] + \mu_2\left[\frac{\partial \varepsilon}{\partial r}\right]^2 = 0,$$

which is the required evolution equation commonly called the *amplitude equation*. If it is solved, then jumps $[\partial V/\partial r]$ and $[\partial \varepsilon_P/\partial r]$ are easily found from (4.27). The coefficients of the amplitude equation are obtained after a tedious calculation in the following form:

$$(4.31)\qquad \mu_1 = \frac{1}{2c}\left(\frac{\partial c}{\partial t} + \eta\,\frac{c_0^2}{c}a_{13}\,\frac{\partial a_{31}}{\partial t}\right) + \mu_1^\# + m^T\frac{\partial \mathcal{U}^+}{\partial r},$$

with notations:

$$\mu_1^\# = -\frac{c_0^2}{2c^2}\eta\,T\,a_{13}\left(\frac{\partial b^\#}{\partial \varepsilon} + a_{31}\frac{\partial b^\#}{\partial \varepsilon_P}\right),\quad m^T \equiv \{\mu_{1V}\ \mu_{1\varepsilon}\ \mu_{1\varepsilon_P}\},$$

$$\mu_{1V} = \frac{\partial c}{\partial \varepsilon} + \eta\,a_{31}\frac{\partial c}{\partial \varepsilon_P} - \eta\,\frac{c_0^2}{c}a_{13}\left(\frac{\partial a_{31}}{\partial \varepsilon} + a_{31}\frac{\partial a_{31}}{\partial \varepsilon_P}\right),$$

$$\mu_{1\varepsilon} = -\frac{\partial c}{\partial \varepsilon} + \frac{c_0^2}{c}\left(\frac{\partial a_{12}}{\partial \varepsilon} + \eta a_{31}\frac{\partial a_{13}}{\partial \varepsilon} - \eta a_{13}\frac{\partial a_{31}}{\partial \varepsilon}\right) - \frac{c_0^2}{c}\left(\frac{\partial a_{12}}{\partial \varepsilon} + \eta a_{31}\frac{\partial a_{12}}{\partial \varepsilon_P} - \frac{1}{c}\left(\frac{\partial c}{\partial \varepsilon} + \eta a_{31}\frac{\partial c}{\partial \varepsilon_P}\right)\right),$$

$$\mu_{1\varepsilon_P} = -\eta a_{31}\frac{\partial c}{\partial \varepsilon_P} + \eta\frac{c_0^2}{c}a_{31}\left(\frac{\partial a_{12}}{\partial \varepsilon_P} + a_{31}\frac{\partial a_{13}}{\partial \varepsilon_P} - a_{13}\frac{\partial a_{31}}{\partial \varepsilon_P}\right) + \frac{c_0^2}{2c}\left(\frac{\partial a_{13}}{\partial \varepsilon} + \eta a_{31}\frac{\partial a_{13}}{\partial \varepsilon_P} - \frac{1}{c}a_{13}\left(\frac{\partial c}{\partial \varepsilon} + \eta a_{31}\frac{\partial c}{\partial \varepsilon_P}\right)\right),$$

as well as

$$\mu_2 = -\frac{\partial c}{\partial \varepsilon} - \eta a_{31}\frac{\partial c}{\partial \varepsilon_P} + \frac{c_0^2}{2c}\left(\frac{\partial a_{12}}{\partial \varepsilon} + \eta a_{31}\frac{\partial a_{13}}{\partial \varepsilon_P}\right) + \frac{c_0^2}{2c}\eta a_{31}\left(\frac{\partial a_{13}}{\partial \varepsilon} + \eta a_{31}\frac{\partial a_{13}}{\partial \varepsilon_P}\right) - \frac{c_0^2}{2c}\eta a_{13}\left(\frac{\partial a_{31}}{\partial \varepsilon} + \eta a_{31}\frac{\partial a_{31}}{\partial \varepsilon_P}\right). \tag{4.32}$$

The term $\mu_1^{\#}$ is shown separately in order to demonstrate that it vanishes for the quasi-rate-independent model (3.12). If a loading wave enters into an undisturbed region we have $\partial \mathcal{U}^+/\partial r = 0$ so that the amplitude equation becomes significantly simplified. However, under such an assumption, caution must be observed since in front of a plastic wave there exists the corresponding elastic precursor wave.

Finally, let us remark that if the indirect wave with the speed $\lambda_{(3)} = -c$ is considered, then for such a wave $\mathcal{U} = \mathcal{U}_0 \exp(Z + c\,t)$ and analogous calculations with the corresponding left eigen-vector $l_{(3)}^T$ (cf. (4.18) would give a new amplitude equation, similar to (4.30) but with other coefficients (4.31) and (4.33).

5. Numerical simulation of a Hopkinson bar

5.1. A solution algorithm and its accuracy

Consider now a Hopkinson bar as an experimental apparatus consisting of two very long and thick cylindrical coaxial elastic bars with a cylindrical, very thin and short viscoplastic cylindrical specimen (cf.[1]). The left bar is preloaded by a constant elastic tensile strain on a major part of its length such that the remaining part of the left bar is initially immobilized by a clamp which suddenly becomes broken at the beginning of the wave motion (cf. [1]). Let their material coordinates as well as time be normalized in the way shown in the previous section, i.e. by

$$t = \frac{\tau}{T},\quad t \in [0,1],\quad Z_k = \frac{\zeta_k}{L_k},\quad Z_k \in [0,1],\quad k \in \{1,2,3\}, \tag{5.1}$$

such that their non-dimensional linearized elastic wave speeds are

$$(c_{0k}^{el})^2 = \frac{E_k}{\rho_{0k}}\left(\frac{T}{L_k}\right)^2,\quad k \in \{1,2,3\}, \tag{5.2}$$

where indices $1,3$ stand for elastic bars, and the index 2 serves to denote the tension specimen.

Boundary conditions between the bars and the specimen must include equality of normal contact forces leading to the corresponding relationships connecting their first Piola-Kirchhoff stresses. Taking into account values of the nondimensional material and temporal coordinates t and Z_k, the boundary conditions in stresses read

$$(5.3)_1 \qquad T_{R22}(0,t) = T_{R11}(1,t)\frac{A_{01}}{A_{02}} \text{ and } T_{R33}(0,t) = T_{R22}(1,t)\frac{A_{02}}{A_{03}},$$

where A_{0k}, $k \in \{1,2,3\}$, are areas of undeformed cross-sections. Similarly, boundary conditions for nondimensional velocities have to take the following form:

$$(5.3)_2 \qquad V_2(0,t) = V_1(1,t)\frac{L_1}{L_2} \text{ and } V_3(0,t) = V_2(1,t)\frac{L_2}{L_3}.$$

For a numerical solution of the wave equations of the type (4.11), the following numerical method [5] is applied here. Time and material coordinates are discretized as follows:

$$t \in [0,1], \quad \Rightarrow \text{temporal index } K \in [1,M], \ \Delta t = (M-1)^{-1}$$

$$Z \in [0,1], \quad \Rightarrow \text{spatial index } J \in [1,N], \ \Delta Z = (N-1)^{-1}$$

Implicit integration in the quasi rate-independent case (cf. (3.11)) is shown by the following scheme. Its initiation at time step $K+1$ is determined by the last iteration values of the previous step i.e.

$$\varepsilon^{(i)}(J,K+1) = \varepsilon(J,K)$$

with $i = 1$ at the initial iteration position and $\mathcal{U}^{(0)}(J,K+1) = \mathcal{U}(J,K)$.

$$\boxed{\varepsilon^{(i)}(J,K+1)}$$

$$\Downarrow$$

$$\varepsilon_P^{(i)}(J,K+1) = \varepsilon_P(J,K) + \eta^{(i-1)}(J,K+1)\, a_{31}^{(i-1)}(J,K+1)\left(\varepsilon^{(i)}(J,K+1) - \varepsilon(J,K)\right)$$

$$\Downarrow$$

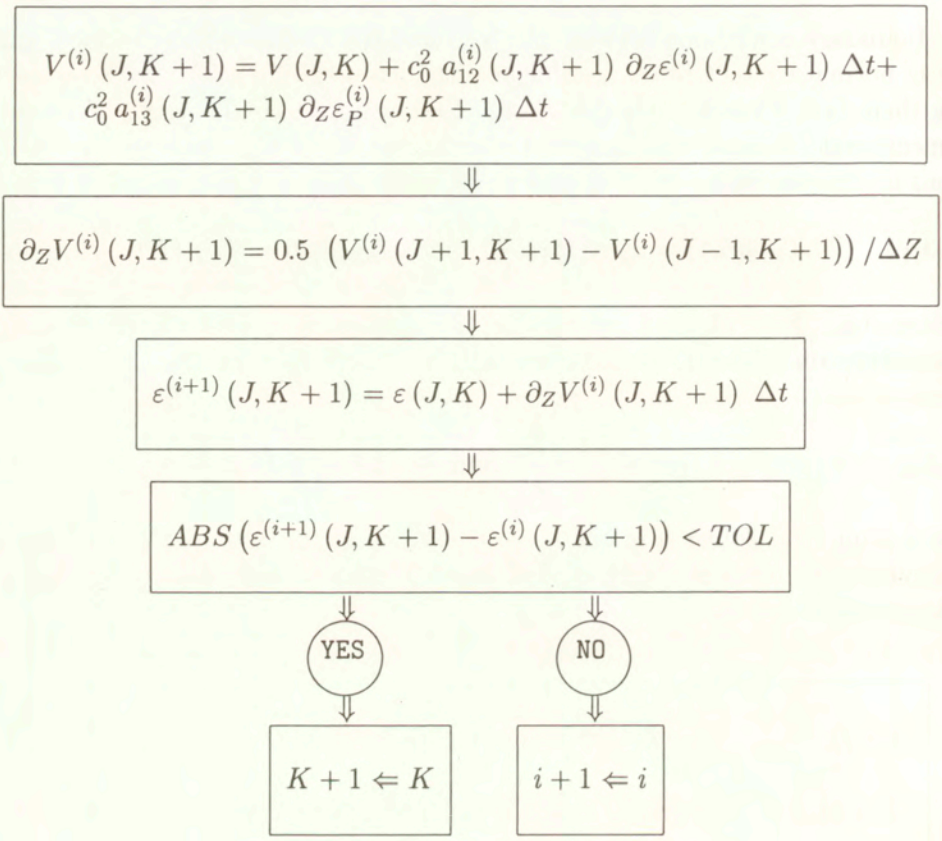

From the above algorithm we are able to derive its order of accuracy following the procedure explained in [11]. To do this we recall that (4.11) is here approximated by:

$$(5.4)_1 \quad \frac{1}{\Delta t}\left(\mathcal{U}_J^{K+1} - \mathcal{U}_J^K\right) + \frac{1}{2\Delta Z}\mathcal{A}\left(\mathcal{U}_J^{K+1}\right)\left(\mathcal{U}_{J+1}^{K+1} - \mathcal{U}_{J-1}^K\right) = \mathcal{B}^{\#}\left(\mathcal{U}_J^{K+1}\right).$$

Now, taking into account that the expansion of

$$(5.4)_2 \qquad \mathcal{U}_{J+\beta}^{K+\alpha} \equiv \mathcal{U}(J\Delta Z + \beta\Delta Z, K\Delta t + \alpha\Delta t)$$

into power series and substitution of the obtained expression into $(5.4)_1$ gives the approximation of order $O(\Delta t + \Delta Z^2)$, we see that the algorithm is linear in time but it is of second order in material coordinate.

On the other hand, von Neumann stability analysis (cf. e.g. [25]) requires that $\xi < 1$ in the following solution

$$(5.4)_3 \qquad \mathcal{U}_J^K = \xi^K \exp(i\chi J\Delta Z)\mathcal{U}_0$$

of $(5.4)_1$. Substituting $(5.4)_3$ into $(5.4)_1$ we arrive at the following form of the characteristic Eq. (4.18):

$$(5.4)_4 \qquad \det\left(\mathcal{A} - i\frac{\Delta Z}{\Delta t}\frac{\xi - 1}{\xi}\frac{1}{\sin(\chi \Delta Z)}\mathcal{I}\right) = 0,$$

such that its solutions lead to the following inequality:

$$(5.4)_5 \qquad \Delta t \geq \left|1 - \frac{1}{\xi}\right| \frac{\Delta Z}{|c|} \sim \frac{\alpha_{BK}\Delta Z}{c^{el}},$$

where plastic wave speed c is determined by (4.19). Therefore, the proposed procedure is unconditionally stable permitting unbounded time increments. In the paper [6] the value $\alpha_{BK} = 5^{1/2}$ is suggested to be convenient.

Practically, for meeting some accuracy requirement by choosing $\xi \in [0.9, 1)$ we may reduce Δt as much as necessary. For instance, if the specimen is divided into 100 elements, then a convenient nondimensional time interval could be $\Delta t \sim 10^{-4}$ for the above established accuracy.

5.2. Appropriate boundary conditions

A very delicate point in this numerical routine is initialization due to the fact that geometrical changes in the apparatus are abrupt with large values of A_{01}/A_{02} as well as of L_1/L_2. Moreover, the length of specimen is more than one hundred times smaller than lengths of the elastic bars. This means that only at the beginning of the plastic wave motion, plastic waves might be clearly recognized whereas during numerous subsequent reflections, the state of specimen strain becomes practically homogeneous.

Thus, a more realistic initialization simulating a background wave-type space-time values of velocity and strain is needed. Otherwise, a disturbance at the end of the specimen becomes numerically "frozen" and does not propagate at all along the specimen. In this paper we proceed in the following way.

For the time being, suppose that a very small disturbance of the type:

$$(5.5) \qquad \varepsilon_1(0,t) = \varepsilon_0\, \eta(-Z_1 + \Theta L_1), \quad \text{with } \Theta = \text{const} < 1$$

is imposed to the left (so-called *"incident-reflected"* bar), so that the corresponding induced strain in the specimen stays inside its initial elastic range. Here $\eta(Z) = 1$, for $Z > 0$ and $\eta(Z) = 0$ otherwise, while magnitude of ε_0 is chosen to be small enough to provoke only linear elastic wave inside the specimen due to approximately constant value of a_{12} for the wave speed c_{02}^{el} in (4.20). Then after P reflections, the incident and reflected stresses and velocities in the bars

as well as in the specimen (under the assumption of linearity of the elastic wave equation) would have the following forms:

$$\sigma_{1I} = \frac{E_1}{2}\,\varepsilon_0\,\eta\left(t + \frac{-Z_1 + \Theta L_1}{c_{01}}\right) + \frac{E_1}{2}\,\varepsilon_0\,\eta\left(-t + \frac{-Z_1 + \Theta L_1}{c_{01}}\right), \tag{5.6}$$

$$\sigma_{1R} = -\frac{E_1}{2}\varepsilon_0\,\frac{r_{12}-1}{r_{12}+1}\eta\left(t + \frac{Z_1 - (1+\Theta)\,L_1}{c_{01}}\right) - 2E_1\varepsilon_0\,\frac{r_{12}}{(r_{12}+1)^2} \times \frac{r_{23}-1}{r_{23}+1}\sum_{\alpha=1}^{P-1}(-r_{123})^{\alpha-1}\,\eta\left(t + \frac{Z_1 - (1+\Theta)\,L_1}{c_{01}} - \frac{2\alpha L_2}{c_{02}}\right), \tag{5.7}$$

$$\sigma_{2I} = E_2\,\varepsilon_0\,\frac{c_{01}L_1}{c_{02}L_2}\frac{r_{12}}{r_{12}+1}\sum_{\alpha=1}^{P-1}(-r_{123})^{\alpha-1} \times \eta\left(t + \frac{Z_1 - (1+\Theta)\,L_1}{c_{01}} - \frac{2\alpha L_2}{c_{02}}\right), \tag{5.8}$$

$$\sigma_{2R} = E_2\,\varepsilon_0\,\frac{c_{01}L_1}{c_{02}L_2}\frac{r_{12}}{r_{12}+1}\frac{r_{23}-1}{r_{23}+1} \times \sum_{\alpha=1}^{P-1}(-r_{123})^{\alpha-1}\,\eta\left(t + \frac{Z_1 - (1+\Theta)\,L_1}{c_{01}} - \frac{2\alpha L_2}{c_{02}}\right), \tag{5.9}$$

$$\sigma_{3I} = 2E_3\,\varepsilon_0\,\frac{c_{01}L_1}{c_{03}L_3}\frac{r_{12}}{r_{12}+1}\frac{r_{23}}{r_{23}+1} \times \sum_{\alpha=1}^{P-1}(-r_{123})^{\alpha-1}\,\eta\left(t - \frac{Z_3}{c_{03}} - \frac{\Theta L_1}{c_{01}} - \frac{(1+2\alpha)\,L_2}{c_{02}}\right), \tag{5.10}$$

with the following notations based on elastic impedances [2)]

$$r_{12} = \frac{E_1A_1}{E_2A_2}\frac{c_{02}L_2}{c_{01}L_1}, \quad r_{23} = \frac{E_2A_2}{E_3A_3}\frac{c_{03}L_3}{c_{02}L_2}, \quad r_{123} = \frac{r_{12}-1}{r_{12}+1}\frac{r_{23}-1}{r_{23}+1}.$$

[2)] At the first sight, a special case of (5.8) when elastic impedance $r_{12} = 1$ leads to $r_{123} = 0$ so that σ_{2I} disappears which, obviously, is a nonsense. Such a conclusion comes from the above compact notation. In fact, when $r_{123} \to 0$, then for $\alpha = 1$ we have $\lim_{r_{123}\to 0} r_{123}^0 = 1$ so that

$$\sigma_{2I} = 0.5E_2\,\varepsilon_0\,\frac{c_{01}L_1}{c_{02}L_2}\eta\left(t + \frac{Z_1 - (1+\Theta)\,L_1}{c_{01}} - \frac{2L_2}{c_{02}}\right).$$

Similar result holds true for σ_{2R} and σ_{3I} given by the next two formulae, (5.9) and (5.10).

The corresponding velocities would have the values:

$$V_{1I} = \frac{1}{2}\, c_{01}\varepsilon_0\, \eta\left(t + \frac{-Z_1 + \Theta L_1}{c_{01}}\right) - \frac{1}{2}\, c_{01}\varepsilon_0\, \eta\left(-t + \frac{-Z_1 + \Theta L_1}{c_{01}}\right),$$

$$V_{1R} = \frac{c_{01}}{E_1}\sigma_{1R}, \quad V_{2I} = -\frac{c_{02}}{E_2}\sigma_{2I}, \quad V_{2R} = \frac{c_{02}}{E_2}\sigma_{2R}, \quad V_{3I} = -\frac{c_{03}}{E_3}\sigma_{3I}. \tag{5.11}$$

Due to the assumed linearity of the elastic wave equation (which is fulfilled for very small elastic strains), the additivity condition

$$\sigma_k = \sigma_{kI} + \sigma_{kR}\ , \quad V_k = V_{kI} + V_{kR}$$

would hold.

5.3. Results of plastic waves inside the specimen

Let us imagine that the initial strain of the left bar, ε_0, in (5.5) – (5.10) is now augmented enough to cause plastic straining of the specimen and that after $P = 2$, the stresses and strains in elastic bars remain unchanged. In other words, this means that during the first two reflections inside the specimen it stays inside the elastic range. Then these formulae with $P = 2$ will serve as an input into the numerical routine shown above. With this type of initiation of plastic strain of the specimen, being calculated by the proposed algorithm as a function of time and its material longitudinal coordinate, is depicted in the following figure.

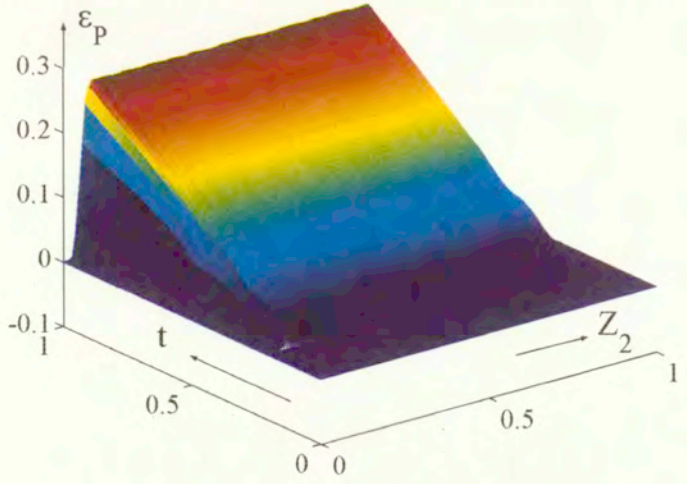

FIG. 1. Plastic wave inside the specimen as a function of space and time.

In order to underline that at initial time interval we have to deal with inhomogeneous distributions along the specimen whereas at advanced strains we

have almost constant strain along its gauge field, we show the following two figures. From the whole history, two characteristic regions are here chosen for presentation: the initial transition time interval and only the last segment of the subsequent steady time interval.

The considered example was made for the following data: $T = 0.001[s]$, $A_{01}/A_{02} = 25$, $L_1/L_2 = 250$, $E_1 = 210\ GPa$, $E_2 = 190\ GPa$, $A_{03} = A_{01}$, $L_3 = L_1$, $E_3 = E_1$, $\varepsilon_0 = 0.0016$, while ρ_0 is the mass density of steel. Taking into account the above accuracy analysis, the specimen was divided into 100 equally spaced elements. The initial time increment was taken to be slightly smaller than the corresponding Courant value [11]. The geometric transition from elastic bars to the specimen was assumed to be gradual with change of rounded corners radius in order to diminish the stress concentration [1] such that the gauge part of the specimen has two times smaller radius than its mounting ends. The initial as well as the yield stress at a non-zero plastic strain are taken respectively to be [3)]

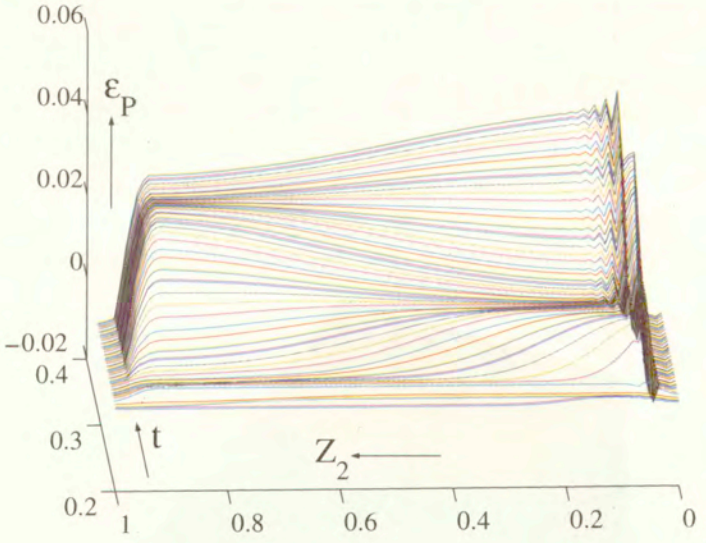

FIG. 2. Initial transition interval of plastic wave.

$$\frac{Y_0}{a} = 1 + b\left(\ln\left[\sqrt{\frac{3}{2}}E\frac{\partial\varepsilon}{\partial t}\right]_{t_0=0}\right)^c, \quad Y = Y_0 + ad\pi^e. \tag{5.12}$$

[3)]The meaning of normalizing constant a is that it is used to denote the initial yield stress at zero plastic strain and equivalent stress rate equal to $1\,[MPa/s]$. The other constants appearing in (5.12) except the Young modulus as well as the "evolution" constants c_1 and c_2 are nondimensional.

These as well as material constants appearing in (3.11) are taken from [19]:

$$a = 251.2\,[MPa], \quad b = 0.015, \quad c = 1.44, \quad d = 17.23, \; e = 0.5,$$
$$c_1 = 1.095\,[MPa^{-1}], \quad c_2 = -0.244\,[MPa^{-2}], \quad \lambda = 0.223.$$

It is worth to note that unlike (2.7), the triggering relationship (5.12) for plasticity commencement at diverse loading-unloading paths takes into account the combined strain-strain rate hardening. Thus, for strain-controlled experiments, curves $Y_0(\pi)$ are not parallel when the strain rate is varied (cf. [1, 2]).

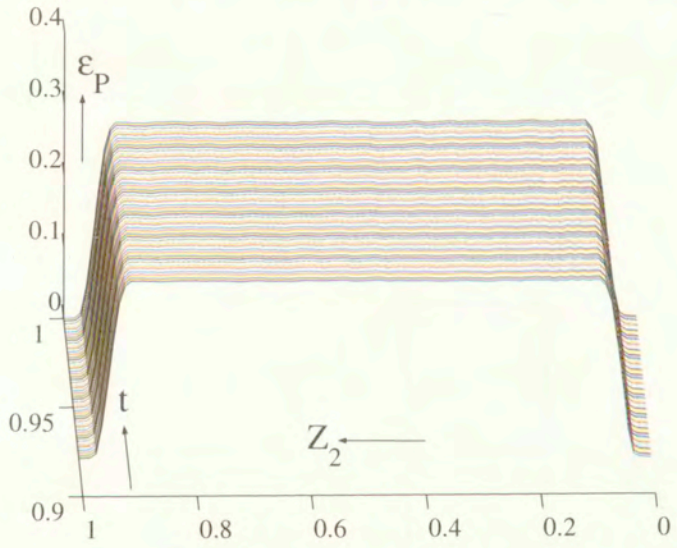

FIG. 3. Ending steady interval of plastic wave.

4.4 A discussion of Lindholm's procedure

At the end of this section, let us consider carefully the standard determination of the stress-strain state inside the specimen by means of measurements made on the elastic bars only. Suppose that two strain gauges, $SG1$ and $SG3$, are situated symmetrically at the same distance from the specimen i.e. $\vartheta L_1 = \vartheta L_3$, where $\vartheta < \Theta < 1$.In other words, $SG1$ has a position between the fixing clamp on the left (incident-reflected) bar and the left end of the specimen. Let the elastic waves in the left and the right elastic bar be:

$$u_1 = f_1\left(t - \frac{Z_1}{c_{01}}\right) + g_1\left(t + \frac{Z_1}{c_{01}}\right), \quad u_3 = f_3\left(t - \frac{Z_3}{c_{03}}\right)$$

where f_1 is the *incident* wave, g_1 – the *reflected* wave and f_3 – the *transmitted* wave. Neglecting the length of the specimen we may assume that time delays at

$SG1$ and $SG3$ are approximately the same and equal to

$$\Delta t = \vartheta L_1/c_{01} = \vartheta L_3/c_{03}.$$

Let us denote the incident, reflected and transmitted strains by means of $\varepsilon_I(Z_1,t) = \partial f_1(\cdot)/\partial Z_1, \varepsilon_R(Z_1,t) = \partial g_1(\cdot)/\partial Z_1$ and $\varepsilon_T(Z_3,t) = \partial f_3(\cdot)/\partial Z_3$ respectively. Then we have

$$\begin{aligned} \varepsilon_1(1,t) &= \varepsilon_I^{SG1}(t-\Delta t) + \varepsilon_R^{SG1}(t+\Delta t) \equiv \varepsilon_I(t) + \varepsilon_R(t), \\ \varepsilon_3(0,t) &= \varepsilon_T^{SG3}(t+\Delta t) \equiv \varepsilon_T(t), \end{aligned}$$

where ε with superscripts $SG1$ and $SG3$ show readings on the strain gauges. For only two prescribed reflections caused by the augmented input ($P = 2$ in formulae (5.7) – (5.10)) as well as stresses and strains subsequently kept at fixed values, we would get the following picture for incident, reflected and transmitted strain histories at the strain gauges. Having such kind of readings as inputs, Lind-

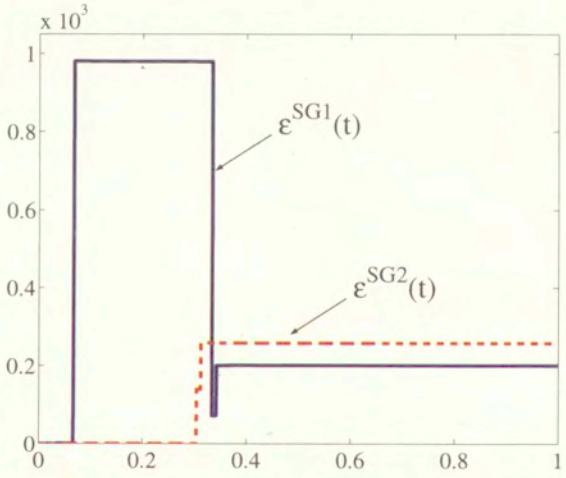

FIG. 4. Incident, reflected and transmitted strains from the left (SG1) and right (SG2) strain gages as functions of nondimensional time.

holm proposed the approximate formulae for the Cauchy stress and presumably homogeneous linear strain (cf. [12]) as follows:

$$\begin{aligned} (5.13)\quad \sigma_2(0.5,t) &\approx 0.5\,(\sigma_2(0,t) + \sigma_2(1,t)) \\ &= 0.5\,E_2\,(A_{01}(\varepsilon_I(t) + \varepsilon_R(t)) + A_{03}\,\varepsilon_T(t))/A_{02}, \end{aligned}$$

$$(5.14)\quad \varepsilon_2(0.5,t) = \frac{1}{L_2}\int_0^t \left(L_1 c_{01}\left(\varepsilon_I\left(t'\right) - \varepsilon_R\left(t'\right)\right) - L_3 c_{03}\,\varepsilon_T\left(t'\right)\right) dt'.$$

Comparing the above two functions of time with the corresponding values calculated by the applied numerical routine yields the following figure which shows that Lindholm's approach should be applied with caution, having in mind that the corresponding error is considerably high. Similar conclusion, but following from some other considerations, has been drawn recently by WU and GORHAM in [29].

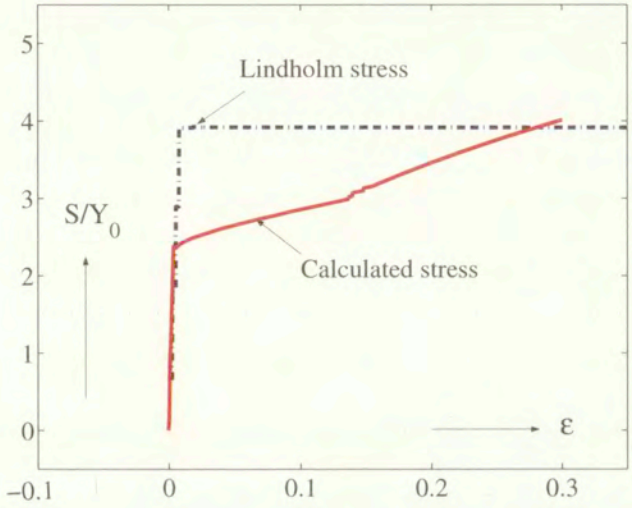

FIG. 5. Check of Lindholm's approximate formulae

6. Concluding remarks

At the end of this paper we could draw the following conclusions:

- It has been previously shown that the so-called universal flow curve and associate flow rule based on the yield function relating only scalars like equivalent stress and equivalent plastic strain was not capable of describing simultaneously the tension and shear, even in the range of only small strain rates (compare for instance [16, 19]). Although commonly used for its simplicity, such an equation is intrinsically scalar since it can describe successfully only a tension test up to large strains. The simplest yet approximately correct approach is to combine the loading function orthogonality with tensor functions.
- At present, it may be concluded that the standard Lindholm's approach to Hopkinson bar analysis does not give satisfactory answers to the assumed homogeneous stress and strain states until failure. Instead, despite the

numerical difficulties met at time and space normalization the approach which accounts explicitly for plastic waves has obvious advantages.

- It is important to underline that the flat horizontal line in the last figure follows either from the applied numerical scheme nor from the constitutive assumptions. On the contrary, boundary conditions at both ends of the specimen are assumed to fulfil Eqs. (5.5) – (5.10) dictating a fixed form of strains and stresses at the left and right end of the specimen. Then the determination of stress and strain by application of (5.13) and (5.14) necessarily lead to such a line. The point is that in such a procedure which eliminates plastic waves and reflections, the specimen is considered as a "black box".
- However, it must be taken into account that ingenious Lindholm's assumption has to be accepted at the beginning of a test analysis. Then, an interactive procedure should be applied to improve agreement between the theory and test, especially at the initial transition range of inelastic strains.

Acknowledgement

Research done in this paper was motivated and made possible by experimental setups and techniques developed by our friends Dr. C. Albertini and late Dr. M. Montagnani to whom our gratitude must be addressed. The authors are grateful to Prof. V. Kukudzanov for valuable comments concerning numerical solving of dynamical inelastic problems. Discussions with Prof. W. Kosiński about the subject were very helpful to us. Mr. D. Stanic made considerable effort in practical solution of the finite difference problem.

The accuracy analysis, the last two conclusions as well as the notes in the text are inserted in the revised version of the paper thanks to reviewer's remarks.

Support of the Serbian Ministry of Science and Technology to M. M. (within grants MNTS-1309 and MNTS-0035) is gratefully acknowledged.

References

1. C. ALBERTINI and M. MONTAGNANI, *Testing techniques in dynamic biaxial loading*, Inst. Phys. Conf. Ser., **47/1** , 21–34, 1979.

2. C. ALBERTINI, M. MONTAGNANI, E. PIZZINATO and A. RODIS, *Comparison of the equivalent flow curves in tension and shear at high strain rate for AISI 316 and ARMCO iron* [in:] Proc. of Mech. Behaviour of Mater. VI, M. JONO and T. INOUE [Eds.], Pergamon, Kyoto 1991.

3. C. ALBERTINI, M. MONTAGNANI and M. MIĆUNOVIĆ, *Viscoplastic behavior of AISI 316 H: multiaxial experimental results and preliminary numerical analysis*, Nuclear Engineering and Design, **130**, 205–210, 1991.

4. C. ALBERTINI, L. J. GRIFFITHS, M. MONTAGNANI, A. RODIS, P. MARIOTTI, A. PALUFFI and G. PAZIENZA, *Material characterization by an innovative biaxial shear experiment at very large strains and at very high strain rates*, Journal de Physique IV, **1/C3**, 435–440, 1991.

5. A. BALTOV, *Investigation of dynamic processes of straining and fracture of inelastic bodies* (in Russian), Bulgarian Acad. Theoretical and Applied Mechanics, **IV/1**, Sofia 1983.

6. A. BALTOV, S. TODOROV *Application of the finite system method in the case of longitudinal bar oscillations*, Theor. Appl. Mechanics, **3**, 56–73, Sofia 1978.

7. J. KLEPACZKO, *Some experimental investigations of the elastic-plastic wave propagation in bars*, [in:] Foundations of plasticity, A. SAWCZUK [Ed.], Noordhoff Publ., Groningen 1972.

8. W. KOSIŃSKI, *Field singularities and wave analysis in continuum mechanics*, PWN, Warsaw 1986.

9. E. KRÖNER, *Allgemeine Kontinuumstheorie der Versetzungen und Eigen-spannungen*, Arch. Rational Mech. Anal., **4**, 273–334, 1970.

10. V. N. KUKUDZANOV *A numerical method for solution of nonsteady elastoviscoplastic problems at large strains*, [in:] Finite inelastic deformations - theory and applications, D. BESDO and E. STEIN [Eds.], IUTAM Proc., Springer, Berlin 1992.

11. V. N. KUKUDZANOV *Finite difference methods in solving solid mechanics problems*, (in Russian), MFTI Publications, Moscow 1992.

12. U. S. LINDHOLM, *Some experiments in dynamic plasticity under combined stress*, [in:] Symposium on the mechanical behavior of metals under dynamic loading, U. S. LINDHOLM [Ed.], San Antonio, Texas, 1967.

13. M. MIĆUNOVIĆ, *A Geometrical treatment of Thermoelasticity of simple inhomogeneous bodies: I) Geometrical and kinematical relations, Bulletin de l'Academie Polonaise des Sciences-Serie des sciences tecniques*, **22/11**, 579–588, Warsaw 1974.

14. M. MIĆUNOVIĆ, C. ALBERTINI and M. MONTAGNANI, *Viscoplastic material properties at non-proportional strain histories of AISI 316 H stainless steel.* [in:] Proc. of MECAMAT, CAILLETAUD *et al.* [Eds.], Mecamat, Besancon 1988.

15. B. MARUSZEWSKI and M. MIĆUNOVIĆ, *On neutron irradiation of an isotropic thermoplastic body*, Int. J. Engng. Sci., **27/8**, 955–965, 1989.

16. M. MIĆUNOVIĆ, *Normality rule from plastic work extremals?*, [in:] Proc. of CMDS-7, K H ANTHONY [Ed.], Materials Science Forum (Trans Tech Publ.), **123–125**, 609–616, 1992.

17. M. MIĆUNOVIĆ, *On viscoplasticity of irradiated steels*, **20**, J. Teor. Appl. Mech., Belgrade, 167–176, 1994.

18. M. MIĆUNOVIĆ, *Multiaxial dynamic experiments versus tensor function representation* [in:] Proc. of CMDS-8, K. Z. MARKOV [Ed.], World Scientific, 564–572, 1996.

19. M. MIĆUNOVIĆ, C. ALBERTINI and M. MONTAGNANI, *High strain rate viscoplasticity of AISI 316H stainless steel from tension and shear experiments,* [in:] Solid Mechanics, P. MILJANIC [Ed.], Serbian Acad. Sci.-Sci. Meetings, Vol. LXXXVII, Dept. Techn. Sci., **3.**, 97–106, 1997.

20. M. MIĆUNOVIĆ, *On viscoplasticity of ferromagnetics*, J. Teor. Appl. Mech., **26**, 107–126, Belgrade, 2001.

21. S. MURAKAMI, *Tensor function approach to constitutive equations of inelasticity*, [in:] Transactions of SMIRT-5, A. SAWCZUK, Z. ZUDANS [Eds.], North-Holland, **L.**, L1/4, 1979.

22. W. K. NOWACKI, *Stress waves in non-elastic solids*, Pergamon, Oxford 1978.

23. P. PERZYNA, *Fundamental problems in viscoplasticity*, Advances in Applied Mechanics, **11**, 313–387, 1971.

24. P. PERZYNA, *Interactions of elastic-viscoplastic waves and localization phenomena in solids*, [In:] Proc. IUTAM Symposium on Nonlinear Waves in Solids, J. L. WEGNER, F. R. NORWOOD [Eds.], Victoria, Canada, ASME Book No AMR137, 114–121,1995.

25. W. H. PRESS, B. P. FLANNERY, S.A. TEUKOLSKY and W. T. VETTERLING, *Numerical recipes in C*, Cambridge Univ. Press 1990.

26. YU. N. RABOTNOV, *Elements of hereditary solid mechanics*, Mir Publishers, Moscow 1980.

27. J. R. RICE, *Inelastic constitutive relations for solids: an internal variable theory and its application to metal plasticity*, J. Mech. Phys. Solids, **19**, 433–455, 1971.

28. C. TRUESDELL and W. NOLL, *The non-linear field theories of mechanics*, [in:] Handbuch der Physik, III/3, S. FLUEGGE [Ed.], Springer, Berlin 1965.

29. X. J. WU and D. A. GORHAM, *Stress equilibrium in the split Hopkinson pressure bar test*, J. de Physique IV **7**, C3 91-96, 1997.

Received February 14, 2002; revised version April 11, 2002.

Arch. Mech., **54**, 5-6, pp. 603–620, Warszawa 2002

Plastic strain in metals by shear banding. I. Constitutive description for simulation of metal shaping operations

R. B. PĘCHERSKI[1], K. KORBEL[2]

[1] *Institute of Fundamental Technological Research, Polish Academy of Sciences, Warsaw*

[2] *University of Mining and Metallurgy, Kraków*

Dedicated to Professor Piotr Perzyna on the occasion of his 70^{th} birthday

THE AIM of the paper is to study the description of plastic strain in metals produced by a hierarchy of plastic slip and shear banding processes: from slip lamellae and slip bands to coarse slip bands, which may further transform into transgranular micro-shear bands and form clusters of micro-shear bands. Constitutive description accounting for the contribution of shear banding was proposed and possible simplifications are discussed from the point of view of applications for numerical simulation of metal shaping operations.

1. Introduction

MULTISCALE MODELLING of large deformations of metals requires the identification of physical mechanisms of plastic strain, careful analysis of averaging procedures and proper setting of the resulting description within continuum theory of materials. The analysis and interpretation of available experimental results obtained with the application of different techniques at different scales reveal a hierarchy of plastic slip processes: from slip lamellae and slip bands to coarse slip bands, which may further transform into transgranular micro-shear bands and form clusters of micro-shear bands. This shows that crystalline solid subjected to plastic deformation is a multi-scale hierarchically organised system. It is a difficult task to describe and predict theoretically the behaviour of such a complex structure. Only partial solutions are available up to now. The mechanism of shear banding was studied in [1], where also the derivation of related macroscopic measure of the rate of deformation was presented. The continuum mechanics description of the kinematics due to shear banding made a basis for constitutive

description proposed in [2-5]. The important question, which remains unsolved, is formulation of a condition of the onset of micro-shear banding. One could expect, that such a criterion should specify at which instant of a considered loading path micro-shear bands start to contribute to plastic deformation. In [3, 4] a theoretical description of small elastic and large plastic deformations within the framework of a two-surface plasticity model, with the internal yield surface connected to back stress anisotropy and the external surface related to micro-shear band formation, was proposed.

On the other hand, the attempts to identify the proposed model for simple case of symmetric shear banding occurring in the case of channel die test made possible to specify the contribution of shear banding as a logistic function of equivalent plastic strain [5, 6]. Such a function accounts for smooth increase of a contribution of micro-shear bands, from zero for very small values of equivalent plastic strain to rapid growth within certain narrow strain interval up to the ultimate value, which is always lower than one. This result led us to the conclusion that it is possible to formulate a simpler form of flow law with a single Huber-Mises yield surface without the necessity of defining the second limit surface related with the onset of micro-shear banding. The aim of the paper is to study afresh the description of plastic strain in metals and to propose such a constitutive description of plastic strain accounting for the contribution of shear banding. In the companion paper [6], the identification and verification of the proposed model are discussed. The results presented herein show the predictive power of the model and the possibilities of applications for numerical simulation of metal shaping operations.

2. Physical motivation

The available results of metallographic observations reveal that in heavily deformed metals, or even at small strains if they are preceded by a properly controlled change of deformation path, a multiscale hierarchy of shear localization modes replaces the crystallographic multiple slip or twinning. Different terminology is used depending on the level of observation. In our study, the term micro-shear band is understood as a long and very thin (of order of 0.1 μm) sheet-like region of concentrated plastic shear crossing grain boundaries without deviation and forming a definite pattern in relation to the principal directions of strain. It bears very large shear strains and lies in a "non-crystallographic position". The term "non-crystallographic" means that micro-shear bands are usually not parallel to a particular densely packed crystallographic plane, of conventionally possible active slip system, in the crystallites they intersect. In such a case, a polycrystalline sample deforms as a "pseudocrystal" subjected to a single or double shear. This change of deformation mode modifies remarkably the ma-

terial properties and makes a basis for the development of new technologies of metal shaping operations [7]. The detailed experimental information about mechanical behaviour and related structural features is reviewed in [2-9], where also comprehensive lists of references are given. The experimental observations reveal the time and spatial organisation of dislocations. This results in the hierarchy of plastic slip processes: from coplanar dislocation groups moving collectively along active slip systems, through slip lamellae and slip bands to coarse slip bands, which may further transform into transgranular micro-shear bands and form clusters (packets) of micro-shear bands of the thickness of order $(10 \div 100)$ μm. At this level of observation, the clusters become elementary carriers of plastic strain.

New information on this phenomenon, showing that it appears even more complex, provide the recent observations of the correlation of temporal instabilities and spatial localization during propagation of Portevin-Le Chatelier deformation bands with use of a novel multizone laser scaning extensometer [10, 11]. The analysis of the extensometer data reveal three types of the PLC bands: type A with continuous propagation of single band along the specimen, type B characterizing with discontinuous band propagation and type C of stochastic nucleation of single bands along the specimen. The clusters of micro-shear bands, produced for instance in rolling, form the planar structures, which are usually inclined by about $\pm 35°$ to the rolling plane and are orthogonal to the specimen lateral face. There can be, however, considerable deviations from this value within the range of 15° to 50°. As it was already stressed in [3, 5], it is typical of the clusters of active micro-shear bands that their planes are rotated relative to the respective planes of maximum shear stress by a certain angle β, which is usually of the order $(5 \div 15)°$. It is worthy to stress that the problem of specifying the angle is complicated by the difficulty of distinguishing the most recently formed micro-shear bands from those that were formed earlier and subsequently rotated with material towards the rolling plane. This is related with the important observation, discussed in [2], that a particular micro-shear band operates only once and develops fully in very short time. As it was discussed in [1], the head of micro-shear band can propagate with the velocity, which is close to the elastic shear wave speed (velocity of sound) in the considered metal or alloy. The micro-shear bands, once formed, do not contribute further to the increase in plastic shear strain. They leave characteristic traces in the structure of the material but it is irrelevant for the constitutive description of plastic flow. We assume that the successive generations of active micro-shear bands competing with the mechanism of multiple crystallographic slips are responsible for the process of advanced plastic flow.

3. Physical model of shear strain rate produced by active micro-shear bands

The physical constraint on any continuum mechanics approach to metal plasticity, i.e. the physical dimension of the smallest representative volume element (RVE) of crystalline material, for which it is possible to define significant overall measures of stress and strain during plastic deformation and the assumptions of the averaging procedure, were thoroughly discussed in [1, 2]. The known in the literature averaging procedure is valid under the general assumption that the dominant mechanism of plastic deformation corresponds to multiple crystallographic slip. In such a case, the theory describing kinematics and constitutive structure of finite elastic-plastic deformation of crystalline solids is well established and the transition between the microscopic and macroscopic levels is well understood. In particular, relations between macro-measures of stress, strain and plastic work are related with the volume averages of their micro-measures. As it was stressed in [2, 4], the situation changes, when an additional mechanism of micro-shear banding is taken into consideration. To solve the problem of proper setting of the effects of micro-shear banding within the continuum mechanics, the description of shear strain rate produced by active micro-shear bands should be given and the concept of RVE should be redefined.

Consider the RVE containing the region of progressive shear banding, depicted schematically in Fig.1a. An active shear band consists of the clusters of micro-shear bands, which at this level of observation can be considered as elementary carriers of plastic strain. On the other hand, an active micro-shear band is produced as the effect of spatial and time organisation of large number of dislocations. They are generated and move collectively within a long and thin sheet-like regions, crossing grain boundaries without deviation and having the thickness of the order of 0.1 μm. Therefore, from the point of view of kinematics, the micro-shear band can be considered as a thin region of concentrated plastic shear. During the passage of the active zone, of thickness h_{ms} and width l_{ms}, the local perturbation B_{ms} of the microscopic displacement field is produced which travels at the head of the micro-shear band with the speed v_{ms} as a distortion wave, cf. Fig 1c. In Fig. 1, two successive "magnifications" of the shear-banding zone are "zoomed in" and the related fundamental mechanisms of plastic shear are illustrated. The first one, depicted in Fig. 1b, corresponds to the cluster of micro-shear bands, in which the passage of large number of active micro-shear bands results in the local perturbation Δ_{MS} of the mezoscopic displacement field$\mathbf{u}_M = \mathbf{x}_M - \mathbf{X}_M$, which moves with the speed V_S. The second "magnification", shown in Fig.1c, represents the aforementioned active zone of a single micro-shear band.

Consider an elementary dislocation model of plastic shear produced in the active zone at the head of a single micro-shear band, as it is depicted in Fig. 1c. According to the known approach, the shear strain γ_{ms} results from the generation and movement of large number of dislocations within the active zone [1]

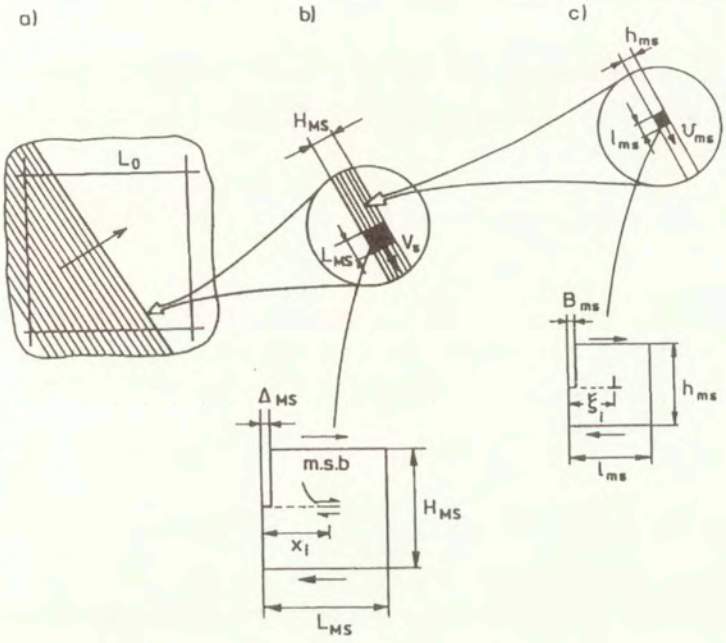

FIG. 1. Schematic view of the multiscale, hierarchically organized system of shear banding: (a) The RVE of the dimension of $L_0 \approx 1$ mm traversed by the region of shear banding progressing in the direction pointed by the arrow. (b) The cluster of active micro-shear bands with the active zone of the thickness $H_{MS} \approx (10 \div 100)$ μm and the width L_{MS} being of the same order. Beneath, the fundamental mechanism of plastic shear strain generated by the active micro-shear bands operating within the active zone, moving along distances x_i, $i = 1 \ldots N_{MS}$ during their "lifetime", and producing the total displacement Δ_{MS} is depicted. (c) The active zone of a single micro-shear band of the thickness $h_{ms} \approx 0.1$ μm and the width l_{ms} of the same order. Below the picture of an elementary dislocation model of plastic shear in the active zone is shown. The displacement B_{ms} is produced by n dislocations moving at the distances $\xi_i, i = 1 \ldots n$.

$$\gamma_{ms} = \frac{B_{ms}}{h_{ms}} = \frac{bn}{l_{ms} h_{ms}} \bar{\xi}, \quad B_{ms} = \frac{b}{l_{ms}} \sum_i^n \xi_i, \quad \bar{\xi} = \frac{\sum_i^n \xi_i}{n}, \tag{3.1}$$

where b is the length of Burgers vector and $\bar{\xi}$ is the average distance that dislocations have moved. If the distance $\bar{\xi}$ and the number of dislocations n can change

with the variable τ, corresponding to the duration of the microscopic process of plastic shear, we have

$$\frac{d\gamma_{ms}}{d\tau} = \frac{b}{l_{ms}h_{ms}}\left(nv_d + \bar{\xi}\frac{dn}{d\tau}\right) \tag{3.2}$$

where $v_d = \dfrac{d\bar{\xi}}{d\tau}$ is the average dislocation velocity. Finally, the shear strain rate, produced in a single micro-shear band, is expressed in terms of the head of micro-shear band speed v_{ms}

$$\frac{d\gamma_{ms}}{d\tau} = \frac{v_{ms}}{h_{ms}}, \quad v_{ms} = \frac{b}{l_{ms}}\left(nv_d + \bar{\xi}\frac{dn}{d\tau}\right). \tag{3.3}$$

According to (3.3), generation and movement of new dislocations contribute to the plastic strain rate. If we assume that the movement of a constant number of mobile dislocations plays the prevalent role, (3.4) transforms into the well known form of the Orowan relation

$$\frac{d\gamma_{ms}}{d\tau} = b\rho v_d, \quad \rho = \frac{n}{l_{ms}h_{ms}}, \tag{3.4}$$

where ρ denotes the dislocation density. In the case of micro-shear bands propagation, the systems, which are not necessarily parallel to densely packed crystallographic planes, are activated. The critical stress in such planes is very high and therefore, the generation of new dislocations may contribute remarkably to plastic shear strain rate. Therefore, it is possible that (3.3) supplemented with proper form of evolution equation for n should be taken into considerations.

Consider a number of active micro-shear bands N_{MS} of similar orientation and produced within certain time interval, $\Delta\tau = \tau_f - \tau_i$, which can be considered as a "time-like" variable or rescaled length of deformation path in the macroscopic description of plastic flow. The interval $\delta\tau$ corresponds to the Representative Time Increment of the process considered earlier in [12]. Such a cluster of "simultaneously" activated (averaged over $\Delta\tau$) micro-shear bands, as it is depicted in Fig. 1b, produces the shear strain on the mezoscopic level

$$\gamma_{MS} = \frac{\Delta_{MS}}{H_{MS}}, \quad \Delta_{MS} = \frac{\bar{B}_{ms}N_{MS}}{L_{MS}}\bar{x}_{MS}, \quad \bar{B}_{ms} = \int_{\tau_i}^{\tau_f} v_{ms}d\tau \tag{3.5}$$

where $\bar{B}_{ms}$ is the total displacement produced by a single micro-shear band and $\bar{\chi}_{MS}$ denotes the average distance that N_{MS} micro-shear bands have moved, during their "lifetime" in the active zone. Assuming that the distance and the

number of micro-shear bands can change during propagation of the active zone of the cluster, we have from (5)

$$\dot{\gamma}_{MS} = \frac{V_S}{H_{MS}}, \qquad V_S = \frac{\bar{B}_{ms}}{L_{MS}} \left(N_{MS} v_{ms} + \bar{x}_{MS} \dot{N}_{MS} \right), \tag{3.6}$$

where the dot denotes differentiation with respect to the "time-like" variable t. Let us observe that the rate $\dot{\bar{x}}_{MS}$ can be identified with the speed v_{ms} of the head of a single micro-shear band under the simplifying assumption that v_{ms} is approximately the same for each micro-shear band in the active zone of the cluster. V_S corresponds to the speed of propagation of the disturbance of the microscopic displacement field, produced in the active zone of the cluster of N_{MS} active micro-shear bands. If the number of active micro-shear bands in the active zone can be assumed constant, the formula similar to the aforementioned Orowan relation is obtained

$$\dot{\gamma}_{MS} = \bar{B}_{ms} \rho_{MS} v_{ms}, \quad \rho_{MS} = \frac{N_{MS}}{L_{MS} H_{MS}}, \tag{3.7}$$

where ρ_{MS} denotes the active micro-shear bands density in the cluster. It is a matter of further investigations upon the evolution of clusters of micro-shear bands to confirm the usefulness of this hypothesis. If we assume that N_{MS} is of the order 100, and the width and thickness of the active zone is of about 100 μm, then the density ρ_{MS} can be estimated for about 10^{10} (m^{-2}).

4. System of active micro-shear bands as a hierarchy of discontinuity surfaces

The discussed process of shear banding can be idealized mathematically as a hierarchy of singular surfaces. The necessary mathematical formalism of the theory of propagating singular surfaces is given in [13-15]. The singular surface of order zero corresponds to the local perturbation of the microscopic displacement field produced by the passage of a single micro-shear band. The passage of large number of micro-shear bands within the active zone of the cluster smoothes out the discontinuity on the micro-level and results in the perturbation of the mezoscopic displacement field traveling with the speed, which produces a discontinuity of the velocity field in the RVE it traverses. This corresponds to the singular surface of order one, called also the surface of strong discontinuity. The discussion of physical nature of the micro-shear banding process, as well as the results of the microscopic observations *in situ*, presented in [16] support the following hypothesis:

The passage of micro-shear bands within the active zone of the cluster results in perturbation of the mezoscopic displacement field traveling with the speed V_S,

which produces a discontinuity of the mezoscopic velocity field v_M in the RVE it traverses. The progression of the sequences of clusters can be idealized mathematically by means of a singular surface of order one propagating through the macro-element (RVE) of the continuum.

The theory of singular surfaces allows identifying the postulated discontinuity surface of the mezoscopic velocity field v_M in RVE as a singular surface $\Sigma(t)$ moving in the reference configuration of the RVE and its dual counterpart $S(t)$ moving in the spatial configuration of the RVE. There exists the jump discontinuity of derivatives of the function of motion χ_M, i.e. of the mezoscopic velocity field $\dot{\chi}_M$ and gradient of deformation $\mathbf{f} = \mathrm{Grad}\chi_M$

$$[\dot{\chi}_M] = \dot{\chi}_M^+ - \dot{\chi}_M^- \neq 0, \quad [\mathbf{f}] = \mathbf{f}^+ - \mathbf{f}^- \neq 0. \tag{4.1}$$

According to the study in [1, 4] the considered surface of strong discontinuity of mezoscopic velocity field fulfills the properties of a vortex sheet with the jump discontinuity of the first derivatives of χ_M given in the spatial configuration by

$$[v_M] = V_S\mathbf{s}, \quad [\mathbf{f}] = -\frac{V_S}{U}\mathbf{s}\otimes\mathbf{nf}, \quad \text{for } U \neq 0, \tag{4.2}$$

where $\mathbf{s}$ and $\mathbf{n}$ are, respectively, the unit tangent and the unit normal vectors to the discontinuity surface $S(t)$, while U corresponds to the local intrinsic speed of propagation of $S(t)$, (cf. [13], p. 508). Similarly, for the material counterpart of a singular surface, the compatibility relations take the form

$$[\dot{\chi}_M] = V_S\mathbf{s}, \quad [\mathbf{f}] = -\frac{V_S}{U_N}\mathbf{s}\otimes\mathbf{N} \quad \text{for } U_N \neq 0, \tag{4.3}$$

where $\mathbf{N}$ is the unit normal to the discontinuity surface $\Sigma(t)$ in the reference configuration of the body and U_N is the normal component of the surface velocity (cf. [4], Fig.2). The progression of large number of clusters of micro-shear bands extending the region of shear banding can be idealized mathematically by means of the singular surface of order two propagating through the macro-element of the continuum as an acceleration wave. The application of the theory of stationary acceleration waves opens the possibility of the analysis of plastic flow instabilities, e.g. strain localization or flutter [17], in relation with shear banding. Application of the results presented in the study [18] upon the mathematical justification of the extension of the concepts of divergence and flutter instabilities to elastic-plastic materials described by incrementally nonlinear constitutive law can appear to be helpful by that.

5. Macroscopic measure of the rate of deformation by micro-shear banding

According to the analysis in [1,4], application of the generalized form of Gauss' theorem for the gradient of the mezoscopic velocity field, which is sufficiently smooth in each point of RVE except the singular surface, where the discussed discontinuity jump appears, results in the following relation for the rate of deformation gradient $\dot{\boldsymbol{F}}$ in the reference configuration:

$$\dot{\boldsymbol{F}} = \frac{1}{V_0}\int\limits_{V_0} \mathrm{Grad}\dot{\chi}_M dV_0 + \frac{1}{V_0}\int\limits_{\Sigma(t)} V_S \mathbf{s}\otimes\mathbf{N} dA_0. \tag{5.1}$$

If we choose the current configuration of RVE at time t as the reference one, the rate of deformation gradient $\dot{F}$ becomes then the rate of the relative deformation gradient (cf. [19], p. 54), and the averaging formula (5.1) takes the following spatial form, [1]:

$$\boldsymbol{L} = \frac{1}{V}\int\limits_{V} \mathrm{grad} v_M dV + \frac{1}{V}\int\limits_{S(t)} V_S \mathrm{s}\otimes \mathrm{n} dA\,, \tag{5.2}$$

where $\boldsymbol{L}$ denotes the macroscopic measure of velocity gradient averaged over the macro-element V traversed by the discontinuity surface $S(t)$. For $V_S = 0$ the known relation is retrieved

$$\boldsymbol{L} \equiv \mathbf{L} = \frac{1}{V}\int\limits_{V} \mathrm{grad}\, v_M dV \tag{5.3}$$

The averaging formula (5.2) enables us to account for the contribution of micro-shear banding in the macroscopic measure of velocity gradient produced at finite elastic-plastic deformations:

$$\boldsymbol{L} = \mathbf{L} + \mathbf{L}_{SB}, \quad \mathbf{L}_{SB} = \frac{1}{V}\int\limits_{S(t)} V_S \mathbf{s}\otimes\mathbf{n} dA. \tag{5.4}$$

Assuming that the singular surface $S(t)$ forms a plane traversing volume V with the unit vectors $\mathbf{s}$ and $\mathbf{n}$ held constant, we have $\mathbf{L}_{SB} = \dot{\gamma}_{SB}\mathbf{s}\otimes\mathbf{n}$, where $\dot{\gamma}_{SB}$ is the averaged macroscopic shear strain rate produced by micro-shear bands

$$\dot{\gamma}_{SB} = \frac{1}{V}\int\limits_{S(t)} H_{MS}\rho_{MS}\bar{B}_{ms} v_{ms} dA. \tag{5.5}$$

Considering the idealized situation, in which the total displacement produced by a single micro-shear band $\bar{B}_{ms}$ and the speed v_{ms} of the head of a single micro-shear band are held constant, we arrive at the following Orowan-type relation for the level of macro-element (RVE) traversed by shear banding zone

$$\dot{\gamma}_{SB} = \rho_{SB}\bar{B}_{ms}v_{ms}\,, \quad \rho_{SB} = \frac{1}{V}\int\limits_{S(t)} H_{MS}\rho_{MS}dA, \tag{5.6}$$

where ρ_{SB} is the macroscopic measure of the density of micro-shear bands operating in the sequences of clusters contributing to the progression of shear banding zone within the RVE. If we take into account that the density ρ_{MS}can change from cluster to cluster in the course of shear banding, then the shear strain rate can be also expressed in terms of the mean rate $\dot{\rho}_{SB}$

$$\dot{\gamma}_{SB} = \dot{\rho}_{SB}\bar{B}_{MS}L_{MS}. \tag{5.7}$$

The derived relation (5.7) is valid for a single system of micro-shear bands. This can be generalized for the case of a double shear, where

$$\mathbf{L}_{SB} = \sum_{i=1}^{2} \dot{\gamma}_{SB}^{(i)}\mathbf{s}^{(i)} \otimes \mathbf{n}^{(i)}. \tag{5.8}$$

The generalization is possible if we assume that the period of time (or the deformation path length), within which the active micro-shear bands operate in both systems, is sufficiently long. Such a period can be considered, on the other hand, as an infinitesimal increment of "time-like" variable, corresponding to the Representative Time Increment, in the macroscopic description. In such a case, the "simultaneous" operation of both systems (clusters) i.e. the double shear is considered. Otherwise, the sequence of single shear systems should be taken into considerations. The derivation of kinematical relations for the rate of deformation and material spin, composed of elastic and plastic parts and accounting for the contribution of micro-shear bands in the double shear (5.8) are given in [1, 4]. The mathematical foundations, which are necessary to describe finite plastic deformation due to the sequence of single shear systems, are given in [20, 21].

6. Constitutive description

According to R. HILL [22], the macroscopic constitutive equations describing elastic-plastic deformations of polycrystalline aggregates are either thoroughly or partially incrementally non linear. Depending on the contribution of the mechanisms involved in plastic flow, a region of fully active loading, called also a

fully active range, separated from the total unloading (elastic) range by a truly nonlinear zone corresponding to the partially active range, may exist. The connection of the fully active range and partially active range with the geometric pattern of micro-shear bands is necessary to specify the relation for the rate of plastic deformations for different loading paths. Because multiple sources of plasticity are dealt with, the theory of multimechanisms with multiple plastic potentials can be considered. The concept of multiple potential surfaces forming a vertex on the smooth limit surface was studied earlier by Z. MRÓZ [23] within the framework of non-associated flow laws. In our case, the existence of the following plastic potentials related to the mechanisms responsible for plastic flow can be postulated [2, 4].

- The plastic potential g_0 that reproduces at the macroscopic level the crystallographic multiple slips and is associated with the limit surface approximated by means of the Huber-Mises locus $F = g_0$.
- The non-associated plastic potentials g_1 and g_2 that approximate at the macroscopic level the multiplicity of plastic potential functions related with the clusters of active micro-shear bands.

The plastic potential functions $g_1$and g_2 display the geometry of the micro-shear bands systems considered and result in two separate planes that form in the space of principal stresses τ_k $(k = 1, 2, 3)$ a vertex at the loading point on the smooth Huber-Mises cylinder F. The planes are defined by normals $\mathbf{N}_i$, which can be expressed in terms of the unit vectors $\mathbf{s}^{(i)}$, $\mathbf{n}^{(i)}$ $(\mathbf{i} = 1, 2)$ defining the "i" th system (cluster) of micro-shear bands

$$\mathbf{N}_i = \frac{\sqrt{2}}{2}\left(\mathbf{s}^{(i)} \otimes \mathbf{n}^{(i)} + \mathbf{n}^{(i)} \otimes \mathbf{s}^{(i)}\right). \tag{6.1}$$

The normals $\mathbf{N}_i$ can be expressed in terms of the unit normal $\boldsymbol{\mu}_F$ to the Huber-Mises yield surface $\frac{1}{2}\boldsymbol{\tau}' : \boldsymbol{\tau}' = k^2$, expressed by deviators of the Kirchhoff stress tensor $\boldsymbol{\tau}'$, and the unit tangent $\mathbf{T}$ to the limit surface at the loading point

$$\mathbf{N}_1 = \cos 2\beta \boldsymbol{\mu}_F + \sin 2\beta \mathbf{T}, \quad \mathbf{N}_2 = \cos 2\beta \boldsymbol{\mu}_F - \sin 2\beta \mathbf{T}, \quad \boldsymbol{\mu}_F = \frac{1}{\sqrt{2}k}\boldsymbol{\tau}'. \tag{6.2}$$

The tensor $\mathbf{T}$ is coaxial with the tangent to the Huber-Mises locus in the deviatoric plane at the loading point

$$\mathbf{T} = T\left(\frac{\overset{\circ}{\boldsymbol{\tau}}'}{\bar{\tau}}\right) = T\left[\overset{\circ}{\boldsymbol{\tau}}' - \left(\overset{\circ}{\boldsymbol{\tau}} : \boldsymbol{\mu}_F\right)\boldsymbol{\mu}_F\right], \quad \bar{\tau} = \sqrt{\frac{1}{2}\boldsymbol{\tau}' : \boldsymbol{\tau}'}. \tag{6.3}$$

For the pressure-insensitive Huber-Mises yield locus $\overset{\circ}{\boldsymbol{\tau}}{}' : \boldsymbol{\mu}_F = \overset{\circ}{\boldsymbol{\tau}} : \boldsymbol{\mu}_F$ holds, whereas T is a normalization factor

$$T = \left\| \overset{\circ}{\boldsymbol{\tau}}{}' - \left(\overset{\circ}{\boldsymbol{\tau}}{}' : \boldsymbol{\mu}_F \right) \boldsymbol{\mu}_F \right\|^{-1}, \tag{6.4}$$

which due to

$$\begin{gathered} \left\| \overset{\circ}{\boldsymbol{\tau}}{}' - \left(\overset{\circ}{\boldsymbol{\tau}}{}' : \boldsymbol{\mu}_F \right) \boldsymbol{\mu}_F \right\|^2 = \overset{\circ}{\boldsymbol{\tau}}{}' : \overset{\circ}{\boldsymbol{\tau}}{}' - \left(\overset{\circ}{\boldsymbol{\tau}}{}' : \boldsymbol{\mu}_F \right)^2, \\ \overset{\circ}{\boldsymbol{\tau}}{}' : \boldsymbol{\mu}_F = \left\| \overset{\circ}{\boldsymbol{\tau}}{}' \right\| \cos\delta' = \left\| \overset{\circ}{\boldsymbol{\tau}} \right\| \cos\delta \end{gathered} \tag{6.5}$$

is given by $T = \left(\left\| \overset{\circ}{\boldsymbol{\tau}}{}' \right\| \sin\delta' \right)^{-1}$. The symbol $\overset{\circ}{\boldsymbol{\tau}}$ denotes the objective rate of stress, which reads

$$\overset{\circ}{\boldsymbol{\tau}} = \dot{\boldsymbol{\tau}} - \mathbf{W}^e\boldsymbol{\tau} + \boldsymbol{\tau}\mathbf{W}^e, \quad \mathbf{W}^e = \mathbf{W} - \mathbf{W}^p, \tag{6.6}$$

where $\mathbf{W}$ is the material spin and $\mathbf{W}^p$ is the plastic spin, which was derived in the following form [2]:

$$\mathbf{W}^p = \frac{1}{2\bar{\tau}\sin 2\beta} \left(\boldsymbol{D}^p\boldsymbol{\tau} - \boldsymbol{\tau}\boldsymbol{D}^p \right). \tag{6.7}$$

Due to the above derivations, the relation for the rate of plastic deformation takes the form

$$\boldsymbol{D}^p = \mathbf{D}^p + \frac{\sqrt{2}}{2} \sum_{i=1}^{2} \dot{\gamma}_{SB}^{(i)} \mathbf{N}_i. \tag{6.8}$$

Assuming that $\mathbf{D}^p$, representing the rate of plastic deformation produced by the crystallographic multiple slips, can be expressed in the simplest case by means of the classical J_2 plasticity theory, we have

$$\mathbf{D}^p = \frac{\sqrt{2}}{2} \dot{\gamma}_s \boldsymbol{\mu}_F, \quad \dot{\gamma}_s = \frac{\sqrt{2}}{2} \frac{\overset{\circ}{\boldsymbol{\tau}} : \boldsymbol{\mu}_F}{h}. \tag{6.9}$$

Due to equations (6.1), (6.2) and (6.8), (6.9), the relation for the rate of plastic deformation takes the form

$$\boldsymbol{D}^p = \frac{\sqrt{2}}{2} \dot{\gamma}^* \boldsymbol{\mu}_F + \frac{\sqrt{2}}{2} \dot{\varepsilon}_{SB} \mathbf{T}, \tag{6.10}$$

where

$$\dot{\gamma}^* = \dot{\gamma}_s + \dot{\gamma}_{SB},$$

$$\dot{\gamma}_{SB} = \cos 2\beta \left(\dot{\gamma}_{SB}^{(1)} + \dot{\gamma}_{SB}^{(2)} \right), \tag{6.11}$$

$$\dot{\varepsilon}_{SB} = \sin 2\beta \left(\dot{\gamma}_{SB}^{(1)} - \dot{\gamma}_{SB}^{(2)} \right).$$

The scalar functions: $f_{SB}^{(1)}$, $f_{SB}^{(2)}$, representing the contributions of the shear banding system (1) and (2), respectively, in the total plastic shear strain rate $\dot{\gamma}^*$, are introduced

$$\dot{\gamma}_{SB}^{(1)} \cos 2\beta = f_{SB}^{(1)} \dot{\gamma}^*, \quad \dot{\gamma}_{SB}^{(2)} \cos 2\beta = f_{SB}^{(2)} \dot{\gamma}^*, \tag{6.12}$$

which are subjected to the following constraints:

$$\frac{\dot{\gamma}_s}{\dot{\gamma}^*} + f_{SB}^{(1)} + f_{SB}^{(2)} = 1, \quad \dot{\gamma}^* \neq 0, \quad f_{SB}^{(1)} + f_{SB}^{(2)} \in [0, 1), \quad f_{SB}^{(1)}, f_{SB}^{(2)} \in [0, 1]. \tag{6.13}$$

Let us note, that this is the formal statement of the experimental observation that shear banding never appears without even slight contribution of crystallographic slips [2]. Basing also on the observation that micro-shear bands can be active only in the case of continued plastic flow, i.e. when the loading condition is fulfilled, it is assumed that for $\dot{\gamma}^* = 0$, $f_{SB}^{(1)} = f_{SB}^{(2)} = 0$.

According to the foregoing discussion and due to (6.11) and (6.12), equation (6.10) is specified for two situations:

- For the case in which the loading direction described by the objective rate of stress $\overset{\circ}{\boldsymbol{\tau}}$ is pointing at partially active range, i.e. for $\delta \in \left(\delta_c, \frac{\pi}{2} \right]$

$$\boldsymbol{D}^p = \frac{\overset{\circ}{\boldsymbol{\tau}} : \boldsymbol{\mu}_F}{2h(1 - f_{SB})} \boldsymbol{\mu}_F + \frac{\overset{\circ}{\boldsymbol{\tau}} : \boldsymbol{\mu}_F}{2h(1 - f_{SB})} \frac{\Delta f_{SB} \tan 2\beta}{\left\| \overset{\circ}{\boldsymbol{\tau}}' \right\| \sin \delta'} \left[\overset{\circ}{\boldsymbol{\tau}}' - \left(\overset{\circ}{\boldsymbol{\tau}} : \boldsymbol{\mu}_F \right) \boldsymbol{\mu}_F \right]. \tag{6.14}$$

- For the case in which the objective rate of stress $\overset{\circ}{\boldsymbol{\tau}}$ is pointing at fully active range, i.e. for $\delta \in [0, \delta_c]$

$$\boldsymbol{D}^p = \frac{\overset{\circ}{\boldsymbol{\tau}} : \boldsymbol{\mu}_F}{2h(1 - f_{SB})} \boldsymbol{\mu}_F + \frac{\overset{\circ}{\boldsymbol{\tau}} : \boldsymbol{\mu}_F}{2h(1 - f_{SB})} \frac{\Delta f_{SB} \tan 2\beta}{\tan \delta_c} \left[\overset{\circ}{\boldsymbol{\tau}}' - \left(\overset{\circ}{\boldsymbol{\tau}} : \boldsymbol{\mu}_F \right) \boldsymbol{\mu}_F \right], \tag{6.15}$$

where $f_{SB} = f_{SB}^{(1)} + f_{SB}^{(2)}$, $\Delta f_{SB} = f_{SB}^{(1)} - f_{SB}^{(2)}$, $\Delta f_{SB} \in [-1, 1]$ and h is the plastic hardening modulus obtained from the simple tensile or compression test. It is confirmed experimentally that in such tests the contribution of shear banding is negligible, [24].

7. Possible simplifications of constitutive description for numerical simulations of metal shaping operations

Among many possible realizations of shear banding processes, which are described by (6.14) and (6.15), one can single out the group of processes characterizing, at lest approximately or for sufficiently long deformation paths, with the same contribution of both systems $f_{SB}^{(1)} = f_{SB}^{(2)}$. Then we have $\Delta f_{SB} = 0$ and (6.14) simplifies. On the other hand, the non-symmetric activation of shear banding can be induced by the sufficiently large change of the loading direction or rotation of the principal axes of stress tensor in the inhomogeneous deformation process caused by boundary conditions. Therefore, we postulate that:

$$\Delta f_{SB} = 0 \ \textit{for} \ \delta \in [0,\ \delta_c] \ \text{and} \ \Delta f_{SB} = A(\delta) \ \text{for} \ \delta \in \left(\delta_c,\ \frac{\pi}{2}\right]. \tag{7.1}$$

The function $A(\delta)$ being a measure of the mentioned asymmetry of shear banding should be identified from numerical simulations of the experiment accounting for the change of loading direction.

As a result of the above assumptions, the flow laws (6.14) and (6.15) read respectively:

- For the case in which the loading direction described by the objective rate of stress $\overset{\circ}{\boldsymbol{\tau}}$ is pointing at partially active range, i.e. for $\delta \in \left(\delta_c, \frac{\pi}{2}\right]$

$$\boldsymbol{D}^p = \frac{\overset{\circ}{\boldsymbol{\tau}} : \boldsymbol{\mu}_F}{2h(1 - f_{SB})}\boldsymbol{\mu}_F + \frac{\overset{\circ}{\boldsymbol{\tau}} : \boldsymbol{\mu}_F}{2h(1 - f_{SB})} \frac{A(\delta)\ \tan 2\beta}{\left\| \overset{\circ}{\boldsymbol{\tau}}' \right\| \sin\delta'} \left[\overset{\circ}{\boldsymbol{\tau}}' - \left(\overset{\circ}{\boldsymbol{\tau}} : \boldsymbol{\mu}_F \right) \boldsymbol{\mu}_F \right], \tag{7.2}$$

- For the case in which the objective rate of stress $\overset{\circ}{\boldsymbol{\tau}}$ is pointing at fully active range, i.e. for $\delta \in [0,\ \delta_c]$:

$$\boldsymbol{D}^p = \frac{\overset{\circ}{\boldsymbol{\tau}} : \boldsymbol{\mu}_F}{2h(1 - f_{SB})}\boldsymbol{\mu}_F. \tag{7.3}$$

The above-mentioned assumptions leading to simplified formula (7.3) finds confirmation in experiment, for the experimental observations reveal that the spatial pattern of micro-shear bands does not change for loading conditions that deviate within limits from the proportional loading path, i.e. the load increments are confined to a certain cone (fully active range) the angle of which can be determined experimentally. For instance, according to [25] in polycrystalline Cu the critical angle δ_c of this cone is of the order of 22°. A more drastic change of the loading scheme produces, however, the change of the spatial orientation of micro-shear bands. This is supported by the results presented in [26], where after cross-rolling two families of micro-shear bands inclined by about ±35°to the most recent rolling direction were observed. The possible applications of the plastic flow law (7.3) for numerical simulation of metal shaping operations are discussed in the companion paper [6].

8. Conclusions

It is worth mentioning that the existence of the deviation angle β, which plays an essential rôle in the non-linear flow law (7.2), is typical for the micro-shear bands produced in the deformation processes carried out under nearly isothermal conditions. Thermal shear bands, i.e. the mode of plastic localization governed by a coupled thermoplastic mechanism, have also been studied by many authors (cf. e.g. [27–29]). In particular, the so-called "adiabatic shear bands" are often reported to coincide with the trajectories of maximum shear stress, which result in β=0. In our view, such a qualitative difference can be attributed to the influence of internal micro-stresses, which control the formation of micro-shear bands. The micro-stresses perturb locally the applied macroscopic state of stress deviating the principal axes of stress tensor. According to the hypothesis on a micro-shear band formation presented in [8], within a suitably oriented grain the critical coarse slip band is activated, which can further transform, under appropriate dynamical conditions, in a transgranular "non-crystallographic" micro-shear band propagating in the planes that are usually deviated from the planes of applied maximum shear stress. On the other hand, the effect of micro-stresses decreases while thermoplastic coupling becomes operative and "adiabatic shear bands" develop. The experimental investigations of the thermomechanical coupling during a simple shear test with use of the thermovision system show the temperature distribution along the shearing paths and reveal a misorientation of the shear-banding zone with respect to the plane of maximum shear stress for non-adiabatic conditions [30]. This confirms, at least qualitatively, the aforementioned interpretation of the deviation angle β. The constitutive description of plastic strain for the angle β=0 reduces to the simple form of plastic flow law (7.3), which can be applied for the numerical simulations of cold as well as hot

metal forming operations. Some results of the relevant applications are reported in [31]. The extension of the proposed description of plastic strain in metals with an account of shear banding under dynamic loading conditions was recently proposed in [32]. The main idea was the modification of the viscoplasticity equation in the form proposed originally by P. PERZYNA [33] in such a way that the viscosity parameter depends on the contribution of shear banding f_{SB}.

Acknowledgement

The State Committee for Scientific Research of Poland supported this work within the framework of the research projects PBZ-KBN-009/T08/1998 and KBN 5 T07 031 22 (the results presented in Sec. 7).

References

1. R. B. PĘCHERSKI, *Macroscopic measure of the rate of deformation produced by micro-shear banding*, Arch. Mech., **49**, 385–401, 1997.
2. R. B. PĘCHERSKI, *Modelling of large plastic deformations based on the mechanism of micro-shear banding. Physical foundations and theoretical description in plane strain*, Arch. Mech., **44**, 563–584, 1992.
3. R. B. PĘCHERSKI, *Finite deformation plasticity with strain induced anisotropy and shear banding*, J. Mat. Processing Technol., **60**, 35–44, 1996.
4. R.B. PĘCHERSKI, *Macroscopic effects of micro-shear banding in plasticity of metals*, Acta Mechanica, **131**, 203–224, 1998.
5. R. B. PĘCHERSKI, *Continuum mechanics description of plastic flow produced by micro-shear banding*, Technische Mechanik, **18**, 107–115, 1998.
6. Z. NOWAK, R. B. PĘCHERSKI, *Plastic strain in metals by shear banding. II. Numerical identification and verification of plastic flow law accounting for shear banding*, Arch. Mech., 603–620, 2002.
7. A. KORBEL, W. BOCHNIAK, *Mechanically induced structure instability – The new opportunity in metal forming*, Proc. of the 1^{st} French-Russian Symposium on Physics and Mechanics of Large Plastic Strains, St. Petersburg, Russia, 4-7 June 2002 (C. TEODOSIU, V. RYBIN, [Eds.] – in print, Problems of Materials Science, **33**, No 1, 2003.
8. A. KORBEL, *The mechanism of strain localization in metals*, Arch. Metall., **35**, 177–203, 1990.
9. A. KORBEL, *Structural and mechanical aspects of homogeneous and non-homogeneous deformation in solids*, In: Localization and Fracture Phenomena in Inelastic Solids, P. PERZYNA [Ed.], CISM Courses and Lectures – No. 386, Udine 1997, Springer Wien New York, 21–98, 1998.
10. A. ZIEGENBEIN, P. HÄHNER, H. NEUHÄUSER, *Correlation of temporal instabilities and spatial localization during Portevin-LeChatelier deformation of Cu-10 at%Al and Cu-15at%Al*, Comput. Mat. Sci., **19**, 27–34, 2000.

11. A. ZIEGENBEIN, P. HÄHNER, H. NEUHÄUSER, *Propagation Portevin-LeChatelier deformation bands in Cu-15at%Al polycrystals: experiments and theoretical description*, Mat. Sci. Engng., **A309-310**, 336–339, 2001.

12. H. PETRYK, *Thermodynamics stability of equilibrium in plasticity*, J. Non-Equlib. Thermodyn. **20**, 132–149, 1995.

13. C. TRUESDELL and R. A. TOUPIN, In: Encyclopaedia of Physics, III/1:The Classical Field Theories, S. FLÜGGE [Ed.], Springer, 226–793, 1960.

14. A. C. ERINGEN and E. S. SUHUBI, *Elastodynamics*, vol. I, Academic Press, 1974.

15. W. KOSINSKI, *Field singularities and wave analysis in continuum mechanics*, PWN, Warszawa & Ellis Horwood, 1986.

16. S. YANG and C. REY, *Shear band postbifurcation in oriented copper single crystals*, Acta Metall. 42, 2763–2774, 1994.

17. J. R. RICE, *The localization of plastic deformation*, in: Theoretical and Applied Mechanics W.T. KOITER [Ed.], North-Holland, 207–220, 1977.

18. D. BIGONI, H. PETRYK, *A note on divergence and flutter instabilities in elastic-plastic materials*, Int. J. Solids Structures, 2001.

19. C. TRUESDELL, W. NOLL, In: Encyclopaedia of Physics, III/3: The non-linear field theories of mechanics, S.FLÜGGE, [Ed.] Springer, 1965.

20. A. KORBEL, R. B. PĘCHERSKI, K. KORBEL, *Sequential slip in the description of plastic deformation of crystals*, (in Polish) Rudy Metale, **R42**, 458–461, 1997 .

21. K. KORBEL, R. B. PĘCHERSKI, A. KORBEL, *Analysis of finite plastic deformation due to the sequence of slips*, Proc. of the 1^{st} French-Russian Symposium on Physics and Mechanics of Large Plastic Strains, St. Petersburg, Russia, 4-7 June 2002 C. TEODOSIU, V. RYBIN [Eds.], – in print.

22. R. HILL, *The essential structure of constitutive laws for metal composites and polycrystals*, J. Mech. Phys. Solids, **14**, 779–795, 1967.

23. Z. MRÓZ, *Non-associated flow laws in plasticity*, J. de Mécanique, **2**, 21–42, 1963.

24. C. A. BRONKHORST, S. T. KALIDINDI, L. ANAND, *Polycrystalline plasticity and the evolution of crystallographic texture in FCC metals*, Phil. Trans. R. Soc. London, **A341**, 443–477, 1992.

25. H. DYBIEC, private communication.

26. K. PIEŁA, A. KORBEL, *The effect of shear banding on spatial arrangement of the second phase particles in the aluminum alloy*, Mat. Sci. Forum, **217-222**, 1037–1042, 1996.

27. M. DUSZEK, P. PERZYNA, *The localization of plastic deformation in thermoplastic solids*, Int. J. Solids Struct., **27**, 1419–1443, 1991.

28. Y. BAI, B. DODD, *Adiabatic Shear Localization*, Pergamon Press, Oxford, 1992.

29. H. V. NGUYEN, W. NOWACKI, *Simple shear of metal sheets at high strain rates*, Arch. Mech., **49**, 369–384, 1997.

30. S. P. GADAJ, W. K. NOWACKI, E. A. PIECZYSKA, *Changes of temperature during the simple shear test of stainless steel*, Arch. Mech., **48**, 779–788, 1996.

31. D. SZELIGA, P. MATUSZYK, V. PIDVYSOTSKYY, M. PIETRZYK, *3D model of cube compression for inverse analysis*, Proc. The 5th Int. ESAFORM Conference, Akademia Górniczo-Hutnicza, Kraków, April 14-17, 2002, M. PIETRZYK *et al.* [Eds.], 171–174, Publishing House "Akapit", Kraków, 2002.

32. R. B. PĘCHERSKI, P. PERZYNA, Z. NOWAK, *Identification of viscoplasticity model accounting for micro-shear banding*, presented at the Workshop on New Experimental Methods in material Dynamics and Impact, NEM-2001, Radziejowice, September 23-26, 2001– under preparation for publication.

33. P. PERZYNA, *Fundamental problems in viscoplasticity*, Advances in Mechanics, **9**, 243–377, 1966.

Received August 8, 2002; revised version November 21, 2002.

Arch. Mech., **54**, 5-6, pp. 621–634, Warszawa 2002

Plastic strain in metals by shear banding. II. Numerical identification and verification of plastic flow law

Z. NOWAK and R. B. PĘCHERSKI

Institute of Fundamental Technological Research, Polish Academy of Sciences, Warsaw

Dedicated to Professor Piotr Perzyna on the occasion of his 70^{th} birthday

THE PAPER IS DEVOTED to the identification and verification of the constitutive description of plastic flow accounting for the hierarchy of shear banding, which is proposed in the companion paper [1]. The numerical identification was carried out with use of the experimental results obtained in channel-die test for polycrystalline copper [2]. To verify the identified model, numerical simulation of the forging process was made and the calculated values of load subjected to the punch versus its displacement were compared with pertinent experimental data given in [11].

Key words: plastic flow with an account of shear bands, channel-die test

1. Introduction

THE AIM OF THE PAPER is to present the results of identification procedure of constitutive equations of plasticity accounting for the hierarchy of shear banding proposed in the companion paper [1]. As a model example, the problem of constrained plain strain compression is considered, which approximates the known channel-die test [2, 3]. Numerical calculations were carried out with application of the finite element program ABQUS/Standard [4]. Preliminary results of the mentioned above identification were discussed in [5-7]. The results presented in this paper have been obtained with the application of new algorithms developed in [8, 9]. The algorithms are based on the solution of nonlinear regression problem with use of the method of global optimization of C. G. BOENDER *et al.* [10]. The automatic procedure of the identification of the unknown scalar function, which describes the contribution of shear bands in plastic shear strain rate, was elaborated. An attempt of verification of the proposed constitutive description is also presented. To verify the plastic flow law with the identified contribution function, the experimental results of forging, presented in [11], were used. The discussed verification shows that the proposed description of plastic flow with an account of shear banding is well suited for the application of numerical simulation of a certain class of metal shaping operations.

2. Discussion of the available experimental data and the results of numerical simulations of channel-die test

In the mentioned above papers [2, 3] the experimental results of the channel-die test for polycrystalline copper were presented. The main subject of the study was the evolution of texture and development of micro-shear bands. The geometry of the matrix and experimental setting are depicted in Fig. 1. The following dimensions of the sample were assumed:

- the height corresponding to the direction of compression: $e_3 - 6.35$mm,
- the width corresponding to the direction of the free plastic flow:$e_2 - 9.53$mm,
- the length corresponding to the direction of matrix constraints: $e_1 - 14.73$mm.

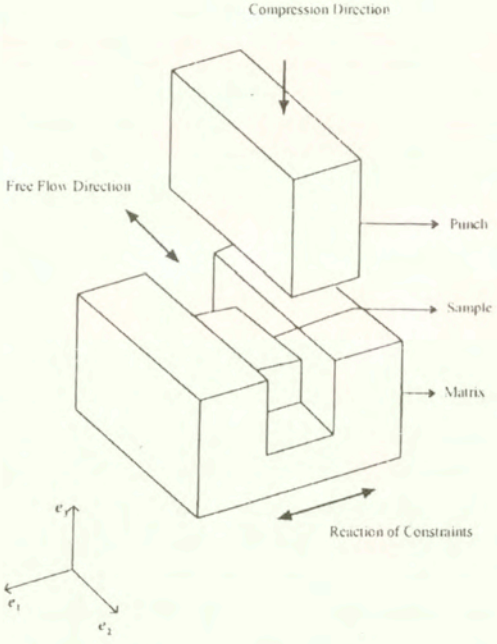

FIG. 1. Scheme of constrained plane strain compression in channel-die test.

The effects of friction were reduced with application of teflon plates covering the contact surfaces of the matrix and the sample. This motivated the authors to assume in numerical calculations that the contact between the sample and the matrix is frictionless. In the experimental investigations described in [2, 3], four series of experiments in which the samples were compressed for the value of: –0.21; –0.52; –1.0 and –1.54 of logarithmic strain ε_3, with the strain rate 0,001 s^{-1}, were conducted. The surface of deformed samples was subjected

to metallographic observations. The results were summarized in [3], p. 234, in the following way: "*... at a true strain of –0.21, the grains are still reasonably equiaxed. Figure 10a shows the microstructure at a true strain of –0.52. At this stage the grains have been flattened, and localized bands, which are 0.1÷0.5 μm in thickness and inclined at ~ ±30÷40° to the horizontal can be observed within individual grains. The initiation of such micro-shear bands occurs somewhere between true strain levels of –0.21 and –0.52. The intensity of these micro-shear bands continues to increase as deformation progresses, and by a strain level of –1.00, Fig. 11a, macro-shear bands which cross grain boundaries have formed.*"

In works [2, 3] the results of calculations were also presented. The authors simulated numerically the similar process of constrained plaine strain compression, approximated by plane strain state, for polycrystalline aggregate with the application of finite element program ABAQUS. The aggregate consists of a large number of grains with assumed crystal lattice orientations, in which the three-dimensional activation of all potential slip systems is allowed. The viscoplastic flow law at the level of a single slip system was assumed. A separate finite element corresponds to a single crystal or a part of it. In the analysis of constrained plane compression problem an aggregate of 400 grains was assumed, which was represented by 400 quadrilateral continuum plane strain 4-node elements – CPE4. In order to reduce the computational time, the lack of friction between the surfaces of sample, matrix and punch was assumed. The detailed information concerning the algorithm and its implementation into finite element program ABAQUS one can find in [2]. The confrontation of the results of numerical calculations and experimental measurement is given in Fig. 2, which displays the relation between the absolute value of compression stress $|\sigma_3|$ and the absolute value of logarithmic strain $|\varepsilon_3|$. The experimental results are represented by points, taken from the plot of experimental data presented in [2], p. 457 – Fig. 7, which shows also the comparison with the results of numerical simulation - presented in our Fig. 2 as a curve labelled by 2. Let us observe, following the remark in [2], that for strain values taken from the range 0.21-0.52, in which the metallographic observations reveal intensive development of micro-shear bands, the discrepancy between the experimental points and the curve displaying the results of numerical calculations becomes visible. The discrepancy increases in the increase of strain, reaching about 22% for the value of logarithmic strain $|\varepsilon_3|$=1.4. The observed inconsistency of numerical simulation and experimental observations was attributed in [2] to the development of micro-shear banding and increasing contribution of this new mechanism in the process of constrained compression in channel-die test. The mechanism of micro-shear banding has not been taken into account in the constitutive model applied for numerical simulation of channel-die test presented in [2]. This might be the reason, according to our opinion, of the observed discrepancy.

3. Identification of plastic flow law accounting for micro-shear banding with application of numerical calculations of channel-die test

The discussed results presented in [2, 3] made a basis for identification of the plastic flow law accounting for micro-shear bands, proposed in the companion paper [1]. Using finite element program ABAQUS/Standard [4], the homogeneous plane strain compression process was calculated, which simulates the idealized, frictionless, channel-die test. The continuum plane strain eight node finite element of type CPE8 was implemented. Plastic flow law accounting for the contribution of symmetric system of micro-shear bands was used (cf. [1]). The specification of Eq. (35) in [1] for infinitesimal elastic strains gives the following rate-type equation:

$$\overset{\circ}{\sigma}_{ij} = C_{ijkl} D_{kl}, \qquad C_{ijkl} = 2G\left(\delta_{ik}\delta_{jl} + \frac{\nu}{1+\nu}\delta_{ij}\delta_{kl} - \frac{1}{\alpha\sigma_Y^2}\sigma'_{ij}\sigma'_{kl}\right), \tag{3.1}$$

where

$$\alpha = \frac{2}{3}\left[1 + \frac{h(1-f_{SB})}{3G}\right], \tag{3.2}$$

σ_{ij} and σ'_{ij} denote, respectively, the components of the Cauchy stress tensor and its deviator in an orthonormal basis, whereas h is plastic modulus. Let us observe that the contribution of shear banding $f_{SB} \in [0,1]$ is accounted in the scalar parameter α, affecting elasto-plastic moduli and, at the same time, the stiffness matrix of the considered numerical scheme. The symbol $\sigma^{\circ}{}_{ij}$ denotes the components of Zaremba-Jaumann derivative of the Cauchy stress tensor. The results of calculations based on the classical model of elastic-plastic deformation with isotropic hardening (called in [4] J_2-theory) are represented in Fig. 2 by curve 1. One can observe the large discrepancy between the curve 1 and the experimental data shown in Fig. 2. For the strain $|\varepsilon_3|$=1.4 the difference reaches about 53%. The results of numerical simulation for elasto-plasticity model defined by Eq. (1) are represented by curve 3. In this case the calculations were conducted for such a form of function $f_{SB} = F_{SB}(\varepsilon^p)$, describing the dependence of shear banding contribution versus equivalent plastic strain ε^p, which assures possibly close fitting of the curve 3 with respect to the experimental points. The possibility provided by the program ABAQUS/Standard was used, which enabled modification of material description by the user procedure UMAT. In the procedure UMAT the simple version of the known algorithm of radial return was implemented, which is used typically for integration of constitutive equations of elasto-plasticity with the Huber-Mises yield condition and isotropic hardening (cf. e.g. [12], part. II, chapter 6). The calculations were made for the following

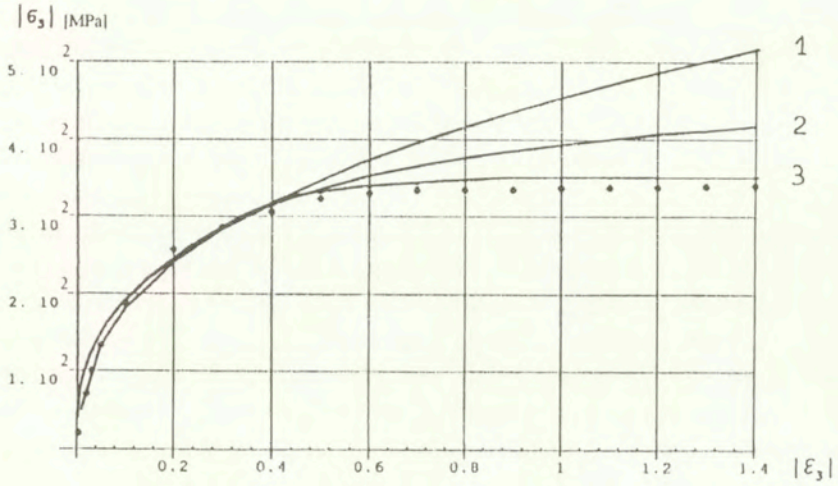

FIG. 2. Plot of the absolute value of compression stress $|\sigma_3|$ as a function of logarithmic strain $|\varepsilon_3|$ for different models of plastic flow versus the experimental results of channel-die test: points representing experimental data of C.A. BRONKHORST *et al.* [2] - •; curve 1 – results of Prandtl-Reuss model for isotropic hardening; curve 2 – numerical simulation of the aggregate of grains according to [2]; curve 3 – results of plastic flow law model expressed by Eqs. (1-4).

approximation of hardening curve taken from the free compression test of Cu polycrystalline samples presented in [2], p. 450, Fig. 2:

$$\sigma = \sigma_Y \left(\frac{E}{\sigma_Y} \varepsilon^p \right)^{\frac{1}{m}}, \tag{3.3}$$

where the yield limit $\sigma_Y = 0.02$ GPa, Young modulus $E = 126.0$ GPa, $m = 2.93$. The shape of the sought function of shear banding contribution, $F_{SB}(\varepsilon^p)$, which provides the required fitting of experimental points with the 3% error, is given in Fig. 3. The function is assumed as a logistic function of the form

$$F_{SB}(\varepsilon^p) = \frac{f_{SB_0}}{1 + \exp(a - b|\varepsilon_3|)} \tag{3.4}$$

where $f_{SB_0} = 0.95$, $a = 7.5$, $b = 13.6$.

Such a method of identification relies on an intuitive selection of the form of the sought function and fitting of relevant constants by means of repeated calculations of the process of homogeneous constrained plane strain compression and comparison of the computed values of compression stress σ_3, displayed in Fig. 3 – curve 3, with experimental points taken from the experimental data

presented in [2]. To make the identification more efficient and independent of intuitive guess, an automatic procedure has been proposed by application of the iteration method. Certain starting value of the shear banding contribution function is assumed, e.g. $f_{SB}^{\text{start}} = 0,5$ and then one executes the series of calculations of the mentioned above problem of constrained plain strain compression. On each step, defined by a given strain increment $|\Delta\varepsilon_3|$, one checks if the stress values σ_3 calculated for different values of $\in[0,1)$, lay sufficiently near, with an assumed error, to the values taken from the curve representing the experimental data (cf. Fig. 2). The presented in Fig. 3 results of the automatic identification procedure were obtained for the assumed error equal to 5%. It appears that an attempt of diminishing of this value leads to the rapid increase of the number of iterations and the resulting cost of computations. In the presented automatic identification procedure the new algorithms developed in [8, 9] were implemented. The algorithms are based on the solution of nonlinear regression problem with use of the method of global optimization of C. G. BOENDER *et al.* [10].

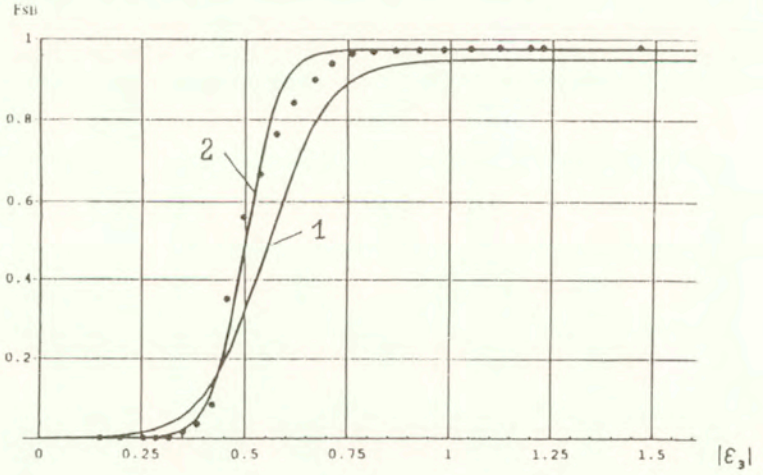

FIG. 3. Comparison of the results of simple identification with the assumed function F_{SB}, Eq. (4), and fitted constants $f_{SB_0} = 0.95$, $a = 7.5$, $b = 13.6$ – curve 1, with the results of automatic iterative identification – filled points and its approximation – curve 2 and with use of the function Eq. (4) and specified constants: $f_{SB_0} = 0.975$, $a = 12.5$, $b = 25.0$.

The details of the automatic identification procedure are discussed in [13], whereas in this paper the results of calculations are considered only. Fig. 3 displays the set of points representing the calculated values of f_{SB}, which satisfy the assumed compatibility condition with experimental data. The points can be fitted with use of a curve shown also in Fig. 3. Let us observe that the intuitively

guessed logistic function $F_{SB}(\varepsilon^p)$ does not differ much from the points obtained from automatic identification.

4. Numerical verification of plastic flow law accounting for shear banding on the example of forging process

The identification of shear banding contribution function $F_{SB}(\varepsilon^p)$ makes possible to apply, as proposed in the companion paper [1], the model of elasto-plastic deformation accounting for shear banding for numerical solution of boundary value problems simulating different processes of metal shaping operations. It remains, however, an open problem of determination of the influence of the change of deformation path or loading scheme on the shape of the identified function $F_{SB}(\varepsilon^p)$. The first attempt to verify the proposed model is the numerical simulation of plane strain micro-forging process of an annealed copper polycrystalline sample, which was studied earlier experimentally and numerically in [11]. The material was chosen the same, as for the discussed above channel die test reported in [2, 3]. The scheme of matrix, the initial geometry of the sample and matrix, and finite element mesh were displayed in Fig. 4. In the upper part of the punch, which at the beginning of the test is in the contact with the sample, small indentation was made in order to prevent the displacement of the points on its upper surface in the direction x_1. The remaining surfaces of the sample and tool were carefully polished and lubricated in order to minimize the effects of friction. Due to the symmetry of the experimental setup of matrix and sample, the calculations were made only for the one half of it. In [11] the finite element program ABAQUS was used with assumption of 17 continuum plane strain eight-node elements of the type CPE8R. The contact between the upper part of the sample and the punch is modelled by assuming the constraints of the displacements in the direction of x_1, while the interaction between the remaining surfaces of the sample, punch and matrix is assumed as contact without friction. In the numerical simulation presented in [11] the authors devoted much attention to the evolution of texture in polycrystalline aggregate assuming certain modified form of the Taylor model. In our considerations we shall focus on the results presented in [11], which are related with global reaction of the system during forging operation. In Fig. 5 the plots of the force applied to the punch in dependence on the displacement of the punch with upper surface of the sample are displayed. The curve with full triangles corresponds to experimental data, whereas the plot with light triangles shows the results of numerical calculations taken from [11].

The problem discussed above was applied for verification of the plasticity model described by Eqs. (3.1)–(3.4). The similar geometry, boundary conditions and the type of finite element have been assumed. Fig. 6 shows the initial and de-

formed finite element mesh. For numerical calculations the program ABAQUS/Standard [4] was implemented with the modified UMAT, as described in the previous section. The results of calculations were displayed in Fig. 5. The curve with filled circles corresponds to the classical Prandtl-Reuss flow law with isotropic hardening (called in [4] J_2-theory), while the curve drawn with heavy line pertains to the flow rule accounting for shear banding given by Eqs. (3.1)–(3.4). Comparison of the results assembled in Fig. 5 shows that the new plasticity model described by Eqs. (3.1)–(3.4) provides quite good accordance with the experimental data and the results of numerical simulation obtained in [11] for the modified Taylor model, which requires much larger computational time. It is also visible that the classical plasticity model leads to increasing discrepancies in comparison with experiment. This is due to the fact that classical model does not account for the new mechanism of plastic deformation, i.e. shear banding, which changes qualitatively material response.

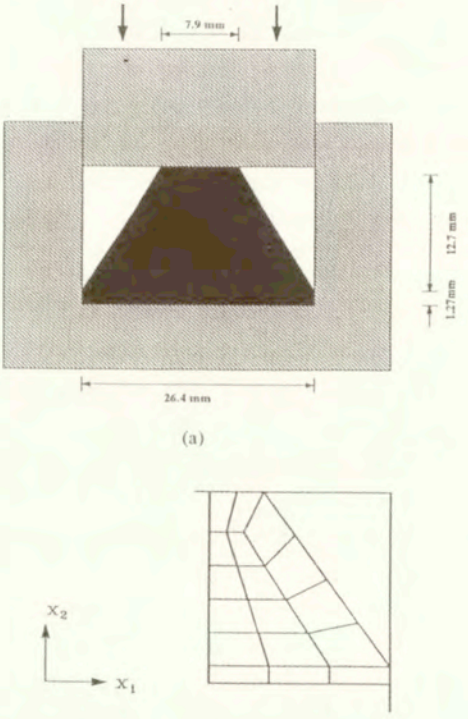

FIG. 4. Scheme of matrix, geometry of initial configuration of sample and matrix together with finite element mesh, according to [11], which were applied for numerical simulation of forging process.

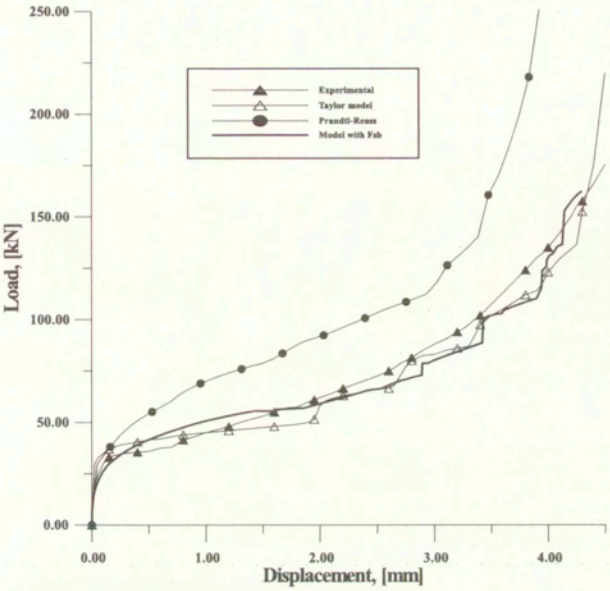

FIG. 5. Plots of load applied to the punch as a function of displacement of the punch with the upper part of the sample.

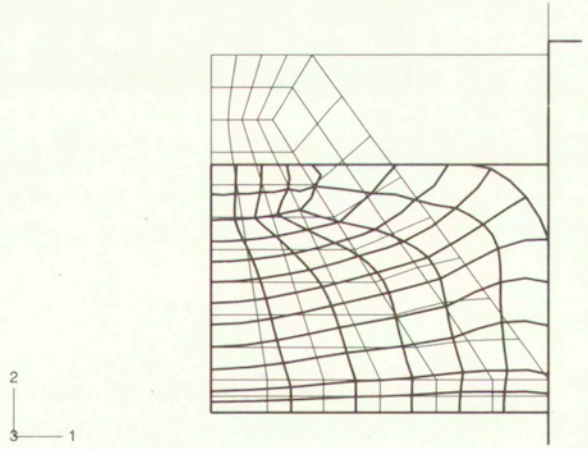

FIG. 6. Finite element mesh in initial and deformed configurations of one half of the specimen.

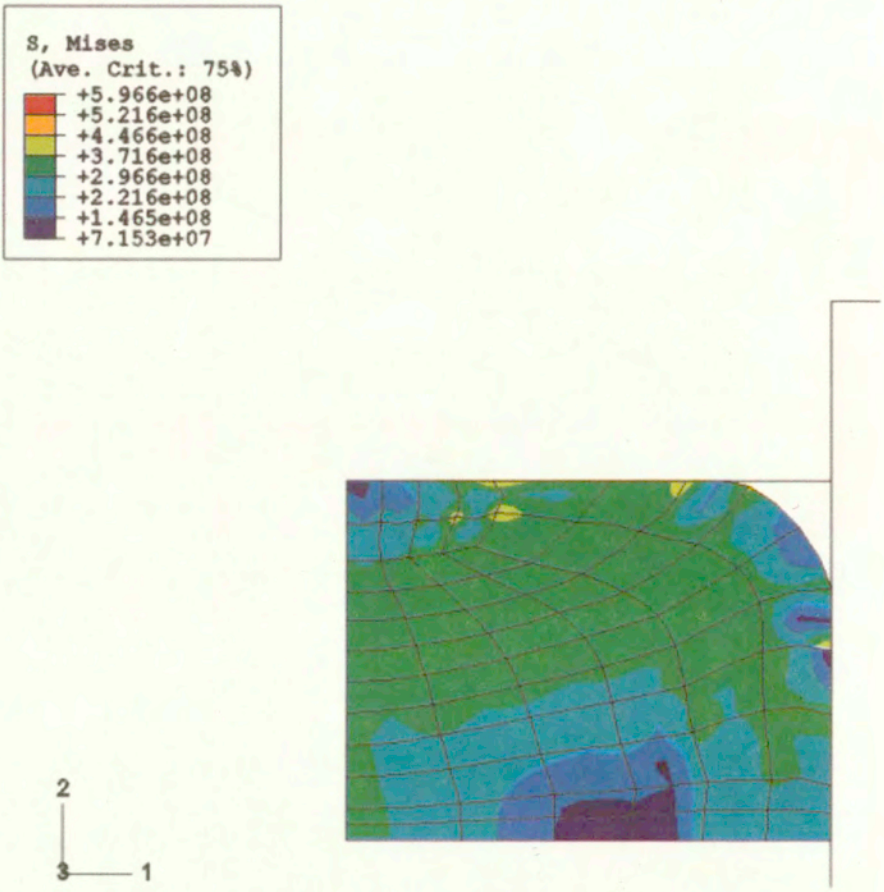

FIG. 7. Distribution of equivalent stress in the deformed configuration.

5. Conclusions

As it was stressed in [5], the motivation for the assumption of the form of function (3.4) was based on the experimental observations, which suggest that micro-shear bands contribute in shear strain rate, as a sequence of generations of active micro-shear bands. The logistic growth law for active micro-shear bands, which is well known in population dynamics, was proposed originally in [14]. The logistic function given in (3.4) may be considered as a solution of such an evolution equation. In future investigations the evolution equation for density of

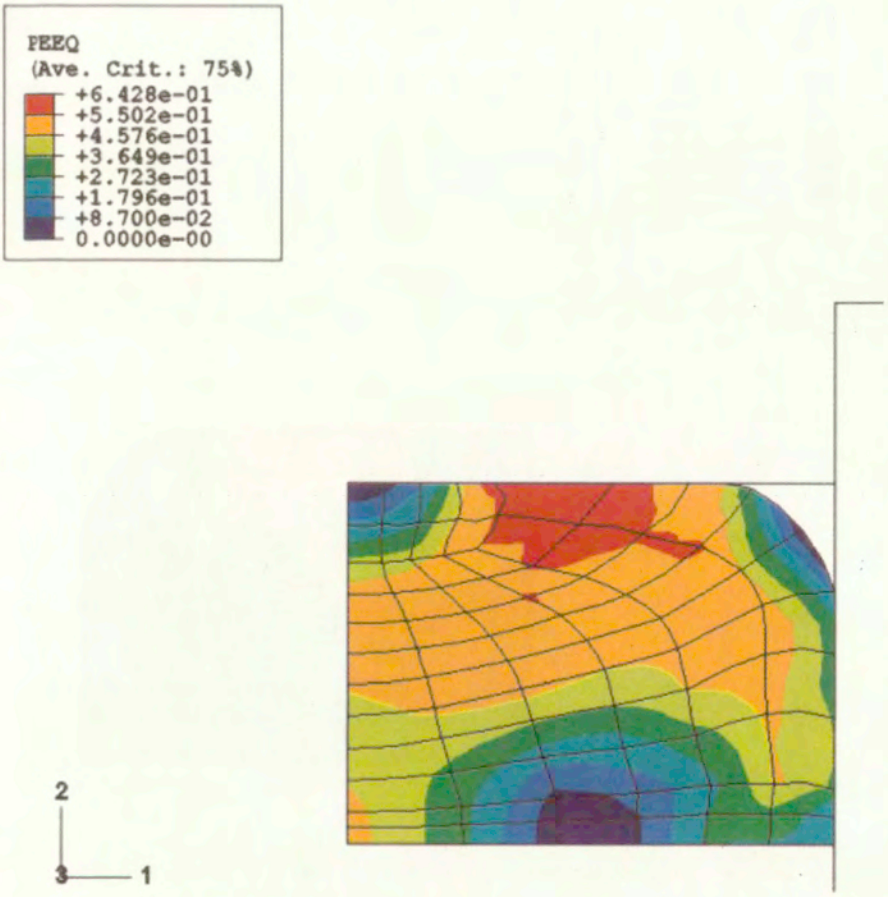

FIG. 8. Distribution of equivalent plastic strain in the deformed configuration.

active micro-shear bands should be sought. Such an evolution equation should take into account the influence of the changes of strain path and loading scheme on the contribution of shear banding f_{SB}. Identification and verification of such an evolution equation needs further studies.

The analysis of the discussed results of numerical calculations and experimental data collected in Fig. 5 leads to the observation that application of the simple model given by Eqs. (3.1)–(3.4), which is based on the flow law for symmetric system of shear banding gives reasonably good accordance with experiment, in spite of appearing inhomogeneities of stress and strain fields. The distribution of equivalent stress is illustrated in Fig. 7, while the inhomogeneous distribution

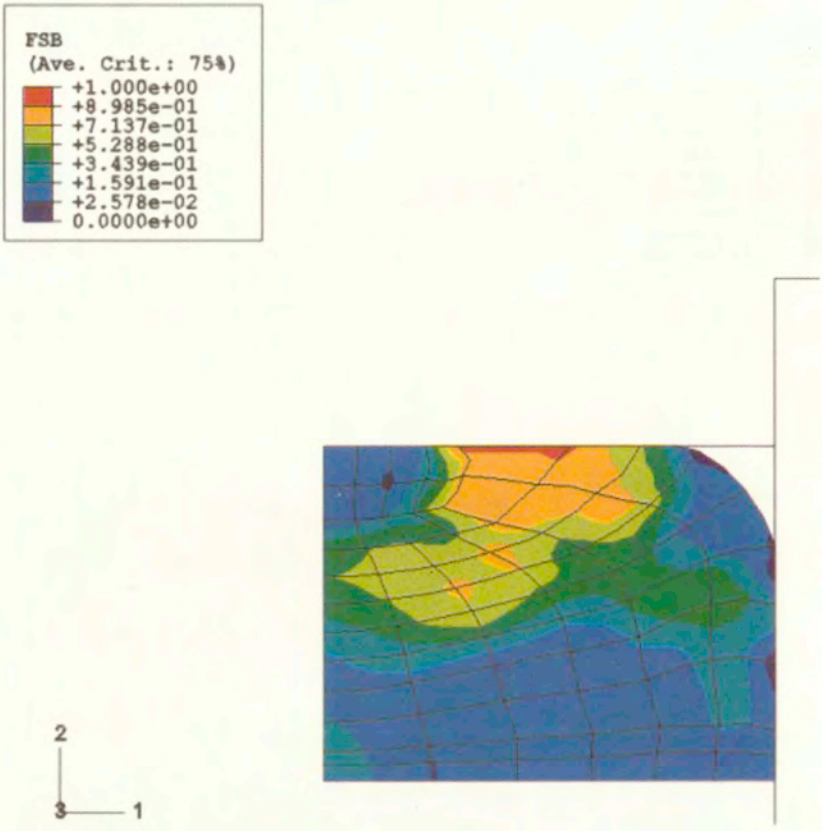

FIG. 9. Distribution of shear banding contribution function F_{SB} in the deformed configuration.

of equivalent plastic strain is displayed in Fig. 8 and the distribution of values of shear banding contribution function f_{SB} at the final stage of deformation is shown in Fig. 9. The mentioned inhomogeneous fields, produced by the assumed geometry of experimental setup and boundary conditions, are related with local rotations of principal axes of the stress tensor and rate of the deformation tensor. The results shown in Fig. 5 suggest that the simple model (3.1–3.3.4) can be also applied for certain class of problems, in which local rotations of principal axes of stress and rate of deformation are admissible. Further studies are necessary to determine the class of processes, in which the application of the simplified constitutive description could appear to be admissible. Otherwise, the more general flow law presented in [1] by Eq. (7.2) should be applied. In

such a case, an additional function being a measure of the asymmetry of shear banding discussed in [1] should be specified and identified numerically with use of the experimental tests taking into account changes of the loading direction. Some preliminary results of such a tests and discussion of possible identification procedure are given in [15].

Acknowledgement

The State Committee for Scientific Research of Poland supported this work within the framework of the research projects PBZ-KBN-009/T08/1998 and KBN 5 T07 031 22 (the results presented in Sec. 3).The numerical calculations have been carried out in Computational Centre of the Warsaw University of Technology (COI-URAN) with use of SUN HPC E10000 computer.

References

1. R. B. PĘCHERSKI and K. KORBEL, *Plastic strain in metals by shear banding. I. Constitutive description for simulation of metal shaping operations*, 603–620, Arch. Mech., 2002.
2. C. A. BRONKHORST, S. T. KALIDINDI and L. ANAND, *Polycrystalline plasticity and the evolution of crystallographic texture in FCC metals*, Phil. Trans. R. Soc. London, **A341**, 443–477, 1992.
3. L. ANAND and S. R. KALIDINDI, *The process of shear band formation in plane strain compression of fcc metals: Effects of crystallographic texture*, Mechanics of Materials, **17**, 223–243, 1994.
4. *ABAQUS/STANDARD - Ver. 6.2, Reference Manuals*, Hibbit, Karlsson and Sorensen Inc., Providence, 2001.
5. R. B. PĘCHERSKI, *Description of plastic deformation with an account of micro-shear bands*, (in Polish) IFTR Reports, Warsaw, 2/1998 – habilitation thesis.
6. R. B. PĘCHERSKI, *Continuum mechanics description of plastic flow produced by micro-shear bands*, Technische Mechanik, **18**, 107–115, 1998.
7. R. B. PĘCHERSKI, Z. NOWAK and K. KORBEL, *Plasticity accounting for micro-shear bands. Application of numerical analysis of channel-die test for the model identification*, Rudy Metali, **R45**, 238-244, 2000 (in Polish).
8. Z. NOWAK and A. STACHURSKI, *Nonlinear regression problem of material functions identification for porous media plastic flow*, Engng. Trans., **49**, 637-661, 2001.
9. Z. NOWAK and A. STACHURSKI, *Global optimization in material functions identification for voided media plastic flow*, Comp. Assisted Mech. Engn. Sci., **9**, 205-221, 2002.
10. C. G. BOENDER, A. H. G. RINNOYKAN, L. STROUGIE and G.T. TIMMER, *A stochastic method for global optimization*, Mathematical Programming, **22**, 125-140, 1982.
11. S. R. KALIDINDI, C. A. BRONKHORST and L. ANAND, *Crystallographic texture evolution in bulk deformation processing of FCC metals*, J. Mech. Phys. Solids, **40**, 537-569, 1992.

12. M. KLEIBER, *Solid state mechanics computational methods*, Mechanika Techniczna, vol. XI, M. KLEIBER [Ed.], WN PWN, Warszawa 1995 (in Polish).

13. Z. NOWAK, P. PERZYNA and R. B. PĘCHERSKI, *Identification of viscoplasticity model accounting for micro-shear bands* – under preparation.

14. R. B. PĘCHERSKI, *A model of plastic flow with an account of micro-shear banding*, ZAMM, **72**, T246-T250, 1992.

15. W. BOCHNIAK, R. B. PĘCHERSKI and K. PANTOŁ *Change of loading scheme under conditions of constrained plane strain compression*(in Polish), Rudy Metale, 2002 – submitted for publication.

Received August 8, 2002; revised version November 14, 2002.

Arch. Mech., **54**, 5-6, pp. 635–646, Warszawa 2002

Some effects of phase transitions on heat propagation

K. SAXTON[1] and R. SAXTON[2]

[1] *Department of Mathematics and Computer Science*
Loyola University
New Orleans, LA 70118, USA

[2] *Department of Mathematics*
University of New Orleans
New Orleans, LA 70148, USA

Dedicated to Professor Piotr Perzyna
on the occasion of his 70^{th} birthday

WE CONSIDER PHASE transitions in solids due to heat propagating through crystalline materials at low temperatures. These are considered in a steady state context where, at the transition temperature, the specific heat becomes singular and the heat conductivity has a maximum. Several consequences are found for the heat capacity having finite or infinite jump discontinuities.

1. Introduction

IN THIS INTRODUCTION, we outline the main features of the low-temperature heat propagation model found in [6, 12] and [13]. An important aspect of the model is a hyperbolic to parabolic change of type which occurs at the temperature of maximum heat conductivity, ϑ_λ. This is associated with the appearance (as temperature decreases) of an internal variable acting as an order parameter. In the steady state limit this change of type disappears, however a second order phase transition takes place, with the specific heat of the material undergoing an abrupt change at ϑ_λ. The model is based strongly on experimental results of [4, 5, 9] and [10] in the context of thermodynamics with internal state variables, [13]. The experimental results give evidence of second sound - hyperbolic or wavelike thermal effects - in crystals of sodium fluoride and bismuth, as has been observed previously in liquid helium, [1]. Significantly, these features are only present at temperatures below which the materials reach their peak thermal conductivities (approximately 18.5 K and 4.5 K for NaF and Bi, respectively). Wavelike thermal phenomena are not seen at higher temperatures, where only diffusive heat propagation is found. We represent this as follows.

Heat conduction in rigid solids is governed by balance of energy

$$\varepsilon_\lambda + q_x = 0, \quad \varepsilon'(\vartheta) = c_v(\vartheta) \tag{1.1}$$

where ϵ is the internal energy per unit volume, c_v is the specific heat at constant volume and q is the heat flux. In the region U_+ in $(x,t) \in \mathbb{R} \times \mathbb{R}^+$ where $\vartheta > \vartheta_\lambda$, heat propagation is understood using (1.1) together with the constitutive relation

$$q = k(\vartheta)\vartheta_x\,, \tag{1.2}$$

while in the region U_- where $\vartheta < \vartheta_\lambda$, heat propagation is instead controlled by (1.1) together with the system

$$p_t = g_1(\vartheta)\vartheta_x + g_2(\vartheta)p, \tag{1.3}$$

$$q = -\alpha(\vartheta)p. \tag{1.4}$$

Here ϑ and ϑ_λ are absolute temperatures, p is the internal state variable, ε, α, k, g_1 and g_2 are constitutive functions with α, k, $g_1 : \mathbb{R}^+ \to \mathbb{R}^+ \cup \{0\}$, $g_2 : \mathbb{R}^+ \to \mathbb{R}^-$.

Let $\psi = \varepsilon - \eta\vartheta$ where ψ and η represent the Helmholtz free energy and the entropy density per unit volume. We will assume that the Helmholtz free energy function takes the form

$$\psi(\vartheta, p) = \psi_1(\vartheta) + \frac{1}{2}\psi_{20}\vartheta p^2. \tag{1.5}$$

The constitutive functions α, g_1, g_2, k are then subject to restrictions arising from the second law of thermodynamics,

$$\eta_t + (q/\vartheta)_x \geq 0. \tag{1.6}$$

These are found to be

$$\alpha(\vartheta) = \psi_{20}\vartheta^2 g_1(\vartheta), \quad g_2(\vartheta) \leq 0. \tag{1.7}$$

The function g_1 can be determined from the speed of second sound pulses while g_2 can be found by steady state conductivity measurements, [12], [13]. Since the presence of low temperature wavelike features is a relatively short time effect, [8], we are interested in pursuing steady state features further here.

The steady state condition is defined by $p_t = 0$ in (1.3), which gives

$$g_1(\vartheta)\vartheta_x = -g_2(\vartheta)p, \tag{1.8}$$

and the steady-state conductivity coefficient, $\mathcal{K}(\vartheta)$, is given by

$$q(\vartheta) = \Big(\frac{\psi_{20}\vartheta^2 g_1^2(\vartheta)}{g_2(\vartheta)}\Big)\vartheta_x = -\mathcal{K}(\vartheta)\vartheta_x. \tag{1.9}$$

We will make the following hypotheses concerning the constitutive functions, $g_1, g_2 \in C(\mathbb{R}^+)$,

$$-\infty < \lim_{\vartheta\to\vartheta-} \frac{g_1^2(\vartheta)}{g_2(\vartheta)} < 0 \quad \text{and} \quad g_i(\vartheta) = 0, \quad i = 1,2, \quad \vartheta \geq \vartheta_\lambda, \tag{1.10}$$

to allow the possibility of a conductivity peak for $\mathcal{K}(\vartheta)$ as $\vartheta \to \vartheta-$. Examples of g_1 and g_2 include

$$g_1(\vartheta) = a\vartheta^{\frac{1}{2}}(\vartheta - \vartheta)_+^{r_1}, \quad a > 0, \tag{1.11}$$

and

$$g_2(\vartheta) = -b(1 + \epsilon\vartheta^4)(\vartheta_\lambda - \vartheta)_+^{r_2}, \quad b > 0, \quad |\epsilon| << 1, \tag{1.12}$$

with $2r_1 = r_2 > 0$, where $z_+^r \equiv z^r H(z)$ and $H(z)$ denotes the step function.

Let us define the steady state conductivity, $K(\vartheta)$, for all temperatures, as

$$K(\vartheta) = \begin{cases} \mathcal{K}(\vartheta) & \text{if} \quad \vartheta < \vartheta_\lambda, \\ k(\vartheta) & \text{if} \quad \vartheta \geq \vartheta_\lambda. \end{cases} \tag{1.13}$$

Experimental observations reveal $K(\vartheta)$ to be continuous, in particular across $\vartheta = \vartheta_\lambda$, from which it follows $k(\vartheta_\lambda+) = \mathcal{K}(\vartheta_\lambda-)$. We will assume that $K'(\vartheta_\lambda) = 0$. Reasonable choices in (1.11), (1.12) are $r_1 = 1/5$ for NaF ($\vartheta_\lambda = 18.5K$), $r_1 = 1/4$ for Bi ($\vartheta_\lambda = 4K$), and $\epsilon = 3/\vartheta_\lambda^4$, with a useful empirical example of $K(\vartheta)$ given by

$$K_{\text{emp}}(\vartheta) = \frac{\psi_{20}a^2}{b}\frac{\vartheta^3}{1 + 3\vartheta^4/\vartheta_\lambda^4}. \tag{1.14}$$

The aim of this paper is to investigate some properties of phase transitions connecting the states U_- and U_+ under the steady state condition $p_t = 0$. Let Γ denote a curve $x = \varphi(t)$ in $\mathbb{R} \times \mathbb{R}^+$ separating the regions and consider the equations

$$\varepsilon(\vartheta)_t - (\mathcal{K}(\vartheta)\vartheta_x)_x = 0, \text{ in } U_- \tag{1.15}$$

and

$$\varepsilon(\vartheta)_t - (k(\vartheta)\vartheta_x)_x = 0, \text{ in } U_+. \tag{1.16}$$

Our interest in these equations comes from the jump in the specific heat, $c_v(\vartheta) = \varepsilon'(\vartheta)$, across Γ. We are unaware of observational indications for a latent heat contribution in the present context, but it is important that we allow the possibility of c_v becoming unbounded, at least locally, in U_-. Letting u be a generic function, we denote limits of u, as $x \to \varphi(t)$ from below and above ϑ_λ, by $u|_{\Gamma-}$ and $u|_{\Gamma+}$ respectively, and write the jump $u|_{\Gamma+} - u|_{\Gamma-}$ across Γ as $[u]$. This means that if $[\vartheta] = 0$ then $[\varepsilon] = 0$. We will however have a second order phase transition, $[c_v] \neq 0$, and to examine this we list some simple consequences.

Equation (1.1) implies the jump relation

$$-s[\varepsilon] + [q] = 0, \tag{1.17}$$

where $s = \dot{\varepsilon}(t)$.

If $[\vartheta] = 0$, then $[q] = 0$ and so $[K(\vartheta)\vartheta_x] = 0$. By the continuity of $K(\vartheta)$ then, assuming $k(\vartheta_\lambda) > 0$, $[\vartheta_x] = 0$, and so $[\vartheta_t] = 0$ because $[\vartheta] = 0$ implies $[\vartheta_t] + s[\vartheta_x] = 0$. Therefore

$$[\varepsilon_t] = [c_v]\vartheta_t|_\Gamma. \tag{1.18}$$

Similarly, $[\varepsilon_t] + s[\varepsilon_x] = 0$ because $[\varepsilon] = 0$. Combining this with the jump of Eq. (1.1), $[\varepsilon_t] + [q_x] = 0$, implies $[q_x] = s[\varepsilon_x]$ or

$$[q_x] = s[c_v]\vartheta_x|_\Gamma. \tag{1.19}$$

Since ϑ_λ is the temperature of maximum heat conductivity ($K'(\vartheta_\lambda) = 0$), (1.19) shows

$$[\vartheta_{xx}] = -\frac{s}{k(\vartheta_\lambda)}[c_v]\vartheta_x|_\Gamma. \tag{1.20}$$

If we more generally allow $[\vartheta] \neq 0$, we have from (1.17)

$$s[\varepsilon(\vartheta)] + [K(\vartheta)\vartheta_x] = 0. \tag{1.21}$$

An appropriate interpretation of (1.21) is important also when $[\vartheta] = [\varepsilon(\vartheta)] = 0$ but $[c_v]$ is undefined in (1.18). In this case s may be defined by computing the ratio of the jumps in (1.21) in terms of limits. For example, (1.21) implies that if one state, say $\vartheta_x|_{\Gamma+}$, is zero, then

$$s = k(\vartheta_\lambda) \lim_{\delta \to 0+} \frac{\vartheta_x(\varphi(t) - \delta, t)}{\varepsilon(\varphi(t) + \delta, t)) - \varepsilon(\vartheta(\varphi(t) - \delta, t))} \tag{1.22}$$

while if either state of ϑ_x is nonzero then in order for s to be finite, the solution must cross ϑ_λ.

We will examine several forms of discontinuity in c_v since it is hard to obtain empirical evidence to determine whether or not specific heat contains a genuine singularity at ϑ_λ. Our aim is to derive mathematical consequences of these assumptions.

In Sec. 2, we begin by considering the case of $[c_v]$ being finite, with c_v piecewise constant (a second order phase transition) and K constant, then allow c_v to become infinite within U_-. Section 3 deals with nonlinear constitutive laws having infinite, but locally integrable c_v ('lambda' phase transitions), following which we examine the speed of propagation of solutions with compactly supported data about $\vartheta = 0$ and $\vartheta = \vartheta_\lambda$.

2. Piecewise constant constitutive terms

In this section we examine the case $K(\vartheta) \equiv 1$. It is convenient to introduce the normalized temperature

$$T = \frac{\vartheta}{\vartheta_\lambda} - 1, \tag{2.1}$$

with equations (1.15) and (1.16) taking the form

$$T_t - \frac{1}{\tilde{c}_v} T_{xx} = 0, \tag{2.2}$$

where

$$\tilde{c}_v(T) = \begin{cases} c_-, & \text{if} \quad T < 0, \\ c_+, & \text{if} \quad T \geq 0, \end{cases} \tag{2.3}$$

and $c_- > c_+ > 0$. We take initial conditions

$$T(x,0) = \begin{cases} T_c, & \text{if} \quad x < 0, \\ T_h, & \text{if} \quad x \geq 0, \end{cases} \tag{2.4}$$

with $T_c \leq 0\,(\vartheta(x,0) \leq \vartheta_\lambda, x < 0)$ and $T_h \geq 0\,(\vartheta(x,0) \geq \vartheta_\lambda, x \geq 0)$, together with the conditions

$$T(\varphi(t),t) = 0, \quad [T_x(\varphi(t),t)] = 0, \quad [T_{xx}(\varphi(t),t)] = -s[\tilde{c}_v]T_x(\varphi(t),t), \tag{2.5}$$

(see (1.20).

2.1. Phase transitions

Consider similarity solutions of the form

$$T(x,t) = \begin{cases} f(\eta), & \text{if } (x,t) \in U_-, \\ g(\eta), & \text{if } (x,t) \in U_+, \end{cases} \tag{2.6}$$

where $\eta = \dfrac{x}{\sqrt{t}}$. Since $\left.\dfrac{dT}{dt}\right|_\Gamma = 0$, clearly

$$\varphi(t) = \gamma\sqrt{t}, \quad s = \frac{\gamma}{2\sqrt{t}} \tag{2.7}$$

for some value of γ.

We write (2.3), (2.4), (2.5) and (2.6) as

$$f''(\eta) + \frac{1}{2}c_- f'(\eta)\eta = 0, \quad -\infty < \eta < \gamma, \tag{2.8}$$

$$g''(\eta) + \frac{1}{2}c_+ g'(\eta)\eta = 0, \quad \gamma < \eta < \infty, \tag{2.9}$$

$$f(-\infty) = T_c, \quad g(\infty) = T_h, \quad f(\gamma) = g(\gamma) = 0, \quad f'(\gamma) = g'(\gamma), \tag{2.10}$$

$$f''(\gamma) - g''(\gamma) = -\frac{1}{2}\gamma f'(\gamma)(c_- - c_+). \tag{2.11}$$

Solving, we obtain

$$f(\eta) = T_c\left(1 - \frac{1 + erf(\sqrt{c}_-\eta/2)}{1 + erf(\sqrt{c}_-\gamma/2)}\right), \quad -\infty < \eta < \gamma, \tag{2.12}$$

and

$$g(\eta) = T_h\left(1 - \frac{1 - erf(\sqrt{c}_+\eta/2)}{1 - erf(\sqrt{c}_+\gamma/2)}\right), \quad \gamma < \eta < \infty, \tag{2.13}$$

where $erf(z) = \dfrac{2}{\sqrt{\pi}}\displaystyle\int_0^z \exp(-x^2)\,dx$. Consequently, the location of Γ is found via $(2.10)_4$,

$$-\sqrt{c}_- \frac{T_c}{1 + erf(\sqrt{c}_-\gamma/2)} e^{-c_-\gamma^2/4} = \sqrt{c}_+ \frac{T_h}{1 - erf(\sqrt{c}_+\gamma/2)} e^{-c_+\gamma^2/4} \tag{2.14}$$

from which, having used (2.7), (2.11) is identically satisfied. We remark on two limiting cases of (2.14).

a) If $T_c \to 0$ $(\vartheta(x,0) \to \vartheta_\lambda, x < 0)$ and $T_h > 0$, then $\gamma \to -\infty$.

b) If $T_h \to 0$ $(\vartheta(x,0) \to \vartheta_\lambda, x \geq 0)$ and $T_c < 0$, then $\gamma \to \infty$.

2.2. The unbounded limit

Now we examine the case $c_- \to \infty$, with c_+ constant, with $T_c < 0 < T_h$. Although this form of c_v is clearly not integrable, it is instructive to compare the features of the solutions to those in the following sections.

Rewriting (2.14) as

$$-\frac{T_c}{T_h}\frac{e^{-c_-\gamma^2/4}}{e^{-c_+\gamma^2/4}} = \frac{\sqrt{c}_+}{\sqrt{c}_-}\left(\frac{1+erf(\sqrt{c}_-\gamma/2)}{1-erf(\sqrt{c}_+\gamma/2)}\right) \tag{2.15}$$

it is easy to see that as $c_- \to \infty$, $c_-\gamma^2 \to \infty$ while $\gamma \to 0$, the phase transition becoming stationary. (A little further investigation shows that, asymptotically, $\gamma \sim \frac{2}{\sqrt{c}_-}\sqrt{\ln\sqrt{c}_- - \ln\left|\frac{2\sqrt{c}_+ T_h}{T_c}\right|}$.)

In particular, we observe from (2.12) that in the limit

$$f(\eta) = T_c, \quad -\infty < \eta < 0, \tag{2.16}$$

while (2.13) becomes

$$g(\eta) = T_h\, erf(\sqrt{c}_+\eta/2), \quad 0 < \eta < \infty. \tag{2.17}$$

Thus we obtain a jump of $[T] = -T_c$ across Γ. Noting that this limiting solution no longer satisfies $(2.10)_{2,3}$, we remark that it may be considered consistent with (1.21) in a sense provided $s = 0$, $[\epsilon]$ not being defined but the second term being finite by (2.16), (2.17).

3. Locally integrable specific heat

In this section, we employ nonlinear constitutive relations which allow analysis using similarity solutions. For this reason we will assume that, for ϑ in a neighbourhood of ϑ_λ, all functions can be represented in terms of the normalized temperature T (this will however not be assumed when we examine $\vartheta \to 0$ at the end of the final section). We will also assume that c_v is unbounded at, but locally integrable about $T = 0$, monotone increasing for $T < 0$ and monotone decreasing for $T > 0$. Since ϑ_λ is a maximum for the continuous function $K(\vartheta)$, $\tilde{K}(T) = K(\vartheta_\lambda(T+1))$ is similarly monotone increasing below, and monotone decreasing above $T = 0$. c_v and K are both considered to be positive for all

$\vartheta > 0$ and so ε and W, defined by $W'(T) = \tilde{K}(T), W(0) = 0$, are both invertible on their domain. Setting $\tilde{c}_v(T) = c_v(\vartheta_\lambda(T+1))$ we will, for simplicity, adopt the power law form $\tilde{c}_v(T) = c|T|^{-\nu}$, $c > 0$ with $0 < \nu < 1$ for $T \in (T_c, T_h)$, $-\delta < T_c \leq 0 \leq T_h < \delta$ and $\delta > 0$ sufficiently small. (1.13), (1.14), (1.16) may be rewritten as

$$\tilde{\varepsilon}(T)_t - W(T)_{xx} = 0. \tag{3.1}$$

Since $W(T) = w$ is an invertible function of T, (3.1) can similarly be rewritten in the form

$$e(w)_t - w_{xx} = 0, \tag{3.2}$$

where $e = \tilde{\varepsilon} \circ W^{-1}$. For simplicity, we now use the fact that $K(T) \approx K(0) \equiv 1$ (in normalized units) for $T_c \leq 0 \leq T_h$ and small δ, and employ the power law hypothesis to express (3.2) as

$$|w|^{-\nu} w_t - w_{xx} = 0, \quad 0 < \nu < 1, \tag{3.3}$$

where we have set $c = 1$ for convenience. (3.3) is a slow-diffusion porous medium equations ([2, 3, 7, 11]) as can be seen by substituting $w = (1-\nu)^{1/1-\nu}|e|^{\nu/1-\nu}e$, which gives

$$e_t - (1-\nu)^{\nu/1-\nu}(|e|^{\nu/1-\nu}e_x)_x = 0. \tag{3.4}$$

We will consider self-similar solutions to (3.3) of the form $w(x,t) = f(t)g(xh(t))$. Substituting into (3.3) and assuming $f(t) > 0, h(t) > 0, g = g(z)$ and $z = xh(t)$, implies that for certain constants λ, μ, we have

$$\lambda|g|^{-\nu}g + \mu|g|^{-\nu}g'z - g'' = 0, \tag{3.5}$$

where

$$\frac{\dot{f}}{f^{\nu+1}h^2} = \lambda, \quad \frac{\dot{h}}{f^\nu h^3} = \mu, \tag{3.6}$$

and up to a constant factor,

$$f(t) = h(t)^{\lambda/\mu}. \tag{3.7}$$

3.1. Examples of continuous solutions and blowup

First consider the case $\lambda = 0, f(t) = 1$. Equations (3.5), (3.6) then give

$$\mu|g(z)|^{-\nu}g'(z)z - g''(z) = 0, \quad \frac{dh(t)}{dt} = \mu h^3(t). \tag{3.8}$$

Considering monotone increasing solutions to $(3.8)_1$ of the form $g(z) = a|z|^{\beta-1}z$ with $a > 0$ gives $\mu \geq 0, a = (\mu/(\beta-1))^{1/\nu}$ and $\beta = 2/\nu$, where we take the particular solution $h(t) = (1-2\mu t)^{-1/2}$ for $(3.8)_2$ so that

$$g(xh(t)) = ax|x|^{2/\nu-1}(1-2\mu t)^{-1/\nu}, \quad 0 \leq t < 1/2\mu. \tag{3.9}$$

This allows us to construct two families of solutions, $w(x,t)$:

$$w_-(x,t) = \begin{cases} a_- \dfrac{x|x|^{2/\nu-1}}{(1-2\mu_- t)^{1/\nu}}, & x < 0, \\ 0, & x \geq 0, \end{cases} \tag{3.10}$$

$$w_+(x,t) = \begin{cases} 0, & x < 0, \\ a_+ \dfrac{x|x|^{2/\nu-1}}{(1-2\mu_+ t)^{1/\nu}}, & x \geq 0. \end{cases} \tag{3.11}$$

These (unbounded) solutions have a maximal time of existence, $t < 1/2\mu_\pm$, at which point they develop infinite jump discontinuities. Both satisfy $s = 0$, corresponding to (1.21) in the sense of (1.22). In view of the smallness of δ discussed above, this class of solution can only be considered as a first approximation to solutions of the full model since, as x leaves the vicinity of the origin, the solutions leave the region where $K \approx 1$.

Another class of solutions exists for the case $\mu = 0, h(t) = 1$, which is bounded. Here (3.5) and (3.6) become

$$\lambda|g(x)|^{-\nu}g(x) - g''(x) = 0, \quad \frac{df(t)}{dt} = \lambda f^{\nu+1}(t). \tag{3.12}$$

For $\lambda < 0, g(x)$ is periodic since the quantity $E = \frac{1}{2}g'^2 - \frac{\lambda}{2-\nu}|g|^{2-\nu}$ is a data-dependent constant in x. This delivers an x-periodic solution

$$w(x,t) = ag(x)(1-\nu a^\nu \lambda t)^{-1/\nu}, \tag{3.13}$$

where we can choose $0 < a = f(0) < \delta/E$ to meet the smallness requirement.

In the following, we will only consider solutions which are both a priori bounded and have compact support.

3.2. Finite and infinite speeds of propagation

An important motivation for introducing hyperbolicity into heat conduction models is that of finite speed of propagation. Since the linear heat equation violates this condition, one can attempt to correct the situation by more detailed modelling, for instance as sketched earlier. In the steady state regime under

consideration here, hyperbolic effects are no longer a feature and one might expect propagation speed to be infinite again. The fact that this is not entirely the case turns out to be a result of the discontinuity in c_v.

Consider again the selfsimilar solution $w(x,t) = f(t)g(xh(t))$ to (3.3), now with $\mu/\lambda = 1-\nu$. Equation (3.5) then gives

$$\lambda(|g|^{-\nu}gz)' = g'' \tag{3.14}$$

from which we have either $g(z) = 0$ or, specializing to $w(x,t)$ lying in $U_- \cup \{0\}$,

$$g(z) = -\nu^{1/\nu}(\frac{\lambda}{2}z^2 + b)^{1/\nu}, \quad b > 0, \tag{3.15}$$

where we choose $\lambda < 0$. Since (3.7) gives $f(t) = h(t)^{1/(1-\nu)}$, (3.6) can be solved to give

$$f(t) = ((2-\nu)(d-\lambda t))^{-\frac{1}{2-\nu}}, \quad d > 0, \tag{3.16}$$

and

$$h(t) = ((2-\nu)(d-\lambda t))^{-\frac{1-\nu}{2-\nu}}. \tag{3.17}$$

This implies

$$w(x,t) = \begin{cases} -f(t)\nu^{1/\nu}\Big(\frac{\lambda}{2}x^2h(t)^2 + b\Big)^{1/\nu}, & |x| < \Big|\frac{2b}{\lambda h^2(t)}\Big|^{1/2}, \\ 0, & |x| \geq \Big|\frac{2b}{\lambda h^2(t)}\Big|^{1/2}, \end{cases} \tag{3.18}$$

which is a compact support Barenblatt-Pattle solution. Thus, given an initial 'cold pulse' ($\vartheta(x,0) \leq \vartheta_\lambda$) coming directly below the temperature of the phase transition, with

$$w(x,0) = \begin{cases} -f(0)\nu^{1/\nu}\Big(\frac{\lambda}{2}x^2h(0)^2 + b\Big)^{1/\nu}, & |x| < \Big|\frac{2b}{\lambda h^2(0)}\Big|^{1/2}, \\ 0, & |x| \geq \Big|\frac{2b}{\lambda h^2(0)}\Big|^{1/2}, \end{cases} \tag{3.19}$$

we obtain an expanding cold region whose support about $\vartheta = \vartheta_\lambda$ never becomes unbounded.

Finally, for $\mu/\lambda = (1-\nu)/2$, we remark on a 'dipole' solution (cf. [3]) which changes sign once, going from cold to hot temperatures or vice-versa. Here $g(z) = 0$, or

$$g(z) = \pm(1-\nu)^{\frac{1}{1-\nu}}z(c - \frac{\nu}{2(2-\nu)}|z|^{2-\nu})^{1/\nu}, c > 0, \tag{3.20}$$

while

$$f(t) = (h(t))^{\frac{2}{1-\nu}} = (1-\lambda t)^{-1},\ \lambda = -(1-\nu)^{\frac{\nu}{1-\nu}}, \tag{3.21}$$

giving

$$w(x,t) = \begin{cases} \pm(1-\nu)^{\frac{1}{1-\nu}} x f(t) h(t) \Big(c - \dfrac{\nu}{2(2-\nu)} |x h(t)|^{2-\nu}\Big)^{1/\nu}, \\ \qquad\qquad |x| < \dfrac{(2c(2-\nu)/\nu)^{\frac{1}{2-\nu}}}{h(t)}, \\ 0, \qquad\qquad |x| \geq \dfrac{(2c(2-\nu)/\nu)^{\frac{1}{2-\nu}}}{h(t)}. \end{cases} \tag{3.22}$$

We have tried to capture finite speed of propagation as well as other features of the physics for temperatures below ϑ_λ, but we have been less motivated in doing so elsewhere due to the fact that wavelike features have only been observed clearly in this one region. We have however considered only a simple model here, for which we have taken c_v to be a symmetric function about ϑ_λ, which need not generally be the case. Consequently, the behaviour of the periodic and dipole solutions may be somewhat different to that which might be found experimentally. All of these results should be contrasted with the behaviour of solutions at temperatures well below ϑ_λ. If we consider similar (small) data to that in (3.19), except with a 'cold pulse' below $\vartheta = \vartheta_\lambda$ being replaced by a 'hot pulse' above $\vartheta = 0$, we may use, for example, the empirical form (1.14) to find that close to $\vartheta = 0, K(\vartheta) \approx \vartheta^3$, where we have dropped inessential constants. For many materials including those under consideration, Debye's law has, similarly, $c_v(\vartheta) \approx \vartheta^3$. Therefore, (1.15) takes the form

$$(\vartheta^4)_t - (\vartheta^4)_{xx} = 0, \tag{3.23}$$

a linear parabolic equation in $u = \vartheta^4$, with the usual infinite speed of propagation.

References

1. C. C. ACKERMAN, B. BERTMAN, H. A. FAIRBANK, and R. A. GUYER, *Second sound in solid helium*, Phys. Rev. Letters, **16**, 789–791, 1966.
2. M. BERTSCH, and D. HILHORST, *The interface between regions where $u < 0$ and $u > 0$ in the porous medium equation*, Appl. Anal., **41**, 111–130, 1991.
3. J. HULSHOF, *Similarity solutions of the porous medium equation with sign changes*, J. Math. Anal. App., **157**, 75–111, 1991.

4. H. E. JACKSON, C. T. WALKER, and T. F. MCNELLY, *Second sound in NaF*, Phys. Rev. Letters, **25**, 1, 26–28, 1970.

5. H. E. JACKSON, and C. T. WALKER, *Thermal conductivity, second sound, and phonon-phonon interactions in NaF*, Physical Review B, **3**, 4, 1428–1439, 1971.

6. W. KOSIŃSKI, K. SAXTON, and R. SAXTON *Second sound speed in a crystal of NaF at low temperature*, Arch. Mech., **49**, 1, 189–196, 1997.

7. A. A. LACEY, J. R. OCKENDON, and A. B. TAYLOR, *"Waiting-time" solutions of a nonlinear diffusion equation*, SIAM J. Appl. Math, **42**, 6, 1252–1264, 1982.

8. H. LI and K. SAXTON, *Large-asymptotic behaviour of solutions to quasilinear hyperbolic equations with nonlinear damping*, Q. App. Math., to appear.

9. T. F. MCNELLY,S. J. ROGERS, D. J. CHAMIN, R. J. ROLLEFSON, W. M. GOUBAU, G. E. SCHMIDT, J. A. KRUMHANSI, and R. O. POHL, *Heat pulses in NaF: onset of second sound*, Phys. Rev. Letters, **24**, 3, 100–102, 1970.

10. V. NARAYANAMURTI, and R. C. DYNES, *Observation of second sound in bismuth*, Phys. Rev. Letters, **28**, 22, 1461–1465, 1972.

11. S. SAKAGUCHI, *Regularity of the interfaces with sign changes of solutions of the one-dimensional porous medium equation*, J. Diff. Equations, **178**, 1–59, 2002.

12. K. SAXTON, R. SAXTON, and W. KOSIŃSKI, *On second sound at the critical temperature*, Q. App. Math., 57, 723–740, 1999.

13. K. SAXTON, and R. SAXTON, *Nonlinearity and memory effects in low temperature heat propagation*, Arch. Mech., 52, 127–142, 2000.

Received June 7, 2002, revised version September 11, 2002..

Arch. Mech., **54**, 5-6, pp. 647–661, Warszawa 2002

Planar frictional motion of highly elastic bodies

G. SZEFER

Institute of Structural Mechanics,
Cracow University of Technology, Poland,
e-mail: szefer@limba.wil.pk.edu.pl

Dedicated to Professor Piotr Perzyna
on the occasion of his 70^{th} birthday

THE PROBLEM OF MOTION of a beam-like elastic body along a horizontal plane in terms of friction, large displacements and finite strains will be considered. The equations of motion are derived using GIBBS-APPELL approach. Deformations of the body and sliding velocity distribution are presented.

1. Introduction

THE MAJORITY of problems considered in dynamics of flexible and movable objects have been solved by using the finite-dimensional approach (systems with finite number of degrees of freedom) and analytical mechanics methods. On the other hand, the strain and stress analysis of flexible elements is based on infinite-dimensional formalism of elastic and inelastic continua. Many flexible dynamical systems considered in structural mechanics, robotics, biomechanics etc. need application of both these descriptons.

In the present paper a problem of planar motion of a highly deformable elastic body resting on a flat, rough and rigid foundation will be considered. The body in form of a beam treated as a three-dimensional continuum (the dimensions of the body are assumed to be arbitrary, thus assumption of the beam theory are neglected) is loaded by its own weight and then, due to application of control torques, starts to move along the plane. We assume very large displacements (movable object) and finite strains (in-plane self-contact may occur). The problem under consideration corresponds to snake-like motion of biologically inspired manipulators. A simplification of this model in the form of a multilink lumped mass system was considered by CHERNOUSKO[1]. The planar contact of beams resting on a rough surface was discussed also by FISCHER and RAMMERSTORFER [2], NIKITIN [7][8], NIKITIN *et al.* [9], MOGILEVSKY and NIKITIN [6] and further by STUPKIEWICZ and MRÓZ [10].

The paper is organized as follows: we begin with a finite-dimensional description of continua using an analytical mechanics approach based on the GIBBS-

APPELL equations, rather seldom applied in continuum mechanics. This will be given in Sec. 2. Next, in Sec. 3, we pass to the statement and solution of the snake-like motion of the beam. Figures with deformations and sliding velocities illustrate the results of the paper.

2. GIBBS-APPELL equations for discretized continua

Consider a deformable body B which, under action of external body forces with density $\mathbf{b}$ and prescribed surface traction $\mathbf{p}_R$ starts to move from its reference configuration B_R, producing contact stresses $\mathbf{t}_C$. Assuming large displacements and finite strains let us denote by $\mathbf{u}(\mathbf{X},t)$ the displacement, its gradient by $\mathbf{H}(\mathbf{X},t)$, by $\mathbf{E}(\mathbf{X},t)$ the Green strain tensor and by $\mathbf{S}(\mathbf{X},t)$ the second Piola-Kirchhoff stress tensor. Here $\mathbf{X}$ and t stands for the particle and time instant, respectively. Assume that there is a common global reference system $\{OX^K\}$, $\{Ox^i\}$ i, K=1,2,3 for the material as well as for the spatial coordinates, respectively. Assume furthermore that, because of the complexity of the problem we want to pose and solve, a space discretization is preferred. Therefore let us express the function of motion $\mathbf{u}(X^K,t)$ approximatively in terms of generalized coordinates $q_\alpha(t)$, $\alpha = 1,2,...,N$ (being the nodal displacements in the Finite Element Technique or time dependent coefficient in series expansion) as follows [4, 5]:

$$\mathbf{u} = [u_K(\mathbf{X},t)] = \left[\sum_{\alpha=1}^{N} N_{K\alpha}(\mathbf{X})\, q_\alpha(t)\right] = \left[N_{K\alpha}\right]\left[q_\alpha\right] = \mathbf{Nq}, \tag{2.1}$$

where $N_{K\alpha}(\mathbf{X})$ are the shape or basic functions, respectively.

Thus, the necessary kinematical quantities of the displacement gradient $\mathbf{H}$ and strain tensor $\mathbf{E}$ are of the form:

$$\mathbf{H} = \nabla\mathbf{u} = [u_{K,L}] = [N_{K\alpha,L}]\,[q_\alpha] = \nabla\mathbf{N}\mathbf{q}, \quad \nabla\mathbf{N} = [N_{K\alpha,L}],$$

$$\mathbf{E} = [E_{KL}] = \frac{1}{2}\left[\mathbf{H} + \mathbf{H}^{\mathbf{T}} + \mathbf{H}^{\mathbf{T}}\mathbf{H}\right]$$

$$= \left[\frac{N_{K\alpha,L} + N_{L\alpha,K}}{2}\right]\,[q_\alpha] + \frac{1}{2}\,[N_{M\alpha,K}N_{M\beta,L}]\,[q_\alpha]\,[q_\beta].$$

To derive the equations of motion for a discretized continuum, the GIBBS-APPELL equations will be used [3].This approach, seldom used in continuum mechanics, is very well known and useful in analytical mechanics, especially in dynamics of nonholonomic systems. The derivation of equations of motion for discretized continua is very simple. Thus introducing the acceleration functional [3]

$$G(t) = \frac{1}{2}\int_{V_R} \rho_R\,(\ddot{\mathbf{u}})^2\, dV_R, \tag{2.2}$$

the principle of motion reads

$$\frac{\partial G}{\partial \ddot{q}_\alpha} = Q_\alpha \quad \alpha = 1,2,...,N, \tag{2.3}$$

where $Q_\alpha(\mathbf{q})$ denotes the generalized forces. For a discretized continuum these quantities take the form [12]

$$\mathbf{Q} = [Q_\alpha] = \int_{V_R} \rho_R \mathbf{b} \frac{\partial \mathbf{u}}{\partial \mathbf{q}} dV_R + \int_{S_R} \mathbf{p}_R \frac{\partial \mathbf{u}}{\partial \mathbf{q}} dS_R + \int_{\Gamma_C} \mathbf{t_C} \frac{\partial \mathbf{u}}{\partial \mathbf{q}} d\Gamma - \int_{V_R} \mathbf{S}(\mathbf{1}+\mathbf{H}) : \frac{\partial \mathbf{H}}{\partial \mathbf{q}} dV_R. \tag{2.4}$$

Here is

V_R – the volume domain of the body in B_R

S_R – the boundary surface

Γ_C – the contact zone.

The left-hand side of (2.3) gives

$$\frac{\partial G}{\partial \ddot{\mathbf{q}}} = \int_{V_R} \rho_R \ddot{\mathbf{u}} \frac{\partial \ddot{\mathbf{u}}}{\partial \mathbf{q}} dV_R = \int_{V_R} \rho_R \mathbf{N}\mathbf{N}^{\mathbf{T}} dV_R \ddot{\mathbf{q}} = \mathbf{M}\ddot{\mathbf{q}} \tag{2.5}$$

where $\mathbf{M} = \int_{V_R} \rho_R \mathbf{N}\mathbf{N}^{\mathbf{T}} dV_R$ – the positive definite mass matrix. Introducing then (2.1) into the right-hand side of (2.3) and denoting by

$$\mathbf{F}^{\mathbf{ext}}(t) = \int_{V_R} \rho_R \mathbf{b} \frac{\partial \mathbf{u}}{\partial \mathbf{q}} dV_R + \int_{S_R} \mathbf{p}_R \frac{\partial \mathbf{u}}{\partial \mathbf{q}} dS_R = \int_{V_R} \mathbf{N}\mathbf{b} dV_R + \int_{S_R} \mathbf{N}\mathbf{p}_R dS_R \tag{2.6}$$

– the external force vector,

$$\mathbf{F_C}(t) = \int_{\Gamma_C} \mathbf{t}_C \frac{\partial \mathbf{u}}{\partial \mathbf{q}} \Gamma$$

– the contact force vector

one obtains a nonlinear equation

$$\mathbf{M}\ddot{\mathbf{q}} = \mathbf{F}^{\mathbf{ext}}(t) + \mathbf{F_C}(t) - \int_{V_R} \mathbf{S}(\mathbf{1}+\mathbf{H}) : \nabla \mathbf{N} dV_R. \tag{2.7}$$

The integral term is nonlinear even if the material is linear elastic. Therefore to omit computational difficulties, the incremental approach will be introduced. Thus considering the sequence of configurations $B_0 = B_R, B_1, ..., B_N, B_{N+1}, B_t = B_M$ which correspond to partition of the prescribed loads

$$\mathbf{b}_{N+1}=\mathbf{b}_N+\Delta\mathbf{b},\quad \mathbf{p}_R^{N+1}=\mathbf{p}_R^N+\Delta\mathbf{p}_R,\quad N=0,1,...,M,$$

one obtains

$$\mathbf{u}_{N+1}=\mathbf{u}_N+\Delta\mathbf{u},\quad \Delta\mathbf{u}=\mathbf{N}\Delta\mathbf{q},\quad \mathbf{H}_{N+1}=\mathbf{H}_N+\Delta\mathbf{H},\quad \Delta\mathbf{H}=\nabla\mathbf{N}\Delta\mathbf{q},$$

$$\begin{aligned}
&\mathbf{E}^{N+1}=\mathbf{E}^N+\Delta\mathbf{E},\quad \Delta\mathbf{E}=\frac{1}{2}\left(\Delta\mathbf{H}+\Delta\mathbf{H}^T+\mathbf{H}^T\Delta\mathbf{H}+\Delta\mathbf{H}^T\mathbf{H}\right),\\
&\mathbf{S}^{N+1}=\mathbf{S}^N+\Delta\mathbf{S},\quad \Delta\mathbf{S}=\mathbf{C}\Delta\mathbf{E},\\
&\mathbf{t}_C^{N+1}=\mathbf{t}_C^N+\Delta\mathbf{t}_C.
\end{aligned}\tag{2.8}$$

Writing (2.7) for the configuration B_{N+1} and using formula (2.8) we obtain

$$\mathbf{M}\Delta\ddot{\mathbf{q}}=\Delta\mathbf{F}^{\mathbf{ext}}+\Delta\mathbf{F}_{\mathbf{C}}-\int_{V_R}\left[\Delta\mathbf{S}\left(\mathbf{1}+\mathbf{H}\right)+\mathbf{S}\Delta\mathbf{H}\right]:\nabla\mathbf{N}\mathbf{d}\mathbf{V}_R.\tag{2.9}$$

To compute the integral it is worth to note that all the terms after simple calculations lead to a symmetric matrix. This fact results immediately when we decompose the matrices $\nabla\mathbf{N}$ and $\mathbf{H}$ into their symmetric and skew-symetric parts, and when we use the known result that the product of symmetric and skew-symmetric matrices is equal to zero. Thus, considering the respective members by using (2.8) it will be:

$$\Delta\mathbf{S}\cdot\mathbf{1}:\nabla\mathbf{N}=[C_{KLMN}]\left[\frac{N_{M\alpha,N}+N_{N\alpha,M}}{2}+\frac{N_{R\alpha,M}N_{R\gamma,N}+N_{R\gamma,M}N_{R\alpha,N}}{2}\right].$$

$$\begin{aligned}
[\Delta q_\alpha]\,[N_{K\beta,L}]&=[C_{KLMN}]\left[B^0_{MN\alpha}+B^1_{MN\alpha\gamma}q_\gamma\right][\Delta q_\alpha]\left[B^0_{KL\beta}\right]\\
&=\mathbf{B^0CB^0}\Delta\mathbf{q}+\mathbf{B^0C}\left(\mathbf{B^1q}\right)\Delta\mathbf{q}.
\end{aligned}$$

Here for simplicity the symmetric matrices

$$\begin{aligned}
&\mathbf{B^0}=\left[B^0_{MN\alpha}\right]=\left[\frac{N_{M\alpha,N}+N_{N\alpha,M}}{2}\right],\\
&\mathbf{B^1}=\left[B^1_{MN\alpha\gamma}\right]=\left[\frac{N_{R\alpha,M}N_{R\gamma,N}+N_{R\gamma,M}N_{R\alpha,N}}{2}\right],
\end{aligned}\tag{2.10}$$

have been introduced. It is next

$$\begin{aligned}
\Delta\mathbf{S}\cdot\mathbf{H}:\nabla\mathbf{N}&=[C_{KLMN}]\left[B^0_{MN\alpha}+B^1_{MN\alpha\gamma}q_\gamma\right][\Delta q_\alpha][N_{i\delta,K}][q_\delta][N_{i\beta,L}]\\
&=\mathbf{B^0CB^0}\left(\mathbf{B^0q}\right)\Delta\mathbf{q}+\mathbf{B^0C}\left(\mathbf{B^1q}\right)\left(\mathbf{B^0q}\right)\Delta\mathbf{q},
\end{aligned}$$

$$\mathbf{S}\Delta\mathbf{H} : \nabla\mathbf{N} = \mathbf{S}\nabla\mathbf{N}\Delta\mathbf{q}\nabla\mathbf{N} = [S_{KL}]\ \ [N_{i\alpha,K}]\ \ [\Delta q_\alpha]\ \ [N_{i\beta,L}] = \mathbf{B}^0\mathbf{S}\mathbf{B}^0\Delta\mathbf{q}.$$

Finally, the integral yields

$$\int_{V_R} [\Delta\mathbf{S}\,(\mathbf{1}+\mathbf{H}) + \mathbf{S}\Delta\mathbf{H}] : \nabla\mathbf{N} dV_R = \int_{V_R} [\mathbf{B}^0\mathbf{C}\mathbf{B}^0 + \mathbf{B}^0\mathbf{C}\,(\mathbf{B}^1\mathbf{q}) + \mathbf{B}^0\mathbf{C}\mathbf{B}^0\,(\mathbf{B}^0\mathbf{q}) + \mathbf{B}^0\mathbf{C}\,(\mathbf{B}^1\mathbf{q})\,(\mathbf{B}^0\mathbf{q}) + \mathbf{B}^0\mathbf{S}\mathbf{B}^0]\, dV_R\Delta\mathbf{q}.$$

Denoting the matrices

$$\mathbf{K} = \int_{V_R} \mathbf{B}^0\mathbf{C}\mathbf{B}^0 dV_R = [K_{\alpha\beta}] = \int_{V_R} [B^0_{KL\beta}]\ \ [C_{KLMN}]\ \ [B^0_{MN\alpha}]\, dV_R,$$

$$\mathbf{K_{NL}}\,(\mathbf{q}) = \int_{V_R} [\mathbf{B}^0\mathbf{C}\,(\mathbf{B}^1\mathbf{q}) + \mathbf{B}^0\mathbf{C}\mathbf{B}^0\,(\mathbf{B}^0\mathbf{q}) + \mathbf{B}^0\mathbf{C}\,(\mathbf{B}^1\mathbf{q})\,(\mathbf{B}^0\mathbf{q})]\, dV_R$$

$$= [K^{NL}_{\alpha\beta}]$$

$$(2.11) \qquad = \int_{V_R} \Big\{ [B^0_{KL\beta}]\,[C_{KLMN}]\,[B^1_{MN\alpha\gamma}]\,[q_\gamma] + [B^0_{MN\alpha}]\,[C_{KLMN}]\ \ [B^0_{SK\gamma}]\,[q_\gamma]\,[B^0_{SL\beta}] + [B^0_{SL\alpha}]\,[C_{KLMN}]\,[B^1_{MN\beta\gamma}]\,[B^0_{SK\delta}]\,[q_\gamma]\,[q_\delta] \Big\} dV_R,$$

$$\mathbf{K_S}\,(\mathbf{q}) = \int_{V_R} \mathbf{B}^0\mathbf{S}\,(\mathbf{q})\,\mathbf{B}^0 dV_R = [K^S_{\alpha\beta}] = \int_{V_R} [B^0_{MK\alpha}]\ \ [S_{KL}]\ \ [B^0_{ML\beta}]\, dV_R$$

we obtain finally the equation of motion

$$(2.12) \qquad \mathbf{M}\Delta\ddot{\mathbf{q}} + (\mathbf{K} + \mathbf{K}_{NL} + \mathbf{K}_S)\,\Delta\mathbf{q} = \Delta\mathbf{F}^{\mathbf{ext}} + \Delta\mathbf{F}_C,$$

which coincides with the form obtained by other methods, e.g. by means of the virtual work principle or by using the Lagrangian equations of second kind. In our opinion, the method based on the GIBBS-APPELL equations seems to be especially preferred in case of very complex systems, e.g. systems composed of rods, beams, plates or shells and three-dimensional blocks. The contact term $\Delta\mathbf{F}_C$ (following $(2.6)_2$) requires separate and careful considerations. This will be the subject of the next section.

3. Snake-like motion of a beam

The following problem is under consideration: a highly elastic beam-like body with density ρ_R in the reference configuration, rests on a fixed, rough and rigid plane (Fig.1). Due to in-plane torques $M_1(t)$ and $M_2(t)$ applied to the beam, the body starts to move. Since the dead weight presses the beam onto the rough surface, planar friction occurs. As mentioned in the introduction, a multilink lumped mass system in snake-like motion was considered by CHERNOUSKO [1]. A continuous highly-elastic description (also in discretized version) in terms of large displacements and finite strains is still open. The aim of this chapter is to fill this gap and to show, that by using suitable torques such kind of motion of beam is possible. To realize the motion of the beam in a demanded direction (e.g. a longitudinal or lateral motion of the centre of mass), a control problem must be stated. This will be the subject of a separate paper.

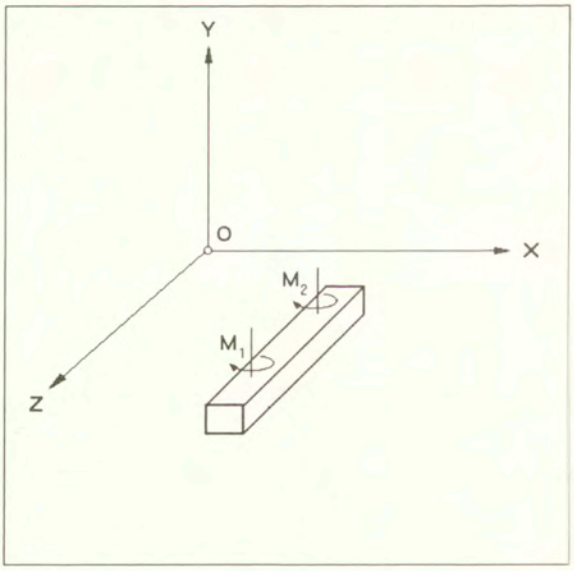

FIG. 1. Scheme of the beam

Consider the contact stress vector $\mathbf{t}_C$. Decomposing it into the sum of normal and tangential components we obtain

$$\mathbf{t}_C = t_n\mathbf{n} + \mathbf{t}_T = t_n\mathbf{n} - \mu t_n \mathbf{e}_T, \quad \mathbf{e}_T = \frac{\dot{\mathbf{u}}_T}{|\dot{\mathbf{u}}_T|}, \tag{3.1}$$

where

$\mathbf{n}$ – the outward unit vector, normal to the plane,
μ – the friction coefficient,
$\dot{\mathbf{u}}_T$ – the sliding velocity.

The contact force $(2.6)_2$ takes the form

$$\mathbf{F_C} = \int_{\Gamma_C} t_n \frac{\partial u_n}{\partial \mathbf{q}} d\Gamma + \int_{\Gamma_C} \mathbf{t_T} \frac{\partial \mathbf{u_T}}{\partial \mathbf{q}} d\Gamma.$$

Here the notations are used

$$u_n = \mathbf{un} = \mathbf{Nqn} = N_{\mathrm{i}\alpha} q_\alpha n_i,$$

$$\mathbf{u}_T = \mathbf{u} - u_n \mathbf{n} = (\mathbf{1} - \mathbf{n} \otimes \mathbf{n})\, \mathbf{u} = [\delta_{ij} - n_i n_j]\, \mathbf{u}, \tag{3.2}$$

$$= \left[P_{\mathrm{ij}} N_{i\alpha} q_\alpha\right] = \mathbf{Pu} = \mathbf{PNq},$$

where $\mathbf{P}=\mathbf{1}-\mathbf{n}\otimes\mathbf{n}$ is the second order projection tensor which maps any vector $\mathbf{u}$ onto its projection on the plane. Thus it will be further

$$\mathbf{F}_C = \int_{\Gamma_C} t_n \mathbf{N}\mathbf{n} d\Gamma + \int_{\Gamma_C} \mathbf{P}\mathbf{N}\mathbf{t}_T d\Gamma. \tag{3.3}$$

The corresponding increments take the form

$$\Delta \mathbf{F}_C = \int_{\Gamma_C} \Delta t_n \mathbf{N}\mathbf{n} d\Gamma + \int_{\Gamma_C} \mathbf{P}\mathbf{N}\Delta\mathbf{t}_T d\Gamma, \tag{3.4}$$

$$\Delta \mathbf{t}_T = \Delta\left(-\mu t_n \mathbf{e}_T\right) = \Delta\left(-\mu t_n \mathbf{\Phi}_\varepsilon\right) = -\mu \Delta t_n \mathbf{\Phi}_\varepsilon - \mu t_n \Delta \mathbf{\Phi}_\varepsilon,$$

where for computational reasons, the regulatization of the friction law by using the function

$$\mathbf{\Phi}_\varepsilon\left(\dot{\mathbf{u}}_T\right) = \begin{cases} \dfrac{\dot{\mathbf{u}}_T}{\varepsilon} = \dfrac{1}{\varepsilon}\mathbf{P}\mathbf{N}\dot{\mathbf{q}} & |\dot{\mathbf{u}}_T| \leq \varepsilon \\ \mathbf{e}_T & |\dot{\mathbf{u}}_T| > \varepsilon \end{cases} \tag{3.5}$$

has been introduced. Symbol ε denotes a positive, sufficiently small number. Hence

$$\Delta\mathbf{\Phi}_\varepsilon = \begin{cases} \dfrac{\Delta\dot{\mathbf{u}}_T}{\varepsilon} = \dfrac{1}{\varepsilon}\mathbf{P}\mathbf{N}\Delta\dot{\mathbf{q}} & |\dot{\mathbf{u}}_T| \leq \varepsilon \\ \Delta\mathbf{e}_T & |\dot{\mathbf{u}}_T| > \varepsilon \end{cases} \tag{3.6}$$

where from $(3.1)_2$ it follows that

$$\Delta \mathbf{e}_T = \Delta\left(\frac{\dot{\mathbf{u}}_T}{|\dot{\mathbf{u}}_T|}\right) = \frac{\Delta\dot{\mathbf{u}}_T\,|\dot{\mathbf{u}}_T| - \dot{\mathbf{u}}_T\,|\Delta\dot{\mathbf{u}}_T|}{\dot{\mathbf{u}}_T^2}$$

$$= \frac{\Delta\dot{\mathbf{u}}_T}{|\dot{\mathbf{u}}_T|} - \frac{\dot{\mathbf{u}}_T}{|\dot{\mathbf{u}}_T|^2}\frac{\Delta\dot{\mathbf{u}}_T\Delta\dot{\mathbf{u}}_T}{|\dot{\mathbf{u}}_T|} = \frac{\Delta\dot{\mathbf{u}}_T}{|\dot{\mathbf{u}}_T|} - \dot{\mathbf{u}}_T\frac{\mathbf{e}_T\Delta\dot{\mathbf{u}}_T}{|\dot{\mathbf{u}}_T|^2} = (\mathbf{1} - \mathbf{e}_T \otimes \mathbf{e}_T)\frac{\Delta\dot{\mathbf{u}}_T}{|\dot{\mathbf{u}}_T|}.$$

The first term of $\Delta\mathbf{e}_T$ demonstrates the local change of the sliding velocity, whereas the second one shows the change of its direction.

Taking (2.1) into account it is generally

$$\dot{\mathbf{u}}_T = \mathbf{PN}\dot{\mathbf{q}}, \qquad \Delta\dot{\mathbf{u}}_T = \mathbf{PN}\Delta\dot{\mathbf{q}},$$

$$|\dot{\mathbf{u}}_T| = \sqrt{\mathbf{PN}\dot{\mathbf{q}}\cdot\mathbf{PN}\dot{\mathbf{q}}}, \qquad \mathbf{e_T} = \frac{\mathbf{PN}\dot{\mathbf{q}}}{\sqrt{\mathbf{PN}\dot{\mathbf{q}}\cdot\mathbf{PN}\dot{\mathbf{q}}}},$$

and then

$$(3.7)\qquad \Delta\mathbf{e}_T = \frac{1}{|\dot{\mathbf{u}}_T|}[\mathbf{1} - \mathbf{e}_T \otimes \mathbf{e}_T]\,\mathbf{PN}\Delta\dot{\mathbf{q}} = \frac{1}{|\dot{\mathbf{u}}_T|}[\delta_{ik} - e_{Ti}e_{Tk}]\,P_{kj}N_{j\alpha}\Delta\dot{q}_\alpha.$$

Thus finally the regularization function Φ_ε and its increment $\Delta\Phi_\varepsilon$ yields

$$(3.8)\qquad \mathbf{\Phi}_\varepsilon(\dot{\mathbf{q}}) = \mathbf{PN}\dot{\mathbf{q}}\phi_\varepsilon \quad \text{where} \quad \phi_\varepsilon = \begin{cases} \dfrac{1}{\varepsilon} & |\dot{\mathbf{u}}_T| \le \varepsilon, \\ \dfrac{1}{|\dot{\mathbf{u}}_T|} & |\dot{\mathbf{u}}_T| > \varepsilon, \end{cases}$$

$$(3.9)\qquad \Delta\mathbf{\Phi}_\varepsilon(\Delta\dot{\mathbf{q}}) = \mathbf{PN}\Delta\dot{\mathbf{q}}\psi_\varepsilon \quad \text{where} \quad \psi_\varepsilon = \begin{cases} \dfrac{1}{\varepsilon} & |\dot{\mathbf{u}}_T| \le \varepsilon, \\ \dfrac{1}{|\dot{\mathbf{u}}_T|} - \dot{\mathbf{u}}_T\dfrac{\mathbf{e}_T}{|\dot{\mathbf{u}}_T|^2} & |\dot{\mathbf{u}}_T| > \varepsilon. \end{cases}$$

Substituting these expressions into (3.4) we obtain finally the increment of the contact force

$$(3.10)\qquad \Delta\mathbf{F}_C = \int_{\Gamma_C}\Big[\Delta t_n\mathbf{Nn} - \mathbf{PN}\left(\mu\Delta t_n\phi_\varepsilon\mathbf{PN}\dot{\mathbf{q}} + \mu t_n\psi_\varepsilon\mathbf{PN}\Delta\dot{\mathbf{q}}\right)\Big]d\Gamma.$$

Introducing now the matrices

$$\Delta \mathbf{F_n} = \int_{\Gamma_C} \Delta t_n \mathbf{N} \mathbf{n} d\Gamma = \int_{\Gamma_C} \Delta t_n N_{i\beta} n_i d\Gamma,$$

$$\Delta \mathbf{F_{nT}} = \mu \phi_\varepsilon \int_{\Gamma_C} \Delta t_n \mathbf{P} \mathbf{N} (\mathbf{P} \mathbf{N} \dot{\mathbf{q}}) \, d\Gamma = \mu \phi_\varepsilon \int_{\Gamma_C} \Delta t_n P_{ik} N_{k\alpha} P_{ij} N_{j\beta} \dot{q}_\beta d\Gamma, \tag{3.11}$$

$$\mathbf{K_T} = \mu \psi_\varepsilon \int_{\Gamma_C} t_n \mathbf{P} \mathbf{N} (\mathbf{P} \mathbf{N}) \, d\Gamma \Delta \dot{\mathbf{q}} = \mu \psi_\varepsilon \int_{\Gamma_C} t_n P_{ik} P_{ij} N_k \alpha N_{j\beta} d\Gamma \Delta \dot{q}_\beta,$$

and substituting it into (3.10) and next into (2.12), one obtains the final form of the incremental equation

$$\mathbf{M} \Delta \ddot{\mathbf{q}} + \mathbf{K}_T \Delta \dot{\mathbf{q}} + (\mathbf{K} + \mathbf{K}_{NL} + \mathbf{K}_S) \Delta \mathbf{q} = \Delta \mathbf{F}^{\mathrm{ext}} + \Delta \mathbf{F}_n + \Delta \mathbf{F}_{nT} \tag{3.12}$$

It is worth making the following remarks:

- In the case of planar motion along a flat and fixed foundation it is $\mathbf{P}\dot{\mathbf{u}} = \dot{\mathbf{u}}$ for any $\dot{\mathbf{u}}$. Hence the increment (3.7) yields
  $\Delta \mathbf{e}_T = \frac{1}{|\dot{\mathbf{u}}_T|} [\mathbf{1} - \mathbf{e}_T \otimes \mathbf{e}_T] \Delta \dot{\mathbf{u}} = \frac{1}{|\dot{\mathbf{u}}_T|} [\delta_{ij} - e_{Ti} e_{Tj}] N_{j\alpha} \Delta \dot{q}_\alpha, \quad i, j = 1, 2.$
- In our case the contact area Γ_C is known
- The normal contact stresses t_n resulting from the own weight of the beam are known and are equal to $\rho \mathbf{g}$ – where $\mathbf{g}$ means the gravity acceleration. Thus Δt_n is also known and is distributed uniformly
- In a general case the increments $\Delta t_n = \Delta(\mathbf{Tnn}) = \Delta(\mathbf{T}{:}\mathbf{n}\otimes\mathbf{n})$ (where $\mathbf{T}$ is the Cauchy stress tensor) are unknown and depend on $\Delta \mathbf{q}$. Thus instead of the column matrices $\Delta \mathbf{F}_n$ and $\Delta \mathbf{F}_{nT}$ suitable matrices $\mathbf{K}_{CN}$ and $\mathbf{K}_{nT}$ appears, being additional terms of the stiffness matrix. The matrix $\mathbf{K}_{nT}$ is then non-symmetric (see [11]). These circumstances should be taken into account when the beam has dimensions of a slab or of a block.
- Because the only loads applied to the beam consist of normal pressure and in-plane torques producing lateral in-plane bending with planar friction (sliding along the axis of the beam is excluded) – a loss of contact does not appear. It means that the body moves in terms of bilateral contact with the plane.

To illustrate the behaviour of the considered system, numerical examples for a linear elastic isotropic material with the following data are presented (numerical calculations were performed by M. Sci. D. Kedzior of the Institute of Structural Mechanics, CUT): ρ_R=1.7*10^{3}kg/m^3, Young's modulus E=1.7*10^{8}N/m^2, ν=0.48, coefficient of friction μ=1.0, cross-section of the beam $b \times h = 0.005 \times 0.005$m and its length l=0.1m. The torques M_1 and M_2 are modelled as couple

forces with a time program given in Fig. 2. The respective deformation pictures at considered time instants are shown in Fig. 3. Figure 4 shows lateral displacement of the centre of mass of the beam whereas Fig. 5 illustrates its longitudinal motion (in z direction). The diagram u_z versus u_x presented in Fig. 6 illustrates the trajectory of the mass centre. The second example concerns the case $M_1 = M_2$ with the time program given in Fig. 7. The corresponding deformation pictures with visible snake-like character of motion are given in Figs. 8 and 9.

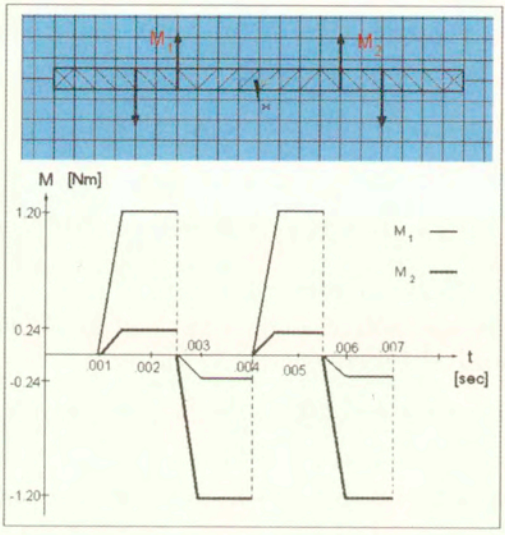

FIG. 2. Time Program I of the applied torques.

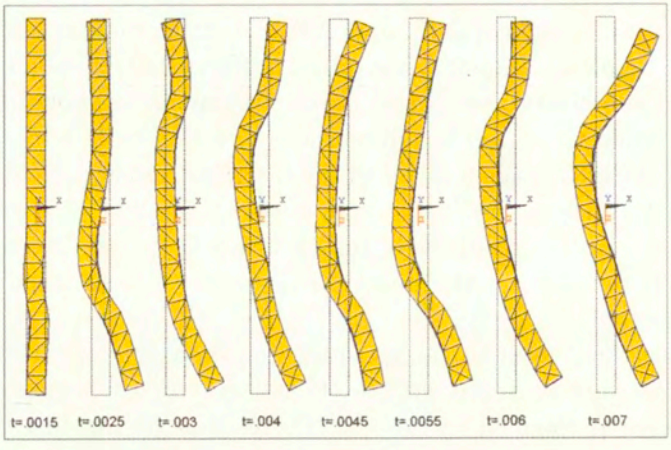

FIG. 3. Deformations caused by Program I.

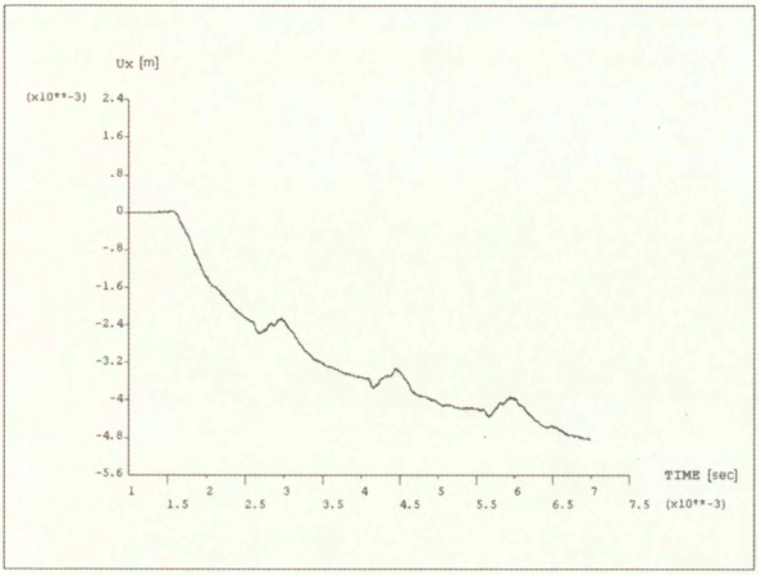

FIG. 4. Lateral displacement of the centre of mass.

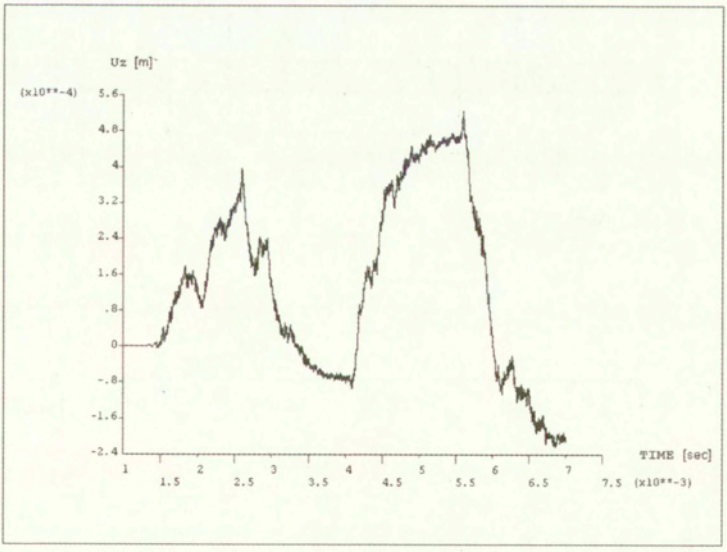

FIG. 5. Longitudinal displacement of the centre of mass.

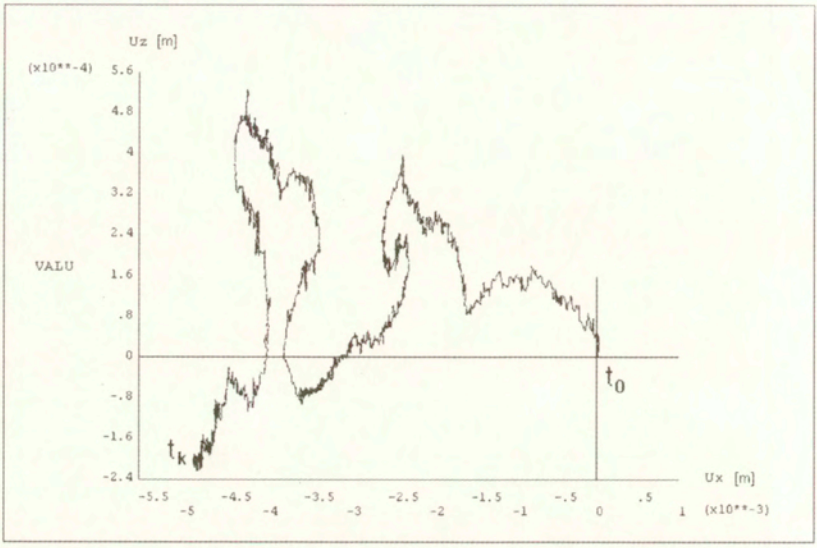

FIG. 6. Trajectory of the centre of mass.

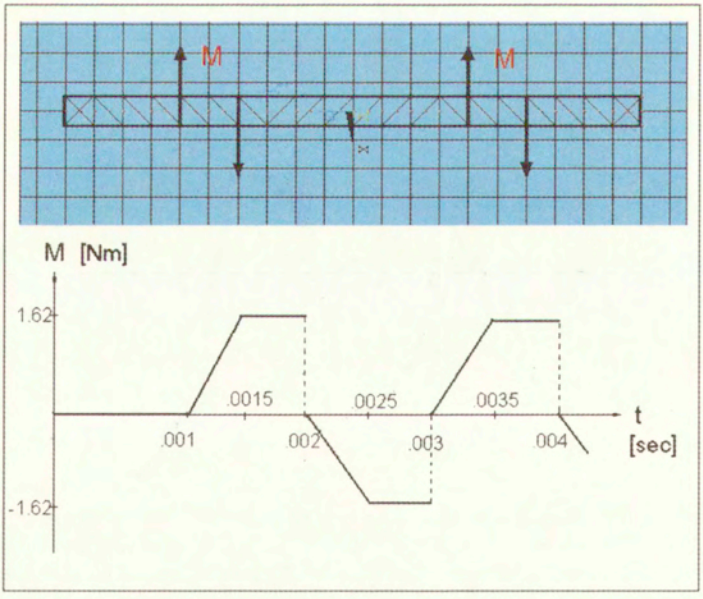

FIG. 7. Time Program II of the torques.

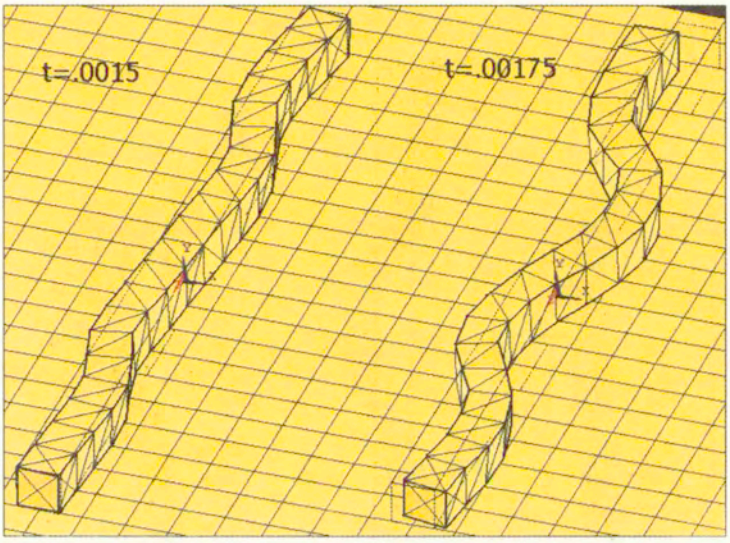

FIG. 8. Deformations caused by Program II.

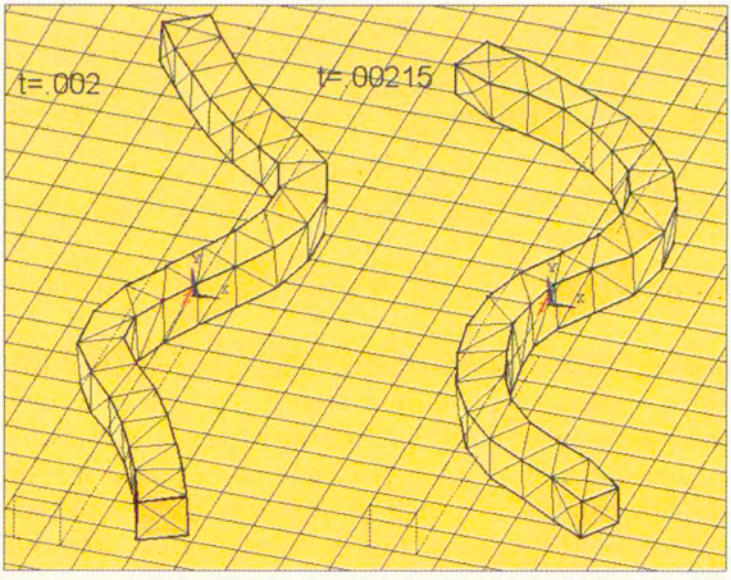

FIG. 9. Deformations caused by Program II.

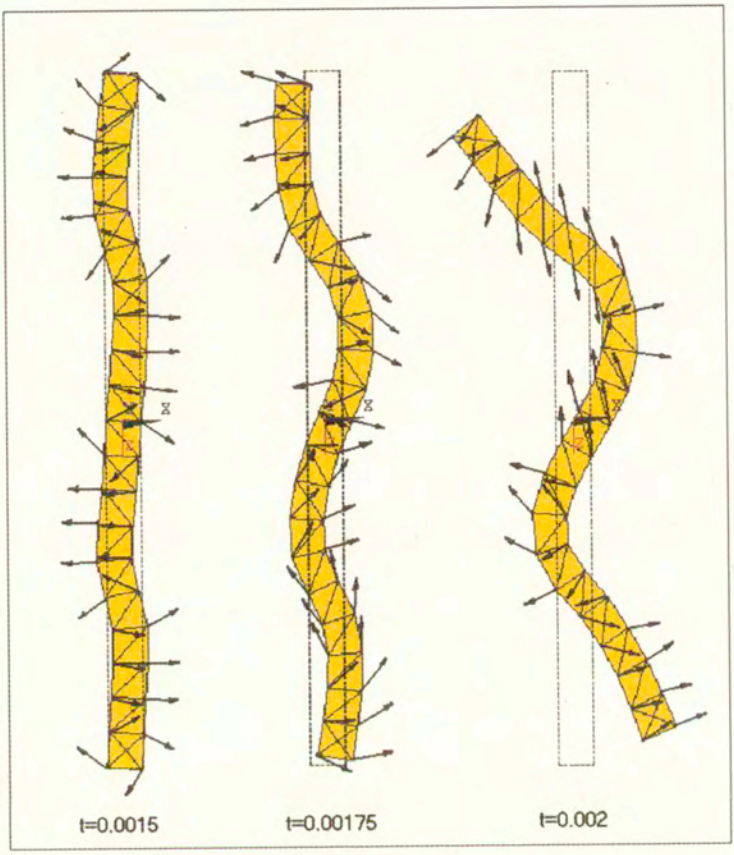

FIG. 10. Sliding velocities for Program II.

4. Conclusions

Equations of motion of a discretized continuum by using the GIBBS-APPELL formalism of analytical mechanics has been derived. As one can see, this proposal is one of the simplest ways to construct equations of motion of discretized continua. A dynamic problem of motion in terms of planar friction was considered. It has been shown that, owing to friction, a high elastic beam can move along a plane under the action of programmable torques perpendicular to the plane of motion. The Figs. 4-6 show the movement of the centre of mass. This kind of motion of the body undergoing in-plane bending and being all the time in contact with the plane, enables us to find such a programme of the control torques, that the centre of mass of the body will be moved in a given direction. Thus an optimal control problem can be formulated.

References

1. F.L.CHERNOUSKO, *The motion of a multilink system along a horizontal plane*, J. Appl. Math. Mech. **64**, 1, 5-15, 2000.
2. F. FISCHER, F. RAMMERSTORFER, *The thermally loaded heavy beam on a rough surface*, Trends in Appl. of Mathem. to Mech. W. SCHNEIDER, H. TROGER, F. ZIEGLER, [Eds.] Longman Higher Educ. Burnt Mill, 10-21, 1991.
3. R. GUTOWSKI, *Analytical Mechanics* [in Polish] PWN, Warsaw 1971.
4. M.KLEIBER, *Technical Mechanics. Computer methods in mechanics of solids* [Ed.], [in Polish], PWN, Warsaw 1995.
5. M. KLEIBER, H. ANTUNEZ, T. HIEN, P. KOWALCZYK, *Parameter Sensitivity in Nonlinear Mechanics*, J.Wiley&Sons, Chichester 1997.
6. R. MOGILEVSKY, L. NIKITIN, *In-plane bending of a beam resting on a rigid rough foundation*, Ing. Arch. **67**, 535-542, 1997.
7. L. NIKITIN, *Bending of a beam on a rough surface* [in Russian], Dokl. Russ. Ac. Sci. **322**, 1057-1061 1992.
8. L. NIKITIN, *Statics and dynamics of solids with dry friction* [in Russian], Moskovskii Licei p. 272, 1998.
9. L. NIKITIN, F. FISCHER, E. OBERAIGNER, F. RAMMERSTORFER, M. SIETZBERGER, R. MOGILEVSKY, *On the frictional behaviour of the thermally loaded beams resting on a plane*, Int. J. Mech. Sci. **38**, 11, 1219-1229, 1996.
10. S. STUPKIEWICZ, Z. MRÓZ, *Elastic beam on a rigid frictional foundation under monotonic and cyclic loading*, Int. J. Sol. Struct. **31**, 24, 3419-3442, 1994.
11. G. SZEFER, D. JASIŃSKA, *Dynamic analysis of large deformation contact of elastic bodies*, J. Theor. Appl. Mech. **1**, 40, 235-257, 2002.
12. C. WOŹNIAK, *Foundation of dynamics of deformable bodies* [in Polish], PWN, Warsaw 1969.

Received June 17, 2002; revised version August 6, 2002.

Arch. Mech., **54**, 5-6, pp. 663–690, Warszawa 2002

Extremum principles for nonpotential and initial-value problems

J. J. TELEGA

Institute of Fundamental Technological Research,
Polish Academy of Sciences,
Świętokrzyska 21, 00-049 Warsaw, Poland
e-mail: jtelega@ippt.gov.pl

Dedicated to Professor Piotr Perzyna
on the occasion of his 70^{th} birthday

THE AIM of this paper is to derive extremum and saddle-point principles for a class of nonpotential and initial-value problems.The procedure used is based on an extension of the procedure primarily used by BREZIS and EKELAND [7, 8] to classical parabolic equations. In essence, this approach exploits some fundamental notions of convex analysis.

1. Introduction

CONSIDER AN OPERATOR equation, not necessarily linear,

$$N(u) = f. \tag{1.1}$$

One can distinguish, grosso modo, three possible approaches to variational formulation of (1.1):

(i) The weak formulation, being a rather general form of the virtual work principle

$$< N(u), v >=< f, v > \qquad \forall v \in V. \tag{1.2}$$

Here $< \cdot, \cdot >$ stands for the duality pairing on $V^* \times V$. The space V is a properly chosen function space, like a Lebesgue or Sobolev space, whilst V^* stands for its dual.

(ii) Stronger is the stationary principle

$$J(u) \to \text{stationary} \quad \text{over} \quad V. \tag{1.3}$$

Then necessarily

$$\delta J =< N(u) - f, \delta u >= 0 \quad \Rightarrow \quad N(u) = f.$$

(iii) The strongest are extremum principles (minimum or maximum principles and min-max principles or saddle-point principles).
For instance,

$$J(u) \longrightarrow \min \quad \text{over} \quad V \tag{1.4}$$

where

$$J = J_1 + I_C. \tag{1.5}$$

Here C is a set of constraints and I_C denotes its indicator function [16, 32, 33]:

$$I_C(v) = \begin{cases} 0 & \text{if} \quad v \in C, \\ +\infty & \text{otherwise.} \end{cases} \tag{1.6}$$

Min-max principle is formulated as follows:

$$\min_{u \in V} \max_{p \in Y} L(u,p) = L(\overline{u}, \overline{p}). \tag{1.7}$$

Here Y is another function space. The point $(\overline{u}, \overline{p})$ may be a saddle-point, see the next section.

It is commonly believed that no general approach allowing for the derivation of extremum principles in the case of nonpotential and initial-value problems is available. For the available results the reader is referred to [5, 17, 19, 20, 34, 35, 37, 38, 40, 41, 42, 48] and the references therein. On the other hand in a series of papers [9–13], extremum and saddle-points principle have been derived in an ad hoc manner for a class of nonpotential and initial-value problems of solid mechanics. In fact, these new principles can be derived by using the general approach developed in the present paper. At the root of our method to the formulation of minimum and saddle-points principles lie the pioneering papers by BREZIS and EKELAND [7, 8]. These authors formulated extremum principles for parabolic heat equation. The approach used exploits fundamental notions of convex analysis. Similar approach was used by NAYROLES [27] and RIOS [29, 31]. Afterwards these papers seem to have been forgotten. Fortunately, AUCHMUTY [3, 4] recalled the ideas due to BREZIS and EKELAND [7, 8] and developed the general framework enabling to derive extremum principles for nonpotential operator equations and parabolic-type problems. Hyperbolic-type (second order in time) equations have not been considered.

The aim of the present paper is threefold. First, inspired by solid mechanics, the approach used by Auchmuty [3, 4] is extended to more general differential inclusions.

Second, having at our disposal the general framework allowing for the formulation of extremum principles of operator and parabolic-type equations, we derive extremum and saddle-points principles for nonlinear, nonconservative and nonpotential elasticity, stationary and nonstationary quasi-linear heat equation.Comments on non-associated plasticity and GAO'S papers [23, 24] are also provided.

Third, a general extremum and saddle-points principles are derived for hyperbolic abstract differential inclusion. This general formulations enables one to derive extremum principles for the Lagrange equations in two important cases: (i) the system studied is subject to conservative forces yet the initial-value problem is to be solved. Usually the boundary value problems are investigated provided that variational principles are used; (ii) the system is subject to nonconservative forces. Extremum principles for the dynamic linear elasticity are also derived.

The approach develop allows for further generalization. For instance, one can develop extremum principle for a coupled system of abstract parabolic-hyperbolic differential inclusion. Then one can derive extremum principles for the nonstationary equations of thermoelasticity. Such coupled problems will be investigated in a separate paper [47]. Thermopiezoelectricity requires still a more general framework: a coupled hyperbolic-parabolic-elliptic differential inclusion, cf. [47].

To facilitate the reading of the paper, in Sec. 2 we introduce the indispensable notions of convex analysis. The approach developed in the present paper or its variants and modifications can likewise be used to the formulation of extremum principles in contact and structural mechanics. We have in mind contact problems with frictions, and beams, plates and shells subject to nonconservating loadings or this type of structures in the dynamic case.

2. Elements of convex analysis

For details the reader is referred to [16, 32, 33]. Let V be a function space and

$$f : V \longrightarrow \overline{\mathbb{R}} = \mathbb{R} \cup \{+\infty\}$$

a functional. For instance, in the case of finite-dimensional problems $V = \mathbb{R}^m$. In the case of continuous systems V is a suitably chosen function space like the Lebesgue space L^p or Sobolev space $W^{m,p}$.

The conjugate of f is defined by

$$f^*(v^*) = \sup\{< v^*, v > - f(v) \mid v \in V\}, v^* \in V^*. \tag{2.1}$$

Here V^* denotes the dual space of V, see [16, 32, 33, 49]. For instance, if A is a linear self-adjoint operator and

$$\exists c > 0 \ \forall v \in V, < Av, v > \geq c \parallel v \parallel_V^2 \tag{2.2}$$

then A is invertible. If

$$f(v) = \frac{1}{2} < Av, v >, v \in V \tag{2.3}$$

then

$$f^*(v^*) = \frac{1}{2} < A^{-1}v^*, v^* >, \quad v^* \in V^*. \tag{2.4}$$

Let us introduce the *subdifferential*. An element $u^* \in V^*$ is said to be a *subgradient* of f at a point $u \in V$ if

$$f(v) - f(u) \geq < u^*, v - u > \quad \forall v \in V. \tag{2.5}$$

We denote

$$\partial f(u) = \{\text{the set of all subgradients of } f \text{at } u\}.$$

The multivalued mapping

$$\partial f : v \longrightarrow \partial f(v)$$

is called the subdifferential of f. The standard example is the subdifferential of the function

$$f(x) = \mid x \mid, \quad x \in \mathbb{R}.$$

It can easily be shown that

$$\partial f(x) = \begin{cases} -1 & \text{if} \quad x < 0, \\ [-1, 1] & \text{if} \quad x = 0, \\ +1 & \text{if} \quad x > 0. \end{cases}$$

The notions of convex and concave functions are elementary and their definitions are well - known, cf. [16, 32, 33].

A convex function f is said to be *proper* if $f \not\equiv +\infty$ and

$$f(v) > -\infty \qquad \forall v \in V.$$

The definition (2.1) of f^* implies that if f is proper then one has

$$f(v) + f^*(v^*) \geq < v^*, v > \tag{2.6}$$

for each $v \in V$ and each $v^* \in V^*$. Just this inequality will play an essential role in the derivation of minimum principles. In (2.6) the equality holds if and only if $v^* \in \partial f(v)$, or equivalently if and only if $v \in \partial f^*(v^*)$.

Let us pass now to concave functions, since the above notions are typical for convex functions.

The *conjugate* of a concave function g is defined by

$$g^*(v^*) = \inf\{< v^*, v > -g(v) \mid v \in V\}, \quad v^* \in V^*. \tag{2.7}$$

Caution: in general

$$g^* \neq -(-g^*).$$

For the convex function $f = -g$, one has not $g^*(v^*) = -f^*(v^*)$, but

$$g^*(v^*) = -f^*(-v^*).$$

The set $\partial g(u)$ consists, by definition, of the elements u^* such that

$$g(v) \leq g(u) + < u^*, v - u > \quad \forall v \in V.$$

We shall call such elements u^* *subgradients* of g at u, and the mapping $u \longrightarrow \partial g(u)$ the subdifferential of g, for simplicity, even though terms like "supergradients" and "superdifferential" might be more appropriate.
One has

$$\partial g(u) = -\partial(-g)(u).$$

If g is proper, i. e. if $(-g)$ is proper, one has

$$g(v) + g^*(v^*) \leq < v^*, v >, \forall v \in V, \forall v^* \in V^*, \tag{2.8}$$

with equality holding if and only if $v^* \in \partial g(v)$.

Let $\Lambda : V \to Y$ be a linear operator, let g be a function on Y, and let f be a function on V. The functions $g\Lambda$ and Λf defined by

$$(g\Lambda)(v) = g(\Lambda v), \tag{2.9}$$

$$(\Lambda f)(y) = \inf\{f(v) \mid v \in V, \ \Lambda v = y\} \tag{2.10}$$

are called the *inverse image* of the function g and the *image* of the function f under the mapping Λ, respectively [25,32,33].

Let us pass to dual functions. The following theorem was proved in IOFFE and TIHOMIROV [25].

THEOREM 1. *Let $\Lambda : V \to Y$ be a continuous linear operator. If g is a function on V, and if f is a function on Y then*

$$(\Lambda g)^* = g^* \Lambda^*, \quad (f\Lambda)^* \leq \Lambda^* f^*.$$

If f is a convex function continuous at a point of the set $Im\Lambda$, then

$$(f\Lambda)^* = \Lambda^* f^*.$$

Moreover, for every $v^* \in dom(f\Lambda)^*$, there exists a vector $y^* \in Y^*$ such that

$$v^* = \Lambda^* y^*, \quad (f\Lambda)^*(v^*) = f^*(y^*). \qquad \square$$

The operator Λ^* is defined by

$$\langle \Lambda^* y^*, v \rangle_{V^* \times V} = \langle y^*, \Lambda v \rangle_{Y^* \times Y} \quad \text{for all } y^* \in Y^* \text{ and all } v \in V. \tag{2.11}$$

We recall that $\Lambda^* : Y^* \to V^*$ stands for the operator adjoint to the operator Λ, $\mathrm{Im}\Lambda$ is the image of Λ and $\mathrm{dom}f$ is the effective domain of the function f; $\mathrm{dom}f = \{v \in V |\ f(v) < +\infty\}$.

We proceed now to saddle-functions. Let C and C_1 be subsets of V and Y, respectively, and let L be a function from $C \times C_1$ to $[-\infty, +\infty]$. We say that L is a *convex - concave* function if $L(u, z)$ is a convex function of $u \in C$ for each $z \in C_1$ and a concave function of $z \in C_1$ for each $u \in C$. Concave - convex functions are defined similarly. Both kinds of functions are called *saddle-functions.*

A point $(\hat{u}, \hat{z})$ is said to be a saddle-point of L on $C \times C_1$ if

$$L(\hat{u}, z) \leq L(\hat{u}, \hat{z}) \leq L(u, \hat{z}) \quad \forall (u, z) \in C \times C_1. \tag{2.12}$$

Particularly we may have $C = V$, $C_1 = Y$. We observe that saddle - functions are naturally appropriate for piezoelectricity [47].

Given any convex - concave function on $V \times Y$, we define

$$\partial_1 L(u, z) = \partial_u L(u, z)$$

to be the set of all subgradients of the convex function $L(\cdot, z)$ at u, i.e. the set of all $u^* \in V^*$ such that

$$L(u', z) - L(u, z) \geq < u^*, u' - u > \quad \forall u' \in V.$$

Similarly, we define

$$\partial_2 L(u, z) = \partial_z L(u, z)$$

to be the set of all subgradients of the concave function $L(u,\cdot)$ at z, i. e. the set of all $z^* \in Y$ such that

$$L(u,z') - L(u,z) \leq < z^*, z' - z > \quad \forall z' \in Y.$$

The elements (u^*, z^*) of the set

$$\partial L(u,z) = \partial_1 L(u,z) \times \partial_2 L(u,z)$$

are then defined to be the *subgradients* of L at (u,z), and the multivalued mapping

$$\partial L : (u,z) \longrightarrow \partial L(u,z)$$

is called the *subdifferential* of L.

The last notion we need is that of conjugate saddle-functions. We define the *lower conjugate* $\underline{L}^*$ of L by

$$\underline{L}^*(u^*,z^*) = \sup_{u\in V} \inf_{z\in Y} \{< u^*, u > + < z^*, z > -L(u,z)\}$$

and the *upper conjugate* $\overline{L}^*$ of L by

$$\overline{L}^*(u^*,z^*) = \inf_{z\in Y} \sup_{u\in V} \{< u^*, u > + < z^*, z > -L(u,z)\}$$

We have $\underline{L}^* \leq \overline{L}^*$, cf. [32,33]. Both these functions are convex-concave. Under rather weak assumptions, specified in Corollary 37.1.2 by ROCKAFELLAR [32], we have

$$\underline{L}^*(u^*,z^*) = \overline{L}^*(u^*,z^*). \tag{2.13}$$

For the initial-boundary value problems studied in the paper [47] the property (2.13) holds true since the saddle-functionals assume only finite values on appropriately defined spaces.

Define now the functional $G : V \longrightarrow \overline{\mathbb{R}}$ by

$$G(u) = \sup_{z\in Y} \mathcal{L}(u,z) \tag{2.14}$$

where $\mathcal{L} : V \times Y \longrightarrow \overline{\mathbb{R}}$ is not necessarily a convex-concave functional. A point $(\hat{u}, \hat{z})$ is a *min-max* point for $\mathcal{L}$ on $V \times Y$ provided $\hat{u}$ minimizes G on V and

$$G(\hat{u}) = \mathcal{L}(\hat{u},\hat{z}) = \sup_{z\in Y} \mathcal{L}(\hat{u},z) \tag{2.15}$$

holds. Consequently, when $(\hat{u},\hat{z})$ is a min-max point of $\mathcal{L}$ on $V \times Y$, then

$$\mathcal{L}(\hat{u},z) \leq \mathcal{L}(\hat{u},\hat{z}) = G(\hat{u}) \leq G(u) \tag{2.16}$$

for all $(u, z) \in V \times Z$. Since $G(u) \geq \mathcal{L}(u, \hat{z})$ for each $u \in V$, a saddle-point will be a min-max point of $\mathcal{L}$. The converse need not hold. Indeed, take the function $\mathcal{L} : \mathbb{R}^2 \to \mathbb{R}$ defined by, cf. [4]

$$\mathcal{L}(x, y) = xy - \frac{1}{3}x^2 - \frac{1}{2}y^2.$$

Then $G(x) = \frac{1}{6}x^2$ and $(0, 0)$ is a min-max point of $\mathcal{L}$. It is not a saddle-point in the sense of (2.12) since

$$\mathcal{L}(0, y) \leq \mathcal{L}(0, 0) \text{ and } \mathcal{L}(x, 0) \leq \mathcal{L}(0, 0)$$

for all (x, y).

3. Minimum principle for nonpotential operator equations

In this section we shall derive minimum principles for a class of boundary-value problems of solid mechanics.

To this end we follow the approach primarily used for the parabolic heat equation by BREZIS and EKELAND [7, 8].

3.1. Abstract framework

It seems that the first attempt to exploit the idea due to Brezis and Ekeland [7, 8] to elliptic-type problems should be attributed to Auchmuty [3], cf. also [4]. Now we shall briefly summarize his results and propose also an extended framework, more suitable to problems of continuum mechanics.

Let V be a locally convex topological space and V^* be its dual space with respect to bilinear pairing $\langle ., \rangle_{V^* \times V}$, usually denoted by $\langle ., . \rangle$.

Auchmuty [3, 4] confines his considerations to V being a Banach space.

Suppose $F : V \longrightarrow V^*$ is a continuous map and $\Phi : V \longrightarrow \overline{\mathbb{R}} = \mathbb{R} \cup \{+\infty\}$ be a proper functional on V. Consider the problem of solving the *differential inclusion*

$$F(u) + f \in \partial\Phi(u) \tag{3.1}$$

with $f \in V^*$.

We recall that when Φ is proper, its conjugate function Φ^* is convex and l.s.c. (lower semi-continuous) in the weak, weak-* or strong topologies on V^* [16].

Define now the functional J on V by

$$J(u) = \Phi(u) + \Phi^*(F(u) + f) - \langle F(u) + f, u \rangle. \tag{3.2}$$

The minimum principle associated with (3.1) means evaluating

$$\alpha = inf\{J(u) |\ u \in V\}. \tag{3.3}$$ $(\mathcal{P})$

An element $\hat{u} \in V$ is said to be a minimizer of J on V if $J(\hat{u}) = \alpha$.

The following theorem has been formulated in [3].

THEOREM 2. *Assume that V, Φ, F and f as above and J defined by (3.2) is a proper functional. Then $\alpha \geq 0$ and $J(\hat{u}) = 0$ if and only if $\hat{u}$ is a solution of (3.1).*

P r o o f. The definition of J^* yields

$$\Phi(u) + \Phi^*(u^*) \geq \langle u^*, u\rangle \quad \forall u \in V,\ \forall u^* \in V^*.$$

Equality holds if and only if $u^* \in \partial\Phi(u)$, cf. [16].

Setting now $u^* = F(u) + f$ we conclude that $J(u) \geq 0$ for all $u \in V$, and $J(u) = 0$ if and only if (3.1) holds. □

Relation (3.2) yields

$$J(u) = \Phi(u) - \langle F(u)+f, u\rangle + sup\{\langle F(u)+f, v\rangle - \Phi(v) \mid v \in V\} = sup\{L(u,v) \mid v \in V\},$$

where $L : V \times V \to \mathbb{R}$ is defined by

$$L(u,v) = \langle F(u) + f, v - u\rangle + \Phi(u) - \Phi(v). \tag{3.4}$$

We observe that L is a Lagrangian of type I for problem $(\mathcal{P})$, cf. [3, 21, 44]. The standard dual principle is to find

$$\alpha^* = \sup\{\mathcal{H}(v) \mid v \in V\}, \tag{3.5}$$ $(\mathcal{P}^*)$

where $\mathcal{H} :\longrightarrow \mathbb{R}$ is defined by

$$\mathcal{H}(v) = \inf\{L(u,v) \mid u \in V\}. \tag{3.6}$$

It is worth noting that the Lagrangian L given by Eq. (3.4) is defined on $V \times V$. Thus its two arguments are of "the same" type.

A point $(\hat{u}, \hat{v}) \in V \times V$ is a saddle point of L if, cf. Sec. 2,

$$L(\hat{u}, v) \leq L(\hat{u}, \hat{v}) \leq L(u, \hat{v}) \quad \text{for all } u, v \text{ in } V. \tag{3.7}$$

It can easily be shown that:

(i) If $(\mathcal{P})$ and $(\mathcal{P}^*)$ are nontrivial, then α and α^* are finite with $\alpha^* \leq \alpha$. If $\alpha^* > 0$, then (3.1) does not possess a solution.

(ii) If there exists a solution $\hat{v}$ in V of $(\mathcal{P}^*)$ with $\mathcal{H}(\hat{v}) = 0$ and a $\hat{u}$ in V such that $(\hat{u}, \hat{v})$ is a saddle point of L, then $\hat{u}$ will be a solution of (3.1).

(iii) If $(\hat{u}, \hat{v})$ is a saddle point of L, then

$$0 = \mathcal{H}(\hat{v}) = L(\hat{u}, \hat{v}).$$

3.2. Generalized framework

Consider now the following differential inclusion

$$F_1(N(u)) + f \in \partial\Phi_1(\Lambda u) \tag{3.8}$$

where $\Lambda : V \to Y$ is a continuous linear operator, Y is another locally convex topological space, Y^* denotes its dual, $N : V \to V_1$ is continuous operator, not necessarily linear, and $F_1 : V_1 \to V^*$ is a continuous mapping. Once again, V_1 is a locally convex topological space.

In applications the operator Λ may be a gradient, the linear strain tensor $\mathbf{e}(\mathbf{u})$ or $\Lambda(\mathbf{u}) = (\underline{e}(\underline{u}), \nabla\underline{u})$ in the case of the Green strain tensor $E_{ij}(\mathbf{u}) = \frac{1}{2}(e_{ij}(\mathbf{u}) + u_{i,k}u_{k,j})$.

The minimum principle associated with (3.8) means evaluating

$$\beta = \inf\{K(u) \mid u \in V\} \quad (Q) \tag{3.9}$$

where, cf. Theorem 2,

$$\begin{aligned} K(u) &= \Phi_1(\Lambda u) + (\Phi_1\Lambda)^*[F(N(u)) + f] - \langle F(N(u)) + f, u\rangle \\ &= \Phi_1(\Lambda u) + (\Lambda^*\Phi_1^*)[F(N(u)) + f] - \langle F(N(u)) + f, u\rangle \\ &= \Phi_1(\Lambda u) + inf\{\Phi_1^*(q^*) \mid q^* \in Y^*, \Lambda^*q^* = F(N(u)) + f\} \\ &\quad - \langle F(N(u)) + f, u\rangle. \end{aligned} \tag{3.10}$$

Now the conjugate functional Φ_1^* is defined by

$$\Phi_1^*(q^*) = \sup\{< q^*, q >_{Y^*\times Y} - \Phi_1(q) \mid q \in Y\}.$$

REMARK 1. Formally, the setting of Sec. 3.1 is recovered provided that

$$F(u) = F_1(N(u)), \quad \Phi(u) = \Phi_1(\Lambda u).$$

However, in many applications the form (3.9) is more convenient. For instance, as we shall see below, in the case where $\Phi(u)$ is a quadratic functional in order to find Φ^* we have to calculate an inverse operator.

The minimum principle (Q) can be reformulated as follows

$$\left|\begin{array}{l} \text{Find} \\ \inf\{K_1(u, q^*) \mid u \in V,\ q^* \in Y^*,\ \Lambda^*q^* = F(N(u)) + f\} \end{array}\right. \tag{Q_1}$$

where

$$K_1(u, q^*) = \Phi_1(\Lambda u) + \Phi_1^*(q^*) - \langle F(N(u)) + f, u\rangle. \tag{3.11}$$

We observe that the last principle involves the adjoint operator Λ^* which usually can easily be calculated.

A theorem similar to Theorem 2 can readily be formulated and proved by the reader.

Let us pass to the formulation of Lagrangian functional, now denoted by L_1:

$$L_1(u, q^*; q) = \Phi_1(\Lambda u) - \Phi_1(q) + \langle q^*, q\rangle_{Y^* \times Y} - \langle F(N(u)) + f, u\rangle_{V^* \times V}. \tag{3.12}$$

We have

$$K_1(u, q^*) = \sup\{L_1(u, q^*; q) \mid q \in Y\}.$$

The dual problem means evaluating

$$\sup\{\mathcal{H}_1(q) \mid q \in Y\},$$

where

$$\mathcal{H}_1(q) = \inf\{L_1(u, q^*; q) \mid u \in V,\ q^* \in Y^*,\ \Lambda^* q^* = F(N(u)) + f\}. \tag{3.13}$$

One can now readily formulate a counterpart of inequalities (3.7) and properties corresponding to (i)-(iii) formulated in Sec. 3.2.

3.3. Applications

The abstract framework presented in Secs. 3.1 and 3.2 can be applied to a wide range of elliptic-type problems of continuum mechanics. Due to limitation of space only selected applications are studied.

3.3.1. Non-self-adjoint linear elliptic equation. In my paper [39], cf. also [15, 35], the following non-self-adjoint equation was considered

$$Qu = Lu + Ru = f, \tag{3.14}$$

where $L = L^*, R = -R$. Moreover, it is assumed that

$$Lu = P^* C P u, \quad R = Q - L \tag{3.15}$$

with $C^* = C$.

We take two real Hilbert spaces H_1 and H. Let P be a linear operator $P : H \to H_1$, with the domain $D(P)$ of P dense in H. We assume that $\mathcal{N}(P)$, the null space of P, is $\mathcal{N}(P) = \{0\}$, 0 being the zero element in H. Suppose that $C : H_1 \to H_1$ is linear bounded and self-adjoint, and $C^* = C$, $(Cu_1, u_1)_{H_1} > 0$ for all $u_1 \in H_1$, $u_1 \neq 0$. We have $D(CP) = D(P)$. Furthemore we assume that the adjoint $P^* : H_1 \to H$ of P exists with a domain $D(P^*)$ dense in H_1. Then

the operator $L = P^*CP : H \to H$ is a positive self-adjoint operator with $D(L)$ dense in H.

In [39] a pair of dual extremum principles for Eqs. (3.15), (3.16) was derived. In essence, the basic idea consists in considering the pair of operator equations

$$\begin{cases} Lu + Ru = f \\ Q^*v = Lv - Rv = g \end{cases} \tag{3.16}$$

with $f, g \in H$. Next we set

$$w_1 = \frac{1}{2}(u+v), \quad w_2 = \frac{1}{2}(u-v) \tag{3.17}$$

$$F = \frac{1}{2}(f+g), \quad G = \frac{1}{2}(f-g). \tag{3.18}$$

Thus (3.16) becomes

$$\begin{cases} Lw_1 + Rw_2 = F \\ Lw_2 + Rw_1 = G. \end{cases} \tag{3.19}$$

Such a formulation was used in [39] to derive dual extremum principles for non-associated plasticity.

Let us briefly show that the formulation proposed in [39] is a specific case of our general setting.

Consider now this setting in the particular case of linear, non-self-adjoint equation (3.14). Any equation of the form

$$Qu = f \tag{3.20}$$

can be written in the form (3.14). It suffices to set

$$L = \frac{1}{2}(Q + Q^*), \quad R = Q - L. \tag{3.21}$$

We assume that L is positive definite.

We define the functional Φ by

$$\Phi(u) = \frac{1}{2}(Lu, u) \tag{3.22}$$

where $(\cdot, \cdot)$ denotes the scalar product in the space H. Then Eq. (3.20) can be written in the form

$$f - Ru \in \partial\Phi(u) \tag{3.23}$$

where $\partial\Phi(u) = \{Lu\}$. The functional J defined by (3.2) becomes

$$J(u) = \Phi(u) + \Phi^*(f - Ru) - (f, u) = \frac{1}{2}(L^{-1}(Qu - f), Qu - f). \tag{3.24}$$

Since the operator L is positive therefore J is convex. Theorem 2 implies that $J(\hat{u}) = 0$ if and only if $\hat{u}$ solves (3.20).

From (3.24) we conclude that

$$Q^*L^{-1}(Qu - f) = 0. \tag{3.25}$$

The Lagrangian is now given by

$$L(u, v) = \Phi(u) - \Phi(v) + (f - Ru, v - u). \tag{3.26}$$

This Lagrangian is obviously a convex-concave functional. Its saddle-point $(\hat{u}, \hat{v})$ obeys

$$G_u L(\hat{u}, \hat{v}) = G_v L(\hat{u}, \hat{v}) = 0, \tag{3.27}$$

where G_u and G_v denote partial Gâteux derivatives.
Hence

$$\begin{cases} L\hat{u} + R\hat{v} = f \\ L\hat{v} + R\hat{u} = f. \end{cases} \tag{3.28}$$

Since L is positive therefore $\hat{u} = \hat{v}$.

The extremum principles derived in [39] are recovered provided that $g = f$.

The conjugate (dual) functional (3.6) now becomes

$$\mathcal{H}(v) = (v, f) - \Phi(v) + \Phi^*(f - Rv). \tag{3.29}$$

REMARK 2. The dual extremum principles derived in [15, 39] are based, ab initio, on the study of Eq. $(3.16)_1$ and the adjoint equation $(3.16)_2$. It means that the following system was considered:

$$\begin{cases} f - Ru \in \partial\Phi(u) \\ g + Rv \in \partial\Phi(v), \end{cases} \tag{3.30}$$

or equivalently

$$\{f - Ru, g + Rv\} \in \partial\Psi(u, v) \tag{3.31}$$

where

$$\Psi(u, v) = \Phi(u) + \Phi(v). \tag{3.32}$$

The functional (3.2) becomes

$$\begin{aligned} J(u, v) &= \Psi(u, v) + \Psi^*(f - Ru, g + Rv) - (f - Ru, u) - (g + Rv, v) \\ &= \Phi(u) + \Phi(v) + \Phi^*(f - Ru) + \Phi^*(g + Rv) - (f, u) - (g, u). \end{aligned}$$

3.3.2. Stationary quasi-linear transport equation. We shall now derive a minimum principle for the following transport equation:

$$\begin{cases} -\mathrm{div}[\mathbf{a}(x,u(x))\nabla u(x)] = f & \text{in } \Omega, \\ u = 0 & \text{on } \Gamma. \end{cases} \tag{3.33}$$

Here Ω is a bounded domain in $\mathbb{R}^3$ and $\Gamma = \partial\Omega$ its boundary. For the sake of simplicity only the homogeneous boundary condition is considered. Mixed -boundary condition can also be taken into account.

The problem of solutions to (3.33) was studied by ARTOLA and DUVAUT [1]. For $f \in W^{-1,q}(\Omega)$, $p > 2$, $\dfrac{1}{p} + \dfrac{1}{q} = 1$, a solution exists in the space $W_0^{1,p}(\Omega)$. In [1] it is assumed that $a_{ij}(x,r) = a_{ji}(x,r)$. No such symmetry condition is required in our setting.

Suppose that

$$a_{ij}(x,r) = a_{ij}^0(x) + a_{ij}^1(x,r), \quad a_{ij}^0 = a_{ji}^0, \tag{3.34}$$

where a_{ij}^0 is positive definite for almost every $x \in \Omega$. We assume that $a_{ij}^0 \in L^\infty(\Omega)$. The conditions to be specified by $\mathbf{a}^1$ are specified in [1,22]. Taking account of Eq. (3.31), problem (3.30) is written as follows

$$f + \mathrm{div}(\mathbf{a}^1(x,u)\nabla u) \in \partial\Phi(u) \tag{3.35}$$

where

$$\Phi(u) = \frac{1}{2}\langle -\mathrm{div}\mathbf{a}^0(x)\nabla u, u\rangle_{W^{-1,q}(\Omega)\times W_0^{1,p}(\Omega)} = \frac{1}{2}\int_\Omega a_{ij}^0(x)u_{,i}u_{,j}dx = \frac{1}{2}\langle \mathbf{a}^0(x)\nabla u, \nabla u\rangle. \tag{3.36}$$

For a mixed-boundary value problem a boundary term in the functional $J(u)$ will appear. Here $u_{,i} = \partial u/\partial x_i$ and the summation convention has been applied.

The functional (3.2) becomes

$$J(u) = \Phi(u) + \Phi^*\big[f + \mathrm{div}(\mathbf{a}^1(x,u)\nabla u)\big] - \langle f + \mathrm{div}(\mathbf{a}^1(x,u)\nabla u), u\rangle, \tag{3.37}$$

where Φ is defined by Eq. (3.36), the duality pairing is defined on $W^{-1,q}(\Omega)\times W_0^{1,p}(\Omega)$ and

$$\Phi^*(v^*) = \sup\{\langle v^*, v\rangle - \Phi(v) \mid v \in W_0^{1,p}(\Omega)\} = \frac{1}{2}\langle L^{-1}v^*, v^*\rangle_{W_0^{1,p}(\Omega)\times W^{-1,q}(\Omega)}, \tag{3.38}$$

where $L^{-1} = (-\mathrm{div}\mathbf{a}\nabla)^{-1}$.

Employing the Lagrangian of type (3.4) we increase the number of variables twice but avoid calculating the inverse operator L^{-1}.

3.3.3. Nonconservative finite elasticity. Let $\mathcal{B}$ denote a hyperelastic solid occupying in its undeformed state the closure $\overline{\Omega}$ of a bounded domain $\Omega \subset \mathbb{R}^3$. Consider the following static problem:

$$\begin{cases} \mathrm{div}\mathbf{T} + \mathbf{f}(x, \mathbf{u}, \mathbf{F}) = \mathbf{0} & \text{in } \Omega, \\ \mathbf{u} = \mathbf{0} & \text{on } \Gamma. \end{cases} \tag{3.39}$$

with $\det \mathbf{F} > 0$.

Here $\mathbf{T}$ denotes the first Piola-Kirchhoff stress tensor and $\mathbf{F} = \nabla \mathbf{u}$ is the deformation gradient [14, 26, 28]. We recall that $\det \mathbf{F} > 0$, where det denotes the determinant. The hyperelastic constitutive equation is given by

$$\mathbf{T} = \frac{\partial W}{\partial \mathbf{F}}. \tag{3.40}$$

The stored energy function $W(x, \mathbf{F})$ is nonconvex in $\mathbf{F}$, cf. [14, 26] for a detailed discussion.

The problem of finding a deformation $\mathbf{u} \in W_0^{1,p}(\Omega)^3$, with p sufficiently large [14, 26], such that (3.39) and (3.40) are formally satisfied, is equivalent to

$$\begin{cases} \mathbf{N}(\mathbf{u}, \nabla \mathbf{u}) \in \partial \Phi_1(\nabla \mathbf{u}) & \text{with } \det \nabla \mathbf{u} > 0, \\ \mathbf{u} = \mathbf{0} & \text{on } \Gamma, \end{cases} \tag{3.41}$$

where

$$\Phi_1(\nabla \mathbf{u}) = \int_\Omega W(x, \nabla \mathbf{u}) dx \tag{3.42}$$

and $\mathbf{N}(\mathbf{u}, \nabla \mathbf{u}) = f(x, \mathbf{u}, \nabla \mathbf{u})$ stands for Nemytskii operator, cf. [14, 18].

One could use the variational approach developed in Sec. 3.2 with $\Lambda = \nabla$. However, the functional Φ_1^* is always convex and this facts leads to the conclusion that the broad class of loadings is precluded, cf. [6, 21, 44]. Therefore we propose a different, quite general approach, similar to the one used for the transport equation. Let

$$\mathbf{T} = \frac{\partial \phi}{\partial \mathbf{F}} + \mathbf{T}_1 \tag{3.43}$$

where ϕ is a *convex* function, for instance a quadratic one. ϕ may depend on $x \in \Omega$. If $\mathbf{T}$ is given by (3.40) then

$$\mathbf{T}_1 = \frac{\partial W}{\partial \mathbf{F}} - \frac{\partial \phi}{\partial \mathbf{F}}. \tag{3.44}$$

Then $(3.41)_1$ is rewritten as follows:

$$\begin{cases} \operatorname{div}\left(\dfrac{\partial \phi}{\partial \mathbf{F}}\right) + \operatorname{div}\mathbf{T}_1 + \mathbf{f}(x, \mathbf{u}, \nabla \mathbf{u}) = \mathbf{0} \quad \text{in } \Omega, \\ \mathbf{u} = \mathbf{0} \quad \text{on } \Gamma. \end{cases} \tag{3.45}$$

We set

$$\Phi(\mathbf{u}) = \int_{\Omega} \phi(x, \nabla \mathbf{u}) dx.$$

Then (3.35) is written as follows:

$$\mathbf{N}(\mathbf{u}, \nabla \mathbf{u}) + \operatorname{div}\mathbf{T}_1 \in \partial \Phi(\mathbf{u}), \quad \det \nabla \mathbf{u} > 0 \tag{3.46}$$

and the functional (3.2) becomes

$$J(\mathbf{u}) = \Phi(\mathbf{u}) + \Phi^*[\mathbf{N}(\mathbf{u}, \nabla \mathbf{u}) + \operatorname{div}\mathbf{T}_1] - \langle \mathbf{N}(\mathbf{u}, \nabla \mathbf{u}) + \operatorname{div}\mathbf{T}_1, \mathbf{u} \rangle. \tag{3.47}$$

The minimization problem (3.3) now takes the form

$$\inf\{J(\mathbf{u}) \mid \mathbf{u} \in W_0^{1,p}(\Omega)^3, \ \det \nabla \mathbf{u}(x) > 0\}.$$

REMARK 3.

(i) One can formulate the extremum principle of type (3.9).

(ii) In the case of Cauchy elasticity there exists a response function $\hat{\mathbf{T}}(x, \mathbf{F})$ such that [14, 26]

$$\mathbf{T} = \hat{\mathbf{T}}(x, \mathbf{F}), \quad \det \mathbf{F} > 0. \tag{3.48}$$

Such a law is in general nonpotential. Employing the results of Secs. 3.1, 3.2, one can formulate extremum principles for Cauchy elastic solids subject to non-conservative forces. The study is left to the reader.

(iii) The minimum and min-max principles proposed by CARINI [11] fall within the general framework considered in Sec. 3.1. This author considered the following nonlinear behaviour:

$$\sigma_{ij}(x, t) = D_{ijkl}(x, t) e_{ij}(\mathbf{u}(x, t)) + \psi_{ij}^n(\mathbf{e}(x, t)).$$

The inverse relation has the form

$$e_{ij} = B_{ijkl}(x, t) \sigma_{kl}(x, t) + \Phi_{ij}^n(\boldsymbol{\sigma}(x, t)).$$

Here $\mathbf{e}$ denotes the small strain tensor, $\boldsymbol{\sigma}$ is the stress tensor t, stands for time (quasi-static evolution), and $\mathbf{B} = \mathbf{B}^T, \mathbf{D} = \mathbf{D}^T$; the subscript T denotes the

transposition. The response function Φ_{ij}^n and ψ_{ij}^n are not necessarily derivable from potential functions.

In the case of nonassociated plasticity we have, cf. [39, 40],

$$\dot{\sigma}_{ij} = E_{ijkl}\dot{e}_{kl}, \quad E_{ijkl} \neq E_{klij}.$$

Here $\dot{\mathbf{e}}$ denotes the strain rate tensor and

$$E_{ijkl} = D_{ijkl} - cD_{ijkl}^n$$

with

$$\begin{cases} c = 1 \text{ if } f = 0 \text{ end } \dot{f} = 0 \\ c = 0 \text{ if } f < 0 \text{ or } f = 0 \text{ and } \dot{f} < 0. \end{cases} \tag{3.49}$$

By $f(\boldsymbol{\sigma}, \boldsymbol{\alpha}) \leq 0$ we denote the yield condition where $\boldsymbol{\alpha}$ stands for a set of internal variables.

The formulation of minimum and saddle point principles for both small deformation and finite nonassociated plasticity deserves a separate study.

REMARK 4. GAO [24] claims to have solved the problem of duality for finite elasticity. Such statement can hardly be taken seriously since his formulation of the primal problem does not take into account the most significant constraint like $\det \mathbf{F} > 0$, where $\mathbf{F}$ stands for the gradient of deformation, cf. [14, 26, 28].

Also in [23] the same author claims that my approach to duality, used in [43] is erroneous. Such a statement is false. It is shown in many papers published mostly with my coworkers that one can use the Rockafellar theory of duality to nonconvex problems, cf. [6, 21, 44, 46] and the references therein. It amounts to finding the dual problem to the convexified or bidual to the primal one. Then, however, additional constraints appear. For instance, in the case of von Kármán plates the membrane forces tensor has to be semi-positive. Otherwise a duality gap arises. It seems that a new framework to coping with nonconvex duality has been proposed in [46]. There an approach developed by ROCKAFELLAR and WETS [33] for finite-dimensional problems has been extended to infinite-dimensional setting. In essence, the approach used exploits augmented Lagrangian method. The study of specific cases has shown that other approaches to nonconvex duality always lead to restrictions on applicability. For instance, Auchmuty's approach to nonconvex duality is not as general as the author believes, cf. [21, 44]. The same pertains to Gao's [24] uncritical statements.

4. Parabolic differential inclusions and extremum principles

4.1. General setting

The aim of this section is to provide a general extremum and saddle point principles for the following problem:

$$\begin{cases} \dot{u}(t) + \partial\Phi(t, u(t)) \ni F(t, u(t)) & \text{on } 0 < t < T, \\ u(0) = u_0 \in X. \end{cases} \tag{4.1}$$

Here $\dot{u} = \dfrac{du}{dt}$ and B is a real Banach space which is dense in X, being also a Banach space.

The procedure which follows extends the original approach due to BREZIS and EKELAND [7, 8] and is more general than the one studied by AUCHMUTY [3].

We make the following assumptions:

(a) For each $t \in [0, T]$, $\Phi(t, \cdot) : B \to \mathbb{R}$ is a proper, convex and weakly lower semicontinuous function,

(b) $F : [0, T] \times B \to B^*$ is a Nemytskii operator.

Let $Y = L^p(0, T; B)$ be the Lebesgue space of measurable functions $u : [0, T] \to B$ endowed with the norm

$$||u||_Y^p = \int_0^T ||u(t)||_B^p dt.$$

The dual space Y^* of Y is $L^q(0, T; B^*)$, cf. [18]. As usual, $\dfrac{1}{p} + \dfrac{1}{q} = 1$.

Let V be the space of all functions v in Y with $\dot{v} \in Y^*$. We recall that $\dot{v}$ is the time derivative of v defined in the distributional sense [18]. V is a Banach space under the norm [18]

$$||u||_V = \left(\int_0^T ||u(t)||_B^p dt \right)^{1/p} + \left(\int_0^T ||\dot{u}(t)||_{B^*}^q dt \right)^{1/q}.$$

Consequently, v is a continuous function from $[0, T]$ to X and the initial condition $(4.1)_2$ is meaningful.

Let

$$\mathcal{K} \equiv \{u \in V | u(0) = u_0 \in X\}. \tag{4.2}$$

$\mathcal{K}$ is obviously a closed manifold of V.

Generalizing the variational functional introduced by Auchmuty we define $J : \mathcal{K} \to \overline{\mathbb{R}}$ by

$$(4.3)\quad J(v) = \int_0^T \left[\Phi(t, v(t)) + \Phi^*\left[(t, F(t, v(t)) - \dot{v}(t)\right] - \langle F(t, v(t)) - \dot{v}(t), v(t)\rangle_{B^* \times B}\right] dt.$$

Usually in applications X is a Hilbert space, cf. [18]. The minimum principle associated with problem (4.1) means evaluating

$$(4.4)\qquad \alpha = \inf\{J(v) \,|\, v \in \mathcal{K}\} \qquad (P_t).$$

The functional J assumes either finite or positively infinite values provided that, cf. [3],

(i) if $v \in Y$, $v^* \in Y^*$ then $\Phi(\cdot, v(\cdot))$ and $\Phi^*(\cdot, v(\cdot))$ are Lebesgue measurable on $[0, T]$;

(ii) there exist finite constants c_1, c_2, not necessarily positive, such that $\Phi(t, v) \geq c_1$ and $\Phi^*(t, v^*) \geq c_2$ on $[0, T] \times B$ and $[0, T] \times B^*$ respectively;

(iii) v in $\mathcal{K}$ implies that $F(\cdot, v(\cdot))$ is in Y^*.

Now we can formulate a counterpart of Theorem 2.

THEOREM 3. *Let J, V and K be as above and (i)-(iii) hold. Then $\alpha \geq 0$ and $J(u) = 0$ if and only if u is a solution to (4.1).*

P r o o f. The proof is similar to the elliptic-type problem (3.1). The definition of the conjugate functional yields

$$\Phi(t, v(t)) + \Phi^*(t, v^*(t)) \geq \langle v^*(t), v(t)\rangle$$

for all $v^*(t) \in B$, $v^* \in B^*$ and $t \in [0, T]$.

Integrating over $[0, T]$ we get

$$(4.5)\qquad \int_0^T [\Phi(t, v(t)) + \Phi^*(t, v^*(t))]\, dt \geq \int_0^T \langle v^*(t), v(t)\rangle\, dt$$

for all $v \in Y$, $v^*(t) \in Y^*$. In (4.5) equality holds if and only if

$$v(t) \in \partial\Phi(t, v(t))$$

for almost everywhere (a.e.) $t \in [0,T]$. Setting $v^*(t) = F(t,v(t)) - \dot{v}(t)$ we obtain

$$(4.6) \quad \int_0^T \{\Phi(t,v(t)) + \Phi^*[F(t,v(t)) - \dot{v}(t)]\}\, dt \geq \int_0^T \langle F(t,v(t)) - \dot{v}(t), v(t)\rangle\, dt.$$

Moreover, in (4.6) equality holds if and only if $v = u$ obeys (4.1) a.e. on $[0,T]$.

If $p = 2$ and X is a Hilbert space with the norm $||\cdot||_X$ induced by the scalar product then we additionally have

$$\int_0^T \langle \dot{v}(t), v(t)\rangle\, dt = \frac{1}{2}||v(t)||^2\Big|_0^T = \frac{1}{2}\left[||v(T)||_X^2 - ||v(0)||_X^2\right].$$

In this specific, practically important case, the functional J takes the form

$$(4.7) \quad J(v) = \int_0^T \Big\{\Phi(t,v(t)) + \Phi^*\big[t, F(t,v(t)) - \dot{v}(t)\big] - \langle F(t,v(t)), v(t)\rangle\Big\} dt + \frac{1}{2}\left(||v(T)||_X^2 - ||u_0||_X^2\right).$$

□

REMARK 5. The functional J involves the conjugate function Φ^*. Similarly to Secs. 3.1 and 3.2 one can formulate Lagrangian and saddle-point principles.

4.2. Applications

Some illustrative examples of application of the extremum principle (P_t) in the case where $p = 2$ and X is a suitably chosen Hilbert space were provided by AUCHMUTY [2,3], cf. also RIOS [29–31]. An alternative approach was used by NAYROLES [27]. More precisely, in [2] an autonomous, nonlinear ordinary differential equation with periodic boundary condition was studied. A general setting for linear initial value problems was elaborated in [3].

The general approach presented in Sec. 4.1 offers many possibilities of finding minimum principles for boundary-initial value problems of solid and fluid mechanics or heat transfer. Particularly, one can formulate minimum and saddle-point principles for heat transfer of biomechanics [36,45]. To mention but a few other possibilities, we think of applications to quasi-static contact problems with friction, adaptive elasticity (biomechanics), nonassociated plasticity and viscoplasticity, linear and nonlinear heat equations and Navier-Stokes equations.

4.2.1. Nonstationary quasi-linear heat equation. We recall that the stationary transport equation has been investigated in Sec. 3.3.2. Consider now the following parabolic equation:

$$\begin{cases} \kappa \dfrac{d\theta}{dt} - \operatorname{div}\left[\mathbf{a}(x,t,\theta)\nabla\theta\right] = f(x,t), & \text{in } \Omega \times (0,T), \\ \theta(x,t) = 0 \quad \text{on } \Gamma \times (0,T), \\ \theta(x,0) = \theta^0(x), \quad x \in \Omega. \end{cases} \tag{4.8}$$

Here $\theta(x,t)$ denotes the temperature.

Now we set

$$X = L^2(\Omega), \quad B = W_0^{1,p}(\Omega), \quad Y = L^2(0,T;W_0^{1,p}(\Omega)).$$

Hence

$$X^* = X = L^2(\Omega), \quad B^* = W^{-1,q}(\Omega), \quad \frac{1}{p} + \frac{1}{q} = 1.$$

We assume that $\theta^0 \in L^2(\Omega)$. The assumptions on the material coefficients are similar to those specified in [1, 22], except that now they hold for all $t \in [0,T]$ and the function $a_{ij}(x,\cdot,\theta)$ is continuous (in the second argument). Consider two cases.

CASE 1. The coefficients a_{ij} have the form similar to (3.34):

$$a_{ij}(x,t,\theta) = a_{ij}^0(x,t) + a_{ij}^1(x,t,\theta) \tag{4.9}$$

and the matrix $\mathbf{a}^0(x,t)$ is symmetric and positive definite. Then we set, cf. (3.36),

$$F(t,\theta) = f + \operatorname{div}\,(\mathbf{a}^1\nabla\theta),$$

$$\Phi(t,\theta) = \frac{1}{2}\left\langle -\operatorname{div}\,(\mathbf{a}^0\nabla\theta), \theta\right\rangle = \frac{1}{2}\left\langle \mathbf{a}^0\nabla\theta, \nabla\theta\right\rangle.$$

Here we use the notation which is normally used in the study of evolution partial differential equations:

$$\theta(t) = \{\theta(x,t)\,|x \in \Omega\}.$$

The minimum principle takes now the form

$$|\ \text{Find } \inf\{J(\theta)\,|\theta \in K\}.$$

The variational function J has now the form (4.7) with $v = \theta$ and $\dot{v}$, u_0 being replaced by $\kappa\dot{\theta}$, θ^0 respectively.

Moreover we have

$$K = \left\{\theta \in L^2(0,T;W_0^{1,p}(\Omega)) \,\middle|\, \dot{\theta} \in L^2(0,T;W^{-1,q}(\Omega), \theta(0) = \theta^0\right\}.$$

We observe that the coefficient κ may be a function of $x \in \Omega$.

REMARK 6. One can consider a slightly more general equation than (4.1):

$$\frac{d}{dt}(a(t)u(t)) + \partial\Phi(t, u(t)) \ni F(t, u(t)).$$

Then the last differential inclusion is written as follows

$$a(t)\dot{u}(t) + \partial\Phi(t, u(t)) \ni F_1(t, u(t))$$

where $F_1(t, u(t)) = F(t, u(t)) - \dot{a}(t)u(t)$.

CASE 2. A positive definite, symmetric matrix $b_{ij}(x, t)$ is introduced and we set

$$F(t, \theta) = f - \operatorname{div}(\mathbf{b}\nabla\theta) + \operatorname{div}(\mathbf{a}\nabla\theta),$$

$$\Phi(t, \theta) = \frac{1}{2}\langle \mathbf{b}\nabla\theta, \nabla\theta\rangle.$$

For instance, we may take $b_{ij}(x, t) = b(x, t)\delta_{ij}$ where (δ_{ij}) is the Kronecker delta.

5. Second-order differential inclusion

5.1. General setting

Consider the problem of solving

$$\begin{cases} \dfrac{d^2u(t)}{dt^2} + \partial\Phi(t, u(t)) \ni F(t, u(t), \dot{u}(t)) \\ u(0) = u^0, \quad \dot{u}(0) = u^1. \end{cases} \tag{5.1}$$

Here we confine our considerations to the case where B is a real Banach space which is dense in H, a Hilbert space with the scalar product denoted by $(\cdot, \cdot)$.

The space Y is defined by, cf. Sec. 4.1,

$$Y = L^2(0, T; B).$$

Now the space V is chosen as follows

$$V = \left\{ v \in Y \,\middle|\, \dot{v} \in L^2(0, T; H), \ddot{v} \in Y^* \right\}. \tag{5.2}$$

We recall that $Y^* = L^2(0, T; B^*)$. The set $\mathcal{K}_h$ of admissible fields is defined by

$$\mathcal{K}_h = \left\{ v \in V \,\middle|\, v(0) = u^0 \in B, \dot{v}(0) = u^1 \in H \right\}. \tag{5.3}$$

The functions Φ, Φ^*, F satisfy assumptions similar to assumptions (i)—(iii) specified in Sec. 4.1.

We introduce the variational functional

$$(5.4)\quad J(v) = \int_0^T \{\Phi(t,u(t)) + \Phi^*[t, F(t,v(t),\dot{v}(t)) - \ddot{v}(t)]$$

$$- \langle F(t,v(t),\dot{v}(t)), v(t)\rangle_{B^*\times B}\}\, dt - \int_0^T ||\dot{v}(t)||_H^2 dt + (\dot{v}(T), v(T)) - (u^1, u^0).$$

The minimum principle associated with (5.1) means evaluating

$$\alpha = \inf\{J(v)\,|\,v \in \mathcal{K}_h\}.$$

THEOREM 4. *Assume that J, V, Φ, Φ^*, F and $\mathcal{K}_h$ are as above. Then $\alpha \geq 0$ and $J(\hat{v}) = 0$ if, and only if $\hat{v}$ is a solution to (5.1).*

P r o o f. We have

$$\Phi(t,v(t)) + \Phi^*(t,v^*(t)) \geq \langle v^*(t), v(t)\rangle$$

for all $v(t) \in B$; $v^*(t) \in B^*$ and $t \in [0,T]$. Integrate over $[0,T]$ and take $v^*(t) = F(t,v(t),\dot{v}(t)) - \ddot{v}(t)$, then

$$(5.5)\quad \int_0^T \{\Phi(t,v(t)) + \Phi^*[t, F(t,v(t),\dot{v}(t)) - \ddot{v}(t)]\}\, dt$$

$$\geq \int_0^T \langle F(t,v(t),\dot{v}(t)) - \ddot{v}(t), v(t)\rangle\, dt.$$

Equality holds here if and only if $\hat{v}$ obeys (5.1) a.e. on $(0,T)$. Moreover, we have

$$(5.6)\quad \int_0^T \langle \ddot{v}(t), v(t)\rangle\, dt = (\dot{v}(T), v(T)) - (u^1, u^0) - \int_0^T (\dot{v}(t), \dot{v}(t))dt.$$

Substituting (5.6) into (5.5) we get (5.4). □

REMARK 7.

(i) Lagrangian formulation is likewise possible.

(ii) The formulation similar to that presented in Sec. 3.2 will be presented elsewhere both for the parabolic and hyperbolic inclusions.

5.2. Applications

The variational formulation presented in Sec. 5.1 offers a possibility of many applications in analytical, solid and structural mechanics. To mention but a few, we think of linear and nonlinear dynamic elasticity, Lagrange equations in the nonconservative case, vibrating structures like beams, plates and shells.

5.2.1. Dynamic linear elasticity. To provide a nontrivial, illustrative example consider the following system of dynamic elasticity:

$$\begin{cases} \rho\ddot{\mathbf{u}} - \operatorname{div}\left[\mathbf{C}(x,t)\mathbf{e}(\mathbf{u}(x,t))\right] = \mathbf{f}(x,t) \quad \text{in } \Omega \times [0,T], \\ \mathbf{u} = \mathbf{0} \quad \text{on} \quad \Gamma \times [0,T], \\ \mathbf{u}(x,0) = \mathbf{u}^0(x), \quad \dot{\mathbf{u}}(x,0) = \mathbf{u}^1(x) \quad \text{in } \Omega. \end{cases} \tag{5.7}$$

Here $\mathbf{u}(x,t)$ denotes the displacement vector, $\mathbf{e}(\mathbf{u})$ is the small strain tensor, ρ denotes the density, not necessarily constant, and C_{ijkl} are components of the elasticity tensor satisfying usual symmetry and coercivity requirements [14, 26].

We set

$$\Phi(t,\mathbf{u}) = \frac{1}{2}\langle -\operatorname{div}\mathbf{C}(x,t)\mathbf{e}(\mathbf{u}), \mathbf{u}\rangle = \frac{1}{2}\int\limits_{\Omega} C_{ijkl}(x,t)e_{ij}(\mathbf{u}(x,t))e_{kl}(\mathbf{u}(x,t))dx. \tag{5.8}$$

The functional spaces are

$$B = H_0^1(\Omega)^3,\ B^* = H^{-1}(\Omega)^3, H = L^2(\Omega)^3,$$
$$V = \Big\{\mathbf{v} \in L^2(0,T;H_0^1(\Omega))^3 \,\Big|\, \dot{\mathbf{v}} \in L^2(0,T;L^2(\Omega))^3\ , \ \ddot{\mathbf{v}} \in L^2(0,T;H^{-1}(\Omega)^3)\Big\}. \tag{5.9}$$

Then the variational functional (5.4) becomes

$$J(\mathbf{u}) = \int\limits_0^T \{\Phi(t,\mathbf{u}(t)) + \Phi^*[t,\mathbf{f}(t) - \rho\ddot{\mathbf{u}}(t)] - \langle \mathbf{f}(t),\mathbf{u}(t)\rangle_{H^{-1}(\Omega)^3 \times H_0^1(\Omega)^3}\Big\}\,dt - \iint\limits_{0\,\Omega}^{T} \rho\dot{u}_i(x,t)\dot{u}_i(x,t)dxdt + \int\limits_{\Omega} \rho\dot{u}_i(x,T)\dot{u}_i(x,T)dx - \int\limits_{\Omega} \rho u_i^1(x)u_i^0(x)dx. \tag{5.10}$$

6. Final remarks

We have developed a general procedure for finding extremum and saddle-point principles applicable to nonpotential and nonconservative problems of mechanics as well as to first- and second-order differential inclusions. Illustrative examples show the flexibility and versatility of the approach used. This approach allows for: (i) finding minimum and saddle point principles for problems usually believed to possess no such principles, (ii) the study of existence of solutions, cf. RIOS [29–31], (iii) the development of new approximation schemes.

In a separate paper extremum principles for dynamic thermoelasticity and piezoelectricity and thermopiezoelectricity will be derived. Our approach offers also a possibility of the derivation of extremum principles for bio-heat equations, cf. [36]. This problem will be studied in [45]. The papers [45,47] will offer a further development of the general variational approach used in the present paper. Particularly, extremum principles for coupled parabolic-hyperbolic differential inclusion will be derived.

Another field of possible applications is the fluid mechanics, thermodynamics and mechanics of porous media.

I would like to stress that it has not been possible to present in a single paper as many comprehensive examples as I would like to. Also, theoretical considerations have been shortened.

Acknowledgement

The author is indepted to Drs. B. Gambin and A. Gałka for their help in the preparation of the manuscript.

References

1. M. ARTOLA, G. DUVAUT, *Un resultat d'homogénéisation pour une classe de problèmes de diffusion non linéaires stationaires,* Ann. Fac. Sci. Toulouse, **4**, 1–27, 1982.
2. G. AUCHMUTY, *Variational principles for periodic solutions of autonomous ordinary differential equations,* in: Proc. Conf. Nonlinear Oscillations in Chemistry and Biology, Lecture Notes in Biomathematics, vol. 66, pp. 252–260, Springer Verlag, New York 1986.
3. G. AUCHMUTY, *Variational principles for operator equations and initial value problems,* Nonlinear Anal., Theory, Methods & Appl., **12**, 531–564, 1988.
4. G. AUCHMUTY, *Min–max problems for non-potential operator equations,* Contemporary Math., **209**, 19–28, 1997.
5. F. BAMPI, A. MORRO, *Topics in the inverse problem of the calculus of variations,* Fisica Matematica, Suppl. B.U.M.I., **5**, 93–115, 1986.

6. W. R. BIELSKI, J. J. TELEGA, *The complementary energy principle in finite elasticity,* in : Finite Rotations in Structural Mechanics, W. PIETRASZKIEWICZ, [Ed.], Lecture Notes in Engineering, **19**, pp. 62–81, Springer-Verlag, Berlin 1986.

7. H. BREZIS, I. EKELAND, *Un principle variationnel associé à certaines équations paraboliques. Le cas independant du temps,* C. R. Acad. Sci. Paris, **282A**, 971–974, 1976.

8. H. BREZIS, I. EKELAND, *Un principle variationnel associé à certaines équations paraboliques. Le cas dependant du temps,* C. R. Acad. Sci. Paris, **282A**, 1197–1198, 1976.

9. A. CARINI, *Colonnetti's minimum principle extension to generally nonlinear materials,* Int. J. Solids Structures, **33**, 121–144, 1996.

10. A. CARINI, *Saddle-point principles for general nonlinear material continua,* J. Appl. Mech., **64**, 1010–1014, 1997.

11. A. CARINI, O. DE DONATO, *A comprehensive energy formulation for general nonlinear material continua,* J. Appl. Mech., **64**, 353–360, 1997.

12. A. CARINI, F. GENA, *Some variational formulation for continuum nonlinear dynamics,* J. Mech. Phys. Solids, **46**, 1253–1277, 1998.

13. A. CARINI, G. MAIER, *Extremum and saddle-point theorems for elastic solids with dissipative displacement discontinuities,* Arch. Mech., **52**, 523-545.

14. P. G. CIARLET, *Mathematical Elasticity, vol. I: Three-dimensional Elasticity,* North-Holland, Amsterdam 1988.

15. W.D. COLLINS, *Dual extremum principles for the heat equation,* Proc. Roy. Soc. Edinb., **77A**, 273–293, 1977.

16. I. EKELAND, R. TEMAM, *Convex Analysis and Variational Problems,* North-Holland, Amsterdam 1976.

17. V. M. FILIPPOV, V. M. SAVCHIN, S. G. SHOROHOV, *Variational principles for nonpotential operators,* (in Russian), Itogi Nauki i Tekhniki, Sovriemennye Problemy Matematiki, Vol. **40**, pp. 3–176, VINITI, Moskwa 1992.

18. H. GAJEWSKI, K. GRÖGER, K. ZACHARIAS, *Nichtlineare Operatorengleichungen und Operatordifferetialgleichungen, Akademie-Verlag,* Berlin 1974.

19. A. GAŁKA, J. J. TELEGA, *A variational method for finite elasticity in the case of non - potential loadings I. First Piola - Kirchhoff stress tensor,* Bull. Acad. Pol. Sci., Série sci. tech., **30**, 1982, 121 - 128; II. Symmetric stress tensor and some comments, ibid., pp.129-135.

20. A. GAŁKA, J. J. TELEGA, *On variational principles and conservation laws in finite non - potential elasticity,* in: Variational Methods in Engineering, C. A. BREBBIA [Ed.], pp. (3–13) – (3–22), Springer - Verlag, Berlin 1985.

21. A. GAŁKA, J. J. TELEGA, *Duality and the complementary energy principle for a class of non – linear structures. Part I. Five - parameter shell model,* Arch. Mech., **47**, 1995, 677 - 698; Part II. Anomalous dual variational principles for compressed elastic beams, ibid., pp. 699—724.

22. A. GAŁKA, J. J. TELEGA, S. TOKARZEWSKI, *Nonlinear transport equation and macroscopic properties of microheterogeneous media,* Arch. Mech., **49**, 293 - 319, 1997.

23. D. Y. GAO, *Dual extremum principles in finite deformation theory with application in post-buckling analysis of nonlinear beam model*, Appl. Mech. Rev., **50**, 564–571, 1997.

24. D. Y. GAO, *Duality, triality and complementary extremum principles in non-convex parametric variational problems with applications*, IMA J. Appl. Math., **61**, 199–235, 1998.

25. A. D. IOFFE, V. M. TIHOMIROV, *Theory of Extremal Problems*, North-Holland, Amsterdam, 1979.

26. J. E. MARSDEN, T.J.R. HUGHES, *Mathematical Foundations of Elasticity*, Prentice-Hall, Englewood Cliffs, New Jersey, 1983.

27. B. NAYROLES, *Un théorème de minimum pour certains systèms dissipatifs. Variante hilbertienne*, Séminaire d'Analyse Convexe, Exposé No 2, Université de Montpellier, 1976; sea also: C.R. Acad. Sci. Paris, **282A**, 1035–1038, 1976.

28. R. W. OGDEN, *Non-linear Elastic Deformations*, Ellis Horwood, Chichester, and John Wiley, 1984.

29. H. RIOS, *Étude de la question d'existence pour certains problèmes d'evolution par minimisation d'une fouctionnelle convexe*, C.R. Acad. Sci. Paris, Série A, **283**, 83–86, 1976.

30. H. RIOS, *Étude de certains problèmes paraboliques: existence et approximations des solutions*, Séminaire d'Analyse Convexe, Exposé No 1, Thèse de specialité, Université de Montpellier, 1978.

31. H. RIOS, *Une étude d'existence sur certains problèmes paraboliques*, Annales Fac. Sci. Toulouse, **1**, 235–255, 1979.

32. R. T. ROCKAFELLAR, *Convex Analysis*, Princeton University Press, Princeton 1970.

33. R. T. ROCKAFELLAR, R.J.-B. WETS, *Variational Analysis*, Springer, Berlin 1998.

34. R. M. SANTILLI, *Foundations of Theoretical Mechanics. I. The Inverse Problem in Newtonian Mechanics*, Springer-Verlag, New York 1978; II. Birkhoffian Generalization of Hamiltonian Mechanics, ibid.

35. M. J. SEWELL, *Maximum and Minimum Principles: A Unified Approach, with Applications*, Cambridge University Press, Cambridge 1987.

36. M. STAŃCZYK, J. J. TELEGA, *Thermal problems in biomechanics: from soft tissues to orthopaedics*, Russian J. Biomechanics, **5**, 30–75, 2001.

37. J. J. TELEGA, *Variational principles for an incompressible, perfectly plastic material with non - associated flow law*, Bull. Acad. Pol. Sci., Série sci. tech., **25**, 357 - 363, 1977.

38. J. J. TELEGA, *On variational formulations for non-linear, non-potential operators*, J. Inst. Maths Applics, **24**, 175 - 195, 1979.

39. J. J. TELEGA, *Dual extremum principles in rate boundary value problems of non - associated plasticity*, Int. J. Eng. Sci., **17**, 215 - 226, 1979.

40. J. J. TELEGA, *Variational principles for rate boundary-value problems in non-associated plasticity*, Zeitschr. Ang. Math. Mech., **60**, 71-82, 1980.

41. J. J. TELEGA, *Determination of potential form of operators*, (in Polish), Matematyka Stos., **18**, 1982, 107 - 122, in Polish.

42. J. J. TELEGA, *Derivation of variational principles for rigid - plastic solids obeying non - associated flow laws. I. Further development of the nonlinear method of adding the adjoint operator. Prescribed jumps,* Int. J. Eng. Sci., **20**, 913 - 933, 1982; II. Unprescribed jumps, ibid., pp. 935–945.

43. J. J. TELEGA, *On the complementary energy principle in non-linear elasticity. Part I: von Kármán plates and three-dimensional solids,* C.R. Acad. Sci. Paris, Série II, **308**, 1193-1198, 1989.

44. J. J. TELEGA, *On anomalous dual variational principles and application to compressed nonlinear beams,* Vestnik RUDN, Ser. Mat., **2**, 136 - 147, 1995.

45. J. J. TELEGA, M. STAŃCZYK, *Extremum principles for linear and nonlinear bio-heat equations,* in preparation.

46. J. J. TELEGA, A. GAŁKA, W. BIELSKI, *Augmented Lagrangian methods for a class of convex and nonconvex problems,* J. Theoret. Appl. Mech., **39**, 741–768, 2001.

47. J. J. TELEGA, A. GAŁKA, B. GAMBIN, *Extremum principles for dynamic piezoelectricity, thermoelasticity and thermopiezoelectricity, in preparation.*

48. E. TONTI, *Variational formulations for every nonlinear problem,* Int. J. Eng. Sci., **22**, 1343–1371, 1984.

49. K. YOSIDA, *Functional Analysis,* Springer-Verlag, Berlin 1978.

Received July 5, 2002; revised version September 26, 2002.

Arch. Mech., **54**, 5-6, pp. 691–707, Warszawa 2002

Dependence of instability strain upon damage in thermoviscoplastic materials

Z.G. WEI and R.C. BATRA

Department of Engineering Science and Mechanics, MC 0219
Virginia Polytechnic Institute and State University
Blacksburg, VA 24061
e-mail: zwei@vt.edu; rbatra@vt.edu

Dedicated to Professor Piotr Perzyna
on the occasion of his 70^{th} birthday

BASED ON THE FIELD EQUATION for the number density of voids and the expression for the expansion of a spherical void in a perfectly plastic infinite body subjected to a uniform hydrostatic tensile stress, an expression for the rate of dilatation of voids is derived. Damage is defined as the volume density of voids. The flow stress of the material is assumed to decrease affinely with an increase in the damage. It is used to find the instability strain in a thermoviscoplastic body deformed in simple shear and simultaneously subjected to a uniform hydrostatic tensile stress. The instability strain is determined by two methods: (i) the Considère condition, i.e., when the shearing traction becomes maximum, and (ii) by studying the stability of a slightly perturbed homogeneous solution of equations governing thermomechanical deformations of a thermoviscoplastic body. Both techniques give essentially the same value of the instability strain. Assuming that failure occurs when the accumulated damage equals 0.3, the failure strain is computed. For a 4340 steel, values of the instability and the failure strains as a function of the nominal strain rate and the hydrostatic pressure are computed.

1. Introduction

TYPICAL DAMAGE MECHANISMS that have been studied are the development of micro-cracks, micro-voids, and adiabatic shear localization. Many investigations [1–4] have revealed that the ductile failure of a body deformed at a high strain rate generally involves the initiation and development of adiabatic shear bands (ASBs), nucleation of micro-voids either within an ASB or by the separation of the matrix material from inclusions or both, growth and coalescence of micro-voids to form micro-cracks, the coalescence of micro-cracks to form cracks, and the propagation of cracks to the boundaries of the body. MCCLINTOCK [5] has analyzed the expansion of a long circular cylindrical cavity embedded in a non-hardening material that is pulled along the cavity axis and also subjected to

transverse tensile stresses. He found that the relative void expansion per unit applied strain increment increases exponentially with the transverse normal stress. Rice and Tracey [6] studied the effect of stress triaxiality on the growth of a spherical void embedded in a perfectly plastic infinite body and found that the relative void volume grows exponentially with the stress triaxiality. Hancock and Mackenzie [8] postulated that the failure process in ductile metals involved the nucleation, growth and coalescence of voids. Thus the effective cross-sectional area is gradually reduced and the load carrying capacity of the member is decreased. They did not incorporate the reduction in the elastic moduli and the flow stress caused by the voids. Gurson [7] has proposed a plastic potential or a yield criterion for an isotropic microporous solid that accounts for the decrease in the flow stress of the material induced by voids. Batra and Jin [9], Batra and Jaber [10] and Batra *et al.* [34] used Gurson's flow potential coupled with the reduction in the elastic moduli, caused by the porosity to study the development of ASBs and the transition of the failure mode from brittle to ductile in plane strain deformations of prenotched thermoviscoplastic plates. Perzyna and coworkers [11–13] have developed a theory of heat conducting microporous thermoviscoplastic solids that accounts for various dissipative mechanisms. Constitutive relations are derived by exploiting the Clausius-Duhem inequality. The material moduli degrade with the damage evolved which is equated to the density of voids.

A few models based on continuum damage mechanics (CDM) theory have been developed to account for the nucleation, the coalescence, and the growth of voids in a ductile body. In the CDM, these phenomena are generally represented by a macroscopic damage variable whose growth rate is taken to be a function of measurable macroscopic variables such as the stress triaxiality, effective plastic strain etc. The material moduli are presumed to decrease with an increase in the damage and the material is assumed to fail when the damage attains a critical material-dependent value. Lemaitre [14] has summarized damage mechanics for elastoplastic deformations. Except for the degradation of material moduli, the theory is similar to that of internal variables developed by Coleman and Gurtin [15]. With the porosity regarded as the damage variable, Perzyna and coworker's theory [11–13] and equations used by Batra *et al.* [9, 10, 34] describe CDM models.

Statistical approach has been employed, amongst others, by Curran *et al.* [16] and Bai *et al.* [17] to derive macrolevel damage relations. From the conservation law of micro-cracks in phase-space, Bai *et al.* [17–20] derived a damage model for ideal cracks. Li *et al.* [21] adopted this method to study the damage due to void expansion in a ductile metal tube with the inner surface subjected to explosive loads.

Adiabatic shear banding is an important failure mechanism in dynamic deformations of ductile materials. An ASB is a narrow region, usually a few microns wide, of intense plastic deformation. TRESCA [22] observed these during the hot forging of a platinum bar. The activity in the field grew rapidly subsequent to their observations by ZENER and HOLLOMON [23] during the punching of a hole in a low carbon steel plate. They proposed that ASBs form when thermal softening overcomes the combined hardening due to strain and strain rate effects. Subsequent experimental [24] and numerical investigations [25] have revealed that an ASB developes in earnest after the load has attained its peak value. Whereas earlier investigations [1] employed the CONSIDÈRE criterion [26] to find the instability strain, BAI [27] used the perturbation method to find the strain when the homogeneous solution upon perturbation will become unstable. BATRA and CHEN [28] showed that these two techniques give essentially the same value of the instability strain. Here we prove that this holds even when damage evolution is considered and the effective stress required to deform the material plastically decreases affinely with the damage evolved.

2. Damage evolution equation due to growth of voids

Following BAI *et al.*'s work [17] on ideal microcracks, we make the following simplifying assumptions: (i) microvoids are spherical and are sparsely distributed, thus the interaction among them is negligible, (ii) no new voids nucleate but the volume of existing voids can change, (iii) the growth of a void is governed by macroscopic deformations, and (iv) the material is rigid perfectly plastic. Since voids of all shapes occur in a material, our assumption of voids being spherical will necessarily give us an approximate expression for the damage. Let v represent the volume of a microvoid and $n(v, t, \sigma_{eq})$ the number density at time t of voids of volume v. Here σ_{eq} is the effective or the von Mises stress in the matrix surrounding a void. Then the number of microvoids at time t in a unit volume of physical space of volume between v and $v + dv$ equals $n(v, t, \sigma_e)dv$. Thus the total volume, V_v, of microvoids is given by

$$V_v = \int_0^\infty n(v, t, \sigma_e) v dv. \tag{2.1}$$

The number density of voids of volume v changes with time according to the relation [17–19]

$$\frac{\partial n}{\partial t} + \frac{\partial (n\dot{v})}{\partial v} = 0, \tag{2.2}$$

where a superimposed dot indicates the material time derivative. This equation is analogous to the continuity equation for an incompressible body.

We define a damage variable, D, by

$$D = \frac{V_v}{V} = \frac{V - V_m}{V}, \tag{2.3}$$

where V and V_m equal, respectively, the total volume of the body and the matrix or the solid phase. Assuming that the body as a whole is incompressible, Eq. (2.3) gives

$$\dot{D} = \frac{\dot{V}_v}{V}. \tag{2.4}$$

Assumptions $\dot{V} = 0$ and $\dot{V}_v \neq 0$ imply that the mass density of the matrix will change. However, in [9, 10] it was assumed that the matrix is incompressible and thus its mass density does not change. Accordingly, the evolution equation for $\dot{V}_v$ derived here differs from that used in Refs. 9 and 10. Substitution from (2.1) and (2.2) into (2.4) yields

$$\dot{D} = \frac{1}{V}\int_0^\infty \frac{\partial n}{\partial t} v dv = -\frac{1}{V}\int_0^\infty \frac{\partial (n\dot{v})}{\partial v} v dv, \tag{2.5}$$

$$= -\frac{1}{V}\left[n\dot{v}v\Big|_0^\infty - \int_0^\infty n\dot{v}dv \right] = \frac{1}{V}\int_0^\infty n\dot{v}dv,$$

since there are no voids of zero volume and no voids of infinite volume.

RICE and TRACEY [6] derived the following expression for the rate of change of radius, r, of a spherical void in a rigid perfectly plastic infinite body subjected to hydrostatic tension at infinity:

$$\dot{r} = Cr\,\dot{\varepsilon}_e \exp\left(\frac{\sigma_{kk}}{2\sigma_y}\right) \tag{2.6}$$

where $\dot{\varepsilon}_e$ equals the effective plastic strain rate, σ_{ij} is the Cauchy stress tensor, a repeated index implies summation over the range of the index, σ_y is the static yield stress of the material in simple tension and the value of the constant C depends upon the loading conditions at infinity. Within about one per cent error, C can be taken to be 0.279. For a spherical void, $v = 4\pi r^3/3$. Thus

$$\frac{\dot{v}}{v} = 0.837\dot{\varepsilon}_e \exp\left(\frac{\sigma_{kk}}{2\sigma_y}\right). \tag{2.7}$$

Equations (2.5) and (2.7) give

$$\dot{D} = 0.837\dot{\varepsilon}_e D \exp\left(\frac{\sigma_{kk}}{2\sigma_y}\right), \tag{2.8}$$

for the rate of evolution of the damage D.

For a two-dimensional problem the damage variable, D_s, is usually determined in terms of the surface area of voids divided by the total area of cross-section. Since for a spherical void of surface area s, $\dot{s}/s = (2/3)\,\dot{v}/v$, therefore, for a two-dimensional problem we take

$$\dot{D}_s = 0.558\dot{\varepsilon}_e D_s \exp\left(\frac{\sigma_{kk}}{2\sigma_y}\right). \tag{2.9}$$

When σ_{kk}/σ_y is independent of ε_e and $D_{s0} = D_s(0)$, we can integrate Eq. (2.9) to obtain

$$D_s = D_{s0}\exp(k\varepsilon_e), \tag{2.10}$$

where

$$k = 0.558\exp\left(\frac{\sigma_{kk}}{2\sigma_y}\right). \tag{2.11}$$

Thus the failure strain, ε_f, corresponding to the critical value, D_{sc}, of the damage is given by

$$\varepsilon_f = \frac{1}{k}\ln\left(\frac{D_{sc}}{D_{s0}}\right). \tag{2.12}$$

It is clear that the failure strain decreases exponentially with an increase in the hydrostatic tension. Damage given by (2.10) depends upon the effective plastic strain ε_e and the hydrostatic tension. The only material parameter appearing in (2.10) is the yield stress of the material in a quasistatic simple tension test because the matrix material has been assumed to be rigid perfectly plastic.

For a thermoviscoplastic material JOHNSON and COOK [29] postulated that

$$D = \sum \Delta\varepsilon_e/(D_1 + (D_2\exp(D_3\sigma_{kk}/3\sigma_{eq})(1 + D_4\ln(\dot{\varepsilon}_e/\dot{\varepsilon}_{e0}))(1 + D_5\theta^{*b}) \tag{2.13}$$

where $\Delta\varepsilon_e$ is the increment in the effective plastic strain which occurs at the effective plastic strain rate $\dot{\varepsilon}_e$, σ_{eq} the effective stress, $\theta^* = (\theta - \theta_r)/(\theta_m - \theta_r)$, θ is the current temperature, θ_m the melting temperature, θ_r the room temperature, and b, D_1, D_2, D_3, D_4, D_5 and $\dot{\varepsilon}_0$ are material parameters; $\dot{\varepsilon}_{e0}$ is generally taken to equal 1/s. For $D_1 = D_4 = D_5 = 0$, the expression in the denominator of (2.13) reduces to the expression for the failure strain proposed by HANCOCK and MACKENZIE [8].

In Secs. 3 and 4 we will use Eq. (2.10) with σ_y replaced by σ_{eq} to ascertain the instability strain in a thermoviscoplastic body. Since this equation has been derived for mechanical deformations of a rigid perfectly plastic body, its application to thermoviscoplastic deformations necessarily involves unproven approximations. Furthermore, σ_{kk}/σ_{eq} will not, in general, be independent of ε_e. Nevertheless, the instability strain derived in Secs. 3 and 4 highlights the importance of considering damage evolution.

3. Instability strain derived from the Considère condition

We study locally adiabatic, simple shearing, and quasistatic thermomechanical deformations of an isotropic and homogeneous thermoviscoplastic body also subjected to uniform hydrostatic tensile tractions σ_∞, and assume that the shear strain rate is constant. In the absence of body and inertia forces, the balance of linear momentum requires that the shear stress, τ, be uniform throughout the body. We assume that

$$\tau = \tau(\gamma, \dot{\gamma}, \theta, D_s) \tag{3.1}$$

where γ is the plastic shear strain, and D_s the damage parameter. Here elastic deformations have been neglected which is reasonable since at the onset of instability, elastic shear strain will be very small as compared to the plastic shear strain. Recall that the area of the face on which tangential tractions act does not change, and uniform hydrostatic stresses do not cause any volume change. Thus Considère's condition, which states that a structure becomes unstable when the load reaches a peak value, in this case implies that an instability will occur when the shear stress given by Eq. (3.1) reaches a maximum value. That is, an instability will occur when

$$\frac{d\tau}{d\gamma} = \frac{\partial \tau}{\partial \gamma} + \frac{\partial \tau}{\partial \dot{\gamma}}\frac{d\dot{\gamma}}{d\gamma} + \frac{\partial \tau}{\partial \theta}\frac{d\theta}{d\gamma} + \frac{\partial \tau}{\partial D_s}\frac{dD_s}{d\gamma} = 0. \tag{3.2}$$

In Eq. (3.2) $\partial\tau/\partial\gamma$ represents work hardening or strain hardening of the material, $\partial\tau/\partial\dot{\gamma}$ its strain-rate hardening, $\partial\tau/\partial\theta$ its thermal softening and $\partial\tau/\partial D_s$ its softening due to the damage evolution.

For locally adiabatic simple shearing deformations, the balance of internal energy gives

$$\frac{d\theta}{d\gamma} = \frac{\beta\tau}{\rho c} \tag{3.3}$$

where β is the Taylor-Quinney parameter that equals the fraction of the plastic work converted to heat, ρ is the mass density and c the specific heat.

For constant shear strain rate $\dot{\gamma}$, $d\dot{\gamma}/d\gamma = 0$. Recalling that $\varepsilon_e = \gamma/\sqrt{3}$, and substituting from (2.10) and (3.3) into (3.2), we conclude that an instability will occur when

$$\frac{\partial \tau}{\partial \gamma} + \frac{\partial \tau}{\partial \theta}\left(\frac{\beta\tau}{\rho c}\right) + \frac{\partial \tau}{\partial D_s} D_{s0} k^* e^{k^*\gamma} = 0, \tag{3.4}$$

where $k^* = k/\sqrt{3}$. In terms of the effective stress σ_{eq} and the effective plastic strain ε_e, equation (3.4) becomes

$$\frac{\partial \sigma_{eq}}{\partial \varepsilon_e} + \frac{\partial \sigma_{eq}}{\partial \theta}\frac{\beta\sigma_{eq}}{\rho c} + \frac{\partial \sigma_{eq}}{\partial D_s} D_{s0} k e^{k\varepsilon_e} = 0. \tag{3.5}$$

We now assume that the thermoviscoplastic behavior of the material is represented by the JOHNSON-COOK relation [30], viz.,

$$\sigma_{eq} = (1 - D_s)(A + B\varepsilon_e^n)\left(1 + C\ln\frac{\dot{\varepsilon}_e}{\dot{\varepsilon}_{e0}}\right)(1 - \theta^{*m}) \tag{3.6}$$

where $A, B, n, C, \dot{\varepsilon}_{e0}$ and m are material parameters. For most materials, $m \simeq 1$; here we study materials for which $m = 1$. We substitute for σ_{eq} from (3.6) into (3.5) and obtain

$$\frac{\varepsilon_e^{n-1}}{(A + B\varepsilon_e^n)^2} = \frac{\beta(1 - D_{so}e^{k\varepsilon_e})}{n\rho Bc(\theta_m - \theta_r)}\left(1 + C\ln\frac{\dot{\varepsilon}_e}{\dot{\varepsilon}_{e0}}\right) + \frac{kD_{so}}{nB(A + B\varepsilon_e^n)(e^{-k\varepsilon_e} - D_{so})}. \tag{3.7}$$

For a given value of the prescribed strain rate, the hydrostatic tension and the initial damage D_{so}, equation (3.7) gives the value of the effective plastic shear strain when the material will become unstable. In deriving (3.7), $k = \sigma_\infty/\sigma_{eq}$ has been assumed to be independent of γ or ε_e. Thus the uniform hydrostatic tension has been assumed to vary so that k is essentially constant during the deformation process. The variation of k with γ can be readily incorporated into the analysis; it will make equation (3.7) more complicated.

4. Instability strain derived by the perturbation method

In the absence of body forces, the equations governing simple shearing deformations of the thermoviscoplastic body are

$$\rho\ddot{\gamma} = \frac{\partial^2\tau}{\partial y^2}, \tag{4.1}$$

$$\rho c\dot{\theta} = \kappa\frac{\partial^2\theta}{\partial y^2} + \beta\tau\dot{\gamma}, \tag{4.2}$$

$$\dot{\gamma} = v_{,y} = \sqrt{3}\,\dot{\varepsilon}_{e0}\exp\left(\left(\frac{\sqrt{3}\,\tau}{(1 - D_s)(A + B\varepsilon_e^m)(1 - \theta^{*m})} - 1\right)/C\right), \tag{4.3}$$

$$D_s = D_{s0}\exp(k^*\gamma). \tag{4.4}$$

Here v is the velocity of a material particle in the direction of shearing, κ is the thermal conductivity, and y is the position of a material particle. Equations (4.1) and (4.2) express, respectively, the balance of linear momentum and the balance of internal energy. Equation (4.3) is the Johnson-Cook relation (3.6). As in the previous section, we have neglected elastic deformations. Since we study

the stability of an infinitesimally perturbed homogeneous solution of equations (4.1)–(4.4), initial conditions are not specified.

Let the homogeneous solution, $\mathbf{s}^0 = [\gamma^0,\ \tau^0,\ \theta^0,\ D_s^0]$, of Eqs. (4.1)–(4.4) at time t_0 be given an infinitesimal perturbation

$$\delta\mathbf{s}(y,t,t_0) = \delta\mathbf{s}^0 e^{\eta(t-t_0)}e^{i\xi y},\ t \geq t_0, \tag{4.5}$$

where

$$\delta\mathbf{s}^0 = [\delta\gamma^0,\ \delta\tau^0,\ \delta\theta^0,\ \delta D_s^0]^T \tag{4.6}$$

is a small disturbance, ξ is the wave number and η the initial growth rate of the perturbation. Implicit in equation (4.5) is the assumption that surface tractions are prescribed on the bounding surfaces $y = \pm\text{const}$; otherwise only those perturbations are admissible for which $\mathbf{s}^0+\delta\mathbf{s}$ satisfies the prescribed essential boundary conditions. $\mathrm{Re}(\eta) > 0$ implies that the homogeneous solution at time t_0 is unstable; otherwise it is stable. Substituting $\mathbf{s} = \mathbf{s}^0 + \delta\mathbf{s}$ into equations (4.1)–(4.4) and linearizing the resulting equations in $\delta\mathbf{s}^0$, we obtain $\mathbf{A}(\mathbf{s}^0,\xi,\eta,t_0)\delta\mathbf{s}^0 = \mathbf{0}$ which has a nontrivial solution only if $\det(\mathbf{A}) = 0$. This gives the following cubic equation for the growth rate η:

$$\begin{aligned}\rho^2 c\eta^3 + \rho(\beta\dot\gamma^0 P_0 + \kappa\xi^2 + cR_0\xi^2)\eta^2 + (-\beta\tau^0 P_0 \\ + \rho c(Q_0 - \hat D_s^0 S_0) + \kappa R_0\xi^2)\xi^2\eta + \kappa(Q_0 - \hat D_s^0 S_0)\xi^4 = 0,\end{aligned} \tag{4.7}$$

where

$$\begin{aligned} P_0 &= -\left.\frac{\partial\tau}{\partial\theta}\right|_{\mathbf{s}=\mathbf{s}^0},\ Q_0 = \left.\frac{\partial\tau}{\partial\gamma}\right|_{\mathbf{s}=\mathbf{s}^0},\ R_0 = \left.\frac{\partial\tau}{\partial\dot\gamma}\right|_{\mathbf{s}=\mathbf{s}^0}, \\ S_0 &= -\left.\frac{\partial\tau}{\partial D_s}\right|_{\mathbf{s}=\mathbf{s}^0},\ \hat D_s^0 = \left.\frac{dD_s}{d\gamma}\right|_{\mathbf{s}=\mathbf{s}^0}, \end{aligned} \tag{4.8}$$

and $\dot\gamma^0$ is the nominal or the average shear strain rate. For materials exhibiting strain hardening, strain-rate hardening and thermal softening, $P_0 \geq 0$, $Q_0 \geq 0$, $R_0 \geq 0$. We presume that the material softens because of the damage evolved and the damage is a nondecreasing function of the plastic strain, i.e., $S_0 \geq 0$ and $\hat D_s^0 \geq 0$. Hence if $P_0 = 0$ and $\hat D_s^0 = 0$, then the homogeneous solution will be always stable. For perturbations of the homogeneous solution to grow, the material must soften either due to heating or due to damage evolution or both.

In terms of non-dimensional variables

$$\begin{aligned} \bar\eta &= \frac{\kappa\eta}{cQ_0},\ \bar\xi = \frac{\kappa\xi}{c\sqrt{\rho Q_0}},\ I = \frac{cR_0}{\kappa},\ J = \frac{\beta\tau^0 P_0 + \rho c\hat D_s^0 S_0}{\rho c Q_0}, \\ \Gamma &= \frac{\beta\kappa P_0\dot\gamma^0}{\rho c^2 Q_0},\ E = 1 - \frac{\hat D_s^0 S_0}{Q_0}, \end{aligned} \tag{4.9}$$

equation (4.7) becomes

$$\bar{\eta}^3 + [\Gamma + (1+I)\bar{\xi}^2]\bar{\eta}^2 + (I\bar{\xi}^2 + 1 - J)\bar{\xi}^2\bar{\eta} + E\bar{\xi}^4 = 0. \tag{4.10}$$

For given values of t_0 and $\bar{\xi}$, equation (4.10) has three roots. The root with the largest real part will make the homogeneous solution most unstable; this root is denoted by $\bar{\eta}_d$. For fixed t_0, $\bar{\eta}_d$ depends upon $\bar{\xi}$. We seek the wave number $\bar{\xi}_m$ for which $\bar{\eta}_d$ assumes the maximum value $\bar{\eta}_m$. Thus $\bar{\eta}_m$ and $\bar{\xi}_m$ satisfy Eq. (4.10) and

$$0 = \left.\frac{d\bar{\eta}}{d\bar{\xi}}\right|_{(\bar{\eta}=\bar{\eta}_m, \bar{\xi}=\bar{\xi}_m)}. \tag{4.11}$$

Equations (4.10) and (4.11) give

$$\bar{\xi}_m^2 = \bar{\eta}_m \frac{(J-1) - (1+I)\bar{\eta}_m}{2(I\bar{\eta}_m + E)}. \tag{4.12}$$

Since $\bar{\xi}_m^2 \geq 0$, therefore,

$$0 \leq \bar{\eta}_m \leq \frac{(J-1)}{(I+1)}. \tag{4.13}$$

Substitution for $\bar{\xi} = \bar{\xi}_m$ from (4.12) into (4.10) yields

$$4(I\bar{\eta}_m + E)(\bar{\eta}_m + \Gamma) = [(J-1) - (1+I)\bar{\eta}_m]^2. \tag{4.14}$$

Thus, whenever

$$J > 1 + 2\sqrt{E\Gamma}, \tag{4.15}$$

or

$$\frac{\beta\tau^0 P_0}{\rho c Q_0} + \frac{\hat{D}_s^0 S_0}{Q_0} > 1 + 2\left[\left(1 - \frac{\hat{D}_s^0 S_0}{Q_0}\right)\frac{\beta\kappa P_0 \dot{\gamma}^0}{\rho c^2 Q_0}\right]^{1/2}, \tag{4.16}$$

equation (4.10) will have a solution $\bar{\eta}_m$ with a positive real part. Equation (4.16) generalizes BAI'S [27] criterion to materials in which the dependence of the flow stress upon the damage is accounted for. If D_s is interpreted as an internal variable and the dependence of τ upon D_s is through the factor $(1 - D_s)$, then equation (4.16) can be deduced from equation (20) of BATRA and CHEN [28]. For $\hat{D}_s^0 = 0$ or $S_0 = 0$, equation (4.16) reduces to Bai's instability criterion. For isothermal deformations, $P_0 = 0$, and the instability will occur when the softening induced by damage evolution exceeds the strain hardening of the material.

DODD and ATKINS [31] have shown that flow localization in shear is possible under isothermal conditions if voids are present within the shear band. For plane strain thermomechanical deformations of a typical steel studied by BATRA and JIN [9], material softening due to void nucleation and growth was found to be greater than that induced by the temperature rise.

For locally adiabatic deformations, $\kappa = 0$, and the instability condition (4.16) becomes

$$\frac{\beta \tau^0 P_0}{\rho c} + \hat{D}_s^0 S_0 > Q_0. \tag{4.17}$$

Thus the material becomes unstable when the material softening due to the combined effects of thermal heating and damage evolution exceeds the work hardening of the material. For a unit increment in the shear strain γ, the first term on the left-hand side of (4.17) represents the magnitude of the decrease in τ due to the thermal softening of the material, and the second term equals the decrease in τ due to the magnitude of the softening of the material caused by the damage evolution, and the term on the right-hand side of (4.7) equals the increase in τ due to work hardening of the material. Even though strain rate hardening does not explicitly appear in equations (4.16) and (4.17), it affects the value of τ^0 and hence of P_0, Q_0 and S_0. In the presence of heat conduction, higher values of $\hat{D}_s^0$ and S_0 reduce the shear strain at instability but higher values of the nominal strain rate $\dot{\gamma}^0$ delay it. BATRA and CHEN [28] have delineated the effect of strain rate on the instability strain.

Let

$$\delta = 2\left[\left(1 - \frac{\hat{D}_s^0 S_0}{Q_0}\right)\frac{\beta \kappa P_0 \dot{\gamma}^0}{\rho c^2 Q_0}\right]^{1/2}. \tag{4.18}$$

In order to estimate the magnitude of δ we use the following values, taken from Batra and Kim [32], of material parameters for a 4340 steel and set

$$3\sigma_\infty/2\sigma_{eq} = 1, \quad D_{s0} = 10^{-5}, \quad \beta = 0.9, \quad \theta \simeq \beta A \varepsilon_e/\rho c, \quad \sigma_{eq} = A.$$

Table 1. Values of material parameters for a 4340 steel.

A(MPa)	B(MPa)	C	n	m	ρ(kg/m^3)
792.2	509.5	0.014	0.26	1.0	7,860

c(J/kg K)	κ(W/m^{2}K)	θ_m(°C)	θ_r(°C)	$\dot{\varepsilon}_{e0}$(s^{-1})
477	49.73	1520	25	10^{-3}

Figures 1a and 1b show, respectively, the variation of δ with $\dot{\varepsilon}_e^0$ for $\varepsilon_e^0 = 0.4$ and the variation of δ with ε_e^0 for $\dot{\varepsilon}_e^0 = 10^3$/s. For the range of values of $\dot{\varepsilon}_e^0$ and

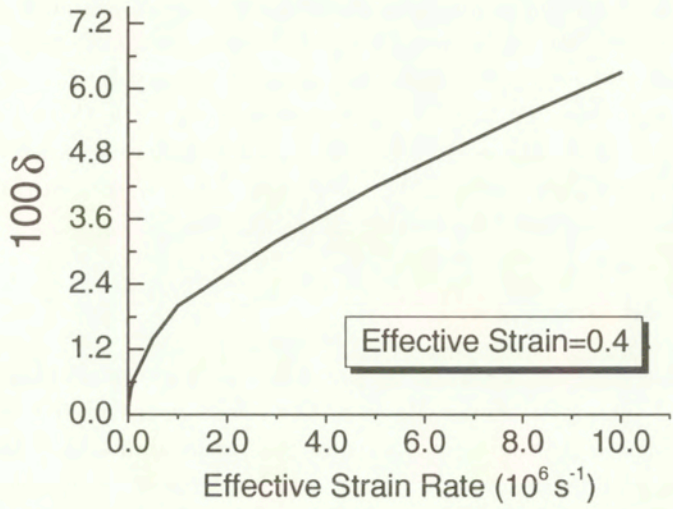

FIG. 1a. At an average effective strain of 0.4, variation of δ defined by Eq. (4.18) with the nominal effective strain rate.

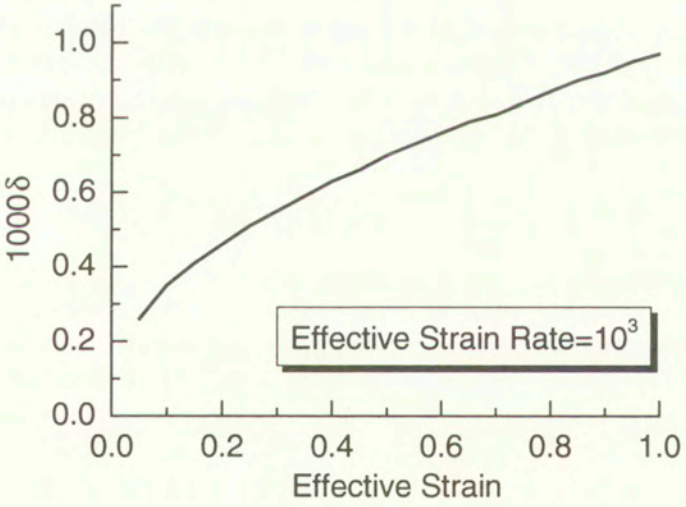

FIG. 1b. For a nominal effective strain rate of $10^3/s$, variation of δ defined by equation (4.18) with the effective strain.

ε_e^0 considered, the maximum value 0.06 of δ occurs for $\dot{\varepsilon}_e^0 = 10^7/s$ and $\varepsilon_e^0 = 0.4$. Thus $\delta \ll 1$ for typical values of strains and strain rates within a shear band, and the instability criterion (4.16) can be simplified to (4.17) even in the presence of heat conduction. This is also supported by the numerical experiments of BATRA and KIM [35] who found that thermal conductivity had a negligible effect on

the onset of an ASB but influenced significantly the subsequent deformations. Since the instability strain, γ_i, equals the minimum value of the shear strain for which inequality (4.17) holds, thus the value of γ_i may be found by replacing inequality in (4.17) by equality. A comparison of (4.17) with (3.5) reveals that the perturbation analysis and the Considère condition give essentially identical values of the instability strain. We note that for a homogeneous solution of equations (4.1)–(4.4), heat conduction plays no role.

5. Results and Discussion

For the 4340 steel deformed in simple shear with a superimposed hydrostatic tension, Fig. 2 shows the dependence of the effective instability strain ε_i upon the nominal strain rate for three values of the initial damage. It is evident that ε_i is an almost affinely decreasing function of $\log \dot{\varepsilon}_e$. Also, the initial value of the damage significantly affects the instability strain; it is because the accumulated damage is directly proportional to the initial damage. Figure 3 exhibits that the instability strain decreases exponentially with an increase in the initial damage. However, when the evolution of damage is neglected, then the instability strain is an increasing affine function of the initial damage. To illucidate this we neglect the third term on the left-hand side of (3.4) since it represents a contribution from the damage evolution. For the 4340 steel, the instability strain is then given by (e.g. cf. equation (3.7))

$$\frac{\varepsilon_i^{-0.74}}{(1+0.643\varepsilon_i^n)^2} = 1.0437\beta(1-D_{s0}).$$

It is clear that a higher value of D_{s0} results in a lower value of ε_i. A positive value of D_{s0} may be viewed as decreasing β which equals the fraction of plastic working converted into heating. A lower heating rate reduces the temperature rise and hence the thermal softening effect which in turn increases the instability strain.

The effect of the hydrostatic tension on the instability strain ε_i and on the failure strain ε_f is shown in Fig. 4; ε_f is computed from equation (2.12) by setting $D_{sf} = 0.3$. It implies that the material ruptures when the surface area of voids equals 30% of the area of cross-section of the specimen. Plate impact experiments of SEAMAN *et al.* [33] suggest that copper specimens fail at a point where the porosity equals 0.3. Results plotted in Fig. 4 show that $\log(\varepsilon_f)$ decreases affinely with an increase in the hydrostatic tension. However, $\log(\varepsilon_i)$ is insensitive to the hydrostatic tension so long as it is small and below a certain value which depends upon the initial damage. Beyond this value of the hydrostatic tension, $\log(\varepsilon_i)$ decreases rather rapidly with an increase in the hydrostatic tension. Should the

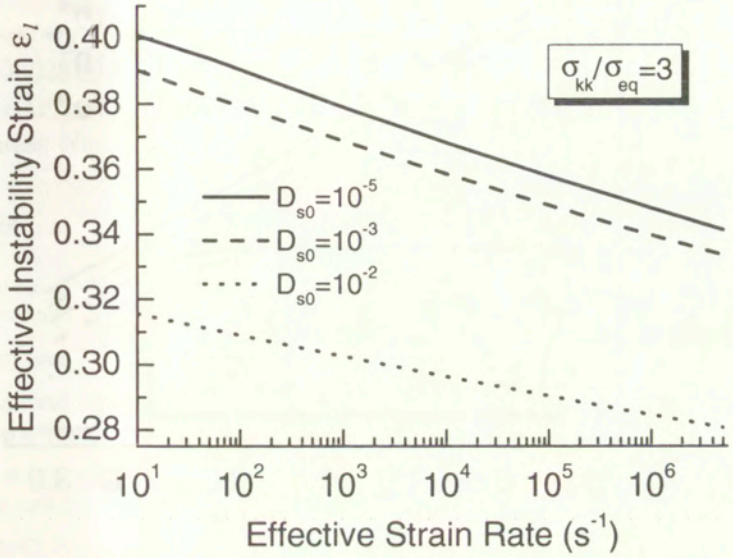

FIG. 2. For three values of the initial damage, variation of the effective instability strain with the nominal effective strain rate.

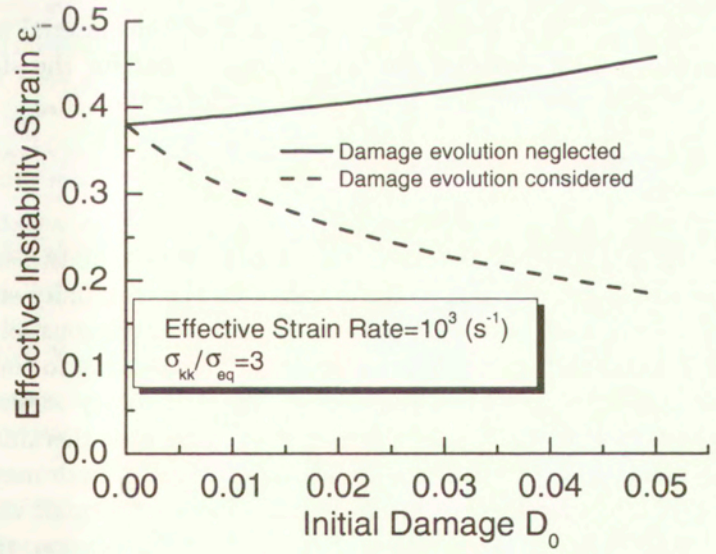

FIG. 3. For nominal strain rate of 10^3/s, variation of the effective instability strain with the initial damage.

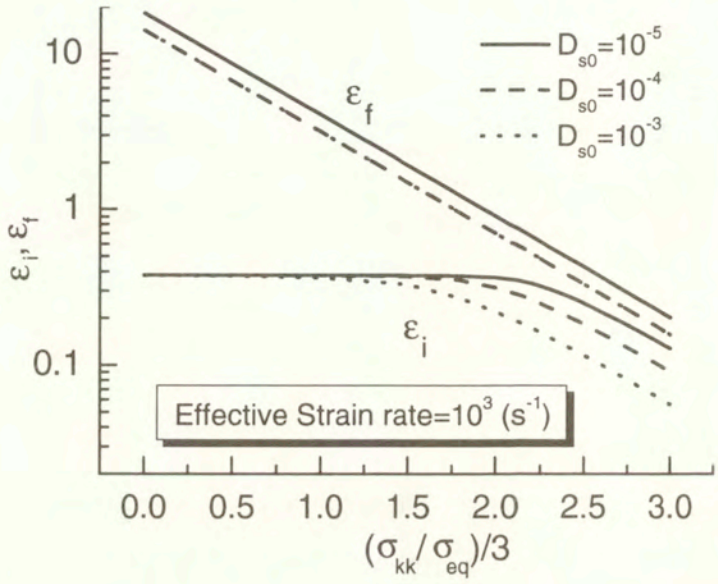

FIG. 4. For the effective nominal strain rate of 10^3/s and a prescribed value of the initial damage, variation of the instability and the failure strains with the normalized hydrostatic tension.

plots of ε_i vs. σ_{kk}/σ_{eq} and ε_f vs. σ_{kk}/σ_{eq} intersect, then the material will fracture before it becomes unstable. Results in Fig. 4 evince that for the steel studied here and $D_{sf} = 0.3$ it will happen only for large values of σ_{kk}/σ_{eq}.

6. Conclusions

For simple shearing deformations of a thermoviscoplastic body also subjected to a uniform hydrostatic tension, we have computed the instability strain by using the Considère criterion and also by examining if a homogeneous solution when perturbed will become unstable. The evolution of damage due to the growth of existing spherical voids has been considered. The instability strain found by the two methods is essentially the same. In the absence of thermal softening, the softening induced by the void and hence the damage growth may make the material unstable. The instability strain is not sensitive to small values of the hydrostatic tension but for large values of the hydrostatic tension, the instability strain decreases rather rapidly with an increase in the hydrostatic tension. However, the logarithm of the failure strain decreases rapidly with an increase in the hystrostatic tension. For the 4340 steel studied and assumed to fail when the accumulated damage equals 0.3, the material becomes unstable before it fails.

Acknowledgements

This work was partially supported by the US National Science Foundation grant CMS0002849 and the ONR grant N00014-98-1-0300 to Virginia Polytechnic Institute and State University. Z. G. Wei's work was also partially supported by the Chinese National Science Foundation grant 10002017.

References

1. L. SEAMAN, D.R. CURRAN and D.A. SHOCKEY, *Computational models for ductile and brittle fracture*, J. Appl. Phys., **17**, 4814–4826, 1976.
2. B. DODD and T.L. BAI, *Ductile fracture and ductility*, Academic Press, London 1987.
3. Y.L. BAI and B. DODD, *Adiabatic shear localization, occurrence, theories, and applications*, Pergamon Press, 1992.
4. A.J. ROSAKIS and G. RAVICHANDRAN, *Dynamic failure mechanics*, International Journal of Solids and Structures, **37**, 331–348, 2000.
5. F.A. MCCLINTOCK, *A criterion for ductile fracture by growth of holes*, J. Appl. Mech., **35**, 363–371, 1968.
6. J.R. RICE and D.M. TRACEY, *On the ductile enlargement of voids in triaxial stress field*, J. Mech. Phys. Solids, **17**, 210–217, 1969.
7. A.L. GURSON, *Plastic flow and fracture behavior of ductile materials incorporating void nucleation, growth and interaction*, Ph.D. Thesis, Brown University, 1975.
8. J.W. HANCOCK and A.C. MACKENZIE, *On the mechanisms of ductile failure in high strength steels subjected to multiaxial stress states*, J. Mech. Phys. Solids, **24**, 147–169, 1976.
9. R.C. BATRA and X.S. JIN, *Analysis of dynamic shear bands in porous thermally softening viscoplastic materials*, Archives of Mechanics, **41**, 13–36, 1994.
10. R.C. BATRA and N.A. JABER, *Failure mode transition speeds in an impact loaded prenotched plate with four thermoviscoplastic relations*, Int. J. Fracture, **110**, 47–71, 2001.
11. P. PERZYNA, *Constitutive modelling of dissipative solids for localization and fracture*, [in:] *Localization and Fracture Phenomena in Inelastic Solids*, P. PERZYNA [Ed.], Springer, Wien, New York, 99–241, 1998.
12. W. DORNOWSKI and P. PERZYNA, *Localized fracture phenomena in thermo-viscoplastic flow processes under cyclic dynamic loadings*, Acta Mechanica, **155**, 233–255, 2002.
13. W. DORNOWSKI and P. PERZYNA, *Constitutive modeling of inelastic solids for plastic flow processes under cyclic dynamic loadings*, J. Engr. Mater., **121**, 210–220, 1999.
14. J.A. LEMAITRE, *Course on damage mechanics*, Springer-Verlag, Berlin, Heidelberg, 1996.
15. B.D. COLEMAN and M.E. GURTIN, *Thermodynamics with internal state variables*, J. Chem. Phys., **47**, 597–613, 1967.
16. D.R. CURRAN, L. SEAMAN and D.A. SHOCKEY, *Dynamic failure of solids*, Phys. Rep., **147**, 253–388, 1987.

17. Y.L. Bai, F.J. Ke and M.F. Xia, *Formulation of statistical evolution of microcracks in solids*, Acta Mechanica Sinica, **7**, 59–66, 1991.

18. Y.L. Bai, Z. Ling, L.M. Luo and F.J. Ke, *Initial development of microdamage under impact loading*, Journal of Applied Mechanics, **59**, 622–627, 1992.

19. Y.L. Bai, J. Bai, H.L. Li, F.J. Ke and M.F. Xia, *Damage evolution localization and failure of solids subjected to impact loading*, Int. J. Impact Eng., **24**, 685–701, 2000.

20. Y.L. Bai, M.F. Xia, F.J. Ke and H.L. Li, *Statistical microdamage mechanics and damage field evolution*, Theoretical and Applied Fracture Mechanics, **37**, 1–10, 2001.

21. Y.C. Li, D.H. Li, Z.G. Wei and Y.X. Sun, *Research on the deformation, damage and fracture rules of circular tubes under inside-explosive loading*, Acta Mechanica Sinica, **31**, 442–449, 1999.

22. H. Tresca, *On further aplications of the flow of solids*, Proc. Inst. Mech. Engrs., **30**, 301–345, 1878.

23. C. Zener and J.H. Hollomon, *Effect of strain rate upon plastic flow of steel*, J. Appl. Phys., **15**, 22–32, 1944.

24. A. Marchand and J. Duffy, *An experimental study of the formation process of adiabatic shear bands in a structural steel*, J. Mechs. Phys. Solids, **36**, 251–283, 1988.

25. R.C. Batra, *Numerical solutions of initial-boundary-value problems with shear strain localization*, [in:] *Localization and Fracture Phenomena in Inelastic Solids*, P. Perzyna [Ed.], Springer, Wien, New York, 301–389, 1998.

26. M. Considère, *Die Anwendung von Eisen und Stahl bei Konstruktionen*, Gerold-Verlag, Wien 1888.

27. Y.L. Bai, *Thermo-plastic instability in simple shear*, J. Mech. Phys. Solids, **30**, 195–207, 1982.

28. R.C. Batra and L. Chen, *Effect of viscoplastic relations on the instability strain, shear band initiation strain, the strain corresponding to the minimum shear band spacing, and the band width in a thermoviscoplastic material*, International Journal of Plasticity, **17**, 1465–1489, 2001.

29. G.R. Johnson and W.H. Cook, *Fracture characteristics of three metals subjected to various strains, strain rates, temperatures and pressures*, Engng. Fract. Mech., **21**, 31–48, 1985.

30. G.R. Johnson and W.H. Cook, *A constitutive model and data for metals subjected to large strain rates and high temperatures*, Proceedings of the Seventh International Symposium on Ballistics, The Hague, The Netherlands, 541–548, 1983.

31. B. Dodd and A.G. Atkins, *Flow localization in shear deformation of solids containing voids and of void-free solids*, Acta Metallurgica, **31**, 9–15, 1983.

32. R.C. Batra and C.H. Kim, *Analysis of shear bands in twelve materials*, Int. J. Plasticity, **8**, 425–452, 1992.

33. L. Seaman, T.W. Barbee, J R. and D.R. Curran, *Dynamic fracture criteria of homogeneous materials*, AFWAL-TR-71-156, Stanford Research Institute.

34. R.C. Batra, N.A. Jaber and M.E. Malsbury, *Analysis of failure modes in an impact loaded thermoviscoplastic prenotched plate*, Int. J. Plasticity, **19**, 139–196, 2003.

35. R.C. BATRA and C.H. KIM, *Effect of thermal conductivity on the initiation, growth and band width of adiabatic shear bands*, Int. J. Engng. Sci., **29**, 949–960, 1991.

Received August 29, 2002; new version December 9, 2002.

Arch. Mech., **54**, 5-6, pp. 709–736, Warszawa 2002

Thermodynamical admissibility of Biot's model of poroelastic saturated materials

K. WILMAŃSKI

Weierstrass Institute for Applied Analysis and Stochastics, Berlin, Germany,
www.wias-berlin.de/private/wilmansk

Dedicated to Professor Piotr Perzyna on the occasion of his 70^{th} birthday

THE PAPER is devoted to the analysis of nonlinear elastic two-component models of saturated porous media, which in a linear form, reproduce as closely as possible the classical Biot's model [1]. We present a full evaluation of the second law of thermodynamics for four classes of nonlinear models. It is proven that two of them in which there is no dependence on higher gradients cannot lead to the Biot's model. On the other hand, two other models in which a dependence on the gradient of porosity is introduced, yield linear constitutive relations but not the field equations appearing in the Biot's model. However, a recombination of partial stresses and momentum sources leads to Biot's equations. This analysis together with earlier publications on the subject exhausts the discussion of the question of thermodynamical admissibility of the Biot's model.

1. Introduction

Continuous models of porous and granular materials which account for the relative motion of components (diffusion) rely on the theory of two-component immiscible mixtures in which one of the components is a solid. The first linear model of this type has been developed by M. A. Biot in early 40ies (see: [1] for the full account of Biot's papers on this subject). This model had an enormous success among engineers and geophysicists who applied it in soil mechanics, mechanics of sediments on the see bottom, propagation of waves in porous and granular materials, experimental testing of such materials etc. Many phenomena of practical importance such as tortuosity which did not appear in the original model of Biot, have been added *ad hoc* to the model mostly by reinterpretation of original contributions.

Unfortunately, the attempts to verify foundations of the Biot's model and to develop such models in the spirit of modern continuum thermodynamics have been vehemently criticized by admirers of the Biot's model, since such attempts were a blasphemy in the holy shrine of infallibility. It is, certainly, true that the

Biot's model provides an explanation of many important observations in porous materials such as the existence of the second sound called Biot's slow wave or the structure of surface waves (existence of additional modes of propagation). Simultaneously it is rather easy to observe that the Biot's field equations violate fundamental laws of thermodynamics: the second law of thermodynamics and the principle of material objectivity.

The classical Biot's model relies on two partial momentum balance equations

$$\begin{aligned} \rho_0^S \frac{\partial \mathbf{v}^S}{\partial t} + \rho_{12} \frac{\partial \mathbf{v}^F}{\partial t} &= \mathrm{div}\mathbf{T}^S + \pi \left(\mathbf{v}^F - \mathbf{v}^S \right), \\ \rho_0^F \frac{\partial \mathbf{v}^F}{\partial t} + \rho_{12} \frac{\partial \mathbf{v}^S}{\partial t} &= \mathrm{div}\mathbf{T}^F - \pi \left(\mathbf{v}^F - \mathbf{v}^S \right), \end{aligned} \tag{1.1}$$

with the following constitutive relations for stresses (e.g. [2])

$$\begin{aligned} \mathbf{T}^S &= Ae\mathbf{1} + 2G\mathbf{e}^S + Q\epsilon\mathbf{1}, \\ \mathbf{T}^F &= \sigma\mathbf{1}, \quad \sigma \equiv -p^F = Qe + R\epsilon, \end{aligned} \tag{1.2}$$

where we use the following notations appearing also further in this work: ρ_0^S, ρ_0^F are constant partial mass densities of the solid component (skeleton) and of the fluid component, respectively, ρ_{12} is the acceleration coupling constant ("added mass"), $\mathbf{v}^S, \mathbf{v}^F$ are macroscopic velocities of components, A, G, Q, R, π are material parameters, $\mathbf{e}^S$ describes small deformations of the skeleton (Almansi-Hamel deformation tensor), and ϵ descibes volume changes of the fluid component[1)]

In my earlier works on this subject (e.g. [3], [4]) I have presented a rather immediate proof that the Biot's model indeed violates the principle of material objectivity. This is related to the coupling through accelerations, i.e. to the existence of the added mass ρ_{12}.

The thermodynamical admissibility is a more subtle issue. It will be presented in this work and it concerns the coupling constant Q.

One should distinguish two cases. The first one appears when changes of porosity are described by an additional field equation. It may be a second order equation proposed in the model of GOODMANN and COWIN [5], a first order evolution equation proposed by BOWEN [6] or a balance equation proposed in

[1)] Within the frame of macroscopical description, all these fields must possess a purely macroscopical interpretation. In our case the volume changes of the skeleton are described by the third invariant of the deformation tensor of the skeleton. This reduces to $tr\mathbf{e}^S$ for small deformations. For the fluid, the mass ϵ of volume changes are related to changes of partial (smeared-out) mass densities

$$\epsilon = \frac{\rho_0^F - \rho^F}{\rho_0^F}.$$

We return to other quanities describing volume changes further in this paper (e.g. Subsec. 2. 3).

my own papers (e.g. [7]). In these models the coupling between partial stresses cannot have the form proposed by Biot due to identities following from the second law of thermodynamics. The second case appears when changes of porosity are described by a constitutive law (see: [8]). This case has not been systematically investigated and it is the subject of this work.

We prove that a nonlinear poroelastic model without contributions of higher gradients cannot produce the Biot's model. We mean by higher gradients of constitutive variables a gradient of porosity n, a gradient of the deformation gradient of skeleton $\mathbf{F}^S$, or a gradient of one of the partial velocities. A model in which the gradient of the deformation gradient $\mathbf{F}^S$ appears leads to the necessity of introducing couple stresses and it becomes a Cosserat–type continuum. On the other hand, the gradients of velocities introduce viscous effects which in turn destroy the hyperbolicity of field equations. This is not desired in the wave analysis. In addition, none of these effects appears in the case of Biot's model. Consequently it remains the gradient of porosity as a reasonable possibility. We shall prove that a correction of a dependence on the gradient of porosity is sufficient for thermodynamical admissibility of Biot's stress relations. However such a correction yields automatically additional contributions to momentum balance equations. They must contain a term with the gradient of porosity as well and this is not the case in the Biot's model.

These considerations seem to exhaust the available possibilities and yield the conclusion that only constitutive relations for stresses in the Biot's model can be constructed in a thermodynamically admissible way provided a classical multicomponent model is extended to higher gradients. Field equations must be different.

We complete the paper with a remark on acoustic waves. We show that linear models constructed in Subsection 2.3 yield the existence of bulk acoustic P1-, S-, and P2-waves as predicted by Biot's model but their speeds of propagation are different.

2. Thermodynamic construction of models

2.1. Fields and field equations

In order to appreciate couplings between partial stresses of a poroelastic saturated medium we consider the two following two-component prototypes of the "Biot's" model for large deformations.

For the first class of models labeled (I) we assume that the real fluid in pores is incompressible. This assumption means that we have two possibilities to control changes of the geometry of the medium. On the one hand we can macroscopically deform the skeleton, and we measure this deformation by the macroscopic

deformation gradient $\mathbf{F}^S$. Doing so we keep the porosity constant, i.e. the fraction n of the volume of the representative volume element (*REV*) corresponding to the fluid component does not change ("undrained conditions"). We can also deform pores by drainage and in this way change the porosity n. Simultaneously we keep unchanged the macroscopic geometry, i.e. $\mathbf{F}^S = \text{const}$. Under the incompressibility assumption the latter deformation is solely related to changes of mass densities. For the fluid component these changes are given by the relation

$$\rho_t^F = n\rho^{FR}, \quad \rho^{FR} = \text{const}, \tag{2.1}$$

where ρ^{FR} is the so-called true mass density. The incompressibility assumption yields this quantity to be constant. The index t means that the mass density refers to the unit volume of the mixture in the current configuration.

In the second class of models labeled (C) we allow for arbitrary changes of mass densities ρ_t^F, ρ_t^S but the porosity is assumed to be given by a "constitutive" relation. It has been shown [9] that in *thermodynamical equilibria* such a relation must have the form $n = \hat{n}\left(\dfrac{\rho_t^F}{\rho_t^S}\right)$. In the simplest case which we consider in this work we assume this relation to have the following form

$$n = n_0 \frac{\rho_t^F}{\rho_0^F} \frac{\rho_0^S}{\rho_t^S}, \tag{2.2}$$

where ρ_0^F, ρ_0^S, n_0 denote reference constant values of partial mass densities and of the porosity. The above relation is assumed to hold also in thermodynamical nonequilibrium.

Let us note that in general the porosity n may change as well without accompanying changes of macroscopic mass densities ρ_t^F, ρ_t^S. This happens when changes of n are compensated by changes of real mass densities ρ^{FR}, ρ^{SR} in such a way that their products $n\rho^{FR}, (1-n)\,\rho^{SR}$ remain constant. Such changes are not controllable on the macroscopic level. They must proceed spontaneously. Consequently they yield a **relaxation** of porosity characteristic for microstructural variables. Relaxation properties are always dissipative and do not appear in thermodynamical equilibria. These phenomena require a source term in an equation describing changes of porosity. Such a general model was discussed elsewhere (e.g. [7]).

We shall discuss further properties of the relation (2.2) when we linearize the model.

For technical reasons it is easier to work in a so-called Lagrangian description (e.g. [7],[8]). In this description we refer all quantities to a chosen reference configuration $\mathcal{B}_0$ of the skeleton for which $\mathbf{F}^S = \mathbf{1}$.

Fields which describe mechanical processes in such a system are as follows:

1. The reference partial mass density of the fluid component

$$\rho^F = \rho^F(\mathbf{X}, t) = \rho_t^F J^S \equiv n J^S \rho^{FR}, \quad J^S := \det \mathbf{F}^S, \quad \mathbf{X} \in \mathcal{B}_0. \tag{2.3}$$

2. The field of partial velocity of the skeleton $\dot{\mathbf{x}}^S(\mathbf{X}, t)$ on the macroscopic level of description.
3. The field of partial velocity of the fluid $\dot{\mathbf{x}}^F(\mathbf{X}, t)$ on the macroscopic level of description.
4. The macroscopic deformation gradient of the skeleton $\mathbf{F}^S(\mathbf{X}, t)$.

By means of the velocity fields one can define the macroscopic filter velocity $\mathbf{w}(\mathbf{X}, t)$, and its corresponding Lagrangian image $\dot{\mathbf{X}}^F(\mathbf{X}, t)$ appearing in balance equations

$$\mathbf{w} := \dot{\mathbf{x}}^F - \dot{\mathbf{x}}^S, \quad \dot{\mathbf{X}}^F := \mathbf{F}^{S-1}\mathbf{w}. \tag{2.4}$$

The reference partial mass density of the skeleton $\rho^S \equiv \rho_0^S$ does not appear among those fields because it is constant in time if we assume that there is no mass exchange between components. Its current value is given by the relation

$$\rho_t^S = \rho_0^S J^{S-1}, \tag{2.5}$$

which satisfies identically the partial mass conservation law in Eulerian description.

Summing up we can write the following relations for the porosity in the two above classes of the models

$$\begin{aligned} &\text{(I)-models} \quad : \quad n = J^{S-1}\frac{\rho^F}{\rho^{FR}}, \quad \rho^{FR} = \text{const}, \\ &\text{(C)-models} \quad : \quad n = \frac{\rho^F}{\rho_0^{FR}}, \quad \rho_0^{FR} = \frac{\rho_0^F}{n_0} = \text{const}. \end{aligned} \tag{2.6}$$

The fields must fulfil the following balance equations in Lagrangian description

1. **Mass conservation of the fluid component**

$$\frac{\partial \rho^F}{\partial t} + Div\left(\rho^F \dot{\mathbf{X}}^F\right) = 0. \tag{2.7}$$

2. **Momentum balance for the skeleton**

$$\rho^S \frac{\partial \dot{\mathbf{x}}^S}{\partial t} = Div\mathbf{P}^S + \hat{\mathbf{p}}. \tag{2.8}$$

3. Momentum balance for the fluid

$$\rho^F \left(\frac{\partial \hat{\mathbf{x}}^F}{\partial t} + \hat{\mathbf{X}}^F \cdot \operatorname{Grad} \hat{\mathbf{x}}^F \right) = Div \mathbf{P}^F - \hat{\mathbf{p}}. \tag{2.9}$$

In addition, the deformation gradient $\mathbf{F}^S$ must fulfil **integrability conditions** yielding the existence of the field of motion of the skeleton. They consist of two parts.

4. Kinematic compatibility condition relates the time derivative and the gradient of velocity

$$\frac{\partial \mathbf{F}^S}{\partial t} = \operatorname{Grad} \hat{\mathbf{x}}^S. \tag{2.10}$$

The second part – a geometrical compatibility condition is a symmetry relation

$$\operatorname{Grad} \mathbf{F}^S = \left(\operatorname{Grad} \mathbf{F}^S \right)^{\overset{23}{T}}, \tag{2.11}$$

or, in Cartesian coordinates

$$\frac{\partial F^S_{kK}}{\partial X^L} = \frac{\partial F^S_{kL}}{\partial X^K}, \tag{2.12}$$

where the small index refers to Eulerian coordinates, and the capital index to Lagrangian coordinates.

Obviously, all operators Grad, Div, $\dfrac{\partial}{\partial X^K}$ refer to Lagrangian variables.

As we have mentioned conditions (2.10),(2.11) yield the existence of the field of motion of skeleton, say $\chi^S(\mathbf{X}, t)$, whose derivatives give the deformation gradient and the partial velocity, vis.

$$\mathbf{F}^S = \operatorname{Grad} \chi^S, \quad \hat{\mathbf{x}}^S = \frac{\partial \chi^S}{\partial t}. \tag{2.13}$$

Momentum balance equations contain partial Piola-Kirchhoff stresses $\mathbf{P}^S, \mathbf{P}^F$ which are related to the usual Cauchy stresses by the following transformation rules

$$\mathbf{T}^S = J^{S-1} \mathbf{P}^S \mathbf{F}^{ST}, \quad \mathbf{T}^F = J^{S-1} \mathbf{P}^F \mathbf{F}^{ST}. \tag{2.14}$$

Momentum equations contain as well the source $\hat{\mathbf{p}}$ which is the diffusion force.

We have to perform a closure in order to obtain field equations from the above balance relations. For poroelastic materials we consider further two models following from two choices of constitutive variables. Namely we choose either

$$\mathcal{C}^{(1)} = \left\{\rho^F, \mathbf{F}^S, \dot{\mathbf{X}}^F\right\}, \tag{2.15}$$

or

$$\mathcal{C}^{(2)} = \left\{\rho^F, \mathbf{F}^S, \dot{\mathbf{X}}^F, \mathrm{Grad} n\right\}. \tag{2.16}$$

The porosity n does not appear among these variables because it is either given by the relation (2.2) or by the relation (2.3). Consequently it can be eliminated from the set of independent constitutive variables.

The following functions must be given in terms of constitutive relations:

$$\mathcal{F} = \left\{\mathbf{P}^S, \mathbf{P}^F, \hat{\mathbf{p}}, \psi^S, \psi^F\right\}, \tag{2.17}$$

where ψ^S, ψ^F denote partial Helmholtz free energies appearing further in the second law of thermodynamics.

For reasons of material objectivity we should choose not only the *relative* velocity as the variable but also one of the *objective measures* of deformation. We shall do so further in this note. However the exploitation of the second law of thermodynamics is easier if we impose the objectivity after the exploitation of the entropy inequality.

For any of the choices of constitutive variables, the constitutive relations are assumed to have the form of the relation

$$\mathcal{F} = \mathcal{F}\left(\mathcal{C}^{(\alpha)}\right), \quad \alpha = 1, 2, \tag{2.18}$$

which is sufficiently smooth for all operations which we perform in the sequel.

Let us make two methodological remarks. Our interest in comparison with the Biot's model as well as in the analysis of acoustic waves is limited to linear models. Consequently the above presented nonlinear models are an overkilling. We do so on purpose because the exploitation of the second law of thermodynamics for a model with linear constitutive laws cannot be made consistent with explicit nonlinear contributions to field equations. This yields serious flaws of the thermodynamical analysis known in all nonlinear field theories.

Secondly we should point out that the restriction to incompressible real fluids in the class (I) of models **does not lead to any constraints.** This may be simply interpreted as a change of variables: changes of the partial mass density of the fluid are replaced by corresponding changes of the porosity. There is no reaction force on such a "constraint". This is different from the cases which

were considered previously (e.g. [10], [9]). In those cases the model possesses an additional equation for porosity which, in turn, is considered to be a real microstructural variable with spontaneous relaxation properties. In such models the incompressibility assumption yields the existence of the reaction pressure, and it requires a special structure of constitutive relations. We shall not discuss this problem in this work.

Let us mention in passing that the above change of variables may lead to some mathematical problems due to the restriction $0 < n < 1$. As we are primarily interested in a linear model changes of porosity with respect to its initial value n_0 are small. The choice of a real value of n_0, say between 0.1 and 0.6, guarantees that this restriction is indeed fulfilled. In addition thermodynamical restrictions are derived by means of the partial mass density for which such a restriction does not appear.

2.2. Thermodynamic admissibility

2.2.1. Second law of thermodynamics. We present here solely the second law of thermodynamics for two-component systems for which the temperature is constant. If this is the case it may be formulated as follows (e.g. [11]). For any solution of field equations (i.e. for any *thermodynamical process*) the following inequality

$$\rho^S \frac{\partial \psi^S}{\partial t} + \rho^F \left(\frac{\partial \psi^F}{\partial t} + \dot{\mathbf{X}}^F \cdot \operatorname{Grad} \psi^F \right) - \mathbf{P}^S \cdot \frac{\partial \mathbf{F}^S}{\partial t} - \mathbf{P}^F \cdot \operatorname{Grad} \dot{\mathbf{x}}^F - \hat{\mathbf{p}} \cdot \mathbf{w} \leq 0, \tag{2.19}$$

must be satisfied identically.

The main technical problem with the exploitation of this inequality is the limitation to solutions of field equations. This can be eliminated by means of Lagrange multipliers introduced to thermodynamics by I-SHIH LIU ([7]). Namely it can be shown that the following inequality

$$\begin{aligned} \rho^S \frac{\partial \psi^S}{\partial t} + \rho^F \left(\frac{\partial \psi^F}{\partial t} + \dot{\mathbf{X}}^F \cdot \operatorname{Grad} \psi^F \right) & - \mathbf{P}^S \cdot \frac{\partial \mathbf{F}^S}{\partial t} - \mathbf{P}^F \cdot \operatorname{Grad} \dot{\mathbf{x}}^F - \hat{\mathbf{p}} \cdot \mathbf{w} \\ & - \Lambda^n \left\{ \frac{\partial \rho^F}{\partial t} + Div \left(\rho^F \dot{\mathbf{X}}^F \right) \right\} - \boldsymbol{\Lambda}^F \cdot \left\{ \frac{\partial \mathbf{F}^S}{\partial t} - \operatorname{Grad}, \dot{\mathbf{x}}^S \right\} \end{aligned} \tag{2.20}$$

$$
\begin{aligned}
(2.20)\ [\text{cont.}] \qquad & - \boldsymbol{\Lambda}^{vS} \cdot \left\{ \rho^S \frac{\partial \dot{\mathbf{x}}^S}{\partial t} - \operatorname{Div} \mathbf{P}^S - \hat{\mathbf{p}} \right\} \\
& - \boldsymbol{\Lambda}^{vF} \cdot \left\{ \rho^F \left(\frac{\partial \dot{\mathbf{x}}^F}{\partial t} + \dot{\mathbf{X}}^F \cdot \operatorname{Grad} \dot{\mathbf{x}}^F \right) - \operatorname{Div} \mathbf{P}^F + \hat{\mathbf{p}} \right\} \leq 0,
\end{aligned}
$$

must hold for any fields and not only for solutions of field equations. The multipliers $\Lambda^n, \boldsymbol{\Lambda}^F, \boldsymbol{\Lambda}^{vS}, \boldsymbol{\Lambda}^{vF}$ are functions of constitutive variables $\mathcal{C}^{(\alpha)}$ for α equal either to 1 or to 2. We proceed to discuss the consequences of the above condition for these two different models.

2.2.2. $\mathcal{C}^{(1)}$–models. We consider the model with constitutive variables given by the relation (2.15). It is not necessary to distinguish between (I)-models and (C)-models because the only difference appears in the final results due to the substitution of either $(2.6)_1$ or $(2.6)_2$.

It is easy to check that the chain rule of differentiation in the inequality (2.21) yields the linearity of this inequality with respect to the following derivatives

$$
(2.21) \qquad \left\{ \frac{\partial \rho^F}{\partial t}, \frac{\partial \mathbf{F}^S}{\partial t}, \frac{\partial \dot{\mathbf{x}}^S}{\partial t}, \frac{\partial \dot{\mathbf{x}}^F}{\partial t} \right\},
$$

as well as

$$
(2.22) \qquad \left\{ \operatorname{Grad} \rho^F, \operatorname{Grad} \mathbf{F}^S, \operatorname{Grad} \dot{\mathbf{x}}^S, \operatorname{Grad} \dot{\mathbf{x}}^F \right\}.
$$

Consequently, as the inequality must hold for **all fields**, the coefficients of these derivatives have to vanish. We obtain from the contributions of time derivatives (2.21) the following relations:

$$
\begin{aligned}
\Lambda^n &= \rho^S \frac{\partial \psi^S}{\partial \rho^F} + \rho^F \frac{\partial \psi^F}{\partial \rho^F}, \\
\mathbf{P}^S + \boldsymbol{\Lambda}^F &= \rho^S \frac{\partial \psi^S}{\partial \mathbf{F}^S} + \rho^F \frac{\partial \psi^F}{\partial \mathbf{F}^S} \\
&\quad - \rho^S \left(\mathbf{F}^{S-T} \frac{\partial \psi^S}{\partial \dot{\mathbf{X}}^F} \right) \otimes \dot{\mathbf{X}}^F - \rho^F \left(\mathbf{F}^{S-T} \frac{\partial \psi^F}{\partial \dot{\mathbf{X}}^F} \right) \otimes \dot{\mathbf{X}}^F, \\
\rho^S \boldsymbol{\Lambda}^{vS} &= - \rho^F \boldsymbol{\Lambda}^{vF} = - \rho^S \frac{\partial \psi^S}{\partial \dot{\mathbf{X}}^F} - \rho^F \frac{\partial \psi^F}{\partial \dot{\mathbf{X}}^F}.
\end{aligned} \qquad (2.23)
$$

On the other hand, the coefficients of spatial derivatives (2.22) lead to the following identities:

$$
\left(\rho^F \frac{\partial \psi^F}{\partial \rho^F} - \Lambda^n \right) \dot{\mathbf{X}}^F + \frac{\partial \mathbf{P}^{ST}}{\partial \rho^F} \boldsymbol{\Lambda}^{vS} + \frac{\partial \mathbf{P}^{FT}}{\partial \rho^F} \boldsymbol{\Lambda}^{vF} = 0,
$$

$$\overset{23}{\operatorname{sym}}\left(\frac{\partial\psi^F}{\partial\mathbf{F}^S}+\Lambda^n\mathbf{F}^{S-T}\right)\otimes\dot{\mathbf{X}}^F=0,$$

$$\mathbf{\Lambda}^F=\mathbf{P}^F=-\rho^F\Lambda^n\mathbf{F}^{S-T}. \tag{2.24}$$

It remains the residual inequality

$$\hat{\mathbf{p}}\cdot\mathbf{w}\geq 0, \tag{2.25}$$

which defines the *dissipation density* of the system.

For technical reasons we make the following simplifying assumption:

$$\frac{\partial\psi^S}{\partial\dot{\mathbf{X}}^F}=\frac{\partial\psi^F}{\partial\dot{\mathbf{X}}^F}=0. \tag{2.26}$$

One could proceed also without this simplification but we aim at the construction of a linear model for which such contributions would be neglected anyway.

Combination of relations $(2.23)_1$ and $(2.24)_1$ yields now

$$\Lambda^n=\rho^F\frac{\partial\psi^F}{\partial\rho^F},\quad \frac{\partial\psi^S}{\partial\rho^F}=0. \tag{2.27}$$

The second part of this relation has the most important bearing on the structure of interactions described by the model. Namely the partial free energy of the skeleton does not react on changes of the porosity. We see in a moment what is the reaction of partial stresses on this property. Such a conclusion would be impossible if we performed the exploitation of the second law for a linear model.

Relation $(2.24)_2$ leads after easy calculations to the relation

$$\frac{\partial\psi^F}{\partial\mathbf{F}^S}=-\Lambda^n\mathbf{F}^{S-T}. \tag{2.28}$$

Hence relations $(2.23)_2$ and $(2.24)_2$ yield the following relations for partial Piola-Kirchhoff stresses:

$$\mathbf{P}^S=\rho^S\frac{\partial\psi^S}{\partial\mathbf{F}^S},\quad \mathbf{P}^F=-\rho^{F2}\frac{\partial\psi^F}{\partial\rho^F}\mathbf{F}^{S-T},$$

or, after the transformation to partial Cauchy stresses, described by (2.14)

$$\mathbf{T}^S=\rho_t^S\frac{\partial\psi^S}{\partial\mathbf{F}^S}\mathbf{F}^{ST},\quad \mathbf{T}^F=-p^F\mathbf{1},\quad p^F:=\rho_t^{F2}\frac{\partial\psi^F}{\partial\rho_t^F}. \tag{2.29}$$

These are classical thermodynamical relations for elastic materials and ideal fluids, respectively. The most important property of these relations is the fact that identities $(2.27)_2$ and (2.28) yield

$$\mathbf{T}^S=\mathbf{T}^S\left(\mathbf{F}^S\right),\quad p^F=p^F\left(\rho_t^F\right). \tag{2.30}$$

The latter requires an assumption on isotropy and it shall be proven in the next subsection.

Consequently one **cannot obtain Biot's model** by linearization of the above model. Couplings between partial stresses which are appearing in the original Biot's model with the material constant Q would have to violate the second law of thermodynamics. This property seems to be common for all multicomponent models of poroelastic materials which do not contain higher gradients among constitutive variables (see also remarks in [4]). It is also a known property of miscible mixtures of fluids. In the latter case the lack of constitutive dependence on gradients of partial mass densities leads to a model called **simple mixtures** in which partial stresses are not coupled in a constitutive way [12].

Obviously the model contains coupling due to the relative motion of components and described by the source $\hat{\mathbf{p}}$. For this reason, solutions of the boundary – initial value problems and consequently local values of partial stresses follow from the **coupled** field equations.

We should also mention that the similarity of the relation for p^F for incompressible real fluids ((I)-models) to the relation for compressible fluids ((C)-models) is misleading. This relation has an entirely different physical interpretation. For compressible fluids the relation $(2.29)_2$ yields the following **linear form** of the constitutive relation for the partial pressure

$$p^F = p_0^F + \kappa \left(\rho^F - \rho_0^F\right), \tag{2.31}$$

where p_0^F is the reference pressure and ρ_0^F – the corresponding reference partial mass density. In such a case the compressibility coefficient κ describes elastic properties of the fluid. Simultaneously its square root specifies the speed of the longitudinal wave in the fluid. This is not the case for the model with the incompressibility assumption. Since the real fluid in this case is incompressible, it has no elastic properties. Consequently the relation for p^F describes its dependence on changes of porosity which are due to microscopical morphological changes of the skeleton such as a redistribution of grains. Hence the acoustic properties related to such a constitutive relation for the pressure cannot be extracted from microscopic properties of the real fluid component.

Incidentally such a model supports the views advocated by W. G. GRAY (e.g. see: [13]) that macroscopic constitutive relations of components in the macroscopic model cannot be directly related to constitutive properties of real components, and even less, they can be derived by any averaging procedure for a single real microscopic component. Macroscopic constitutive properties reflect for each component microscopic properties of both real components as well as microscopic interactions between them.

In the next subsection we consider a higher gradient model which allows for interactions in constitutitve relations for partial stresses.

2.2.3. $\mathcal{C}^{(2)}$–models. We proceed to consider the model based on constitutive variables (2.16). However we limit the attention to the simplest case in which the model is *linear* with respect to the gradient of porosity. In such a case it may appear solely in the constitutive relation for the source $\hat{\mathbf{p}}$ because this is the only vectorial constitutive function. We simplify the model even further and assume linearity of the source with respect to both the filter velocity $\mathbf{w}$ and $gradn$. Consequently

$$\hat{\mathbf{p}} = \pi \mathbf{w} - N \operatorname{grad} n, \tag{2.32}$$

where material parameters π and N may still depend on ρ^F and $\mathbf{F}^S$. We have left out a possible nonlinear contribution proportional to the vector product $\mathbf{w} \times gradn$ which would appear in a general nonlinear isotropic model. In contrast to linear contributions, such a term would be nondissipative. The minus sign in (2.32) is related to the property of incompressible models (e.g. [10]) in which N coincides with the pore pressure. In general it may not be the case. This parameter seems to be always positive. However, such a property does not follow from the second law of thermodynamics. We assume also the relation (2.26) to hold.

Bearing the relation (2.6) in mind we obtain the following contribution of the source to the inequality (2.20):

$$\begin{aligned} &(I) - \text{models} : \hat{\mathbf{p}} \cdot \mathbf{w} \\ &\qquad = \pi \mathbf{w} \cdot \mathbf{w} - N \frac{1}{\rho^{FR} J^S} \left\{ \operatorname{Grad} \rho^F - \rho^F \mathbf{F}^{ST} \operatorname{Div} \mathbf{F}^{S-1} \right\} \cdot \dot{\mathbf{X}}^F, \\ &(C) - \text{models} : \hat{\mathbf{p}} \cdot \mathbf{w} = \pi \mathbf{w} \cdot \mathbf{w} - N \frac{1}{\rho_0^{FR}} \operatorname{Grad} \rho^F \cdot \dot{\mathbf{X}}^F, \quad \mathbf{w} \equiv \mathbf{F}^S \dot{\mathbf{X}}^S. \end{aligned} \tag{2.33}$$

Contributions appearing with the parameter N in these relations change the identities of the previous subsection following from coefficients of spatial derivatives. Namely relations $(2.24)_1$ and $(2.24)_2$ will be influenced. We collect all these results of the second law of thermodynamics in the juxtaposition.

After easy manipulations we obtain the following relations for the partial Piola-Kirchhoff stresses in both classes of models

$$
\begin{aligned}
&\text{(I)-models}: \quad \mathbf{P}^S = \rho^S \frac{\partial \psi^S}{\partial \mathbf{F}^S} + nN\mathbf{F}^{S-T}, \\
&\text{(C)-models}: \quad \mathbf{P}^S = \rho^S \frac{\partial \psi^S}{\partial \mathbf{F}^S},
\end{aligned} \tag{2.34}
$$

$$
\text{(I)-models and (C)-models:} \quad \mathbf{P}^F = -\left(\rho^{F2} \frac{\partial \psi^F}{\partial \rho^F} + nN\right) \mathbf{F}^{S-T}, \tag{2.35}
$$

as well as the following identities for partial free energy functions

$$
\begin{aligned}
&\text{(I)} - \text{models}: \quad \frac{\partial \psi^{\mathrm{F}}}{\partial \mathbf{F}^{\mathrm{S}}} = -\rho^{\mathrm{F}} \frac{\partial \psi^{\mathrm{F}}}{\partial \rho^{\mathrm{F}}} \mathbf{F}^{\mathrm{S-T}}, \quad \rho^{\mathrm{S}} \frac{\partial \psi^{\mathrm{S}}}{\partial \rho^{\mathrm{F}}} = \frac{\mathrm{N}}{\rho^{\mathrm{FR}} \mathrm{J}^{\mathrm{S}}}, \\
&\text{(C)} - \text{models}: \quad \frac{\partial \psi^{\mathrm{F}}}{\partial \mathbf{F}^{\mathrm{S}}} = -\left(\rho^{\mathrm{F}} \frac{\partial \psi^{\mathrm{F}}}{\partial \rho^{\mathrm{F}}} + \frac{\mathrm{N}}{\rho_0^{\mathrm{FR}}}\right) \mathbf{F}^{\mathrm{S-T}}, \quad \rho^{\mathrm{S}} \frac{\partial \psi^{\mathrm{S}}}{\partial \rho^{\mathrm{F}}} = \frac{\mathrm{N}}{\rho_0^{\mathrm{FR}}}.
\end{aligned} \tag{2.36}
$$

Table 1.

(I)-models	(C)-models
$\Lambda^n = \rho^S \frac{\partial \psi^S}{\partial \rho^F} + \rho^F \frac{\partial \psi^F}{\partial \rho^F},$	$\Lambda^n = \rho^S \frac{\partial \psi^S}{\partial \rho^F} + \rho^F \frac{\partial \psi^F}{\partial \rho^F},$
$\mathbf{P}^S = \rho^S \frac{\partial \psi^S}{\partial \mathbf{F}^S} + \rho^F \frac{\partial \psi^F}{\partial \mathbf{F}^S} - \mathbf{P}^F,$	$\mathbf{P}^S = \rho^S \frac{\partial \psi^S}{\partial \mathbf{F}^S} + \rho^F \frac{\partial \psi^F}{\partial \mathbf{F}^S} - \mathbf{P}^F,$
$\mathbf{P}^F = -\rho^F \Lambda^n \mathbf{F}^{S-T},$	$\mathbf{P}^F = -\rho^F \Lambda^n \mathbf{F}^{S-T},$
$\rho^S \frac{\partial \psi^S}{\partial \rho^F} - \frac{N}{\rho^{FR}} J^{S-1} = 0, \quad \rho^{FR} = \text{const}$	$\rho^S \frac{\partial \psi^S}{\partial \rho^F} - \frac{N}{\rho_0^{FR}} = 0,$
$\frac{\partial \psi^F}{\partial \mathbf{F}^S} + \rho^F \frac{\partial \psi^F}{\partial \rho^F} \mathbf{F}^{S-T} = 0,$	$\frac{\partial \psi^F}{\partial \mathbf{F}^S} + \left(\rho^F \frac{\partial \psi^F}{\partial \rho^F} + \frac{N}{\rho_0^{FR}}\right) \mathbf{F}^{S-T} = 0.$

Then for the partial Cauchy stresses follow the relations of the form

(2.37)
$$\text{(I)-models:}$$
$$\mathbf{T}^S = \rho^S J^{S-1} \frac{\partial \psi^S}{\partial \mathbf{F}^S} \mathbf{F}^{ST} + nNJ^{S-1}\mathbf{1}, \quad \mathbf{T}^F = -p^F \mathbf{1},$$
$$p^F := \rho^{F2} J^{S-1} \frac{\partial \psi^F}{\partial \rho^F} + nNJ^{S-1},$$
$$\text{(C)-models:}$$
$$\mathbf{T}^S = \rho^S J^{S-1} \frac{\partial \psi^S}{\partial \mathbf{F}^S} \mathbf{F}^{ST}, \quad \mathbf{T}^F = -p^F \mathbf{1},$$
$$p^F := \rho^{F2} J^{S-1} \frac{\partial \psi^F}{\partial \rho^F} + nNJ^{S-1}.$$

It is seen that both models contain couplings of stresses which may lead to Biot's constitutive relations for stresses (e.g. [2]) of the linear model. We proceed to investigate this question.

In order to simplify the construction of the linear model we evaluate the above nonlinear relations for isotropic materials. In such a case free energies ψ^S, ψ^F satisfying the principle of material objectivity depend on the deformation gradient $\mathbf{F}^S$ solely through the invariants of its symmetric part. For instance we can choose the invariants of the right Cauchy - Green deformation tensor $\mathbf{C}^S$

(2.38)
$$\mathbf{C}^S := \mathbf{F}^{ST}\mathbf{F}^S, \quad I := \mathrm{tr}\mathbf{C}^S,$$
$$II := \frac{1}{2}\left(I^2 - \mathrm{tr}\mathbf{C}^{S2}\right), \quad III \equiv J^{S2} := \det \mathbf{C}^S.$$

Then

$$\psi^S = \psi^S\left(I, II, III, \rho^F\right), \quad \psi^F = \psi^F\left(I, II, III, \rho^F\right). \tag{2.39}$$

Let us exploit the identity $(2.36)_1$ under the above assumption. Bearing the following relation in mind

$$\frac{\partial \psi^F}{\partial \mathbf{F}^S} = 2\mathbf{F}^S \frac{\partial \psi^F}{\partial \mathbf{C}^S}, \tag{2.40}$$

we obtain

(2.41)
$$\frac{\partial \psi^F}{\partial \mathbf{F}^S}\mathbf{F}^{ST} = 2\left(\frac{\partial \psi^F}{\partial I}\mathbf{B}^S + \frac{\partial \psi^F}{\partial II} I\mathbf{B}^S - \frac{\partial \psi^F}{\partial II}\mathbf{B}^{S2} + \frac{\partial \psi^F}{\partial III} III\mathbf{1}\right),$$
$$\mathbf{B}^S := \mathbf{F}^S\mathbf{F}^{ST}, \quad III \equiv J^{S2},$$

where the symmetric tensor $\mathbf{B}^S$ is called the left Cauchy-Green deformation tensor. Now we can write $(2.36)_1$ in the form

(2.42)
(I)-models :

$$\left(2III\frac{\partial\psi^F}{\partial III}+\rho^F\frac{\partial\psi^F}{\partial\rho^F}\right)\mathbf{1}+2\left(\frac{\partial\psi^F}{\partial I}+\frac{\partial\psi^F}{\partial II}I\right)\mathbf{B}^S-2\frac{\partial\psi^F}{\partial II}\mathbf{B}^{S2}=0,$$

(C)-models :

$$\left(2III\frac{\partial\psi^F}{\partial III}+\rho^F\frac{\partial\psi^F}{\partial\rho^F}+\frac{N}{\rho_0^{FR}}\right)\mathbf{1}+2\left(\frac{\partial\psi^F}{\partial I}+\frac{\partial\psi^F}{\partial II}I\right)\mathbf{B}^S$$

$$-2\frac{\partial\psi^F}{\partial II}\mathbf{B}^{S2}=0.$$

These relations must hold for arbitrary deformations $\mathbf{B}^S$. Consequently, according to the corollaries of the Cayley-Hamilton theorem in the tensor analysis, coefficients of tensors $\mathbf{1},\mathbf{B}^S,\mathbf{B}^{S2}$ have to vanish independently. Hence in both cases the free energy ψ^F must be independent of invariants I,II, and, consequently (comp. relations for N in Table. 1) N must be independent of these two invariants in (C)-models but not necessarily in (I)-models. In addition we have

$$\text{(2.43) (I)-models} \quad : \quad \psi^F=\psi^F\left(J^S,\rho^F\right), \quad J^S\frac{\partial\psi^F}{\partial J^S}+\rho^F\frac{\partial\psi^F}{\partial\rho^F}=0;$$

$$\text{(2.44) (C)-models} \quad : \quad \psi^F=\psi^F\left(J^S,\rho^F\right), \quad J^S\frac{\partial\psi^F}{\partial J^S}+\rho^F\frac{\partial\psi^F}{\partial\rho^F}=-\frac{N}{\rho_0^{FR}},$$

$$N = N\left(J^S,\rho^F\right).$$

The differential equation $(2.43)_2$ for (I)-models can be easily solved by the method of characteristics. If we denote the variable along the characteristic by ξ then we can write this equation in the characteristic form

$$\text{(2.45)} \qquad \frac{dJ^S}{d\xi}=J^S, \quad \frac{d\rho^F}{d\xi}=\rho^F, \quad \frac{d\psi^F}{d\xi}=0.$$

Consequently ψ^F is constant along the characteristics, and these are labelled by the following initial values

$$\text{(2.46)} \qquad \rho^F J^{S-1}=\text{const},$$

which follows from $(2.45)_{1,2}$. It means that the solution of the identity $(2.36)_1$ for isotropic materials with incompressible real fluid is of the form

$$\text{(2.47)} \qquad \text{(I)-models: } \psi^F=\psi^F\left(\rho_t^F\right).$$

The problem is more complicated for compressible materials. However we can simplify the equation $(2.44)_2$ if we change the variables in a way suggested by the above solution for the (I)-model. Namely we obtain

$$\text{(2.48)} \qquad \text{(C)-models}: \quad \left(\rho^F, J^S\right) \to \left(\rho_t^F, J^S\right) \quad \Longrightarrow \quad \psi^F = \psi^F\left(\rho_t^F, J^S\right)$$

and

$$\text{(2.49)} \qquad J^S \frac{\partial \psi^F}{\partial J^S} = -\frac{N}{\rho_0^{FR}} \quad \Longrightarrow \quad \psi^F = \psi^F_{ideal}\left(\rho_t^F\right) - \frac{1}{\rho_0^{FR}} \int_1^{J^S} \frac{N\left(\rho_t^F, \xi\right)}{\xi} d\xi.$$

It is instructive to apply the relation $(2.36)_2$ in the formulae (2.37) for Cauchy stresses. For isotropic materials we obtain immediately

(I)-models:

$$\text{(2.50)} \qquad \begin{aligned} \mathbf{T}^S = \rho^S J^{S-1} \Bigg\{ & \left(J^S \frac{\partial \psi^S}{\partial J^S} + \rho^F \frac{\partial \psi^S}{\partial \rho^F} \right) \mathbf{1} + 2 \left(\frac{\partial \psi^S}{\partial I} + I \frac{\partial \psi^S}{\partial II} \right) \mathbf{B}^S \\ & - 2 \frac{\partial \psi^S}{\partial II} \mathbf{B}^{S2} \Bigg\}, \end{aligned}$$

$$\mathbf{T}^F = -\rho^F J^{S-1} \left(\rho^F \frac{\partial \psi^F}{\partial \rho^F} + \rho^S \frac{\partial \psi^S}{\partial \rho^F} \right) \mathbf{1},$$

(C)-models:

$$\text{(2.51)} \qquad \begin{aligned} \mathbf{T}^S &= \rho^S J^{S-1} \left\{ J^S \frac{\partial \psi^S}{\partial J^S} \mathbf{1} + 2 \left(\frac{\partial \psi^S}{\partial I} + I \frac{\partial \psi^S}{\partial II} \right) \mathbf{B}^S - 2 \frac{\partial \psi^S}{\partial II} \mathbf{B}^{S2} \right\}, \\ \mathbf{T}^F &= -\rho^F J^{S-1} \left(\rho^F \frac{\partial \psi^F}{\partial \rho^F} + \rho^S \frac{\partial \psi^S}{\partial \rho^F} \right) \mathbf{1}. \end{aligned}$$

Let us discuss first the structure of stress relations for (I)-models. As indicated by (2.47), the first contribution to the partial stress $\mathbf{T}^F$ cannot contain any coupling to the deformation of the skeleton. Consequently it is the derivative of the partial Helmholtz free energy ψ^S with respect to ρ_t^F which relates $\mathbf{T}^F$ to the deformation of the skeleton. According to the relation $(2.36)_2$ for the existence of this coupling, the coefficient N must be different from zero. For the symmetry required in the Biot's model it is necessary to introduce a rather complicated dependence of the partial free energy function ψ^S on the mass density ρ^F which would create a term in $\rho^S \dfrac{\partial \psi^S}{\partial J^S}$ canceling out the contribution $\rho^S \rho^F J^{S-1} \dfrac{\partial \psi^S}{\partial \rho^F}$ to the stress $\mathbf{T}^S$ (the wrong sign!) and simultaneously produces another one introducing the coupling to the deformation of the fluid. Even though it is possible

in principle, such a model does not seem to be very plausible and we do not investigate it any further.

Let us mention in passing that in a particular case of the constant partial free energy ψ^F, the relation $(2.37)_2$ for incompressible real fluids yields $N = \frac{p^F}{n}$ which is the pore pressure of classical models. Hence in this particular case the coefficient in the diffusion force (2.32) coincides with that of classical models of consolidation. This structure has been indicated in the work [14] on nonlinear sources.

The structure of stress relations for (C)-models is simpler. As thermodynamical requirements do not lead to any restrictions of the free energy ψ^S on ρ_t^F and the free energy ψ^F on J^S, we may produce as a particular case a desired dependence and symmetry. We shall do so for the linear model.

Concluding the above thermodynamical considerations we see that the Biot's constitutive relations for stresses can be derived from nonlinear $\mathcal{C}^{(2)}$-models by a specific choice of partial free energies. It means that such a transition requires a higher gradient model as a background.

2.3. Linear models

The relations derived in the previous subsection yield immediately the constitutive relations of the fully linear model. Let us introduce the Almansi-Hamel deformation measure $\mathbf{e}^S$ commonly used in the linear theory of elasticity (e.g. [7])

$$\mathbf{e}^S := \frac{1}{2}\left(\mathbf{1} - \mathbf{B}^{S-1}\right). \tag{2.52}$$

The linearity follows from the assumption that deformations of the skeleton are small, and that changes of porosity are small

$$\begin{aligned} \max\left\{\left|\lambda^{(\alpha)}\right|\right\}_{\alpha=1,2,3} &\ll 1, \quad \det\left(\mathbf{e}^S - \lambda^{(\alpha)}\mathbf{1}\right) = 0, \\ |\varsigma| &\ll 1, \quad \varsigma := \frac{n - n_0}{n_0}, \end{aligned} \tag{2.53}$$

where $\lambda^{(\alpha)}$ are eigenvalues of $\mathbf{e}^S$, and they are called principal deformations while n_0 denotes the reference constant value of porosity.

We construct the linear version of the (C)-model. In this model, also in its fully nonlinear version, the porosity is related to the mass density by the relation $(2.9)_2$, i.e.

$$n = \frac{\rho_t^F J^S}{\rho_0^{FR}}. \tag{2.54}$$

The variable ς can be now coupled to changes of the partial mass density ρ_t^F and to volume changes of the skeleton $J^S \approx 1 + \mathrm{tr}\mathbf{e}^S$. We have

$$\varsigma = \frac{n}{n_0} - 1 \approx \frac{\rho_t^F - \rho_0^F}{\rho_0^F} + \mathrm{tr}\,\mathbf{e}^S, \quad \rho_0^F \equiv n_0 \rho_0^{FR}. \tag{2.55}$$

The first contribution describes the macroscopic volume changes of the fluid component, i.e it is the (macroscopic) negative fluid *dilation* ϵ while the second contribution describes changes of the macroscopic volume e. Hence

$$\varsigma \approx e - \epsilon, \quad e := \mathrm{tr}\,\mathbf{e}^S, \quad \epsilon := -\frac{\rho_t^F - \rho_0^F}{\rho_0^F}. \tag{2.56}$$

Let us note that the macroscopic model constructed in this way does not require any reference to the microscopic description.

Before we proceed with the linearization of constitutive relations it is convenient to change the variables in (2.51) from (ρ^F, J^S) to (ρ_t^F, J^S). Bearing identities of the previous section in mind we obtain

$$\begin{aligned} \mathbf{T}^S &= \rho_t^S \left\{ J^S \frac{\partial \psi^S}{\partial J^S} + 2\left(\frac{\partial \psi^S}{\partial I} + I \frac{\partial \psi^S}{\partial II} \right) \mathbf{B}^S - 2 \frac{\partial \psi^S}{\partial II} \mathbf{B}^S \right\} - n_0 N \frac{\rho_t^F}{\rho_0^F} \mathbf{1}, \\ \mathbf{T}^F &= -\left(\rho_t^{F2} \frac{\partial \psi^F}{\partial \rho_t^F} + n_0 N \frac{\rho_t^F}{\rho_0^F} \right) \mathbf{1}. \end{aligned} \tag{2.57}$$

Obviously the stress tensor in the skeleton possesses already the structure desired in the comparison to Biot's model. The last contribution can be written in terms of the variable ϵ which reflects the coupling with the fluid. Such a contribution does not appear in the stress tensor for the fluid. However the free energy ψ^F may be still dependent on both variables (ρ_t^F, J^S). Consequently we can choose this dependence in such a way that the symmetry required by the Biot's model remains preserved. It is easy to check that the following choice:

$$\psi^F = \psi^F_{\mathrm{ideal}}\left(\rho_t^F\right) + n_0 N \frac{e}{\rho_t^F}, \quad N = \mathrm{const}, \quad J^S \equiv 1 + e, \tag{2.58}$$

indeed yields the desired coupling and it is compatible with the relation (2.49) provided the coupling coefficient N in the fully nonlinear model possesses a specific dependence on volume changes of the skeleton J^S

$$N = \frac{N_0}{J^S}, \quad N_0 = \mathrm{const}. \tag{2.59}$$

This yields indeed the relation (2.58) because in the linear model we do not have to distinguish between N and N_0 in the above relation. Such a dependence is

solely motivated by the requirement of the linear model and cannot be derived from any thermodynamical relations.

Let us make an important observation that the coupling in the partial stress tensor $\mathbf{T}^F$ cannot be corrected any more because the contribution ψ^F_{ideal} is independent of volume changes of the skeleton. Hence the coupling constant must be of the order of the constant N.

The standard linearization procedure leads now to the following linear constitutive relations for partial stresses:

$$\begin{aligned} \mathbf{T}^S &= \mathbf{T}^S_0 + \lambda^S e\mathbf{1} + 2G^S\mathbf{e}^S + n_0 N\epsilon\mathbf{1}, \\ \mathbf{T}^F &= -p^F\mathbf{1}, \quad p^F := p^F_0 - (R\epsilon + n_0 Ne), \end{aligned} \tag{2.60}$$

where $\mathbf{T}^S_0, p^F_0$ are initial values of the stress in the skeleton: $\mathbf{F}^S = \mathbf{1}$, or equivalently $\mathbf{e}^S = \mathbf{0}$, as well as $\epsilon = 0$, and of the partial pressure in the fluid, respectively. The material parameters λ^S, G^S, R, N may depend solely on the initial porosity n_0.

In order to obtain Biot's stress relations (1.2) we have to identify $\lambda^S = A$, $G^S = G$, $Q = n_0 N$ and to assume that initial stresses are zero (stresses in Biot's relations are the so-called excess stresses):

In contrast to customary **macroscopic** thermodynamical models of multicomponent systems, the deformation measures $\mathbf{e}^S$ and ϵ appearing in the Biot's model do not have the meaning of macroscopic quantities. They represent some macroscopic averages of real **microscopic** deformations which are not clearly specified for the Biot's model. One can solely presume their interpretation from Gedankenexperiments provided by BIOT and WILLIS [2] and quoted later on in many works on this subject. Some rather vague remarks[2)] about the effect of microscopic interactions on such an interpretation do not influence the construction of the Biot's model.

Let us mention that the physical interpretation of Biot's displacement fields $\mathbf{u}$ for the skeleton and $\mathbf{U}$ for the fluid which define the variables $\mathbf{e}^S$ and ϵ do not clear the interpretation of the latter either. The reason is that they were introduced for small deformations of the skeleton, again without any clear distinction between real microscopic deformations and macroscopic deformations. Simultaneously, a motion of the fluid component has never been considered in a manner similar to that which is customary in the fluid mechanics. Such a

[2)] e.g.: "... It should be pointed out that this expression (i.e. defining ϵ by the divergence of the fluid displacement $\mathbf{U}$; K.W.) is not the actual strain in the fluid but simply the divergence of the fluid-displacement field which itself is derived from the average volume flow through the pores..." or "... the dry specimen may not exhibit the same properties as the saturated one. As an example of this we may cite the case where the elastic properties result from surface forces of a capillary nature at the interface of the fluid and the solid" ([2], p. 595).

quantity as the displacement of the fluid $\mathbf{U}$ can be solely introduced localy in time by integrating the ordinary differential equation $\frac{\partial \mathbf{x}}{\partial t} = \mathbf{v}^F(\mathbf{x}, t)$ with an initial condition $\mathbf{x}(t = t_0) = \mathbf{x}_0$ and $\mathbf{U} = \mathbf{x} - \mathbf{x}_0$. t_0 should not be too far from the present instant of time t. This is an unnecessary complication of the model. In addition, the microstructural variable ς in the Biot's model is sometimes defined in a different way than this presented above. It may be introduced by the following definition (e.g. [15])

$$\zeta := n_0 \mathrm{div}(\mathbf{u} - \mathbf{U}), \tag{2.61}$$

where $\mathbf{u}, \mathbf{U}$ denote *microscopic average* displacements of the skeleton and the fluid, respectively. Even though a motivation of this formula and an interpretation of $\mathbf{u}$ and $\mathbf{U}$ is missing it seems to be based on the argument that the following relations hold true:

$$e \equiv \mathrm{tr}\mathbf{e}^S = \mathrm{div}\mathbf{u}, \quad \epsilon = \mathrm{div}\mathbf{U} \quad \Longrightarrow \quad \varsigma = \frac{\zeta}{n_0}. \tag{2.62}$$

Using these deformation measures, Biot and Willis introduce an alternative description by conjugate dynamical quantities: the bulk stress tensor $\mathbf{T}$ and the pore pressure p for which the constitutive relations (1.2) transform as follows:

$$\begin{aligned} \mathbf{T} &:= \mathbf{T}^S + \mathbf{T}^F = (\lambda + \alpha^2 M) e\mathbf{1} + 2G\mathbf{e}^S - \alpha M \zeta \mathbf{1}, \\ p &:= \frac{p^F}{n_0} = -\alpha M e + M\zeta, \end{aligned} \tag{2.63}$$

where[3)]

$$\begin{aligned} \lambda &:= A - \frac{Q^2}{R}, \quad G := G^S, \quad A \equiv \lambda^S, \quad Q \equiv n_0 N, \\ M &:= \frac{R}{n_0^2}, \quad \alpha := n_0 \frac{Q + R}{R}. \end{aligned} \tag{2.64}$$

In the literature on Biot's model it is not always clear which stresses and variables are being used.

[3)] In [15] the following notation is used

$$H := \lambda + \alpha^2 M + 2G, \quad C := \alpha M.$$

It is rather common for the literature on Biot's model that the notation varies from paper to paper.

We have considered in this section the simplest version of a linear higher gradient model but it is almost obvious that neither the contributions of relative velocities to free energies nor the nonlinear contributions of the gradient of porosity can change anything in the structure of a linearized model.

Field equations of the model follow from partial balance equations of mass and momentum. For the linear model considered in this section they have the form

$$
\begin{aligned}
&\frac{\partial \rho_t^S}{\partial t} + \rho^S \operatorname{div}\mathbf{v}^S = 0, \quad \rho^S \frac{\partial \mathbf{v}^S}{\partial t} = \operatorname{div}\mathbf{T}^S + \pi\left(\mathbf{v}^F - \mathbf{v}^S\right) - n_0 N \operatorname{grad}\varsigma, \\
&\frac{\partial \rho_t^F}{\partial t} + \rho_0^F \operatorname{div}\mathbf{v}^F = 0, \quad \rho_0^F \frac{\partial \mathbf{v}^F}{\partial t} = \operatorname{div}\mathbf{T}^F - \pi\left(\mathbf{v}^F - \mathbf{v}^S\right) + n_0 N \operatorname{grad}\varsigma.
\end{aligned} \tag{2.65}
$$

These equations differ from the equations used in the Biot's model due to the presence of the source term with the gradient of porosity. However in the linear model in which the coefficient N is **constant** and the relation (2.54) holds true, the contribution of the source can be formally incorporated into the constitutive relations for partial stresses. After the transformation

$$
\mathbf{T}^S \to \mathbf{T}^S - n_0 N \varsigma \mathbf{1}, \quad \mathbf{T}^F \to \mathbf{T}^F + n_0 N \varsigma \mathbf{1}, \tag{2.66}
$$

we obtain new constitutive laws similar to the relations derived by CIESZKO and KUBIK in [18], and repeated in [19], which possess the same symmetry as the original Biot relations and the field equations do not contain sources. Instead of the coupling coefficient $n_0 N$ we have then $2n_0 N$ and, of course, the elastic coefficients λ^S and R must be corrected on $-n_0 N$. We investigate in the next section the influence of these relations on the propagation of sound waves in porelastic materials.

3. Fundamentals of acoustic waves in linear poroelastic media

3.1. Wave front

Let us remind a few elementary properties of the description of wave fronts in continua. Acoustic waves in continua are related to the propagation of a nonmaterial singular surface – the *wave front* σ – on which acceleration fields are discontinuous but the velocity fields remain continuous. If the latter does not hold, we deal either with shock waves or with vortex sheets.

Let us assume that the instantaneous geometry of the front σ is given by the following equation

$$
f(\mathbf{x}, t) = 0, \quad \mathbf{x} \in \mathcal{B}_t \subset \Re^3, \quad t \in \mathcal{T}, \tag{3.1}
$$

which is at least of the class $\mathcal{C}^2$ with respect to $\mathbf{x}$, and of the class $\mathcal{C}^1$ with respect to time t. $\mathcal{B}_t$ denotes the current configuration of the skeleton. The smoothness requirements mean that changes of the normal vector to the surface are differentiable, and changes of curvatures are continuous. Simultaneously there exists a smooth speed of propagation of the surface. In order to see these properties we use the identity

$$df \equiv d\mathbf{x}\cdot\operatorname{grad} f + dt\frac{\partial f}{\partial t} = 0. \tag{3.2}$$

As the gradient of f is orthogonal to the surface (f is constant along the surface, i.e. the vector $\operatorname{grad} f$ may possess solely an orthogonal component), we can define a unit normal vector by the relation

$$\mathbf{n} := \frac{\operatorname{grad} f}{|\operatorname{grad} f|}. \tag{3.3}$$

The second gradient of f, i.e. a quantity proportional to $\operatorname{grad}\mathbf{n}$ is related to curvatures. Bearing the relation (3.2) in mind we obtain for the speed of propagation

$$v_n := \frac{d\mathbf{x}}{dt}\cdot\mathbf{n} = -\frac{\dfrac{\partial f}{\partial t}}{|\operatorname{grad} f|}. \tag{3.4}$$

It is easy to see that the relation (3.1) does not impose any conditions on the tangential component of the velocity of the surface. This means that kinematics of slip motions cannot be described by such a relation. However this is immaterial in the theory of waves.

If the speed of propagation v_n is given then the relation (3.4) is the nonlinear differential equation for the funcion f

$$\frac{\partial f}{\partial t} + v_n\,|\operatorname{grad} f| = 0. \tag{3.5}$$

With an appropriate initial condition for the position of the front (i.e. $f(\mathbf{x}, t = 0)$ – given) this equation forms a nonlinear Cauchy problem.

3.2. Kinematic and dynamic compatibility conditions, speeds of propagation

The behaviour of various kinematic quantities on singular surfaces has been studied since 150 years and the modern theory follows the way proposed by Hadamard. An excellent presentation of this subject can be found in the classical book of C. TRUESDELL and R. A. TOUPIN [16] (Chapter IV). We use here a

particular case of these kinematic compatibility conditions following under the assumption of continuity of both motions and velocities.

We have for the skeleton

$$
\begin{gathered}
[[\rho_t^S]] = 0, \quad [[\mathbf{v}^S]] = 0, \quad [[\mathbf{e}^S]] = 0, \\
[[\ldots]] := \sigma^+ \lim(\ldots) - \sigma^- \lim(\ldots),
\end{gathered} \tag{3.6}
$$

where limits are evaluated on the positive and negative sides of the front.

Introducing the notation

$$
R^S := \left[\left[\frac{\partial \rho_t^S}{\partial t}\right]\right], \quad \mathbf{A}^S := \left[\left[\frac{\partial \mathbf{v}^S}{\partial t}\right]\right], \tag{3.7}
$$

we arrive at the following relations for discontinuities of various derivatives appearing in field equations of the linear model.

$$
\begin{aligned}
&[[\operatorname{grad} \rho_t^S]] = -\frac{1}{v_n} R^S \mathbf{n}, \quad [[\operatorname{grad} \mathbf{v}^S]] = -\frac{1}{v_n} \mathbf{A}^S \otimes \mathbf{n}, \\
&[[\operatorname{grad} \mathbf{e}^S]] = -\frac{1}{v_n} \left[\left[\frac{\partial \mathbf{e}^S}{\partial t}\right]\right] \otimes \mathbf{n}.
\end{aligned} \tag{3.8}
$$

It follows from the kinematic relation between $\mathbf{v}^S$ and $\mathbf{e}^S$ (compare (2.10) for such a relation in the nonlinear model)

$$
\frac{\partial \mathbf{e}^S}{\partial t} = \frac{1}{2}\left(\operatorname{grad} \mathbf{v}^S + (\operatorname{grad} \mathbf{v}^S)^T\right), \tag{3.9}
$$

and this yields

$$
[[\operatorname{grad} \mathbf{e}^S]] = \frac{1}{2v_n^2}\left(\mathbf{A}^S \otimes \mathbf{n} + \mathbf{n} \otimes \mathbf{A}^S\right) \otimes \mathbf{n}. \tag{3.10}
$$

Similarly we have on the wave front σ for the fluid component

$$
[[\rho_t^F]] = 0, \quad [[\mathbf{v}^F]] = 0 \quad \Rightarrow \quad [[\varsigma]] = 0. \tag{3.11}
$$

With the following notation

$$
R^F := \left[\left[\frac{\partial \rho_t^F}{\partial t}\right]\right], \quad \mathbf{A}^F := \left[\left[\frac{\partial \mathbf{v}^F}{\partial t}\right]\right], \tag{3.12}
$$

we obtain the kinematic compatibility conditions for the fluid component in the form

$$
\begin{aligned}
&[[\operatorname{grad} \rho_t^F]] = -\frac{1}{v_n} R^F \mathbf{n}, \quad [[\operatorname{grad} \mathbf{v}^F]] = -\frac{1}{v_n} \mathbf{A}^F \otimes \mathbf{n} \quad \Rightarrow \\
&[[\operatorname{grad} \varsigma]] = \left(-\frac{1}{\rho_0^F v_n} R^F + \frac{1}{v_n^2} \mathbf{A}^S \cdot \mathbf{n}\right) \mathbf{n}, \quad [[\operatorname{grad} \epsilon]] = \frac{1}{\rho_0^F v_n} R^F \mathbf{n}.
\end{aligned} \tag{3.13}
$$

These relations yield the following relations for jumps of partial stress gradients implied by constitutive relations (2.60)

$$
\begin{aligned}
[[\operatorname{grad}\mathbf{T}^S]] &= \lambda^S \frac{1}{v_n^2}\left(\mathbf{A}^S\cdot\mathbf{n}\right)\mathbf{1}\otimes\mathbf{n} + G^S\frac{1}{v_n^2}\left(\mathbf{A}^S\otimes\mathbf{n}+\mathbf{n}\otimes\mathbf{A}^S\right)\otimes\mathbf{n} \\
&\quad + n_0 N\frac{1}{\rho_0^F v_n}R^F\mathbf{1}\otimes\mathbf{n}, \qquad (3.14)\\
[[\operatorname{grad}\mathbf{T}^F]] &= R\frac{1}{\rho_0^F v_n}R^F\mathbf{1}\otimes\mathbf{n} + n_0 N\frac{1}{v_n^2}\left(\mathbf{A}^S\cdot\mathbf{n}\right)\mathbf{1}\otimes\mathbf{n},
\end{aligned}
$$

where material constants λ^S, G^S, N, R are assumed to be continuous across the front σ.

We use these relations in the balance equations of the linear model (2.65). Evaluation of jumps of these equations on the wave front σ gives rise to the conditions

$$
R^S = \rho^S\frac{1}{v_n}\mathbf{A}^S\cdot\mathbf{n}, \quad R^F = \rho_0^F\frac{1}{v_n}\mathbf{A}^F\cdot\mathbf{n}, \tag{3.15}
$$

$$
\begin{aligned}
v_n^2\mathbf{A}^S &= \left(\frac{\lambda^S+G^S-n_0N}{\rho^S}\right)\left(\mathbf{A}^S\cdot\mathbf{n}\right)\mathbf{n} + \frac{G^S}{\rho^S}\mathbf{A}^S + \frac{2n_0N}{\rho^S}\left(\mathbf{A}^F\cdot\mathbf{n}\right)\mathbf{n},\\
v_n^2\mathbf{A}^F &= \frac{R-n_0N}{\rho_0^F}\left(\mathbf{A}^F\cdot\mathbf{n}\right)\mathbf{n} + \frac{2n_0N}{\rho_0^F}\left(\mathbf{A}^S\cdot\mathbf{n}\right)\mathbf{n}.
\end{aligned} \tag{3.16}
$$

Relations (3.15) imply that neither mass density of the skeleton ρ_t^S nor mass density of the fluid ρ_t^F yield their own modes of propagation. Rather their amplitudes R^S, R^F are determined by the normal component of the acceleration discontinuity in the skeleton $\mathbf{A}^S\cdot\mathbf{n}$, and by the normal component of the corresponding acceleration in the fluid $\mathbf{A}^F\cdot\mathbf{n}$, respectively.

The second relation (3.16) shows that the amplitude $\mathbf{A}^F$ possesses solely the component in the direction of propagation $\mathbf{n}$. It means that this is related to a longitudinal wave.

The amplitude $\mathbf{A}^S$ possesses both the normal component as well as the transversal component. Separating these contributions we can write (3.16) in the the following form:

$$
\begin{pmatrix}
\dfrac{\lambda^S+2G^S-n_0N}{\rho^S}-v_n^2 & \dfrac{2n_0N}{\rho^S}\\[2ex]
\dfrac{2n_0N}{\rho_0^F} & \dfrac{R-n_0N}{\rho_0^F}-v_n^2
\end{pmatrix}
\begin{pmatrix}
\mathbf{A}^S\cdot\mathbf{n}\\ \mathbf{A}^F\cdot\mathbf{n}
\end{pmatrix} = 0, \tag{3.17}
$$

$$\left(v_n^2 - \frac{G^S}{\rho^S}\right)\mathbf{A}_\perp^S = 0, \quad \mathbf{A}_\perp^S := \mathbf{A}^S - (\mathbf{A}^S \cdot \mathbf{n})\,\mathbf{n}, \quad \text{i.e.} \quad \mathbf{A}_\perp^S \cdot \mathbf{n} = 0. \tag{3.18}$$

Relation (3.18) means that the discontinuity $\mathbf{A}_\perp^S$ may be different from zero solely on the front σ which propagates with the speed

$$v_n^S = \sqrt{\frac{G^S}{\rho^S}}. \tag{3.19}$$

Certainly, this is the classical relation for the transversal wave in a solid. The corresponding wave is called S-wave in geophysics. Obviously in the model we consider in this section this speed of propagation of the S-wave witch is not influenced by the presence of the fluid component.

Relation (3.17) forms the eigenvalue problem typical for problems of wave propagations. It yields the following dispersion relation for the speeds of propagation:

$$\left(\frac{\lambda^S + 2G^S - n_0 N}{\rho^S} - v_n^2\right)\left(\frac{R - n_0 N}{\rho_0^F} - v_n^2\right) - \frac{4n_0^2 N^2}{\rho^S \rho_0^F} = 0. \tag{3.20}$$

Eigenvalues v_n^2 determine the speeds of propagation, and the eigenvectors – amplitudes of the corresponding modes of propagation. We obtain two solutions of this problem:

$$v_n^2 = \frac{1}{2}\left\{(c^{S2} + c^{F2}) \pm \sqrt{(c^{S2} - c^{F2})^2 + 16\frac{n_0^2 N^2}{\rho^S \rho_0^F}}\right\}, \tag{3.21}$$

$$c^S := \sqrt{\frac{\lambda^S + 2G^S - n_0 N}{\rho^S}}, \quad c^F := \sqrt{\frac{R - n_0 N}{\rho_0^F}}. \tag{3.22}$$

The first one – v_n^{P1} – corresponds to the P1 longitudinal wave, while the second one – v_n^{P2} – to the P2 longitudinal wave (Biot's wave).

In the limit case $N = 0$ the speed of the P1-wave is equal to $c^S = \sqrt{\dfrac{\lambda^S + 2G^S}{\rho^S}}$, and the speed of the P2-wave is equal to $c^F = \sqrt{\dfrac{R}{\rho_0^F}}$. These are the relations which follow from the linearized $\mathcal{C}^{(1)}$-model without contributions of porosity gradient (comp. [17]).

Let us mention that in spite of constitutive relations identical with those of Biot the relations (3.21), (3.22) are different from the results of Biot's propagation condition due to the influence of the gradient of porosity on the source of momentum.

The above presented analysis of propagation of wave fronts may deviate considerably from the observations of waves in soils. Apart from flaws of the model, the discrepancies may result from the fact that *in situ* measurements are made usually in the range of low frequencies (a few Hz) where the attenuation of waves is relatively small. In addition, one measures the phase velocities rather than speeds of propagation which correspond to phase velocities in the limit of very high (theoretically infinite) frequencies. These may differ by 5–10%.

4. Conclusion

The thermodynamical analysis presented in this work seems to close the issue of thermodynamical admissibility of the classical Biot's model of saturated poroelastic materials. We conclude in general that Biot's field equations violate the second law of thermodynamics. A part of the model – constitutive relations for stresses – may contain a coupling between deformations of components described by the material parameter Q provided we introduce a constitutive dependence on higher gradients. However this correction yields a change in the structure of momentum source appearing in partial momentum balance equations which has been ignored by Biot.

Simultaneously we have shown that the original Biot's model as well as a corrected version with the gradient of porosity lead to the same modes of propagation of acoustic bulk waves. There appear numerical discrepancies in the values of speeds of propagations which may be of the order of accuracy of the *in situ* measurements.

The subject which has not been discussed in any details in this work but seems to worry people working on granular materials is the structure of the speed of propagation of shear waves. Both the Biot's model and the model discussed in this paper yield the speed of shear waves given by the formula (3.19). This is questioned by experimentalists investigating S-waves in soils. This seems to be the main issue requiring a correction of a linear model independently of its thermodynamical admissibility.

References

1. I. TOLSTOY, *Acoustics, elasticity, and thermodynamics of porous media: Twenty-one Papers by M. A. Biot*, Acoustical Society of America, 1991.

2. M. A. BIOT, D. G. WILLIS, *The elastic coefficients of the theory of consolidation*, Jour. Appl. Mech., **24**, 594–601, 1957.

3. K. WILMAŃSKI, *Some questions on material objectivity arising in models of porous materials*, [in:] M. BROCATO [Ed.], *Rational Continua, classical and new*, Springer-Verlag, Italia Srl, Milano, 149–161, 2001.

4. I. EDELMAN, K. WILMAŃSKI, *Asymptotic analysis of a surface waves at vacuum/porous medium and liquid/porous medium interfaces*, Continuum Mech. Thermodyn., **14**: 25–44, 2002.

5. M. A. GOODMANN, S. C. COWIN, *A continuum theory for granular materials*, Arch. Rat. Mech. Anal., **44**, 249–266, 1972.

6. R. M. BOWEN, *Compressible porous media models by use of the theory of mixtures*, Int. J. Engn. Sci, **20**, 697–763 1982.

7. K. WILMAŃSKI, *Thermomechanics of continua*, Springer, Berlin (1998).

8. K. WILMAŃSKI, *Lagrangean Model of two-phase porous material*, J. Non–Equilib. Thermodyn., **20**, 50–77, 1995.

9. K. WILMAŃSKI, *Mass exchange, diffusion and large deformations of poroelastic materials*, [in:] *Modeling and mechanics of granular and porous materials*, G. CAPRIZ, V. N. GHIONNA, P. GIOVINE [Eds.], 213–244, Birkhäuser 2002.

10. K. WILMAŃSKI, *Note on the notion of incompressibility in theories of porous and granular materials*, ZAMM, **81**, 37–42, 2001.

11. K. WILMA NSKI, *Thermodynamics of multicomponent continua*, [in:] *Earthquake thermodynamics and phase transformations in the earth's interior*, J. MAJEWSKI, R. TEISSEYRE [Eds.], 567–655, Academic Press, San Diego 2001.

12. I. MÜLLER, *Thermodynamics*, Pitman 1985.

13. W. G. GRAY, *Elements of a systematic procedure for the derivation of macroscale conservation equations for multiphase flow in porous media*, [in:] *Kinetic and continuum theories of granular and porous media*, K. HUTTER, K. WILMAŃSKI [Eds.], CISM Courses and Lectures No. 400, Springer WienNewYork, 67–130, 1999.

14. T. WILHELM, K. WILMAŃSKI, *On the Onset of Flow Instabilities in granular media due to porosity inhomogeneities*, Int. Jour. Multiphase Flows, in print 2002.

15. R. D. STOLL, *Sediment acoustics*, Lecture Notes in Earth Sciences, vol. 26, Springer-Verlag, Berlin 1989.

16. C. TRUESDELL, R. D. TOUPIN, *The Classical field theories*, [in:] *Handbuch der Physik*, S. FLÜGGE [Ed.], Springer-Verlag, Berlin, 226–793, 1960.

17. K. WILMAŃSKI, *Waves in porous and granular materials*, [in:[*Kinetic and continuum theories of granular and porous media*, K. HUTTER, K. WILMAŃSKI [Eds.], CISM Courses and Lectures No. 400, Springer WienNewYork, 131–186, 1999.

18. M. CIESZKO, J. KUBIK, *Constitutive description of fluid-saturated porous media with immiscible elastic constituens*, [in:] *Problems of environmental and damage mechanics* Proc. of the XXXI Polish Solid Mechanics Conference SolMec'96, Mierki near Olsztyn, September 9-14, 1996, W. KOSIŃSKI, R. DE BOER and D. GROSS [Eds.], IPPT PAN, Warszawa, 39–57 1997.

19. M. CIESZKO, J. KUBIK, M. KACZMAREK, (in Polish) 2000, *Fundamentals of dynamics of saturated porous media*, IPPT PAN, Warszawa, 2000.

Received May 10, 2002; revised version November 14, 2002.

Arch. Mech., **54**, 5-6, pp. 737–750, Warszawa 2002

On the macroscopic modelling of elastic/viscoplastic composites

CZ. WOŹNIAK and E. WIERZBICKI

Institute of Mathematics and Informatics
Technological University of Częstochowa,
Dąbrowskiego 73, 42-200 Częstochowa, Poland
e-mail: wozniak@matinf.pcz.czest.pl

Dedicated to Professor Piotr Perzyna
on the occasion of his 70^{th} birthday

THE AIM of this contribution is to formulate a macroscopic model for the analysis of dynamic problems in micro-periodic composites made of elastic/viscoplastic and/or linear viscoelastic materials. The proposed modelling approach is based on the concept of tolerance averaging which so far was applied to the linear elastodynamics and heat transfer in periodic materials and structures. The obtained model equations, in contrast to homogenized equations, describe the effect of microstructure size on the overall behaviour of a composite solid.

1. Introduction

THIS PAPER is devoted to macroscopic modelling of certain inelastic micro-periodic composites. This modelling problem has been investigated for viscoelastic and elastic-plastic materials in a series of papers [2,4,5,10–15]. In this contribution we propose a unified method of macroscopic modelling for dynamic problems in micro-periodic composites made of elastic/viscoplastic and/or linear viscoelastic components. The motivation for writing this paper is an important role which recently play elastic/viscoplastic materials both from the theoretical and engineering point of view; among the leading papers on this subject we have to mention those by PERZYNA [6–9], to whom this work is dedicated. An alternative approach to the concept of elastic/viscoplastic materials can be found in [1] (cf. also [12] for the discussion of different models of viscoplasticity). In contrast to macroscopic models derived by homogenization, we look for models that make it possible to describe the effect of microstructure size on the overall dynamic behaviour of a micro-periodic solid. To this end we extend the tolerance averaging technique which so far has been applied to the problems of elastodynamics and heat conduction, [17,18,19]. In order to make the paper self-consistent, in the subsequent section, following [17], we outline some basic concepts of the tolerance averaging.

Throughout the paper we use the absolute tensor notation; by small bold letters, $\mathbf{a}$, $\mathbf{b}$, $\mathbf{v}$, $\mathbf{w}$,... we denote vectors and vector fields and by capital boldface letters $\mathbf{S}$, $\mathbf{D}$,... we denote the second order tensors and tensor fields. The block letters $\mathbb{A}$, $\mathbb{B}$, $\mathbb{C}$ are reserved for the fourth order tensors and tensor fields. Symbol $sym(\mathbf{a} \otimes \mathbf{b})$ stands for a symmetric part of the second order tensor $\mathbf{a} \otimes \mathbf{b}$ and $\varepsilon(\mathbf{v})$ is a symmetrized gradient of an arbitrary differentiable vector field $\mathbf{v}$.Superscripts $a, b, ...$ and $A, B, ...$ run over sequences $1, ..., n$ and $1, ..., N$, respectively; summation convention holds unless otherwise stated. It is assumed that all introduced functions satisfy the smoothness conditions required in subsequent considerations.

2. Preliminaries

In this section we recall some basic concepts and statements related to the tolerance averaging, which will be used subsequently; for a detailed discussion the reader is referred to [17] (see also [18,19]). We begin with the statement that in the problem under consideration, every physical quantity (measured in a fixed system of units) can be specified only to within a certain tolerance. It means that the values F_1, F_2 of this quantity will be not discerned provided that $|F_1 - F_2| \leq \varepsilon_F$, where ε_F is a certain positive constant which is referred to as a tolerance parameter related to this quantity (cf. also [3], where ε_F is called "upper bound for negligibles"). In this case we shall tacitly assume that ε_F is known and we shall write $F_1 \cong F_2$. Hence $\cong$ is a certain tolerance relation, i.e. a binary relation defined on $\mathbb{R}$ which is symmetric and reflexive but not transitive. By a tolerance system we shall mean a mapping T which assigns to every unknown field F in the problem under consideration a tolerance parameter ε_F. Subsequently, we shall deal with fields which for every time t are defined in the region Ω in E^3 occupied by the composite. Let $\Delta = (-l_1/2, l_1/2) \times (-l_2/2, l_2/2) \times (-l_3/2, l_3/2)$ be a unit cell of the periodic structure of the composite and let $l = \mathrm{diam}\Delta$. Let us denote by $\|\mathbf{x} - \mathbf{y}\|$ the distance between points $\mathbf{x}$ and $\mathbf{y}$ in E^3, and by $B(\mathbf{x},l)$ – the ball in E^3 with a center $\mathbf{x}$ and a radius l. Setting $\Delta(\mathbf{x}) = \mathbf{x} + \Delta$, $\Omega_\Delta = \{\mathbf{x} \in \Omega : \Delta(\mathbf{x}) \subset \Omega\}$ we define the averaging operator of an arbitrary integrable function $f : \Omega \to \mathbb{R}$ by means of

$$\langle f \rangle(\mathbf{x}) = \frac{1}{|\Delta|} \int\limits_{\Delta(\mathbf{x})} f(\mathbf{y}) dy_1 dy_2 dy_3, \quad \mathbf{x} \in \Omega_\Delta,$$

where $|\Delta|$ is the measure of Δ. If $f(\cdot)$ is a Δ-periodic function then $\langle f \rangle = \mathrm{const}$. If $f(\cdot)$ depends also on time t then we shall write $\langle f \rangle(\mathbf{x},t)$. Let DF stand for a function F as well as for all its derivatives (including time derivatives) which occur in the problem under consideration.

Function $F : \Omega \to \mathbb{R}$ will be called *slowly-varying*, $F \in SV_\Delta(T)$, if for every $\mathbf{x}, \mathbf{y} \in \Omega$ condition $\|\mathbf{x} - \mathbf{y}\| \leq l$ implies $|DF(\mathbf{x}) - DF(\mathbf{y})| \leq \varepsilon_{DF}$.

Function $G : \Omega \to \mathbb{R}$ will be called *periodic-like*, $G \in PL_\Delta(T)$, if for every $\mathbf{x} \in \Omega$ there exists Δ-periodic function $G_{\mathbf{x}}(\cdot)$ satisfying for every $\mathbf{y} \in B(\mathbf{x},l) \cap \Omega$ condition $|G(\mathbf{y}) - G_{\mathbf{x}}(\mathbf{y})| \leq \varepsilon_G$. Function $G_{\mathbf{x}}(\cdot)$ will be called a *Δ-periodic approximation* of $G(\cdot)$ near $\Delta(\mathbf{x})$.

A periodic-like function will be called *oscillating*, $G \in PL^*_\Delta(T)$, if $G \in PL_\Delta(T)$ and if condition $\langle G_{\mathbf{x}} \rangle(\mathbf{x}) = 0$ holds for every $\mathbf{x} \in \Omega_\Delta$.

It can be shown that every periodic-like function G can be uniquely decomposed into a sum of slowly varying function G^o and oscillating function G^*, [17]. Under the aforementioned denotations, bearing in mind the meaning of the tolerance parameter and the corresponding tolerance relation, for every $\mathbf{x} \in \Omega_\Delta$ we obtain the following approximation formulae

$$
\begin{aligned}
&\langle fF \rangle(\mathbf{x}) \cong \langle f \rangle F(\mathbf{x}), \qquad F \in SV_\Delta(T), \\
&\langle fG \rangle(\mathbf{x}) \cong \langle fG_{\mathbf{x}} \rangle(\mathbf{x}), \quad G \in PL_\Delta(T),
\end{aligned}
\tag{2.1}
$$

where f is an arbitrary integrable Δ-periodic function.

The tolerance averaging of equations with Δ-periodic functional coefficients is based on the assumption that there exists a certain tolerance system T so that formulae (2.1) can be used as approximations in the averaging procedure, [17]. It has to be emphasized that a tolerance system T may be not specified in the course of modelling; all we need is that this system exists. Moreover, the tolerance parameters can be calculed *a posteriori* as certain residuals determining the degree of accuracy of obtained solutions to the special problem under consideration.

3. Modelling approach

Let Ω stand for a region in E^3 occupied by a Δ-periodic elastic-viscoplastic composite solid in its reference configuration. It is assumed that the diameter l of the periodicity cell Δ is sufficiently small when compared to the minimum characteristic length dimension of Ω. Denoting by $\mathbf{u}(\mathbf{x},t), \mathbf{S}(\mathbf{x},t)$, the displacement and stress fields, respectively, defined in Ω for every time t, by $\varrho(\mathbf{x})$ the mass density field in Ω, and assuming that the body force $\mathbf{b}$ is constant, we obtain the well known form of the equations of motion

$$
\nabla \cdot \mathbf{S} - \varrho \ddot{\mathbf{u}} + \varrho \mathbf{b} = 0 \tag{3.1}
$$

which have to be satisfied in Ω for every time t together with the known stress continuity conditions on the interfaces between constituents.

To simplify the subsequent considerations we shall restrict ourselves to materials subjected to small strains. The elastic/viscoplastic components are assumed to obey the Huber-Mises yield condition. For the sake of simplicity we shall neglect the hardening effect. Setting

$$\mathbf{S}^D = \mathbf{S} - \frac{1}{3}\mathbf{1}tr\mathbf{S}, \quad \sigma(\mathbf{S}) = \frac{1}{2}\mathbf{S}^D : \mathbf{S}^D$$

we introduce the concept of the yield surface in the form $\sigma(\mathbf{S}) - k^2 = 0$. Let us denote

$$H(a) = \begin{cases} 0 & \text{if} \quad a < 0 \\ 1 & \text{if} \quad a \geq 0 \end{cases}$$

for every real a. Let μ be a viscous parameter representing the relaxation time and define

$$\mathbf{D} = H(\sigma(\mathbf{S}) - k^2)\frac{\sqrt{\sigma(\mathbf{S})} - k}{2\mu\sqrt{\sigma(\mathbf{S})}}\mathbf{S}^D \tag{3.2}$$

as the viscoplastic strain rate. We shall also assume that viscoelastic component materials are obeying the linear Maxwell's law. Combining together the constitutive equations of elasto/viscoplasticity with the equations of linear viscoelasticity, we obtain

$$\varepsilon(\dot{\mathbf{u}}) = \mathbb{A} : \dot{\mathbf{S}} + \mathbb{B} : \mathbf{S} + \mathbf{D} \tag{3.3}$$

where $\mathbb{A}$, $\mathbb{B}$ are the compliance tensors describing respectively the elastic and viscous properties of the material. Neglecting in (3.3) the term $\mathbb{B} : \mathbf{S}$ we shall deal with the elastic/viscoplastic component materials. Setting in (3.3) $\mathbf{D} \equiv \mathbf{0}$ we shall describe the behaviour of the linear viscoelastic components. For the solid under consideration $\mathbb{A}$, $\mathbb{B}$, μ, k are Δ-periodic functions of $\mathbf{x}$ which attain constant values in every constituent of the composite.

The main aim of this contribution is to derive from Eqs. (3.1)–(3.3), which describe the composite solid on the micro-level, a certain system of equations with constant (averaged) coefficients. The derived equations will be interpreted as describing the composite solid on the macroscopic level. To this end we apply the tolerance averaging approach using the concepts outlined in Sec. 2.

The tolerance averaging is based on the heuristic assumption that in an arbitrary periodicity cell $\Delta(\mathbf{x})$, $\mathbf{x} \in \Omega_\Delta$, which is located away from the boundary of Ω, the displacement $\mathbf{u}(\cdot, t)$ and stress $\mathbf{S}(\cdot, t)$ fields conform to the Δ-periodic structure of the solid under consideration. The above *conformability assumption* states that for every time t fields $\mathbf{u}(\cdot, t)$ and $\mathbf{S}(\cdot, t)$ are periodic-like functions:

$$\mathbf{u}(\cdot, t) \in PL_\Delta(T), \quad \mathbf{S}(\cdot, t) \in PL_\Delta(T); \tag{3.4}$$

the above condition may be violated only near the boundary of the solid. Let us observe that the condition similar to that formulated above is also used in homogenization, cf. [14], p. 204.

Following the results of Sec. 2 we conclude that (3.4) implies the decomposition

$$\mathbf{u}(\cdot,t) = \mathbf{w}(\cdot,t) + \mathbf{v}(\cdot,t), \quad \mathbf{w}(\cdot,t) \in SV_{\Delta}(T), \quad \mathbf{v}(\cdot,t) \in PL^{*}_{\Delta}(T), \tag{3.5}$$

where $\mathbf{w}(\mathbf{x},\mathbf{t}) = \langle \mathbf{u} \rangle(\mathbf{x},t)$, $\mathbf{x} \in \Omega$, is the averaged displacement field and $\mathbf{v}(\mathbf{x},t)$, $\mathbf{x} \in \Omega$, will be referred to as the displacement fluctuation field. Denoting by $\mathbf{v}_{\mathbf{x}}$ and $\mathbf{S}_{\mathbf{x}}$ the Δ-periodic approximations near $\Delta(\mathbf{x})$ of $\mathbf{v}$ and $\mathbf{S}$, respectively, defining $\mathbf{D}_{\mathbf{x}}$ by (3.2) for $\mathbf{S} = \mathbf{S}_{\mathbf{x}}$ and introducing $\bar{\mathbf{v}}$ and $\bar{\mathbf{S}}$, with $\langle \bar{\mathbf{v}} \rangle = \mathbf{0}$, as arbitrary Δ-periodic test functions, by means of (2.1) we obtain from (3.1) and (3.5) the following variational conditions:

$$\begin{aligned} &\langle \nabla \bar{\mathbf{v}} : \mathbf{S}_{\mathbf{x}} \rangle(\mathbf{x},t) + \langle \varrho \bar{\mathbf{v}} \rangle \cdot \ddot{\mathbf{w}}(\mathbf{x},t) + \langle \varrho \bar{\mathbf{v}} \cdot \ddot{\mathbf{v}}_{\mathbf{x}} \rangle(\mathbf{x},t) - \langle \varrho \bar{\mathbf{v}} \rangle \cdot \mathbf{b} = 0, \\ &\langle \bar{\mathbf{S}} : \varepsilon(\dot{\mathbf{v}}_{\mathbf{x}}) \rangle(\mathbf{x},t) + \langle \bar{\mathbf{S}} \rangle : \varepsilon(\dot{\mathbf{w}})(\mathbf{x},t) \\ &\qquad = \langle \bar{\mathbf{S}} : \mathbb{A} : \dot{\mathbf{S}}_{\mathbf{x}} \rangle(\mathbf{x},t) + \langle \bar{\mathbf{S}} : \mathbb{B} : \mathbf{S}_{\mathbf{x}} \rangle(\mathbf{x},t) + \langle \bar{\mathbf{S}} : \mathbf{D}_{\mathbf{x}} \rangle(\mathbf{x},t) \end{aligned} \tag{3.6}$$

which hold for every $\mathbf{x} \in \Omega_{\Delta}$ provided that $\mathbf{x}$ is not situated near the boundary $\partial\Omega$ of Ω.

In order to apply the second one of the conformability assumptions (3.4), we introduce a partition of Δ into a set of n not intersecting elements (regions) Δ_a, $a = 1, ..., n$, $\bar{\Delta} = \cup \bar{\Delta}_a$, so that every element Δ_a is homogeneous, i.e., it consists of only one constituent of the composite. Let $(\mathbf{e}_1, \mathbf{e}_2, \mathbf{e}_3)$ be the orthonormal basis in E^3 and let us denote by Λ the Bravais lattice $\Lambda = \{\mathbf{z} \in E^3 : \mathbf{z} = n_1 l_1 \mathbf{e}_1 + n_2 l_2 \mathbf{e}_2 + n_3 l_3 \mathbf{e}_3;\ n_i = 0, \pm 1, \pm 2, ...\}$. Define

$$\Xi^a = \{\mathbf{y} \in \Delta_a + \mathbf{z};\ \mathbf{z} \in \Lambda\}, \quad \Omega^a = \Xi^a \cap \Omega$$

and let $\eta^a(\cdot)$ be the characteristic function of $\Xi^a, a = 1, ..., n$. Obviously, $\eta^a(\cdot)$ is a Δ-periodic function. Taking into account that $\mathbf{S}(\cdot,t)$ is a periodic-like function, we shall introduce n sufficiently smooth functions $\mathbf{S}^a(\cdot,t)$ defined in Ω which are slowly varying and every $\mathbf{S}^a(\mathbf{z},t)$, $\mathbf{z} \in \Lambda \cap \Omega_{\Delta}$, is a mean value of $\mathbf{S}(\cdot,t)$ in $\Delta(\mathbf{z}) \cap \Xi^a$. The subsequent considerations will be based on the extra modelling assumption that in the course of averaging procedure we can use the approximations

$$\mathbf{S}_{\mathbf{x}}(\mathbf{y},t) \cong \eta^a(\mathbf{y}) \mathbf{S}^a(\mathbf{x},t);\ \mathbf{y} \in \Delta(\mathbf{x}),\ \mathbf{x} \in \Omega_{\Delta},$$

where $\mathbf{S}_{\mathbf{x}}(\cdot,t)$ is a Δ-periodic approximation of $\mathbf{S}(\cdot,t)$ near $\Delta(\mathbf{x})$. This approximation holds with a sufficient accuracy provided that the partition of Δ into

elements Δ_a, $a = 1, ..., n$, is sufficiently fine. Fields $\mathbf{S}^a(\cdot, t)$ describe the stresses on the micro-level but, as slowly varying functions, they will also describe a behaviour of the composite in the framework of a proposed macroscopic model. Following [14], p. 253, we recall that in modelling problems under consideration it is not possible to eliminate entirely the microscopic description from the macroscopic one.

Fields $\mathbf{S}^a$ will be referred to as the mean local stresses. Substituting into (3.6) $\mathbf{S}_{\mathbf{x}}(\mathbf{y}, t) = \eta^a(\mathbf{y})\mathbf{S}^a(\mathbf{x}, t)$, $\mathbf{y} \in \Delta(\mathbf{x})$ and $\bar{\mathbf{S}} = \eta^a(\mathbf{y})\mathbf{C}^a$ where $\mathbf{C}^a$ are arbitrary constant second-order tensors, we obtain

$$\langle \eta^a \nabla \bar{\mathbf{v}} \rangle : \mathbf{S}^a(\mathbf{x}, t) + \langle \varrho \bar{\mathbf{v}} \rangle \cdot \ddot{\mathbf{w}}(\mathbf{x}, t) + \langle \varrho \bar{\mathbf{v}} \cdot \ddot{\mathbf{v}}_{\mathbf{x}} \rangle(\mathbf{x}, t) - \langle \varrho \bar{\mathbf{v}} \rangle \cdot \mathbf{b} = 0,$$

$$\langle \eta^a \eta^b \mathbb{A} \rangle : \dot{\mathbf{S}}(\mathbf{x}, t) + \langle \eta^a \eta^b \mathbb{B} \rangle : \mathbf{S}(\mathbf{x}, t) + \langle \eta^a \eta^b \rangle \mathbf{D}^b(\mathbf{x}, t) \tag{3.7}$$

$$= \langle \eta^a \rangle \varepsilon(\dot{\mathbf{w}})(\mathbf{x}, t) + \langle \eta^a \varepsilon(\dot{\mathbf{v}}_{\mathbf{x}}) \rangle(\mathbf{x}, t)$$

where (no summation over b!)

$$\mathbf{D}^b = H(\sigma(\mathbf{S}^b) - k_b) \frac{\sqrt{\sigma(\mathbf{S}^b)} - k_b}{2\mu_b \sqrt{\sigma(\mathbf{S}^b)}} (\mathbf{S}^b)^D \tag{3.8}$$

and moduli k_b, μ_b are related to the material components occupying part Ω^b of the region Ω. Fields $\mathbf{D}^b$ will be referred to as the mean local viscoplastic strain rates. Equation $(3.7)_1$ represents the variational condition which has to hold for every oscillating Δ-periodic test function $\bar{\mathbf{v}}$. By means of the approximation $\mathbf{S} = \eta^a \mathbf{S}^a$ and after restricting the domain Ω of (3.1) to an arbitrary but fixed cell $\Delta(\mathbf{x})$, $\mathbf{x} \in \Omega_\Delta$, we obtain the averaged form of equations of motion

$$\langle \eta^a \rangle \nabla \cdot \mathbf{S}^a(\mathbf{x}, t) - \langle \varrho \rangle \cdot \ddot{\mathbf{w}}(\mathbf{x}, t) - \langle \varrho \ddot{\mathbf{v}}_{\mathbf{x}} \rangle(\mathbf{x}, t) + \langle \varrho \rangle \mathbf{b} = \mathbf{0}. \tag{3.9}$$

Equations (3.7)–(3.9) constitute the system of equations for averaged displacements $\mathbf{w}$, mean local stresses $\mathbf{S}^a$ and displacement fluctuations $\mathbf{v}$ (which in every $\Delta(\mathbf{x})$, $\mathbf{x} \in \Omega_\Delta$, are represented by their local periodic approximations $\mathbf{v}_{\mathbf{x}}$). The above equations have a physical sense only if $\mathbf{w}(\cdot, t)$, $\mathbf{S}^a(\cdot, t)$ are slowly-varying functions.

In order to obtain from (3.7)–(3.9) the macroscopic model of the composite medium under consideration we apply the procedure used in [17]. To this end we shall look for the approximate solution to the periodic variational problem (3.7) for $\mathbf{v}_{\mathbf{x}}$ in the form

$$\mathbf{v}_{\mathbf{x}}(\mathbf{y}, t) = h^A(\mathbf{y})\mathbf{v}^A(\mathbf{x}, t), \quad \mathbf{y} \in \Delta(\mathbf{x}) \tag{3.10}$$

where $h^A(\cdot)$ are the postulated a priori linear independent Δ-periodic shape functions and $\mathbf{v}^A(\cdot)$ are new unknowns which will be referred to as fluctuation

variables. Because $\mathbf{v}(\cdot,t) \in PL^*_\Delta(T)$, then $\mathbf{v}^A(\cdot,t)$ have to be slowly varying functions. It is assumed that the shape functions lead to the positive definite matrix $\langle \varrho h^A\ h^B\rangle$ and satisfy conditions $\langle h^A\rangle = 0$, $h^A \in O(l)$, $l\nabla h^A \in O(l)$. Let us substitute the right-hand sides of (3.10) into (3.7), (3.9). Using the orthogonalization method we substitute $\bar{\mathbf{v}} = h^A\mathbf{c}^A$ into $(3.7)_1$; here $\mathbf{c}^A$ are arbitrary independent constant vectors. After simple manipulations, we obtain finally

$$
\begin{aligned}
&\langle\varrho\rangle\ddot{\mathbf{w}}(\mathbf{x},t) + \langle\varrho h^A\rangle\ddot{\mathbf{v}}^A(\mathbf{x},t) - \langle\eta^a\rangle\nabla\cdot\mathbf{S}^a(\mathbf{x},t) - \langle\varrho\rangle\mathbf{b} = \mathbf{0},\\
&\langle\varrho h^A h^B\rangle\ddot{\mathbf{v}}^B(\mathbf{x},t) + \langle\varrho h^A\rangle\ddot{\mathbf{w}}(\mathbf{x},t) + \langle\eta^a\nabla h^A\rangle\cdot\mathbf{S}^a(\mathbf{x},t) - \langle\varrho h^A\rangle\mathbf{b} = \mathbf{0},\\
&\langle\eta^a\eta^b\mathbb{A}\rangle : \dot{\mathbf{S}}^b(\mathbf{x},t) + \langle\eta^a\eta^b\mathbb{B}\rangle : \mathbf{S}^b(\mathbf{x},t) + \langle\eta^a\eta^b\rangle\mathbf{D}^b(\mathbf{x},t)\\
&\qquad - \langle\eta^a\rangle\varepsilon(\dot{\mathbf{w}})(\mathbf{x},t) - sym(\langle\eta^a\nabla h^A\rangle\otimes\dot{\mathbf{v}}^A) = \mathbf{0}
\end{aligned}
\tag{3.11}
$$

where the mean local viscoplastic strain rates $\mathbf{D}^b$ are defined by condition (3.8). It has to be remembered that fields $\mathbf{S}^a(\cdot,t)$, $\mathbf{D}^a(\cdot,t)$ are defined in Ω but have a physical meaning only in Ω^a.

Formulae (3.11) together with (3.8) constitute a system of relations for unknown averaged displacements $\mathbf{w}$, fluctuation variables $\mathbf{v}^A$ and mean local stresses $\mathbf{S}^a$. The aforementioned equations have constant coefficients and can be treated as representing a certain *averaged (macroscopic) model of the composite made of elastic/viscoplastic and/or viscoelastic components.* This model has a physical sense if all unknowns for every instant t are slowly-varying functions:

$$
\mathbf{w}(\cdot,t) \in SV_\Delta(T), \quad \mathbf{v}^A(\cdot,t) \in SV_\Delta(T), \quad \mathbf{S}^a(\cdot,t) \in SV_\Delta(T). \tag{3.12}
$$

The above conditions can be verified only *a posteriori.*, i.e., after obtaining a solution to the problem under consideration. In this way we can evaluate on the basis of (3.12) the tolerance parameters related to functions $\mathbf{w}$, $\mathbf{v}^A$, $\mathbf{S}^a$ and their derivatives, and hence to determine residuals of approximation for the derived solution. The characteristic feature of the derived model is that it describes the effect of the microstructure size on the macroscopic dynamic behaviour of a solid due to terms $\langle\varrho h^A h^B\rangle \in O(l^2)$, $\langle\varrho h^A\rangle \in O(l)$ in (3.11). It has to be remembered that the length-scale effect for the problem under consideration is also due to the presence of viscous parameters μ_b in (3.8).

The form and number of equations (3.11) depends on the form and number of shape functions h^A and on the partition of the cell Δ into elements Δ_a. It means that the derived model can be formulated on different levels of accuracy. For a discussion of the problem of finding functions h^A the reader is referred to [17].

4. Special cases

Setting $\mu_a \to 0$ for $a = 1, ..., n$ and neglecting in (3.11) the terms involving $\mathbb{B}$ we obtain equations of a composite solid with elastic-perfectly plastic constituents. In this case instead of (3.8) we obtain

$$\mathbf{D}^b = H(\sigma(\mathbf{S}^b) - k_b)\mathbf{D}_p^b$$

where $\mathbf{D}_p^b$ is a rate of the plastic strain in Ω^b. Let us observe that, in contrast to homogenization where we deal with one averaged yield condition for a macroscopic stress, [13,14], here we have separate yield conditions

$$\sigma(\mathbf{S}^a(\mathbf{x}, t)) - k_a = 0$$

for mean local stresses related to different parts Ω^a of Ω. Obviously, if parts Ω^a and Ω^b are occupied by one elastic/viscoplastic constituent then $k_a = k_b$.

Let $\mathbf{S}^a(\mathbf{x}, t) < k_a$, $a = 1, ..., n$, hold for every $\mathbf{x} \in \Omega$ and every time t. In this case the mean local viscoplastic strain rates $\mathbf{D}^a$ disappear. For the time being let us also neglect in $(3.11)_3$ the terms involving $\mathbb{B}$. Under notations (in the definition of ξ^a no summation over a!):

$$\xi^a = \eta^a \langle \eta^a \rangle^{-1}, \quad \mathbf{G}^{AB} = \langle \eta^a \nabla h^A \rangle \cdot \langle \xi^a \xi^b \mathbb{C} \rangle \cdot \langle \eta^b \nabla h^B \rangle,$$

where $\mathbb{C}$ is a tensor of elastic moduli, we can eliminate from (3.11) mean local stresses $\mathbf{S}^a$. After simple manipulations we obtain

$$\langle \varrho \rangle \ddot{\mathbf{w}} + \langle \varrho h^A \rangle \ddot{\mathbf{v}}^A - \langle \eta^a \rangle \nabla \cdot [\langle \xi^a \mathbb{C} \rangle : \varepsilon(\mathbf{w}) + \langle \xi^a \xi^b \mathbb{C} \rangle : sym(\langle \eta^b \nabla h^A \rangle \otimes \mathbf{v}^A)] - \langle \varrho \rangle \mathbf{b} = \mathbf{0},$$

$$\langle \varrho h^A h^B \rangle \ddot{\mathbf{v}}^B + \langle \varrho h^A \rangle \ddot{\mathbf{w}} + \mathbf{G}^{AB} \cdot \mathbf{v}^B - \langle \eta^a \nabla h^A \rangle \cdot \langle \xi^a \mathbb{C} \rangle : \varepsilon(\mathbf{w}) - \langle \varrho h^A \rangle \mathbf{b} = \mathbf{0}.$$

It can be shown that the above equations, for a sufficiently fine partition of Δ into Δ_a, lead to the equations obtained in [16] for the macroscopic model of Δ-periodic linear elastic composites.

For a homogeneous solid $\langle \varrho h^A \rangle = \varrho \langle h^A \rangle = 0$, $\langle \eta^1 \nabla h^A \rangle + \langle \eta^2 \nabla h^A \rangle + ... + \langle \eta^n \nabla h^A \rangle = \langle \nabla h^A \rangle = 0$ and introducing a sufficiently small cell Δ (which for a homogeneous solid may be taken as infinitesimal) we can also assume that $\mathbf{S} = \eta^a \mathbf{S}^a$ and $\mathbf{D} = \eta^a \mathbf{D}^a$ are slowly-varying functions. In this case from equations $(3.11)_1$, $(3.11)_3$ we derive equations (3.1) and (3.3), respectively, and under homogeneous initial conditions equations $(3.11)_2$ yield $\mathbf{v}^B = \mathbf{0}$.

5. Illustrative example

The general model equations (3.11) with conditions (3.8) will be now illustrated and discussed on a simple example of the uniaxial stress in a rod made of two periodically distributed materials, see Fig. 1. In this case equations (3.1), (3.3), after neglecting body forces and denoting $(\cdot)' = \partial(\cdot)/\partial x$, can be reduced to the form

$$s'(x,t) - \varrho(x)\ddot{u}(x,t) = 0,$$

$$\dot{u}'(x,t) = \frac{1}{E(x)}\dot{s}(x,t) + B(x)s(x,t) + d(x,t) \tag{5.1}$$

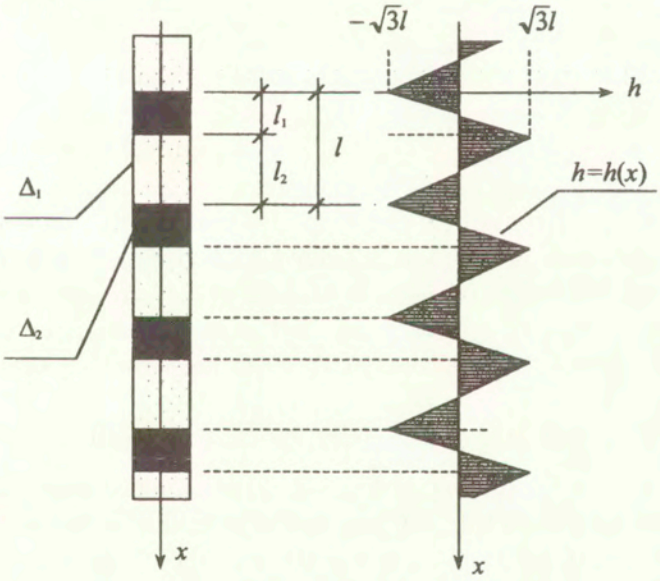

FIG. 1. Scheme of the rod and diagram of the shape function.

and equation (3.2) yields

$$d = (H(|s| - \sqrt{3}k(x))\frac{1}{3\mu(x)}(s - \sqrt{3}k(x)\operatorname{sgn} s) \tag{5.2}$$

The mass density $\varrho(x)$, Young's modulus $E(x)$ and moduli $B(x)$, $k(x)$, $\mu(x)$ are assumed to attain the constant values ϱ_1, E_1, B_1, k_1, μ_1 and ϱ_2, E_2, B_2, k_2, μ_2, respectively, in the intervals of the x-axis with lengths l_1, l_2, see Fig. 1. The cell Δ

now reduces to the interval $(-l/2, l/2)$, $l = l_1 + l_2$. Let us introduce a partition of this cell into two elements $\Delta_1 = (-l/2, -l/2 + l_1)$, $\Delta_2 = (-l/2 + l_1, l/2)$. Following [17] we introduce only one shape function $h = h(x)$, the diagram of which is shown on the right-hand side of Fig. 1. In this case we deal with one fluctuation variable $v = v(x,t)$. Let us also define $\nu_1 = l_1/l$, $\nu_2 = l_2/l$ and denote by s_1, s_2 the mean local stresses. Under the above notation, the model equations (3.11) will take the form

$$\langle\varrho\rangle\ddot{w}(x,t) - \nu_1 s_1'(x,t) - \nu_2 s_2'(x,t) = 0,$$

$$l^2\langle\varrho\rangle\ddot{v}(x,t) + 2\sqrt{3}[s_1(x,t) - s_2(x,t)] = 0,$$

$$\frac{\nu_1}{E_1}\dot{s}_1(x,t) + \nu_1 B_1 s_1(x,t) + \nu_1 d_1(x,t) - \nu_1\dot{w}'(x,t) - 2\sqrt{3}\dot{v}(x,t) = 0, \tag{5.3}$$

$$\frac{\nu_2}{E_2}\dot{s}_2(x,t) + \nu_2 B_2 s_2(x,t) + \nu_2 d_2(x,t) - \nu_2\dot{w}'(x,t) + 2\sqrt{3}\dot{v}(x,t) = 0$$

and condition (3.8) for the uniaxial stress will be given by

$$d_\alpha = \frac{1}{3\mu_\alpha} H(|s_\alpha| - \sqrt{3}k_\alpha)(s_\alpha - \sqrt{3}k_\alpha \operatorname{sgn} s_\alpha), \quad \alpha = 1,2. \tag{5.4}$$

Equations (5.3), (5,4) constitute the proposed macroscopic model for problems described by equations (5.1), (5.2) provided that $B_1 d_1(\cdot,t) \equiv 0$, $B_2 d_2(\cdot,t) \equiv 0$. Bearing in mind (3.5), the total displacements $u(x,t)$ are now described by the formula $u(x,t) = w(x,t) + h(x)v(x,t)$. We have to remember that by means of (4.1), the solutions to equations (5.3), (5.4) have the physical sense only if conditions

$$w(\cdot,t), v(\cdot,t), s_1(\cdot,t), s_2(\cdot,t) \in SV_\Delta(T)$$

hold for every time t. We have stated in Sec. 4 that the proposed model describes the effect of the microstructure cell size on the overall solid behaviour due to the presence of the length parameter l in equation $(5.3)_2$. Neglecting the microstructural term $l^2\langle\varrho\rangle\ddot{v}$ we obtain from (5.3) a simplified model in which $s_1 = s_2 = s$. For this simplified model, equation $(5.3)_1$ takes the form

$$\langle\varrho\rangle\ddot{w}(x,t) - s'(x,t) = 0. \tag{5.5}$$

After denotations

$$E^{\text{eff}} = \left(\frac{\nu_1}{E_1} + \frac{\nu_2}{E_2}\right)^{-1}, \quad \langle B\rangle = \nu_1 B_1 + \nu_2 B_2, \quad \alpha = E^{\text{eff}}\langle B\rangle$$

we obtain the following equation for the stress field

$$\dot{s}(x,t) + \alpha s(x,t) + E^{\text{eff}}[\nu_1 d_1(x,t) + \nu_2 d_2(x,t)] = E^{\text{eff}}\dot{w}'(x,t) \tag{5.6}$$

where

$$
\begin{aligned}
d_1 &= \frac{1}{3\mu_1} H(|s| - \sqrt{3}k_1)(s - \sqrt{3}k_1 \operatorname{sgn} s), \\
d_2 &= \frac{1}{3\mu_2} H(|s| - \sqrt{3}k_2)(s - \sqrt{3}k_2 \operatorname{sgn} s);
\end{aligned} \tag{5.7}
$$

and constant E^{eff} in (5.6) is the well-known effective value of the Young modulus in the uniaxial stress. In this case we have arrived at the system of equations (5.5), (5.6) for $w(\cdot)$ and $s(\cdot)$, where the partial viscoplastic strain rates are given by conditions (5.7). Neglecting in (5.6) the term involving α we pass to the simplified macroscopic model of the problem under consideration for an elastic/viscoplastic material. This problem is governed by equation (5.5) and

$$
\dot{s}(x,t) - E^{\text{eff}}\dot{w}'(x,t) + E^{eff}[\nu_1 d_1(x,t) + \nu_2 d_2(x,t)] = 0
$$

together with conditions (5.7). For viscoelastic composites $d_1 = d_2 \equiv 0$ and equation (5.6) yields

$$
s(x,t) - s(x,0) = E^{\text{eff}}[w'(x,t) - w'(x,0) - \alpha e^{-\alpha t} \int_0^t w'(x,\tau) e^{\alpha\tau} d\tau]. \tag{5.8}
$$

Substituting the right-hand side of (5.8) into (5.5) we obtain the equation for the averaged displacement field $w(\cdot)$. The above results hold only under the assumption that the microstructural term $l^2\langle\varrho\rangle\ddot{v}(x,t)$ in (5.3) is neglected.

If the microstructural term $l^2\langle\varrho\rangle\ddot{v}(x,t)$ in (5.3) is not neglected then $s_1 \neq s_2$ and for viscoelastic composites, under notations

$$
\alpha_1 = E_1 B_1, \quad \alpha_2 = E_2 B_2,
$$

we obtain from (5.3):

$$
\begin{aligned}
s_1(x,t) - s_1(x,0) &= E_1 \Big[w'(x,t) - w'(x,0) + \frac{2\sqrt{3}}{\nu_1} v(x,t) - \frac{2\sqrt{3}}{\nu_1} v(x,0) \\
&\quad + \alpha_1 e^{-\alpha_1 t} \int_0^t (w'(x,\tau) + \frac{2\sqrt{3}}{\nu_1} v(x,\tau)) e^{\alpha_1 \tau} d\tau], \\
s_2(x,t) - s_2(x,0) &= E_2 [w'(x,t) - w'(x,0) - \frac{2\sqrt{3}}{\nu_2} v(x,t) + \frac{2\sqrt{3}}{\nu_2} v(x,0) \\
&\quad + \alpha_2 e^{-\alpha_2 t} \int_0^t (w'(x,\tau) - \frac{2\sqrt{3}}{\nu_2} v(x,\tau)) e^{\alpha_2 \tau} d\tau \Big].
\end{aligned} \tag{5.9}
$$

Substituting the right-hand sides of equations (5.9) into equations $(5.3)_1$ and $(5.3)_2$ we arrive at the system of two governing equations for $w(\cdot)$ and $v(\cdot)$. For

elastic materials $\alpha_1 = \alpha_2 = 0$ and the aforementioned system of equation can be reduced to the form

$$\langle \varrho \rangle \ddot{w}(x,t) - \langle E \rangle w''(x,t) - 2\sqrt{3}(E_2 - E_1)v(x,t) = 0,$$

$$l^2 \langle \varrho \rangle \ddot{v}(x,t) + 2\sqrt{3}\left(\frac{E_2}{\nu_2} + \frac{E_1}{\nu_1}\right)v - 2\sqrt{3}(E_2 - E_1)w'(x,t) = 0$$

which coincides with the known result obtained in [16].

6. Conclusions

We close the paper with a summary of new results and information on the macroscopic modelling of micro-periodic elastic/viscoplastic and linear viscoelastic composites.

1. The proposed macroscopic model of the micro-periodic composites made of elastic/viscoplastic and/or linear viscoelastic components was obtained in the form of equations (3.11) together with conditions (3.8). The above equations involve exclusively constant coefficients. The characteristic feature of the proposed model is that it describes the effect of microstructure size on the dynamic overall behaviour of a composite solid (the microstructure length-scale effect).
2. The aforementioned microstructure length-scale effect takes place only in dynamic problems, i.e., terms describing this effect for the quasi-stationary problems drop out from the governing equations (3.11) of the macroscopic model.
3. The proposed model introduces the concept of mean local stresses and mean local viscoplastic strain rates into the macroscopic description of a micro-periodic composite and hence makes it possible to formulate constitutive equations on the macroscopic level independently for every material constituent, see equations $(3.11)_3$, together with condition (3.8).
4. The proposed modelling approach leads to certain *a posteriori* estimates of solutions which can be derived in every special problem from conditions (3.12).
5. For the sake of simplicity all considerations have been based on the simplest form (3.2), (3.3) of constitutive equations for elastic/viscoplastic materials. However, the modelling approach outlined in the paper can be easily extended to general constitutive equations proposed by Perzyna in [6-9].

The main drawback of the proposed model lies in a possibly large number of unknown fields $\mathbf{v}^A(\cdot)$, $A = 1, ..., N$, and $\mathbf{S}^a(\cdot)$, $a = 1, ..., n$, involved in the macroscopic description of the problem in the framework of the model equations (3.11).

References

1. G. DUVAUT, J.-L. LIONS, *Les inéquations en mécanique et en physique*, Dunod, Paris 1972.
2. G. DVORAK, M. RAO, *Axisymmetric plasticity theory of fibrous composites*, Int. J. Engng. Sci., **9**, 971, 1971.
3. G. FICHERA, *Is the Fourier theory of heat propagation paradoxical?*, Rendiconti del Circolo Matematico di Palermo, Serie II, **XLI**, 5–28, 1992.
4. C. FRANCFORT, D. LEGUILLON, P. SUQUET, *Homogénéisation de milieux viscoélastiques linéarisés de Kelvin Voigt*. C. R. Acad. Sci. Paris, I, **269**, 287–290, 1983.
5. P.V. MC LAUGHLIN, *Limit behaviour of fibrous materials*, Int. J. Solids Structures, **6**, 1357–1376, 1970.
6. P. PERZYNA, *The constitutive equations for rate-sensitive plastic materials*, Quart. Appl. Math., **20**, 321–332, 1963.
7. P. PERZYNA, *Fundamental problems in viscoplasticity*, Advances in Applied Mechanics, **9**, 343–377, 1966.
8. P. PERZYNA, *Thermodynamic theory of viscoplasticity*, Advances in Applied Mechanics, **11**, 313–354, 1977.
9. P. PERZYNA, *Thermo-elasto-viscoplasticity and damage*, [in:] Lemaitre Handbook of material Behaviour Models, Academic Press, 2001.
10. E. SANCHEZ–PALENCIA, J. SANCHEZ–PALENCIA, *Sur certains problémes physiques d'homogénéisation donnant lieu à des phénomènes de relaxation*, C.R. Acad. Sc. Paris (A), **286**, 903–906, 1978.
11. L. S. SHU, B. W. ROSEN, *Strength of fiber reinforced composites by limit analysis method*, J. Composite Materials, **1**, 366–381, 1967.
12. L. J. SLUYS, *Computational modelling of localization and fracture* [in:] Localization and Fracture Phenomena in Inelastic Solids, PERZYNA [Ed.], International Centre for Mechanical Mechanical Sciences, CISM, Courses and Lectures - No. 386, Springer, 243–299, 1998.
13. P. SUQUET, *Local and global aspects in the mathematical theory of plasticity*, [in:] Plasticity Today, BIANCHI and SAWCZUK [Eds.], Elsevier, 1984.
14. P. SUQUET, *Elements of homogenization for inelastic solid mechanics*, [in:] Lecture Notes in Physics 272, Homogenization Techniques for Composite Media E. SANCHEZ-PALENCIA and ZAOUI [Eds.], 194–278, 1984.
15. M. WĄGROWSKA, CZ. WOŹNIAK, *On the modelling of dynamic problems for visco-elastic composites*, Int. J. Engng Sci., **34**, 923–932, 1996.
16. CZ. WOŹNIAK, *Refined macrodynamics of periodic structures*, Arch. Mech., **45**, 295–304, 1993.
17. CZ. WOŹNIAK, E. WIERZBICKI, *Averaging techniques in thermomechanics of composite solids. Tolerance averaging versus homogenization*, Wyd. Politechniki Częstochowskiej, Częstochowa 2000.

18. Cz. WOŹNIAK, E. WIERZBICKI, M. WOŹNIAK, *A macroscopic model for the heat propagation in the microscopic composite solids*, Journal of Thermal Stresses, **25**, 283–293, 2002.

19. Cz. WOŹNIAK, *Macroscopic modelling of multiperiodic composites*, C. R. Mecanique, **330**, 283–293, 2002.

Received May 5, 2002; revised version August 26, 2002.

Arch. Mech., **54**, 5-6, pp. 751–770, Warszawa 2002

On the optimal design of viscoplastic bars under combined torsion with bending

M. ŻYCZKOWSKI, E. CEGIELSKI

Institute of Mechanics and Machine Design
Cracow University of Technology
Warszawska 24, 31-155 Krakow, Poland

Dedicated to Professor Piotr Perzyna on the occasion of his 70^{th} birthday

THE GOVERNING EQUATION for viscoplastic simultaneous torsion and bending of a prismatic bar is derived. Then a certain particular closed–form solution of this equation is found; it corresponds to an elliptic cross–section with the ratio of semi–axes depending on the bending-to-torsion ratio. This solution proves to be optimal if the optimization constraint is imposed on initiation (nucleation) and growth of material damage and if the material properties conform to the Huber–Mises–Hencky failure hypothesis.

1. Introduction

THERE EXISTS a great variety of formulations of optimal design problems of viscoplastic structures. Viscoplasticity – giving the most adequate description of mechanical properties of many materials, particularly under dynamic loadings – brings together the difficulties of the theory of plasticity and of creep mechanics: effective time factor and necessity of separation of plastically–active and plastically-passive processes, not always described by unique and experimentally verified criteria for various viscoplastic materials. Further problems pertain to quasi–static or dynamic loadings, a great variety of constitutive equations, various approaches to damage, their evolution and final rupture. A comprehensive treatment of various aspects of viscoplasticity has been given by Perzyna and his collaborators as a result of his over forty years research, initiated by the most often quoted fundamental papers [27], [29] and his early monograph [30].

Particularly much attention to optimal design of viscoplastic structures, both under quasi-static and dynamic loadings, has been paid by CEGIELSKI (partly with ŻYCZKOWSKI). In most cases the minimal volume served as the design objective, whereas the optimization constraints were divided into global and local ones. In the first group the following quantities were classified: the total energy dissipated during the process, the norm of residual displacements (e.g.

the maximal residual deflection of a beam), the norm of displacements maximal in time under impact etc. Local constraints were imposed on the unit dissipated energy, maximal (in time) reduced stress at individual points of the body, the minimal or maximal dimension of the cross–section, and similar.

In particular, quasi-static loadings were investigated by CEGIELSKI [5], where optimal shapes of a cantilever beam were considered as an example. The author analyzed the dependence of optimal shapes on constitutive equations, on distribution of loading in space and in time, and on the type of constraints adopted. The remaining papers were devoted to dynamic loadings: CEGIELSKI and ŻYCZKOWSKI [8] determined optimal shapes of bars under axial impact, CEGIELSKI [4] considered optimal beams for various impulse shapes, CEGIELSKI and ŻYCZKOWSKI [9] found optimal thickness distribution in circular cylindrical shells under dynamic combined loadings, and ŻYCZKOWSKI and CEGIELSKI [47] optimized beams under transverse impact. CEGIELSKI and ŻYCZKOWSKI [10] discussed optimal bars under dynamic axial loading in the range of finite strains, CEGIELSKI [6] optimized non–prismatic circular bars under dynamic twisting loadings, and finally, CEGIELSKI [7] considered optimal beams under dynamic bending and axial forces.

We mention also several other papers devoted to optimization of viscoplastic structures, based mainly on sensitivity analysis. ARORA *et al.* [1] compared material derivative and control volume approach in the case of the geometrically non–linear viscoplasticity. ZHANG *et al.* [41] derived design sensitivity coefficients by the boundary element method. ARORA *et al.* [2] LEE *et al.* [19] used a Lagrangian description and discussed in detail various constitutive equations of viscoplasticity. JAO and ARORA [14] considered optimization of viscoplastic structures described by an endochronic model. LEU and MUKHERJEE [22, 23] discussed sensitivity in finite–strain viscoplasticity. KULKARNI and NOOR [17] considered two-dimensional viscoplastic structures under dynamic loadings. A detailed review of optimization of viscoplastic structures is given in the survey paper by ŻYCZKOWSKI [43].

The present paper deals with optimal design of viscoplastic bars under simultaneous quasi-static torsion with bending. In view of the neglected dynamic effects it is assumed that both the twisting and bending moments are constant along the axis of the bar, hence optimal design is reduced to optimization of the cross–sectional shape. First the governing equation for viscoplastic torsion with bending for bars of arbitrary cross–section will be derived. Then a particular closed–form solution will be found; it corresponds to an elliptic cross section and generalizes that found by OBERWEIS and ŻYCZKOWSKI [26] for perfectly plastic materials. Then, following the paper by ŻYCZKOWSKI [44] who proved that this elliptic section satisfies the Drucker–Shield necessary condition of optimal plastic design, we are going to analyze the attributes of optimality of this section in

viscoplasticity. In particular we shall prove that according to some approaches to damage mechanics, the initiation (nucleation) of damage starts uniformly along the whole contour line, hence the shape obtained may be called the „shape of uniform viscoplastic strength".

From among the related papers we mention here those by PIECHNIK [35] who solved the problem of simultaneous bending with torsion of a circular bar subject to nonlinear creep, by MEGUID *et al.* [24] on viscoplastic combined tension with torsion, by LAU and LISTVINSKY [18] (bending with torsion of a circular cylinder under creep conditions), finally by RYSZ and ŻYCZKOWSKI [37], who optimized a thin–walled cross–section under bending with torsion for a given creep rupture time (the „shape of uniform creep strength").

The present paper is based on the following assumptions:

1. A straight prismatic bar is subject to twisting moment M_t and bending moment M_b, changing slowly in time t (quasi-static loading). At the beginning no relation is assumed between the moments, but the solution obtained will be valid only for proportional changes of these moments.
2. The supports of the bar allow for free warping of all cross-sections. A particular example of the supports will be described below.
3. The material is viscoplastic and isotropic; in general, elastic strains and plastic hardening are allowed for, but in the first part of the paper a restriction to rigid–perfectly viscoplastic materials will be introduced.
4. The material is incompressible both in elastic and viscoplastic range. It is governed by the Huber–Mises–Hencky (HMH) failure hypothesis.
5. The analysis is confined to small strains.

2. Governing equations for torsion with bending

Consider a prismatic bar of arbitrary solid bisymmetric cross-section with the axis z, subject to simultaneous torsion and bending in the principal plane yz. The twisting and the bending moments are assumed to be constant along the axis. For example, it will be assumed that the cross-section $z = 0$ is clamped (but allowing for free warping), and the cross-section $z = l$ is free (Fig.1). The signs of the moments shown in Fig.1 are assumed to be compatible with the paper [44]. Then the distribution of velocities in engineering notation is given by (Hill [13])

$$
\begin{aligned}
\dot{u} &= -\frac{1}{2}\dot{\varkappa} xy + \dot{\vartheta} yz, \\
\dot{v} &= -\frac{1}{4}\dot{\varkappa}\left(-x^2 + y^2 + 2z^2\right) - \dot{\vartheta} xz, \\
\dot{w} &= \dot{\varkappa} yz + \dot{\vartheta} w_0(x, y),
\end{aligned}
\tag{2.1}
$$

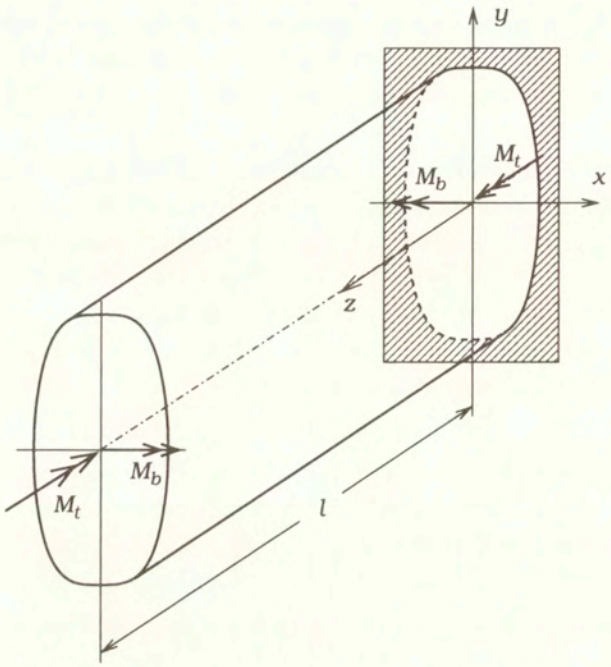

FIG. 1. Scheme of the bar.

for any constitutive equation under the assumption of incompressibility and small strains. In these equations dots denote derivatives with respect to the time t, and namely $\dot{\varkappa}$ the rate of curvature, $\dot{\vartheta}$ – the rate of unit angle of twist, and $w_0(x,y)$ – the warping function. The strain rates are as follows:

$$\begin{aligned} &\dot{\varepsilon}_x = \dot{\varepsilon}_y = -\frac{1}{2}\dot{\varkappa} y, \qquad \dot{\varepsilon}_z = \dot{\varkappa} y, \\ &\dot{\gamma}_{xy} = 0, \qquad \dot{\gamma}_{zy} = \dot{\vartheta}\left(\frac{\partial w_0}{\partial y} - x\right), \qquad \dot{\gamma}_{zx} = \dot{\vartheta}\left(\frac{\partial w_0}{\partial x} + y\right). \end{aligned} \tag{2.2}$$

The equilibrium equations are in this case reduced to one equation

$$\frac{\partial \tau_{zx}}{\partial x} + \frac{\partial \tau_{zy}}{\partial y} = 0 \tag{2.3}$$

with the relevant boundary condition

$$\tau_{zx}\mathrm{d}y - \tau_{zy}\mathrm{d}x = 0. \tag{2.4}$$

The constitutive equations of viscoplasticity are assumed in the form proposed by PERZYNA [27, 28, 30] under additional restriction to the Huber-Mises-Hencky

hypothesis. In tensorial notation they have the form (with slightly changed notation)

$$\dot{e}_{ij} = \frac{1}{2G}\dot{s}_{ij} + \frac{1}{T_m}\left\langle \Phi\left(\frac{\sqrt{s_{kl}s_{kl}}}{\varkappa_h} - 1\right)\right\rangle \frac{s_{ij}}{\sqrt{s_{kl}s_{kl}}}, \tag{2.5}$$

where s_{ij}, $\dot{s}_{ij}$, and $\dot{e}_{ij}$ denote, in turn, the deviatoric stress, deviatoric stress rate, and the deviatoric strain rate components, Φ is the empirical overstress function, $\varkappa_h$ – the isotropic workhardening function, T_m – the relaxation time, G – Kirchhoff's modulus and $\langle\ \rangle$ denotes the Macauley bracket (ramp function). In our case (2.5) yields three scalar equations, hence together with (2.3) we have four equations for four unknowns σ_z, τ_{zx}, τ_{zy}, and w_0; all these functions depend on two spatial variables, x and y, and on the time t.

3. A certain exact solution for rigid-visco-perfectly plastic materials

First we restrict our considerations to rigid-visco-perfectly plastic materials. Then the constitutive equations (2.5) are simplified to the form

$$\dot{e}_{ij} = \frac{1}{T_m}\left\langle \Phi\left(\sqrt{\frac{3}{2}}\frac{\sqrt{s_{kl}s_{kl}}}{\sigma_0} - 1\right)\right\rangle \frac{s_{ij}}{\sqrt{s_{kl}s_{kl}}}, \tag{3.1}$$

where σ_0 denotes the yield-point stress in uniaxial tension. Since the strain rate distribution is given here by (2.2), we are interested in an inverse form of (3.1), in order to calculate the stress components. To this aim we multiply each side of (3.1) by itself and after contraction obtain

$$\dot{e}_{ij}\dot{e}_{ij} = \frac{1}{T_m^2}\left[\left\langle \Phi\left(\sqrt{\frac{3}{2}}\frac{\sqrt{s_{kl}s_{kl}}}{\sigma_0} - 1\right)\right\rangle\right]^2. \tag{3.2}$$

Introducing the strain rate intensity $\dot{\varepsilon}_e$ and the stress intensity σ_e by the formulae

$$\dot{\varepsilon}_e = \sqrt{\frac{2}{3}\dot{e}_{ij}\dot{e}_{ij}}, \qquad \sigma_e = \sqrt{\frac{3}{2}s_{ij}s_{ij}}, \tag{3.3}$$

we rewrite (3.2) in the form

$$\dot{\varepsilon}_e = \frac{1}{T_m}\sqrt{\frac{2}{3}}\left\langle \Phi\left(\frac{\sigma_e}{\sigma_0} - 1\right)\right\rangle. \tag{3.4}$$

The symbol $\dot{\varepsilon}_e$ should not be confused with the time derivative of the strain intensity ε_e; they are equal to each other just in a simple loading processes.

For plastically active processes (loading) we may invert (3.4) to the form

$$\sigma_e = \sigma_0 \left[1 + \Phi^{-1} \left(\sqrt{\frac{3}{2}} T_m \dot{\varepsilon}_e \right) \right], \tag{3.5}$$

where the symbol Φ^{-1} denotes the function inverse with respect to Φ. Equation (3.1) expresses similarity of deviators, hence, taking (3.3) into account, we may write

$$s_{ij} = \frac{2}{3} \frac{\sigma_e}{\dot{\varepsilon}_e} \dot{e}_{ij} = \frac{2\sigma_0}{3\dot{\varepsilon}_e} \left[1 + \Phi^{-1} \left(\sqrt{\frac{3}{2}} T_m \dot{\varepsilon}_e \right) \right] \dot{\varepsilon}_{ij}. \tag{3.6}$$

Now we define the function $\Psi\left(\dot{\varepsilon}_e^2\right)$ as follows:

$$\frac{2\sigma_0}{3\dot{\varepsilon}_e} \left[1 + \Phi^{-1} \left(\sqrt{\frac{3}{2}} T_m \dot{\varepsilon}_e \right) \right] = \Psi\left(\dot{\varepsilon}_e^2\right), \tag{3.7}$$

hence

$$s_{ij} = \Psi\left(\dot{\varepsilon}_e^2\right) \dot{e}_{ij}. \tag{3.8}$$

The argument $\dot{\varepsilon}_e^2$ is here more convenient than $\dot{\varepsilon}_e$. Returning to engineering notation and making use of (2.2) we obtain

$$\begin{aligned} \sigma_z &= \frac{3}{2} \Psi \dot{\varkappa} y, \\ \tau_{zx} &= \frac{1}{2} \Psi \dot{\vartheta} \left(\frac{\partial w_0}{\partial x} + y \right), \\ \tau_{zy} &= \frac{1}{2} \Psi \dot{\vartheta} \left(\frac{\partial w_0}{\partial y} - x \right). \end{aligned} \tag{3.9}$$

The argument $\dot{\varepsilon}_e^2$ of the function Ψ equals

$$\varepsilon_e^2 = \dot{\varkappa}^2 y^2 + \frac{1}{3} \dot{\vartheta}^2 \left[\left(\frac{\partial w_0}{\partial x} + y \right)^2 + \left(\frac{\partial w_0}{\partial y} - x \right)^2 \right]. \tag{3.10}$$

Substituting (3.9) and (3.10) into the equilibrium equation (2.3) we obtain the equation for the warping function (final governing equation of the problem)

$$\begin{aligned} \Psi' \Bigg\{ & \left[\left(\frac{\partial w_o}{\partial y} - x \right) \left(\frac{\partial^2 w_o}{\partial x \partial y} - 1 \right) + \left(\frac{\partial w_o}{\partial x} + y \right) \frac{\partial^2 w_o}{\partial x^2} \right] \left(\frac{\partial w_o}{\partial x} + y \right) \dot{\vartheta}^2 \\ & + \left[\left(\frac{\partial w_o}{\partial y} - x \right) \frac{\partial^2 w_o}{\partial y^2} + \left(\frac{\partial w_o}{\partial x} + y \right) \left(\frac{\partial^2 w_o}{\partial x \partial y} + 1 \right) \right] \left(\frac{\partial w_o}{\partial y} - x \right) \dot{\vartheta}^2 \\ & + 3y \left(\frac{\partial w_o}{\partial y} - x \right) \dot{\varkappa}^2 \Bigg\} + \Psi \left(\frac{\partial^2 w_o}{\partial x^2} + \frac{\partial^2 w_o}{\partial y^2} \right) = 0, \end{aligned} \tag{3.11}$$

where Ψ' denotes the derivative of Ψ with respect to its argument $\dot{\varepsilon}_e^2$. In linear elasticity we have obviously $\Psi' = 0$, in (3.11) just the last term remains, and the warping w_0 is a harmonic function (HUBER [13]).

The nonlinear second-order Eq. (3.11) is rather complicated and its solutions depend, in general, on the shape of the function $\Psi = \Psi(\dot{\varepsilon}_e^2)$, but it may be easily checked that the harmonic function, well-known in elasticity,

$$w_o = Cxy \tag{3.12}$$

may satisfy (3.11) for any Ψ. Indeed, substituting (3.12) into (3.11) we find that the last term vanishes, and all the remaining terms may be divided by $\Psi' xy$. Then we obtain the following algebraic equation:

$$2C(C+1)\dot{\vartheta}^2 + 3\dot{\varkappa}^2 = 0, \tag{3.13}$$

and C may be evaluated for a given ratio $\dot{\vartheta}^2/\dot{\varkappa}^2$. In this case the shearing stresses are equal

$$\begin{aligned} \tau_{zx} &= \frac{1}{2}\Psi\dot{\vartheta}(C+1)y, \\ \tau_{zy} &= \frac{1}{2}\overset{\Psi}{\dot{\vartheta}}(C-1)x, \end{aligned} \tag{3.14}$$

so their effective values depend on the function Ψ. Nevertheless, substituting (3.14) into the boundary condition (2.4) we realize that the final shape of the cross-section does not depend on Ψ, namely

$$(C+1)y\,\mathrm{d}y - (C-1)x\,\mathrm{d}x = 0. \tag{3.15}$$

This equation determines an ellipse, since from (3.13) it is seen that $-1 < C < 0$. If we write equation of this ellipse in the classical form

$$\frac{x^2}{a^2} + \frac{y^2}{b^2} = 1, \tag{3.16}$$

we find

$$C = -\frac{b^2 - a^2}{b^2 + a^2} \tag{3.17}$$

and (3.13) results in

$$\frac{4}{3}\frac{\dot{\vartheta}^2}{\dot{\varkappa}^2} = \frac{(a^2+b^2)^2}{a^2(b^2-a^2)}. \tag{3.18}$$

Equation (3.18) restricts our considerations to simple loading/unloading processes (the strain rates remain proportional to each other at any point of the

body). It coincides with Eq. (13) of the paper by OBERWEIS and ŻYCZKOWSKI [26], where a certain exact solution for combined bending with torsion of a perfectly plastic bar was found. Indeed, if (3.12) is valid for any function Ψ, then it must also be valid for perfect plasticity. Later, ŻYCZKOWSKI [44] proved that the ellipse (3.16) combined with (3.18) determines the optimal shape of the cross-section and in [45] he applied this relation to determine optimal shapes of the beams under the variable bending moment $M_b = M_b(z)$.

For the given ratio $\dot{\vartheta}/\dot{\varkappa}$ we can find from (3.18) the relevant ratio a/b, it means the shape of the elliptical cross-section. Equation (3.18) is biquadratic with respect to a/b and we obtain

$$\frac{a^2}{b^2} = \frac{1}{1+\frac{4}{3}\frac{\dot{\vartheta}^2}{\dot{\varkappa}^2}}\left(\frac{2}{3}\frac{\dot{\vartheta}^2}{\dot{\varkappa}^2} - 1 \pm \sqrt{\frac{4}{9}\frac{\dot{\vartheta}^4}{\dot{\varkappa}^4} - \frac{8}{3}\frac{\dot{\vartheta}^2}{\dot{\varkappa}^2}}\right). \tag{3.19}$$

The radical in (3.19) must be non-negative, hence $\dot{\vartheta}^2/\dot{\varkappa}^2 \geqslant 6$. For $\dot{\vartheta}^2/\dot{\varkappa}^2 = 6$ we obtain one solution $a/b = 1/\sqrt{3}$, whereas for $\dot{\vartheta}^2/\dot{\varkappa}^2 > 6$ formula (3.19) determines two elliptic sections for which the solution (3.12) holds.

Substituting (3.12) and (3.17) into (3.10) we may write

$$\dot{\varepsilon}_e^2 = \frac{b^4}{b^2-a^2}\left(\frac{x^2}{a^2}+\frac{y^2}{b^2}\right)\dot{\varkappa}^2, \tag{3.20}$$

or making use of (3.18),

$$\dot{\varepsilon}_e^2 = \frac{4}{3}\frac{a^2b^4}{(a^2+b^2)^2}\left(\frac{x^2}{a^2}+\frac{y^2}{b^2}\right)\dot{\vartheta}^2. \tag{3.21}$$

4. Evaluation of external loadings

The bar under consideration is subject to twisting moment M_t and bending moment M_b. They are expressed in terms of stresses as follows:

$$M_t = \int\int_A (\tau_{zx}\, y - \tau_{zy}\, x)\, \mathrm{d}A, \tag{4.1}$$

$$M_b = 2\int\int_{A/2} \sigma_z\, y \mathrm{d}A, \tag{4.2}$$

where A is the cross-sectional area. Substituting (3.14) we may write

$$M_t = \frac{1}{a^2+b^2}\,\dot{\vartheta}\int\int_A \Psi\left(\dot{\varepsilon}_e^2\right)\left(a^2y^2+b^2x^2\right)\mathrm{d}x\,\mathrm{d}y. \tag{4.3}$$

It is convenient to introduce the variables ρ and φ by the substitution

$$x = a\,\rho\cos\varphi, \quad y = b\rho\sin\varphi, \quad \mathrm{d}A = ab\,\rho\,\mathrm{d}\rho\,\mathrm{d}\varphi, \tag{4.4}$$

then

$$M_t = \frac{2\pi a^3 b^3}{a^2+b^2}\,\dot{\vartheta}\int_o^1 \Psi\left(\dot{\varepsilon}_e^2\right)\rho^3\mathrm{d}\rho. \tag{4.5}$$

We call the (non–orthogonal) system of coordinates ρ, φ the "polar–elliptic coordinates" since the name "elliptic coordinates" is ascribed to some other, orthogonal system (MORSE and FESHBACH [25]). Stress and strain components are retained in Cartesian system. The normal stresses σ_z are given by (3.9), hence

$$M_b = \frac{3}{2}\pi a b^3 \dot{\varkappa}\int_o^1 \Psi\left(\dot{\varepsilon}_e^2\right)\rho^3\mathrm{d}\rho. \tag{4.6}$$

Introduce the ratio of the moments squared, like in the papers by BOCHENEK *at al.* [3] and by ŻYCZKOWSKI [44]

$$\eta = \left(\frac{M_b}{M_t}\right)^2. \tag{4.7}$$

Substituting (4.5), (4.6) and (3.18), we obtain for any function $\Psi(\dot{\varepsilon}_e^2)$

$$\eta = \frac{3}{4}\,\frac{b^2-a^2}{a^2} \tag{4.8}$$

and hence the ratio of semi-axes of the ellipse may be expressed in terms of external loadings as follows:

$$\frac{b}{a} = \sqrt{1+\frac{4}{3}\,\eta}. \tag{4.9}$$

This result coincides with that obtained by ŻYCZKOWSKI for perfect plasticity [44]. In contradistinction to (3.19), it gives one and only one solution for any value of η.

As an example we consider the power law, being an extension of Norton's creep law to viscoplasticity (PERZYNA [30]).

$$\dot{e}_{ij} = \frac{1}{T_m}\left\langle\left(\sqrt{\frac{3}{2}}\,\frac{\sqrt{s_{kl}s_{kl}}}{\sigma_o}-1\right)^{\delta}\right\rangle\frac{s_{ij}}{\sqrt{s_{kl}s_{kl}}}. \tag{4.10}$$

Then (3.5) and (3.7) take the form

$$\sigma_e = \sigma_o \left[1 + \left(\sqrt{\frac{3}{2}} T_m \frac{b^2}{\sqrt{b^2 - a^2}} \rho |\dot{\varkappa}| \right)^{1/\delta} \right], \tag{4.11}$$

$$\Psi = \frac{2\sigma_o (b^2 - a^2)}{3b^2 \rho |\dot{\varkappa}|} \left[1 + \left(\sqrt{\frac{3}{2}}\, T_m \frac{b^2}{\sqrt{b^2 - a^2}} \rho |\dot{\varkappa}| \right)^{1/\delta} \right] \tag{4.12}$$

(or a similar form expressed in terms of $\dot{\vartheta}$), and the moments are equal to

$$M_b = \frac{\pi}{3}\, ab\sqrt{b^2 - a^2}\, \sigma_o \left[1 + \frac{3\delta}{3\delta + 1} \left(\sqrt{\frac{3}{2}} T_m \frac{b^2}{\sqrt{b^2 - a^2}} |\dot{\varkappa}| \right)^{1/\delta} \right] \operatorname{sign} \dot{\varkappa}, \tag{4.13}$$

$$M_b = \frac{2\pi}{3\sqrt{3}}\, a^2 b\, \sigma_o \left[1 + \frac{3\delta}{3\delta + 1} \left(\sqrt{2}\, T_m \frac{ab^2}{a^2 + b^2} |\dot{\vartheta}| \right)^{1/\delta} \right] \operatorname{sign} \dot{\vartheta}. \tag{4.14}$$

Of course, in view of (3.18) the square brackets are identical to each other and (4.8) holds, but it is more natural to present M_b in terms of $\dot{\varkappa}$ and M_t in terms of $\dot{\vartheta}$, and hence the notation used. For $\delta \to 0$ we obtain the formulae derived in [44] under the assumption of perfect plasticity. Inversion of (4.13) and (4.14) so as to determine the functions $\dot{\varkappa} = \dot{\varkappa}(M_b)$ and $\dot{\vartheta} = \dot{\vartheta}(M_t)$ does not present any difficulties.

5. Extension to additional elastic strains and plastic hardening

In Sec. 3 we derived an exact solution for the problem under consideration but under additional restrictions to perfect plasticity and ommision of elastic strains. The solution is explicit and analytical if the function Φ^{-1} in the formula for Ψ (3.7) may be determined analytically. Now we return to the more general constitutive equation (2.5) and prove that also in this case a similar solution holds, but Ψ must be evaluated numerically.

We make use of the polar–elliptic coordinates (4.4), and assume the warping function w_o in the form (3.12) with C determined by (3.17). Hence Eqs. (2.2) look now as follows:

$$\begin{aligned} &\dot{\varepsilon}_x = \dot{\varepsilon}_y = -\frac{1}{2}\, \dot{\varkappa} \rho b \sin\varphi, \qquad \dot{\varepsilon}_z = \dot{\varkappa} \rho b \sin\varphi, \\ &\dot{\gamma}_{xy} = 0, \quad \dot{\gamma}_{zx} = \dot{\vartheta} \frac{2a^2}{b^2 + a^2}\, \rho b \sin\vartheta, \quad \dot{\gamma}_{zy} = -\dot{\vartheta} \frac{2b^2}{b^2 + a^2}\, \rho a \cos\varphi. \end{aligned} \tag{5.1}$$

where $\dot{\varkappa}$ and $\dot{\varphi}$ are interrelated by (3.18). Now we assume the solution in the form (3.9) with substituted (3.12)

$$
\begin{aligned}
\sigma_z &= \frac{3}{2}\Psi\dot{\varkappa}\rho b\sin\varphi,\\
\tau_{zx} &= \Psi\dot{\vartheta}\frac{a^2}{b^2+a^2}\rho b\sin\varphi,\\
\tau_{zy} &= -\Psi\dot{\vartheta}\frac{b^2}{b^2+a^2}\rho a\ \cos\varphi.
\end{aligned}
\tag{5.2}
$$

Equations (5.2) are regarded as a hypothesis: it will be shown that they can satisfy all the governing equations, and the equation for Ψ, generalizing (3.7), will be derived.

In general, $\Psi = \Psi(\rho, \varphi, t)$, but the equilibrium Eq. (2.3) results in $\partial\Psi/\partial\varphi = 0$, hence we assume $\Psi = \Psi(\rho, t)$. First we discuss plastically passive processes. Neglecting the bracket in (2.5) we realize that all the three independent equations for $\dot{\varepsilon}_z, \dot{\gamma}_{zx}$, and $\dot{\gamma}_{zy}$, are satisfied if

$$\dot{\varkappa} = \frac{1}{2G}\frac{\mathrm{d}}{\mathrm{d}t}(\Psi\dot{\varkappa}). \tag{5.3}$$

We used here the symbol of ordinary derivative, since the spatial variable ρ is not present. Integrating (5.3) we find

$$\varkappa = \frac{\Psi\dot{\varkappa}}{2G} + C. \tag{5.4}$$

In the elastic range preceding viscoplastic deformations the constant C vanishes, and hence

$$\Psi = \frac{2G\varkappa}{\dot{\varkappa}}. \tag{5.5}$$

Further we prove that the plastic hardening depends only on the coordinate ρ, and does not depend on φ. It will be sufficient to restrict our considerations to isotropic hardening: in simple loading/unloading processes enforced by (3.18) other types of hardening (kinematic, distortional, etc.) do not bring any effects. Isotropic hardening is usually expressed in terms of the Odqvist parameter $I_{\varepsilon p}$ (strain–hardening) or of the plastic work W^p (work–hardening). Here we consider only strain–hardening in view of simpler final expressions, but principal conclusions remain valid for work-hardening without change. The Odqvist parameter is defined as the length of the trajectory in the plastic strain space:

$$I_{\varepsilon p} = \int_0^t \sqrt{\dot{\varepsilon}^p_{ij}\dot{\varepsilon}^p_{ij}}\ \mathrm{d}\bar{t} = \int_0^t \sqrt{\dot{e}_{ij}\dot{e}_{ij} - \frac{1}{G}\dot{e}_{ij}\dot{s}_{ij} + \frac{1}{4G^2}\dot{s}_{ij}\dot{s}_{ij}}\ \mathrm{d}\bar{t} \tag{5.6}$$

where $\bar{t}$ is the variable of integration. Making use of (5.1), (5.2) and (3.18) we calculate the invariants appearing in (5.6):

$$\dot{e}_{ij}\,\dot{e}_{ij} = \frac{3}{2}\frac{b^4}{b^2-a^2}\rho^2\dot{\varkappa}^2, \tag{5.7}$$

$$\dot{e}_{ij}\,\dot{s}_{ij} = \frac{3}{2}\frac{b^4}{b^2-a^2}\rho^2\dot{\varkappa}\frac{\mathrm{d}}{\mathrm{d}t}(\Psi\dot{\varkappa}), \tag{5.8}$$

$$\dot{s}_{ij}\,\dot{s}_{ij} = \frac{3}{2}\frac{b^4}{b^2-a^2}\rho^2\left[\frac{\mathrm{d}}{\mathrm{d}t}(\Psi\dot{\varkappa})\right]^2, \tag{5.9}$$

and hence

$$I_{\varepsilon p} = \sqrt{\frac{3}{2}}\frac{b^2\rho}{\sqrt{b^2-a^2}}\int_0^t \left|\dot{\varkappa} - \frac{1}{2G}\frac{\mathrm{d}}{\mathrm{d}t}(\Psi\dot{\varkappa})\right| \mathrm{d}\bar{t} \tag{5.10}$$

or after integration, for monotonically increasing $|\varkappa|$,

$$I_{\varepsilon p} = \sqrt{\frac{3}{2}}\frac{b^2\rho}{\sqrt{b^2-a^2}}\left|\varkappa - \frac{\Psi\dot{\varkappa}}{2G}\right|\Bigg|_0^t = I_{\varepsilon p}(\rho, t). \tag{5.11}$$

It is seen from (5.5) that in the elastic range the bracket vanishes, hence the integration starts in the viscoplastic range, and we may simply omit the limits of integration $0, t$. The most important conclusion is that $I_{\varepsilon p}$ depends on ρ and t, but does not depend on φ.

In order to have notation similar to (3.1) we present now the strain-hardening function in the form

$$\varkappa_h = \sigma_o\sqrt{\frac{2}{3}}\left[1 + f_h\left(I_{\varepsilon p}\right)\right] \tag{5.12}$$

$$= \sigma_o\sqrt{\frac{2}{3}}\left[1 + f_h\left(\sqrt{\frac{3}{2}}\frac{b^2\rho}{\sqrt{b^2-a^2}}\left|\varkappa - \frac{\Psi\dot{\varkappa}}{2G}\right|\right)\right]$$

where f_h is a function to be determined experimentally. In applications, f_h is often assumed as a linear function. Now we return to (2.5), substitute (5.1), (5.2), (5.12) and the expression resulting from (5.2) for the stress intensity

$$\sigma_e = \sqrt{\frac{3}{2}s_{ij}s_{ij}} = \frac{3}{2}\frac{b^2}{\sqrt{b^2-a^2}}\Psi\rho\,|\dot{\varkappa}| \tag{5.13}$$

and realise, that all three equations for the components $\dot{\varepsilon}_z$, $\dot{\gamma}_{zx}$, and $\dot{\gamma}_{zy}$ cancelled, in turn, by $\sin\varphi$, $\sin\varphi$ and $\cos\varphi$, may simultaneously be satisfied. It takes place if the function $\Psi = \Psi(\rho, t)$ satisfies the nonlinear ordinary differential equation

$$\dot{\varkappa} = \frac{1}{2G}\frac{\mathrm{d}}{\mathrm{d}t}(\Psi\dot{\varkappa}) + \sqrt{\frac{2}{3}}\frac{\sqrt{b^2-a^2}}{T_m b^2 \rho}\left\langle \Phi\left\{\frac{\frac{3}{2}\frac{b^2}{\sqrt{b^2-a^2}}\Psi\rho\dot{\varkappa}}{\sigma_o[1+f_h(I_{\varepsilon p})]} - 1\right\}\right\rangle. \tag{5.14}$$

The symbol of partial derivative was not introduced into (5.13) since the variable ρ may be regarded as a parameter and the differentiation with respect to ρ does not appear.

The elastic-viscoplastic interface is determined by vanishing of the bracket in (5.14). We obtain the equation

$$\frac{3}{2}\frac{b^2}{\sqrt{b^2-a^2}}\Psi\rho\dot{\varkappa} = \sigma_o\left[1 + f_h\left(\sqrt{\frac{3}{2}}\frac{b^2\rho}{\sqrt{b^2-a^2}}\left|\varkappa - \frac{\Psi\dot{\varkappa}}{2G}\right|\right)\right]. \tag{5.15}$$

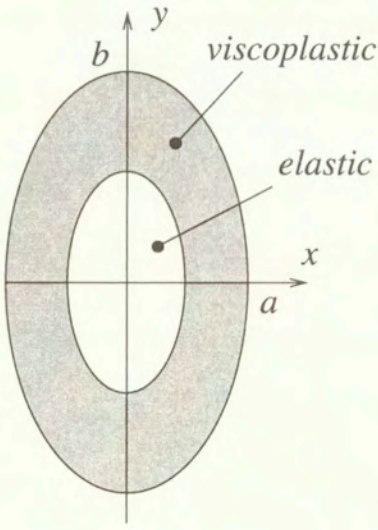

FIG. 2. The elastic and viscoplastic zones in the cross-section.

Considering the first plastification we substitute Ψ determined for the elastic range (5.5), hence the elastic-viscoplastic interface is an ellipse, geometrically similar to the contour, and is described by the coordinate $\rho = \rho_b$

$$\rho_b = \frac{\sqrt{b^2-a^2}}{3b^2}\frac{\sigma_o}{G\varkappa} \tag{5.16}$$

(Fig.2). Of course, this ellipse decreases with increasing $\varkappa$.

6. Attributes of optimality of the solution obtained

In the introduction we pointed out the variety of optimization problems in viscoplasticity. Now we are going to prove that the solution obtained, namely the elliptic shape (3.16) satisfying the conditions (3.19) or (4.9), is indeed an optimal solution if we impose constraints on damage evolution and restrict the class of materials under consideration.

Strength of a viscoplastic structure is usually determined by reaching by the upper bound of the damage parameter a certain prescribed value, regarded as critical. There exist many various approaches to the concepts of damage and to relevant evolution equations. For our purposes any of them may be employed, provided the material of the structure (of the bar under torsion with bending) is governed exclusively by the HMH failure hypothesis. Indeed, from (5.13) it is seen that the stress intensity $\sigma_e = \sigma_{HMH}$ is constant along the contour $\rho = 1$ at any time t, hence the elliptic shape is the "shape of uniform viscoplastic strength". Though the shapes of uniform strength are not always optimal (for example, if the geometry changes are taken into account, ŚWISTERSKI *at al.* [40]), but in the case under consideration nothing like that takes place.

First we consider Kachanov's approach who introduced the damage parameter D connected with formation of microcracks. He described the damage evolution under uniaxial tension by the equation

$$\dot{D} = \overline{C}\left(\frac{\sigma}{1-D}\right)^{\mu}, \tag{6.1}$$

where $\overline{C}$ and μ are temperature-dependent material constants. Several generalizations of (6.1) for multiaxial states were introduced. HAYHURST [12] proposed to replace σ by the following stress invariant σ_{red} (reduced stress)

$$\sigma_{red} = \alpha\sigma_{\mathrm{I}} + \beta J_{1\sigma} + \gamma\sigma_e \tag{6.2}$$

with $\alpha + \beta + \gamma = 1$; in this equation σ_{I} denotes the maximal principal stress (Galileo's hypothesis), and $J_{1\sigma} = \sigma_{kk}$ – the first stress invariant. Some particular cases of (6.2) were considered eariler by SDOBYRIEV [38] with $\beta = 0$, $\alpha = \gamma = \frac{1}{2}$, and by RABOTNOV [36] with $\beta = 0$. $\alpha + \gamma = 1$. It is seen that (6.1) with substituted (6.2) gives constant damage rate at the boundary of the elliptic cross–section under consideration if $\alpha = \beta = 0$, $\gamma = 1$. This takes place for example, for aluminium alloys Al-Mg-Si [12], and then the ellipse may be regarded as optimal.

In a series of papers Perzyna considered the damage as nucleation and growth of microvoids (porosity). In the papers [31, 32] he proposed to describe nucleation

of the porosity parameter ξ by the evolution equation

$$(\dot{\xi})_{nucl} = \frac{1}{T_m} h^*(\xi,\ \vartheta) \left[\exp \frac{m^*(\vartheta)|I_n - \tau_n(\xi,\ \vartheta,\ I_{\varepsilon\rho})|}{k\vartheta} - 1 \right], \tag{6.3}$$

where ϑ denotes temperature (not to be confused with the notation introduced in Sec. 2 for the unit angle of twist), k – the Boltzmann constant, $h^*(\xi, \vartheta)$ is a material function describing the microvoid interaction, $m^*(\vartheta)$ is a temperature-dependent coefficient, τ_n is the threshold stress for microvoid nucleation, and I_n denotes the following stress invariant, similar to (6.2),

$$I_n = a_1 J_{1\sigma} + a_2 \sigma_e + a_3 (J_{3d})^{1/3}, \tag{6.4}$$

a_i $(i = 1, 2, 3)$ are the material constants, and J_{3d} is the third invariant of the stress deviator. Further, in a paper with DRABIK [34], the following evolution equation for the growth mechanism of ξ was postulated:

$$(\dot{\xi})_{grow} = \frac{1}{T_m} \frac{g^*(\xi,\ \vartheta)}{x_o} [I_g - \tau_{eq}(\xi,\ \vartheta,\ I_{\varepsilon p})], \tag{6.5}$$

where $T_m x_o$ denotes dynamic viscosity of the material, $g^*(\xi, \vartheta)$ – the function describing the microvoid interaction, I_g – the stress invariant like (6.4) with some other coefficients b_i, and τ_{eq}, the void growth threshold stress. Finally, the evolution equation for ξ is determined by the sum of (6.3) and (6.5). The details are presented by PERZYNA [33] in his contribution to the Handbook of Materials Behaviour Models [21]. It is seen that in the case $a_1 = a_2 = 0$ the microvoid nucleation is governed by the HMH hypothesis, and then the elliptic contour is optimal with respect to nucleation. Moreover, if $b_1 = b_2 = 0$, then the optimality pertains also to the microvoids growth. Unfortunately, not too many values of material constants a_i and b_i are available. Paper [33] quotes the relevant values for the AISI 4340 steel. The constant $b_3 = 0$ and b_1 is smaller than b_2, but b_1 is different from zero and for that steel the optimality of (3.16) does not take place.

In [46] ŻYCZKOWSKI proposed to express the damage evolution equations in terms of the unit dissipated power $\overline{\Psi}$, namely

$$\dot{D} = \frac{1}{C_d} \sqrt{\frac{\overline{\Psi}}{1 - D}}, \tag{6.6}$$

where C_d is called the damage modulus. In the case of Perzyna's Eq. (2.5), for viscoplastic materials we obtain

$$\overline{\Psi} = s_{ij}\, \dot{e}^p_{ij} = \frac{1}{T_m} \left\langle \Phi \left(\frac{\sqrt{s_{kl} s_{kl}}}{\varkappa_h} - 1 \right) \right\rangle \sqrt{s_{ij} s_{ij}} \tag{6.7}$$

and hence

$$\dot{D} = \frac{1}{C_d}\sqrt{\frac{1}{(1-D)T_m}\left\langle \Phi\left(\frac{\sqrt{s_{kl}s_{kl}}}{\varkappa_h} - 1\right)\right\rangle \sqrt{s_{ij}s_{ij}}}. \tag{6.8}$$

It is seen that in this case $\dot{D}$ depends only on the second deviatoric stress invariant and hence the shape (3.16) is optimal. The hypothesis (6.6) was relatively well confirmed for various materials subject to nonlinear creep in uniaxial tension, but a similar confirmation for viscoplastic materials is lacking, and undoubtedly it may take place for a certain restricted class of materials only.

Extensive reviews of damage evolution equations are given by LEMAITRE [20], KRAJCINOVIC [16], SKRZYPEK and GANCZARSKI [39]. Many of them are expressed just in terms of the stress intensity σ_e and then the shape (3.16) is optimal for viscoplastic bars under simultaneous torsion with bending if the strength expressed by damage evolution is assumed as the optimization constraint.

7. Conclusions

1. The paper gives a simple closed-form solution to the complicated nonlinear governing equation of viscoplastic bars under torsion with bending (3.11). It corresponds to an elliptic cross-section with the ratio of semi-axes depending on the ratio of twist to curvature, (3.19), or on the ratio of bending to twisting moment (4.9). This solution may be regarded as a bench mark to verify numerical methods applied for other shapes of the cross-section.

2. In his habilitation thesis GAJEWSKI [11] considered the dependence of optimal shapes on the constitutive equations adopted. In general, the optimal shapes depend on them, but Gajewski separated many cases of structural elements, loadings and constraints in which the final shape does not depend on constitutive equations. The present paper shows probably the first case of optimal design under combined loadings in which the solution also does not depend on constitutive equations.

3. The solution obtained is shown to be optimal if the constraints are imposed on initiation and growth of damage, considered as responsible for strength of the bar. Optimality takes place if the constitutive equations and the damage evolution equations are based on the HMH failure hypothesis, it means on the second deviatoric stress invariant.

4. Extension to linear combination with other stress invariants, like (6.2) or (6.4), is not possible. However, ŻYCZKOWSKI [42] considered general, non-

linear functions of the basic invariants leading to the "ad hoc" elliptic yield condition, namely, in the case under consideration,

$$\sigma_z^2 + c\,(\tau_{zx}^2 + \tau_{zy}^2) = \sigma_o^2, \tag{7.1}$$

with arbitrary positive constant c. Then the chances of deriving similar formulae as in the present paper are quite realistic.

5. Optimization of the viscoplastic bars subjected to torsion with bending with the constraints imposed on stiffness is undoubtedly much more difficult. However, if we express that stiffness (or rather compliance) by the total dissipated power, then one may expect that (3.16) with (3.19) or (4.9) gives also in this case the optimal solution, since we proved in Sec. 6 that the unit dissipated power is constant along any line ρ =const. The proof of such a statement should be based on the general Eq. (3.11) and hence it seems rather complicated.

Acknowledgement

The Grant 7T07A 03819 from the State Committee for Scientific Research KBN Poland is gratefully acknowledged.

References

1. J. S. ARORA, T. H. LEE and J. B. CARDOSO, *Structural shape sensitivity analysis: relation between material derivative and control volume approaches*, AIAA Journal, **30**, 1638–1648, 1992.
2. J. S. ARORA, T. H. LEE and V. KUMAR, *Design sensitivity analysis of non-linear structures III: shape variation of viscoplastic structures*, publ. AIAA, Washington, 447–485, 1993.
3. B. BOCHENEK, Z. KORDAS and M. ŻYCZKOWSKI, *Optimal plastic design of a cross section under torsion and small bending*, J. Struct. Mech., **11**, 3, 383–400, 1983.
4. E. CEGIELSKI, *Optimization of rigid-viscoplastic bars and beams under dynamic loadings*, in Proc. IV Bulg. Congr. Mech. Varna, vol. 1, 484–489, 1981.
5. E. CEGIELSKI, *Problems of optimization of a cantilever viscoplastic beam under quasistatic load* [in Polish], Mech. Teor. Stos., **23**, 3/4, 381–396, 1985.
6. E. CEGIELSKI, *Parametric optimization of viscoplastic bars under dynamic twisting loadings*, Mech. Teor. Stos., **28**, 1/2, 35–44, 1990.
7. E. CEGIELSKI, *Optimal design of rigid-viscoplastic beams subject to dynamical bending and axial forces*, Z. Angew. Math. Mechanik, **72**, 6, 540–542, 1992.
8. E. CEGIELSKI and M. ŻYCZKOWSKI, *Parametric optimization of viscoplastic bars under dynamic axial loading*, Rozprawy Inż., **29**, 1, 27–37, 1981.

9. E. CEGIELSKI and M. ŻYCZKOWSKI, *Optimization of some viscoplastic structures under variable loads*, in Proc. Euromech Coll. 174 on Inelastic Structures, Palerno 1983, COGRAS, 105 – 116, Palermo 1984,

10. E. CEGIELSKI and M. ŻYCZKOWSKI, *Optimal design of viscoplastic structures uider dynamic loadings*, in Proc. GAMM Seminar Discretization Meth. and Struct. Optimiz., Siegen 1988, Springer 1989. 102 – 109.

11. A. GAJEWSKI, *Optymalne kształtowanie wytrzymałościowe w przypadku matıriału o nieliniowości fizycznej*, Zeszyty Nauk. Polit. Krak. 5, Kraków 1975 (Polish ful text); Effect of physical nonlinearities on optimal design of structures, in Proc. IUTAM Symp. on Physical Nonlinearities, Senlis 1980, publ. Springer 1981, 81 – 84 (English summary).

12. D. R. HAYHURST, *Creep rupture under multiaxial state of stress*, J. Mech. Phys Solids, **20**, 6, 381 – 390, 1972.

13. R. HILL, *The mathematical theory of plasticity*, Clarendon Press, Oxford 1950.

14. M. T. HUBER, *Theory of elasticity* [in Polish:], vo. I, PAU, Kraków 1948.

15. S. Y. JAO and J. S. ARORA, *Design optimization of non-linear structures with rate-dependent and rate-independent constitutive models*, Int. J. Numer. Meth. Eng., **36** 2805 – 2823, 1993.

16. L. M. KACHANOV, *Time of the rupture process under creep conditions* [in Russian], Izv. AN SSSR, Otd. Tekh. Nauk. 8, 26-31, 1958.

17. D. KRAJCINOVIC, *Damage mechanics*, Elsevier, Amsterdam, 1996.

18. M. KULKARNI and A. K. NOOR, *Sensitivity analysis of the non-linear dynamic viscoplastic response of 2D - structures with respect to material parameters*, Int. J. Numer Meth. Eng., **38**, 2, 183-198, 1995.

19. J. H. LAU and G. K. LISTVINSKY, *Bending and twisting of internally pressurized thin-walled cylinder with creep*, J. Appl. Mech., **48**, 2, 439-441, 1981.

20. T. H. LEE, J. S. ARORA and V. KUMAR, *Shape design sensitivity analysis of viscıplastic structures*, Comp. Meth. Appl. Mech. Eng., **108**, 237-259, 1993.

21. J. LEMAITRE, *A course on damage mechanics*, Springer, Berlin 1992.

22. J. LEMAITRE [Ed.], *Handbook of materials behavior models*, vol. 1/3, Academic Press, San Diego 2001.

23. K. J. LEU and S. MUKHERJEE, *Sensitivity analysis and shape optimization in nonlinear solid mechanics*, Eng. Anal. Bound. Elements, **12**, 4, 251 – 260,1993.

24. K. J. LEU and S. MUKHERJEE, *Implicit objective integration for sensitivity analysis in nonlinear solid mechanics*, Int. J. Numer. Meth. Eng., **37**, 3843-3868, 1994.

25. S. A. MEGUID, J. D. CAMPBELL and L. E. MALVERN, *On the elastic-viscoplastic proportional combined twist and stretch of a circular bar of rate-sensitive material*, J. Mech. Phys. Solids, **27**, 4, 331 – 343, 1979.

26. P. M. MORSE and H. FESHBACH, *Methods of theoretical physics*, Mc Graw-Hill, Nev York - Toronto - London, 1953.

27. P. OBERWEIS and M. ŻYCZKOWSKI, *On Pala's method for plastic bending with tırsion*, J. Appl. Mech., **64**, 2, 435 – 437, 1997.

28. P. PERZYNA, *The constitutive equations for rate sensitive plastic materials,* Quart. Appl. Math., **20**, 321–332, 1963.

29. P. PERZYNA, *The constitutive equations for work-hardening and rate sensitive plastic materials,* Bull. Acad. Pol. Sci., Ser.Sci. Techn., **12**, 199–206, 1964.

30. P. PERZYNA, *Fundamental problems in viscoplasticity,* Adv. Appl. Mech., **9**, 243–377, 1966.

31. P. PERZYNA, *Theory of viscoplasticity,* (in Polish), IPPT PAN-PWN, Warszawa 1966.

32. P. PERZYNA, *Internal state variable description of dynamic fracture of ductile solids,* Int. J. Sol. Structures, **22**, 797–818, 1986.

33. P. PERZYNA, *Constitutive modelling for brittle dynamic fracture in dissipative solids,* Arch. Mechanics, **38**, 725–738, 1986.

34. P. PERZYNA, *Thermo-elasto-viscoplasticity and damage,* in [21], Sec. 9.5, 821–834, 2001.

35. P. PERZYNA and A. DRABIK, *Description of micro-damage process by porosity parameter for nonlinear viscoplasticity,* Arch. Mechanics, **41**, 895–908, 1989.

36. S. PIECHNIK, *Steady-state creep of solid bar under combined load,* Kungl. Tekniska Högskolans Handlingar, Mech. Engng., 7, Stockholm 1962.

37. YU. N. RABOTNOV, *Creep of structural elements,* Nauka, Moskva 1966 (Russian original); North Holland, Amsterdam 1969 (English translation).

38. M. RYSZ and M. ŻYCZKOWSKI, *Optimal design of a thin-walled cross-section subject to bending with torsion against creep rupture,* Int. J. Mech. Sci., **30**, 2, 127–136, 1988.

39. V. P. SDOBYREV, *A long-time strength criterion for heat-resisting alloys under multiaxial states of stress* [in Russian], Izv. AN SSSR, Otd. Tekhn. Nauk., 6, 93–99, 1959.

40. J. SKRZYPEK and A. GANCZARSKI, *Modeling of material damage and failure of structures,* Springer, Berlin 1999.

41. W. ŚWISTERSKI, A. WRÓBLEWSKI and M. ŻYCZKOWSKI, *Geometrically nonlinear eccentrically compressed columns of uniform creep strength vs. optimal columns,* Int J. Nonlinear Mech., **18**, 4, 287–296, 1983.

42. O. ZHANG, S. MUKHERJE and A. CHANDRA, *Design sensitivity coefficients for elasto-viscoplastic problems by boundary element methods,* Int. J. Numer. Meth. Eng., **34**, 3, 947-966, 1992.

43. M. ŻYCZKOWSKI, *Combined loadings in the theory of plasticity,* PWN–Nijhoff, Warszawa–Alphen aan den Rijn 1981.

44. M. ŻYCZKOWSKI, *Optimal structural design under creep conditions,* Appl. Mech. Rev., **49**, 9, 433–446, 1996.

45. M. ŻYCZKOWSKI, *Optimal plastic design for combined torsion with bending,* Proc. Second World Congr. Str. Optimiz., Zakopane, W. GUTKOWSKI and Z. MRÓZ [Eds.], vol.2, 809–814, 1997.

46. M. ŻYCZKOWSKI, *Optimal plastic design of statically indeterminate beams under bending with torsion,* Festschrift Prof. Peter Gummert, TU Berlin, 251–262, 1998.

47. M. ŻYCZKOWSKI, *Creep damage evolution equations expressed in terms of dissipated power*, Int. J. Mech. Sci., **42**, 755–769, 2000.

48. M. ŻYCZKOWSKI and E. CEGIELSKI, *Parametric optimization of rigid-viscoplastic beams under dynamic loads* (in Polish), Arch. Inż. Lądowej, **32**, 1, 95–104, 1986.

Received June 7, 2002; revised version August 26, 2002.

Archives of Mechanics

Contents of issue 5-6 vol. 54

(Continued on cover III)

Dedicated to Professor Piotr Perzyna

For technical reasons two subsequent papers will be published in the next issue

Arch. Mech., **54**, nr 5-6, str. 353–770, Warszawa 2002